Springer Series in Biophysics

Editor: P.M. Bayley, London

3

# Springer Series in Biophysics

U. Aebi      J. Engel (Eds.)

# Cytoskeletal and Extracellular Proteins

Structure, Interactions and Assembly

The 2nd International EBSA Symposium

With 149 Figures

Professor Dr. UELI AEBI
Maurice E. Müller-Institut
Biozentrum der Universität Basel
Klingelbergstraße 70
CH-4056 Basel

Professor Dr. JÜRGEN ENGEL
Abteilung für Biophysikalische Chemie
Biozentrum der Universität Basel
Klingelbergstraße 70
CH-4056 Basel

# Preface

Cytoskeletal and extracellular matrix proteins have many features in common regarding their 3-dimensional structure, interactions and assembly properties. In- and outside the cell filaments, fibres and more complex supramolecular assemblies are in dymanic equilibrium with molecular building blocks exhibiting many common structural motifs and having a high potential for *in vitro* self-assembly. In addition, the two systems can communicate with each other through receptor molecules spanning the plasma membrane and interacting via their extracellular and cytosolic domains with specific components of the two.

Biophysical research has made substantial contributions to our present knowledge and understanding of the often complex biological functions and interactions of the cytoskeleton and the extracellular matrix. The three-dimensional structure of the constituent proteins, the dynamics of their interactions, the thermodynamics of assembly and the mechanisms of regulatory processes, as well as the architecture and molecular organization of complex structures all represent problems that are approached by a large repertoire of biophysical methods. The polymerization mechanisms underlying actin filament formation, the regulation of their spatial and temporal distribution by actin-binding proteins, their interaction with myosin in force generation, the growth and dynamic remodelling of micotubules, collagen fibrillogenesis, the multidomain structure of cell attachment molecules such as laminin, the supramolecular organization of basement membranes and of the nuclear pore complex are only a few examples for successful biophysical research. The fascinating discoveries of receptor molecules establishing a link between components of the extracellular matrix and the cytoskeleton, and the observation of dramatic changes in the cytoskeleton in response to extracellular stimuli represent a new challenge to biophysicists for exploring the underlying molecular events and mechanisms.

The present book is based on the contributions made at a recent Symposium of the **European Biophysical Societies Association (EBSA)** held in Gwatt, Switzerland, from 4th to 7th September, 1988 which was supported by the Swiss National Science Foundation, the Swiss Academy of Sciences, the Maurice E. Müller Foundation of Switzerland, and the Interpharma Association in Basel. The Symposium was organized with the idea to bring together researchers from "both sides of the cell membrane" to present to and discuss with each other the current research in the two fields, to exchange experience and

ideas, and to stimulate collaboration. Not only the related methodologies and approaches but also the need for a more integral approach to systematically evaluate the structure, function and interactions of the proteins of the cytoskeleton and the extracellular matrix made such a symposium timely. We intentionally did not limit the scope to "pure" biophysics but tried to incorporate relevant biochemical and cell biological work. To all of us this Symposium was very informative and stimulating and we are hoping that this also holds true for the present book which is trying to give a representative sampling and up-to-date picture of current research in the two fields. Each section contains a number of articles written by experts which, in addition to just presenting new data, also try to review the state of knowledge in a particular area. This, we hope, will make the book useful also to non-experts and will help to follow the many new results reported in 65 contributions. We obviously had to be selective and were unable to cover all interesting ongoing work in the two fields. To help bridge this gap, sufficient references and an index are provided with the hope of the editors to make this book an useful source for gathering information and stimulate further reading in these two exciting and rapidly evolving fields of research.

Basel, November 1988                                     Ueli Aebi and Jürgen Engel

# Contents

## SECTION III: Structural Motifs of Multi-Domain Proteins

## SECTION IV: Biophysical Methods for Elucidation of the Structure and Assembly of Cytoskeletal and Extracellular Constituents

## SECTION V: Thermodynamics and Kinetics of Assembly

# List of Contributors

You will find the addresses at the beginning of the respective contribution

Aebi, U.  33, 51, 57
Affolter, M.  312
Akey, C.W.  307
Atkinson, S.J.  150
Aubery, M.  110
Audenaert, R.  222
Aumailley, M.  92
Avigad, G.  203
Bächinger, H.P.  171
Bärmann, M.  233
Bailey, R.T.  169
Bayley, P.M.  249
Beck, K.  102, 106, 117
Bennett, V.  319
Bigner, D.  114
Bisher, M.E.  15
Blake, C.C.F.  137
Blumberg, A.  355
Blumberg, B.  347
Bollag, D.M.  3
Bruch, M.  108
Brunner, J.  345
Brunner, U.T.  163
Burger, M.M.  345
Butler, J.A.  341
Campbell, A.G.  347
Carlier, M.-F.  264
Chapman, J.A.  292
Chiquet, M.  102, 117
Chiquet-Ehrismann, R.  117
Chu, M.-L.  92
Clarke, S.R.  150
Codogno, P.  110
Colombo, R.  289
Combeau, C.  264
Conway, J.F.  140
Cross, R.A.  160
Dardik, R.  119
Davis, J.  319
Davis, J.M.  171
Deutzmann, R.  92
Doberstein, S.  271
Dölz, R.  81, 182
Doglia, S.  289
Doyennette-Moyne, M.-A.
   110

Edelstein, S.J.  3
Edgar, D.  92
Eikenberrry, E.F.  203
End, P.  117
Engel, A.  33, 39, 51, 187
Engel, J.  81, 106, 108, 182
Engelborghs, Y.  222, 249,
   262
Eppenberger, H.M.  39
Erickson, H.P.  54, 114, 259
Feldmann, B.  166
Fessler, J.H.  347, 355
Fessler, L.I.  347, 355
Flocke, K.  110
Foisner, R.  166
Fowler, V.M.  337
Gaill, F.  302
Gal, V.  249
Garrison, K.  347, 355
Gaub, H.E.  228, 233
Gebhard, W.  48
Gehr, P.  235
Geiser, M.  235
Gerl, M.  92
Giordano, P.  289
Goldschmidt-Clermont, P.
   271
Gross, H.  39
Hagestedt, T.  9
Häner, M.  33
Hartmann, H.  60
Hemphill, A.  312
Heremans, K.  222
Heremans, L.  222
Hinssen, H.  65
Hojima, Y.  81
Holland, S.K.  137
Holmes, K.C.  48
Holt, C.  169
Huber, P.  163
Huckriede, A.  65
Hulmes, D.J.S.  292
Hunter, I.  106
Im Hof, V.  235
Isenberg, G.  228, 233
Jagla, A.  212

Jauch, A.  163
Jokusch, B.M.  65
Kabsch, W.  42, 48
Kadler, K.E.  81, 292
Kaiser, D.A.  271
Kaiser, H.  319
Karecla, P.  249
Koch, M.H.J.  27
Kordeli, E.  319
Kühn, K.  69
Lahav, J.  119
Landwehr, R.  108
Lange, G.  212
Lichtenberg, B.  9
Lightner, V.A.  114
Lin, S.  341
Lutz, H.U.  328
Machesky, L.  271
Maciver, S.  271
Mack, J.W.  15
MacKrell, A.J.  347, 355
Magnus, K.A.  271
Mann, K.  92
Mandelkow, E.  9, 212
Mandelkow, E.-M.  9, 212
Mannherz, H.G.  42, 110
March, J.L.  33
Maretzki, D.  328
Mariani, M.  328
Martin, S.R.  249
Marugg, R.  235
Masuda-Nakagawa, L.  102
McCarthy, R.A.  102
Melki, R.  264
Meyer, R.K.  57
Michon, A.M.  27
Millonig, R.  51
Milzani, A.  289
Moir, R.D.  150
Mörgelin, M.  123
Morris, N.P.  171
Mould, A.P.  292
Nelson, R.E.  347
Niggli, V.  345
Noegel, A.A.  60, 62
Nurcombe, V.  92

# SECTION I
## Cytoskeletal Proteins and Their Supramolecular Assemblies

# Functional Properties of β-Tubulin In Vivo

Daniel M. Bollag, Michael D. Rozycki and Stuart J. Edelstein
Department of Biochemistry
University of Geneva
1211 Geneva 4, Switzerland

Microtubules, cytoskeletal organelles composed of αβ tubulin heterodimers, are implicated in a wide variety of cell functions including nuclear division, intracellular transport and cell motility (Dustin, 1984). Neither the specific roles nor the detailed structure of the individual tubulin subunits have been established, since the conditions necessary for separating the heterodimer result in loss of the subunits' ability to repolymerize. We have used plasmids which allow regulated overexpression of ß-tubulin alone or both tubulin subunits in the yeast Saccharomyces cerevisiae to dissect the properties of the tubulin subunits *in vivo*. Under conditions of tubulin induction, ß-tubulin overproducing cells are shown to accumulate fibrous structures associated with the cell membrane, as revealed by immunofluorescence microscopy. Simultaneous overexpression of both α- and ß-tubulin subunits also yields membrane-associated filamentous arrays. We conclude that ß-tubulin subunits are competent to assemble into elongated supramolecular structures, essentially devoid of α-tubulin subunits.

A high level expression plasmid for use in the budding yeast S. cerevisiae was constructed by fusing the cloned yeast tubulin gene TUB2 (Neff et al., 1983) to the GAL10 promoter (Fig. 1a). Exonuclease digestion was used to remove tubulin regulatory sequences which had been shown to interfere with introduction of high copy numbers of the ß-tubulin gene into yeast cells. The resulting multicopy $2\mu$ plasmid, pGT2, was transformed into yeast strain F808 (Rose & Fink, 1987) for these studies. A similar $2\mu$ plasmid, pDB68, containing both TUB1 (α-tubulin; Schatz et al., 1986) and TUB2 genes under control of the GAL10 promoter was a kind gift from D. Burke, Univ. of Virginia, Charlottesville (Fig. 1b). Induction of yeast cells containing these plasmids was carried out in minimal media by transferring the cells from a glucose to a galactose carbon source. Cells were induced for 10-14h before being harvested for analysis. Levels of induction were estimated in lysed cell extracts by gel immunoblotting and detection with specific α- or ß-tubulin antibodies (Fig. 2). By comparing the antibody signal intensity in a dilution series of crude extract protein, the amount of soluble tubulin

protein relative to that in uninduced cells could be estimated. In FLT12 cells simultaneously overproducing both subunits, α- tubulin was induced up to twenty-fold (Fig. 2 left, lane 4) and ß-tubulin fifty-fold (Fig. 2 right, lane 6) compared to the levels in uninduced cells. Strain FUT2, expressing ß- tubulin, contained similar levels of the induced protein with no corresponding increase in α-tubulin expression.

Cells overproducing only ß- or both α- and ß-tubulin subunits were examined by immunofluorescence microscopy (Kilmartin & Adams, 1984). Induction resulted in a 20-30% increase in cell size and a markedly stronger fluorescence (Fig. 3). Uninduced cells usually displayed tubulin fluorescence only in the nucleus or as cytoplasmic microtubules connecting nuclei in replicating cells (Fig. 3 a and b). However, in cells overproducing either ß-tubulin alone or both subunits, three classes of unusual structures were observed, all colocalizing with a membrane. Primarily, a ring or halo was seen closely following the cell
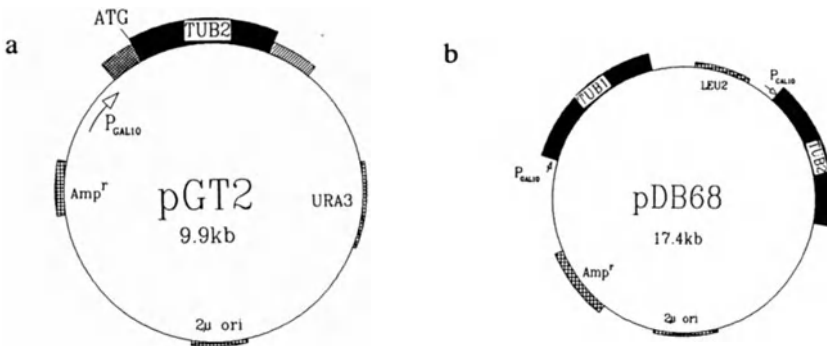


Fig. 1. Plasmids used for tubulin overexpression. a, Plasmid pGT2 contains the yeast ß-tubulin gene TUB2 (Neff et al., 1983) under the regulated control of the GAL10 promoter in plasmid pCGS109, a multicopy 2μ shuttle vector with the URA3 selectable marker gene (obtained from J. Schaum and J. Mao, Collaborative Research). pGT2 was transformed into yeast strain F808 (Rose & Fink, 1987) and the resultant strain was called FUT2. b, Plasmid pDB68 contains both the yeast α-tubulin gene TUB1 (Schatz et al., 1986) and the yeast ß-tubulin gene TUB2 fused to the regulated GAL10 promoter. The LEU2 gene is used as a selectable marker and the 2μ origin maintains the plasmid in multiple copies in the yeast cell. pDB68 was transformed into yeast strain F808 and the strain was called FLT12.

membrane. Tubulin fluorescence was also observed, but less frequently, at the neck between budding cells or forming a ring around the nuclear membrane. In FLT12 cells overproducing both tubulin subunits (Fig. 3c, d and e), the fluorescent rings contained α- and ß- tubulin, whereas ß-tubulin overproducing FUT2 cells appeared to contain essentially no α-tubulin in these structures (Fig. 3f). The tubulin fluorescence at the bud neck in both FLT12 and FUT2 cells was detected only with the ß-tubulin antibody, suggesting that this subunit possesses a special affinity for this region. Additional evidence for a bundled fiber
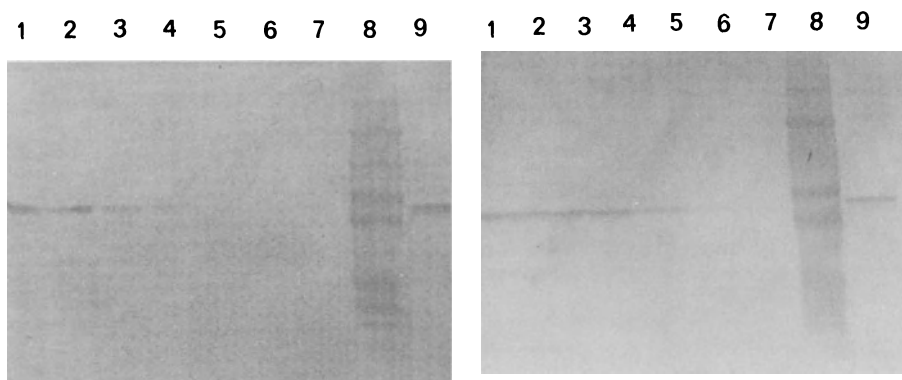


Fig. 2. Immunoblots of crude extracts from galactose-induced FLT12 yeast cells expressing both α-and ß-tubulin. Induction followed published methods (West et al., 1984) and will be described in detail elsewhere. Extracts from tubulin-overproducing cells were obtained by glass bead lysis, subjected to electrophoresis on polyacrylamide gels (Laemmli, 1970) and electrophoretically transferred to nitrocellulose filters (Towbin et al., 1979). The filters were probed with rat monoclonal α-tubulin antibody YOL1/34 (Kilmartin et al., 1982) or rabbit polyclonal ß-tubulin antibody 124C (Bond et al., 1986) and subsequent binding of a horseradish peroxidase-conjugated goat anti-rat or anti-rabbit second antibody (Sigma or Bio-Rad, respectively) permitted detection of tubulin protein. The gels were loaded with 20, 10, 5, 3, 1, 0.5, and $0.1\mu g$ of crude extract protein (lanes 1-7), prestained molecular weight markers of 180kD, 116kD, 84kD, 58kD, 48.5kD, 36.5kD, and 26.6kD (lane 8), and partially purified yeast tubulin protein (lane 9). Left, immunoblot probed with YOL1/34 (α-tubulin). Right, immunoblot probed with 124C (ß-tubulin). At least $20\mu g$ of crude extract protein from uninduced cells were needed to obtain an antibody signal on immunoblots.
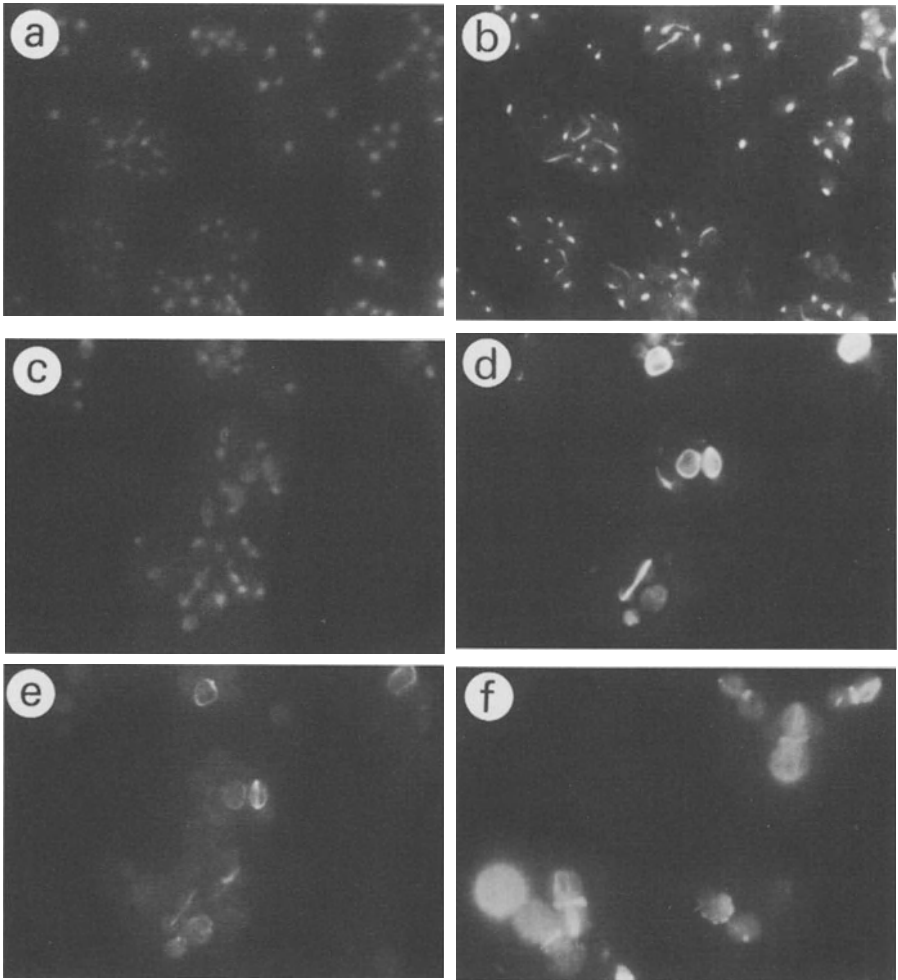
Fig. 3. Tubulin localization in <u>Saccharomyces</u> <u>cerevisiae</u> cells by indirect immunofluorescence microscopy. Cells were harvested and prepared for immunofluorescence as described (Kilmartin & Adams, 1984). Monoclonal rat α-tubulin antibody YOL1/34 (Kilmartin <u>et al.</u>, 1982) or polyclonal rabbit ß-tubulin antibody 124C (Bond <u>et al.</u>, 1986) were used in combination with DAPI staining of DNA. Fluorescein- and rhodamine-conjugated goat anti-rat or anti-rabbit second antibodies (Sigma) served to visualize the anti-tubulin antibodies. a and b: uninduced F808 cells containing plasmid pCGS109. DAPI staining is shown in a and the corresponding fluorescein staining of α-tubulin is shown in b. c, d and e: induced FLT12 cells. DAPI staining is shown in c, fluorescein staining of α-tubulin is shown in d, and rhodamine staining of ß-tubulin is shown in e. f: induced FUT2 cells. Fluorescein staining of ß-tubulin is shown in f.

arrangement of tubulin in the rings of overproducing cells was obtained when such cells were treated with zymolyase, an enzyme which disrupts the yeast cell wall, prior to fixation. The rings observed after this treatment appeared frayed, and a fluorescence signal resembling individual fibers liberated from the main bundle gave the impression of a gyroscope when focussing through such cells.

Before the advent of recombinant DNA techniques, it had not been possible to isolate individual tubulin subunits in a functional form, making it difficult to dissect the contributions of the α- and ß-tubulin subunits to microtubule formation. Our demonstration of a filamentous structure almost entirely comprised of ß-tubulin suggests that this subunit possesses an essential property for the formation of fibers. A likely candidate for a catalytic property controlling assembly is the binding site of an exchangeable and hydrolyzable GTP located on the ß subunit (Nath et al., 1985). Since the α-and ß-tubulin genes are thought to be derived from a single ancestral gene, ß-tubulin may possess the salient structural features needed for polymerization while α-tubulin may have evolved to provide regulatory regions needed for organizing microtubules into specialized structures. The localization of the ß-tubulin subunit alone at the bud neck is interesting in light of recent reports of arrays of microtubules emanating from the bud neck in other yeasts (Hagan & Hyams, 1988 and Barton & Gull, in the press) and may suggest a role of ß-tubulin in the initiation of microtubule formation. Work in progress with individual tubulin subunits purified from yeast should permit new insights into the contributions of individual α- and ß-tubulin subunits to microtubule structure and regulation.

References

Barton R, Gull K (in the press) Variation in cytoplasmic microtubule organization and spindle length between the two forms of the dimorphic fungus Candida albicans. J Cell Sci

Bond JF, Fridovich-Keil JL, Pillus L, Mulligan RC, Solomon F (1986) A chicken-yeast chimeric ß-tubulin protein is incorporated into mouse microtubules in vivo. Cell 44:461-468

Dustin P, (1984) Microtubules. Springer-Verlag Berlin

Hagan IM, Hyams JS (1988) The use of cell division cycle mutants to investigate the control of microtubule distribution in the fission yeast Schizosaccharomyces pombe. J Cell Sci 89:343-357

Kilmartin JV, Adams AEM (1984) Structural rearrangements of tubulin and actin during the cell cycle of the yeast Saccharomyces. J cell Biol 98:922-933

Kilmartin JV, Wright B, Milstein C (1982) Rat monoclonal antitubulin antibodies derived by using a new nonsecreting rat cell line. J cell Biol 93:576-582

Laemmli UK (1970) Cleavage of structural proteins during the assembly of the head of bacteriophage T4. Nature 277:680-685

Nath JP, Eagle GR, Himes RH (1985) Direct photoaffinity labeling of tubulin with guanosine 5'-triphosphate. Biochemistry 24:1555-1560

Neff NF, Thomas JH, Grisafi P, Botstein D (1983) Isolation of the ß-tubulin gene from yeast and demonstration of its essential function in vivo. Cell :33, 211-219

Rose MD, Fink GR (1987) KAR1, A gene required for function of both intranuclear and extranuclear microtubules in yeast. Cell 48:1047-1060

Schatz PJ, Pillus L, Grisafi P, Solomon F, Botstein D (1986) Two functional α-tubulin genes of the yeast Saccharomyces cerevisiae encode divergent proteins. Molec cell Biol 6:3711-3721

Towbin H, Staehelin T, Gordon J (1979) Electrophoretic transfer of proteins from polyacrylamide gels to nitrocellulose sheets: procedure and some applications. Proc natn Acad Sci U.S.A. 76:4350-4354

West RW, Yocum RR, Ptashne M (1984) Saccharomyces cerevisiae GAL1 - GAL10 divergent promoter region: location and function of the upstream activating sequence UAS$_G$. Molec cell Biol 4:2467-2478

# Paracrystals of Tau Protein – A Molecular Accordion

B. Lichtenberg, E.-M. Mandelkow, T. Hagestedt and E. Mandelkow
Max-Planck-Unit for Structural Molecular Biology
c/o DESY, Notkestraße 85, D-2000 Hamburg 52, F.R.G.

## ABSTRACT

Tau is one of the microtubule-associated proteins (MAPs) in mammalian brain (Weingarten et al., 1975). It occurs mainly in axons and is a component of the neurofibrillary tangles of Alzheimers disease (Kosik et al., 1986; Wood et al., 1986). In this report we summarize some structural features of paracrystals of tau studied by electron microscopy and image processing at a resolution of 5-6 nm (Lichtenberg et al., 1988). The paracrystals are polar, indicating that the subunits are aligned with the same orientations. Up to seven regions of protein density can be distinguished. In contrast to other known paracrystals, the repeats of tau vary over a wide range (from 22 nm to 68 nm) while retaining the relative positions of their protein domains. This suggests that tau has unusual elastic properties.

## METHODS

The methods of protein preparation, paracrystal formation, and image analysis are described in more detail elsewhere. Briefly, microtubule protein was prepared from porcine brain by a modified temperature cycle method (Mandelkow et al., 1985), boiled for 15 min (Fellous et al., 1977), followed by a clearing spin. The supernatant was then applied to a Pharmacia FPLC Mono-S column and eluted with a NaCl gradient. The protein was precipitated with 2.5% perchloric acid to remove the non-tau MAPs (Lindwall & Cole, 1984). The supernatant containing tau was precipitated in 45% ammonium sulfate, and the pellet was redissolved in 20 mM PIPES pH 6.9 with 1 mM each of EGTA, $MgSO_4$,

dithiothreitol, and 50 mM NaCl. SDS-PAGE shows the usual 4-5 isotypes in the range 50-70 kDal (Weingarten et al., 1975). Paracrystals were grown by grid dialysis (Van Bruggen et al., 1986) against 10-50 mM Na acetate buffer, pH 5.4-6.5, 20-50 mM $MgCl_2$, using copper grids coated with collodion/carbon. Staining was done with 1% uranyl acetate. The specimens were examined on a Philips CM12 microscope at 35-45,000 magnification. For the image analysis the electron micrographs were screened by optical diffraction, digitized, and computer processed (Fourier transformation, noise filtering, reconstruction).

## RESULTS

The paracrystals are usually straight (Fig. 1), but highly coiled ones are also observed (Fig. 2), indicating that the structures can accomodate internal stress. They show patterns of light and dark transverse bands, typical of structures where elongated molecules are aligned parallel to one another along the axis. The structures with the largest repeats (above about 60 nm) show the most detailed pattern, with up to 7 transverse striations per repeat. The most prominent bands (termed 0 and 2, Fig. 1) are separated by roughly 1/3 of the repeat. Between them one observes two faint striations (bands 1a and 1b); three more bands (3, 4, 5) occur between band 2 and 6 (equivalent to band 0). The polarity of the pattern is most easily seen from the dark "gap" preceding band 0 in Fig. 1a. The polarity means that the molecules must be arranged in the same direction. In this regard the paracrystals are similar to those of collagen (Doyle et al., 1975), but different from tropomyosin where subunits are packed with antiparallel orientations (Caspar et al., 1969). As the repeat decreases the banding pattern changes gradually; for example, bands 1a and 1b merge into one another, and bands 3-5 become more evenly spaced. Thus the contracted pattern usually shows less polarity (Fig. 1b). Nevertheless the relative positions of the striations remains roughly the same. Evidence described elsewhere (Lichtenberg et al., 1988) suggests that the ends of the molecules are near the bright bands (0 and/or 2); this is incorporated into the model

discussed later.

A striking feature is the wide range of repeats (between 22 and 68 nm). The variation is observed not only by comparing different particles (Fig. 1a, b), but is also within a given particle; for example, the repeats tend to shrink towards the ends (not shown). In the coiled specimen of Fig. 2 the repeat on the outside is 45 nm, but on the inside it is only 22 nm, i.e. half of the outside repeat. In spite of this compression the banding pattern is preserved. This suggests that the molecules themselves are elastic, i.e. the structure behaves like an accordion.

Diffraction patterns of well-ordered paracrystals show reflections up to the 11th order. Thus the density distribution can be reconstructed to 5-6 nm resolution (not shown). When scaling different reconstructions to the same repeat it becomes apparent that the bands can be nearly superimposed. In other words, the reconstructed densities can be transformed into one another simply by stretching or compressing. This can only be explained if the molecules are highly elastic, consistent with the flexibility of the paracrystals (e.g. Fig. 2).

These observations lead to the working model of tau protein in Fig. 3. It consists of several domains connected by springs. In the paracrystals different molecules are joined roughly head-to-tail, with the same polarities, and with little overlap. The maximum length would be given roughly by the maximum repeat, about 68 nm (top diagram). The bottom diagram shows a contracted state; all domains move towards one another with little change in their relative positions.

12

Fig. 1: Paracrystals of tau protein. (a) Periodicity 63 nm. The two most prominent bands (0 and 2) are marked. There are two faint striations between bands 0 and 2 (1a and 1b), and three striations between band 2 and the next band 0 (3, 4, 5). The dark gap to the left of band 0 allows the polarity to be observed by eye (long arrow). (b) Periodicity 53 nm. Bands 1a and 1b are no longer resolved, and the gap preceding band 0 has largely disappeared, resulting in a more symmetrical appearance. A given paracrystal may contain more than one type of banding pattern. Bar = 100 nm.
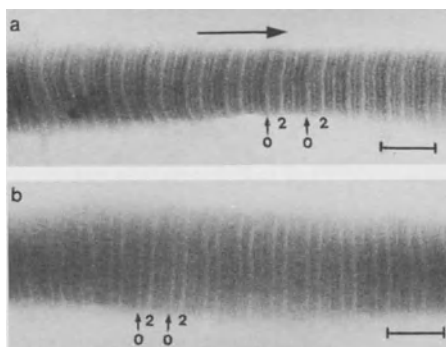


Fig. 2: Coiled paracrystal. The periodicity varies from 22 nm at the inner edge to 45 nm at the outer edge (reminiscent of an accordion). Note that the relative arrangement of the striations remains unchanged and is similar in the coiled and straight portions. Blurred regions showing no striations are probably explained by internal disorder.
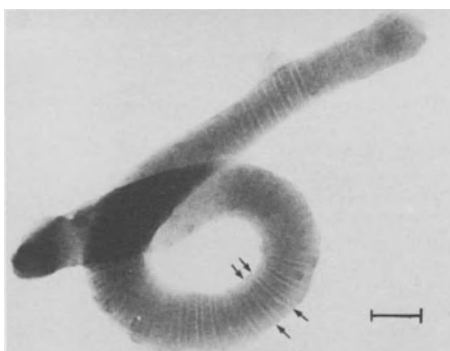


Fig. 3: Model of the structure of tau molecules and their packing in the paracrystal. The filled blocks represent high protein density ( = bands in the paracrystals), the springs indicate the elasticity of the molecule. The distinction between structural and elastic elements is exaggerated for clarity. The top and bottom diagrams show the molecules in an extended and contracted state. A single tau molecule begins roughly at band 0 and ends roughly at the next band 0. The overlap between successive molecules is probably small, so that the maximum repeat (68 nm) is close to the maximum molecular length (all springs extended). This is consistent with the observation that the separation of the bands changes nearly proportionally to the overall repeat (Fig. 3). All Figures reprinted from Lichtenberg et al., 1988.
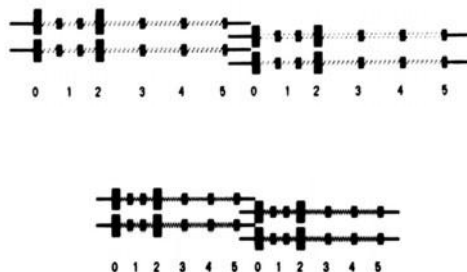
## DISCUSSION

Tau is an abundant microtubule-associated protein in mammalian brain; thus far it is the only one whose sequence is known (Lee et al., 1988) and which forms ordered arrays amenable to structure analysis (Lichtenberg et al., 1988). In the paracrystals up to seven striations can be discerned per repeat, two of which are particularly prominent (bands 0, 2). This could mean that tau consists of several structural domains. This would be consistent with the idea that tau has regions responsible for binding to the microtubule surface and others that project away from it, and with the observation that tau contains three internal sequence repeats (possibly microtubule-binding regions). However, it is not yet possible to assign such functions to the densities detected in the paracrystals.

Perhaps the most interesting and unusual property of tau is the flexibility and elasticity. The structure can extend and/or contract by more than 300%, i.e. from a minimum of 22 nm to a maximum of 68 nm. This variability is not due to a change in overlap between adjacent tau molecules, but reflects an intrinsic property of the protein. In this regard tau differs from all other paracrystal-forming proteins known to us so far. One would expect that this is somehow related to the unusual amino acid sequence which contains a high proportion of Pro, Gly, and hydrophilic residues. However, the way in which this composition might be translated into elasticity is unclear at present. There is some similarity to the elastic protein elastin in that both have a high proportion of Pro (Raju & Anwar, 1987), but otherwise there are no obvious sequence homologies. In any case it is likely that the elasticity of tau observed in vitro is important for its function in vivo. For example, the protein could stabilize microtubules (by virtue of its interaction with the microtubule surface) and at the same time confer elasticity to the cytoplasmic ground substance. Such a property would be important for allowing the passage of vesicles and organelles along microtubule tracks during axoplasmic transport.

14

Another notable feature of tau is that it forms a major component of the
neurofibrillary tangles observed in Alzheimer's senile dementia (Kosik et al.,
1986; Wood et al., 1986). These structures contain paired helical filaments
twisting around one another (Crowther & Wischik, 1985). The crossover points
are spaced about 70-80 nm apart, a value close to the maximum repeat of the tau
paracrystals. At present there is still a debate on whether the paired helical
filaments consist of tau and/or some other protein(s); and on the other hand we
have not detected helical structures in the tau paracrystals. Nevertheless, the
fact that tau protein can associate into regular structures in vitro suggests a
possible relationship with the tangles occurring in vivo which merits a more
detailed investigation.

## REFERENCES

Caspar, D.L.D., Cohen, C. & Longley, W. (1969). Tropomyosin: Crystal structure, polymorphism and molecular interactions. J. Mol. Biol. 41, 87-107.

Crowther,R.A. and Wischik, C.M. (1985). Image reconstruction of the Alzheimer paired helical filament. EMBO J. 4, 3661-3665.

Doyle, B., Hukins, D., Hulmes, D., Miller, A. and Woodhead-Galloway, J. (1975). Collagen polymorphism: Its origins in the amino acid sequence. J. Mol. Biol. 91, 79-99.

Fellous, A., Francon, J., Lennon, A.M. and Nunez, J. (1977). Microtubule assembly in vitro: Purification of assembly promoting factors. Eur. J. Biochem. 78, 167-174.

Kosik, K., Joachim, C. and Selkoe, D. (1986). Microtubule-associated protein tau is a major antigenic component of paired helical filaments in Alzheimer disease. Proc. Natl. Acad. Sci. U.S.A. 83, 4044-4048.

Lee, G., Cowan, N. and Kirschner, M. (1988). The primary structure and heterogeneity of tau protein from mouse brain. Science 239, 285-288.

Lichtenberg, B., Mandelkow, E.-M., Hagestedt, T. & Mandelkow, E. (1988). Structure and elasticity of microtubule-associated protein tau. Nature 334, 359-362.

Lindwall, G. and Cole, R.D. (1984). The purification of tau protein and the occurrence of two phosphorylation states of tau in brain. J. Biol. Chem. 259, 12241-12245.

Mandelkow, E.-M., Herrmann, M. and Rühl, U. (1985). Tubulin domains probed by subunit-specific antibodies and limited proteolysis. J. Mol. Biol. 185, 311-327.

Raju, K. and Anwar, R.A. (1987). Primary structures of bovine elastin a, b, and c deduced from the sequences of cDNA clones. J. Biol. Chem. 262, 5755-5762.

Van Bruggen, E., van Breemen, J., Keegstra, W., Boekema, E. and van Heel, M. (1986). Two-dimensional crystallization experiments. J. Microsc. 141, 11-20.

Weingarten, M.D., Lockwood, A.H., Hwo, S.Y. and Kirschner, M.W. (1975). A protein factor essential for microtubule assembly. Proc. Natl. Acad. Sci. U.S.A. 72, 1858-1862.

Wood, J., Mirra, S., Pollock, N. and Binder, L. (1986). Neurofibrillary tangles of Alzheimer disease share antigenic determinants with the axonal microtubule-associated protein tau. Proc. Natl. Acad. Sci. U.S.A. 83, 4040-4043.

# Structure and Assembly of Intermediate Filaments: Multi-Faceted, Myosin-like (But Non-Motile) Cytoskeletal Polymers

A C Steven, J W Mack[†], B L Trus[*], M E Bisher and P M Steinert[†]
Laboratory of Physical Biology
National Institute of Arthritis, Musculoskeletal and Skin Diseases
National Institutes of Health
Bethesda, MD 20892
U. S. A.

## INTRODUCTION

Intermediate filament (IF) proteins, actin, and tubulin are the troika of the eukaryotic cytoskeleton, in that fibrous polymers of these three classes of protein abound in virtually all kinds of cells. However, as our knowledge of their molecular properties grows, it is becoming increasingly apparent that IF proteins (Steinert & Roop, 1988) differ in many respects from actin (Pollard & Cooper, 1986) and tubulin (Kirschner & Mitchison, 1986), but have much in common with another important and long-studied component of the cytoskeleton, albeit one that is somewhat less ubiquitous - myosin (Harrington & Rodgers, 1984; Warrick & Spudich, 1987). It is the purpose of this contribution to summarize some recent lines of evidence emerging from biophysical and molecular biological experiments concerning both static and dynamic properties of IF proteins; to examine how far their resemblance to myosin extends; and to explore its implications for the functions - still rather vaguely defined - that are exercised by IF in cells.

Actin and tubulin are filamentous proteins only at the supramolecular level, having globular monomers. In contrast, IF proteins are already filamentous at the molecular level (Fig. 1), and the structural hierarchy that leads to fully assembled IF entails several further levels of filamentous organization (Aebi et al, 1983). Moreover, unlike actin and tubulin which are evolutionarily very conservative, IF proteins are notably diverse, forming a family of about 40 different members per mammalian species, whose monomer molecular weights run from ~ 44 kDa to ~ 115 kDa. However, each cell expresses only a few members of the family, and based primarily on this criterion, IF proteins have been operationally assigned to six different classes: desmin (muscle), vimentin (mesenchymal cells), glial fibrillary acidic protein - GFAP (astrocytes), neurofilament NF proteins (neurons), keratins (epithelia), and lamins (constitutive expression).

Now-abundant amino-acid sequence information on IF subunits has clarified the molecular basis of this diversity and suggested another more fundamental classification of these proteins. The hallmark of an IF polypeptide chain is the presence of a characteristic "rod domain" sequence that is conserved in length (~ 314 residues, extended to ~ 356 in the case of lamins (McKeon et al, 1985; Fisher et al, 1986), and secondary structure (segmented α-helix with a propensity to form

-----------------

Correspondence : Bldg. 6, Rm. 114, NIH, Bethesda MD 20892, U.S.A.
[†] Dermatology Branch, National Cancer Institute, NIH
[*] Computer Systems Laboratory, Division of Computer Research and Technology, NIH

coiled-coils) and, to a greater or lesser extent, homology. This rod domain is bounded by "end-domain" sequences which are highly variable in length (thus accounting for the spread in subunit molecular weights) and amino-acid composition; moreover, they are generally not $\alpha$-helical. On the basis of proximity of homology of the rod domains and, to a somewhat lesser extent, end-domain properties, IF proteins fall into the following Types (Hanukoglu & Fuchs, 1983; Steinert et al, 1985a): Type I (acidic keratins); Type II (neutral/basic keratins); Type III (vimentin, desmin, GFAP); Type IV (neurofilaments NF-L, NF-M, NF-H); and Type V (lamins A,B,C).

## OLIGOMERIC COMPLEXES OF IF PROTEINS

**(a) The 2-chain Molecule:**    The first level of higher-order structure is the dimeric molecule whereby the rod domains of two IF polypeptide chains come together in parallel and in axial register to form a 2-stranded coiled-coil rope (Ahmadi et al, 1980; Geisler & Weber, 1982; Woods & Inglis, 1984; Parry et al, 1985). The expected length of this molecule is about 46nm (314 residues x 0.149nm axial rise per residue), but is not known precisely because of 3-4 helix-breaking interruptions in the coiled-coil (Conway & Parry, 1988) and uncertainty as to the contribution of the end-domains. The major interruption is a "linker" peptide (L12), 16 or 17 residues in length, that divides the rod domain into two segments of approximately equal length, "segment 1" and "segment 2" (for a more detailed account, see Conway and Parry - this volume). The absence of stagger between the paired rod domains has the advantage of ensuring that all of their coiled-coil interruptions are in phase, thereby maximizing the length of the coiled-coil tracts, and presumably contributing to their stability. It appears that all IF polypeptide chains pair into molecules in essentially the same way via their conserved rod domains.

**(b) 4-chain Complexes and Higher Oligomers:**   The next level in the hierarchy involves combinations of molecules, of which the simplest case is a pair of molecules (4-chain complex). There are numerous reports of such complexes (or proteolytic fragments thereof) obtained by exposing IF to dissociating conditions. Electron microscopy of such preparations has visualized rod-like particles 40-50nm in length, suggesting a side-by-side pairing of molecules with little if any axial offset; however, these data do not distinguish between parallel or antiparallel arrangements. Addressing this point, Geisler et al (1985) found a majority of dumbell-shaped particles in electron micrographs of desmin labelled with an antibody against a determinant located near one end of the rod, implying labelling at both ends, and therefore an antiparallel association of molecules. On the other hand, Ip (1988) also applied an antibody-labelling technique to desmin and rarely encountered double-ended labelling. Accordingly, the issue of this complex's polarity - which has important implications for whether or not the filament itself is a polar or a non-polar structure (Steinert & Steven, 1985) - cannot be regarded as settled.

It is not, in principle, possible to construct a filament out of IF molecules without employing more than one mode of association between them. Of other possible modes of association, attention has focused on complexes in which the paired molecules are offset by about half a

molecular length (Steinert et al, 1985a). There are three possibilities for such 4-chain complexes, having the molecules oriented - (a) in parallel; (b) antiparallel, with overlapping N-terminal halves (segment 1) ; (c) antiparallel with overlapping C-terminal halves (segment 2). In each case, the particles should be ~ 65-75nm long. Particles in this length range were hypothesized by Ahmadi et al (1980). Experimentally, a particle containing four fragments of helix 1 has been isolated from a proteolytic digest of wool keratins (Woods & Inglis, 1984), pointing to model (b). There is a preliminary report of vimentin particles in the 65nm range (Potschka, 1986). However, the particles of about this length visualized by Ip et al (1985) were interpreted as 8-chain complexes (two half-staggered 4-chain 45nm particles).

We have employed low-angle rotary shadowing electron microscopy to examine particles obtained by solubilizing heteropolymer Type III IF (vimentin + desmin) extracted from BHK cells (Fig. 1). The populations of particles in these preparations are notably heterogeneous, although they contain several recurring types (Fig. 1a-e). These include - short rods 20-25nm long (Fig. 1a); straight particles in the 40-50nm range (Fig. 1b); and particles of the same length, but kinked near their middles (Fig. 1c). We also observe longer (70-80nm) particles that are straight and not necessarily uniform in width (Fig. 1d), as well as other particles of similar length that are kinked, often at points about two thirds along from one end (Fig. 1e). These subsets of particles can all be accounted for as variants of a 45nm particle (or oligomers thereof) with a central hinge or point of flexibility - presumably the linker L12 inferred from rod domain sequence analyses. Thus the 20-25nm particles would be produced by folding 45nm rods through $180^{\circ}$ about their hinge-point, and through a smaller angle to produce the kinked particles (Fig. 1(c)). An approximately half-staggered association of molecules (or 4-chain complexes, or both), with one of these particles bent at its hinge-point would produce the longer asymmetrically kinked particle (Fig. 1(e)). Thus, although these species do not account for all the particles observed in these preparations, they provide evidence in support of a predicted point of flexibility at or near the middle of a 40-50nm particle, and for at least two modes of association between IF molecules that are generally in line with the intra-filament packing schemes advanced by several authors (Geisler et al (1985), Ip et al (1985), Fraser et al (1986). They also point to the existence of states in which several different oligomers and conformers may co-exist, presumably in dynamic equilibrium, which would tend to subvert experiments which presuppose a monodisperse suspension.

Although rotary-shadowing electron microscopy is a straightforward and informative technique for the study of fibrous proteins, it has limitations - in particular, uncertainty as to how many molecules may actually be present in a given complex. This uncertainty arises primarily because shadowing tends to amplify dimensions (especially the width of fibrous particles) through mobility of the incident platinum, and particularly so at room temperature. As a result, their perceived width is several-fold greater than that of an $\alpha$-helical coiled-coil, or small aggregate thereof, making it difficult to distinguish between these alternatives in practice. For this reason, it would be highly desirable to have available a technique in which both the the mass (and hence the number of molecules involved) as well as the length of each particle could be explicitly determined. Initial studies with STEM dark-field microscopy of dissociated vimentin visualized
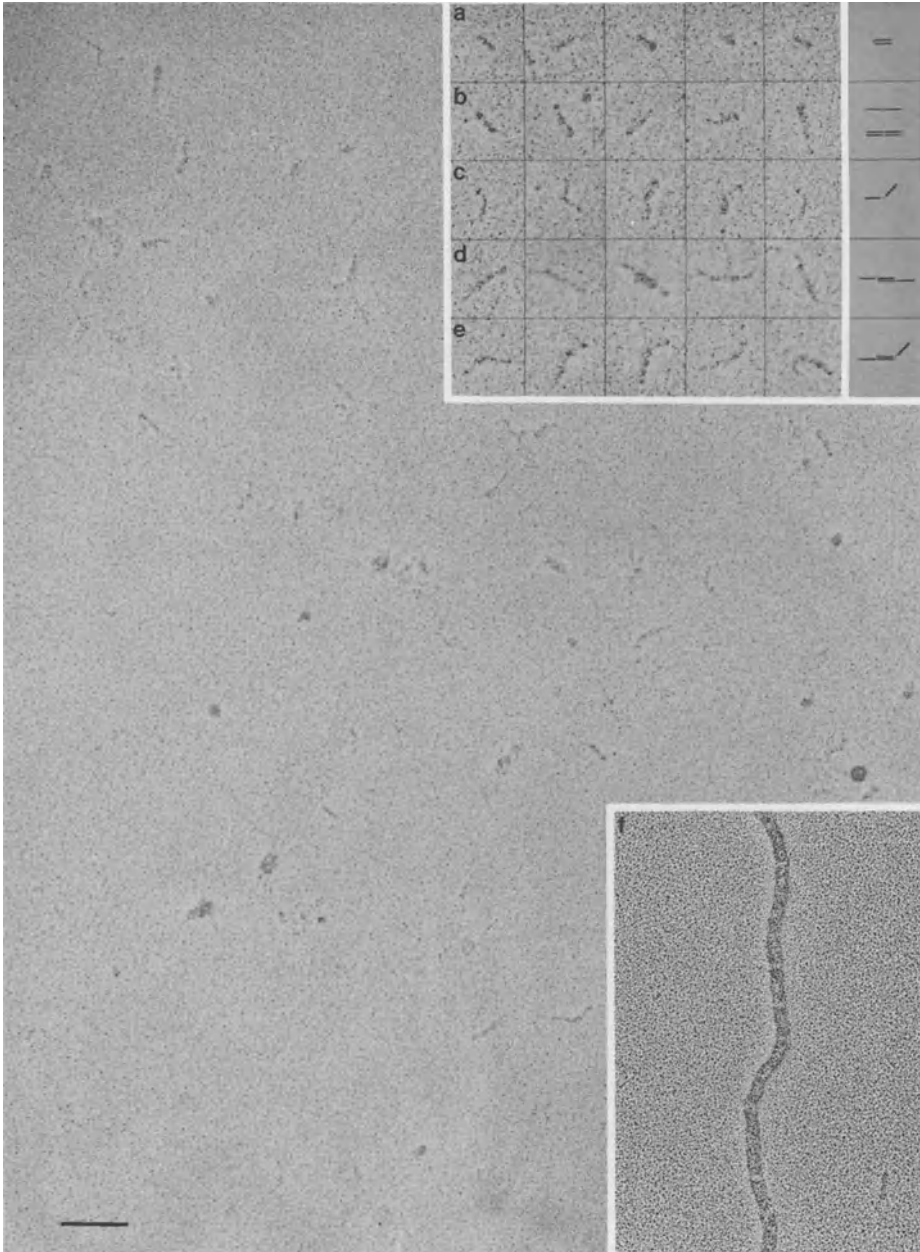
Fig 1: Low-angle rotary shadowing (Pt/C) electron microscopy of IF protein particles (vimentin/desmin) purified from BHK cells as described by Steinert et al, 1980. The gallery (inset, top right) shows five morphological types of particles (a-e) recurrently found in these heterogeneous populations. Inset (f) is an intact IF (in this case, murine epidermal keratin IF reassembled in vitro) visualized by the same technique. Bars = 100nm.

unstained after freeze-drying have given promising results, indicating that this approach may be feasible (S. George, ACS et al - work in progress).

## FILAMENT STRUCTURE : A BUNDLE OF α-HELICAL COILED-COILS SURROUNDED BY A PERIPHERAL SHELL OF END-DOMAINS

Although many specifics remain to be clarified, current evidence strongly favors the proposition that all IF are built according to the same plan, viz. they have backbones that consist of helically packed rod domains oriented approximately parallel to the filament axis, from which the end-domains protrude (Steven et al, 1985; cf. also Fraser & MacRae, 1982). The data on which this model is based are as follows:

(i) There are numerous observations that, with intact IF, end-domains are more susceptible to proteolysis than rod domains, suggesting that they occupy a more exposed location (e.g. Steinert et al, 1983; Kaufmann et al, 1985).

(ii) Contrasting of IF by low-angle shadowing accentuates an intrinsic axial repeat of about 22nm (Fig. 1f) which has, by now, been demonstrated for virtually all kinds of IF (Milam & Erickson, 1982; Henderson et al, 1982; Sauk et al, 1984; Steven et al, 1987). Several considerations imply that this repeat is specified by rod domain properties. In particular, like the size of the rod domain, this axial spacing is essentially the same for IF of all kinds, except for lamins where the repeat is longer in proportion with the extended lamin rod domain (Aebi et al, 1986). Moreover, the 22nm spacing correlates with the expected lengths of segments 1 and 2.

(iii) The mass-per-unit-length values measured by scanning transmission electron microscopy (STEM) for several kinds of Type III and keratin IF were found to be proportional to the average molecular weights of the subunits contained, indicating that a given length of filament contained the same number of molecules in each case (Steven et al, 1985). This proportionality is readily explained if IF of all kinds were to be made up of building-blocks that have modules of conserved length and mass (the rod domains) and modules of variable mass (the end-domains), and that IF are assembled by packing the conserved modules together in essentially the same way.

Interpretation of the above experiments was complicated somewhat by the occurrence of polymorphism, whereby several discrete and seemingly quantized density classes were observed, particularly among reassembled IF (Steven et al, 1982, 1983; Engel et al, 1985). Otherwise stated, the above conclusion (iii) was that these IF all contained the same number of molecules in cross-section, at least within each density class. Native vimentin IF contain about 16 molecules in cross-section, but lower density IF (10-12 molecules in cross-section) are a common and sometimes predominant product of in vitro reassembly.

(iv) Radial density reconstructions from STEM images of unstained frozen-dried IF reveal a core of uniform density, that is 9-10nm in diameter for IF that contain ~16 molecules in cross-section, and ~ 8nm for the lower density species (Steven et al, 1985, 1987). This core is surrounded by diffuse peripheral density that tapers off to an outermost diameter of 15-16nm (respectively, 13-14nm). For the IF examined (vimentin and bovine epidermal keratin), the ratio of the core mass to the periphery mass was found to be the same as the ratio of the rod domain mass and that of the end-domains combined.


## ANALOGY BETWEEN INTERMEDIATE FILAMENTS AND MYOSIN FILAMENTS

The architectural principle of a filament backbone composed of $\alpha$-helical coiled-coils surrounded by protruding end-domains whose foldings involve other conformations is also deployed in the myosin filament. Upon comparison, myosin is found to resemble IF proteins in other ways, although there are also notable differences. The myosin molecule is based on a dimer of "heavy" chains joined via the coiled-coil formed by their respective $\alpha$-helical rod domains. As with IF molecules, a parallel, in register, mode of association is used, although the myosin rod is over three times as long as the IF rods, and is expected to have fewer helix-breaking interruptions. Moreover, the distributions of charged amino-acids in both rods observe a periodicity of about 9.5 residues (Conway & Parry, 1988; McLachlan, 1984). This periodicity is distinct from the 7-residue repeat (and harmonics thereof) of apolar residues that underlies the coiled-coil interactions, and is thought to have a role in specifying higher-order structure. Whereas both IF end-domains are often of comparable size, the myosin end-domains are lop-sided, the amino-terminal end-domain being vestigial whereas the carboxy-terminal end-domain, subfragment 1 (S-1) is very large, ~ 100kDa. This is the domain to which the myosin light chains bind, and where the ATPase activity essential to force generation resides.

In the myosin filament, the respective functions of the rod domain and of the end-domain are well understood. The rod domains are polymerized into a stable inextensible filament backbone, and the S1-crossbridges extend from this matrix to couple cyclically with another cytoskeletal element, the actin filament, thus generating mechanical force (Warrick & Spudich, 1987). This analogy, in addition to other arguments (Steinert et al, 1985a), implies that the end-domains of IF are the functionally important parts of these molecules. There is, however, no evidence that IF play an active role in motility (the involvement of NF in axonal transport, discussed by Lasek (1985), seems to be at most an indirect and passive one). Accordingly, it appears that IF fulfill other functions, and the observed pattern of IF gene expression most likely reflects differentiation-specific changes in their role(s). As to what these functions are, this hypothesis predicts that some clues may be forthcoming from an improved knowledge of end-domain structures.

# STRUCTURAL PROPERTIES OF IF END-DOMAINS

Whereas crystals of myosin S-1 have been obtained, and analysis of them is proceeding (Baker & Winkelmann, 1986), information on the structures of IF end-domains remains sparse. However, some insights are beginning to emerge, largely on the basis of amino-acid sequence information. It is noteworthy that IF end-domain sequences often contain remarkably high concentrations of particular amino-acids, for instance Gly and Ser in epidermal keratin IF, and Glu and Lys in the long carboxy-terminal extensions of NF-M and NF-H (Geisler et al, 1984). Characteristic sets of subdomains have been identified in the end-domains of both Type I and Type II keratins (Steinert et al, 1985b; Zhou et al, 1988). In both cases, the variations in size and amino-acid composition are confined primarily to particular amino-terminal (V1) and carboxy-terminal (V2) subdomains. The largest V1 and V2 keratin subdomains are found in the K1 and K10 subunits expressed in terminally differentiating epidermis: these subdomains contain the high concentrations of Gly and Ser residues mentioned above, interspersed with occasional aliphatic residues, and often configured in tandem pseudo-repeats.

The properties of these domains are reminiscent of the characteristics of a recently proposed secondary structure, the Ω-loop (Leszczynski & Rose, 1986), defined on the basis of a systematic survey of conformations exhibited at the surfaces of globular proteins. Ω-loops are 6 - 16 residues in length; have a particularly high incidence of Gly, and to a somewhat lesser extent, of Ser; are almost invariably found on the surfaces of proteins; and have a high accessibility to solvent. These characteristics all apply to the V1 and V2 subdomains of epidermal keratins. The only dissonance between the properties of the V1 and V2 subdomains and those of archetypal Ω-loops are that the latter tend to have low temperature factors, indicating restricted mobility, whereas the residues in V1 and V2 are highly mobile (see below), at least with isolated protein under in vitro conditions. Nevertheless there are sufficient properties in common to raise the possibility that these subdomains take the form of a loosely associated cluster of Ω-loops or related structures (Zhou et al, 1988) - cf. Fig. 2.

Until recently, little information concerning end-domain structure has emerged from electron microscopic studies, but observations have now been reported of lamin carboxy-terminal end-domains (Aebi et al, 1986; Parry et al, 1987). Moreover, long flexible protrusions have been observed on native and reassembled NF after rotary-shadowing (Hisanaga & Hirokawa, 1988). These structures were identified as the C-termini end-domains of NF-M and NF-H, and their median lengths estimated at 55nm (NF-M)
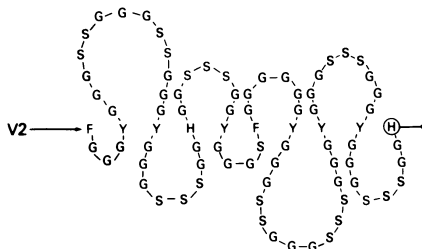


Fig 2: Schematic diagram showing a hypothetical folding of the V2 subdomains of the carboxy-terminal end-domain of human epidermal keratin subunit K10 (Zhou et al, 1988) into a succession of Ω-loops (cf. Leszczynski & Rose, 1986). No particular three-dimensional arrangement of these loops - shown here as linear arrays - is implied, although the aliphatic groups may have a tendency to aggregate, leading to more compact, rosette-like, structures

and 63nm (NF-H). The flexibility of these structures is striking and, intriguingly, this property has also been attributed to the (chemically quite different) end-domains of K-IF on other grounds (see below).


## DYNAMIC PROPERTIES OF KERATIN END-DOMAINS PROBED BY NMR SPECTROSCOPY

Carbon-13 and deuterium nuclear magnetic resonance (NMR) have been used to investigate the molecular ordering and internal dynamics associated with the subdomainal structure of epidermal keratin IF. Solid-state pulsed NMR has been demonstrated to be useful in the study of biological macromolecules, although isotopic labelling is generally necessary (Griffin, 1981; Keniry et al, 1984; Torchia, 1984), and we have applied this technique to mouse epidermal keratins in subfilamentous form, viz. "prekeratin" (Matoltsy, 1965) and in intact IF (Mack et al, 1988). These proteins were metabolically labelled either in vivo (K1,K10) or in vitro (K5,K6,K14,K16) with amino-acids enriched in $^{13}C$ or $^{2}H$ .

The preponderance of glycyl residues in the V1 and V2 regions of the end-domains of these keratins (e.g. over 60% of the total end-domain residues of K1 and K10 are Gly), and their segregation to the end-domains (90-93% of K1 and K10's glycyl residues are in their end-domains) (Steinert et al, 1983; Zhou et al, 1988) led us to choose $^{13}C$-enriched glycines as probes of end-domain ordering and dynamics. A similar degree of confinement of leucyl residues to the rod domains led to the choice of deuterated leucines, incorporated into keratins K5, K6, K14 and K16 synthesized in cell culture, as probes of the structural order of rod domains.

Figure 3A is a $^{13}C$ spectrum, taken at 63MHz, of prekeratin extracted from mouse epidermis after labelling with [1-$^{13}C$] glycine. The glycyl carbonyl signal is the major component of the strong resonance at ~ 175ppm (a portion of this resonance is also contributed by serine residues to which the $^{13}C$ label was metabolized). Figure 3B shows the corresponding spectrum from unlabelled prekeratin and establishes that labelling strongly enhances the glycyl carbonyl signal. The major feature of note about the carbonyl resonance is its narrowness (~ 5ppm full-width at half-height), which contrasts with its
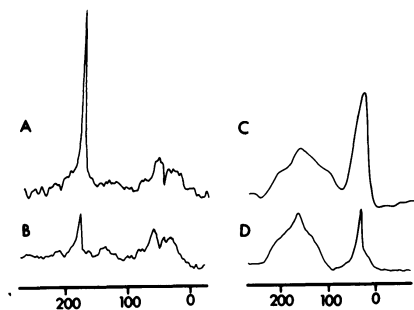


Fig 3: Comparison of $^{13}C$ NMR spectra of epidermal keratin IF (A and B) with those of crystalline polyglycine (C) and collagen fibrils (D). A and B are the respective spectra of IF labelled with [1-$^{13}C$] glycine, and of unlabelled IF. These spectra were recorded at 25°C and 63 MHz; spectrum C was recorded at 74 MHz. The collagen fibrils were labelled with [1-$^{12}C$] glycine and [6-$^{13}C$] lysine, and their spectrum recorded at 15 MHz. Spectra C and D were provided by courtesy of Dr D A Torchia.

counterpart in the NMR spectrum of collagen fibrils labelled with enriched glycine - Fig 3D. Every third residue of the collagen polypeptide chain is Gly, and in the triple-stranded coiled-coil collagen molecule these residues are packed inside, close to the axis of the coiled-coil (Bornstein & Traub, 1979). Here, the carbonyl resonance is ~ 120ppm wide, only about 30% narrower than in crystalline polyglycine (Fig. 3C) where the peptide backbone is quite rigid. The implication for end-domain conformation in these IF is that the mobility about the polypeptide backbone in the immediate vicinity of the glycyl residues is far greater than in another fibrous protein (collagen) or in crystalline polyglycine. Based on a variety of NMR measurements, we find that motions about the glycyl peptide bonds in these keratins are effectively isotropic, and have average correlation times in the range of 0.2 to 20ns. Moreover, this mobility is the same both for the subfilamentous form (prekeratin) and in intact IF (Mack et al. 1988), indicating that the V1 and V2 subdomains of K1 and K10 are not perceptibly constrained as a result of being assembled into filaments, a conclusion that is entirely consistent with the peripheral location previously attributed to these end-domains on other grounds (Steinert et al, 1983; Steven et al, 1985).

As a probe of the rod domains, L-[$^2$H$_{10}$] leucine was incorporated into the pre-keratins of primary mouse tissue culture. Figures 4A & B show deuterium spectra taken at 77MHz of labelled IF at 26$^o$ and -45$^o$C, and of crystalline L-[$^2$H$_{10}$] leucine at 26$^o$C (Fig 4C). It is readily apparent that in contrast to the narrow isotropic $^{13}$C line observed in the glycine spectrum (Fig. 3), the leucine deuterium lineshape is a broad powder pattern distribution, with the major portion of the signal arising from the methyl deuterons. This lineshape is strongly temperature-dependent, and at -45$^o$C, very much resembles that of the crystalline amino-acid. Crystalline leucine is known from X-ray diffraction studies to have essentially a rigidly constrained sidechain. The higher temperature lineshapes of the labelled IF are thus inferred to represent deviations from rigidity of the sidechain. Detailed analysis of the leucyl lineshapes has led to the conclusion that the peptide backbone in the rod domain is far more structured than in the end-domains, although the conformation is sufficiently
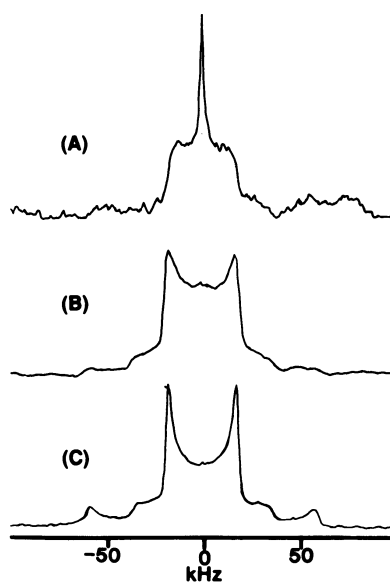


Fig 4: Comparison of the deuterium NMR spectra of L-[$^2$H$_{10}$] leucine-labelled epidermal keratin IF at 26$^o$C (A) and -45$^o$C (B) with that of crystalline leucine (C). All spectra were recorded at 77 MHz using the quadrupolar echo pulse sequence: A and B were each averaged over 25,000 scans, and C over 128 scans.

flexible to accommodate sidechain motions of substantial magnitude (Mack et al, 1988). Computational simulations indicate that the observed lineshapes arise from dynamic isomerization of the leucyl sidechains on temperature-dependent timescales in the range of $10^{-6}$ to $10^{-4}$ s.

In summary, we find that the peptide backbone within the Gly-rich V1 and V2 subdomains of keratins K1 and K10 are extremely flexible, implying a virtually complete lack of long-range order. The rod domains, however, are much more ordered with peptide motions probably limited to torsional oscillations. Nevertheless, sidechain motions of considerable amplitude are observed for leucine, a polar residue supposedly confined to the hydrophobic core of the coiled-coil. This finding indicates that the conformational stability of coiled-coils is relative (to end-domains) rather than absolute. This freedom of movement is, moreover, consistent with a packing of rod domains in IF backbones that is somewhat open and highly hydrated.

## REFERENCES

Aebi U, Fowler W E, Rew P, Sun T-T (1983) The fibrillar structure of keratin filaments unraveled. J Cell Biol 97:1131-1143.

Aebi U, Cohn J, Buhle L, Gerace L (1986) The nuclear lamina is a meshwork of intermediate-type filaments. Nature(Lond) 323:560-564.

Ahmadi B, Boston N M, Dobb M G, Speakman P T (1980) Possible four-chain repeating unit in the microfibril of wool. In: Parry D A D & Creamer L K (eds) Fibrous Proteins: Scientific, Industrial and Medical Aspects, vol 2. Academic Press, London, pp 161-166.

Baker T S, Winkelmann D A (1986) Methodology for determining the three-dimensional structure of myosin S1 from electron microscopy of orthogonal thin sections. Proc 44th Ann Mtg EMSA pp.26-29. San Francisco Press, San Francisco.

Bornstein T, Traub W (1979) The chemistry and biology of collagen. In: Neurath H & Hill R L (eds) The Proteins, vol 4. Academic Press, New York, pp 411-632.

Conway J F, Parry D A D (1988) Intermediate filament structure 3: analysis of sequence homologies. Int J Biol Macromol 10:79-98.

Engel A, Eichner R, Aebi U (1985) Polymorphism of reconstituted human epidermal keratin filaments: determination of their mass-per-length and width by scanning transmission electron microscopy (STEM). J Ultrastruc Res 90:323-335.

Fisher D Z, Chaudhury N, Blobel G (1986) cDNA sequencing of nuclear lamins A and C reveals primary and secondary structure homology to intermediate filament proteins. Proc Nat'l Acad Sci USA 83:6450-6454.

Fraser R D B, MacRae T P (1982) The fine structure of keratin fibers. In: Breuer M M (ed) Milton Harris: chemist, innovator and entrepreneur. American Chemical Society, pp 109-137.

Fraser R D B, MacRae T P, Parry D A D, Suzuki E (1986) Intermediate filaments in α-keratins. Proc Nat'l Acad Sci USA 83:1179-1183.

Geisler N, Kaufmann E, Fischer S, Plessmann U, Weber K (1983) Neurofilament architecture combines structural principles of intermediate filaments with carboxy-terminal extensions increasing in size between triplet proteins. EMBO J 2:1295-1302.

Geisler N, Fischer S, Vandekerckhove J, Plessmann U, Weber, K (1984) Hybrid character of a large neurofilament protein (NF-M): intermediate-type filament sequences followed by a long acidic carboxy-terminal extension. EMBO J 3:2701-2706.

Geisler N, Kaufmann E, Weber K (1985) Antiparallel orientation of the two double-stranded

coiled-coils in the tetrameric protofilament unit in intermediate filaments. J Mol Biol 182:173-177.

Griffin R G (1981) Solid-state nuclear magnetic resonance of lipid bilayers. Meth Enzymol 72:108-174.

Hanukoglu I, Fuchs E (1983) The cDNA sequence of a type II cytoskeletal keratin reveals constant and variable structural domains among keratins. Cell 33:915-924.

Harrington W F, Rodgers M E (1984) Myosin. Ann Rev Biochem 53:35-74.

Henderson D, Geisler N, Weber K (1982) A periodic ultrastructure in intermediate filaments. J Mol Biol 155:173-176.

Hisanaga S-I, Hirokawa N (1988) Structure of the peripheral domains of neurofilaments revealed by low-angle rotary shadowing. J Mol Biol 202:297-305.

Ip W, Hartzer M K, Pang Y-Y S, Robson R M (1985) Assembly of vimentin and its implications concerning the structure of intermediate filaments. J Mol Biol 183:365-376.

Ip W (1988) Modulation of desmin intermediate filament assembly by a monclonal antibody. J Cell Biol 106:735-746.

Kaufmann E, Weber K, Geisler N (1985) Intermediate filament forming ability of desmin derivatives lacking either the amino-terminal 67 or the carboxy-terminal 27 residues. J Mol Biol 185:733-742.

Keniry M A, Gutowski H S, Oldfield E (1984) Surface dynamics of the integral membrane protein bacteriorhodopsin. Nature(Lond) 307:383-386.

Kirschner M W, Mitchison T J (1986) Beyond self-assembly: from microtubules to morphogenesis. Cell 45:329-342.

Lasek R J, Phillips L, Katz M J, Autilio-Gambetti L (1985) Function and evolution of neurofilament proteins. Ann N Y Acad Sci 455:462-478.

Leszczynski J N, Rose G D (1986) Loops in globular proteins: a novel category of secondary structure. Science 234:849-855.

Mack J W, Torchia D A, Steinert P M (1988) Solid-state NMR studies of the dynamics and structure of mouse keratin intermediate filaments. Biochemistry(USA) 27:5418-5426.

McKeon F D, Kirschner M W, Caput D (1986) Homologies in both primary and secondary structure between nuclear envelope and intermediate filament proteins. Nature(Lond) 319:463-468.

McLachlan A D (1984) Structural implications of the myosin amino-acid sequence. Ann Rev Biophys Bioeng 13:167-190.

Milam L, Erickson H P (1982) Visualization of a 21-nm axial periodicity in shadowed keratin intermediate filaments. J Cell Biol 94:592-592.

Parry D A D, Steven A C, Steinert P M (1985) The coiled-coil molecules of intermediate filaments consist of two parallel chains in exact axial register. Biochem Biophys Res Com 127:1012-1018.

Pollard T D, Cooper J A (1986) Actin and actin-binding proteins. Ann Rev Biochem 55:987-1036.

Potschka, M (1986) Structure of intermediate filaments. Biophys J 49:129-130.

Sauk J J, Krumweide M, Cocking-Johnson D, White J G (1984) Reconstitution of cytokeratin filaments in vitro: further evidence for the role of nonhelical peptides in filament assembly. J Cell Biol 99:1590-1597.

Steinert P M, Idler W W, Goldman R D (1980) Intermediate filaments of BHK-21 cells and bovine epidermal keratinocytes have similar ultrastructures and subunit domain structures. Proc Nat'l Acad Sci USA 77:4534-4538.

Steinert P M, Rice R H, Roop D R, Trus B L, Steven A C (1983) Complete amino-acid sequence of a mouse epidermal keratin subunit and implications for the structure of intermediate filaments. Nature(Lond) 302:794-800.

Steinert P M, Steven A C (1985) Splitting hairs and other intermediate filaments. Nature(Lond) 316:767.

Steinert P M, Steven A C, Roop D R (1985a) The molecular biology of intermediate filaments. Cell 42:411-419.

Steinert P M, Parry D A D, Idler W W, Johnson L D, Steven A C, Roop D R (1985b) Amino acid sequences of mouse and human epidermal type II keratins of $M_r$ 67,000 provide a systematic basis for the structural and functional diversity of the end-domains of keratin intermediate filament subunits. J Biol Chem 260:7142-7149.

Steinert P M, Roop D R (1988) Molecular and cellular biology of intermediate filaments. Ann Rev Biochem 57:593-625.

Steven A C, Wall J S, Hainfeld J T, Steinert P M (1982) Structure of fibroblastic intermediate filaments: analysis by scanning transmission electron microscopy. Proc Nat'l Acad Sci USA 79:3101:3105.

Steven A C, Hainfeld J T, Trus B L, Wall J S, Steinert P M (1983) Epidermal keratin filaments assembled in vitro have masses-per-unit-length that scale according to average subunit mass: structural basis for homologous packing of subunits in intermediate filaments. J Cell Biol 97:1939-1944.

Steven A C, Trus B L, Hainfeld J F, Wall J S, Steinert P M (1985) Conformity and diversity in the structures of intermediate filaments. Ann N Y Acad Sci 455:371-380.

Steven A C, Trus B L, Steinert P M (1987) What's where in intermediate filaments? Proc 45th Ann Mtg EMSA pp 802-805. San Francisco Press, San Francisco.

Torchia D A (1984) Solid-state NMR studies of protein internal dynamics. Ann Rev Biophys Bioeng 13:125-144.

Woods E F, Inglis A S (1984) Organization of the coiled-coils in the wool microfibril. Int J Biol Macromol 6:277-283.

Zhou X-M, Idler W W, Steven A C, Roop D R, Steinert P M (1988) The complete sequence of the human intermediate filament chain keratin 10: subdomainal divisions and model for folding of end-domain sequences. J Biol Chem - in the press.

# Structure and Assembly of Calf Hoof Keratin Filaments

Z. Sayers, A.M. Michon and M.H.J. Koch
EMBL Hamburg Outstation c/o DESY
Notkestrasse 85
D - 2000 Hamburg 52

## 1. Introduction

The constituent proteins of keratin, the intermediate filaments
(IF) in all epithelial cells, can be grouped into acidic (pI $<$
5.5) and basic  (pI $>$ 6.0) subfamilies. Expression patterns in
tissues and in vitro reconstitution indicate that at least one
member from each subfamily is required for full filament forma-
tion (Franke et al. 1983). In the early steps of IF assembly the
subunits interact laterally to form two stranded then four
stranded coiled coils (protofilaments) that are 40-50 nm long and
2-3 nm wide (Quinlan et al. 1986). Reconstituted IF are highly
polymorphic. Different models of the packing of protofilaments
are based on different values of filament diameter and mass per
unit length determined by scanning transmission electron micros-
copy (STEM) (Steven et al. 1983, Engel et al. 1985).
We have characterized the keratin filaments reconstituted from
material extracted from calf hoof stratum corneum and determined
their radius of gyration of the cross-section (Rx) and mass per
unit length (M/L) using X-ray solution scattering.

## 2. Materials and Methods

Unfractionated keratin filament polypeptides were purified from
calf hoof stratum corneum following essentially the method of
Steinert and Idler (1975). The urea buffer used for extraction
and disassembly contained 9 M urea, 50 mM Tris. HCl pH 9, 25 mM

2-Mercaptoethanol, 1 mM $NaN_3$ and the assembly buffer had 10 mM

Tris. HCl, 25 mM 2-Mercaptoethanol and 1 mM $NaN_3$. Fractionation of

the polypeptide mixture was carried out on an anion exchange

column and electrophoretic analyses involved nonequilibrium pH

gradient gels and SDS/polyacrylamide gels. X-ray scattering

measurement were carried out on the X33 camera (Koch and Bordas

1983) on the DORIS storage ring of Deutsches Elektronen Synchro-

tron (DESY).


## 3. Results and Discussion


Electrophoretic analysis of the calf hoof keratin filament

proteins in figure 1A reveals eight polypeptides in the range 49

to 64 kD. The elution profile of this polypeptide mixture on an

anion exchange column and the electrophoresis pattern of selected

peak fractions are illustrated in figure 1B. The first peak of

the chromatogram (fraction 39) contains the polypeptides with

molecular weights 64, 60 and 58 kD and the second peak (fraction

44) contains mainly the 51 and 50 kD components. The 60.5 kD

component elutes at the end of second peak and a third small peak

(fraction 53) is enriched in the 54.5 and 49 kD proteins. The

isoelectric behaviour of the unfractionated polypeptide mixture

shown in figure 1C, is in accordance with the elution profile in

that the 64, 60 and the 58 kD proteins appear as relatively basic

and the 60.5, 51, 50 and 49 kD proteins appear as more acidic.

The 54.5 kD that is fractionated on the column together with the

acidic 49 kD polypeptide however, appears on the 2D gel as a

streak across both the acidic and the basic regions. This

behaviour is not fully understood.

Electron micrographs of the assembly products of the unfrac-
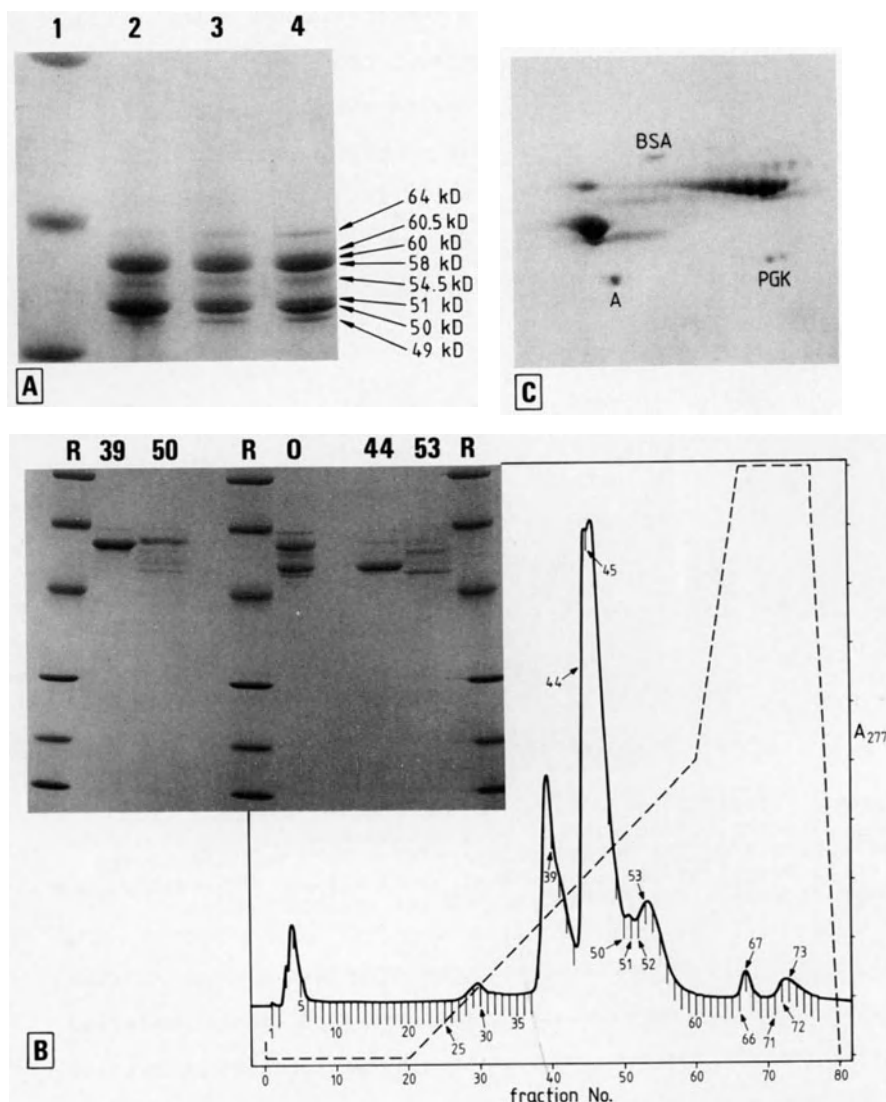
Figure 1.   A:  Migration pattern of calf hoof keratin filament polypeptides on a 7.5 to 17.5% SDS/polyacrylamide gradient gel with the   estimated molecular weights. B: Chromatogram of the Mono Q column. Broken line indicates the 0 to 500 mM salt gradient. Insert shows the electrophoretic analysis of selected fractions, lanes are labelled with the fraction number. Lane 0 is the material applied to the column and lanes labelled R are the reference proteins from top to bottom:  94 kD, 67 kD, 43 kD, 30 kD, 20 kD, 14.4 kD. C: 2D gel of the unfractionated polypeptides. Marker proteins are (A) actin MW 42 kD pI 5.4, (BSA) bovine serum albumin MW 67 kD pI 6.4 and (PGK) phosphoglycerate kinase MW 43 kD pI 7.5.

-tionated sample and fractionated components are shown in figure
2. Under assembly conditions the basic proteins form nonspecific
aggregates whereas the acidic proteins assemble into short
protofilamentous structures. Short stubby structures with
apparently the same diameter as the full filaments can also be
seen on the micrographs of the reassembled acidic proteins. These
could be due to contamination from basic proteins in this fraction.
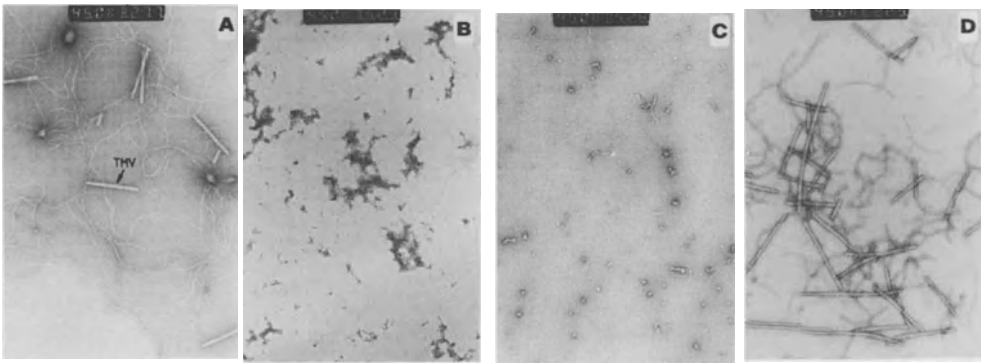


Figure 2. Electron micrographs obtained under assembly conditions
from: A: the unfractionated polypeptide mixture; B: The basic
polypeptides; C: The acidic polypeptides; D: A mixture of the
selected fractions of figure 1B at equal ratios. TMV denotes the
tobacco mosaic virus particles used for calibration.

X-ray scattering patterns of sections of native stratum corneum
display broad and weak intensity features with little preferred
orientation. In contrast, the scattering patterns of reconstitu-
ted filaments in solution or in a gel are featureless in the
range $0.02 < s < 0.50$ nm$^{-1}$. Cross-section plots obtained from the
scattering patterns of filament solutions reconstituted from
unfractionated polypeptides are shown in figure 3 together with
an electron micrograph of the same sample.

**A**                    **B**
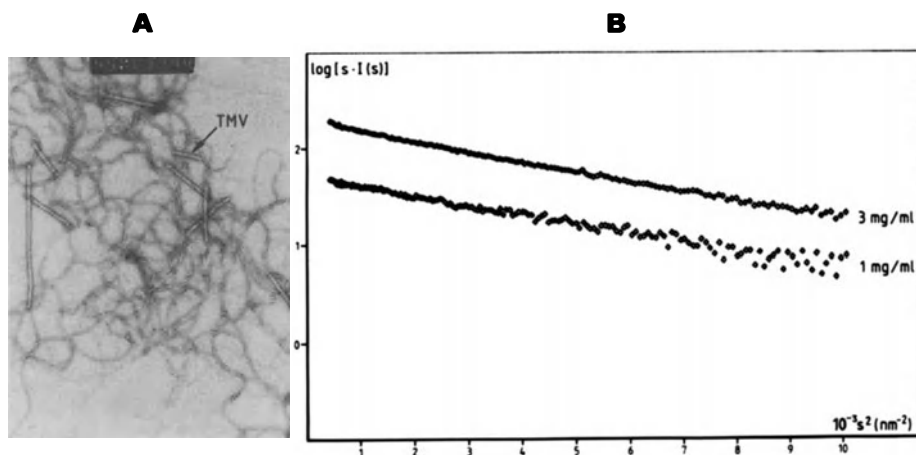


Figure 3. A: Electron micrograph of the filament preparation used for X-ray scattering. B: Cross-section plots of keratin filaments at concentrations of 1 mg/ml and 3 mg/ml. I (s) is the scattered intensity corresponding to s = (2 sin θ) /λ , where 2θ is the scattering angle and   λ the wavelength.

Linearity of the cross-section plots is in agreement with a narrow (gaussian) distribution of filament diameters. The average Rx determined from the slope of the cross section plot is 3.47 nm and corresponds to an equivalent solid cylinder diameter of 9.8 nm. M/L determined relative to that of actin filaments from the intercept of the cross-section plots is 25 kD/nm. The filament diameter determined is smaller than values previously obtained by STEM; 11. 3-12.6 nm by Engel et al. (1985) and 15-16 nm by Steven et al. (1983). M/L as we determine falls in the range reported by the two groups for the major species of human epidermal IF but is smaller than the value given by Steven et al. (1983) for bovine epidermal keratin filaments. No evidence was found in the X-ray patterns of reconstituted calf hoof keratin filaments for the 22-23 nm repeat observed in glycerol sprayed metal shadowed specimens (Henderson et al. 1982). Similarly, we did not find any features corresponding to the 47 nm repeat proposed for         α-

keratin fibres (Fraser and McRae, 1971). Our results suggest that although a similar structure is seen in electron micrographs there may be more subtle structural differences between native and reconstituted filaments. Some caution is thus required in the generalizations made about the 3D structure of IFs.

## 4. References

Engel A, Eichner R, Aebi U (1985) Polymorphism of reconstituted keratin filaments: Determination of their mass-per-length and width by scanning transmission electron microscopy (STEM). J Ultrastr Res 90:323-335

Franke WW, Schiller DL, Hatzfeld M, Winter S (1983) Protein complexes of intermediate filaments: melting of cytokeratin complexes in urea reveals different polypeptide separation characteristics. Proc Natl Acad Sci USA 80:7113-7117

Fraser RDB, MacRae TP (1985) Intermediate filament structure. Boisci Rep 5:573-579

Fraser RDB, MacRae TP (1971) Structure of $\alpha$-keratin. Nature 233:138-140

Henderson D, Geisler N, Weber K (1982) A periodic ultrastructure in intermediate filaments. J Mol Biol 155:173-176

Koch MHJ, Bordas J (1983) X-ray diffraction and scattering on disordered systems using synchrotron radiation. Nuclear Instrum and Methods 208:461-469

Quinlan RA, Hatzfeld M, Franke WW, Lustig A, Schulthess T, Engel J (1986) Characterization of dimer subunits of intermediate filament proteins. J Mol Biol 192:337-349

Steinert PM, Idler WW (1975) The polypeptide composition of bovine epidermal $\alpha$-keratin. Biochem J 151:603-611

Steven AC, Hainfeld JF, Benes LT, Wall JS, Steinert PM (1983) Epidermal keratin filaments assembled in vitro have masses-per-unit-length that scale according to average subunit mass. J Cell Biol 97:1939-1944

# Structure and Assembly of Neurofilaments (NF): Analysis of Native NF and of Specific NF Subunit Combinations

J. C. Troncoso[1], M. Häner[2], J. L. March[1], R. Reichelt[2], A. Engel[2], and U. Aebi[2,3]

[1]Departments of Pathology and Neurology, The Johns Hopkins University School of Medicine,
  Baltimore, MD. 21205, USA
[2]Maurice E. Müller-Institute for High Resolution Electron Microscopy,
  Biocenter, University of Basel, CH-4056 Basel, Switzerland
[3]Department of Cell Biology and Anatomy, The Johns Hopkins University School of Medicine,
  Baltimore, MD. 21205, USA

## Introduction

A large body of information on the primary and secondary structure of intermediate filaments (IF) is now available [Weber et al., 1983; Steinert et al., 1985]. In the quest to ultimately understand IF structure, function and interaction at the molecular level, next steps include: (i) establishing the rules by which IF polypetides assemble into supramolecular structures; (ii) determining the three-dimensional (3-D) molecular architecture of IF; and (iii) establishing correlations between the molecular structure and function of the various IF. Because it has not been possible to obtain crystalline arrays of IF proteins in a consistent manner - which is a prerequisite for X-ray diffraction analysis of proteins - investigators have sought alternative techniques to approach these questions. In our labs we have begun to apply *in vitro* reconstitution of filaments and scanning transmission electron microscopy (STEM) to the study of neurofilaments (NF). This is a preliminary report on our work with NF, including effective and reproducible separation of the three NF polypeptides, *in vitro* reconstitution of NF from individual as well as specific combinations of subunits, and STEM mass measurements of native and reconstituted NF. We have observed that *in vitro* reassembly of NF takes place within strict limits of temperature, pH and salt concentration. In addition, STEM mass measurements disclose a marked polymorphism both of native and reconstituted NF.

## Native NF

Native NF were extracted from fresh or deep-frozen bovine spinal cord in 100 mM Mes, pH 6.5, containing 1 mM EGTA , 0.5 mM $MgCl_2$ and protease inhibitors, basically as described by Delacourte et al., 1980, and suspended in 50 mM MES, 175 mM NaCl, 0.5 mM EGTA, 1 mM DTT, pH 6.5 for further analysis or processing. Gel electrophoresis of this material (Fig. 1, inset) revealed the classical NF polypeptide triplet consisting of NF-L (68 kDa), NF-M (~160 kDa) and NF-H (~200 kDa). As displayed in Fig. 1, negatively stained native NF were studded with globular structures at variable intervals (the shortest intervals being approximately 22 nm) and had apparent

diameters ranging between 10 and 15 nm. We have not observed the thin filamentous structures radially projecting from the core of the filaments (i.e. "sidearms") as has recently been demonstrated after glycerol spraying/low-angle rotary metal shadowing of native NF [Hisanaga and Hirokawa, 1988]. Instead, in our pictures it appears that the sidearms have collapsed into studs along the filament shaft - a situation which may represent a specimen preparation artifact induced by the negative staining.
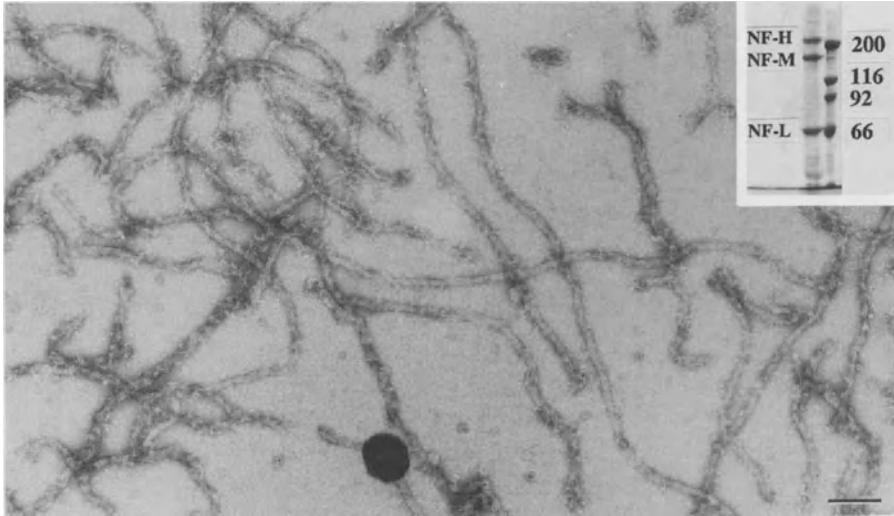


**Fig. 1**: Electron micrograph of native NF isolated from bovine spinal cord after negative staining with 0.75% uranyl formate. Inset: SDS/PAGE (7.5%) of native NF (left) together with gel standards (right). Scale bar, 100 nm.

Following extraction, native NF were dissolved in 6 M urea. Subsequent removal of the urea from the denatured native NF solution by dialysis for ≥3 hours at 37°C against 50 mM Mes, pH 6.25, containing 175 mM NaCl, 0.5 mM EGTA, 1mM DTT, resulted in reassembly of filaments that were significantly less studded than the native filaments, suggesting abnormal - or reduced - incorporation of NF-M and/or NF-H into reconstituted filaments. The optimal pH for reassembly was 7.4 (in this case using Tris or imidazole).

## Separation of NF Polypeptides

Native NF were dissolved in 6 M urea as above, and contaminants were removed by passage over a Sephadex G-25 column. The void peak was then applied to a DEAE anion exchange column which was eluted with a 100-250 mM linear NaCl gradient. By this step we were often unable to achieve good separation of NF-M and NF-L. Better and more reproducible separation of NF-M and NF-L was achieved by FPLC using a Mono Q anion exchange column (Pharmacia, Uppsala, Sweden) and eluting it with a multi-step NaCl gradient (i.e. between 200 and 500 mM NaCl).

Low-speed sedimentation equilibrium centrifugation analysis of separated NF-L, NF-M and NF-H in 6 M urea, using a Beckman Model E analytical ultracentrifuge, yielded a mixture of monomers and dimers for the protein concentrations tried (i.e. 0.2-0.5 mg/ml). To obtain more effective dissociation into monomers, 6 M guanidine-HCl was employed.

## Reconstitution Experiments with Individual NF Subunits
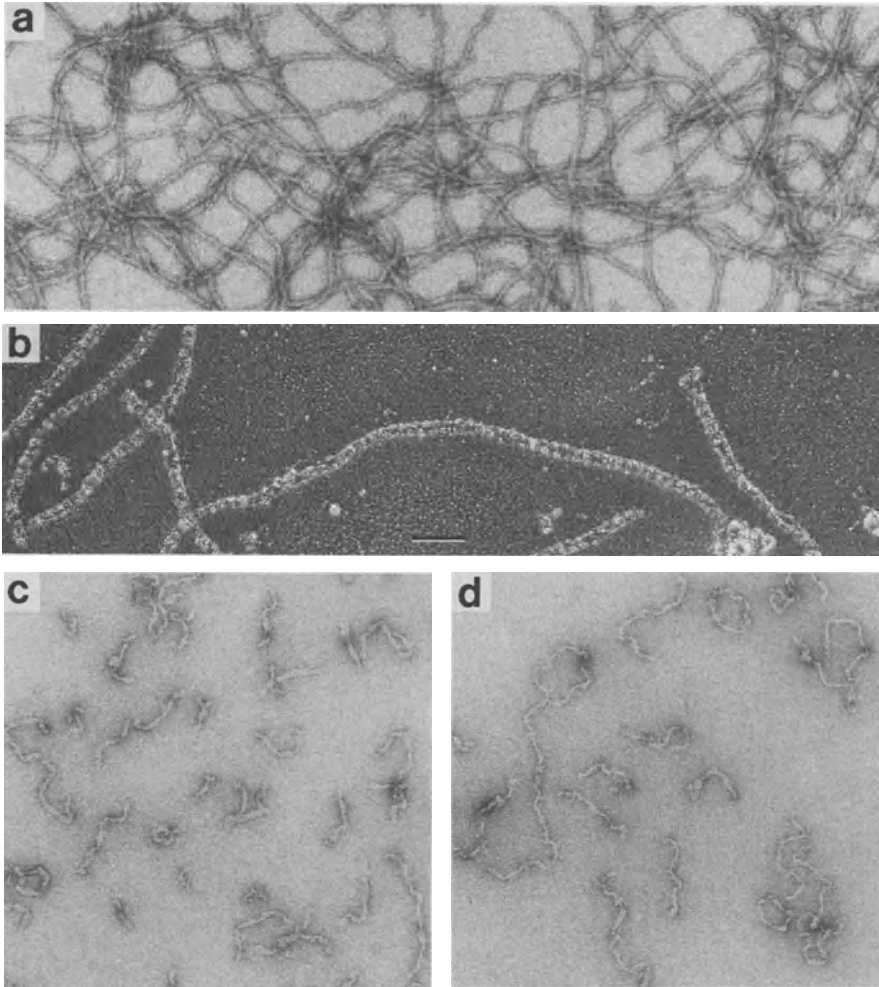


**Fig. 2:** Electron micrographs of individual NF subunits reconstituted under standard filament forming conditions (dialyzed against 50 mM Mes, 175 mM NaCl, 0.5 mM EGTA, 1 mM DTT, pH 6.25 for $\geq 3$ hours at 37°C). (a) Reconstituted NF-L, negatively stained with 0.75% uranyl formate. (b) Dito but glycerol sprayed/low-angle rotary shadowed with platinum-carbon. (c) Reconstituted NF-M, negatively stained as in (a). (d) Reconstituted NF-H negatively stained as in (a). Scale bar, 100 nm (a-d).

6-M-urea solubilized NF-L, NF-M or NF-H fractions were dialyzed for ≥3 hours against "standard filament reconstitution" buffer (50 mM Mes, pH 6.25, containing 175 mM NaCl, 0.5 mM EGTA, 1mM DTT) at 37°C. Filament reconstitution was virtually complete after three hours of dialysis, at which time all three types of subunits had assembled into filamentous structures (Fig. 2): NF-L assembled into long, 8-12 nm wide, filaments which appeared smooth and flexible (Fig. 2a); both NF-M (Fig. 2c) and NF-H (Fig. 2d) formed short s-shaped - and sometimes kinked - filaments, 8-10 nm wide, with a smooth surface. When sprayed with glycerol onto freshly cleaved mica and rotary shadowed at low-angle with platinum-carbon, NF-L filaments looked indistinguishable from other IF and revealed a characteristic 22-23 nm axial "beading".

## Reconstitution Experiments with Specific NF Subunit Combinations

Using the same reconstitution conditions as described above, we attempted reconstitution of various NF subunit combinations. A fraction eluted from the DEAE column containing an approximate 1:1 mixture of NF-L & NF-M formed long filaments, 8-12 nm wide. These filaments did not appear studded and looked similar to reconstituted NF-L filaments (Fig. 2a). Again, glycerol spraying/low-angle rotary metal shadowing of these filaments revealed the 22-23 nm axial beading characteristic for IF (Fig. 2b). Equimolar mixtures of NF-L & NF-M, NF-L & NF-H, or NF-L & NF-M & NF-H led to predominantly "segregated" assembly of NF-L filaments on the one hand, and NF-M or NF-H filaments on the other hand, without significant co-assembly of the different NF subunits into common structures as has previously been reported by some investigators [c.f. Geisler and Weber, 1981; Hisanaga and Hirokawa, 1988].

## Systematic Variation of NF-L Reconstitution Conditions

We have performed a series of experiments to evaluate the effects of pH, temperature, and ionic strength on the reconstitution of 6-M-urea solubilized NF-L. Based on these experiments, we have determined the "optimal" reconstitution conditions for NF-L to be dialysis for ≥3 hrs at 37°C against 50 mM MES containing 0.5 mM EGTA, 1 mM DTT, 175 mM NaCl, pH 6.25. In the range 0.2-2 mM, $MgCl_2$ seems to have no significant effect on NF-L reconstitution both in terms of the length of the NF-L filaments, their compactness and/or apparent width. The permissive pH range for NF-L filament formation is about 5.75 to 6.75. Below pH 5.75, an abrupt change occurs: the filamentous assemblies become shorter (~75 to 300 nm) and wider (~15 to 25 nm) than normal NF-L filaments (Fig. 3a). Most importantly, these structures can no longer be converted into normal looking IF upon restoring the pH to 6.25, meaning that they represent aberrant assemblies. Raising the pH above 6.75 yields progressively shorter filaments with a tendency to laterally dissociate into protofibrils or protofilaments (Fig. 3b). In this case, however, normal looking IF are formed upon lowering the pH to 6.25, indicating that the subfilamentous structures occuring at elevated pH (Fig. 3b) are true IF precursors.
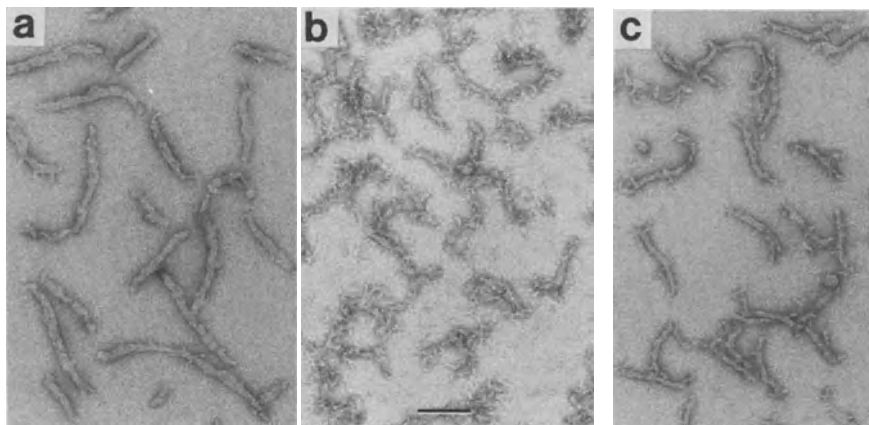
Fig. 3: Electron micrographs of negatively stained samples illustrating the effects of pH (a,b) and temperature (c) on filament reconstitution of NF-L. (a) NF-L, 1 mg/ml, was dialyzed for 12 hours against standard filament reconstitution buffer (50 mM MES, pH 6.25, containing 175 mM NaCl, 0.5 mM EGTA, 1mM DTT, 37°C), except at **pH 5.0**. (b) NF-L was dialyzed against filament reconstitution buffer, except at **pH 7.5**. (c) NF-L was dialyzed against standard filament reconstitution buffer, except at **20°C**.

Temperature appears to be another crucial parameter to achieve correct NF-L assembly: Reconstitution of NF-L at 20°C - under otherwise optimal reconstitution conditions (see above) - results in short filamentous structures (Fig. 3c) which, after raising the temperature back to 37°C, can no longer form normal looking IF. Apparently, lowering the temperature significantly below 37°C leads to "dead-end" precursor structures that cannot be rescued by simply restoring the proper reconstitution temperature.

## Mass Measurements of NF by STEM

Mass-per-length (MPL) values are useful to calculate the number of polypeptides per filament cross-section, an important parameter for understanding the supramolecular organization of IF [Steven et al., 1982; Engel et al., 1985]. We have therefore employed STEM to measure the MPL of native and various types of reconstituted NF. Native NF revealed a histogram exhibiting a wide distribution of MPL values which could be fitted by two Gaussian curves of similar size centered at 53 kDa/nm and 79 kDa/nm (Fig. 4a). In contrast, the MPL histogram of NF reconstituted from 6-M-urea solubilized native NF was narrower and revealed smaller MPL values, which could be fitted by a major Gaussian centered at 47 kDa/nm and a minor Gaussian centered at 74 kDa/nm. Finally, a rather narrow MPL histogram was obtained from filaments reconstituted from 6-M-urea solubilized NF-L which could best be fitted by a single Gaussian centered at 23 kDa/nm, meaning that these filaments contained 16 NF-L polypeptides per filament cross-section. These results, while still preliminary, indicate that the previously observed MPL-polymorphism of IF [Engel et al., 1985; see also Steven et al., this volume] may not be limited to reconstituted IF. On the contrary, our data demonstrate that native NF are the most polymorphic filaments that we have examined, and that
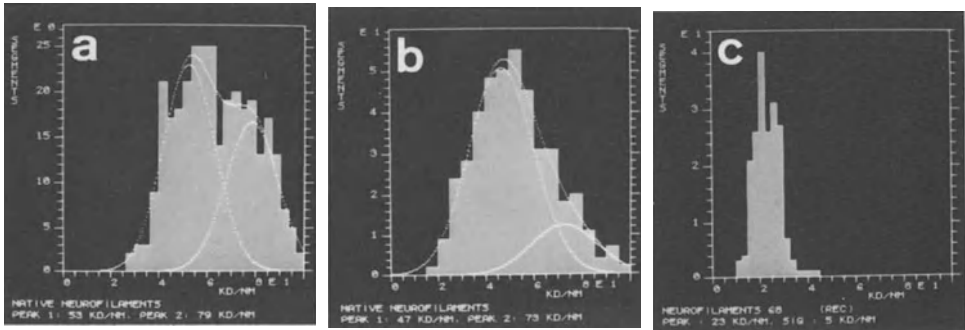
**Fig. 4**: MPL histograms measured from native NF (a), 6-M-urea solubilized/reconstituted NF (b), and reconstituted NF-L (c) filaments by scanning transmission electron microscopy (STEM). Specimen preparation and MPL measurements were performed as described [Engel et al., 1985].

some of the reconstituted forms - e.g. the NF-L filaments - exhibit minimal MPL-polymorphism. Clearly, more work needs to be done for understanding the cause and ultimate significance of the IF MPL-polymorphism.

## Acknowledgements

## References

Aebi, U., W.E. Fowler, P. Rew, and T.-T. Sun (1983). The Fibrillar Substructure of Keratin Filaments Unraveled. *J. Cell Biol.* **97**: 1131-1143.

Aebi, U., M. Häner, J.C. Troncoso, R. Eichner, and A. Engel (1988). Unifying Principles in Intermediate Filament (IF) Structure and Assembly. *Protoplasma* **145**: 73-81.

Delacourte, A., G. Filliatreau, F. Boutteau, G. Biserte, and J. Schrevel (1980). Study of the 10-nm Filament Fraction During the Standard Microtubule Preparation. *Biochem. J.* **191**: 543-546.

Engel, A., R. Eichner, and U. Aebi (1985). Polymorphism of Reconstituted Human Epidermal Keratin Filaments: Determination of their Mass-per-Length and Width by Scanning Transmission Electron Microscopy (STEM). *J. Ultrastruct. Res.* **90**: 323-335.

Geisler, N., and K. Weber (1981). Self Assembly *In Vitro* of the 68,000 Molecular Weight Component of the Mammalian Neurofilament Triplet Protein into Intermediate-Sized Filaments. *J. Mol. Biol.* **151**: 565-571.

Hisanaga, S., and Hirokawa, N. (1988). Structure of the Peripheral Domains of Neurofilaments Revealed by Low Angle Rotary Shadowing. *J. Mol. Biol.* **202**: 297-305.

Steinert, P.M, and D.A.D. Parry (1985). Intermediate Filaments: Conformity and Diversity of Expression and Structure.*Annu. Rev. Cell Biol.* **1**: 41-65.

Steven, A.C., J. Wall, J. Hainfeld, and P.M. Steinert (1982). Structure of Fibroblastic Intermediate Filaments: Analysis by Scanning Transmission Electron Microscopy. *Proc. Natl. Acad. Sci. USA* **79**: 3101-3105.

Weber, K., and N. Geisler (1984). Intermediate Filaments - from Wool α-Keratins to Neurofilaments: a Structural Overview. In: Cancer Cells 1, "The Transformed Phenotype". *Cold Spring Harbor Laboratory Press*: 153-159.

# Mitochondrial Creatine Kinase (Mi-CK) Forms Octameric Molecules: Structure-Function Relationship and Implications for the CP-Shuttle

Thomas Schnyder, Andreas Engel[+], Heinz Gross, Hans M. Eppenberger and Theo Wallimann*

Institute for Cell Biology, ETH-Hönggerberg, CH-8093 Zürich, and [+]Maurice E. Müller Institute, Biocenter, University Basel, CH-4056 Basel, Switzerland
*to whom correspondence should be sent

Creatine kinase (CK) transphosphorylates the phosphoryl group of phospho-creatine (CP) to ADP to regenerate ATP, the primary source of energy in living systems. Besides the "cytosolic" brain-type (BB-CK), muscle-type (MM-CK) and heterodimer-type (MB-CK) isoforms (for review see: Eppenberger et al. 1983), a fourth isoform of CK, the mitochondrial Mi-CK (Jacobs et al. 1984), is also present in significant amounts in tissues with sudden high energy demand, e.g., skeletal and cardiac muscle, brain and photoreceptor cells, and spermatozoa. Mi-CK is restricted to mitochondria and seems to be well adapted to generate CP from ATP produced by oxidative phosphorylation within the mitochondrial matrix (Jacobus and Lehninger, 1973). Mi-CK which is bound at the outer side of the inner mitochondrial membrane (Scholte, 1973) is thought to be functionally coupled to the ATP/ADP-translocator (Saks et al. 1980) and was found to be clearly different in amino acid composition, cDNA sequence and immunological properties from B- and M-CK (Hossle et al. 1988; Schlegel et al. 1988), but conflicting reports on its oligomeric structure (subunit $M_r$ = 43'000) have been published. A mild and efficient scheme for the purification of Mi-CK from chicken cardiac and brain mitochondria was developed which allows the fast isolation of 5-10 mg quantities of the enzyme with a purity of $\geq$ 99.5 % (Schlegel et al. 1988). Characterization by gelpermeation, analytical ultracentrifugation (UC) and direct mass measurement by scanning transmission electron microscopy (STEM) revealed the presence of a major octameric Mi-CK species with a $M_r$ of 328'000$\pm$25'000(UC) and 340'000$\pm$55'000(STEM), and a minor dimer species with a $M_r$ of 83'000$\pm$8'000(UC) (Schnyder et al. 1988). Negative staining of single Mi-CK octamers, both from brain and cardiac mitochondria (Fig. 1a and b, respectively), revealed distinct square-shaped particles with four-fold symmetry, sides of 10 nm and a central cavity of 2,5-3 nm filled by negative stain (Fig. 1: gallery of Mi-CK molecules after linear and rotational alignment (b); and averaged structure by
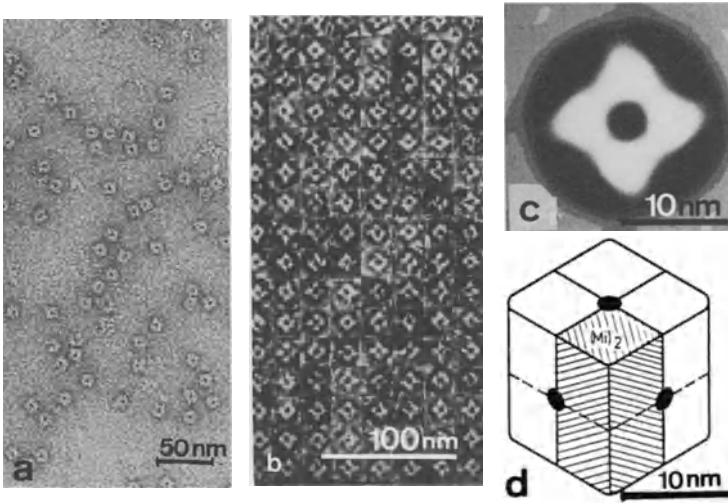
<u>Figure 1:</u> Electron micrograph of a field of Mi-CK octamers after negative staining (a); computer alignment (b); and image processing (c); simple model of the Mi-CK octamer(d).

SEMPER image processing program (c)). Rotary shadowing by heavy metal (Ta/W) at very low temperature (-250$^{\circ}$C) of freeze-dried single Mi-CK molecules (Gross et al. 1985) revealed structural details ($\leq$ 2 nm) of the surface relief of the octamers, e.g. cross-like, radial indentations originating from a central pit that divide Mi-CK octamers into the four dimeric subdomains (Fig. 2a, showing a field of Mi-CK octamers after high-resolution shadowing). Note the regularly sized, well preserved molecules after freeze-drying and the extremely fine heavy metal grain. A simplified model of the Mi-CK octamer by combining the features of negatively stained (Fig. 1) and rotary shadowed molecules (Fig. 2a) is shown in Fig. 1d, where Mi-CK is depicted as a cube-like structure with a central indentation on the surface that is compatible with a pit or channel. The octamer is shown to consist of four dimers (Mi-CK)$_2$ (shaded area in Fig. 1d), dimers being the common structure of the other CK iso-forms as well. The Mi-CK dimers are arranged around a central stain-accumulating cavity. The fact that by each method, negative staining and rotary shadowing, only a single kind of view of the molecule is seen (Fig. 1 and 2) indicates either that Mi-CK octamers adsorb onto the support preferentially by two identical sides (top or bottom) or that all six sides of the cube-like molecules are structurally very similar as depicted in Fig. 1d. Preliminary
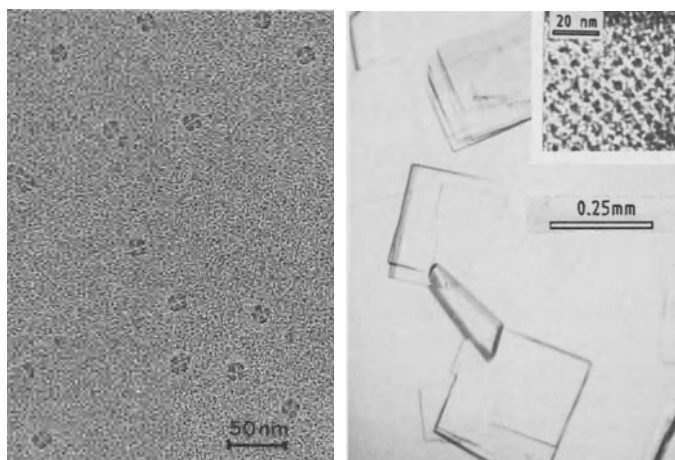
Figure 2: A field of freeze-dried Mi-CK octamers after high-resolution metal (Ta/W) shadowing at very low temperature ($-250^{\circ}$C) (a); Mi-CK crystals (b); and EM pictures of a negatively stained fragment of a Mi-CK crystal (inset).

analysis of the first crystals of Mi-CK by X-ray and negative staining revealed tetragonal packing of octameric Mi-CK within the crystal (Fig. 2, inset). If Mi-CK as an energy channeling molecule forms a multi-enzyme compartment at the contact sites of inner and outer mitochondrial membranes where it is accumulated (Schnyder et al. 1988), then the concept of Mi-CK representing an octamer with a central channel could suggest an attractive structure-function relationship within the CP-shuttle frame-work (Wallimann and Eppenberger 1985). It is tempting to speculate that the total of eight catalytic centers be directed towards the central cavity thus providing the biochemical basis for a cooperative multi-subunit energy channeling protein.

Eppenberger HM, Perriard JC, and Wallimann T (1985) In: Rattazzi et al (eds) Isozymes, AR Liss, Vol 7 pp 19-35
Gross H, Müller T, Wildhaber I, and Winkler H (1985) Ultramicroscopy 16:287-304
Hossle JP, Schlegel J, Wegmann G, Wyss M, Böhlen P, Eppenberger HM, Wallimann T, and Perriard JC (1985) B B R C 151:408-416
Jacobs M, Heldt HW, and Klingenberg M (1964) B B R C 16:516-521
Jacobus WE, and Lehninger AL (1973) J Biol Chem 248:4803-4810
Saks VA, Kupriyanov VV, Elizarova EV, and Jacobus WF (1980) J B C 255:755-763
Schlegel J, Zurbriggen B, Wegmann G, Wyss M, Eppenberger HM, and Wallimann T, (1988) J Biol Chem, in press (Nov 88)
Schnyder T, Engel A, Lustig A, Wallimann T (1988) J Biol Chem, in press (Nov 88)
Scholte HR (1973) B B A 305:413-427
Wallimann T, and Eppenberger HM (1985) In: Shay JW (ed) Cell and Muscle Motility, Plenum Publishing Corporation, Vol 6 pp 239-285

# Current State of the Structural Analysis of the Actin : DNase I Complex

* W. Kabsch, * E.F. Pai, ** H.G. Mannherz and *** D. Suck

* Max-Planck-Institut für medizinische Forschung, Abt. Biophysik, Jahnstr. 29, D-6900 Heidelberg 1, FRG

** Institut für Anatomie und Zellbiologie der Universität, D-3550 Marburg, FRG

*** EMBL, Postfach 102209, D-6900 Heidelberg 1, FRG

The complex between rabbit skeletal muscle actin and bovine pancreatic DNase I (Lazarides & Lindberg, 1974) can be crystallized in three different forms. The x-ray structure of the orthorhombic form III has been solved to a resolution of 0.6nm (Suck, Kabsch & Mannherz, 1981). More recently the resolution has been increased to 0.45nm and the actin molecule has been unambigously identified in the map (Kabsch, Mannherz & Suck, 1985). This identification was derived from knowledge of the DNase I atomic structure (Suck, Oefner & Kabsch, 1984). In addition, only one combination of actin and DNase I density was found which is common to both the monoclinic (form II) and the orthorhombic (form III) crystals. It was concluded that this unique combination must represent the complex as found in solution.

Because of the difficulties of reproducibly preparing isomorphous heavy-atom derivatives it became clear that any further progress could not be acchieved by using the available method of data collection by the rotation / oscillation film technique. Therefore, a large effort was undertaken (Kabsch, 1988a,1988b) to develop algorithms and programs for the automatic collection and processing of diffraction data recorded by an electronic area detector (Nicolet / Xentronics, Madison ,WI,USA) available in our laboratory. It is now possible to collect and process a virtually complete data set to a resolution of 0.3nm from a single actin: DNase I crystal within two days.

Native data sets of good quality were collected from two crystals and subsequently scaled together. After several unsuccessful attempts a useful $Pb(NO_3)_2$ heavy atom derivative was prepared. Because of the reproducibility problem it was found essential to collect a complete data set from one crystal. A second heavy - atom derivative was

# Isomorphous Replacement results of type III actin: DNase I crystals

| Resolution [nm] | 0.6 | 0.45 | 0.35 |
|---|---|---|---|
| **Native** | | | |
| Figure of merit | 0.83 | 0.65 | 0.47 |
| Number of phased reflections | 2280 | 2847 | 4682 |
| Number of observed reflections | 2280 | 2893 | 5092 |
| Number of possible reflections | 2303 | 2980 | 5677 |
| **Pb(NO$_3$)$_2$  [1mM, 1 d]** | | | |
| Phasing power | 1.78 | 1.79 | 1.45 |
| $R_C$ [%] | 49.3 | 55.3 | 71.1 |
| $R_F$ [%] | 17.5 | 17.7 | 18.0 |
| Number of reflections | 2060 | 2695 | 4536 |
| **MMA [1mM, 1h]** | | | |
| Phasing power | 1.56 | 1.46 | 1.23 |
| $R_C$ [%] | 57.5 | 64.6 | 77.8 |
| $R_F$ [%] | 19.9 | 19.8 | 23.1 |
| Number of reflections | 2126 | 2750 | 4555 |

Phasing power $= F_H / E$

$R_C$  =  Cullis R - factor for centric reflections

$R_F$  =  $2\Sigma \mid F_P - F_{PH} \mid / \Sigma \mid F_P + F_{PH} \mid$
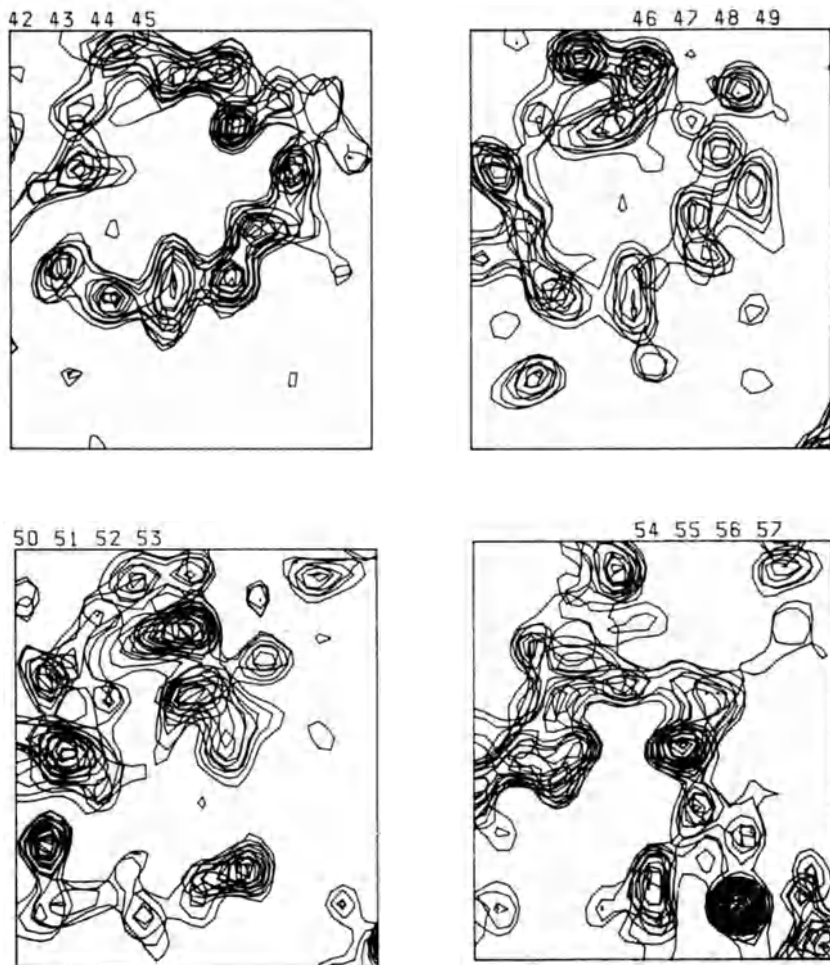
**Fig. 1**

Picture of the actin:DNase I map at 0.35nm resolution when looking through a fixed window of size 2.64nm x 3.02nm in the a,c-plane of the orthorhombic type III unit cell. Distance between two sections is 0.094nm. The highest density in the map appears in the lower right picture and probably represents the phosphate peak of ADP. The density features mainly represent helices.
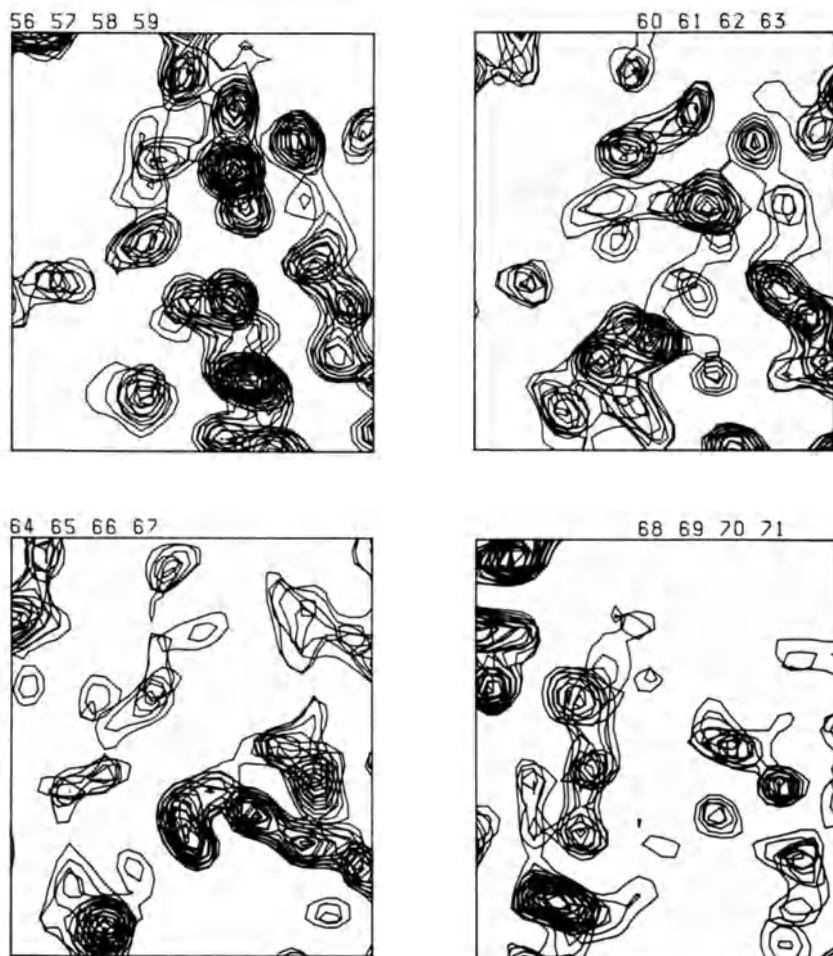
**Fig. 2**

Picture of the actin:DNase I map at 0.35nm resolution when looking through a window of size 2.64nm x 3.02nm in the a,c-plane of the orthorhombic type III unit cell. Distance between two sections is 0.094nm. The highest density appears in the upper left picture and probably represents the phosphate peak of ADP.
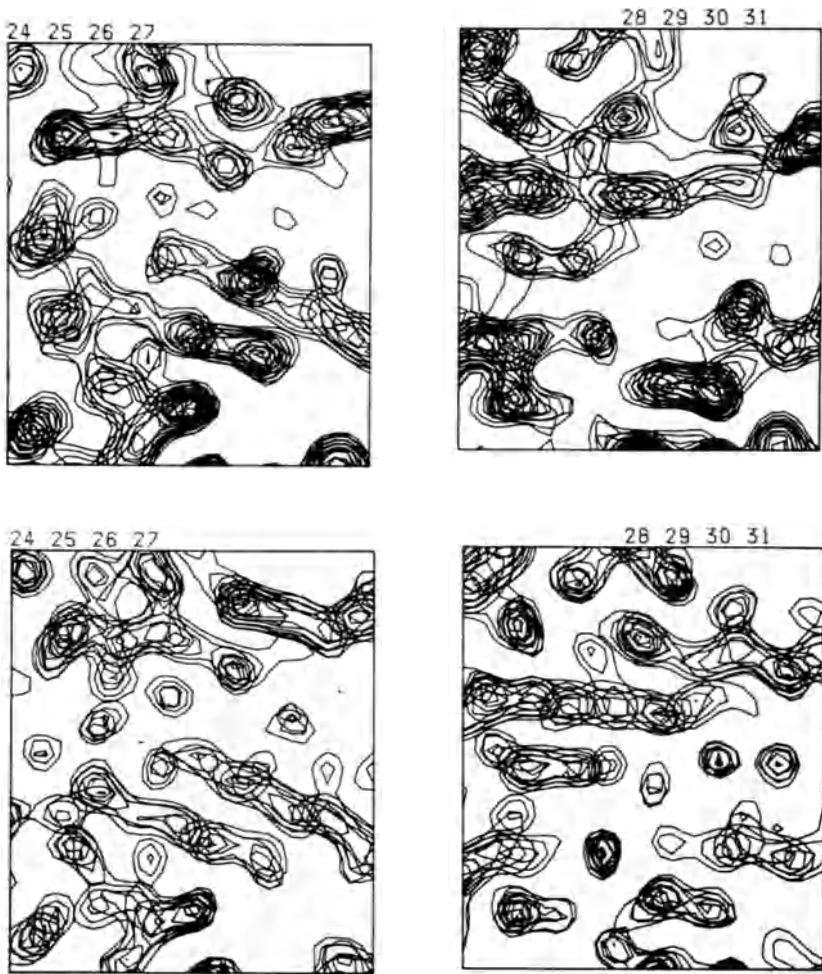
**Fig. 3**

Picture of the actin: DNase I map at 0.35nm resolution when looking to a fixed window of size 2.64nm x 3.02nm in the a, c-plane of the orthorhombic type III unit cell. Distance between two sections is 0.094nm. The density region at the center of the DNase I molecule is shown in the upper two pictures. The two pictures in the lower part of this figure show the same density region when calculated from the atomic coordinates of DNase I.

obtained by soaking in a 1mM methylmercury (MMA) solution for 1 h. The heavy-atom positions of the two derivatives were located by the difference Fourier technique, starting with the known native structure factors at 0.6 nm. A summary of the isomorphous replacement results is given in the table. The numbers for the figure of merit were calculated from the two new heavy-atom derivatives and the low resolution derivatives described earlier (Kabsch, Mannherz & Suck, 1985). A solvent flattening procedure similar to the method of Wang (1985) was applied to improve the phases. An electron density map was calculated at 0.35 nm resolution. The map confirms our results obtained at lower resolution:

Actin consists of a large and a small domain each containing a ß-pleated sheet surrounded by helices. Each sheet  is built up from at least four strands. The ADP-molecule is bound between the two domains stretching across the edges of the ß-sheets. All helices which had been identified earlier are also found in the new map including side chain densities as expected at 0.35 nm resolution. Long stretches of the polypeptide chain can easily be followed in the map.

Fig. 1 displays a sequence of three helices in the large domain starting at the phosphate peak of ADP in the lower right picture. Fig. 2 shows the region surrounding the phosphate peak of ADP (upper left picture). Two helices can be seen at the bottom parts of the upper row of pictures. One of the helices is pointing towards the phosphate peak. Several features in the lower row of pictures represent strands of ß-sheets.

The quality of the map can be judged from Fig. 3. The upper part of this figure shows a portion of electron density at the center of the DNaseI molecule.The lower part displays the same region as calculated from the atomic coordinates of DNaseI. From a visual comparison of the corresponding regions we conclude that our map is of sufficient quality to justify our expectation that an atomic model of actin will be available in the near future.

References

Kabsch, W. (1988a) J. Appl. Cryst. 21,67-71.

Kabsch, W. (1988b) J. Appl. Cryst. (in press).

Kabsch, W., Mannherz, H.G. and Suck, D. (1985) EMBO J. 4,2113-2118.

Lazarides, E. and Lindberg, U. (1974) Proc. Natl. Acad. Sci.71,4742-4746.

Suck, D., Kabsch, W. and Mannherz, H.G. (1981) Proc. Natl, Acad. Sci. USA, 78,4319-4323.

Suck, D., Oefner, C. and Kabsch, W. (1984) EMBO J. 3,2423-2430.

Wang, B.C. (1985) Meth. Enzymol. 115,90-112.

# The Structure of F-Actin Calculated from X-Ray Fibre Diagrams and the 0.6 nm Crystal Structure

K.C.Holmes, D.Popp, W.Gebhard, W.Kabsch
Max Planck Institut für medizinische Forschung, Heidelberg
W. Germany

The structure of the g-actin monomer complexed with DNaseI has been solved by x-ray crystallography to 0.45nm resolution, Fig.1 (Kabsch, Mannherz, & Suck, 1985). In the following we describe the structure of f-actin arrived at by a search procedure: the structure obtained from crystallography at 0.6nm is placed in all possible orientations in the F-actin helix; the fibre diffraction pattern is computed from the resulting structure and compared with the x-ray diffraction data from orientated gels of F-actin (Popp, Lednev, & Jahn, 1986) measured to 0.8 nm resolution. This process yielded five possible solutions at low resolution (2.0nm) only one of which successfully refined to high resolution (0.8nm). A full account of this study is in preparation (Holmes, et al. 1989). The best of the five possible solutions resulting from the low resolution search is shown in Fig. 2. The (intensity) R-factor is 0.12. To refine at high resolution we adopted an iterative least squares procedure. However, no solution would refine satisfactorily. The resulting R-factors ranged from 0.37-0.45.

High R-factors could arise if the structure of the actin monomer complexed with DNase I is different from the structure in F-actin. Inspection of the 0.6nm structure (Fig.1) shows the actin molecule to consist of two domains connected by ·a narrow neck. The neck may also contain the nucleotide binding site. Therefore, we cut the electron density through the narrowest part of the neck and let the two domains refine separately. The five low resolution structures resulting from the three dimensional search were used as starting points for the refinement. Only one starting point, namely the best low resolution solution, refined in a satisfactory manner (i.e. the domains neither overlapped nor drifted apart and retained a plausible stereochemical relationship to each other) to give an acceptable R-factor and the correct radius of gyration.

The final structure is depicted in Fig.3. The orientation of the kidney-shaped actin molecule is approximately at right-angles to the helix axis, as was suggested by Egelmann & DeRosier, 1983). The large domain is at small radius with the long axis of the domain pointing along the steep two-start actin helix. This domain contacts neighbouring domains along the two-start helix as well as making contacts with other large domains across the helix axis. The small domain does not contact neighbouring small domains and lies at large radius. Compared with the position it would have if joined onto the large domain as in the actin-DNase-I complex, the small domain has moved round about 80° and translated through 2.5nm. The maximum diameter is 10.0nm. The N-terminus is probably in the small domain and therefore at large radius; the position of the C-terminus is also thought to be at large radius from energy transfer studies (Taylor et al. 1981) and therefore may also be in the small domain. A comparison with the electron micrograph reconstructions from negative stained actin monolayers (O'Brien et al. 1983) shows that the two structures are very alike
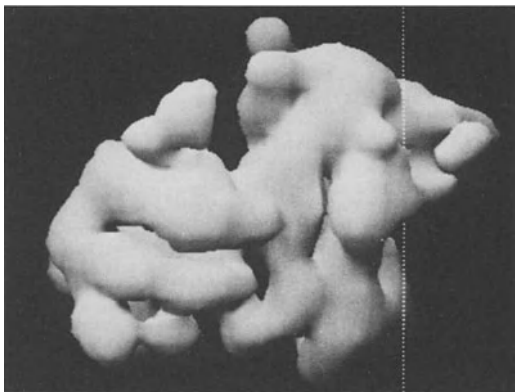
Fig. 1   The 0.6nm resolution structure of g-actin  (Kabsch et al 1983). The dotted line shows the helix axis in the structure shown in Fig. 2. Note the small domain (left) and large domain (right).
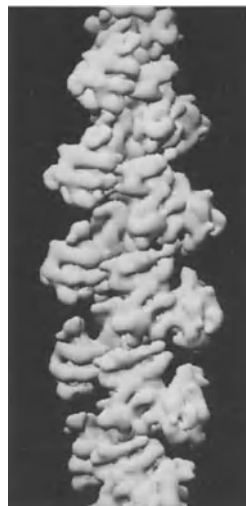


Fig. 2   The best refined structure for f-actin using the form shown in Fig. 1.



Fig. 3   A much better structure can be obtained by letting the large (dark) and small (light) domains refine separately. The actin monomer becomes bent.
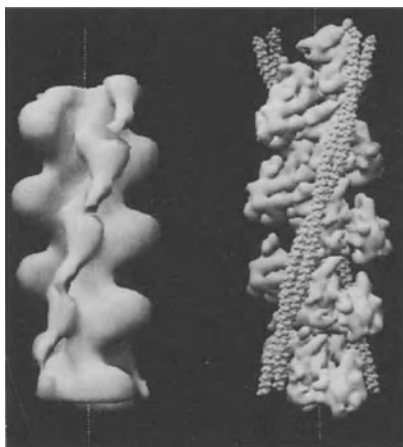


Fig. 4   A comparison with the e.m. reconstruction of O´Brien et al (1983) - left. Tropomyosin has been added to the computed structure (right).

(Fig. 4). It also appears similar to the reconstruction of Trinick et al. (1986) and resembles the structure proposed by Aebi et al (1986). In Fig. 4 tropomyosin has been added. The reconstruction of decorated actin (Amos et al., 1982) shows that the S1 probably binds to the thin filament at two sites. The present study suggests that the rigor S1 makes contact with both sides of the small domain on both sides of the thin filament and in the process bridges the tropomyosin. Chemical evidence (Sutoh, 1982) suggests that myosin S1 binds to a site near the actin N-terminus, whereas the light chain binds to the C-terminus, which, as suggested above, may also be in the small domain.

REFERENCES

Aebi, U., Millonig, R., Salvo, H., & Engel, A. (1986) The three-dimensional structure of the actin filament revisited . Annal. New York Acad. Sci **483**, 100-119.

Amos, L.A. Huxley, H.E., Holmes, K.C., Goody,R.S., & Taylor, K.A. (1982) Structural evidence that myosin heads may interact with two sites on F-actin. Nature (Lond.) **5882**, 467-469.

Egelman, E.H. & DeRosier, D.J. (1983). Structural studies of F-actin. in *Actin: Its structure and function on muscle and non-muscle cells* (ed. dos Remedios & Barden) pp 17-24. Academic Press London.

Holmes,K.C., Popp,D., Gebhard,W., Kabsch,W., Jahn, W., & Bryan,R. (1989) The structure of f-actin as revealed by analysis of the x-ray fibre diffraction pattern. (in preparation)

Kabsch,W., Mannherz,H.G. & Suck,D. (1985) Three dimensional structure of the complex of actin and DNase I at 4.5 A resolution. EMBO Journal **4**, 2113-2118.

Milligan, R.A. & Flicker, P.F. (1987) Structural relationships of actin, myosin, and tropomyosin revealed by cryo-electron microscopy. J. Cell Biology **105**,29-39

O'Brien,E.J., Couch, J., Johnson, G.R.P., & Morris, E.P. (1983) Structure of actin and the thin filament. in *Actin: Its structure and function on muscle and non-muscle cells* (ed. dos Remedios & Barden) pp 3-16. Academic Press , London.

Popp, D., Lednev,V.V., & Jahn, W. (1987) Methods of preparing well-orientated sols of f-actin containing filaments suitable for x-ray diffraction. J. molec. Biol. **197**, 679-684

Sutoh, K. (1982) Identification of myosin binding sites on the actin sequence. Biochemistry **21**, 3654-3661

Taylor,D.L., Reidler,J., Spudich,J.A., & Stryer, L. (1981) Detection of actin assembly by fluorescence energy transfer. J. Cell Biology **89**, 362-367.

Trinick,J., Cooper,J., Seymour,J., & Egelman, E.H. (1986) Cryo-electron microscopy and three-dimensional reconstruction of actin filaments. J. of Microscopy **141**, 349-360.

# The "Lateral Slipping" Model of F-Actin Filaments

R. Millonig[1,2], R. Sütterlin[1], A. Engel[1], T.D. Pollard[2], and U. Aebi[1,2]

[1] Maurice E. Müller-Institute for High Resolution Electron Microscopy,
   Biocenter, University of Basel, CH-4056 Basel, Switzerland
[2] Department of Cell Biology and Anatomy, The Johns Hopkins University School of Medicine
   Baltimore, MD 21205, USA

Actin, one of the most abundant proteins in nature, has been shown to exist as long helical filaments in its functional form. These filaments consist of two linear strands of actin subunits which are helically twisted around each other in a right-handed sense, cross each other every 36 nm, have an axial repeat of 5.5 nm, and are axially staggered by 2.75 nm relative to each other [Hanson and Lowy, 1963; Huxley, 1963]. An alternative description of the same structure is as a one-start "genetic" helix connecting neighbouring subunits on opposite strands with 13 subunits making 6 left-handed turns with a pitch of 5.9 nm. Although the 3-D structure of the actin filament has been investigated for almost 20 years no consensus in the field has yet been reached in terms of its molecular structure [Aebi et al., 1986; Amos, 1985; Holmes et al., this volume]. To avoid interdigitation and superposition artifacts common with F-actin paracrystals [Aebi et al., 1986; Egelman, 1985; Smith et al., 1984], we have utilized negatively stained disperse filaments and have found a significant number of reasonably straight and well preserved filament stretches suitable for processing and reconstruction (Fig. 1a) when a new preparation and staining method [Aebi et al., 1986] was employed.
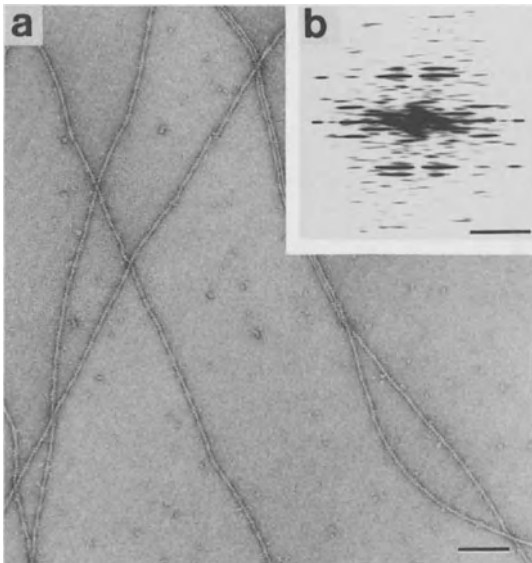


Fig. 1: (a) Synthetic F-actin filaments polymerized with 2 mM $MgCl_2$ & 50 mM KCl, and negatively stained with 0.75% uranyl formate, pH 4.25. The micrograph was recorded under minimal dose conditions at a nominal magnification of 50,000x. (b) Computed diffraction pattern of a 10-helical-repeat long filament stretch after digital straightening. Scale bars, 100 nm (a) and $(5 \text{ nm})^{-1}$ (b).

Computed diffraction patterns (Fig. 1b) of such filament stretches, typically 5 to 10 helical repeats long, reveal strong 1st and 6th layerlines with weaker 2nd and 7th layerlines. Information typically extends to at least the 13th layerline axially (i.e. $(2.75 \text{ nm})^{-1}$) and to about $(2.5 \text{ nm})^{-1}$ radially.

We have found that the following image processing steps are crucial to obtain satisfactory and reproducible reconstructions: (1) Filament stretches chosen for reconstruction have to be digitally *straightened.* (2) The *optimal* helical repeat is determined by minimizing the power loss on linear averaging over this repeat. (3) The *best* helix axis is searched for by minimizing the power loss on helical filtering [Smith et al., 1983] the linearly averaged optimal helical repeat according to the integer selection rule $l = -6n + 13m$. Reproducibly, thus processed and computed 3-D reconstructions (Fig. 2a) exhibit strong connectivity *along* the two long-pitch helical strands and somewhat less connectivity *between* the two strands (i.e. along the genetic helix). The strength of the long-pitch helix contact relative to that along the genetic helix becomes even more apparent when individual sections perpendicular to the helix axis are inspected. As depicted in Fig. 2b, the *interstrand* contact along the genetic helix appears rather tenuous, often absent in several sections, compared to the strong high-density *intrastrand* contact along the two long-pitch helices. The greater physical strength of the intrastrand contact relative to the interstrand contact is further supported by our observation of partially unravelled or splayed filaments [Aebi et al., 1986].

Based on sections such as those presented in Fig. 2b, we have been able to unambiguously and reproducibly "cut-out" monomers from our filament reconstructions (Fig. 2c). Accordingly, the actin molecule exhibits overall dimensions of 5.5 nm x ~6.5 nm x ~3.0 nm and is roughly bilobed, with a massive base and a slender tip in the direction of the helix axis. As this monomer is distinctly polar, it has been possible to orient the actin subunit within the filament relative to the "barbed" and "pointed" filament ends as defined by myosin S1 decoration. To this end, we have found that the massive base of the subunit points toward the barbed end of the filament and the slender tip toward the pointed end (data not shown).

After reconstructing in excess of 50 filaments the only two significant differences we have noted among reconstructions are (i) the degree of "lateral slipping" of the two long-pitch helical strands relative to each other, and (ii) the strength (i.e. in terms of mass density) and spatial extent of the interstrand contact. These differences can most clearly be depicted in helical projections such as shown in Figs. 2d&e. This lateral slipping might explain the variable crossover distances [Egelman et al., 1982], as well as the intrinsic variability in the width of the actin filament [Aebi et al., 1986; Smith et al., 1984; Fowler and Aebi, 1983].

Recently, we have begun processing and reconstructing filaments stabilized with the highly poisonous alkaloid phalloidin [see Cooper, 1987]. The resulting 3-D reconstructions reproducibly exhibit less pronounced lateral slipping and stronger interstrand contacts (Fig. 2f). This suggests that phalloidin might "stiffen" the actin filament by strengthening the genetic-helix contact thereby preventing lateral slipping of the two long-pitch helical strands past each other and, as a consequence, significantly altering the actin-myosin interaction during muscle contraction.
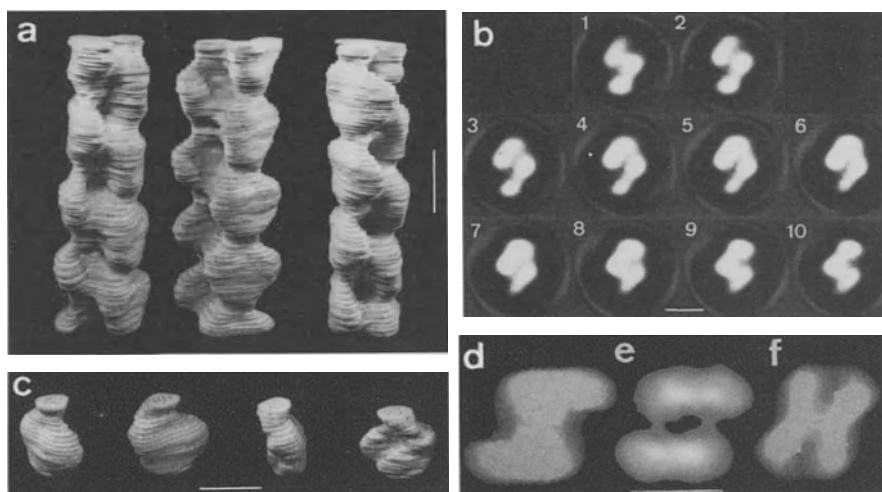
**Fig. 2:** (a) Three different views of a Balsa wood model of an actin filament 3-D reconstruction contoured at a level to include 100% mass. (b) Ten equidistant sections of an actin filament 3-D reconstruction perpendicular to the filament axis and extending over half a subunit (2.75 nm) in the direction of the filament axis. (c) Balsa wood model of an actin subunit "cut-out" from the filament 3-D reconstruction shown in (a). (d) Helical projection of an actin filament 3-D reconstruction exhibiting a large amount of lateral slipping. (e) Dito but from an actin filament 3-D reconstruction exhibiting a relatively small amount of lateral slipping. (f) Dito but from a phalloidin-stabilized actin filament 3-D reconstruction. (d) to (f) have the same angular orientation. Scale bars, 5 nm (a-f).

# References:

Aebi, U., R. Millonig, H. Salvo, and A. Engel (1986). The Tree-Dimensional Structure of the Actin Filament Revisited. *Annals N.Y. Acad. Sci.* **483**: 100-119.

Amos, L.A. (1985). The Structure of Muscle Filaments Studied by Electron Microscopy. *Annu. Rev. Biophys.* **14**: 291-313.

Cooper, J.A. (1987). Effect of Cytochalasin and Phalloidin on Actin Filaments. *J. Cell Biol.* **105**: 1473-1478.

Egelman, E.H. (1985). The Structure of F-Actin. *J. Muscle Res. Cell Motility.* **6**: 129-151.

Egelman, E.H., N. Francis, and D. DeRosier. (1982). F-actin is a Helix with a Random Variable Twist. *Nature* **298**: 131-135.

Fowler, W.E., and U. Aebi (1983). A Consistent Picture of the Actin Filament Related to the Orientation of the Actin Molecule. *J. Cell Biol.* **97**: 264-269.

Hanson, J., and J. Lowy (1963). The Structure of F-actin and of Actin Filaments Isolated from Muscle. *J. Mol. Biol.* **6**: 46-60.

Huxley, H.E. (1963). Electron Microscope Studies on the Structure of Natural and Synthetic Protein Filaments from Striated Muscle. *J. Mol. Biol.* **7**: 281-308.

Smith, P.R., W.E. Fowler, T.D. Pollard, and U. Aebi (1974). Structure of the Actin Molecule Determined from Electron Micrographs of Crystalline Actin Sheets with a Tentative Alignment of the Molecule in the Actin Filament. *J. Mol. Biol.* **167**: 641-660.

Smith, P.R., W.E. Fowler, and U. Aebi (1984). Toward an Alignment of the Actin Molecule in the Actin Filament. *Ultramicroscopy* **13**: 113-124.

# A New Model for Actin – A Rigid Helical Backbone with Flexible Outer Domains

Harold P. Erickson
Department of Cell Biology
Duke University Medical Center
Durham, NC 27710 USA

The polymer F-actin is quite strong with respect to breaking: spontaneous fragmentation is so unfavorable that it is rarely observed except under conditions of shear or sonication. In striking contrast, single subunits appear to be held relatively weakly at the end of the filament, and dissociate readily under most solution conditions.

The subunits of f-actin are connected by two types of bonds: longitudinal bonds connect the subunits within each long pitch helix, and diagonal bonds connect subunits across these helices. These are diagrammed at the left in a flattened, untwisted projection.

**End Association:**

One diagonal bond

One longitudinal bond

Dissociation of a subunit from the end of the filament requires breaking one longitudinal and one diagonal bond. Fragmentation requires breaking these same two bonds plus one additional longitudinal bond. *Can the difference between fragmentation and end dissociation be explained by the one extra longitudinal bond?* A qualitative argument would suggest that this is only possible if the longitudinal bond is relatively strong. I have recently developed this argument quantitatively, deriving an estimate for the intrinsic bond constants for the end association reaction and for fragmentation/ annealing (Erickson, 1989). The longitudinal bond is estimated to be *three times stronger than the diagonal.*

**Fragmentation/anneal.**

One diagonal bond

*Two* longitudinal bonds

The strong longitudinal bond is an important contradiction to some recent structural models for f-actin, which have shown the longitudinal contact to be weak or absent relative to the diagonal (Egelman, 1984; Milligan and Flicker, 1987). It should be noted, however, that the images and model of Aebi et al. (1986) show a prominent longitudinal interface, consistent with the stronger longitudinal bond that is necessary to prevent fragmentation. The question of the existence and strength of the longitudinal bond is particularly important for consideration of the flexibility of the actin filament.

## TORSIONAL FLEXIBILITY OF ACTIN

Egelman et al. (1982) analyzed the torsional flexibility of free actin filaments, as indicated by variations in crossover distances, and by diffraction patterns from electron micrographs. They postulated a very large twist, on the order of $10°$ between each subunit pair, varying randomly from + to - in a random walk fashion. In an entirely different approach, Yoshimura et al. (1984) attached an eosin label attached to cys-373 and measured

flexibility by fluorescence anisotropy decay. They found a very large rotational motion of their label, comparable to the 10° rotation per subunit postulated by Egelman et al. Although the motion of cys-373 could be attributed to the torsional flexibiility proposed by Egelman et al., it is just as well explained by the new model proposed below.

The proposal of Egelman et al., for ± 10° angular shifts at each subunit, suffers primarily from lack of a convincing model based on known principles of protein structure. In the absence of longitudinal bonds, one might have imagined a system of hinges within the subunits that would have supported the flexibility. However, the non-covalent protein-protein bonds must be relatively rigid, permitting movements across these interfaces no more than 1 Å (Erickson, 1989), so the prominent longitudinal bonds proposed here severely limit the possible flexibility.

One might propose that the torsional flexibility is achieved by hinges within the subunit, but I have been unable to construct a reasonable model. The triangular arrangement of longitudinal and diagonal bonds imposes rigidity even if the subunits themselves have hinges: each hinge within a subunit is bridged by (rigid) diagonal and longitudinal bonds on the opposite strand. One might try models with multiple hinges, but there is no evidence for more than two domains.

Finally, one will always have to confront what I believe is the most serious contradiction to the proposal of Egelman et al.: to accommodate the hypothetical large angular flexibility with the well established rigidity to bending. Several measures, reviewed by Oosawa (1980), demonstrate a persistence length to bending of 6 μm, corresponding to a bend of about 0.02° per subunit. This is 500 times less than the 10° per subunit proposed for angular flexibility. I doubt that any mechanical model can produce a filament with this rigidity to bending, and accommodate a torsional flexibility 500 times greater.

## A NEW MODEL FOR THE ACTIN FILAMENT

A resolution to the problem of how to accommodate the observed motion of cys-373 and the other indications for angular disorder, with the arguments and evidence for rigidity, is suggested by the new model for f-actin structure diagrammed below. The actin subunit is known from low resolution x-ray crystallography to comprise two domains (Kabsch et al., 1985). One domain, probably the large one, is at the center of the actin filament in most models (Egelman, 1984; Aebi et al., 1986; Milligan and Flicker, 1987). In the model shown below, this large domain is postulated to be attached to adjacent central domains by diagonal and longitudinal bonds, forming a *rigid helical backbone*. This backbone is rigid because (a) non-covalent protein-protein bonds cannot support bending or sliding flexibility (argued above), and (b) the domain itself is assumed to be a typical, rigid, globular domain (no clefts or hinges are visible in any of the EM or x-ray models). The second feature of the model is that the small domain is shown projecting outward from this helical core. Most important, this outer domain is postulated to be attached to the inner one by a *flexible hinge*. This hinge will be one or more strands of polypeptide chain that pass between the two domains and link them. There are many precedents for such flexible hinges between domains of a protein molecule, supporting angular motions on the order of 10-20° or more. Motions of the outer domain could be both torsional and axial. This model therefore pictures a *rigid helical backbone*, composed of the large domains of the actin connected by (rigid) non-covalent bonds, and a *flexible outer shell*,

composed of the small domains attached to the helical core by flexible hinges of polypeptide chain.

The flexible shell of outer domains can explain most observations previously attributed to torsional flexibility of the entire subunit. First, variation in crossover distance, and more generally many of the "random" features of diffraction patterns, can be attributed to large random movements of the outer domains, perhaps superimposed on a small twist (~1° per subunit) of the helical core. Second, the motion of the residue cys-373 (Yoshimura et al., 1984) is predicted by the flexible shell model. This residue is on the outside of the actin filament, in contact with myosin and almost certainly in the flexible outer domain. One particular observation in that study strongly favors the two domain model: phalloidin, in spite of its effect in stabilizing the actin filament (which should be acting on the inner, core domains in this new model) had no effect on the motion of cys-373 (postulated here to be on the flexible outer domain). Finally, The new model makes one prediction that is quite different from that of Egelman and DeRosier. In the model of Egelman et al. the cumulative twist could, in response to a torsional stress, be as much as 10° per subunit. When actin filaments pack into paracrystalline arrays they could be subject to substantial twist to accommodate favorable packing into the lattice. Several paracrystalline arrays, which could apply various twists, have actually been analyzed (Gillis and O'Brien, 1975; DeRosier et al., 1980), and they all have twists that vary only ± 0.5°, exactly what is predicted for a rigid helical backbone. Thus if actin does have the possibility of 10° torsional motions, neither nature nor biochemistry have yet taken advantage of it to pack actin into bundles.

**Rigid helical core, flexible outer shell**

A flexibly attached outer domain should have an obvious role in the function of actin. The function of the outer domain is presumably to bind the myosin head. Since myosin heads in muscle are directed at the actin subunits from a range of angles, and apparently move through a substantial angle during the power stroke, it makes sense, indeed it is almost essential, for the myosin-binding domain of actin to be flexibly attached to the filament core. *(Supported by NIH grant GM28553).*

**REFERENCES**

Aebi, U., Millonig, R., Salvo, H. & Engel, A. (1986) *Ann. N.Y. Acad. Sci.* **483,** 100-119.
DeRosier, D., Tilney, L. & Flicker, P. (1980) *J. Mol. Biol.* **137,** 375-389.
Egelman, E. H. (1984) *J. Mus. Res. Cell Mot.* **6,** 129-151.
Egelman, E. H., Francis, N. & DeRosier, D. J. (1982) *Nature* **298,** 131-135.
Erickson, H. P. (1989) *J. Mol. Biol. (in Press)*
Gillis, J. M., and O'Brien, E. J., (1975). *J. Mol. Biol.* **99,** 445-459.
Kabsch, W., Mannherz, H. G., & Suck D. (1985) *Embo J.* **4,** 2113-2118.
Milligan, R .A. & Flicker, P. F. (1987) *J.Cell Biol.* **105,** 29-39.
Oosawa, F. (1980) *Biophys. Chem.* **11,** 443-446.
Stokes, D. L., and DeRosier, D. J. (1987) *J. Cell Biol.* **104:** 1005-1017.
Yoshimura, H., Nishio, T., Mihashi, K., Kinosita, K. Jr. Ikegami, A. (1984)
    *J. Mol. Biol.* **179,** 453-467.

# Biochemical and Structural Analysis of the Interaction of α-Actinin with Actin Filaments and Lipids

Rudolf K. Meyer and Ueli Aebi
Maurice E. Müller-Institut für hochauflösende Elektronenmikroskopie am Biozentrum der Universität Basel
Klingelbergstrasse 70, CH-4054 Basel, Switzerland

α-Actinin is a dumb-bell shaped homodimer of 200,000 Da molecular mass. It has an actin binding site at each end and is able to crosslink actin filaments. A specific interaction with free fatty acids and glycerides has been demonstrated (Meyer et al., 1982). Different isoforms of this protein are found in striated muscle (Z-lines), in smooth muscle, and in nonmuscle cells (stressfibers, adhesion plaques). The intracellular localization of α-actinin in nonmuscle cells suggests a direct involvement in cell locomotion. Furthermore, in these cells its distribution is drastically changed after cell transformation.

In this study we have investigated at the biochemical and structural level the specific interaction of α-actinin with actin, as well as the influence of lipids on this interaction. To achive this a centrifugation assay was developed allowing for the separation of α-actinin-F-actin aggregates from unbound protein. Varying amounts of actin and α-actinin where incubated in actin polymerization buffer (5 mM imidazole, 2 mM $MgCl_2$, 150 mM KCl, 0.2 mM ATP, pH 7.5) and centrifuged for 15 min at 20,000xg. The supernatant was carefully separated from the pellet, and the two were analyzed by SDS-PAGE. The relative amounts of actin and α-actinin in each lane were determined by scanning the Coomassie blue stained gels. In Fig. 1 the binding of α-actinin to actin is expressed as the molar ratio of sedimented (bound) α-actinin to actin vs. α-actinin remainig in the supernatant. The sigmoidal binding curve saturates near 0.07 (M/M), i.e. at a ratio of α-actinin dimer to actin of 1:14 (i.e. 7 actin molecules per α-actinin binding site). The apparent $K_d$ for this interaction is 0.426 μM (at 22 °C). Below saturation, the ratio of bound α-actinin to actin vs. free α-actinin follows an exponential law, indicating a highly cooperative interaction.
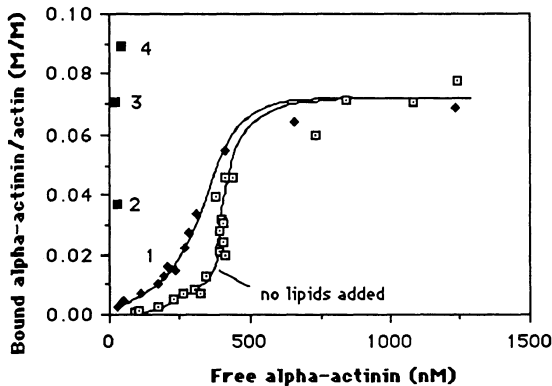


**Fig. 1:** Interaction of α-actinin with F-actin in the presence (filled symbols) or absence (open symbols) of lipids. Various concentrations of α-actinin (0.02-0.5 mg/ml) were incubated with actin (0.05-0.8 mg/ml) and polymerized by addition of 2 mM $MgCl_2$, 150 mM KCl, 0.2 mM ATP in the presence or absence of 1 mg/ml phosphatidylglycerol, 0.5 mg/ml diglycerides and 1 mg/ml palmitic acid. Specifically, at the points denoted the concentration of actin was 0.5 (1), 0.4 (2), 0.3 (3) and 0.2 (4) mg/ml and that of α-actinin was from 0.02 to 0.5 (1) or 0.1 (2-4) mg/ml.

Similar analyses were performed after addition of liposomes composed of free fatty acids, glycerides and phospholipids. In the absence of actin, a strong binding of α-actinin to lipid micelles

could be demonstrated (Fig. 2). Addition of lipids to actin-α-actinin mixtures resulted in a subsequent decrease of the apparent $K_d$, suggesting competitive binding of the lipids to α-actinin (Fig. 1).
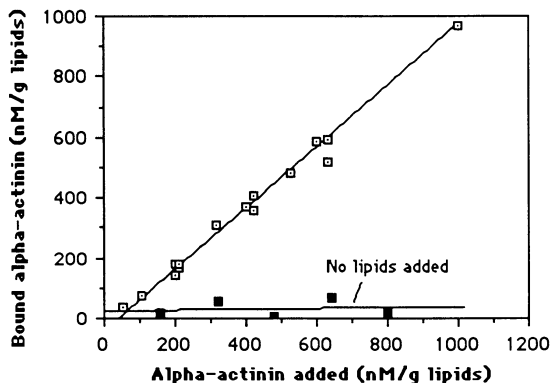


**Fig. 2:** α-Actinin binds to lipid micelles. Varying amounts of α-actinin (0.02-0.2 mg/ml) were added to 1 mg/ml phospholipids, 0.5 mg/ml diglycerides and 1 mg/ml palmitic acid, and incubated. Bound α-actinin was separated from unbound protein by centrifugation at 20,000xg for 15 min.

α-Actinin in the presence or absence of lipids was mixed with actin, incubated and examined by EM. Samples were adsorbed to glow-discharged carbon-coated parlodion films on copper grids and stained with 0.75% uranylformate without any previous washing or dilution. Bundles of actin filaments were observed for all buffer conditions which induced actin polymerization (Fig. 3a). Furthermore, contrary to previous reports (Burn et al. 1985), this bundle formation was independend of the presence or absence of lipids. However, with lipids added, α-actinin molecules with their ends bound to liposomes were observed and some vesicles were even crosslinked to actin filaments by α-actinin (Fig. 3b, arrow).

Bundle formation was highly sensitive to the α-actinin concentration. No bundles were found when the amount of α-actinin was kept below a critical concentration (i.e. below a molar ratio of α-actinin to actin of 1:125). Therefore dilution or washing of unfixed samples had to be avoided. However, α-actinin-F-actin filament bundles could be isolated after glutaraldehyde fixation or after crosslinking with dithiobis(succinimidylproprionate) (DSP). Since DSP was superior to glutaraldehyde with regard to the ultrastructural preservation it was primarly used in this study. For this purpose actin filaments where stabilized with phalloidin (1:2 M/M) prior to fixation. Optimal crosslinking conditions were explored by analysis on SDS-PAGE. A 100-fold molar excess of DSP over actin at pH 8.5 proved to be optimal for crosslinking.

The crosslinked samples were applied to a small Sephadex G-25 column. After washing with buffer, smaller aggregates, unbound protein and unreacted crosslinker passed through the column. Larger bundles which could not penetrate the column, were collected from the top. Examination in the EM revealed actin filament bundles crosslinked by α-actinin (Fig. 3c). The interfilament distance was decreased with increasing $Mg^{2+}$ concentration, probably by changing the orientation of the α-actinin molecules from "perpendicular" to "parallel" relative to the actin filaments (Fig. 3c, arrows).

According to these results α-actinin is a concentration-dependent inducer of F-actin bundling. The molecular structure of α-actinin-actin bundles has not yet been completely resolved but stochiometric and geometric arguments favor a model with parallel actin filaments saturated with likewise parallel arranged α-actinin molecules. The observed perpendicular orientation of α-actinin relative to the actin filaments my therefore be a specimen preperation artifact by which the α-actinin-actin bundles "open up". Certain specific lipids compete with actin for a binding site but do not influence bundle formation. The binding of α-actinin to F-actin and lipids my be significant *in vivo* for stressfiber formation.
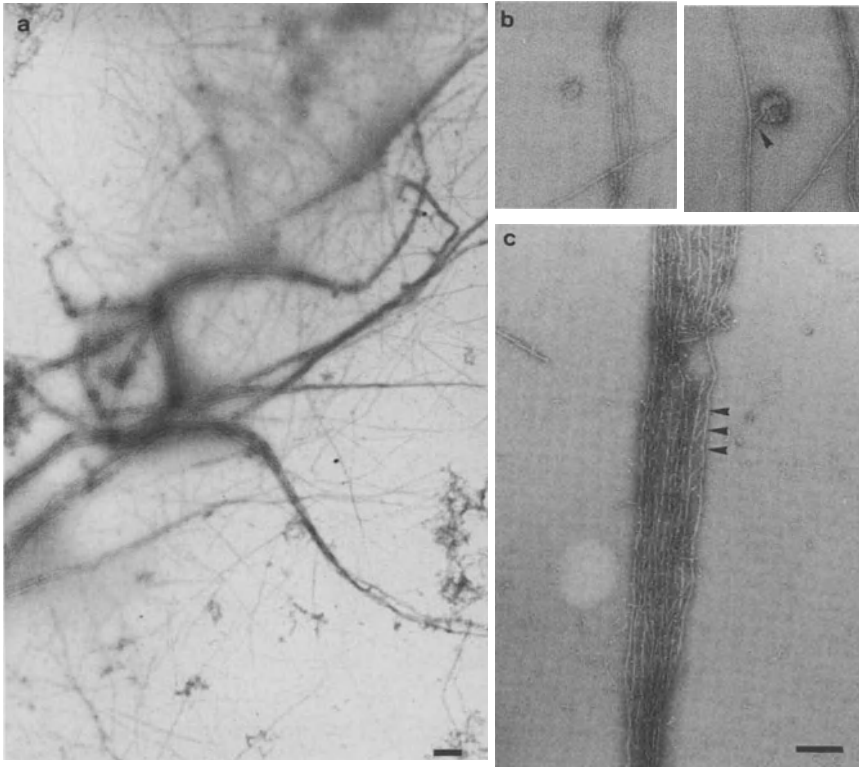
**Fig. 3**: Electron micrographs of α-actinin and actin. 3a) F-actin-α-actinin bundles adsorbed to carbon-coated parlodion films on copper grids without dilution or washing. 3b) α-actinin bound to lipid vesicles and occasionaly crosslinking them to actin filaments (arrow). 3c) F-actin-α-actinin bundles crosslinked with DSP and washed by "sieving" over a Sephadex column. Arrows denote α-actinin molecules. All samples were stained by 0.75% uranylformate. Bar, 0.5 μm (a), 100 nm (b,c).

Burn P, Rotman A, Meyer RK, Burger MM (1985) Diacylglycerol in large α-actinin/actin
    complexes and in the cytoskelton of ativated platelets. Nature 314: 469-472
Meyer RK, Schindler H, Burger MM (1982) α-Actinin interacts specifically with model
    membranes containing glycerides and fatty acids. Proc. Natl. Acad. Sc.79: 4280-428

# Functional Analysis of Actin Binding Proteins In Vitro and In Vivo

A.A. Noegel, K. Ziegelbauer, H. Hartmann, and M. Schleicher

Max-Planck-Institut für Biochemie, 8033 Martinsried, F.R.G.

A large number of actin-binding proteins has been isolated from different organisms. Similar interactions with G- or F-actin indicate that they represent classes of proteins with conserved functions during evolution. Data emerging from comparisons of protein- and DNA-sequences support this notion. We have started a search for novel actin-binding proteins in _Dictyostelium discoideum_ which may reveal new classes of generally important proteins.

From _D. discoideum_ several actin binding proteins have been isolated for which no counterparts in other organisms are known. Among these is a 17kDa protein that has been detected by a gel overlay assay using iodinated G-actin as probe (Schleicher _et al._ 1984, EMBO J. 3:2095-2100). Binding of the 17kDa protein to F-actin was determined by a cosedimentation assay. The protein cosedimented with the F-actin in a strongly pH-dependent manner within a critical range of pH 6.5-7.5. At pH 6.5 binding was essentially complete: no 17kDa protein was detected in the supernatant by electrophoresis and Coomassie blue staining. At pH 7.5 the protein was almost completely recovered in the supernatant whereas sedimentation of F-actin was unaffected. At pH 6.0 or 6.5 the 17kDa protein mediated the enhancement of actin polymerisation in the absence of $Mg^{2+}$ or $K^+$. The protein has been purified from both soluble and particulate fractions of the cells. As judged by the apparent molecular mass in SDS-polyacrylamide gel electrophoresis and 2D-electrophoresis, the 17kDa proteins from the soluble and particulate fraction are indistinguishable. Using monoclonal antibodies directed against the 17kDa protein, cDNA-clones were isolated from a cDNA library in λgt11 that contained the complete coding region. The cDNA sequence codes for a protein with a

molecular weight of 13700 which consists of 118 amino acids. The sequence does not reveal any signal peptide, transmembrane region or N-glycosylation site. The most characteristic feature of the protein is its high content of 31 histidine residues out of 118 amino acids. The 17kDa protein is encoded by a single gene and the corresponding mRNA as well as the protein are present throughout growth and all stages of development. When the cDNAs were expressed in E. coli in a vector that allowed synthesis of a fusion protein which contained four additional amino acids at the N-terminus, a protein was produced that had an apparent molecular weight comparable with the one of the protein isolated from D. discoideum.

The pH-sensitivity of the interaction of the 17kDa protein with actin might be of biological importance since the average cytoplasmic pH determined by $^{31}$P-NMR is between 6.7 - 7.3 and the transition from the binding to the non-binding state of the protein occurs between pH6.5 and 7.5. Changes of intracellular pH during the development of D. discoideum cells have not been unequivocally demonstrated. But short-term changes in response to cAMP stimuli have been reported. It is therefore possible that the 17kDa protein acts as an intracellular pH-sensor that links chemotactic signals to responses in the microfilament system of the cells. A dramatic increase of actin polymerization is observed in cells stimulated with chemoattractant. The 17kDa protein might be involved in this response by nucleating actin polymerization or stabilizing the filaments.

D. discoideum offers the possibility to investigate the in vivo role of the protein by inactivation of genes coding for specific proteins through production of antisense mRNA or gene disruption. Experiments are in progress to inactivate the gene coding for the 17kDa protein in D. discoideum and to investigate the consequences of the lack of this protein for the cell.

# Calcium- and Actin-Binding Sites in F-Actin Crosslinking Molecules from *Dictyostelium Discoideum*

Michael Schleicher and Angelika Noegel

Max-Planck-Inst. f. Biochemistry

8033 Martinsried, FRG

Numerous actin-binding proteins regulate the viscosity and elasticity of the cytoplasm by either interfering directly with the equilibrium of G- and F-actin, or by crosslinking the filaments (for reviews see Stossel et al., 1985; Pollard and Cooper, 1986). F-actin crosslinking proteins are usually dimers that form a three dimensional network via two binding sites for actin. The most prominent F-actin crosslinking activities in Dictyostelium discoideum are due to two proteins with apparent molecular weights of 95.000 ($\alpha$-actinin)(Condeelis and Vahey, 1982; Fechheimer et al., 1982) and 120.000 (gelation factor) (Condeelis et al., 1982). Cloning and sequencing of the genes coding for these cytoskeletal proteins revealed similarities to proteins from other species including mammals. These similarities may help to identify functional domains that are involved in the binding to actin and in the regulation by calcium ions.

## $\alpha$-ACTININ:

D. discoideum harbors a single $\alpha$-actinin gene that codes for a 3.0kb mRNA (Witke et al., 1986). The protein is a homodimer whose subunits assemble in an anti-parallel fashion to form a rod-like structure (Wallraff et al., 1986). The crosslinking activity of D. discoideum $\alpha$-actinin is completely inhibited by sub-micromolar concentrations of $Ca^{2+}$. This calcium sensitivity distinguishes muscle and non-muscle $\alpha$-actinins. The determination of the complete sequence of D. discoideum $\alpha$-actinin allowed the identification of three structural features: i) Two complete EF-hands that may be responsible for the $Ca^{2+}$-regulation; ii) internal repeats that render $\alpha$-actinin a spectrin-like molecule; iii) a striking similarity to chicken fibroblast $\alpha$-actinin near the N-terminus (Noegel et al., 1987).

The recently published complete sequences of chicken fibroblast $\alpha$-actinin (Baron et al., 1987) and dystrophin, the protein product of the Duchenne muscular dystrophy locus (Koenig et al., 1988) show in C-terminal regions significant similarities to the EF-hands of $\alpha$-actinin. A true EF-hand domain scores twelve or better out of sixteen functionally important amino acids (Kretsinger, 1980a).

Fig.1 shows a comparison of corresponding domains from _Trypanosoma_ calmodulin (Tschudi et al., 1985), D. discoideum α-actinin, chicken fibroblast α-actinin and dystrophin. Among the cytoskeletal proteins only D. discoideum α-actinin scores in both EF-hands the required number of matches (12x, 14x), whereas the putative $Ca^{2+}$-binding loops from chicken fibroblast α-actinin (11x, 13x) and dystrophin (8x, 11x) apparently degenerated during evolution.

```
      *   E L'    L'L'     L'D'  D'  D'G   I D'    E L'    L'L'    L'
                           X    Y   Z  -Y  -X   -Z


CAM: (16)  E F K E A F S L F D K D G D G T I T T K E L G T V M R S L
DDA: (12)  E F K A C F S H F D K D N D N K L N R L E F S S C L K S I
CHA: (11)  E F R A S F H N F D R K K T G M M D C E D F R A C L I S M
DYS:  (7)  A C D A L D Q H N L K Q N D Q P M D I L Q I I N C L T T I


CAM: (15)  E V D E M I R E A D V D G D G Q I N Y E E F V K M M M S K
DDA: (14)  Q L N Q V I S K I D T D G N G T I S F E E F I D Y M V S S
CHA: (13)  E F A R I M S I V D P N R M G V V T F Q A F I D F M S R E
DYS: (11)  C L N W L L N V Y D T G R T G R I R V L S F K T G I I S L
```
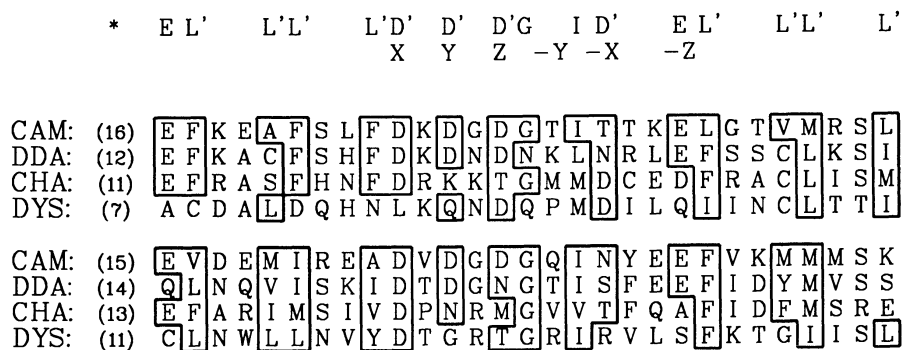
Figure 1: Alignment of EF-hand regions from _Trypanosoma_ calmodulin (CAM), D. discoideum α-actinin (DDA), chicken fibroblast α-actinin (CHA) and dystrophin (DYS). Boxed residues indicate a correct alignment with the 16 characteristic positions building an EF-hand structure (Kretsinger, 1980b).

GELATION FACTOR:

Another F-actin crosslinking molecule from D. discoideum has been described as a dimer with an apparent molecular weight of 120.000 per subunit upon SDS-PAGE (Condeelis et al., 1982). Unlike α-actinin, it is insensitive to $Ca^{2+}$. A complete cDNA clone coding for the gelation factor was isolated from a λgt11-library and its sequence determined (Noegel et al., in preparation). Fig. 2 summarizes some peculiarities of the primary structure. The protein consists of 858 amino acids; the calculated molecular weight is 92.300, which is considerably smaller than the app. molecular weight of 120.000 as jugded by SDS-PAGE. The distribution of certain amino acids is strongly asymmetrical. Especially glycine and proline residues are abundant in the C-terminal 2/3 of the molecule. Accordingly, almost no α-helical structure is predicted. The C-terminal part contains six repeats with about 100 amino acids each. The consensus sequence of the repeating domains is based mainly on common glycine and proline residues.

# DICTYOSTELIUM GELATION FACTOR

AMINO ACIDS:

```
1      100     200     300     400     500     600     700     800  858
```

PROLINE RESIDUES:

GLYCINE RESIDUES:

TRP–( | ), CYS–(*)RESIDUES:

CONSERVED REGION                    REPEATS

**Figure 2:** Organization of the _D. discoideum_ gelation factor. The positions of specific amino acids are indicated by vertical bars or by stars.

The N-terminal third of the molecule is very similar to the putative actin-binding sites of _D. discoideum_ α-actinin, chicken fibroblast α-actinin and dystrophin. To prove that this conserved domain in fact contains an actin-binding activity, the corresponding region of _D. discoideum_ α-actinin was expressed in _E. coli_ and the fusion protein was shown to be able to bind to actin filaments in co-sedimentation assays.

REFERENCES

Baron MD et al. (1987) J Biol Chem 262:17623-17629
Condeelis J et al. (1982) Cell Motil. 2:273-285
Condeelis J, Vahey M (1982) J Cell Biol. 94:466-471
Fechheimer M et al. (1982) Cell Motil. 2:287-308
Koenig M et al. (1988) Cell 53:219-228
Kretsinger RH (1980a) Ann NY Acad Sci 356:14-19
Kretsinger RH (1980b) CRC Crit Rev Biochem 8:119-174
Noegel A et al. (1987) FEBS Letters 221:391-396
Pollard TD, Cooper JA (1986) Ann Rev Biochem 55:987-1035
Stossel TP et al. (1985) Ann Rev Cell Biol 1:353-402
Tschudi C et al. (1985) Proc Natl Acad Sci USA 82:3998-4002
Wallraff E et al. (1986) EMBO J 5:61-67
Witke W et al. (1986) J Cell Biol 103:969-975

# Comparison of Various Gelsolin-Like Proteins and Their Interaction with Actin Filaments

Anke Huckriede, Horst Hinssen and Brigitte M. Jockusch
Developmental Biology Unit, University of Bielefeld
POB 8640, D-4800 Bielefeld 1, FRG

Gelsolins are Ca-dependent actin-binding proteins which modulate the polymer state of actin in vitro by nucleation of polymerization, capping, and severing of actin filaments. Though gelsolins have been isolated from a number of cell types and from blood plasma, the physiological role of these proteins remains unclear.

We have investigated the interaction of various gelsolins with actin in vitro, on detergent-extracted cell models, and by microinjection into living cells. The gelsolins used here were purified from pig stomach smooth muscle, pig and human plasma and human platelets. Fig. 1 shows the effects of the various gelsolins on the viscosity of an F-actin solution. All four gelsolins induced a dramatic decline of viscosity in the presence of Ca indicating the disruption of the preformed filaments. However, the effects varied among the different proteins: The pig plasma protein exhibited a relatively low severing activity and only a limited Ca-dependence, whereas the severing activity of the three other proteins was significantly higher and strictly Ca-dependent. When applied to permeabilized cells, all four proteins degraded stress fibers and rendered the actin extractable. Again, pig plasma gelsolin was found to be partially active also in the presence of EGTA.
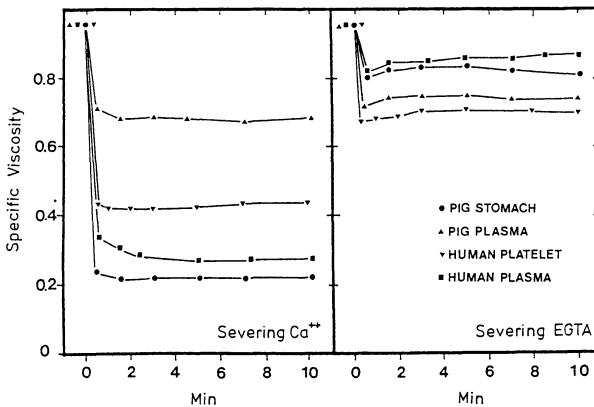


Fig. 1: Severing of F-actin by various gelsolins. To skeletal muscle F-actin (1 mg/ml) in 0.1 M KCl, 2 mM $MgCl_2$, 10 mM imidazole pH 7.4, 1 mM ATP), gelsolins were added at a molecular ratio of 1:100, and the viscosity was measured at various time intervals with an Ostwald viscometer.

When the proteins were microinjected into tissue culture cells, heterogeneous effects on the microfilament system were observed: The prominent stress fibers of rat fibroblasts visualized by rhodamine-phalloidin staining (Fig. 2A, control-injected cell) were destroyed by microinjected extracellular gelsolins (Fig. 2B), whereas the cytoplasmic gelsolins had practically no effect (see table Fig. 2). To determine whether these results were due to subtle differences in

Ca-requirement of the proteins in the cytoplasm, we microinjected purified proteolytic fragments representing the N-terminal half of the pig stomach, e.g. human plasma gelsolin molecule. Both fragments severed actin filaments in vitro in a completely $Ca^{++}$-insensitive manner. In contrast, they behaved differently after microinjection: While the fragment from human plasma gelsolin disrupted stress fibers effectively, the smooth muscle gelsolin fragment was again completely inactive (see table Fig. 2).
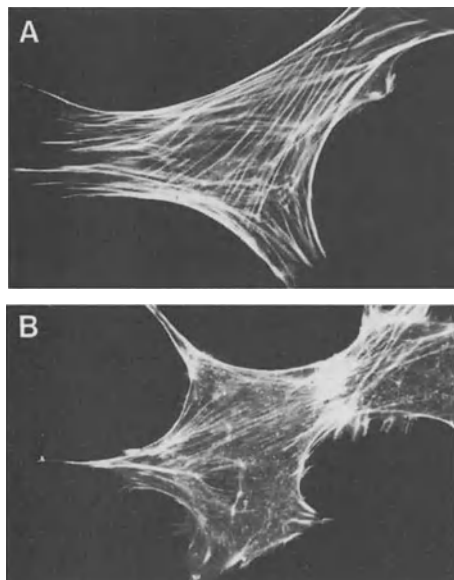


C

| GELSOLINS (CONC.) | CELLS WITH INTACT STRESS FIBERS IN PERCENT OF TOTAL | |
|---|---|---|
| | + CA | - CA |
| HUMAN PLASMA MG/ML) | 40 % | 70 % |
| PIG PLASMA (0.6 MG/ML) | 40 % | |
| HUMAN PLATELET (2 MG/ML) | 70 % | |
| PIG STOMACH (4 MG/ML) | 70 % | 70 % |
| HUMAN PLASMA THERMOLYSIN FRAGMENT TL 45 (0.5 MG/ML) | | 10 % |
| PIG STOMACH CHYMOTRYPSIN FRAGMENT CT 47 (1 MG/ML) | 70 % | 70 % |

Fig. 2: Influence of microinjected gelsolins on the actin skeleton of cultured cells. (A) Rat fibroblast injected with buffer alone (TBS containing 1 mM Ca/EGTA buffer pCa 5) after fixation and staining for F-actin with rhodamine-phalloidin. (B) Fibroblast injected with 1.0 mg/ml human plasma gelsolin. (C) Semi-quantitative evaluation of stress fiber disruption by microinjected gelsolins and gelsolin fragments in a buffer containing either 1 mM EGTA or $10^{-5}$ M $Ca^{++}$. For each number given, the presence or absence of stress fibers in at least one hundred cells was determined. More than 70% of control injected or non-injected cells possessed stress fibers. Gelsolins were regarded as inactive in vivo when the percentage of cells with stress fibers was equivalent to the controls.

Thus, our results show that gelsolin may affect actin filaments in the living cell, but that there is no clear-cut correlation with the activities in vitro and in cell models. We assume that in addition to a possible modulation by intracellular Ca, other mechanisms may regulate the properties of gelsolin in the cytoplasm.

**SECTION II**
**Components and Supramolecular Assemblies of the Extracellular Matrix**

# Basement Membrane (Type IV) Collagen – Its Molecular and Macromolecular Structure

Klaus Kühn

Max-Planck-Institut für Biochemie

Department of Connective Tissue Research

D-8033 Martinsried, FRG

Type IV collagen is the main collagenous constituent of basement membrane (Martin et al., 1988). Its non-fibrillar, network-like macromolecular organization forms the scaffold for the sheet-like basement membrane in which the other basement membrane constituents, such as the laminin-nidogen complex and the heparan sulfate proteoglycan are embedded. The amino acid sequence of the two constituent polypeptide chains, as well as the molecular and the macromolecular structure of type IV collagen have been extensively studied, so that this collagen type is one of the best known members of the collagen family. Its molecule is 400 nm long and bears a globular domain at the C-terminal end (Oberbäumer et al., 1982). It is a heterotrimer of two $\alpha 1$(IV) chains and one $\alpha 2$(IV) chain, 1669 and 1712 amino acid residues in length, respectively (Trüeb et al., 1982; Brazel et al., 1988). The primary structure of both chains, from man and mouse, was completely elucidated by a combination of protein and cDNA sequencing (Brazel et al., 1987; Babel and Glanville, 1984; Pihlajaniemi et al., 1985; Oberbäumer et al., 1985; Nath et al., 1986; Wood et al., 1988; Soininen et al., 1987; Brazel et al., 1988; Siebold et al., 1987; Killen et al., 1987; Hostikka et al., 1987; Schwarz et al., 1986a; Vogeli et al., 1986; Schwarz et al., 1986b; Kurkinen et al., 1987).

Electron microscopical observation of pepsin dissolved type IV collagen fragments led to the socalled network model, in which the molecules are covalently crosslinked via their like ends (Timpl et al., 1981). Four molecules are connected via the N-terminal end region, two molecules are held together by their globular C-terminal domain (Fig.1). Recent studies have shown that during formation of the macromolecular structure the central triple helical area is additionally involved in the lateral aggregation of the molecules (Yurchenco and Ruben, 1987).
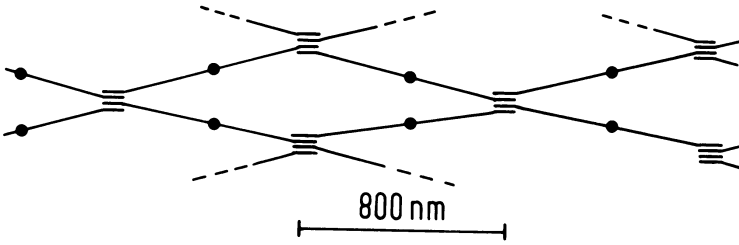
Fig. 1: Schematic representation of the network model. The type IV collagen molecules are covalently crosslinked via their like ends (Timpl et al. 1981).
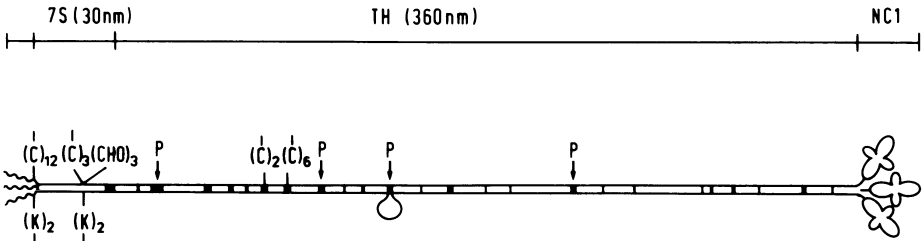


Fig.2: Schematic representation of the collagen IV molecule which consists of two α1(IV) chains and one α2(IV) chain. The 26 non-triple-helical interruptions of the triple helical domain are indicated by black bars. The cysteine (C) residues and lysine or hydroxylysine (K) residues involved in intra- or intermolecular bonds are shown. (CHO) designates a N-glycosidically bound oligosaccharide chain. The subscript numerals indicate the number of residues in a distinct region, summarizing all three α-chains. P designates a main pepsin cleavage site. In interruption XIII the α2(IV) chain forms a 21 residue long loop, stabilized by an interchain disulfide bond. 7S, aminoterminal aggregation and crosslink domain; TH, triple helical domain; NC1, carboxyl-terminal noncollagenous aggregation and crosslink domain (taken from Brazel et al. 1988).

According to these studies, the type IV collagen molecule contains three functionally important domains (Fig.2): the two terminal aggregation and crosslink regions - the N-terminal (7S) domain and the C-terminal (NC1) globular domain - and the central triple helical part. The latter comprises specific sites involved in interactions with other extracellular matrix components and with

**A**

Helical X-linking site

CHO
|
α1 |G I P G C N G T K G Q R|
α2 |G Y D G C N G T Q G D S|
|
CHO

N

α1  K G G C A G S G C - G K C D C H G V K G Q K
α2 K F D V P C G G R D C S G G C Q C Y P E K G G R

Non helical X-linking site

**B**

Overlap Zone

30 nm

S S S

K S      S K   K
  S
K  K S      S K +
  S S S

Fig.3: A. Schematic representation of the N-terminal aggregation and crosslink site. The terminal sequence of the α1(IV) and α2(IV) chains is nonhelical and contains cysteines (C) and lysines (K) which participate in intra- and intermolecular crosslinks. The triple helical overlap region also contains a crosslink site comprising a cysteine and a hydroxylysine (K+) residue.
B: Antiparallel, 80 amino acid residues overlapping arrangement of two type IV molecules with alignment of crosslink sites.

cells. In the following, the structural features of the three domains will be described, which are responsible for the formation of the macromolecular network.


The N-terminal aggregation and crosslink (7S) domain

The amino termini of the α1(IV) and the α2(IV) chains comprise the 15 and 21 residues long non-helical crosslinking sites (Siebold et al., 1987). They contain four cysteine residues at identical positions, presumably involved in intra- and intermolecular disulfide bonds (Fig.3a). Also a lysine residue additionally present in the α1(IV) chain takes part in intermolecular crosslink

dimeric antiparallel aggregation

tetrameric antiparallel aggregation

Fig.4: Scheme of the lateral arrangement of four N-terminal aggregation domains. Broad lines designate the hydrophobic self interacting reaction edge deduced from a interaction matrix. Section A and B at the boundaries of the interaction edge are involved in the contacts between the molecules orientated in an antiparallel fashion. N and C indicate the orientation of the molecules looking down the helix axis from the amino or carboxyl terminal, respectively. Taken from Siebold et al. 1987).

formation. The adjacent triple helical region of 118 residues is responsible for the overlap aggregation of the molecules. It also contains a crosslink region in which both chains comprise a cysteine and again the αl(IV) chain an additional hydroxylysine residue.

Three dimensional evaluation of the amino acid sequence of the triple helical overlap region revealed the highest hydrophobic interaction score for two molecules, arranged in an antiparallel fashion, with an overlap of 80 amino acids residues. This correlates with the electron microscopical data and allows an optimal formation of intermolecular disulfide bridges as well as of a lysine derived aldimine bond between the nonhelical and the helical crosslink sites of two overlapping molecules (Fig.3b) (Siebold et al., 1987).

The azimuthal orientation of the two molecules is determined by a hydrophobic self interacting reaction edge with a width of $90^{o}$ (Fig.4). The first contact between two antiparallel molecules aggregating to a dimer occurs mainly via segment A of the

interaction edge whereas segment B is responsible for the subsequent formation of a tetramer, in which the middle section of the reaction edge points to the interior of the tetragonal arrangement. Thus a potential, unlimited aggregation of antiparallel molecules is prevented Siebold et al., 1987).


## The C-terminal aggregation and crosslink (NC1) domain

The NC1 domains of the α1(IV) and the α2(IV) chains are 227 and 228 residues long, respectively (Siebold et al., 1988). In this C-terminal region the two α-chains are of high homology. Thus 65% of the residues are identical and 16% of the substitutions are conservatives. In the 7S domain and in the triple helical domain the two α-chains show only a low homology (Brazel et al., 1988). Both NC1 domains are divided into two similar repeating units, subdomain I and subdomain II, with 39% identical residues and 21% conservative substitutions (Oberbäumer, 1985). Thus, each subdomain contains an identical set of six cysteins. Isolation of disulfide bridged cyanogen bromide peptides of the unreduced α1(IV)NC1 domain led to the determination of the disulfide bonds in subdomain I (Fig.5). The two cysteins at position 20 from the
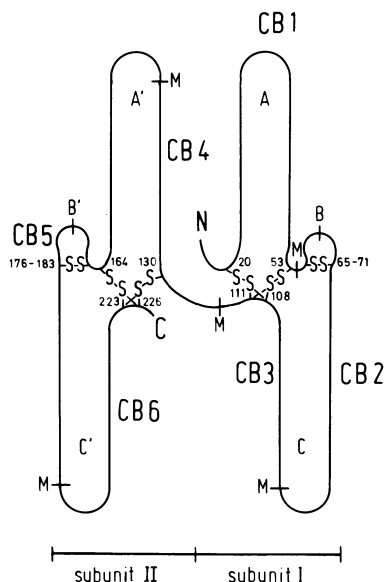


Fig.5: Schematic diagram of the intrachain disulfide bonds which force the α1(IV)NC1 domain into a four leafed clover-like structure. The position of the methionine residues and the numbering of the cyanogen bromide peptides are indicated. The NC1 domain is divided into two homologous subdomains, I and II. The loops A, B and C in subdomain I formed by disulfide bonds are 32,5 and 54 residues long, respectively. The same is true for subdomain II. M, methionine; S-S, disulfide bond; the numbers give the positions of the cysteines within α1(IV)NC1 (taken from Siebold et al. 1988).

N-terminal end, and position 53 from the middle region are connected to the cysteine pair 108 and 111 at the very C-terminal

end of subdomain I. Thus loop A and C with  32  and  54  residues, respectively, are formed. Loop C includes the small loop B of five residues, due to a disulfide bond between cysteine 65 and 71.  The high homology of subdomain I and II suggests the same  arrangement in subdomain II, which  is  supported  by  the  identification  of peptide CB4-5-6. The same arrangement of disulfide bonds has  been shown also for the α2(IV)NC1 domain (Siebold et al., 1988).

The aggregation  of  two  type  IV  collagen  molecules  by  their C-terminal domain leads  to  the  formation  of  a  hexameric  NC1 complex,  which  subsequently  becomes  stabilized  by  disulfide exchange either between two α1(IV)NC1 domains or by another still
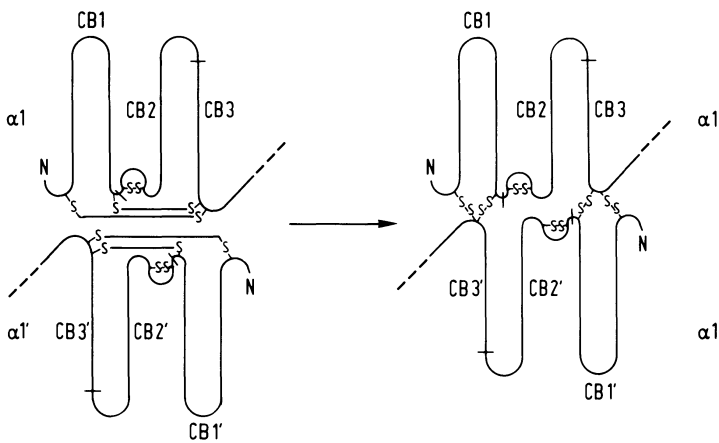


Fig.6: Scheme  of  the  disulfide  exchange  which  leads  to intermolecular bonds during dimerization of two type  IV  collagen molecules via their NC1  domains.  For  reasons  of  clarity  only subdomain I  is  depicted.  All  four  cysteine  residues  of  the disulfide knot are involved in the exchange reaction  (taken  from Siebold et al. 1988).

unknown unreducible covalent bond (Weber et al., 1984; Siebold  et al,  1988).  To  obtain  information  about  the  intermolecular disulfide bridges α1(IV)NC1  dimers  were  treated  with  cyanogen bromide  as  monomeric  α1(IV)NC1.  Surprisingly,  isolation  and characterization of the disulfide  bridged  peptides  resulted  in exactly the same peptides as obtained for the  monomer.  This  can only be the case if the  exchange  has  taken  place  between  two identical  disulfide  knots  either  from  subdomain  I  or  from

subdomain II and if all four cysteines of each knot have been involved in this exchange (Fig.6). The homology between α1(IV)NC1 and α2(IV)NC1 suggests an identical arrangement of disulfide bonds also for the dimeric α2(IV)NC1 domain (Siebold et al. 1988).

Chromatographic separation of the hexameric complex into monomers and dimers, the further separation of monomers in α1(IV)NC1 and α2(IV)NC1 as well as of dimers in $[α1(IV)NC1]_2$ and $[α2(IV)NC1]_2$ allowed a quantitative estimation of crosslinks. 50% of all monomeric NC1 domains were crosslinked to dimers. Trimeric NC1 domains or higher polymers were not observed. The assembly to the hexameric NC1 domain complex occurs in a highly ordered manner which favours the disulfide exchange mainly between two α1(IV)NC1 domains and to a lesser extent also the reaction between two α2(IV)NC1 domains. Thus only 13% of all dimers were α2(IV)NC1 dimers. Another 13% of the dimers (only α1(IV)NC1 dimers) were connected by unknown unreducible bonds. No evidence was obtained for covalent bonds between α1(IV)NC1 and α2(IV)NC1 monomers (Siebold et al 1988).

## The triple helical domain

According to electronmicroscopical investigations the triple helical domain of the type IV collagen molecule is much more flexible than the triple helix of the relatively rigid and stiff fiber forming collagens (Hofmann et al. 1984). This is due to the presence of nontriple helical areas. Thus the tripeptide structure of the α1(IV) chain is interrupted 21 times and of the α2(IV) chain 23 times. This includes the substitution of a glycine by an alanine residue in the Gly-X-Y tripeptide, as well as stretches of as many as 24 residues lacking the Gly-X-Y repeat. Both chains differ in length and to some extent also in the distribution of the non-tripeptide regions. The alignment of the two α-chains led thus to 26 regions in which the triple helical structure is disturbed or disrupted (Schwarz et al. 1986b; Brazel et al. 1988) (Fig.1). To get triple helical segments of maximal length – as well as matching – of the non-tripeptide region, insertions or deletions had to be introduced into the non-tripeptide interruptions of the one or the other chain. Some typical examples are given in Table 1. Interruptions III and X are main cleavage sites for proteolytic enzymes. They simultaneously introduce

flexible areas into the triple helix. Extremely resistant against proteolytic attack is the 13 residues long interruption I, which survives pepsin and trypsin treatment at $37^{\circ}$C. There is electronmicroscopical evidence for a secondary structure of the area which forces the molecule into a kink of $40^{\circ}$ (Hofmann et al 1984). In interruption IX both chains contain cysteine residues involved in intermolecular disulfide bonds, connecting all three α-chains with one another. A special case is interruption XIII where the α2(IV) chain forms a 21 residues long loop, stabilized by a intrachain disulfide bridge. There are some short triple helical imperfections (XIX, XXII) which may introduce kinks into the triple helix.

Table 1. Some nonhelical interruptions of the triple helical domain of the type IV collagen molecule. The nontripeptide sections in the α1(IV) and the α2(IV) chains are indicated by thin lines below and above the sequence, respectively. Numbers above the first **G** are position numbers along the two aligned α-chains (see Brazel et al. 1988).

```
         112
I    α1  G D P G E I L G H V P G M L L K G E R
     α2  G E P   Y A L P K E E R D R Y R G E P
         253
III  α1  G V P G Q A Q V Q E K G D F A T           K G E K
     α2  G I P S D T L H P I I A P T G V T F H P D Q Y K G E K
         551
X    α1  G E F Y       F D L R L K G D K
     α2  G D S R T I T T K G E R G Q P
         487
IX   α1  G E S C L I C D I D G Y R G P P
     α2  G E C R C T E G D E A I K G L P
         661
XIII α1  G K I V P     L P G P P
     α2  G Q I D C - C I G G P K
         D T D V K R A V G G D R Q E A I Q P G
         1034
XIX  α1  G Q P   G P K
     α2  G H I K G V K
         1234
XXII α1  G E V   G F P G L A
     α2  G E A N T L P G P V
```

The macromolecular structure

Comparison of the primary structure of the triple helical domain of the different type IV collagen α-chains, including drosophila type IV collagen (Cecchini et al. 1987; Blumberg et al. 1987),

revealed only a low homology of the amino acid residues in position X and Y of the tripeptide structure. The distribution of the main non-triple helical areas along the molecules appears to be conserved, although the amino acid sequence in the individual, matching interruptions is not homologous. This suggests that the specific distribution of flexible areas and, in some cases also kinks, is a structural feature of the molecule and is important for the formation of the macromolecular network of type IV collagen. In recent electronmicroscopical investigations of human
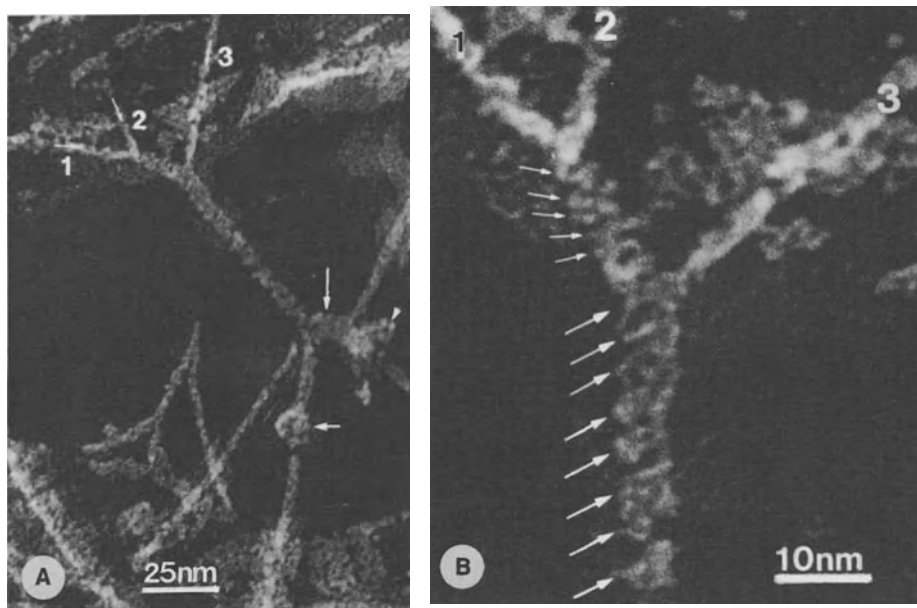


Fig.7: Macromolecular architecture of the type IV collagen network. Three triple helical molecules labelled 1-3 join to form a thicker laterally associated triple filament. A. In the double and triple filament the two and three molecules appear to be twisted around one another. B. Detail of the region where the three filaments join and twist helically (taken from Yurchenco and Ruben, 1987).

amniotic basement membrane by Yurchenco and Ruben (1987), the first detailed knowledge was obtained about the macromolecular structure of the genuine type IV collagen network (Fig.7). They observed that two or three individual triple helical domains join and twist around one another, forming double and triple filaments, and that such branching and twisted supramolecular filaments appeared to be present in many regions of the network. Although

the hexameric NC1 domain marks the position of the joint C-termini of two molecules within the network, the course of the molecule in the complex macromolecular structure is not yet known. It is, however, obvious that a molecule with a continuous, stiff triple helix is unsuitable to form such a network. Only the specific introduction of non-helical areas into the triple helical domain enables the type IV collagen molecules to bend in different regions, to twist to supermolecular helices and to form thus a stable but flexible three dimensional network.

## References

Babel W, Glanville, RW (1984) Structure of human basement membrane (type IV) collagen - complete amino acid sequence of a 914-residue-long pepsin fragment from the $\alpha1(IV)$ chain. Eur J Biochem 143: 545-556

Blumberg B, MacKrell AJ, Olson PF, Kurkinen M, Monson JM, Natzle JE, Fessler JH (1987) Basement membrane procollagen IV and its specialized carboxyl domain are conserved in drosophila, mouse and human. J Biol Chem 262: 5947-5950

Brazel D, Oberbäumer I, Dieringer H, Babel W, Glanville RW, Deutzmann R, Kühn K (1987) Completion of the amino acid sequence of the $\alpha1$ chain of human basement membrane collagen (type IV) reveals 21 non-triplet interruptions located within the collagenous domain. Eur J Biochem 168: 529-536.

Brazel D, Pollner R, Oberbäumer I, Kühn K (1988) Human basement membrane collagen (type IV). The amino acid sequence of the $\alpha2(IV)$ chain and its comparison with the $\alpha1(IV)$ chain reveals deletions in the $\alpha1(IV)$ chain. Eur J Biochem 172: 35-42

Cecchini JP, Knibiehler B, Mirre C, LeParco Y (1987) Evidence for a type IV related collagen in drosophila melanogaster - evolutionary constancy of the carboxyl-terminal noncollagenous domain. Eur J Biochem 165: 587-593

Hofmann H, Voss T, Kühn K, Engel J (1984) Localization of flexible sites in thread-like molecules from electronmicrographs - comparison of interstitial, basement membrane and intima collagens. J Mol Biol 172: 325-343

Hostikka SL, Kurkinen M, Tryggvason K (1987) Nucleotide sequence coding for the human type IV collagen $\alpha2$ chain cDNA reveals extensive homology with the NC1 domain of $\alpha1(IV)$ but not with the collagenous domain or 3'-untranslated region. FEBS Lett 216: 281-286

Killen PD, Francomano CA, Yamada Y, Modi WS, O'Brian SJ (1987) Partial structure of the human $\alpha2(IV)$ collagen chain and chromosomal localization of the gene (Col4a2). Hum Genet 77: 318-324

Kurkinen M, Condon MR, Blumberg B, Barlow DP, Quinones S, Saus J, Pihlajaniemi T (1987) Extensive homology between the carboxyl-ter-

minal peptides of mouse α1(IV) and α2(IV) collagen. J Biol Chem
262: 8496-8499

Martin GR, Timpl R, Kühn K (1988) Basement membrane proteins:
molecular structure and function. Adv Prot Chem 39: in press

Nath P, Laurent M, Horn E, Sobel ME, Zon G, Vogeli G (1986)
Isolation of an α1 type IV collagen cDNA clone using a synthetic
oligodeoxynucleotide. Gene 43: 301-304

Oberbäumer I, Wiedemann H, Timpl R, Kühn K (1982) Shape and
assembly of type IV procollagen obtained from cell culture. EMBO J
1: 905-910

Oberbäumer I, Laurent M, Schwarz U, Sakurai Y, Yamada Y, Vogeli G,
Voss T, Siebold B, Glanville RW, Kühn K (1985) Eur J Biochem 147:
217-224

Pihlajaniami T, Tryggvason K, Myers JC, Kurkinen M, Lebo R, Cheung
MC, Prockop DJ, Boyd CD (1985) cDNA clones coding for the
proα1(IV) chain of human type IV procollagen reveal an unusual
homology of amino acid sequences in two halves of the carboxyl--
terminal domain. J Biol Chem 260: 7681-7687

Siebold B, Deutzmann R, Kühn K (1988) The arrangement of intra-
and intermolecular disulfide bonds in the carboxyterminal,
non-collagenous aggregation and crosslinking domain of basement
membrane type IV collagen. Eur J Biochem, in press

Siebold B, Qian R-Q, Glanville RW, Hofmann H, Deutzmann R, Kühn K
(1987) Construction of a model for the aggregation and
crosslinking region (7S domain) of type IV collagen based upon an
evaluation of the primary structure of the α1 and α2 chains in
this region. Eur J Biochem 168: 569-575

Soininen R, Haka-Risku T, Prockop DJ, Tryggvason K (1987) Complete
primary structure of the α1-chain of human basement membrane (type
IV) collagen. FEBS Lett 225: 188-194

Schwarz U, Schuppan D, Oberbäumer I, Glanville RW, Deutzmann R,
Timpl R, Kühn K (1986a) Structure of mouse type IV collagen -
amino acid sequence of the C-terminal 511-residue-long triple
helical segment of the α2(IV) chain and its comparison with the
α1(IV) chain. Eur J Biochem 157: 49-56

Schwarz-Magdolen U, Oberbäumer I, Kühn K (1986) cDNA and protein
sequence of the NC1 domain of the α2-chain of collagen IV and its
comparison with α1(IV). FEBS Lett 208: 203-207

Timpl R, Wiedemann H, van Delden V, Furthmayr H, Kühn K (1981) A
network model for the organization of type IV collagen molecules
in basement membranes. Eur J Biochem 120: 203-211

Trüeb B, Groebli B, Spiess M, Odermatt BF, Winterhalter KH (1982)
Basement membrane (type IV) collagen is a heteropolymer. J Biol
Chem 257: 5239-5245

Vogeli G, Horn E, Carter J, Kaytes PS (1986) Proposed alignment of
helical interruptions in the two subunits of the basement membrane
(type IV) collagen. FEBS Lett 206: 29-32

Weber S, Engel J, Wiedemann H, Glanville RW, Timpl R (1984)
Subunit structure and assembly of the globular domain of basement

membrane collagen type IV. Eur J Biochem 139: 401-410

Wood L, Theriault N, Vogeli G (1988) cDNA clones completing the nucleotide and derived amino acid sequence of the α1 chain of basement membrane (type IV) collagen from mouse. FEBS Lett 227: 5-8

Yurchenco PD, Ruben GC (1987) Basement membrane structure in situ: evidence for lateral associations in the type IV collagen network. J Cell Biol 105: 2559-2568

# Effects of Mutations that Change Primary Structure of Collagen on the Self-Assembly of the Protein into Fibrils

Darwin J. Prockop[1], Bruce E. Vogel[1], Reinhard Doelz[2],
Jurgen Engel[2], Yoshio Hojima[1] and Karl E. Kadler[1]
[1] Department of Biochemistry and Molecular Biology, and
   Jefferson Institute of Molecular Medicine,
   Jefferson Medical College,
   Philadelphia, PA, USA
[2] The Biocenter of the University of Basel,
   Basel, Switzerland

We have recently observed that a single base mutation in a gene
for type I procollagen converts a glycine residue to cysteine and
that the substitution for the glycyl residue has a remarkable effect
both on the conformation of the molecule and the morphology of the
fibrils that are formed as the mutated procollagen molecule is
processed to collagen (Vogel et al., 1987; 1988; Kadler et al.,
1988b). The observations have largely been made possible through
the development of a new system for examining the self-assembly of
collagen de novo (Kadler et al., 1987; 1988a).

New System for Studying the Self-assembly of Collagen de novo.
      The assembly of collagen fibrils was extensively studied in the
past with collagen extracted from tendon or skin with cold acidic
solutions and then reconstituted into fibrils by neutralizing and
warming the solutions (Gross and Kirk, 1958; Wood, 1960; Cooper,
1970; Leibovich and Weiss, 1970; Comper and Veis, 1977; Williams et
al., 1978; Gelman et al., 1979; Silver et al., 1979; Helseth and
Veis, 1981; Farber et al., 1986; Holmes et al., 1986; Na et al.,
1986). However, the fibrils formed from the extracted collagen tend
to be narrow in diameter and lack the tightly structured appearance
of fibrils in situ (see Cooper, 1970; Miyahara et al., 1982). Also,
extracted collagen does not reproduce fibrils at temperatures above
35°C or without the presence of high concentrations of phosphate in
the buffer (see Cooper, 1970).
      We have recently developed a novel system for studying the
assembly of collagen fibrils de novo in which collagen is generated
enzymically under physiological conditions from an intermediate in
the normal processing of type I procollagen (Fig. 1) to collagen
(Miyahara et al., 1982, 1984; Kadler et al., 1987; 1988a). The
system has two major components. One is the partially processed
precursor of collagen that is known as pCcollagen and retains the

C-propeptides but not the N-propeptides of the procollagen molecule. The second component is highly purified procollagen C-proteinase that can cleave the C-propeptide (Hojima et al., 1985). The pC-collagen itself does not form any aggregates or regular structures in solution at 37°C and in concentrations of up to 0.5 mg/ml (Fig. 2). However, cleavage of pCcollagen to collagen by C-proteinase generates collagen that readily assembles into fibrils. The system has several advantages over previously employed systems involving reconstitution of collagen fibrils. Fibrils can be formed that vary in diameter from thin fibrils to thick fibrils as much as 3 microns in diameter. The process can be examined over temperatures ranging from 25 to 41°C. The system can employ a physiological buffer. Also, all the components of the system are homogeneous and in monomeric form.

We have employed the system to study the thermodynamic parameters of collagen self-assembly (Kadler et al., 1987; 1988a,b). The results demonstrate that polymerization of collagen under physiological conditions is an entropy-driven process with thermo-
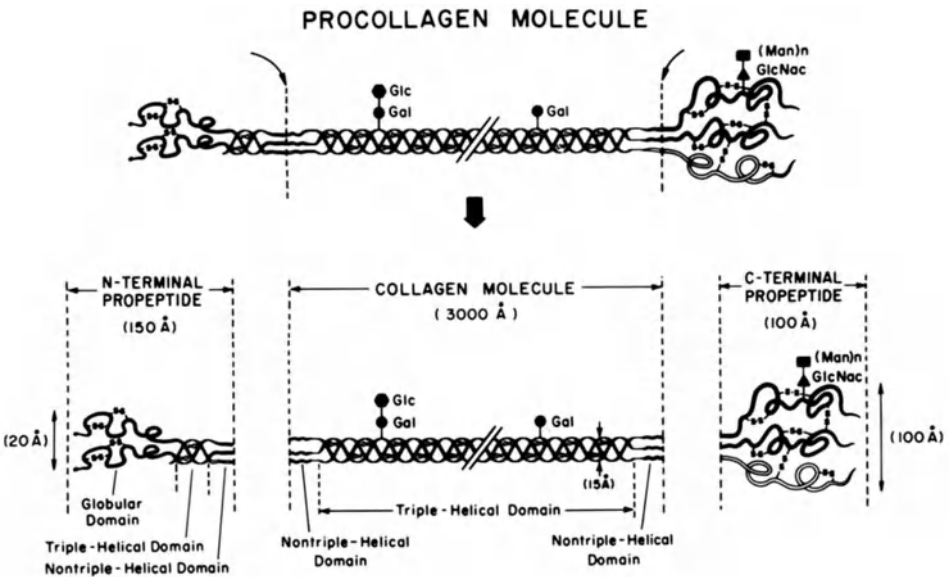


Figure 1. Schematic representation of the type I procollagen molecule. Reproduced with permission from Prockop and Kivirikko (1984).
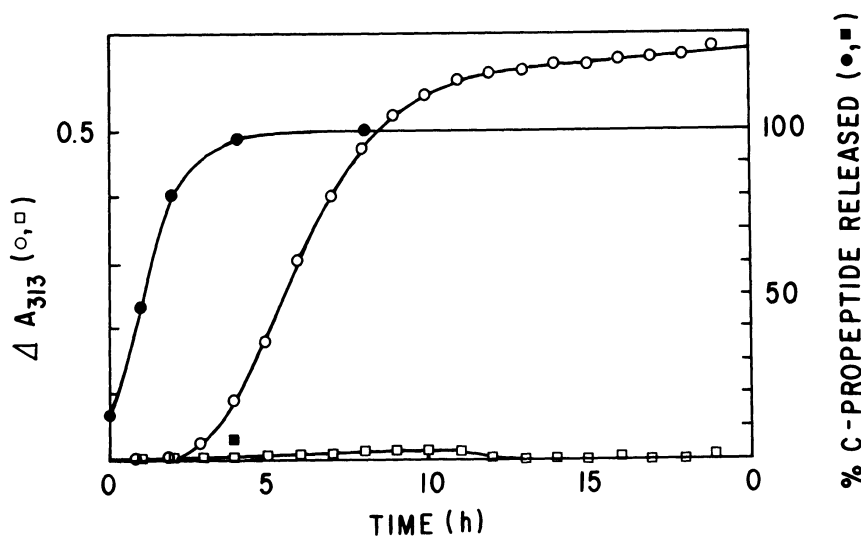
Figure 2. Formation of fibrils by cleavage of type I pCcollagen by procollagen C-proteinase. For experimental conditions, see Kadler et al. (1987).

dynamic parameters similar to those for other protein polymerizations (Table I).

TABLE I. Thermodynamic parameters for systems of protein self-assembly.

| Protein | $\frac{G^a}{kcal.mol^{-1}}$ | H | $\frac{S}{cal.K^{-1}.mol^{-1}}$ | Reference |
|---------|------|------|------|-----------|
| G-actin | | +10-15 | | Asakura et al. (1960) |
| G-ADP-actin | | +10-15 | | Kasai (1969) |
| Flagella | $-1.9^b$ | +101 | +332 | Gerber et al. (1973) |
| Tobacco mosaic virus protein | $-10.0^b$ | +34 | +139 | Paglini and Lauffer (1968) |
| Sickle cell Hb | $-11.4^b$ | +68 | +256 | Murayama (1972) |
| Type I collagen Extracted De novo | -23 -13 | +56 | +220 | Cooper (1970) Kadler et al. (1987) |

[a] At 37°C.

[b] Values calculated here from published data.

## Substitution of a Single Amino Acid that Produces a Kink in the Type I Procollagen Molecule and Generates Dendritic Fibrils.

For several years we and others have been studying the genetic mutations that produce osteogenesis imperfecta, a heritable disorder of connective tissue that is characterized by remarkably brittle bones (see Prockop et al., 1988). Recent data from a number of laboratories have demonstrated that most probands with osteogenesis imperfecta have mutations in the gene for either the proα1(I) or proα2(I) chain of type I procollagen. Some of the mutations in the type I procollagen genes are partial gene deletions. One involves insertion of amino acid sequences, and several involve RNA splicing mutations. Of special interest are a series of mutations that are single-base substitutions that convert codons for glycine to codons for other amino acids in either the α1(I) or α2(I) chain. The presence of the bulkier amino acid for glycine apparently disrupts the triple helix of collagen and lowers the melting temperature of the protein by 4°C. At least five of the glycine substitutions produce lethal phenotypes, in part, because the lower thermal stability of the protein means that it unfolds at body temperatures and is degraded.

We recently identified a point mutation in a lethal variant of osteogenesis imperfecta that changes the codon at amino acid position 748 of the triple helical region of the α1 chain of type I procollagen from glycine to cysteine (Vogel et al., 1987). The type I procollagen synthesized by cultured fibroblasts from the proband was post-translationally over-modified, had a decreased thermal stability, and was secreted slowly as compared to collagen synthesized by fibroblasts from an unaffected individual. Some, but not all, of the type I procollagen appeared to be degraded because of its low thermal stability. In the course of studies with the proband's fibroblasts, we made the unexpected observation that the mutated procollagen was poorly processed to pCcollagen in post-confluent cultures of skin fibroblasts (Vogel et al. 1987). We subsequently demonstrated directly that the procollagen containing the cysteine substitution was cleaved more slowly by purified pro-collagen N-proteinase, the large neutral metalloproteinase that normally cleaves the three proα chains of type I procollagen at a specific site near the N-terminal region of the protein (Vogel et al., 1988). The effect of the mutation on processing by N-proteinase was initially perplexing because the amino acid substitution for glycine 748 was over 225 nanometers distant from the

N-proteinase cleavage site. Procollagen N-proteinase is unusual among proteinases in that it is highly specific for procollagen with a native conformation and it will not cleave procollagen that is even partially unfolded (Tuderman and Prockop, 1982; Dombrowski and Prockop, 1988). However, it was not obvious how the substitution for glycine 748 could alter the conformation of the N-proteinase cleavage site that was so far removed from the mutation itself.

We considered several possible explanations for the observations (Vogel et al., 1988). Our conclusion was that the cysteine substitution for glycine 748 introduced a conformational change that altered the N-proteinase cleavage site located over 225 nm away from the site of the mutation. A shift in phase of the three chains of the collagen triple helix appeared to be the most likely conformational change that could be transmitted over this distance in the protein.

We, therefore, constructed a series of models for the collagen triple helix in which the presence of the cysteine residue instead of glycine produced a phase shift at the site of the amino acid substitution that was propagated to the N-propeptide cleavage site (Vogel et al., 1988). The phase-shift models were based on the generally accepted principles that all the hydrogen bonds in the triple-helix are interchain and that side-chain interactions are of secondary importance. They were also based on the principle that the triple helix requires that each of the three chains is staggered by one residue. Our model-building experiments suggested that two phase-shift models were equally satisfactory, one involving a looping out of one tripeptide unit from one chain and the other involving a looping out of one tripeptide unit from each of two chains (Fig. 3). The two phase-shift models were equally satisfactory by current criteria of conformational energies. They were, in fact, about equal by these criteria to an earlier model for a cysteine substitution for glycine proposed by Traub and Steinmann (1986) that did not involve a phase shift. One consistent feature of all the phase-shift models, however, was that they produced a discernible kink in the collagen molecule at the site of the cysteine mutation.

Therefore, we set out to test the phase-shift models by examining the mutated procollagen by rotary shadowing electron microscopy. The results demonstrated that a large number of the molecules had a kink at the site of the cysteine substitution.

We next examined the question of what effect the kink induced by the cysteine substitution might have on the assembly of collagen fibrils de novo. pCcollagen was prepared from the proband's type I procollagen (Kadler et al., 1988b). The proband was heterozygous for the mutation and the type I procollagen secreted by the proband's cells in culture was a mixture of normal and mutant procollagen. The pCcollagen was therefore a mixture of normal and mutant pCcollagen. Cleavage of the C-propeptides from the proband's
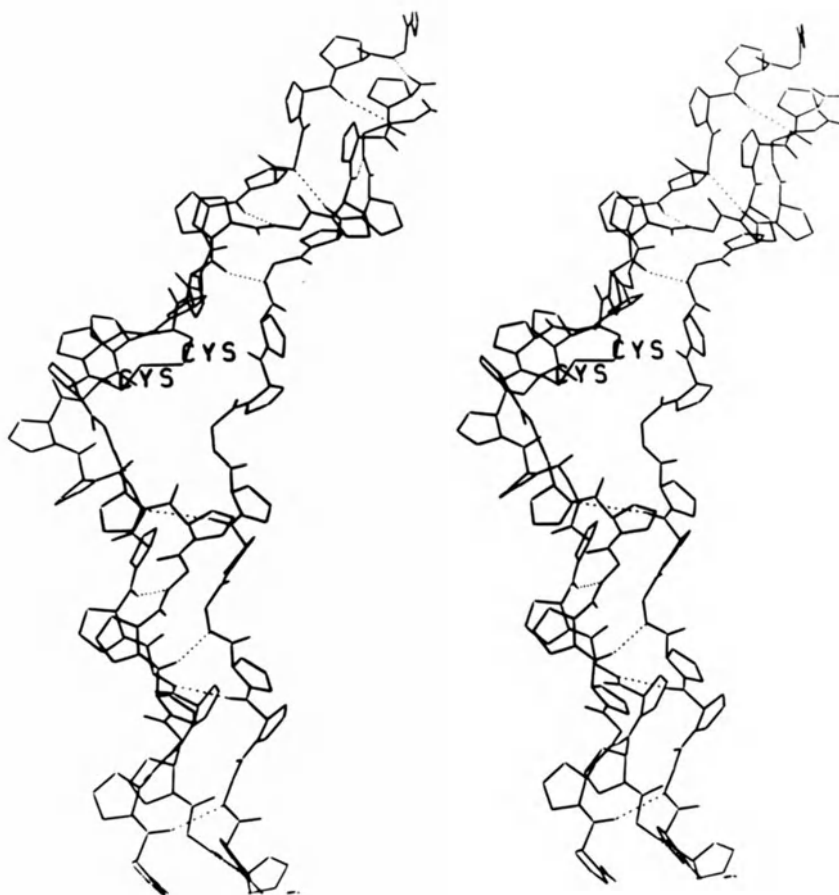


Figure 3. Stereo drawings of the phase shift model II showing a Cys/Gly substitution in the α1 chains. Hydrogens have been omitted for clarity. The two cysteines are labeled. The hydrogen bonds within the intact tripple helices are shown as dashed lines. The C-terminus is on top of the figures. Reproduced with permission from Vogel et al. (1988).

pCcollagen generated readily detectable collagen fibrils. However, the concentration of collagen monomers in equilibrium with fibrils was 34.1±2.2 µg/ml at 32°C of which 14.0±1.0 µg/ml was the normal monomer produced from the proband's procollagen. In contrast, the value was 2.2±0.1 µg/ml with normal type I collagen. Accordingly, one effect of the monomer containing the cysteine substitution was to limit the assembly of the normal monomer into fibrils. These data are consistent with the theories of copolymerization as discussed in detail by Oosawa and Asakura (1975) who demonstrated that in a mixture containing two kinds of actin monomer, the critical concentration of one monomer for the formation of copolymers was affected by the concentration of the other monomer.

In parallel experiments, the fibrils formed were examined using dark- field light microscopy. Control fibrils generated at 32°C were needle-shaped with pointed ends (Fig. 4A). In contrast, fibrils generated by incubating the proband's pCcollagen with C-proteinase were highly branched (Fig. 4B). At 37°C the fibrils were even more branched or dendritic than those formed at 32°C (Kadler et al., 1988b). Examining the fibrils at early time points demonstrated that the fibrils were branched as soon as the structures became visible by light microscopy, and the pattern persisted as the fibrils grew.

The results help to explain why the structure of collagen has been so highly conserved during evolution and why mutations that change the primary structure of the protein drastically alter the phenotype of the organism. Previous observations demonstrated that the effects of synthesis of a structurally abnormal proα chain of type I procollagen involved amplification by the phenomenon of "procollagen suicide" whereby structurally abnormal proα chains become associated at their C-propeptide domains to normal proα chains and lead to degradation of both the normal and abnormal chains. The results here demonstrate that the effects of a change in primary structure can be further amplified during fibril formation. The presence of the cysteine mutation produced a kinked collagen molecule. The kinked collagen molecule greatly decreased the efficiency with which normal collagen synthesized by the same fibroblast was used to assemble collagen fibrils. Also, the fibrils generated had greated distorted morphologies and, therefore, are likely to have altered biological functions in vivo.
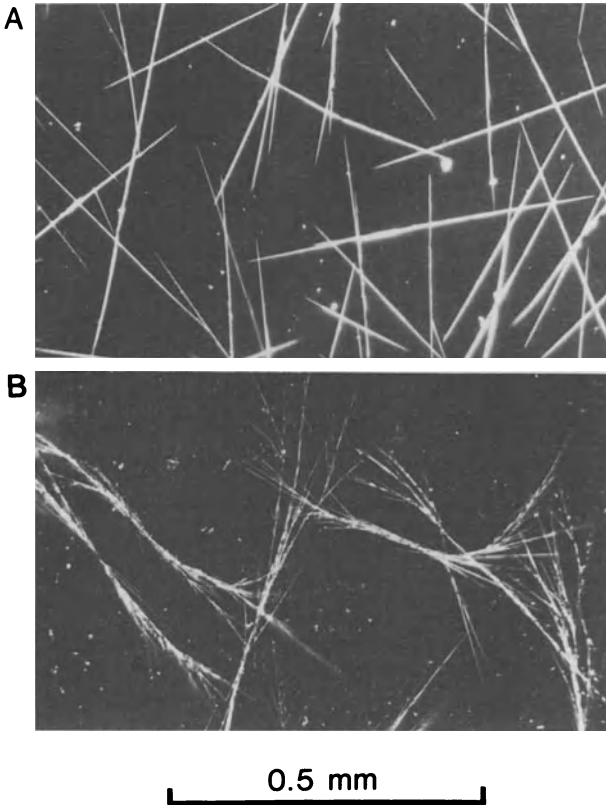
Figure 4. Dark-field light micrographs of control (A) and proband's (B) fibrils. Fibrils were generated by incubating pCcollagen (70 μg/ml) with C-proteinase (50 U/ml) at 32°C.

REFERENCES

Asakura S, Kasai M, and Oosawa F (1960) J Polym Sci Part D Macromol
     Rev 44:35-49
Comper WD and Veis A (1977) Biopolymers 16:2113-2131
Cooper A (1970) Biochem J 118:355-365
Dombrowski KE and Prockop DJ (1988) J Biol Chem, in press
Farber S, Garg AK, Birk DE and Silver FH (1986) Int J Biol Macromol
     8:37-42
Gelman RA, Williams BR and Piez KA (1979) J Biol Chem 254:180-186
Gerber BR, Asakura S and Oosawa F (1973) J Mol Biol 74:467-487
Gross J and Kirk D (1958) J Biol Chem 233:355-360
Helseth DL Jr and Veis A (1981) J Biol Chem 256:7118-7128
Hojima Y, van der Rest M and Prockop DJ (1985) J Biol Chem
     260:15996-16003
Holmes DF, Capaldi MJ and Chapman JA (1986) Int J Biol Macromol 8:
     161-166
Kadler KE, Hojima Y and Prockop DJ (1987) J Biol Chem
     262:15696-15701

Kadler KE, Hojima Y and Prockop DJ (1988a) J Biol Chem
     263:10517-10523
Kadler KE, Vogel BE, Hojima Y and Prockop DJ (1988b) Collagen Rel
     Res, abstract in press
Kasai M (1969) Biochim Biophys Acta 180:399-409
Leibovich SJ and Weiss JB (1970) Biochim Biophys Acta 214:445-454
Miyahara M, Njieha, FK and Prockop DJ (1982) J Biol Chem
     257:8442-8448
Miyahara M, Hayashi K, Berger J, Tanzawa K, Njieha F.K, Trelstad RL,
     and Prockop DJ (1984) J Biol Chem 259:9891-9898
Murayama M. (1972) In: Brewer GJ (eds)  Hemoglobin and Red Cell
     Structure and Function. Plenum Publishing Corp, New York,
     pp.243-251
Na GC, Butz LJ, Bailey DG, and Carroll RT (1986) Biochemistry
     25:958-966
Oosawa F and Asakura S (1975) Thermodynamics of the Polymerization
     of Protein, Academic Press, New York
Paglini S and Lauffer MA (1968) Biochemistry 7:1827-1835
Prockop DJ and Kivirikko KI (1984) New Engl J Med 311:376-386
Prockop DJ, Kadler KE, Hojima Y, Constantinou CD, Dombrowski KE,
     Kuivaniemi H, Tromp G and Vogel B (1988) In: Evered D and
     Harnett S (eds) Cell and Molecular Biology of Vertebrate Hard
     Tissues. CIBA Foundation Symposium No. 136. Wiley Chichester,
     UK, pp. 142-156
Silver FH, Langley KH and Trelstad RL (1979) Biopolymers
     28:2523-2535
Tuderman L and Prockop DJ (1982) Eur J Biochem 125:545-549
Traub W and Steinmann B (1986) FEBS Lett 198:213-216
Vogel BE, Minor RR, Freund M and Prockop DJ (1987) J Biol Chem
     262:14737-14744
Vogel BE, Doelz R, Kadler KE, Hojima Y, Engel J and Prockop DJ
     (1988) Collagen Rel Res, abstract in press
Williams BR, Gelman RA, Poppke DC and Piez KA (1978) J Biol Chem
     253:6578-6585
Wood GC (1960) Biochem J 75:598-605

# Molecular Cloning of Chicken Type VI Collagen

B. Trueb
Biochemie I
ETH Zentrum
CH – 8092 Zürich
Switzerland

Type VI collagen is a dumb-bell-shaped molecule with two large globular domains linked by a short collagenous triple helix. It is composed of three different polypeptide chains that are linked extensively by disulfide bonds. Type VI collagen is synthesized and secreted by most mesenchymal cells. In the extracellular matrix it forms small microfilaments which are often associated with the large banded fibers of interstitial collagens.

Our interest has focused on type VI collagen because its biosynthesis is largely reduced in cells transformed by various tumor viruses. It is conceivable that this reduction may have profound effects on the adhesive properties of transformed cells as type VI collagen is known to promote cell attachment and spreading.

We have isolated and sequenced several overlapping cDNA clones which encode the entire α2 subunit of chicken type VI collagen. The clones hybridize specifically to a 4.2 kb mRNA abundant in chicken and human fibroblasts. Virally transformed fibroblasts contain drastically reduced levels of this mRNA indicating that the synthesis of type VI collagen might be blocked at the transcriptional level in transformed cells.

The cDNA clones cover a total of 4153 base pairs. The deduced amino acid sequence predicts that the α2(VI) polypeptide consists of 1015 amino acid residues which can be divided into four domains: a hydrophobic signal peptide of 20 residues, an amino terminal globular domain of 228 residues, a collagenous segment of 335 residues and a carboxy terminal globular domain of 432 residues.

The collagenous domain contains one interruption in the repetitive Gly-X-Y sequence. In this domain there are seven Arg-Gly-Asp sequences which might function as cell binding sites, one Asn-Gly-Thr sequence allowing the attachment of N-linked carbohydrates within the triple helix and one cysteine residue which might be involved in the formation of type VI collagen dimers. On both sides of the collagenous domain there are short cysteine-rich segments which might connect the three subunits in a type VI collagen molecule by the formation of disulfide bonds. Our sequence data substantiate and refine the structural model of type VI collagen proposed by Furthmayr et al. (Biochem J (1983) 211:303-311, see Fig.1).
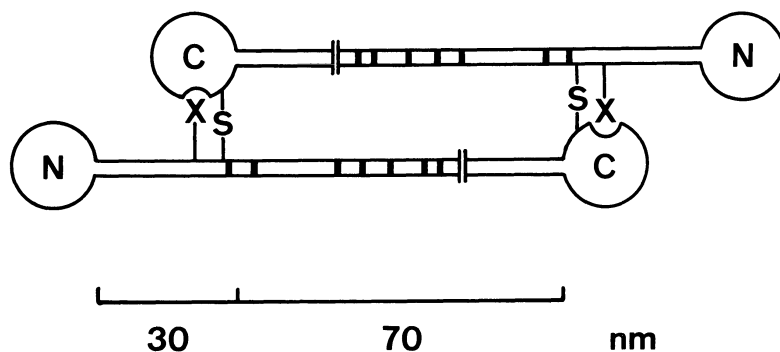
**Fig.1.** Diagram summarizing the characteristic features of the α2(VI) polypeptide in a type VI collagen dimer. The short interruption in the repetitive Gly-X-Y sequence is indicated by two vertical lines, the potential cell binding sites are given as dark boxes. S cystine, X oligosaccharide linked to Asn, N amino terminal globular domain, C carboxy terminal globular domain.

A computer analysis of the globular sequences reveals three homologous repeats, one in the amino terminal and two in the carboxy terminal globular domain. These repeats have an average length of 180 amino acid residues and show a striking similarity to the collagen-binding motifs found in von Willebrand factor and cartilage matrix protein. We therefore speculate that the three homologous repeats of type VI collagen may be able to interact with collagenous sequences as they are found in the center of adjacent type VI collagen molecules. Such an interaction between globular and triple helical domains would lend great stability to the extended microfilaments of type VI collagen.

Our sequence data establish type VI collagen as another member of the growing family of extracellular multidomain proteins that may play a crucial role in cell attachment.

# Structure and Biology of the Laminin-Nidogen Complex

R. Timpl, K. Mann, M. Aumailley, M. Gerl, R. Deutzmann,
V. Nurcombe[a], D. Edgar[a], M.-L. Chu[b] and Y. Yamada[c]

Max-Planck-Institut für Biochemie,
D-8033 Martinsried,
FRG

A large variety of cells in the body are exposed to extracellular
matrices which affect cell function and behavior. Basement
membranes are prominent matrix structures and have been shown to
consist of several collagenous and non-collagenous glycoproteins
and proteoglycans (Martin and Timpl, 1987). Laminin is one of the
major and ubiquitous components that was originally isolated and
characterized from a tumor basement membrane as a cross-shaped,
multidomain protein (Timpl et al., 1979; Engel et al., 1981). It
is considered to be one of the important cell-binding proteins
present in basement membranes and in addition possesses binding
potentials for other matrix components. Another non-collagenous
glycoprotein, nidogen/entactin, was initially discovered as a
sulfated 158kD polypeptide (Carlin et al., 1981) and shown to have
a characteristic dumb-bell structure (Paulsson et al., 1986;
1987). Even though nidogen is also an ubiquitous constituent of
basement membranes its function is not immediately apparent.
However, several pieces of indirect evidence from cell culture and
tissue studies (Dziadek and Timpl, 1985) provided initial clues
about the possible role of nidogen, by showing that it forms
tight, stoichiometric, noncovalent complexes with laminin in situ.
This was confirmed by isolating the intact complex from the EHS

--------------------

[a] Max-Planck-Institut für Psychiatrie, D-8033 Martinsried,
Federal Republic of Germany

[b] Departments of Biochemistry and Molecular Biology and
Dermatology, Thomas Jefferson University, Philadelphia, PA
19107, USA.

[c] Laboratory of Developmental Biology and Anomalies,
National Institute of Dental Research, NIH, Bethesda, MD
20892, USA.

tumor using chelating agents to facilitate extraction (Paulsson et al., 1987). In the following we will discuss the progress made during the past two years to analyze the structures of laminin and nidogen, and their repertoires of interactions both within the matrix and with cells.


## Structure of laminin


As isolated from the mouse EHS tumor and cultured cells laminin has a molecular mass of about 900kD and consists of three disulfide-linked polypeptide chains, B1, B2 and A, which differ in size (Timpl et al., 1979; Cooper et al., 1981). Rotary shadowing has shown these three chains to form a cross-shaped structure with three short arms and one long arm (Engel et al., 1981) comprising in all seven rod-like segments and seven globular domains. There are several indications for isoforms of laminin (Martin and Timpl, 1987) which when isolated from Schwann cells may have a Y-shaped rather than a cross-shaped structure (Davis et al., 1985; Edgar et al., 1988). It was also shown that these materials lack a 400kD A chain but it is still unclear if they are composed solely of B1-B2 chain dimers or contain a smaller A chain variant (Edgar et al., 1988). Such isoforms may not be restricted to neuronal tissue, little if any A chain being found in early embryos (Cooper and McQueen, 1983) or in embryonic kidney prior to induction of tubular epithelium (Klein et al., 1988).

The complete amino acid sequence of mouse tumor laminin has been elucidated from cDNA clones. The data show 1786 amino acid residues for the B1 chain (Sasaki et al., 1987), 1607 residues for B2 chain (Sasaki and Yamada, 1987) and 3084 residues for the A chain (Sasaki et al., 1988) including in each case a typical signal peptide. Portions of these sequences were confirmed by Edman degradation (Hartl et al., 1988; Deutzmann et al., 1988). The data have led to a refined model of laminin domain structure (Fig.1). Several of these domains are shared by all three chains. They include domains I and II in the rod-like long arm with a predicted coiled-coil $\alpha$-helix, and domains III and V which contain several EGF-like repeats and constitute rod-like segments of the three short arms. Further domains (IV, VI and G) with a lower interchain homology are likely to form various globular domains.
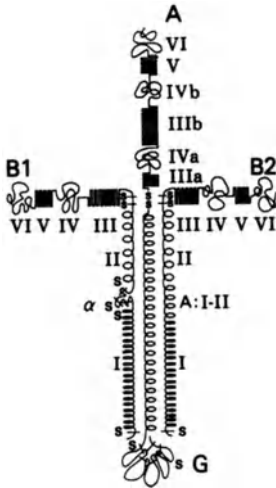
Fig.1: Domain model of laminin and its constituent A, B1 and B2 chains based on cDNA sequences and morphological studies. Domains (roman numbers) include α-helical rods (I,II), EGF-like repeats (III,V) and globular segments (IV, VI). A short, cysteine-rich segment α is unique to the B1 chain. G denotes a large globular domain of A chain at the end of the long arm. The N-termini of the chains are present in domain VI. Reproduced from Sasaki et al. (1988).

The sequence-predicted domain structure is with some exceptions in full agreement with data from morphological studies (Engel et al., 1981) and from proteolytic fragmentation (Martin and Timpl, 1987). Differences include a predicted globular domain IVa which interrupts domain III in the A chain for which no independent evidence so far exists. Unique chain structures include a short cysteine-rich region (α) in the B1 chain and the large (100kD) globular domain G which is located at the distal end of laminins long arm, and consists of A chain sequences showing five internal repeats with 25-30% homology (Deutzmann et al., 1988; Sasaki et al., 1988).

## Structure of nidogen

Intact nidogen (150kD) was isolated initially from 6M guanidine.-HCl extracts of the EHS tumor and more recently by milder dissociating conditions from its complex with laminin (Paulsson et al., 1986; 1987). Electron microscopical and physical data indicate that it consists of two distinct globular domains of about 85kD and 38kD, separated by a 17nm-long rod-like element (Fig.2). This structure was confirmed by studies with proteolytic fragments arising in part by endogenous cleavage. N-terminal sequence analyses of nidogen and its fragments showed it to be a distinct protein (Paulsson et al., 1986; Mann et al., 1988).

## Sites involved in matrix interactions


The high stability of the laminin-nidogen complex ($k_D$<10nM) indicates that it forms a distinct structure within basement membranes, and implicates discrete binding sites on both components as previously suggested by electron microscopy (Paulsson et al., 1987). The laminin-binding site of nidogen was recently localized to its C-terminal globule (Mann et al., 1988), although mapping to a particular sequence within one of the subdomains has not yet been achieved. The nidogen-binding site of laminin has been localized to fragment 1, which comprises the inner rod-like domains III from all three chains (Fig.1). Separation of the constituent chains of fragment 1 by partial reduction showed full binding activity for the B1 chain segment while 10fold lower activities were found for the A and B2 chain segments, respectively. All binding activity was abolished by total reduction of laminin or nidogen demonstrating that binding is conformation-dependent.

In addition to binding laminin, nidogen has recently been shown to bind collagen type IV (Fig.3), indicating that nidogen has a mediator function in matrix assembly. The binding site of nidogen was again localized to the C-terminal globule but is presumably not identical to that structure which binds laminin. Binding to collagen type IV was specific when compared to other types of collagens. The interaction with collagen type IV occurs with a triple-helical segment about 80nm away from the C-terminal globule NC1 (Fig.3). A second, presumably weaker binding site may be about 180nm away from NC1. As expected, the laminin-nidogen complex also binds collagen type IV, although it is not yet clear if the interaction of the complex also involves structures of laminin (Charonis et al., 1986).

Another property of laminin but not of nidogen is its binding activity for heparin and heparan sulfate indicating that this is used in the asssociation to proteoglycans. A major heparin binding site has been localized to laminin fragment 3 (Ott et al., 1982) which corresponds to the 400 C-terminal amino acid residues of A chain domain G (Fig.3). This sequence contains several clusters of basic amino acid residues (Deutzmann et al., 1988; Sasaki et al., 1988) which could be involved in binding.
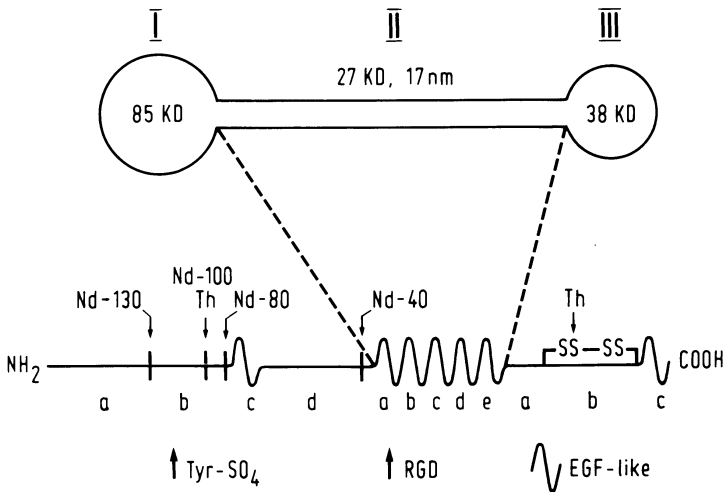
Fig.2: Dumb-bell model of nidogen and correlation with subdomains predicted from amino acid sequences. Major domains (I-III) correspond to the two globular domains and the rod-like segment. Subdomains (small letters) include EGF-like repeats (Ic, IIa-e, IIIc) and those predicted from cleavages by thrombin (Th) and endogenous proteases (Nd) (Paulsson et al., 1986; Mann et al., 1988). Positions of tyrosine sulfation and of cell-binding RGD sequence are indicated.

The amino acid sequence of mouse and human nidogen has been recently elucidated (Mann et al., manuscript in preparation) demonstrating that it consists of some 1217 amino acid residues. The sequence data predict two globular domains in terminal positions which are connected by a rod-like segment in agreement with the proposed model (Fig.2). The sequence shows an irregular distribution of cysteine residues, mainly concentrated in seven EGF-like repeats. Five EGF-like repeats are located in the rod-like segment, but contain six rather than the eight cysteine residues per repeat found in the rod-like elements of laminin. Further division of the two globules into four and three subdomains, respectively, is indicated by two more EGF-like repeats and the presence of peptide bonds susceptible to endogenous proteolysis (Paulsson et al., 1986). The presence of two putative carbohydrate acceptor sites and two tyrosine residues in a consensus sequence predicting sulfation are also apparent. This is of interest because of the previous identification of tyrosine sulfate in the protein (Paulsson et al., 1985).
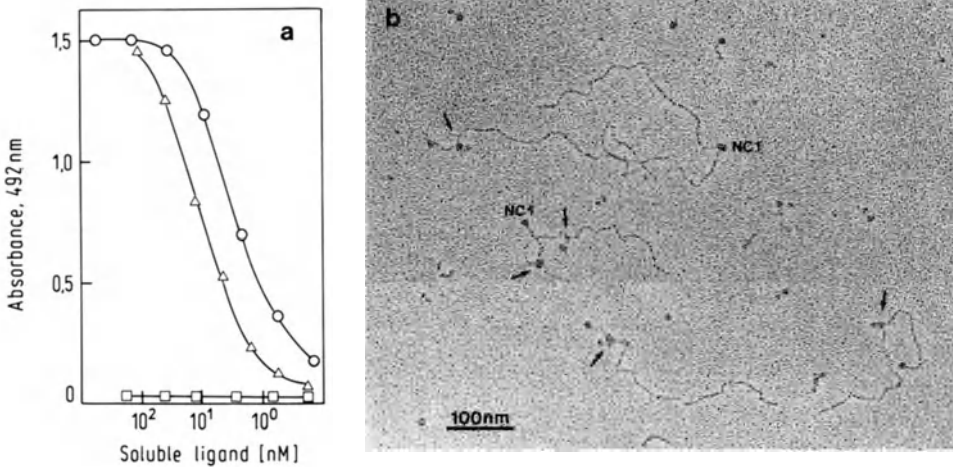
Fig.3: Interaction of nidogen and laminin-nidogen complex with collagen type IV in a binding assay (a) and visualizaton of nidogen-collagen IV complexes by rotary shadowing (b). An ELISA-type of binding assay was used with laminin-nidogen complex ($\triangle$), nidogen (o) and laminin ($\square$) as soluble ligands and collagen IV as insoluble ligand. The electron micrograph shows an overview. Bound nidogen particles are indicated by arrows, NC1 identifies the globular domain of collagen IV.

## Cell-binding sites of the laminin-nidogen complex

Laminin possesses two high affinity ($K_D$=1-5nM) cell binding sites which were localized to fragments 1 (see above) and 8 (Aumailley et al., 1987). Fragment 8 comprises the end of the long arm of laminin including domains I of all three chains and domain G from the A chain (Paulsson et al., 1987; Deutzmann et al., 1988; see Fig.1). Both fragments promote distinct attachment and spreading of most cultured cells (Aumailley et al., 1987; Goodman et al., 1987). Fragment 8 was also identified as stimulating neuron survival and neurite outgrowth (Edgar et al., 1984). Radioligand competition assays demonstrated that these two fragments bind to two distinct cellular receptors (Fig.4). Interestingly, while fragment 1 is capable of binding to many cell types, fragment 1-4 comprising the complete short arms of laminin (Ott et al., 1982) is unable to bind to the fragment 1 receptor. This indicates that fragment 1 binding structures are latent within the intact short arms of laminin (V. Nurcombe et al., manuscript in preparation).
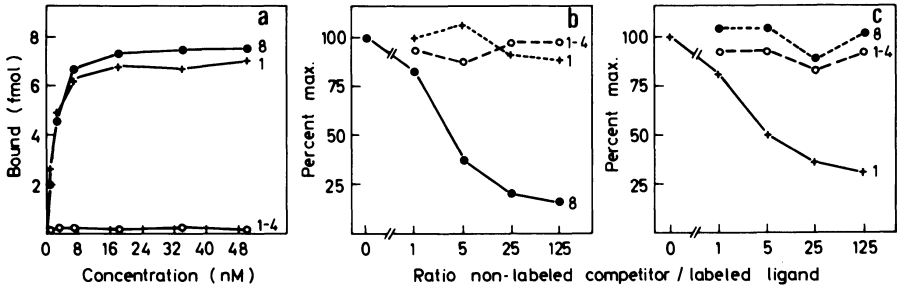
**Fig.4:** Radioligand specific binding curves of $^{125}$I- labelled laminin fragments 8, 1-4 and 1 to HT-1080 cells (a) and cross-inhibitions of binding fragments 8 (b) and 1 (c) by non-labelled fragments. The data show that fragments 1 and 8 bind to two distinct receptors and that fragment 1-4 binds to neither of these receptors (Aumailley et al., 1987; Nurcombe et al., manuscript in preparation).

The data imply that native laminin binds to cells via the site on fragment 8. The importance of fragment 8 sites was also demonstrated by antibody inhibition in vitro (Aumailley et al., 1987) and in vivo where antibodies to this fragment inhibit cell polarization during development of kidney epithelium (Klein et al., 1988). High resolution immuno-electron microscopy showed that fragment 8 epitopes are located close to cells in the corneal epithelium while fragment 1 epitopes were concentrated in the center of the basement membrane (Schittny et al., 1988). These observations emphasize that fragment 8 provides the crucial high affinity cell-binding sites of laminin. The sequence of these sites still remains to be identified. Although the cell-binding site of laminin fragment 1 requires proteolytic activation before being able to associate with cellular receptors, the fact that this fragment nevertheless causes distinct cell attachment and spreading indicates that it is likely to play some sort of physiological role, the nature of which is unknown. A peptide sequence YIGSR present within the fragment 1 structure (B1 chain domain III) has been shown to promote cell attachment (Graf et al., 1987). In addition domain IIIb of the A chain was found to contain a potential RGD cell-binding sequence (Sasaki et al., 1988). Whether these sequences correspond to the latent high-affinity cell-binding site of laminin fragment 1 is unknown.

The two high-affinity binding sites described for fragments 1 and 8 may not account for the complete cellular recognition repertoire of the laminin-nidogen complex. Structures of the short arms of laminin distinct from fragment 1 have been found to promote neurite outgrowth (Edgar et al., 1984) and cell attachment (Goodman et al., 1987). Fragment 1 was also shown to possess growth factor activity which could not be correlated to cell adhesion activity (Panayotou et al., manuscript in preparation). The observation of an RGD sequence in domain IIb of nidogen (Fig.2) has also led to the examination of its cell-binding properties because such sequences are known to promote cell atachment by a variety of proteins (Ruoslahti and Pierschbacher, 1987). Nidogen was in fact found to promote cell attachment and spreading, but with lower efficiency compared to that of laminin. This interaction unlike that of laminin could be inhibited by synthetic RGD-containing peptides.

## Conclusions

The laminin-nidogen complex represents a major structural element of basement membranes. The sequence and domain structure of the complex has been elucidated. A variety of interactions both within the complex, with other basement membrane components and with cellular receptors have been identified. Determination of the particular amino acid sequences responsible is feasible, and will further our understanding of basement membranes at the molecular and biological level.

## References

Aumailley M, Nurcombe V, Edgar D, Paulsson M, Timpl R (1987) The cellular interactions of laminin fragments. Cell adhesion correlates with two fragment-specific high affinity binding sites. J Biol Chem 262: 11532-11538

Carlin B, Jaffe R, Bender B, Chung AE (1981) Entactin, a novel basal lamina associated sulfated glycoprotein. J Biol Chem 256: 5209-5214

Charonis AS, Tsilibary EC, Saku T, Furthmayr H (1986) Inhibition of laminin self-assembly and interaction with type IV collagen by antibodies to the terminal domain of the long arm. J Cell Biol 103: 1689-1697

Cooper AR, McQueen HA (1983) Subunits of laminin are differentially synthesized in mouse eggs and early embryos. Devel Biol 96: 467-471

Cooper AR, Kurkinen M, Taylor A, Hogan BLM (1981) Studies on the biosynthesis of laminin by murine parietal endoderm cells. Eur J Biochem 119: 189-197

Davis GE, Manthorpe M, Engvall E, Varon S (1985) Isolation and characterization of rat Schwannoma neurite promoting factor: evidence that the factor contains laminin. J Neurosci 5: 2662-2671

Deutzmann R, Huber J, Schmetz KA, Oberbäumer I, Hartl L (1988) Structural studies of long arm fragments of laminin: evidence for repetitive C-terminal sequences in the A chain, not present in the B chain. Eur. J Biochem, in press

Dziadek M, Timpl R (1985) Expression of nidogen and laminin in basement membranes during mouse embryogenesis and in terato-carcinoma cells. Devel Biol 111: 372-382

Edgar D, Timpl R, Thoenen, H (1984) The heparin-binding domain of laminin is responsible for the effects on neurite outgrowth and neuronal survival. EMBO J 3: 1463-1468

Edgar D, Timpl R, Thoenen H (1988) Structural requirements for the stimulation of neurite outgrowth by two variants of laminin and their inhibition by antibodies. J Cell Biol 106: 1299-1306

Engel J, Odermatt E, Engel A, Madri JA, Furthmayr H, Rohde H, Timpl R (1981) Shapes, domain organizations and flexibility of laminin and fibronectin, two multifunctional proteins of the extracellular matrix. J Mol Biol 150: 97-120

Goodman SL, Deutzmann R, von der Mark K (1987) Two distinct cell-binding domains in laminin can independently promote non-neuronal cell adhesion and spreading. J Cell Biol 105: 589-598

Graf J, Iwamoto Y, Sasaki M, Martin GR, Kleinman HK, Robey FA, Yamada Y (1987) Identification of an amino acid sequence in laminin mediating cell attachment, chemotaxis and receptor binding. Cell 48: 989-996

Hartl L, Oberbäumer I, Deutzmann R (1988) The N-terminus of laminin A chain is homologous to the B chains. Eur J Biochem 173: 629-635

Klein G, Langegger M, Timpl R, Ekblom P (1988) Role of laminin A chain in the development of epithelial cell polarity. Cell, in press

Mann K, Deutzmann R, Timpl R (1988) Characterization of proteolytic fragments of the laminin-nidogen complex and their affinity in ligand binding assays. Eur J Biochem, in press

Martin GR, Timpl R (1987) Laminin and other basement membrane components. Ann Rev Cell Biol 3: 57-85

Ott U, Odermatt E, Engel J, Furthmayr H, Timpl R (1982) Protease resistance and conformation of laminin. Eur J Biochem 123: 63-72

Paulsson M, Dziadek M, Suchanek C, Huttner WB, Timpl R (1985) Nature of sulfated macromolecules in mouse Reicherts membrane. Evidence for tyrosine-O-sulfate in basement membrane proteins. Biochem J 232: 571-579

Paulsson M, Deutzmann R, Dziadek M, Nowack H, Timpl R, Weber S, Engel J (1986) Purification and properties of intact and degraded nidogen obtained from a tumor basement membrane. Eur J Biochem 156: 467-478

Paulsson M, Aumailley M, Deutzmann R, Timpl R, Beck K, Engel J (1987) Laminin-nidogen complex: extraction with chelating agents and structural characterization. Eur J Biochem 166: 11-19

Ruoslahti E, Pierschbacher MD (1987) New perspective in cell adhesion: RGD and integrin. Science 238: 491-497

Sasaki M, Yamada Y (1987) Structure of the laminin B2 chain shows multidomain structures homologous to the B1 chain. J Biol Chem 262: 17111-17117

Sasaki M, Kato S, Kohno K, Martin GR, Yamada Y (1987) Sequence of cDNA encoding the laminin B1 chain reveals a multidomain protein containing cysteine-rich repeats. Proc Natl Acad Sci USA 84: 935-939

Sasaki M, Kleinman HK, Huber H, Deutzmann R, Yamada Y (1988) Laminin, a multidomain protein: the A chain has a unique globular domain and homology with the basement membrane proteoglycan and the laminin B chains. J Biol Chem, in press

Schittny JC, Timpl R, Engel J (1988) High resolution immunoelectron microscopic localization of functional domains of laminin, of nidogen and heparan sulfate proteoglycan in epithelial basement membrane of mouse cornea reveals different topological orientations. J Cell Biol, in press

Timpl R, Rohde H, Gehron Robey P, Rennard SI, Foidart JM, Martin GR (1979) Laminin - a glycoprotein from basement membranes. J Biol Chem 254: 9933-9937

# Structure of the Basement Membrane Protein Laminin: Variations on a Theme

K. Beck[1], R. A. McCarthy[2], M. Chiquet, L. Masuda-Nakagawa[3] and
W. K. Schlage[4]
Department of Biophysical Chemistry
Biocenter of the University of Basel
Klingelbergstraße 70
CH‑4056 Basel
Switzerland

Laminin is a noncollagenous glycoprotein ($M_r \approx 10^6$) localized specifically in basement membranes. In vertebrates it consists of disulfide-linked polypeptide chains of $M_r \approx 200'000$ (B1- and B2-chain) and $M_r \approx 400'000$ (A-chain). By electron microscopy it is visualized as an asymmetric cross with one long and three short arms each bearing terminal globules (cf Paulsson 1987). By extraction with a physiological buffer containing a metal ion chelator (EDTA) laminin copurifies with nidogen ($M_r \approx 150'000$) which is bound near the middle of one of the short arms (Paulsson et al 1987). To investigate structural variations of laminin during evolution we applied this extraction protocol to some invertebrates covering the main groups of phylogeny: we have chosen sea urchins belonging to the deuterostomia, leeches as an example for the protostomia and anthomedusae for the radiata.

## Sea urchin laminin

Extracts of basal lamina preparations of gastrula stage sea urchin embryos (Sphaerechinus granularis) have been purified by molecular sieve chromatography. SDS-polyacrylamide gels of column fractions collected near the void volume (Superose 6) exhibit one band which migrates slightly more slowly than mouse tumour laminin and one band which comigrates with nidogen. After reduction, the apparent molecular masses of the bands are 480'000, 260'000 and 150'000.

As revealed by electron microscopy, the column fractions contain cross-

---

1) present address: Institut für Biophysik, Universität, A-4040 Linz
2) Dept. Biochemistry, Biocenter of the University of Basel;
   present address: Dept. Anatomy and Cellular Biology, Harvard Medical
   School, Boston, MA 02115
3) Dept. Pharmacology, Biocenter of the University of Basel
4) Institute of Zoology, University of Basel, CH-4051 Basel;
   present address: Institut für biologische Forschung, D-5000 Köln
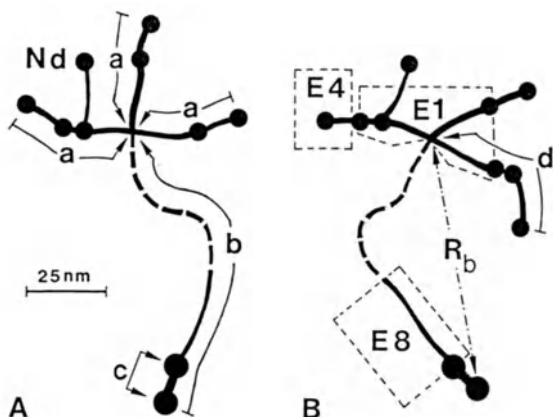
Fig. 1 : General model of the laminin-nidogen complex of invertebrates. The most prominent fraction of molecules exhibits three short arms of equal length (a) as shown in A. The length (b) of the long arm varies between the species. The center-to-center distance (c) between its terminal globules measures about 15 nm. About 20 to 30 percent of sea urchin and leech laminins bear an additional short arm (Nd) resembling nidogen.

A significant portion of molecules (B) has an elongated short arm (d) with two globules near the middle. Digestion of sea urchin laminin with elastase results in fragments similar to those of mouse tumour laminin (boxed; E1 consists of three arms only and does not contain nidogen). The center-to-end distance $R_b$ is a measure for the flexibility of the long arm (cf Table 1).

shaped molecules very similar to vertebrate laminin (McCarthy et al 1987). The cross (Fig. 1) consists of three $39 \pm 10$ nm long arms (length a and d) with globules near the middle and at the ends and one $113 \pm 6$ nm long arm (b) with two distinct terminal globules (center-to-center distance c : $14 \pm 3$ nm). The corresponding lengths for mouse laminin are 36 nm (a) and 77 nm (b); the long arm has one terminal globule only (Engel et al 1981). About one third of sea urchin laminins exhibit an additional dumbbell-shaped extension (Nd) near the middle of one of the short arms similar to the laminin-nidogen complex (Paulsson et al 1987). The large variance in the short arm length results from a heterogeneity of their appearance: For about 20 percent of the molecules one of the short arms (d) measures $48 \pm 7$ nm; the middle of these arms exhibit two globules and their outer rod-like portion is somewhat elongated. A nidogen-like extension has never been observed on the modified short arm. As a measure of the flexibility of the long arm the stiffness parameter $L_0$ was calculated from the contour length b and distance $R_b$; the resulting $L_0 = 62$ nm agrees well with that determined for mouse laminin (Engel et al 1981).

A mild elastase digest of sea urchin laminin results in three prominent classes of fragments (Fig. 1 B) similar to fragment 1, 4 and 8 described for mouse laminin (cf Paulsson 1987). The first class of particles consists of three $25 \pm 5$ nm long rods with terminal globules

resembling the center of the cross ('E 1'); the second class consists
of globules with a $10 \pm 4$ nm long rod which may correspond to the outer
part of one of the short arms ('E 4'); the third class consists of one
globule with a $35 \pm 5$ nm long rod which must result from the terminal
portion of the long arm ('E 8'), but lacks one of the two globules seen
in intact sea urchin laminin.


## Leech laminin

Extracts from leech (Hirudo medicinalis) ganglion capsule extracellu-
lar matrix as well as from leech body wall preparations have been pu-
rified by gel filtration (Masuda-Nakagawa et al 1988). Void volume
column fractions (Biogel A - 1.5 m) contain molecules resembling lami-
nin, tenascin and collagen IV as revealed by electron microscopy. La-
minin could be purified by immunoaffinity chromatography (Chiquet et
al 1988). Under nonreducing conditions, SDS-gels reveal two bands of
$M_r \approx 10^6$. After reduction, bands of $M_r \approx 340'000$, $220'000$, $160 - 180'000$
and about  $120'000$ are detected. In the electron microscope, this mo-
lecule is nearly identical to sea urchin laminin except that the long
arm (b) measures $94 \pm 6$ nm (cf Table 1). 40 percent of the molecules
exhibit a $53 \pm 4$ nm long short arm (d) with two inner globules. About
20 percent bear a nidogen-like extension on one of the 36 nm long arms.


## Anthomedusa laminin

Extracts from entire anthomedusae (Podocoryne carnea) have been puri-
fied on a Superose 6 column. Fractions eluting near the void volume
contain a molecule that comigrates with mouse tumour laminin on SDS-
gels. After reduction protein bands are detected of $M_r \approx 340'000$ and
$260'000$.  Molecules with a similar shape as mouse laminin are visua-
lized by electron microscopy, however, the long arm measures $97 \pm 9$ nm
and has two terminal globules (cf Table 1). No indications for the
existence of nidogen were found. The presence of a laminin-like mole-
cule in the diploblastically organized anthomedusa reflects the highly
conserved nature of an extracellular matrix protein from the onset of
metazoan life.


The main structural difference between the laminins investigated is
the length of their long arms. Whereas several biological activities
have been found to be localized within the short arms and the part

Table 1: Dimensions and molecular masses of invertebrate laminins.

Length a, b and $R_b$ were measured as shown in Fig. 1. The stiffness parameter $L_o$ was calculated acc. Engel et al 1981. $M_r(A)$ and $M_r(B)$ denote the molecular masses of the heavy and light chains, respectively, as determined by SDS-gels upon reduction.

| Source | long arm (nm) | | | short arms | $M_r(A)$ | $M_r(B)$ |
| | b | $\sqrt{\langle R_b^2 \rangle}$ | $L_o$ | a (nm) | | |
|---|---|---|---|---|---|---|
| sea urchin | 113 ± 6 | 87 | 62 | 35 ± 6 | 480'000 | 260'000 |
| leech | 94 ± 6 | 74 | 57 | 36 ± 4 | 340'000 | 220'000 |
| anthomedusa | 97 ± 9 | 76 | 58 | 36 ± 7 | 340'000 | 260'000 |

corresponding to fragment E 8 (cf Paulsson 1987) none is described for the inner part of the long arm. The similarity of the fragmentation pattern of sea urchin laminin with that of mouse laminin let us assume that the inconstancy might be due to modifications within the inner part of the long arm (broken line in Fig. 1). For mouse laminin it has been shown that the long arm is built up of $\alpha$-helices in a coiled-coil conformation (cf Paulsson et al 1987). The carboxy-terminal sequences of the three polypeptide chains which make up the long arm reveal repeating segments of seven residues with hydrophobic ones in position 1 and 4 (cf Parry, this volume). Thus the variability in length may result from a different number of such heptads. The differences in the long arm regions and the essential conservation of the short arm structures is in agreement with the recent finding that the C-terminal parts in mouse and Drosophila B 1 - chains (Montell and Goodman 1988) exhibit a low degree of homology whereas regions comprising one of the short arms are conserved.

## References

Chiquet M, Masuda-Nakagawa L, Beck K (1988) Attachment to an endogenous laminin-like protein initiates sprouting by leech neurons. J Cell Biol 107 : 1189-1198

Engel J, Odermatt E, Engel A, Madri JA, Furthmayr H, Rohde H, Timpl R (1981) Shapes, domain organization and flexibility of laminin and fibronectin, two multifunctional proteins of the extracellular matrix. J Mol Biol 150 : 97 - 120

Masuda-Nakagawa L, Beck K, Chiquet M (1988) Identification of molecules in leech extracellular matrix extracts that promote neurite outgrowth. Proc R Soc Lond B 235 (in press)

McCarthy RA, Beck K, Burger MM (1987) Laminin is structurally conserved in the sea urchin basal lamina. EMBO J 6 : 1587 - 1593

Montell DJ, Goodman CS (1988) Drosophila substrate adhesion molecule: Sequence of laminin B1 chain reveals domains of homology with mouse. Cell 53 : 463 - 473

Paulsson M (1987) Noncollagenous proteins of basement membranes. Collagen Rel Res 7 : 443 - 461

Paulsson M, Aumailley M, Deutzmann R, Timpl R, Beck K, Engel J (1987) Laminin-nidogen complex. Extraction with chelating agents and structural characterization. Eur J Biochem 166 : 11 - 19

# Triple Coiled-Coil Regions of Laminin: Specificity and Chain Stability

I. Hunter, K. Beck[*], T. Schulthess and J. Engel.
Department of Biophysical Chemistry,
Biocentre of the University of Basel,
CH-4056 Basel.
Switzerland.

## INTRODUCTION

Laminin is a large (Mr $\sim$ 800000) extracellular glycoprotein which is a ubiquitous component of basement membranes. It consists of three different polypeptide chains, A (Mr $\sim$ 400000), $B_1$ and $B_2$ (both Mr $\sim$ 200000) which are linked by disulphide bonds to form a characteristic asymmetric cross structure (Engel et al, 1981).

The C-terminal regions of both the $B_1$ and $B_2$ chains are $\alpha$-helical. Sequence data are not yet available for this region of the A chain, but current models (Engel and Furthmayr, 1987) predict that it too is $\alpha$-helical and together with the B chains forms a triple helical coiled-coil, the length of the long arm.

The mechanism of laminin chain assembly remains unknown, but it is possible that recognition and interaction of sequences within the coiled-coil region of the long arm may be important. We have examined the specificity of chain assembly of an $\alpha$-helical fragment of laminin, E8 (Paulsson et al, 1985), after chain separation and $\alpha$-helix denaturation.

## RESULTS

Urea denaturation of E8 (under non-reducing conditions) was monitored by loss of $\alpha$-helix as measured by circular dichroism, and by dissociation of the native molecule into its constituent polypeptide chains during electrophoresis through a transverse linear (0-8 M) urea gradient.

In 1 M urea, there was already a 15 % reduction in the $\alpha$-helix content of E8. This suggests that there may be some unfolding of the structure, which however did not result in chain separation. By 2 M urea, the $\alpha$-helix content was reduced to 50 % and some dissociation of E8 was observed. In 4M urea, E8 dissociation was apparently complete and only 15 % $\alpha$-helix remained. Above 6M urea, no $\alpha$-helix was detected and E8 was fully dissociated into its constituent A and $B_1$-$B_2$ chains.

Urea denaturation of E8 was reversible. Removal of urea by

---

* Institute of Biophysics, University, A-4040 Linz, Austria.

dialysis resulted in virtually complete recovery of α-helix content, regardless of the initial denaturing concentration of urea.

When samples, renatured from completely dissociated E8 (4 M and 8 M urea), were run on native polyacrylamide gels, they had mobilities almost identical to that of the native protein. Second dimension SDS-PAGE, confirmed that the renatured samples had the same composition as the native material.

Native and renatured E8 could not be distinquished by low angle rotary shadowing EM.


CONCLUSIONS

Chain re-assembly in the coiled-coil E8 fragment of laminin is not a random process. When all three chains (A, $B_1$, $B_2$) are urea denatured, they specifically renature into structures which in their α-helix content, chain composition and ultrastructural appearance are indistinguishable from native E8.

These data support the concept of a triple coiled-coil structure in the long arm of laminin and indicate that sequences within this region alone carry sufficient information to direct laminin chain assembly.

Interestingly, native E8 showed a low urea stability, and it may be that other interactions eg disulphide bond formation are important in the stabilization of the laminin structure.

We are currently preparing purified A and B chains of E8 in order to characterise further the specificity and stability of laminin chain assembly. Preliminary data indicate that the B chains alone can form double coiled-coil rod structures, as have been previously reported for the small B chain fragment, 25K isolated directly from EHS tumour (Paulsson et al, 1985).


REFERENCES

Engel J, Odermatt E, Engel A, Madri J.A, Furthmayr H, Rohde H, and Timpl R (1981) Shapes, domain orgainisation and flexibility of laminin and fibronectin, two multifunctional proteins of the extracellular matrix. J Mol Biol 150:97-120.
Engel J, and Furthmayr H (1987) Electron microscopy and other physical methods for the characterisation of extracellular matrix components: Laminin, fibronectin, collagen IV, collagen VI and proteoglycans. Meth Enzymol 145:3-78.
Paulsson M, Deutzmann R, Timpl R, Dalzoppo D, Odermatt E, and Engel J (1985) Evidence for coiled-coil α-helical regions in the long arm of laminin. EMBO J. 4:309-316.

# A Fragment of Laminin Comprising the Entire Long Arm

M. Bruch, R. Landwehr and J. Engel
Department of Biophysical Chemistry
Biocenter of the University of Basel
CH-4056 Basel, Switzerland

## Introduction

Laminin is one of the major noncollagenous protein of the extra-
cellular matrix. It consists of three nonidentical polypeptide
chains (designated A, $B_1$ and $B_2$) which are arranged into the
structure of an elongated cross with three short arms and one long
arm. The organization and insertion of the laminin molecule in the
basement membrane may involve fixation of the divalent cation
calcium, since laminin can be extracted from basement membrane
containing tissues by calcium sequestrating reagents (Paulsson et
al. 1987). In vitro studies have shown that laminin aggregates in
the presence of calcium (Yurchenco et al. 1985).

In recent studies (Paulsson et al. 1988) various proteolytic
enzymes have been used to probe for stabilization of laminin by
calcium. By a similar approach we have investigated the effect of
calcium ions on the proteolytic digestion by cathepsin G, a
cationic proteinase present in polymorphonuclear leukocytes. We
report here on the ability of cathepsin G to produce a long arm
fragment selectively in the presence of calcium.

## Results and Discussion

Cathepsin G a neutral serine-protease was tested for its ability
to produce proteolytic fragments of laminin. The limited
proteolytic digestion was carried out at 37°C at an enzyme to
substrate ratio of 1:100 in the presence of 5 mM calcium or in the
presence of 5 mM EDTA. As revealed by the time course of the
proteolytic digestion, the presence of calcium in the reaction

buffer produces a different peptide pattern than in its absence. Two high molecular fragments which were detectable in the presence of calcium were absent when calcium was removed from the reaction medium by addition of EDTA. This was interpreted as being due to an increased stability of the laminin structure by calcium ions.

The differential susceptibility of laminin to digestion by cathepsin G allowed us to produce a new fragment of laminin comprising the entire long arm. Purification of this fragment was achieved by a two step procedure namely by ion-exchange on a Mono Q column and by gel filtration on a Superose 6 column. According to electron microscopy the new fragment has the shape of the long arm of laminin. The measurements of the length of the arm from the end of the terminal globe to the proteolytic cleavage site results in 77 ± 7 nm. This length corresponds exactly to the length of the long arm of intact laminin. The rod like region reveals a kink probably at the N-terminus of fragment E8. The far ultraviolet circular dichroism spectrum contained a single negative peak with a minimum value of -16'800° $cm^2$/dmol at 208 nm. Evaluation of the secondary structure indicates that this long arm fragment contains a considerable amount of α helix. In previous proteolytic fragmentations of laminin only E8 was isolated and the region between its N-terminus and the cross was lost. The new fragment may be used in exploring the properties and functions of the upper long arm region which so far was not available in a fragment.

Paulsson M, Aumailley M, Deutzmann R, Timpl R, Beck K, Engel J (1987) Laminin-nidogen complex. Extracting with chelating agents and structural characterization. Eur J Biochem 166:11-19

Paulsson M, Saladin K and Landwehr R (1988) Binding of $Ca^{2+}$ influences susceptibility of laminin to proteolytic digestion and interactions between domain-specific laminin fragments. Eur J Biochem, in press

Yurchenco P, Tsilibary E, Charonis A, Furthmayr H (1985) Laminin Polymerization in Vitro. Evidence for a two-step assembly with domain specificity. J Biol Chem 260:7636-7644

# 5'-Nucleotidase as Receptor for the Extracellular Matrix Proteins Laminin and Fibronectin

H.G. Mannherz, U. Stochaj, K. Flocke, P. Codogno*, M.-A. Doyennette-Moyne* and M. Aubery*

Institut für Anatomie und Zellbiologie
Robert-Koch-Str. 5
3550. Marburg, FRG

5'-Nucleotidase is a glycoprotein concentrated in the plasma membranes of many eucaryotic cells. It is an ectoenzyme, i.e. its catalytic center faces the cell exterior. By its enzymatic activity AMP is hydrolysed into adenosine and Pi. 5'-Nucleotidase purified from chicken gizzard exhibits a molecular mass of 79 kDa after SDS-PAGE and behaves like an integral membrane protein, i.e. it is only soluble in the presence of detergents and can be reconstituted into artificial phospholipid vesicles (Dieckhoff et al. 1985, 1987)

Recently evidence has been presented indicating a specific inter-actin of purified chicken gizzard 5'-nucleotidase with laminin and fibronectin, both components of the extracellular matrix (ECM). Thus we observed a modulation of its AMPase-activity by these com-ponents of the ECM, i.e. an inhibition by fibronectin and a stimu-lation by laminin (Dieckhoff et al. 1986). Furthermore, polyclonal and monoclonal antibodies against 5'-nucleotidase were shown to inhibit the spreading process of chick embryonic fibroblasts (CEF) on laminin -,but not on fibronectin substratum (Codogno et al. 1988). Concomitant to the inhibition of CEF spreading the formation of intracellular stress fibres is impaired. From these results it was speculated that 5'-nucleotidase functions as a signal trans-ducer molecule through the plasma membrane connecting certain com-ponents of the ECM to the intracellular microfilament system. This hypothesis appeared to be supported by a number of reports indi-cating a direct interaction of 5'-nucleotidase and actin (Mescher et al. 1981, Dieckhoff & Mannherz 1985). This hypothesis neces-sitates 5'-nucleotidase to be a spanning membrane protein, i.e. to

*Unité INSERM, Biomédicale Saints-Péres, Paris,
 France

possess functionally different domains on both sites of the
phospholipid bilayer. In this report we analyse the mode of attach-
ment of chicken gizzard 5'-nucleotidase to the lipid bilayer and
present further evidence for its direct interaction with laminin
and fibronectin.

Reconstitution of 5'-nucleotidase into artificial unilamellar
phospholipid vesicles produces a mixed liposome population contain-
ing the enzyme in either inside-out or outside-out orientation
(Dieckhoff et al. 1987). These liposomes can be fractionated into
inside-out liposomes by affinity adsorption of the outside-out
liposomes. These inside-out liposomes were anylsed by protein
modifying techniques for the presence of a presumptive cytoplasmic
domain of 5'-nucleotidase. Using such techniques no evidence for a
cytoplasmic domain could be obtained. Therefore we have tested the
possibility of an anchorage of 5'-nucleotidase by a glycan-phos-
phatidylinositol linker (PI - linker). To this aim a number of
phospholipases were tested for their ability to liberate recon-
stituted 5'-nucleotidase from mixed liposomes and plasma membrane
preparations. The results obtained demonstrate that only PI-specific
phospholipase C is able to transform the enzyme from a hydrophobic
into a hydrophilic form. After addition of detergent about 100%
of the reconstituted enzyme is liberated from mixed liposomes
whereas only 50% of the total AMPase activity is liberated from
plasma membranes from chicken gizzard and a human tumor cell line.
Immunoblots of plasma membrane preparations or crude homogenates
of chicken gizzard revealed the presence of immunreactive bands of
higher molecular mass than 79 kDa. Similar observations were made
using chicken myoblasts and myotubes. Therefore the existence of
isoforms of 5'-nucleotidase appears probable differing in their
mode of attachment to the plasma membrane like the N-CAMs (Hemperly
et al. 1986), i.e. the immunreactive forms of about 88 and 116 kDa
could possess a classical proteinaceous membrane spanning domain.
Further experimental evidence will, however, be necessary to
definitively decide this question.

The interaction of purified 5'-nucleotidase with laminin and fibro-
nectin was probed by a number of techniques: cosedimentation by
sucerose gradient centrifugation, affinity adsorption to immobilized
laminin and fibronection. Using these techniques the interaction of
5'-nucleotidase with both laminin and fibronectin could be proved
to be specific, since (i) no binding to or competition with BSA or

other unrelated proteins occurred (affinity adsorption, cosedimen-
tation and a dot blot overlay technique) and (ii) binding of radio-
labelled 5'-nucleotidase to laminin and fibronectin was suppressed
by unlabelled enzyme and an excess of laminin or fibronectin (over-
lay technique). This competition could only be obtained by an excess
of the homologeous ECM component. This result seems to give evidence
for distinct binding sites for laminin and fibronectin on 5'-nucleo-
tidase. Preliminary results seem to indicate that 5'-nucleotidase
binds to the socalled E1' and E8 fragments of laminin.

During the course of these experiments we have tested a number of
different preparations of laminin (from the EHS-tumor) and fibro-
nectin (from human serum). Binding of 5'-nucleotidase to these ECM
components could reproducibly be demonstrated by the techniques
listed above. In contrast the initially reported modulation of
5'-nucleotidase AMPase activity (Dieckhoff et al. 1986) was only
rarely found. The reason for this  inconsistency is at present
unclear. Two explanation are possible: (i) other copurified com-
ponents are reponsible or (ii) the AMPase modulation depends on
labile conformations of these large glycoproteins, which may easily
be lost during their purification and storage.

In summary, our results give evidence for a specific interaction of
purified 5'-nucleotidase with laminin and fibronectin. Purified
5'-nucleotidase is attached to the plasma membrane by a PI-linker,
although the existence of variants with other types of membrane
anchorage appears probable. In vivo experiments with CEF have given
an indication for the involvement of this enzyme in cell spreading
on laminin substratum and for its possible linkage to the micro-
filament system (Codogno et al. 1988). Further experimentation will
be aimed to the characterization of the 5'-nucleotidase isoforms
and their involvement in the cell adhesion process on laminin and
fibronectin.

Codogno P, Doyennette-Moyne M-A, Aubery M, Dieckhoff J, Lietzke R, Mannherz HG (1988) Exp. Cell Res. 174:344-354

Dieckhoff J, Knebel H, Heidemann M, Mannherz HG (1985) Eur. J. Biochem. 151:377-383

Dieckhoff J, Mannherz HG (1985) Biochim. Biophys. Acta 829:209-220

Dieckhoff J, Mollenhauer J, Kühl U, Niggemeyer B, von der Mark K, Mannherz HG (1986) FEBS Lett. 195:82-86

Dieckhoff J, Niggemeyer B, Lietzke R, Mannherz HG (1987) Eur. J. Biochem. 162:451-459

Hemperly JJ, Edelman GM, Cunningham BA (1986) Proc. Natl. Acad. Sci. USA 83:9822-9826

Mescher MF, Jose MJL, Balk SP (1981) Nature 289:139-144

# Monoclonal Antibody 127 Recognizes a Subpopulation of Chicken Hexabrachion/Tenascin

V.A.Lightner, C.Pegram, D.Bigner, and H.P.Erickson

Departments of Cell Biology and Pathology

Duke University Medical Center

Durham, NC  27710  USA

Hexabrachion/tenascin is an extracellular matrix protein with a distinct spatial and temporal distribution in tissue (Erickson and Lightner, 1988).  In chicken embryo fibroblast cultures it is isolated as a hexameric protein with disulfide linked subunits of 250, 225 and 215 Kd (Chiquet and Fambrough, 1984a,b; Erickson and Lightner, 1988). These subunits have very similar proteolytic cleavage patterns, indicating they are related peptides (Chiquet and Fambrough, 1984b). Pulse chase experiments (Chiquet and Fambrough, 1984b) and recently published sequence data (Jones et al.,1988; Pearson et al.,1988) suggest they result from alternative splicing of the tenascin mRNA. However, nothing is known about the functional differences between these subunits or how they are assembled into the hexameric structure.

Recently, we have isolated a monoclonal antibody (Mab) to human tenascin which cross reacts with chicken tenascin.  This Mab, which recognizes only the larger subunit of tenascin, has allowed us to examine the partitioning of the subunits in the assembly of hexabrachion structures.

## Preparation of Mab 127

BALB/AnNcrIBR mice were immunized with 5 µg of purified human tenascin (Erickson and Taylor, 1987) and boosted on days 24, 25 and 26 with 1 µg of protein prior to sacrifice and fusion of spleen cells with myeloma cell line P3X63/Ag8.653 as previously described (Bourdon et al.,1983). After selection, hybridomas were screened by ELISA (Engvall and Perlmann, 1972) on 96 well Falcon plastic plates previously coated with either 0.75 µg/ml human tenascin or 1 µg/ml chicken tenascin. Mab 45.6, an $IgG_{2b}$ immunoglobulin of no known specificity (Bourdon et al.,1983), was used as a control for ELISA, Western blotting and antibody mapping.  Mab 127, an $IgG_1$ subclass, was selected for further study on the basis of its reactivity to both the human and the chicken proteins.  Cloning in methocell and production of ascites was as previously described (Bourdon et al.,1983).

## Mab 127 stains only the large subunit of tenascin

Purified chicken tenascin (Erickson and Taylor, 1987) was Western blotted using Mab M1 (Chiquet and Fambrough, 1984a,b) and Mab 127. As shown in figure 1a, Mab 127 reacts only with the larger subunit of tenascin. Mab M1 recognizes all three bands (the two smaller bands are not resolved in this gel). Other Mab to human tenascin that cross reacted with the chicken protein recognized all three bands (not shown). In addition, Mab 127 reacted on Western blots with human tenascin that had been N-deglycosylated using N-glycanase or O-deglycosylated using a mixture of glycanases, suggesting it recognizes a peptide epitope on the tenascin molecule (not shown).



Figure 1a : Western blotting of chicken tenascin with Mab M1 and 127
Figure 1b : SDS PAGE of chicken tenascin purified with Mab 127 and M1

## Purification of large chicken hexabrachions using Mab 127

Mab 127 was coupled to cyanogen bromide activated Sepharose 2B. The column was used to purify chicken tenascin from culture supernatant of confluent 10 day chicken embryo fibroblasts. As shown in figure 1b, the material eluted from the 127 column differs from that purified by M1 affinity chromatography in lacking the two smaller subunits of tenascin. The 127 purified tenascin also show a higher proportion of cross-linked dimers when compared to the M1 purified tenascin.

## Mapping the Mab 127 epitope by rotary shadowing

Purified human tenascin in 0.2 M ammonium formate, 30% glycerol, pH 7.5 was incubated with Mab 127 at 35 µg/ml overnight at 4°C prior to rotary shadowing as previously described (Erickson and Iglesias, 1984). There was a very small yield of labeling with the antibody (fewer than 1% of the hexabrachions had an attached antibody). Where labeling



Figure 2 : Rotary shadowing of Mab 127 - tenascin complexes. 115,000 X

occurred, the antibody bound approximately 1/3 of the length from the terminal knob of the hexabrachion arm (figure 2). No labeling was seen with the control Mab 45.6. Because of the low number of labeled hexabrachions, this mapping can only be considered provisional.

## Discussion

Mab 127 is a monoclonal antibody to human tenascin which cross reacts with the chicken tenascin. Mab 127 appears to react with a peptide based epitope, suggesting there are regions of conserved sequence between the chicken and human tenascin.

On Western blots, Mab 127 recognizes only the larger subunit of chicken (Fig 1a) and human tenascin (not shown). Several lines of evidence suggest these represent alternatively spliced forms of tenascin (Chiquet and Fambrough, 1984b; Jones et al.,1988; Marton et al.,1987; Pearson et al.,1988). The blots indicate a conservation of spliced domains in the two species. When Mab 127 was used to affinity purify chicken tenascin, only hexabrachions with larger arms were isolated. This suggests that the assembly of subunits has some selectivity allowing the assembly of homogeneous hexamers. Alternatively, there may be subpopulations of embryonic chicken fibroblasts that make the different forms of hexabrachion. The functional differences of these forms of hexabrachions is not known. In contrast to the chicken embryo fibroblast, the shorter subunits of the human hexabrachion are present in small amounts relative to the predominant 320 Kd subunit (Erickson and Lightner,1988). When human tenascin is affinity purified using Mab 81C6 (Bourdon et al.,1983), an antibody that only recognizes the larger subunit, both large and small subunits are seen on reducing gels, suggesting the hexamer incorporates all sizes in its assembly.

Bourdon, M.A., Wikstrand, C.J., Furthmayr, H., Matthews, T.J. and Bigner, D.D. (1983) Cancer Res. 43:2796-2805
Chiquet, M. and Fambrough, D.M. (1984a) J.Cell Biol. 98:1937-1946
Chiquet, M. and Fambrough, D.M. (1984b) J.Cell Biol. 98:1926-1936
Engvall, E. and Perlmann, P. (1972) J.Immunol. 109:129-135
Erickson, H.P. and Iglesias, J.L. (1984) Nature 311:267-269
Erickson, H.P. and Lightner, V.A. (1988) Adv.Cell Biol. 2:in press
Erickson, H.P. and Taylor, H.C. (1987) J.Cell Biol. 105:1387-1394
Jones, F.S., Burgoon, M.P., Hoffman, S., Crossin, K.L., Cunningham, B.A. and Edelman, G.M. (1988) Proc.Natl.Acad.Sci.U.S.A. 85:2186-2190
Marton, L.S., Gulcher, J.R. and Stefansson, K. (1987) J.Cell Biol. 105:135a, (Abstract)
Pearson, C.A., Pearson, D., Shibahara, S., Hofsteenge, J. and Chiquet-Ehrismann, R. (1988) EMBO J. 7:2977-2982

# Functional Domains of Tenascin

Matthias Chiquet[1], Susanne Schenk[1], Peter End[1], Konrad Beck[1], Carolyn Pearson[2], and Ruth Chiquet-Ehrismann[2]

Biozentrum der Universität[1] and Friedrich Miescher Institut[2]

CH-4000 Basel

Switzerland

Tenascin from chick embryos is an extracellular matrix protein with disulfide-linked subunits of $M_r$ = 190-220,000 and a six-armed appearance in the electron microscope (EM) (cf. Chiquet-Ehrismann et al 1988). Its expression during development suggests a function in morphogenesis (Chiquet-Ehrismann et al 1986). Several activities of tenascin can be assayed in vitro: hemagglutination, interference with fibronectin-mediated cell spreading, promotion of neurite outgrowth, and stimulation of DNA synthesis (Chiquet-Ehrismann et al 1986, 1988, Chiquet 1989). We are trying to assign various functions to specific domains on the molecule.

Whereas oligomeric tenascin was obtained from embryonic fibroblasts, we were able to isolate molecules from adult chick gizzard with an $M_r$ of 200,000 on SDS gels under both reducing and nonreducing conditions. Based on mapping with monoclonal antibodies (mAb's) and EM studies, this material represented apparently intact tenascin arms. Monomeric tenascin had no hemagglutinating activity but was active in all other functional assays (Table I).

Fragments of $M_r$ = 80,000, which were still partially disulfide-linked to oligomers, were obtained by pepsin digestion of fibroblast tenascin. These fragments could be isolated by means of mAb M1 which binds to the thin proximal part of the tenascin arms (cf. Chiquet-Ehrismann et al 1988). cDNA sequencing of this region of the tenascin subunit revealed 13 EGF-like repeats in tandem (Pearson et al 1988). The pepsin fragments had none of the tenascin effects on cell adhesion, but still stimulated thymidine incorporation by serum-starved 3T3 fibroblasts (Table I).

Table I: Schematic representation of the structure and function of chick tenascin and of fragments thereof.

| | hexameric | monomeric | pepsin fragment |
|---|---|---|---|
| EM structure |  |  |  |
| $M_r$ nonreduced | $1.2 \times 10^6$ (trimers: 600,000) | 200,000 | 240,000 160,000 80,000 |
| $M_r$ reduced | 190-220,000 | 200,000 | 80,000 |
| Hemagglutination | + | - | - |
| Inhibition of cell spreading | + | + | - |
| Neurite outgrowth | + | + | - |
| Stimulation of DNA synthesis | + | + | + |

Conversely, a cell binding site could be localized on the distal glob-ules of the tenascin arms. mAb 68 which decorated this domain as re-vealed by EM (Chiquet-Ehrismann et al 1988) inhibited hemagglutin-ation, effects on cell spreading, and neurite outgrowth mediated by tenascin.

Thus, we demonstrated that an oligomeric structure of tenascin is needed for its hemagglutinating activity but not for other functions. Moreover, we were able to identify two separate functional domains on the tenascin subunit.

Chiquet-Ehrismann R, Mackie EJ, Pearson CA, Sakakura T (1986) Tenascin: an extracellular matrix protein involved in tissue interactions during fetal development and oncogenesis. Cell 47: 131-139
Chiquet-Ehrismann R, Kalla P, Pearson CA, Beck K, Chiquet M (1988) Tenascin interferes with fibronectin action. Cell 53:383-390
Chiquet M (1989) Tenascin / J1 / cytotactin: the potential function of hexabrachion proteins in neural development. Dev. Neurosci., in press
Pearson CA, Pearson D, Shibahara S, Hofsteenge J, Chiquet-Ehrismann R (1988) Tenascin: cDNA cloning and induction with TGF. EMBO J 7:2677

# Complex Formation of Endothelial Cell Thrombospondin with Heparin and Fibronectin

R. Dardik and J.Lahav

Department of Polymer Research

The Weizmann Institute of Science

Rehovot

Israel

## INTRODUCTION

Thrombospondin (TSP) is a large glycoprotein synthesized, secreted and incorporated into the extracellular matrix by various cell types in culture (see Silverstein et al.,1986 for a recent review). TSP synthesis is inversely proportional to cell density (Mumby et al.,1984a). Its matrix incorporation is age-dependent (Kramer et al.,1985) and can be regulated by specific growth factors (Majack et al.,1985), suggesting that TSP is involved in cell growth and development. A recent report shows that cell-associated TSP is essential for smooth muscle cell proliferation (Majack et al., 1988). TSP was found to promote cell-substrate adhesion of several human sqamous carcinoma cell lines, but not that of melanoma or glioma cell lines (Varani et al.,1986). Among the tumor cell lines tested there was direct correlation between the ability of the cells to synthesize and bind TSP and their ability to utilize the protein as an adhesion factor (Riser et al.,1988). It seems, however, that such correlation is not a general phenomenon, since endothelial cells, capable of both TSP synthesis and binding, do not adhere to TSP covered surfaces. Moreover, TSP was shown to inhibit cell-substrate adhesion of endothelial cells (Lahav et al., 1987; Lahav,1988). TSP is a multifunctional protein capable of interacting with a variety of macromolecules, among them fibronectin (FN) (Lahav et al., 1982; Lahav et al.,1984), heparin (Lawler et al.,1981), collagen (Lahav et al.,1982; Mumby et al.,1984b)˙and sulfated glycolipids (Roberts et al.,1985). It should be noted, that all these molecules are constituents of the extracellular matrix, suggesting that TSP forms complexes with other matrix components when deposited into the extracellular matrix. Indeed, it was shown that TSP codistributes with FN and von Willebrand factor in the extracellular matrix of bovine aortic endothelial cells (Dreyfus and Lahav,1988; submitted for publication). In vivo, TSP was shown to be an endogenous component of extracellular matrices of a variety of human tissues (Wight et al.,1985).

TSP is also stored in resting platelets; it is secreted and can be expressed on platelet surface following platelet activation (Lawler et al.,1978; Phillips et al.,1980). The platelet and cell-derived forms, although indistinguishable on the basis of molecular weight and amino acid composition (McPherson et al.,1981), differ in their susceptibility to proteolysis, the cellular being more resistant (Clezardin et al.,1986; Dardik and Lahav,1987). Our results, reported below, reveal additional important differences between the platelet and cell-originating forms of TSP.

With the aim of understanding the role of TSP in extracellular matrix assembly

and in cell-matrix interaction, we have focused on elucidation of the structure-function relationship of endothelial cell TSP (EC-TSP). In this report we present the results of our study of the interaction between EC-TSP and two extracellular matrix components, namely heparin and FN.

## CHARACTERIZATION OF HEPARIN AND FIBRONECTIN BINDING DOMAINS OF EC-TSP

Being a multifunctional protein, TSP can be proteolyzed under well defined conditions to give separate binding domains which are relatively resistant to proteolysis. Using three serine proteases (thrombin, trypsin and chymotrypsin) in combination with affinity cromatography, we characterized the binding domains of EC-TSP to heparin and FN, both of which are important constituents of the extracellular matrix. We find that EC-TSP has two different binding sites for both heparin and FN. Since TSP has a $Ca^{2+}$-sensitive structure and is much more sensitive to proteolysis in the absence than in the presence of $Ca^{2+}$ (Lawler et al., 1982), we also studied the effect of $Ca^{2+}$ removal on the production and binding activities of the functional domains.

Limited proteolytic digestion of TSP with chymotrypsin (1:20 enzyme to substrate ratio, 5 min at room temperature) in the presence of $Ca^{2+}$ produced four major fragments: 160 kD C-terminal fragment, 27 kD N-terminal fragment and two fragments of 140 kD and 18 kD derived from the 160 kD fragment. Both the 160/140 kD and the 27 kD fragments, which reside on different parts of the molecule and have no overlapping segments, bind to both heparin and FN affinity columns. In the absence of $Ca^{2+}$ under the same incubation conditions chymotrypsin cleaves the 160/140 kD fragments to yield a stable core fragment of 70 kD which has both FN and heparin binding capacities, the latter being very weak. The production and the binding capacities of the 27 kD fragment are not affected by chelation of $Ca^{2+}$ with EDTA. Using a solid-phase binding assay, we quantitated the binding of the 70 kD and the 27 kD chymotryptic fragments to surface-adsorbed FN. We found that the affinity of the 70 kD fragment to FN is somewhat higher than that of the 27 kD fragment. (Dissociation constants for the 70 kD and the 27 kD fragments were $4.1 \times 10^{-7}M$ and $8.8 \times 10^{-7}M$, respectively). In addition, we find that soluble heparin competitively inhibits the binding to surface-immobilized FN of intact TSP and of its 27 kD fragment, but does not affect the binding of the 70 kD fragment. These observations are in good agreement with our results reported earlier, showing that the 27 kD fragment contains the high affinity heparin binding site, whereas the affinity of the 70 kD fragment is low (Dardik and Lahav, 1987).

Thus, EC-TSP has binding sites for both heparin and FN in both the 27 kD N-terminal fragment and in the 70 kD core fragment. In this respect EC-TSP differs from platelet TSP which has only one binding site for each component: a heparin binding site in the 27 kD fragment and a FN binding site in the 70 kD fragment

(Lawler et al.,1986).
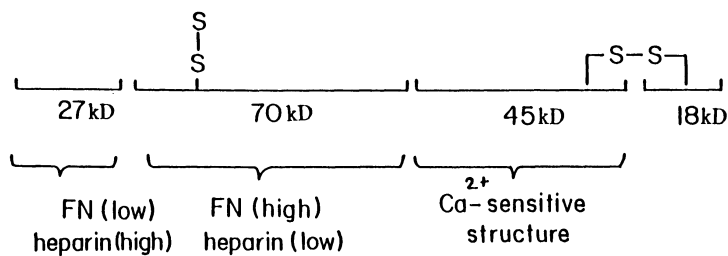


Figure 1. Alignment of the heparin and FN binding fragments of EC-TSP produced by chymotrypsin. High and low binding affinities are indicated by (high) and (low), respectively.


## PROTECTION OF EC-TSP FROM EXTENSIVE DEGRADATION AND LOSS OF BINDING ACTIVITY BY COMPLEXATION.

Thrombin digestion of soluble TSP in the absence of $Ca^{2+}$ produces fragments smaller than those produced under the same conditions in the presence of $Ca^{2+}$. However, cleavage by thrombin of $Ca^{2+}$-depleted TSP prebound to either heparin or FN produces fragments identical to those obtained in the presence of $Ca^{2+}$, suggesting that complexation of TSP prevents the denaturation of its $Ca^{2+}$-sensitive structure caused by removal of $Ca^{2+}$ (Lahav et al.,1987).

Similarly to chymotrypsin, tryptic fragmentation of TSP in the presence of $Ca^{2+}$ can yield large C-terminal fragments of 160 and 140 kD. In contrast, however, and in spite of their large size, tryptic fragments lose both FN and heparin binding capacities. It turns out, that prebinding of TSP to either heparin or FN prior to tryptic digestion preserves the binding capacities of these fragments to both components.

Thus, complexation of TSP to either heparin or FN stabilizes its conformation, resulting in increased resistance to proteolysis and protection of binding capacities.


## SUMMARY

Our results demonstrate that in contrast to platelet TSP, EC-TSP has multiple binding domains to FN and heparin. In addition, we find that complex formation with other matrix components stabilizes the conformation of TSP and protects it from extensive proteolysis and loss of function. We, therefore, suggest that cellular TSP can function differently and under more dire conditions than platelet secreted TSP.

REFERENCES

Clezardin P, Hunter NR, Lawler JW, Pratt DA, McGregor JL, Pepper DS, Dawes J (1986)
Structural and immunological comparison of human thrombospondins isolated from
platelets and from culture supernatants of endothelial cells. Eur J Biochem 159:569-579

Dardik R, Lahav J (1987) The structure of endothelial cell thrombospondin: characterization
of the heparin binding domains. Eur J Biochem 168:347-355

Lahav J, Schwartz MA, Hynes RO (1982) Analysis of platelet adhesion with a radioactive
chemical crosslinking reagent: interaction of thrombospondin with fibronectin and
collagen. Cell 31:253-262

Lahav J, Lawler J, Gimbrone MA (1984) Thrombospondin interactions with fibronectin and
fibrinogen: mutual inhibition in binding. Eur J Biochem 145:151-156

Lahav J, Dardik R, Stein O (1987) Endothelial cell thrombospondin and its possible role in
cell adhesion.In: Gartner TK and Walz DA (eds) Seminars in thrombosis and hemostasis,
vol 13.Thieme Medical Publisher, Inc.,New York, p 352

Lahav J (1988) Thrombospondin inhibits endothelial cell adhesion. Exp Cell Res 177:199-204

Lawler JW, Slayter HS, Colligan JE (1978) Isolation and characterization of a high molecular
weight glycoprotein from human blood platelets. J Biol Chem 253:8609-8616

Lawler JW, Slayter HS (1981) The release of heparin binding peptides from platelet
thrombospondin by proteolytic action of thrombin,
plasmin and trypsin. Thromb Res 22:267-279

Lawler J, Chao FC, Cohen CM (1982) Evidence for calcium-sensitive structure in platelet
thrombospondin. J Biol Chem 257:12257-12265

Lawler J, Conolly JE, Ferro P, Derick LH (1986) Thrombin and chymotrypsin interactions
with thrombospondin. In: Fenton JW II, Shuman D, Walz DA (eds) Ann NY Acad Sci,
vol 485. The New York Academy of Sciences, New York, p 273

Kramer RH, Fuh GH, Bensch KG, Karasek MA (1985) Synthesis of extracellular matrix
glycoproteins by cultured microvascular endothelial cells isolated from dermis of neonatal
and adult skin. J Cell Physiol 123:1-9

Majack RA, Cook SC, Bornstein P (1985) Platelet-derived growth factor and  heparin-like
glycosaminoglycans regulate thrombospondin synthesis and deposition in the matrix by
smooth muscle cells. J Cell Biol 101:1059-1071

Majack RA, Goodman LV, Dixit VM (1988) Cell surface thrombospondin is functionally
essential for smooth muscle cell proliferation. J Cell Biol 106:415-422

McPherson J, Saga H, Bornstein P (1981) Isolation and characterization of a glycoprotein
secreted by aortic endothelial cells in culture: apparent identity with platelet
thrombospondin. J Biol Chem 256:11330-11336

Mumby SM, Abbott- Brown D, Raugi GJ, Bonstein P (1984a) Regulation of thrombospondin
secretion by cells in culture. J Cell Physiol 120:280-288

Mumby SM, Raugi GJ, Bornstein P (1984b) Interactions of thrombospondin with extracellular
matrix proteins: selective binding to type V collagen. J Cell Biol 98:646-652

Phillips DR, Jennings LK, Prasanna HR (1980) Ca-mediated association of glycoprotein G
(thrombin-sensitive protein, thrombospondin) with human platelets. J Biol Chem
255:11629-11632

Riser BL, Varani J, O'Rourke K, Dixit V (1988) Thrombospondin binding by human
squamous carcinoma and melanoma cells:relationship to biological activity. Exp Cell Res
174:319-329

Roberts DD, Haverstick DM, Dixit VM, Frazier WA, Santoro SA, Ginsburg V (1985) The
platelet glycoprotein thrombospondin binds specifically to sulfated glycolipids. J Biol
Chem 260:9405-9411

Silverstein RL, Leung LLK, Nachman RL (1986) Thrombospondin: a versatile multifunctional
glycoprotein. Arteriosclerosis 6:245-253

Varani J, Dixit VM, Fligiel SEG, McKeever PE, Carey TS (1986) Thrombospondin-induced
attachment and spreading of human squamous carcinoma cells. Exp Cell Res 167:376-390

Wight TN, Raugi GJ, Mumby SM, Bornstein P (1985) Light microscopic immunolocation of
thrombospondin in human tissues. J Histochem Cytochem 33:295-302

# Functional Aspects of Proteoglycan Domain Structure

Mats Paulsson and Matthias Mörgelin
Department of Biophysical Chemistry
Biocenter of the University of Basel
Klingelbergstrasse 70
CH 4056 Basel
Switzerland

## Introduction

   Proteoglycans, a class of extracellular macromolecules
characteristically consisting of a protein core substituted with
one or several glycosaminoglycan chains, have a profound
influence on the physical properties of the extracellular matrix
and the pericellular space. Many proteoglycans have a multidomain
structure where distinct biological properties can be assigned to
particular, often well conserved portions of the protein core. In
the present chapter we review the functional aspects of
proteoglycan domain structure using the large aggregating class
of interstitial matrix proteoglycans as an example. These
molecules are abundant in many types of extracellular matrix, but
most pronouncedly so in cartilage. There they do by formation of
large aggregates with hyaluronate fill the space between collagen
fibers and make the tissue resilient to pressure (for review see
Heinegård and Paulsson, 1984). Interstitial matrix does in
addition contain two or more distinct populations of small
proteoglycans. At least certain members of the class of small
proteoglycans have affinity for collagen fibrils and are thought
to regulate collagen fibril formation (Scott and Orford, 1981;
Vogel et al, 1984).

Other important classes of proteoglycans are found at the cell surface as integral membrane proteins or in specialized matrix structures such as basement membranes. Cell surface proteoglycans are likely to be of importance for the interactions of cells with components of the interstitial matrix, and for basement membrane proteoglycans important functions have been proposed in the determination of filtration properties and in matrix assembly (for review see Hassel et al, 1986; Evered and Whelan, 1986).

## Structure of large aggregating cartilage proteoglycans

A typical hyaline cartilage contains up to 100 mg/ml of proteoglycans most of which are of the large aggregating kind. Because of the slow but continuous physiological turnover of the matrix, a large proportion of these are at different stages of degradation as compared to the original biosynthesis product. A major difficulty is therefore to distinguish between metabolically related subpopulations of proteoglycans occurring as a result of degradation and potentially existing subpopulations due to translation of different classes of mRNA or significantly different glycosylation. A number of studies have, however, shown the presence of two distinct populations in tissue samples, which may be separated by composite agarose/acrylamide gel electrophoresis (McDevitt and Muir, 1971) or on a preparative scale by sucrose density gradient centrifugation (Heinegård et al, 1985b). The larger of these has a total $M_r$ of 3.5 x $10^6$ with a core protein of $M_r$ 210 000 and has a large region densely substituted with a total of 100 chains of chondroitin sulphate (Heinegård et al, 1985b). The smaller, $M_r$ 1.3 x $10^6$, has a core protein of $M_r$ 95 000 and appears to contain separate regions substituted with primarily chondroitin sulphate or keratan sulphate. Each of these populations is polydisperse, at least in part due to physiological proteolytic degradation. In foetal tissue only the large population is found, while the smaller one accumulates with maturation (Inerot and Heinegård, 1983). So far

only a single core protein of $M_r$ 220 000 has been identified by cDNA techniques but the presence of alternatively encoded forms of this molecule can not yet be excluded (Doege et al, 1987).

When such large aggregating cartilage proteoglycans were studied by electron microscopy using the glycerol spraying/rotary shadowing technique (Wiedemann et al, 1984; Paulsson et al, 1987) a pronounced domain structure was revealed (Fig. 1). Correlation of the morphological data with the plentitude of earlier biochemical information and the simultaneously emerging cDNA and protein sequences (Doege et al, 1986, 1987; Sai et al, 1986; Oldberg et al, 1987; Neame et al, 1987) has resulted in the structural model depicted in Fig. 2. An N-terminal, globular
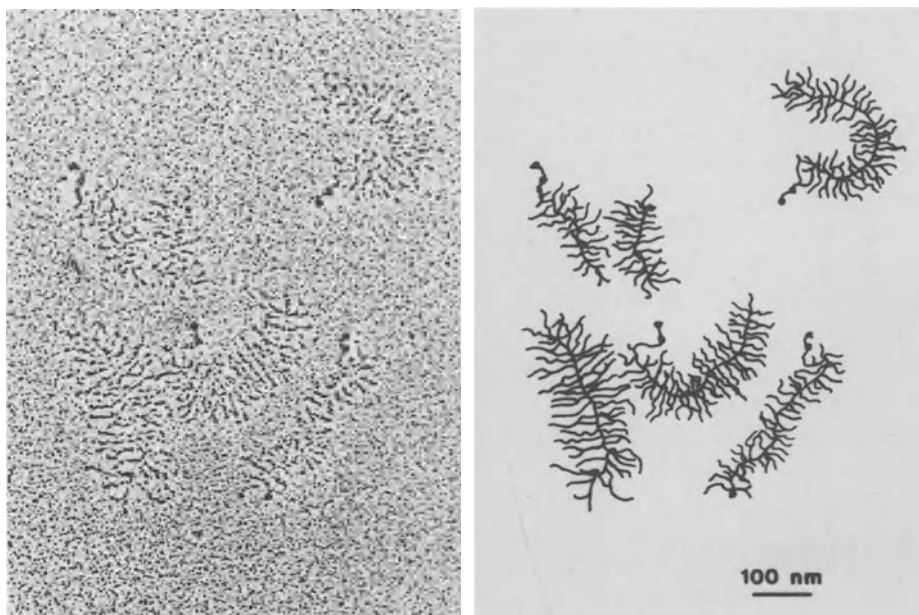


Fig. 1: Electron micrographs of monomeric cartilage proteoglycans of the large aggregating class obtained after glycerol spraying/rotary shadowing.

N-Terminus                                                    C-Terminus

E1(*l*)

G1  G2

E2(*L*)

G3
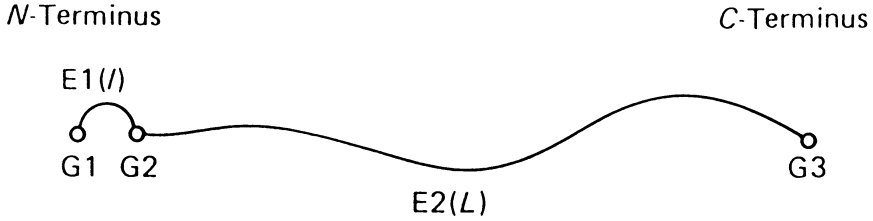
Fig. 2: Schematic representation of the domain structure of the core protein of large aggregating cartilage proteoglycans. The lengths l = 30 nm and L = 280 nm were obtained by measurements of the contour lengths of E1 and E2, respectively (From Paulsson et al, 1987, by courtesy of Biochem. J.).

protein domain G1 corresponds to the previously described hyaluronate binding region (Heinegård and Hascall, 1974). In the direction of the C-terminus this is followed by a 30 nm long extended domain E1 and a second globular domain G2, which shows a high degree of sequence homology to G1. Beyond G2 the 280 nm long, major extended domain E2 follows, carrying the bulk of the glycosaminoglycan side chains. Sequence analysis allows the division of this segment into four distinct subdomains which all contain the Ser-Gly sequences required for glycosaminoglycan substitution but differ with regard to the presence of other internal repeats (Doege et al, 1987). At the C-terminus yet another globular domain G3 follows, distinct from G1 and G2 in sequence but sharing homology with chicken hepatic lectin and related carbohydrate-binding proteins (Doege et al, 1986; Sai et al, 1986; Oldberg et al, 1987). When a cDNA segment corresponding to this domain was in vitro translated it could also be shown to have affinity for carbohydrates, in particular for fucose and galactose (Halberg et al, 1988). This domain G3 is, despite physiological proteolysis, present on 30-50% of the proteoglycans

in a tissue extract (Paulsson et al, 1987) and its lectin
activity is therefore likely to be of relevance in vivo even
though its physiological ligands are not yet known.

## Aggregation of cartilage proteoglycans

Cartilage proteoglycan aggregates can have a length of 4000 nm
and a diameter of 500-600 nm. They are formed by the non-covalent
interaction of typically 50 proteoglycan monomers with a single
strand of hyaluronate (for review see Heinegård and Paulsson,
1984). The interaction is stabilized by the binding of an
accessory component, link protein, which has binding sites for
both proteoglycan (Franzén et al, 1981) and for hyaluronate
(Tengblad, 1981). By proteolytic fragmentation of aggregates a
hyaluronate binding region of the proteoglycan could be defined
(Heinegård and Hascall, 1974) which corresponds to globular
domain G1 in our model (Fig. 2).

In rotary shadowed replicas link-stabilized aggregates reveal
an organization with a heavily stained central filament, made up
from the G1 domains and link proteins bound to the hyaluronate
(Fig. 3, Wiedemann et al, 1984; Mörgelin et al, 1988). This
filament appears as a continuous structure and is surrounded by a
field of fuzzy, thinner filamentous structures, corresponding to
the glycosaminoglycans on the chondroitin sulphate attachment
region E2 of the proteoglycan. In addition, some globular
structures can be seen, in particular adjacent to the central
filament and in the periphery of the aggregate.

The involvement of the various proteoglycan domains in the
formation of aggregates can be studied in more detail if the
chondroitin sulphate chains are removed by enzymatic digestion
prior to formation of the aggregate structure (Fig. 4, Mörgelin
et al, 1988). In such core protein-hyaluronate aggregates formed
in the absence of link protein (Fig. 4a) the N-terminal globules
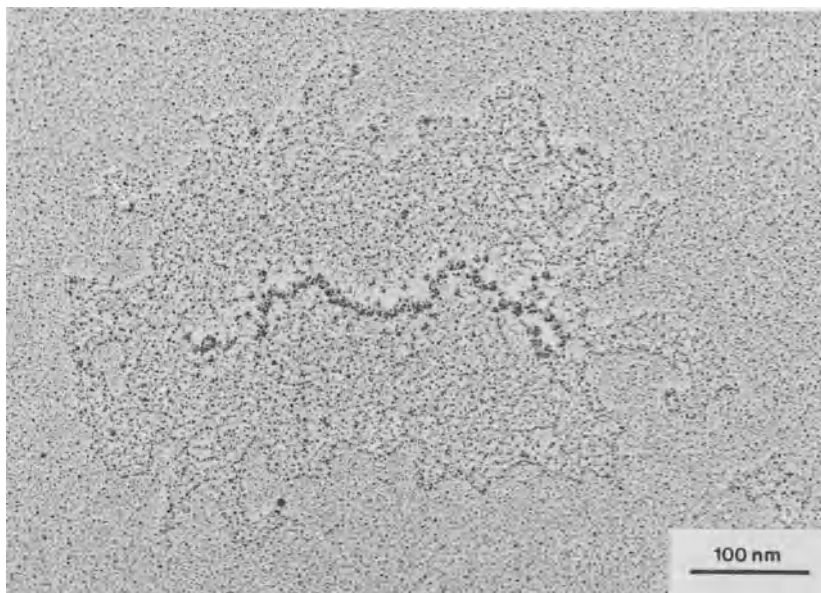
Fig. 3: Rotary shadowed image of a link stabilized cartilage proteoglycan aggregate (From Mörgelin et al, 1988, by courtesy of Biochem. J.).

G1 are seen bound to the hyaluronate with a random spacing depending on the degree of saturation, while the other domains radiate out. This demonstrates that G1 is the only part of the proteoglycan molecule which binds directly to hyaluronate, an observation which is interesting in the light of the pronounced sequence homology between G1 and G2.

When link protein is added prior to aggregate formation (Fig. 4b) the central filament takes on a condensed, continuous appearance, similar to that seen with intact proteoglycans in Fig. 3. In part this is due to the added mass contributed by the link protein to the central filament, especially as link can be incorporated in suprastoichiometric amounts as compared to proteoglycan monomer (Thornton et al, 1987). In addition, link protein might have the ability to connect adjacent G1 globules and thereby induce a cooperative set of protein-protein
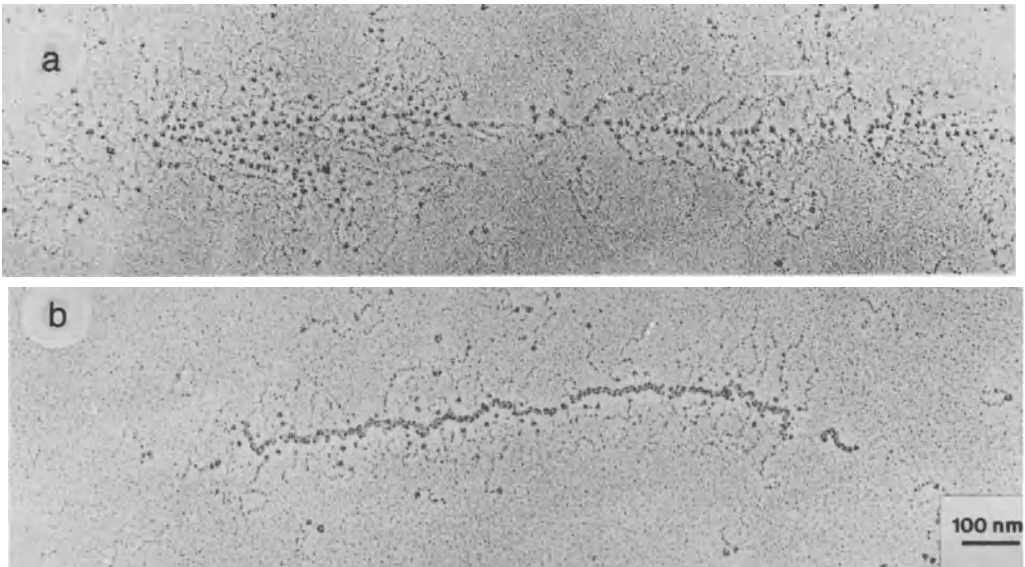
Fig. 4: Aggregates of cartilage proteoglycan core protein and hyaluronate formed in the absence (a) and presence (b) of link protein as seen after glycerol spraying/rotary shadowing (From Mörgelin et al, 1988, by courtesy of Biochem. J.).

interactions along the hyaluronate strand, contracting the whole structure. This is a very different situation from that seen with globule G1 in the absence of link protein. In this case the binding is completely non-cooperative with a minimum center to center distance of 12 nm (Mörgelin et al, 1988).

## Large aggregating proteoglycans from other types of connective tissue

Also other forms of connective tissue, such as tendon, sclera and aortic wall, contain large proteoglycans with the capacity to form aggregates with hyaluronate. When such proteoglycans were compared with those from cartilage, using immunochemical crossreactivity and peptide patterns as criteria, evidence was

found for the presence of a structure similar to the hyaluronate
binding region in all (Heinegård et al, 1985a). At the same time
also differences were noted, with the aorta proteoglycan being
the most aberrant one in this group. More recently, Krusius et al
(1987) determined a partial C-terminal sequence from a large
chondroitin sulphate proteoglycan expressed by fibroblasts. They
found a C-terminal lectin-like domain homologous but not
identical to G3 in cartilage proteoglycans. Further towards the
N-terminus they also found two repeats with an EGF-like cysteine
pattern, a structural motif not found in the cartilage
proteoglycan sequence.

Our studies on the molecular morphology of these molecules
have demonstrated large similarities in domain structure between
in particular those from sclera and tendon and those from
cartilage (Fig. 5; Mörgelin et al, in preparation). The globular
domains G1, G2 and G3 are all present interspaced by extended
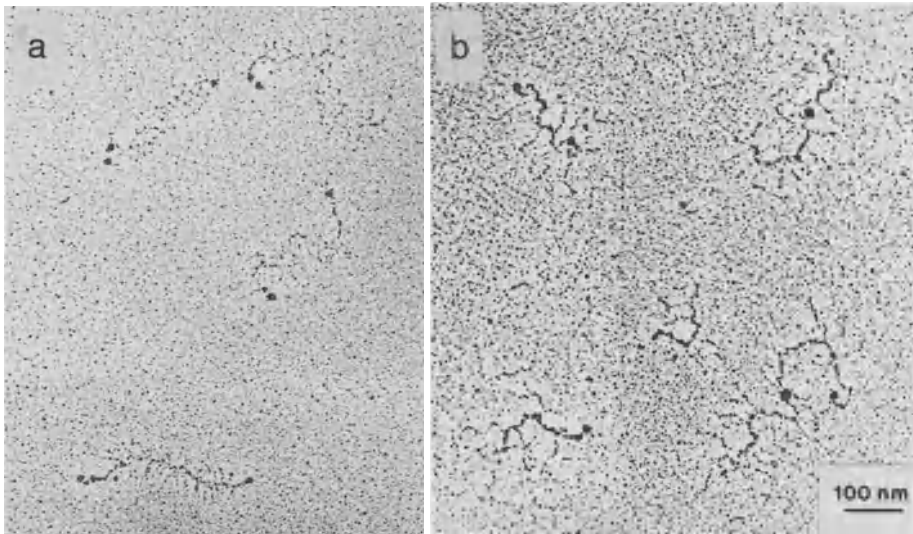


Fig 5: Rotary shadowed images of large proteoglycans from sclera
(a) and aorta (b).

domains similar to El and E2. A marked difference is, however, that the number of glycosaminoglycan side chains is much lower in the proteoglycans from sclera and tendon than in those from cartilage. Aorta proteoglycans differ more, in that even though they contain both N- and C-terminal globular domains connected by a long extended domain they lack a domain corresponding to G2 (Fig. 5). Both aorta and sclera proteoglycans form link-stabilized aggregates of a morphology reminiscent of that of cartilage proteoglycan aggregates which demonstrates also a functional conservation.

## Perspectives

The studies reviewed above contain two new implications with regard to the structure and tissue organization of large aggregating proteoglycans. One important point is that the protein cores are made up from a common set of building blocks or structural domains. These show structural and functional similarity in different proteoglycans, but are probably not identical in their amino acid sequences. It also appears that a building block can be deleted in a certain proteoglycan, as demonstrated by the absence of domain G2 in aorta proteoglycans. Some of these domains are also related to other proteins with functional similarities, as in the case of domains Gl and G2, which shares homologies with link protein (Neame et al, 1987), or domain G3, with its lectin homology (Doege et al, 1986; Sai et al, 1986; Oldberg et al, 1987). Maybe proteoglycans would be a relevant system in which to study the evolution of multidomain protein gene structure.

Another new feature is the observation of an apparently continuous protein shell around the hyaluronate in the central filament of proteoglycan aggregates. Maybe this structure is more ordered than has been assumed and perhaps the central filament even has a defined spatial arrangement in solution. It remains to determine the relative importance of protein-hyaluronate and

protein-protein interactions in the central filament. The
hyaluronate strand is certainly responsible for directing the
growth of a proteoglycan aggregate, but the protein-protein
interactions are likely to have other important functions in
defining the structure and physical characteristics of the
aggregate.

## Acknowledgements

## References

Doege K, Fernandez P, Hassell JR, Sasaki M, Yamada Y (1986)
    Partial cDNA sequence encoding a globular domain at the C
    terminus of the rat cartilage proteoglycan. J Biol Chem
    261:8108-8111
Doege K, Sasaki M, Horigan E, Hassell JR, Yamada Y (1987)
    Complete primary structure of the rat cartilage proteoglycan
    core protein deduced from cDNA clones. J Biol Chem 262:17757-
    17767
Evered D, Whelan J (eds)(1986) Functions of the proteoglycans.
    Ciba Found Symp 124
Franzén A, Björnsson S, Heinegård D (1981) Cartilage proteoglycan
    aggregate formation. Role of link protein. Biochem J 197:669-
    674
Halberg DF, Proulx G, Doege K, Yamada Y, Drickamer K (1988) A
    segment of the cartilage proteoglycan core protein has
    lectin-like activity. J Biol Chem 263:9486-9490
Hassell JR, Kimura JH, Hascall VC (1986) Proteoglycan core
    protein families. Ann Rev Biochem 55:539-567
Heinegård D, Hascall VC (1974) Aggregation of cartilage
    proteoglycans. Characteristics of the proteins isolated from
    trypsin digests of aggregates. J Biol Chem 249:4250-4256
Heinegård D, Paulsson M (1984) Structure and metabolism of
    proteoglycans. In Piez K, Reddi A (eds) Extracellular matrix
    biochemistry, Elsevier, New York, pp. 277-328

Heinegård D, Björne-Persson A, Cöster L, Franzén A, Gardell S, Malmström A, Paulsson M, Sandfalk R, Vogel K (1985a) The core proteins of large and small interstitial proteoglycans from various connective tissues form distinct subgroups. Biochem J 230:181-194

Heinegård D, Wieslander J, Sheehan J, Paulsson M, Sommarin Y (1985b) Separation and characterization of two populations of aggregating proteoglycans from cartilage. Biochem J 225:95-106

Inerot S, Heinegård D (1983) Bovine tracheal cartilage proteoglycans. Variations in structure and composition with age. Collagen Rel Res 3:245-262

Krusius T, Gehlsen KR, Ruoslahti E (1987) A fibroblast chondroitin sulphate proteoglycan core protein contains lectin-like and growth factor-like sequences. J Biol Chem 262:13120-13125

McDevitt CA, Muir H (1971) Gel electrophoresis of proteoglycans and glycosaminoglycans on large pore composite polyacrylamide-agarose gels. Anal Biochem 44:612-622

Mörgelin M, Paulsson M, Hardingham TE, Heinegård D, Engel J (1988) Cartilage proteoglycans. Assembly with hyaluronate and link protein as studied by electron microscopy. Biochem J 253:175-185

Neame PJ, Christner, JE, Baker, JR (1987) Cartilage proteoglycan aggregates. The link protein and proteoglycan amino-terminal globular domains have similar structures. J Biol Chem 262:17768-17778

Oldberg A, Antonsson P, Heinegård D (1987) The partial amino acid sequence of bovine cartilage proteoglycan, deduced form a cDNA clone, contains numerous Ser-Gly sequences arranged in homologous repeats. Biochem J 243:255-259

Paulsson M, Mörgelin M, Wiedemann H, Beardmore-Gray M, Dunham D, Hardingham T, Heinegård D, Timpl R, Engel J (1987) Extended and globular protein domains in cartilage proteoglycans. Biochem J 245:763-772

Sai S, Tanaka T, Kosher RA, Tanzer ML (1986) Cloning and sequence analysis of a partial cDNA for chicken cartilage proteoglycan core protein. Proc Natl Acad Sci USA 83:5081-5085

Scott JE, Orford CR (1981) Dermatan sulphate-rich proteoglycan associates with rat tail tendon collagen at the d band in the gap region. Biochem J 197:213-216

Tengblad A (1981) A comparative study of the binding of cartilage link protein and the hyaluronate-binding region of the cartilage proteoglycan to hyaluronate-substituted Sepharose gel. Biochem J 199:297-305

Thornton DJ, Sheehan JK, Nieduszynski IA (1987) A study of the interaction between cartilage proteoglycan and link protein. Biochem J 248:943-951

Vogel KG, Paulsson M, Heinegård D (1984) Specific inhibition of type I and type II collagen fibrillogenesis by the small proteoglycan of tendon. Biochem J 223:587-597

Wiedemann H, Paulsson M, Timpl R, Engel J, Heinegård D (1984) Domain structure of cartilage proteoglycans revealed by rotary shadowing of intact and fragmented molecules. Biochem J 224:331-333

# SECTION III
## Structural Motifs of Multi-Domain Proteins

# Multi-Domain Proteins: Towards Complete Structures

S.K. Holland and C.C.F. Blake
Laboratory of Molecular Biophysics
Department of Zoology
University of Oxford
South Parks Road
Oxford
England

The basis for constructing many extracellular proteins is the repetition and assembly of a range of small domains to create multi-functional molecules such as fibronectin, integrins and other cellular receptors. The unique combination of small binding units within each protein yields the specificity required for its association with other macromolecules and cell surfaces. In response to different environments or substrate binding this arrangement may adopt many conformations ranging from compact to elongated structures with inherent flexibility or rigidity. Via their structural diversity these molecules can promote the recognition of distant, randomly oriented substrates present in extracellular matrices.

Understanding of the global organization of these systems requires structural analysis of the domain assembly and range of conformations of each multi-domain protein and its orientation within macromolecular complexes. Unlike globular proteins, direct structure determination of the complete proteins is difficult using the established methods of X-ray and NMR analysis due to their large size, inherent flexibility and glycosylation. However the proteolytically cleaved fragments containing one or two domains are suitable for high resolution analysis.

This approach has been successful in determining the structures of domains present in the multi-functional proteins of blood coagulation and fibrinolysis and which contin domains also found in complement, fibronectin, integrins and growth factors (Blake et al., 1988).

High resolution structures of prothrombin Fragment 1 (containing a Vitamin K-dependent calcium-binding unit and a Kringle domain) and epidermal growth factor (EGF) have been determined (Harlos et al., 1987a, 1987b; Cooke et al., 1987). These can be used to model similar domains in other proteins based on their sequence homologies. The Kringle has also been used to derive the generic three-dimensional structure of the fibronectin Type II domain as

138
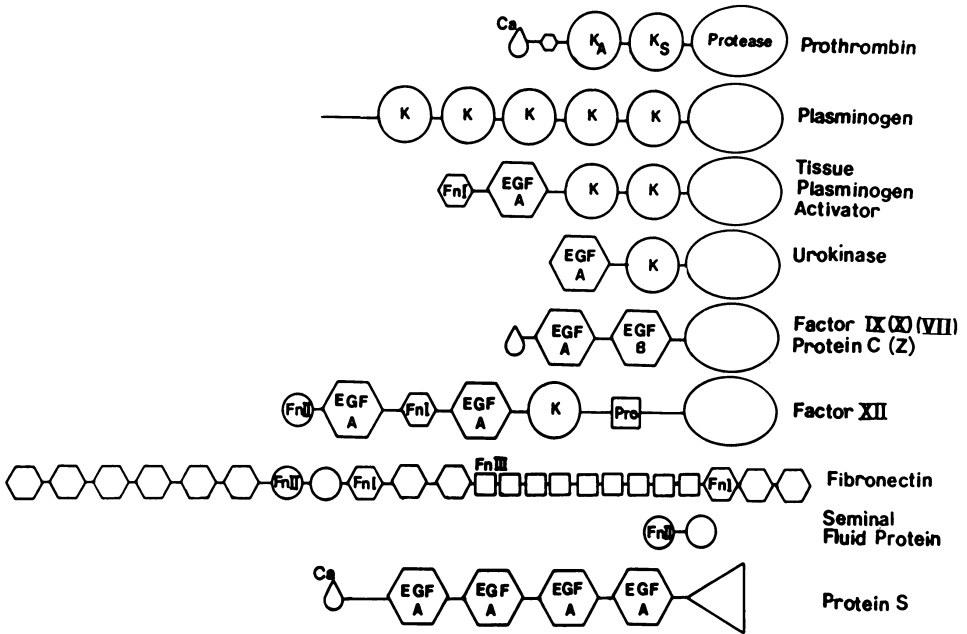


Figure 1. Schematic domain structures of coagulation, fibrinolytic
and related proteins. Ca:calcium binding domain; K:Kringle;
Protease:serine protease domain; EGF:epidermal growth factor unit
(type A/B); Fn:Fibronectin Type I, II & III domains; Pro: proline-
rich unit.

the consensus sequences of these domains exhibit sequence homology
(Holland et al., 1987).

The domains present in the multi-domain molecules are typically
40-90 residues in size and often contain several disulphide
bridges which form complex intra-connections within each domain.
In the EGF and Kringle structures it is apparent that the role of
these bonds is to stabilise the tertiary structures in the absence
of extensive secondary structures. The environment of each protein
may vary significantly and high levels of stability may be
required to maintain structural integrity, e.g. at membrane
surfaces.

For the small multi-domain proteins which often have only one
copy of a particular domain it is apparent that each has a
specific binding function. Multiple copies of a single domain in
a protein may reflect either amplification of a weak binding
function or their role as structural 'spacers'.

The inter-domain linkers constitute the remainder of each
protein and these regions are likely to control the overall

conformation.    Short linke suggest the spatial proximity of
adjacent domains and thus the possibility of domain interfaces,
imparting limited flexibility to the region.    Proteolysis-
sensitive links suggest exposed, mobile regions.    An alternative
to direct study of the whole structure may be a reconstruction of a
molecule from its constituent domains incorporating structural
information about the linkers and analysis of possible domain
interfaces.    Studies of molecular shape using low angle scattering
are aided by such detailed models enabling both accurate inter-
pretation of results and further refinement of the model to
comprehensively describe the protein conformation.

The method has been applied to plasminogen which comprises
five Kringles and a serine protease domain.    All the component
domains can be modelled on known structures.    Evidence from the
prothrombin linker crystal structure, hydropathy, databases and
structure predictions suggests that the plasminogen linkers are
tightly folded brining the Kringles into close proximity about a
regular interface which in one case is strengthened by an inter-
domain disulphide bridge.    The conformation is predicted to be a
stacked domain arrangement forming a solid helical filament with
restricted flexibility rather than a 'beads-on-a-string' assembly
(Holland SK, unpublished observations).    These results are
confirmed by electron micrographs of the plasminogen molecule
(Tranqui et al., 1979) and verify the approach in the structure
determination of these complex proteins.

Blake CCF, Harlos K, Holland SK (1988) Exon and domain evolution
in the proenzymes of blood coagulation and fibrinolysis.   In: Cold
Spring Harbour Symposia on Quantitative Biology.   Vol. LII.   Cold
Spring Harbour Laboratory, New York p925.
Cooke RM, Wilkinson AJ, Baron M, Pastore A, Campbell ID, Gregory
H, Sheard B (1987)   The solution structure of human epidermal
growth factor.    Nature 327:339-341.
Harlos K, Boys CWG, Holland SK, Esnouf MP, Blake CCF (1987a)
Structure and order of the protein and carbohydrate domains of
prothrombin Fragment 1.    FEBS Lett. 224:97-103.
Harlos K, Holland SK, Boys CWG, Burgess AI, Esnouf MP, Blake CCF
(1987b)   Vitamin K dependent blood coagulation proteins form
hetero-dimers.    Nature 330:82-84.
Holland SK, Harlos K, Blake CCF (1987)   Deriving the generic
structure of the fibronectin Type II domain from the prothrombin
Kringle 1 crystal structure.    EMBO J. 6:1875-1880.
Tranqui L, Prandini MH, Chapel A (1979)   The structure of
plasminogen studied by electron microscopy.   Biol. Cellulaire
34:39-42.

# Structure and Spatial Organisation of Intermediate Filament and Nuclear Lamin Molecules

James F Conway and David A D Parry
Department of Physics and Biophysics
Massey University
Palmerston North
New Zealand

## INTRODUCTION

Intermediate filament structure has been investigated extensively and much is now known about the conformation of IF chains, their aggregation into two-stranded molecules, the modes of assembly of the molecules into four-chain structural units and the arrangement of units in the IF (Geisler and Weber, 1982; Hanukoglu and Fuchs, 1982; Crewther et al, 1983; Steinert et al, 1983, 1984; Parry and Fraser, 1985; Steinert and Parry 1985, Parry et al, 1986; McKeon et al, 1986). This knowledge provides the basis for further experimentation and analysis and allows new insights to be presented here on the role of the conserved sequences in the rod domain, the antiparallel arrangement of 1B segments and the flexibilities of the terminal domains.

## CHAIN STRUCTURE

IF chains may be divided into three domains: N-terminal, central and C-terminal. Delineation of these domains arises through the recognition of a central region of homologous sequence with a high α-helical content and a heptad substructure characteristic of α-fibrous proteins. Within the central rod domain four coiled-coil segments (1A, 1B, 2A and 2B) and three linking segments (L1, L12 and L2) have been described (see for example Parry and Fraser 1985; Figure 1). Segment 1 (1A + L1 + 1B) and segment 2 (2A + L2 + 2B) are each about 22 nm long and are connected by a short link L12, thus generating a central rod domain of approximate length 47 nm. Conserved breaks in the phasing of the heptad repeat occur at link L2 and at a point close to the centre of segment 2B. Furthermore, sequences with a high degree of interspecies homology occur close to or at the ends of the rod domain (see Steinert and Parry, 1985 for a complete list of pertinent references).

IF sequences may be classified into five Types on the basis of homology in the rod domain (Hanukoglu and Fuchs, 1982; Parry and Fraser, 1985; Steinert and Parry, 1985; Parry et al, 1986). Type I and Type II chains occur only in keratin IF and may be further subdivided into hard α-keratins - Ia, IIa and soft α-keratins - Ib, IIb (Conway and Parry, 1988). Type III chains occur in glial fibrillary acidic protein, vimentin and desmin IF, and Type IV chains are found solely in neurofilaments. The latter may be further subdivided on the basis of molecular weight (see review by Lazarides, 1982) or sequence homology (Conway and Parry, 1988) into sub-classes known as NF-L,

NF-M and NF-H. Type V chains are localised in the lamina of the nuclear membrane: they differ from Types I-IV chains in that segment 1B has a six heptad insertion; L12 is predicted to be α-helical; and L1 represents only a phase discontinuity in the heptad repeat (for a comparison of the Types I-IV and Type V IF chains see Parry et al, 1986).

| | E1 | V1 | H1 | 1A | L1 | 1B | L12 | 2A | L2 | 2B | H2 | V2 | E2 |
|---|---|---|---|---|---|---|---|---|---|---|---|---|---|
| Ia | ? | ? | ≥7 | 35 | 11 | 101 | 16 | 19 | 8 | 121 | ≥0 | ? | ? |
| Ib | 0-10 | 65-140 | 7 | 35 | 11-14 | 101 | 16 | 19 | 8 | 121 | 0 | 0-110 | 5-30 |
| IIa | ? | ? | ≥32 | 35 | 10 | 101 | 17 | 19 | 8 | 121 | ≥10 | ? | ? |
| IIb | 5-70 | 20-160 | 36 | 35 | 11-14 | 101 | 17 | 19 | 8 | 121 | 20 | 25-125 | 21 |
| III | 19-81 | | 20 | 35 | 8 | 101 | 16 | 19 | 8 | 121 | 58 | 0 | 0 |
| IV-L | 0 | 0 | 91 | 35 | 10 | 101 | 17 | 19 | 8 | 121 | 81 | 60-70 | |
| IV-M | 0 | 0 | 102 | 35 | 10 | 101 | 17 | 19 | 8 | 121 | ≥88 | ? | ? |
| IV-H | 0 | 0 | 97 | 35 | 10 | 101 | 22 | 19 | 8 | 121 | >110 | ? | ? |
| V | 0 | 0 | 30 | 41 | 0 | 148 | 19 | 19 | 8 | 121 | 179 | ? | ? |
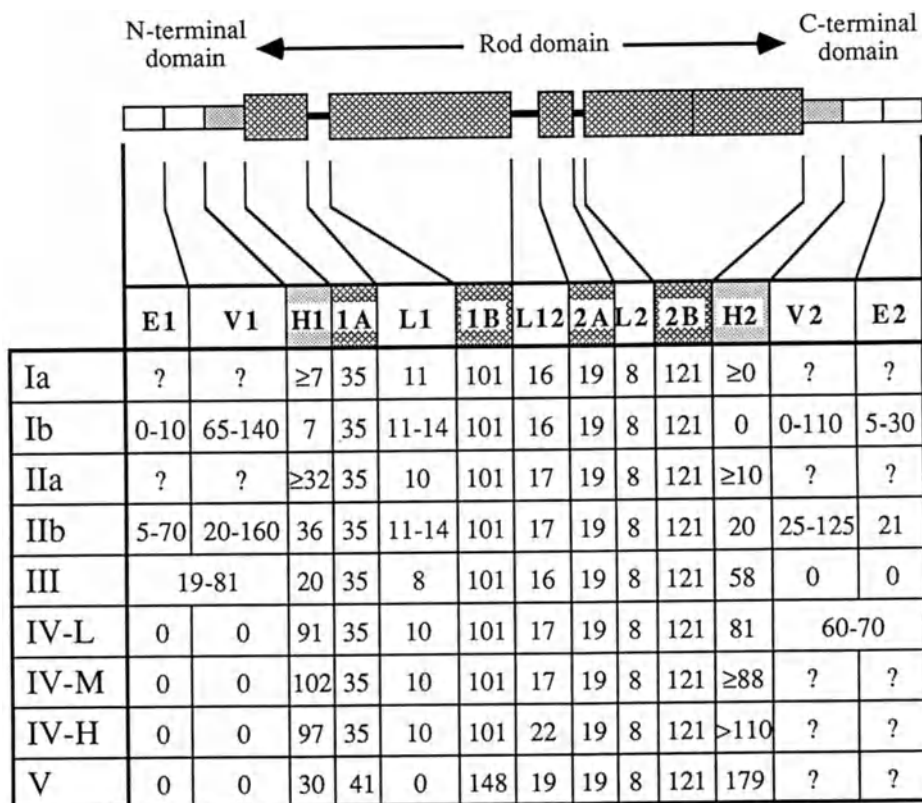
FIGURE 1: Schematic representation of the segmental substructure of mammalian IF chains. Ia and IIa refer to Type I and Type II chains from hard α-keratins while Ib and IIb refer to Type I and Type II chains from epidermal α-keratins; III represents desmin, vimentin and glial fibrillary acidic protein chains; IV-L, IV-M and IV-H refer to the light, medium and heavy chains from neurofilaments; V represents lamin chains A and C. The symbol ? indicates that insufficient sequence data are available for an estimate to be made.

The sequences comprising the N- and C-terminal domains show features of considerable interest. For Type I and Type II chains these domains may be divided into homologous (H1 and H2), variable (V1 and V2) and end segments (E1 and E2) arranged with bilateral symmetry about the central rod domain (Figure 1; Steinert et al, 1985; Steinert and Parry, 1985); a similar, but less pronounced subdivision occurs for other IF chain types. Although the structures and functions of the various subdomains

remain unclear some features of interest are beginning to emerge. For example epithelia generally express specific pairs of Type I and Type II chains. Each of the Type II chains has a molecular weight of about 7-10 kDa greater than its coexpressed partner and this arises predominantly from the disparity of the sizes of the V subdomains of the two chains. The V subdomains are largest and most glycine-rich in terminally differentiating cells, and smallest and most serine-rich in the less differentiated living cell layers: such features have been related to function (Steinert and Parry, 1985).

## MOLECULAR STRUCTURE

Within the rod domain each IF molecule consists of two parallel chains in axial register; the chains coil around one another in a left-handed manner to generate a rope-like structure (see, for example, Parry *et al*, 1977, 1985; Ahmadi and Speakman, 1978; Quinlan and Franke, 1982, 1983; Geisler and Weber, 1982; Woods and Inglis, 1984; Steinert *et al*, 1984; Parry and Fraser, 1985). The pitch length of the supercoil thus generated is unknown but is likely to be in the vicinity of 14 nm (Parry, 1975). Each molecule has a pair of globular structures at each end corresponding to terminal domains of the constituent chains. For keratin molecules the structure is heterodimeric containing a Type I and a Type II chain; in contrast desmin, vimentin and glial fibrillary acidic protein molecules are homodimeric, containing only Type III chains. Type IV chains occur only in neurofilament IF though the three subclasses previously discussed allow the possibility of heterodimers.

A highly significant observation pertaining to the rod domain of Types I-IV IF molecules is the well defined periodicity in the linear disposition of both the acidic and the basic residues in segment 1B (period 9.54 residues ~1.42 nm) and in segment 2 (period 9.84 residues ~1.46 nm) (Parry *et al*, 1977; McLachlan and Stewart, 1982; Crewther *et al*, 1983; Parry and Fraser, 1985). In the Type V lamin molecules the period is 9.9 residues (~1.47 nm) and extends without a break over the entire rod domain (Parry *et al*, 1986). These regularities provide the means by which self-assembly is specified *in vivo* though, naturally, the importance of apolar and hydrogen bond interactions in the final docking process will also be crucial.

## FOUR CHAIN STRUCTURAL UNITS AND THEIR ARRANGEMENT IN IF

Extensive data support the notion that a pair of two-stranded IF molecules comprise a structural unit (Ahmadi and Speakman, 1978; Geisler and Weber, 1982; Woods and Inglis, 1984; Quinlan *et al*, 1984; Parry *et al*, 1985). The two molecules in the unit are antiparallel and are either completely overlapped (Quinlan *et al*, 1984; Geisler *et al*, 1985) or approximately half staggered (Ahmadi *et al*, 1980; Crewther *et al*, 1983; Woods and Inglis 1984; Parry *et al*, 1985). Both modes of assembly are probable *in vivo*.

The packing of the four-chain structural units in IF may be revealed by low resolution X-ray diffraction studies on ordered assemblies. However with the notable exception of the highly detailed fibre X-ray diffraction patterns from hard α-keratin (Fraser *et al*, 1976), the only other X-ray data available are from neurofilaments (Wais-Steider *et al*, 1983). In that case the axial periodicity in the IF was 25.2 nm; in contrast a value of 47 nm has been reported for quill α-keratin (Fraser and MacRae, 1971). Although these data show the axial repeats in the two structures are different this does not necessarily imply that the surface lattice structures are unrelated. Indeed small changes in surface lattice geometry can easily result in structures with widely different symmetries (see, for example, the various surface lattice geometries in myosin-containing thick filaments from muscle). Data from an extensive analysis of IF sequence homologies (Conway and Parry, 1988) support the idea that IF from diverse sources form a family of polymorphic structures with closely related surface lattices. In the case of hard α-keratin, each surface lattice point corresponds to a single tetrameric chain unit (Fraser *et al*, 1986); this has been determined from mass measurements made on related IF using the technique of scanning transmission electron microscopy (Steven *et al*, 1982, 1983*a*).

Steinert *et al* (1983, 1985) have shown that limited enzymatic digestion of epidermal keratin IF produces peptides from both terminal domains without the structural integrity of the IF being compromised. This indicates that part of these domains protrude from the core of the IF, a conclusion which is consistent with the radial mass measurements made using STEM (Steven *et al*, 1983*b*). It has also been established that the terminal domains of the IF chains have an effect on the aggregation of molecules in the IF and on the stability of the assembly thus formed (Geisler *et al*, 1982; Traub and Vorgias, 1983; Kaufmann *et al*, 1985). More specifically it has become clear that, in addition to the rod domain, only the N-terminal domain plays a role in the aggregation of desmin (or vimentin) molecules in the IF. New data to support this conclusion have come from Geisler and Weber (1988) who showed that phosphorylation of chicken desmin *in vitro* occurred within the N-terminal domain and that it inhibited IF formation. Since the terminal domain(s) of keratin, neurofilament and lamin chains are also phosphorylated *in vivo* the hypothesis that phosphorylation could affect intracellular depolymerisation of IF is an attractive one (see also Inagaki *et al*, 1987, 1988), and emphasises the increasing recognition that is attached to phosphorylation as a regulatory mechanism in diverse protein structures.

STRUCTURAL PROGRESS

Protein sequences that are highly conserved have structural and/or functional importance and certainly those in IF chains in segment 1A and at the C-terminal end of segment 2B are no exception. Their role, however, has remained enigmatic though recent data obtained from a study of lamin paracrystals (Goldman *et al*, 1986; Parry *et al*, 1987) have provided the first evidence that these sequences are involved in specifying the axial stagger between similarly directed molecules in the IF (Parry *et al*,
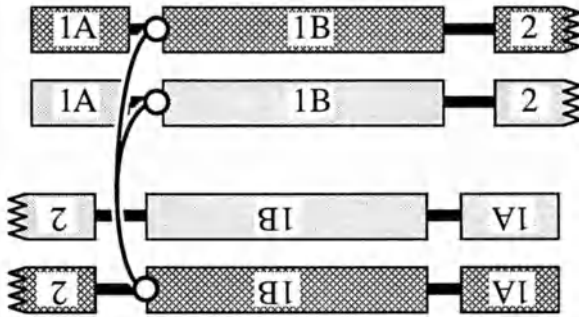
FIGURE 2: Limited chymotryptic digestion of reduced carboxymethylated wool IF protein results in the release of tetrameric particles containing covalently linked 1B segments. This (artefactual) situation is believed to arise as a result of a transpeptidation reaction. Two crosslinking peptides (shown) have been isolated and characterised, and are consistent only with a heterodimeric structure for the keratin molecule (Sparrow *et al*, 1988). Furthermore the reaction would be most probable when the appropriate residues in the antiparallel molecules were in close juxtaposition in the IF. This suggests that a likely axial stagger between oppositely directed 1B segments in α-keratin is about -5 residues (Sparrow *et al*, 1988).

1987). A consequence of the structure proposed by these authors was that the conserved sequences from different molecules became axially aligned. Furthermore the two most apolar regions in the rod domain (one lies in each of the two conserved sequences) were optimally placed to interact and stabilise the molecular arrangement. A similar role is possible in Types I-IV IF provided that a small number of residues (say 3-6) that are predicted to be α-helical on the basis of secondary structure prediction techniques are, in fact, in a more extended conformation. Such a small margin of error lies well within the limitations of the prediction methods used. A further consequence of this study is that segment 1A, although lacking the well defined periodicity in the acidic and basic residues found elsewhere in the rod domain, must be parallel and not antiparallel (or perpendicular) to segments 1B and 2. This is consistent with the observed lengths of Types I-IV IF molecules *in vitro* and with the totally linear structure of lamin molecules (Aebi *et al*, 1986; Parry *et al*, 1987). If this hypothesis proves correct then the importance of highly conserved sequences at both ends of the rod domain becomes self evident for without them the stability of the axial assembly of IF molecules would be significantly reduced and IF formation compromised.

A four-chain particle has been isolated from reduced carboxymethylated wool IF protein after limited chymotryptic digestion (Sparrow *et al*, 1988). As an adjunct to this experiment it was found that 1B segments were covalently linked, probably as a consequence of transpeptidation (Figure 2). From the isolation and characterisation of the crosslinks Sparrow *et al* (1988) have shown that the IF molecules from hard α-keratin are heterodimers (in confirmation of several other lines of less direct data) and that specific physical limitations are implied about possible axial staggers between oppositely directed 1B segments *in vivo*. Four such possible staggers (15, 4, -5 and -15 residues) have been suggested previously by Fraser *et al* (1986) from a consideration of the maximisation of intermolecular ionic

interactions subject to the constraint of the known surface lattice of α-keratin IF. All of these staggers are consistent with the chymotryptic data though one of the smaller values (-5 residues) is currently favoured (Figure 2; Sparrow *et al*, 1988); also, staggers of -5 and -15 residues are those most readily compatible with the conclusion that segments 1A and 1B are colinear.

X-ray diffraction patterns of fibres prepared from purified 1B segments have revealed an axial period of 16 nm (Suzuki *et al*, 1973). Since 1B segments are 15 nm long (ie. 101 x 0.1485 nm) an axial stagger between pairs of segments of ±5 or ±15 residues will yield tetrameric chain structures of lengths 15.7 and 17.2 nm respectively. Both are consistent with the observed X-ray periodicity. Larger axial staggers, however, seem less easily reconciled with the fibre diffraction data.
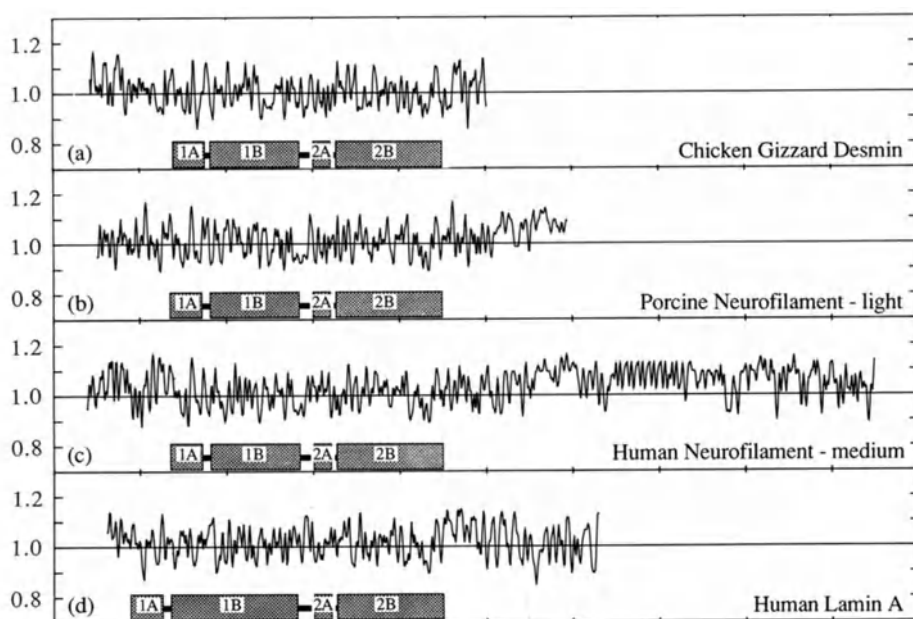


FIGURE 3: Flexibility indices for (a) chicken gizzard desmin (Type III), (b) porcine neurofilament light chain (Type IV-L), (c) human neurofilament medium chain (Type IV-M) and (d) human lamin A chain (Type V) calculated using the method of Karplus and Schulz (1985) but weighted over a three residue window (relative weights 1, 2, 1). Note the higher average flexibility scores for the N- and C-terminal domains compared to those for the rod domain, also the high flexibilities for the L1 segment of chicken gizzard desmin and porcine neurofilament light chain. In contrast, lower than average flexibilities are found in the profile for the L12 segment of desmin and both neurofilament chains. The regularities in the flexibility profile for the C-terminal domain of human NF-M chain correspond to the 13 residue repeat (PVPKSPVEEKGKS). The horizontal scale is marked in intervals of 100 residues.

Temperature factor data collected from the structures of 31 protein crystals have been used by Karplus and Schulz (1985) to assess chain flexibilities in other proteins. On the assumption that this technique is also applicable to fibrous proteins, Conway *et al* (1988) have calculated the flexibility scores for rod domain segments and also for the N- and C-terminal domains of α-keratin chains. The scores obtained for the terminal domains from hard α-keratin did not differ significantly from 1.0 (an "average" value) and were seen to be consistent with the high cysteine content of these domains and their involvement in the formation of disulphide bonds with both matrix and other IF protein chains to generate a highly crosslinked and inert structure. In contrast the terminal domains of the soft (epidermal) α-keratins revealed significantly higher than average flexibility scores, the high scoring portions of which relate closely to glycine-serine rich segments. The interpretation of the flexibility data can be made in terms of the requirement that these domains interact with and form part of a flexible barrier - the skin - between an animal and its environment. The terminal domains of Type III chains from chicken gizzard desmin, however, show the lowest flexibility scores of any IF chain, though these values still indicate a flexibility above that of the rod domain (Figure 3a, Table 1). High flexibility is exhibited by several sizeable segments in the C-terminal domains of both the light and medium molecular weight neurofilament chains (Figure 3b, c; Table 1). This again can be rationalised by consideration of the role that similar segments in NF-H chains play in acting as part of extended bridges between IF and microtubules. The flexibility profile of lamin (Figure 3d) shows higher flexibility in the N-terminal domain than in the C-terminal (Table 1). Interestingly the N-terminal domain of the lamin chains is the smallest of any of the IF chains whereas the C-terminal domain is amongst the largest.

|     | CGD* | PNF-L* | HNF-M* | LAMIN* |
| --- | --- | --- | --- | --- |
| N | 1.028 ± 0.077 | 1.016 ± 0.073 | 1.044 ± 0.083 | 1.053 ± 0.061 |
| 1A | 0.982 ± 0.074 | 0.989 ± 0.077 | 0.998 ± 0.080 | 1.007 ± 0.073 |
| L1 | 1.064 ± 0.074 | 1.058 ± 0.074 | 1.003 ± 0.085 | – |
| 1B | 1.001 ± 0.068 | 1.005 ± 0.072 | 1.000 ± 0.071 | 1.011 ± 0.067 |
| L12 | 0.983 ± 0.070 | 0.976 ± 0.079 | 0.988 ± 0.074 | 1.041 ± 0.074 |
| 2A | 0.979 ± 0.072 | 0.986 ± 0.074 | 1.038 ± 0.059 | 0.984 ± 0.049 |
| L2 | 1.001 ± 0.068 | 1.002 ± 0.046 | 0.967 ± 0.073 | 1.040 ± 0.052 |
| 2B | 0.992 ± 0.079 | 1.006 ± 0.072 | 1.007 ± 0.068 | 1.007 ± 0.071 |
| C | 1.015 ± 0.085 | 1.047 ± 0.064 | 1.055 ± 0.068 | 1.027 ± 0.083 |
| Rod | 0.998 ± 0.070 | 1.003 ± 0.073 | 1.003 ± 0.071 | 1.010 ± 0.069 |

TABLE 1
Mean Flexibility Indices (± sd) for Types III, IV and V IF Chain Segments

* CGD – chicken gizzard desmin (III); PNF-L – porcine neurofilament chain of lowest molecular weight (IV-L); HNF-M – human neurofilament chain of medium molecular weight (IV-M); LAMIN – human lamin A (V).

The terminal domains of IF chains all show greater flexibility than their rod domains, sometimes to a marked degree. Such features are to be expected of structures containing close packed rods within their cores whilst placing their terminal domains externally in an aqueous environment in positions where they may interact with other intracellular elements.

## CONCLUSIONS

Much remains to be done before the detailed structure of IF molecules and their precise packing in the IF is known. Two problems are in need of particular attention at the molecular level – the supercoil pitch length and the nature of the coiled-coil deformation at the two points in the structure where the heptad phasing undergoes a discontinuity. At higher levels of structure, detailed X-ray diffraction studies on ordered assemblies of desmin and vimentin IF will be required to ascertain the surface lattice of these structures *in vivo*. Crosslinking studies also have the potential to place limitations on the possible axial staggers between the various coiled-coil segments.

Since the basic framework of IF structure is now well established increasing effort is being devoted to refining specific details of the molecular structure and the nature of molecular packing. It is to be hoped, and indeed expected, that such studies will yield a medium resolution model of the IF within the next decade.

## REFERENCES

Aebi U, Cohn J, Buhle L and Gerace L (1986) The nuclear lamina is a meshwork of intermediate-type filaments. Nature (London) 323:560-564

Ahmadi B and Speakman PT (1978) Suberimidate crosslinking shows that a rod-shaped, low-cystine, high-helix protein prepared by limited proteolysis of reduced wool has four protein chains. FEBS Lett 94:365-367

Ahmadi B, Boston NM, Dobb MG and Speakman PT (1980) Possible four chain repeating unit in the microfibril of wool. In: Parry DAD and Creamer LK (eds) Fibrous Proteins: Scientific, Industrial and Medical Aspects, vol 2. Academic Press, London, pp 161-166

Conway JF and Parry DAD (1988) Intermediate filament structure 3: Analysis of sequence homologies. Int J Biol Macromol 10:79-98

Conway JF, Fraser RDB, MacRae TP and Parry DAD (1988) Protein chains in wool and epidermal keratin IF: Structural features and spatial arrangement. In: Rogers GE, Reis PJ, Ward KA and Marshall RC (eds) The Biology of Wool and Hair, Chapman and Hall, London and New York (in press)

Crewther WG, Dowling LM, Steinert PM and Parry DAD (1983) Structure of intermediate filaments. Int J Biol Macromol 5:267-274

Fraser RDB and MacRae TP (1971) Structure of α-keratin. Nature (London) 233:138-140

Fraser RDB, MacRae TP and Suzuki E (1976) Structure of the α-keratin microfibril. J Mol Biol 108:435-452

Fraser RDB, MacRae TP, Parry DAD and Suzuki E (1986) Intermediate filaments in α-keratins. Proc Natl Acad Sci USA 83:1179-1183

Geisler N and Weber K (1982) The amino acid sequence of chicken muscle desmin provides a common structural model for intermediate filament proteins. EMBO J 1:1649-1656

Geisler N and Weber K (1988) Phosphorylation of desmin *in vitro* inhibits formation of intermediate filaments; identification of three kinase A sites in the aminoterminal head domain. EMBO J 7:15-20

Geisler N, Kaufmann E and Weber K (1982) Proteinchemical characterization of three structurally distinct domains along the protofilament unit of desmin 10 nm filaments. Cell 30:277-286

Geisler N, Kaufmann E and Weber K (1985) Antiparallel orientation of the two double-stranded coiled-coils in the tetrameric protofilament unit of intermediate filaments. J Mol Biol 182:173-177

Goldman AE, Maul G, Steinert PM, Yang HY and Goldman RD (1986) Keratin-like proteins that coisolate with intermediate filaments of BHK-21 cells are nuclear lamins 83:3839-3843

Hanukoglu I and Fuchs E (1982) The cDNA sequence of a human epidermal keratin: Divergence of sequence but conservation of structure among intermediate filament proteins. Cell 31:243-252

Inagaki M, Nishi Y, Nishizawa K, Matsuyama M and Sato C (1987) Site-specific phosphorylation induces disassembly of vimentin filaments *in vitro*. Nature (London) 328: 649-652

Inagaki M, Gonda Y, Matsuyama M, Nishizawa K, Nishi Y and Sato C (1988) Intermediate filament reconstitution *in vitro*. The role of phosphorylation on the assembly-disassembly of desmin. J Biol Chem 263:5970-5978

Karplus PA and Schulz GE (1985) Prediction of chain flexibility in proteins. Naturwissenschaften 72:212-213

Kaufmann E, Weber K and Geisler N (1985) Intermediate filament forming ability of desmin derivatives lacking either the amino-terminal 67 or the carboxy-terminal 27 residues. J Mol Biol 185:733-742

Lazarides E (1982) Intermediate filaments: A chemically heterogeneous, developmentally regulated class of proteins. Ann Rev Biochem 51:219-250

McKeon FD, Kirschner MW and Caput D (1986) Homologies in both primary and secondary structure between nuclear envelope and intermediate filament proteins. Nature (London) 319:463-468

McLachlan AD and Stewart M (1982) Periodic charge distribution in the intermediate filament proteins desmin and vimentin. J Mol Biol 162:693-698

Parry DAD (1975) Double helix of tropomyosin. Nature (London) 256:346-347

Parry DAD and Fraser RDB (1985) Intermediate filament structure 1. Analysis of IF protein sequence data. Int J Biol Macromol 7:203-213

Parry DAD, Crewther WG, Fraser RDB and MacRae TP (1977) Structure of α-keratin: Structural implication of the amino acid sequences of the Type I and Type II chain segments. J Mol Biol 113:449-454

Parry DAD, Steven AC and Steinert PM (1985) The coiled-coil molecules of intermediate filaments consist of two parallel chains in exact axial register. Biochem Biophys Res Commun 127:1012-1018

Parry DAD, Conway JF and Steinert PM (1986) Structural studies on lamin: Similarities and differences between lamin and intermediate filament proteins. Biochem J 238:305-308

Parry DAD, Conway JF, Goldman AE, Goldman RD and Steinert PM (1987) Nuclear lamin proteins: Common structures for paracrystalline, filamentous and lattice forms. Int J Biol Macromol 9:137-145

Quinlan RA and Franke WW (1982) Heteropolymer filaments of vimentin and desmin in vascular smooth muscle tissue and cultured baby hamster kidney cells demonstrated by chemical crosslinking. Proc Natl Acad Sci USA 79:3452-3456

Quinlan RA and Franke WW (1983) Molecular interactions in intermediate-sized filaments revealed by chemical cross-linking. Eur J Biochem 132:477-484

Quinlan RA, Cohlberg JA, Schiller DL, Hatzfeld M and Franke WW (1984) Heterotypic tetramer ($A_2D_2$) complexes of non-epidermal keratins isolated from cytoskeletons of rat hepatocytes and hepatoma cells. J Mol Biol 178:365-388

Sparrow LG, Dowling LM, Loke VY and Strike PM (1988) Amino acid sequences of wool keratin IF proteins. In: Rogers GE, Reis PJ, Ward KA and Marshall RC (eds) The Biology of Wool and Hair, Chapman and Hall, London and New York (in press)

Steinert PM and Parry DAD (1985) Intermediate filaments: Conformity and diversity of expression and structure. Ann Rev Cell Biol 1:41-65

Steinert PM, Rice RH, Roop DR, Trus BL and Steven AC (1983) Complete amino acid sequence of a mouse epidermal keratin subunit and implications for the structure of intermediate filaments. Nature (London) 302:794-800

Steinert PM, Parry DAD, Racoosin EL, Idler WW, Steven AC, Trus BL and Roop DR (1984) The complete cDNA and deduced amino acid sequence of a type II mouse epidermal keratin of 60 000 Da: Analysis of sequence differences between type I and type II keratins. Proc Natl Acad Sci USA 81:5709-5713

Steinert PM, Parry DAD, Idler WW, Johnson LD, Steven AC and Roop DR (1985) Amino acid sequences of mouse and human epidermal Type II keratins of $M_r$ 67 000 provide a systematic basis for the structural and functional diversity of the end domains of keratin intermediate filament subunits. J Biol Chem 260:7142-7149

Steven AC, Wall J, Hainfeld J and Steinert PM (1982) Structure of fibroblastic intermediate filaments: Analysis by scanning transmission electron microscopy. Proc Natl Acad Sci USA 79:3101-3105

Steven AC, Hainfeld JF, Trus BL,Wall JS and Steinert PM (1983a) Epidermal keratin filaments assembled *in vitro* have masses-per-unit-length that scale according to average subunit mass: Structural basis for homologous packing of subunits in intermediate filaments. J Cell Biol 97:1939-1944

Steven AC, Hainfeld JF, Trus BL, Wall JS and Steinert PM (1983b) The distribution of mass in heteropolymer intermediate filaments assembled *in vitro*. J Biol Chem 258:8323-8329

Suzuki E, Crewther WG, Fraser RDB, MacRae TP and McKern NM (1973) X-ray diffraction and infrared studies of an $\alpha$-helical fragment from $\alpha$-keratin. J Mol Biol 73:275-278

Traub P and Vorgias CE (1983) Involvement of the N-terminal polypeptide of vimentin in the formation of intermediate filaments. J Cell Sci 63:43-67

Wais-Steider C, Eagles PAM, Gilbert DS and Hopkins J (1983) Structural similarities and differences amongst neurofilaments. J Mol Biol 165:393-400

Woods EF and Inglis AS (1984) Organization of the coiled-coils in the wool microfibril. Int J Biol Macromol 6:277-283

# The Role of Repeating Sequence Motifs in Interactions Between α-Helical Coiled-Coils such as Myosin, Tropomyosin and Intermediate-Filament Proteins

Murray Stewart, Roy A. Quinlan* Robert D. Moir, Simon R. Clarke and Simon J. Atkinson.
*Medical Research Council Laboratory of Molecular Biology,*
*Hills Rd., Cambridge CB2 2QH, ENGLAND.*

SUMMARY

Many fibrous proteins have repeating sequence motifs that are associated with macromolecular interactions. We discuss here some of these motifs in α-helical coiled-coils found in muscle and cytoskeletal proteins. The motifs are most conveniently detected and analysed using Fourier methods which, if the data is appropriately scaled, can also be used to assess the statistical significance of a particular feature. Tropomyosin has a repeating motif in its acidic residues that occurs every 19.7 residues and which is associated with the interaction between tropomyosin and actin that plays a key role in the regulation of contraction in vertebrate skeletal muscle. The tails of myosin molecules have a pattern of alternating positive and negative zones that repeats every 28 residues and which is important in the interactions between myosin tails that result in the formation of thick filaments. Electron microscopy of 2-dimensional crystals of proteolytic fragments of myosin rod showed the coiled-coil pitch was near 14.3 nm and also indicated the likely interaction geometry between coiled-coils in thick filaments. The assembly of intermediate filament proteins also seems to involve the complementation of alternating zones of charge in an analogous way to that seen with myosin. The actual assembly of intermediate filament proteins appears to involve the formation of molecular dimers (that is, two molecules or four chains) often referred to as "tetramers". We have been able to produce paracrystals from fragments of glial fibrillary acidic protein (the intermediate filament type present in astrocytes) that we have produced by recombinant DNA methods. These paracrystals indicated that the two molecules within a tetramer overlap their N-termini by approximately 33 nm, which would be consistent with models of intermediate filament structure proposed on the basis of X-ray diffraction data.

* *Present Address: Department of Biochemistry, University of Dundee,*
*Dundee DD1 4HN, SCOTLAND.*

# INTRODUCTION

Most fibrous proteins function in cells by forming aggregates, and so the molecular nature of the interactions between the proteins in these assemblies is of fundamental importance in relating their structure and function *in vivo*. One important class of fibrous proteins is based on an α-helical coiled-coil and includes the keratins and associated intermediate filament forming proteins, a number of muscle proteins such as myosin, tropomyosin and paramyosin, fibrinogen and a range of silks (see Fraser & MacRae, 1973 for a review). These molecules all have a very extended structure and so interact with a number of molecules in their assemblies *in vivo*. A common feature of these molecules is the presence of repeating sequence motifs that are involved in these molecular interactions. These motifs have probably arisen by a series of gene duplication events, but have then been retained in the sequence because of their importance in molecular interactions. In this article we will illustrate the role of these sequence repeats in molecular interactions between a range of cytoskeletal and muscle proteins including tropomyosin, myosin rod and intermediate filaments.

# THE COILED-COIL CONFORMATION

The coiled-coil conformation is based on two α-helices that coil around one another to produce a superhelix. This conformation was first proposed by Crick (1953) who noted that such a structure could be stabilised by an interaction between residues on the complementary faces of the helices. In particular, Crick observed that when two α-helices came into contact, the protruding residues from one helix were opposite the gaps between residues in the other helix. This "knobs-in-holes" interaction would then enable a very close packing of the two α−helices in the coiled-coil. Because the α-helix has approximately 7 residues in 2 turns, this knobs in holes interaction produces a marked "heptad" repeat in these sequences, with every 1st and 4th residue in the heptad tending to be hydrophobic. Thus, if consecutive residues are denoted by *a-b-c-d-e-f-g,* residues *a* and *d* are usually hydrophobic, whereas the remainder are often charged or hydrophilic. Although hydrophobic interactions between residues in positions *a* and *d* are primarily responsible for stabilising the interaction between the two α-helices, ionic interactions between residues in positions *e* and *g* probably also have a role, at least in tropomyosin (McLachlan & Stewart, 1975). This sort of heptad pattern was first analysed in detail in tropomyosin (see McLachlan & Stewart, 1975 and references therein), but has subsequently be seen in a range of coiled-coil proteins such as myosin (McLachlan & Karn, 1982) and intermediate filament proteins (reviewed by Conway & Parry, 1988). If the α-helix had exactly 7 residues in 2 turns, then the two interacting helices would lie parallel to one another. However,

as first noted by Crick (1953), because there are slightly more than 7 residues in 2
turns, the two helices will tend to wrap around one another to form a left-handed
supercoil. The precise relationship between the helical parameters of the $\alpha$-helix
and the helical parameters of the coiled-coil have been discussed in detail by Fraser
and MacRae (1973). An ideal $\alpha$-helix should give a coiled-coil pitch of 18.6 nm,
but very small changes in the $\alpha$-helix symmetry can produce large changes in the
coiled-coil pitch (see Fraser & MacRae, 1973) and the two coiled-coil pitches that
have been determined (tropomyosin and myosin rod) are instead close to 14 nm
(Phillips, *et al.*, 1986; 1987; Quinlan & Stewart, 1987).

FOURIER ANALYSIS

Because most of the repeating sequence motifs associated with molecular
interactions are spaced regularly along the sequences of fibrous proteins, Fourier
analysis is usually an efficient method for both detecting these periodic features
and for assessing their significance. Fourier analysis is a general mathematical
procedure in which functions are analysed in terms of sums of *sine* and *cosine*
functions. Although any well-behaved function can be analysed in this way,
periodic functions have the special property that only *sine* and *cosine* waves that
have the same wavelength as the periodic feature or which have wavelengths that
are integral fractions of the period can contribute. This is because the contribution
to each repeat must be the same  and so waves that were not an integral fraction of
the repeat distance would make a different contribution to each motif in the repeat.
This property allows sequence data to be analysed in a manner analogous to that
employed for image analysis of electron micrographs of regular biological
specimens (see Stewart, 1988, for an introduction): in the Fourier transform,
periodic features contribute to the peaks, whereas the non-periodic features
contribute to the continuous background.

The Fourier transform of a sequence can be computed by first converting the
chemical sequence into a mathematical one by scoring the different residues in
some convenient way. For example, acidic residues could be scored as 1 and all
other residues as 0 (see, for example, Stewart & McLachlan, 1975). The Fourier
transform of the mathematical sequence is then computed using standard
algorithms and a simple graphical representation of the intensity of the transform
against frequency then enables any peaks to be identified. If the mathematical
sequence is scaled appropriately (McLachlan & Stewart, 1976), the statistical
significance of any peak in the Fourier transform is easily calculated. Figure 1
shows a Fourier spectrum from the $\alpha$-tropomyosin sequence, in which there are
very clear peaks at frequencies corresponding to approximately 20 residues and at
7/2 and 7/3 residues. The peaks at 7/2 and 7/3 are overtones (the fundamental or

1st-order peak at 7 residues is absent because the structure repeats at half this distance) of the 7-residue heptad repeat characteristic of an $\alpha$-helix (see above), whereas the repeat at approximately 20 residues is associated with the actin-tropomyosin interaction (see below).
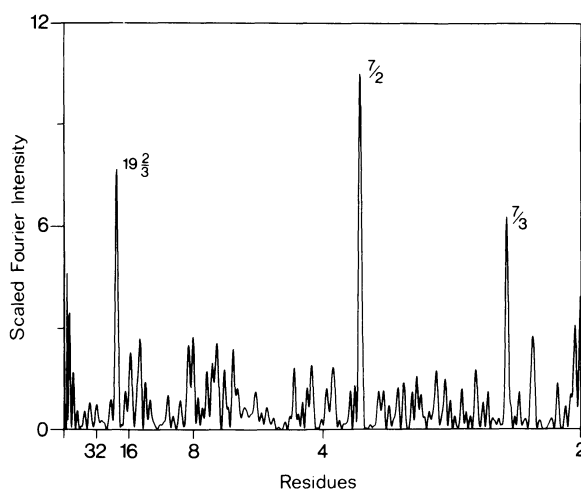


**Fig. 1.** Fourier transform of the acidic residues in the protein sequence of rabbit $\alpha$-tropomyosin (Stone & Smillie, 1978) showing strong peaks at 7/2 and 7/3 residues, associated with the coiled-coil heptad repeat, and also a peak at about 19.7 residues. This latter peak derives from the zones of negative charge that are thought to be related to actin binding (see Stewart & McLachlan, 1975).

## TROPOMYOSIN

Tropomyosin is a component of the actin-containing filaments of muscle and many non-muscle cells. It is a rod shaped molecule which, in vertebrate skeletal muscle, is constructed from two 284-residue chains arranged parallel and in register (Caspar, *et al.*, 1969; Stewart, 1975). In skeletal muscle it forms an important component of the Ca-operated control of contraction. The molecule lies in the grooves of the actin helix of thin filaments and changes its azimuthal position in response to Ca-related changes in troponin, another constituent of thin filaments (reviewed by Phillips, *et al.*, 1987). Each tropomyosin molecule is associated with 7 actin units and so one might expect there to be 7 equally-spaced actin binding sites along tropomyosin. In fact, Fourier analysis (Stewart & McLachlan, 1975; McLachlan & Stewart, 1976) shows a strong and significant peak corresponding to approximately 14.7 repeats in the acidic residues along the sequence (see Fig. 1). The non-integral number of repeats is a consequence of the overlapping of the ends of consecutive tropomyosin molecules along the thin filament and, if the molecules

overlap by 8-9 residues, then there would be 14 repeats along the sequence. Close analysis of these repeats indicates that alternate repeats are slightly different and probably represent the sites for the two different tropomyosin azimuthal binding positions to actin (McLachlan & Stewart, 1976; Phillips, *et al.*, 1986). As illustrated in Figure 2, these zones of negative charge would be arranged in quasi-equivalent positions to successive actin units in the thin filament if the tropomyosin had a coiled-coil pitch of 13.7 nm (Stewart & McLachlan, 1975) and recent X-ray diffraction studies on crystals (Phillips, *et al.*, 1986; 1987) have confirmed that the tropomyosin coiled-coil pitch does indeed have this value.



troponin       tropomyosin       actin
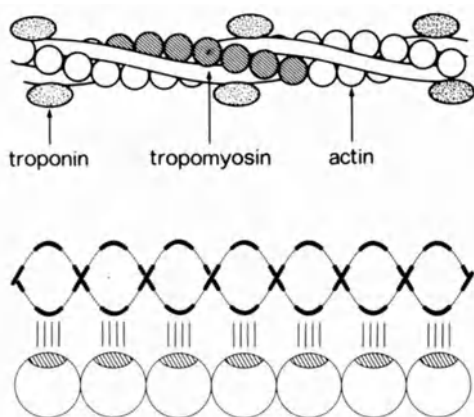
**Fig. 2.** Schematic illustration of how the zones of negative charge in tropomyosin can interact with actin if the coiled-coil pitch is 13.7 nm. With this coiled-coil pitch, the zones form 4 groups of 7 arranged in stripes parallel to the tropomyosin's axis and separated azimuthally by $\pi/2$. One set of 7 zones can interact with actin in the "on" position and another in the "off" position. Reproduced, with permission, from Stewart & McLachlan, *Nature (London)*, **257**:331-333 (1975).

## MYOSIN ROD

The myosin molecule has a long rod-like tail and two globular heads. The heads interact with actin in thin filaments to produce the crossbridges that develop tension and result in the relative sliding of filaments in muscle contraction, whereas the rod-like tails associate to form the shaft of the thick filaments. The myosin tail is an $\alpha$-helical coiled-coil in which the two chains are arranged parallel and in register (Stewart, 1982). In addition to the characteristic coiled-coil heptad repeat of hydrophobic residues in positions *a* and *d*, the myosin rod sequence Fourier transform (Fig. 3) also has a strong periodicity in charged residues with a period of 28 residues (Parry, 1981; McLachlan & Karn, 1982). Furthermore, the

acidic and basic residues within the repeat are segregated so that the rod is traversed by a series of alternating bands of positive and negative charge. These alternating charged bands are thought to play a major role in the interaction between myosin tails in the assembly of thick filaments with adjacent molecules staggered by some odd multiple of 14 residues so that the acidic zones in one molecule are opposite the basic zones of its neighbour (McLachlan & Karn, 1982).
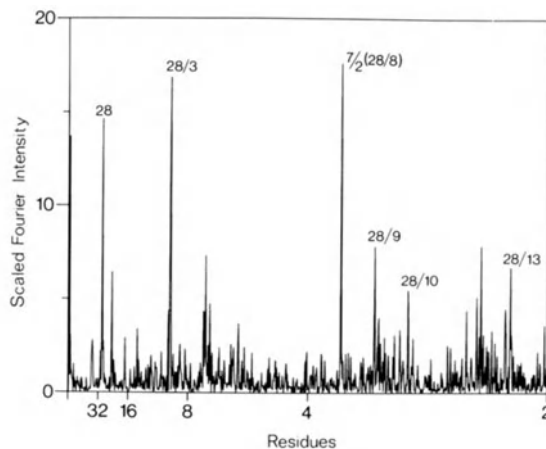


**Fig. 3.** Fourier transform of the acidic residues in the protein sequence of nematode myosin rod, showing again the 7/2 and 7/3 peaks deriving from the heptad repeat, and also peaks at 28 residues and overtones (28/3 and 28/9 are particularly strong) which derive from the bands of alternating charge that are thought to be involved in molecular interactions.

Although the arrangement of myosin heads on the surface of thick filaments has been established in a number of instances (see, for example, Stewart & Kensler, 1987; Stewart, *et al.,* 1985), the detailed packing of the tails in the thick filament shaft has not yet been determined for any species. However, the detailed arrangement of myosin heads determined for frog thick filaments (Stewart & Kensler, 1987) indicates that this arrangement may not be completely straightforward, at least for vertebrate skeletal muscles. One way of investigating the molecular interactions between myosin tails is to examine the behaviour of fragments and, in one instance, it has been possible to form 2-dimensional crystals that, when examined by electron microscopy (Figs 4 and 5), show both the myosin coiled-coil pitch and the molecular interaction geometry (Quinlan & Stewart, 1987). The coiled-coil pitch in these crystals is close to 14.3 nm and adjacent molecules interact in two ways: molecules in the plane of the crystal have their coiled-coils staggered by an odd number of quarter pitches, whereas molecules stacked perpendicular to the plane of the crystal are staggered by an even number of quarter pitches. Only the second of these interaction geometries would be

consistent with the complementation of the alternating charged zones, but the other interaction might possibly be associated with the 3rd and 9th overtones of the basic 28-residue repeat (Quinlan & Stewart, 1987), which give very strong peaks in the
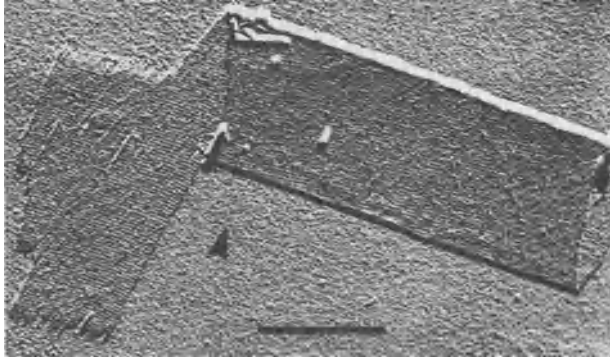


**Fig. 4.** Platinum-shadowed two-dimensional crystalline tube of chicken myosin rod subfragment-2, illustrating how the tube is constructed from a single crystalline sheet rolling up in a right-handed helical manner. Reproduced from Quinlan & Stewart, *J Cell Biol*. **105**:403-415 (1987) by copyright permission of The Rockefeller University Press. Bar 500 nm
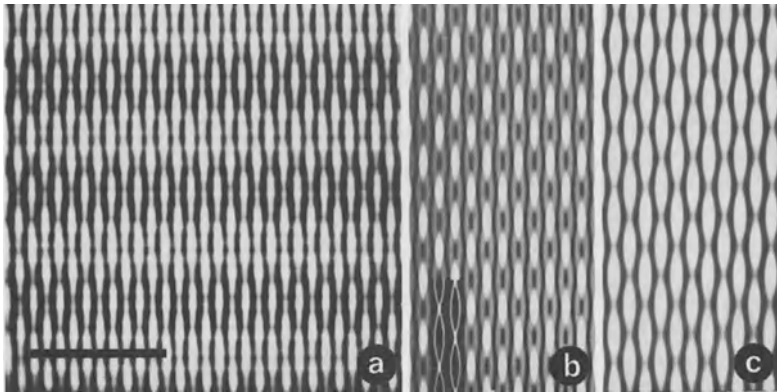


**Fig 5.** Image processing of crystalline tubes to show coiled-coils and interaction geometry. (a) Computer-filtered image of one side of a negatively-stained tube showing long, rod-like molecules with alternating areas of high and low density along them. Computer modelling shows that the areas of high density correspond to the coiled-coil cross-overs. (b) shows ideal coiled-coils whereas (c) shows the model at 2 nm resolution, equivalent to that in the filtered image. These data indicate that the coiled-coil pitch in these crystals is near 14.3 nm and that adjacent molecules across the sheet are staggered by an odd number of quarter-pitches. Molecules stacked perpendicular to the plane of the sheet are staggered by even number of quarter pitches. Reproduced from Quinlan & Stewart, *J Cell Biol*. **105**:403-415 (1987) by copyright permission of The Rockefeller University Press. Bar 20 nm

computed Fourier transform (McLachlan & Karn, 1982). Interestingly, the interaction of the 3rd and 9th order periodicities gives rise to a series of patches of charge on the coil-coil surface and, with a coiled-coil pitch of 14.3 nm successive patches of negative charge are rotated azimuthally by close to $90^o$ so that the charged patches would form 4 rows down the molecule somewhat analogous to the 4 rows of negative charge along the tropomyosin molecule.

The 28-residue repeat of zones of alternating charge may also be important for interactions between the part of the myosin tail that forms the crossbridge in muscle and the thick filament shaft. Bending of the crossbridge portion of the rod allied with attraction between it and the shaft offers an explanation for the elastic crossbridge element detected by mechanical measurements on muscle and may also explain the variation in this parameter as the lateral spacing between filaments is altered (Stewart, *et al.*, 1987).

INTERMEDIATE FILAMENT PROTEINS

Intermediate filaments are a widely-distributed class of cytoskeletal components. The proteins from which they are constituted are members of a large multi-gene family that share considerable amino-acid homologies (reviewed most recently by Conway & Parry, 1988) and includes the keratins, desmin, vimentin, neurofilaments, glial fibrillary acidic protein (GFAP) and the nuclear lamins. All intermediate filament proteins have a common structural basis, with a central coiled-coil rod domain flanked by non-helical N- and C- terminal domains (Geisler & Weber, 1982). The homologies between these proteins are greatest in the rod domain and the specific properties associated with each class of intermediate filament protein derive mainly from differences in the non-helical domains. These proteins all appear to assemble to form filaments primarily through interactions between their rod domains, although interactions involving the remainder of the molecule are also important (see, for example, Kaufmann, *et al.*, 1985). The rod domains of these proteins show a strong 28/3 residue repeat of zones of alternating charge (Parry, *et al,* 1977; McLachlan, 1978; McLachlan & Stewart, 1982) analogous to the strong 3rd order of the 28-residue repeat in myosin rod and it seems likely that a mechanism based on complementation of charged zones is also important in this system. Individual molecules (called "dimers") assemble first to form molecular dimers (called "tetramers") before forming filaments (see, for example, Geisler & Weber, 1982; Quinlan & Franke, 1982; Quinlan, *et al,* 1986; Soellner, *et al.*, 1985), probably by way of subfilaments (see, for example, Aebi, *et al.*, 1983). To investigate the molecular mechanisms of assembly of intermediate filaments in greater detail, we have produced a number of fragments of GFAP by expressing the appropriate c-DNA in *E. coli* . This has enabled the production of a

broad range of fragments that often could not be produced by proteolysis of the whole protein. In addition to enabling the precise role of the non-helical domains in filament formation to be investigated, these fragments also enable the molecular interactions between rods to be investigated using site-directed mutagenesis techniques. One of these fragments, that corresponds broadly to the rod domain of GFAP, forms paracrystals (Fig. 6) that show a characteristic staining pattern.
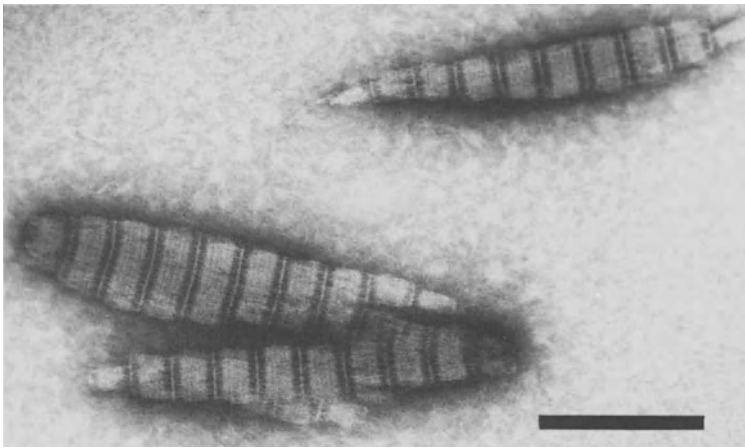


**Fig. 6.** Negatively-stained paracrystal of a fragment of GFAP expressed in *E. coli*. The paracrystal clearly has a gap-overlap structure, in which the two dark bands represent lower protein density and the broad and narrow light bands represent areas of higher protein density. Detailed analysis of this material indicates that the simplest unit cell contains two antiparallel molecules overlapping their N-termini by about 33 nm. Bar 200 nm.

The molecular positions in the paracrystal's unit cell are easily established and correspond to two antiparallel rod molecules overlapping their N-termini by approximately 33 nm. We interpret this as indicating the molecular arrangement within tetramers of this fragment. Interestingly, this sort of arrangement would be consistent with models of intermediate filament structure derived from X-ray diffraction and sequence analysis (Fraser, *et al.*, 1985).

ACKNOWLEDGEMENTS

# REFERENCES

Aebi U Fowler WE, Rew P, Sun T-T (1983) The fibrillar structure of keratin filaments unravelled. *J Cell Biol.* **97**:1131-1143.

Caspar DLD, Cohen C, Longley W (1969) Tropomyosin crystal structure, polymorphism and molecular interactions. *J Mol Biol.* **41**:87-107.

Conway, JF, Parry, DAD (1988) Intermediate filament structure: 3. Analysis of sequence homologies. *Internat J Biol Macromol.* **10**:79-98.

Crick FHC (1953) The Fourier transform of a coiled coil. *Acta Crystallogr.* **6**:685-689.

Fraser RDB, MacRae TP (1973) *Conformation in Fibrous Proteins* , Academic Press, New York.

Fraser RDB, MacRae TP, Suzuki E, Parry DAD (1985) Intermediate filament structure: 2. molecular interactions in the filament. *Internat J Biol Macromol.* **7**:258-274.

Geisler N, Weber K (1982) The amino acid sequence of chicken muscle desmin provides a common structural model for intermediate filament proteins. *EMBO J.* **1**:1649-1656.

Kaufmann E, Weber K, Geisler N (1985) Intermediate filament forming ability of desmin derivatives lacking either the amino-terminal 67 or the carboxy-terminal 27 residues. *J Mol Biol.* **185**:733-742.

McLachlan AD (1978) Coiled-coil conformation  and sequence regularities in the helical regions of alpha-keratin. *J Mol Biol.* **124**:279-304.

McLachlan AD, Karn J (1982) Periodic charge distributions in the myosin rod amino acid sequence match crossbridge spacings in muscle. *Nature (London)* , **299**:226-231.

McLachlan AD, Stewart M (1975) Tropomyosin coiled-coil interactions. *J Mol Biol.* **97**:293-304.

McLachlan AD, Stewart M (1976) The 14-fold periodicity in tropomyosin. *J Mol Biol.* **103**:271-298.

McLachlan AD, Stewart M (1982) Periodic charge distribution in the intermediate filament proteins desmin and vimentin. *J Mol Biol.* **162**:693-698.

Parry DAD (1981) Structure of rabbit skeletal myosin. Analysis of the amino acid sequences of two fragments of the rod region. *J Mol Biol.* **153**:495-464.

Parry DAD, Crewther WG, Fraser RDB, MacRae TP (1977) Structure of alpha-keratin: structural implications of the amino acid sequences of type I and type II chain segments. *J Mol Biol.* **113**:449-454.

Phillips GN, Fillers JP, Cohen C (1986) Tropomyosin crystal structure and muscle regulation. *J Mol Biol.* **192**:111-131.

Phillips GN, Cohen C, Stewart M (1987) Preliminary X-ray diffraction studies and analysis of molecular packing in a new crystalline form of tropomyosin. *J Mol Biol.* **195**:219-223.

Quinlan RA, Franke WW (1982) Heteropolymer filament of desmin and vimentin in vascular smooth muscle tissue and cultured baby hamster kidney cells demonstrated by chemical crosslinking. *Proc Natl Acad Sci USA.* **79**:3452-3456.

Quinlan RA, Stewart M (1987) Crystalline tubes of myosin subfragment-2 showing the coiled-coil and molecular interaction geometry. *J Cell Biol.* **105**:403-415.

Quinlan RA, Hatzfeld M, Franke WW, Lustig A, Schulthess T, Engel J (1986) Characterisation of dimer subunits of intermediate filament proteins. *J Mol Biol.* **192**:337-349.

Soellner P, Quinlan RA, Franke WW (1985) Identification of a distinct soluble subunit of an intermediate filament protein: tetrameric vimentin from living cells. *Proc Natl Acad Sci USA.* **82**:7929-7933.

Stewart M (1975) Tropomyosin: no stagger between chains. *FEBS Letters* **53**:5-7.

Stewart M (1982)  Chain register in myosin rod. *FEBS Letters* **140**:210-212.

Stewart M (1988)  Introduction to the computer image processing of electron micrographs of two-dimensionally ordered biological material. *J EM Tech..* **9**:301-324.

Stewart M, Kensler RW (1986) The arrangement of myosin heads in relaxed thick filaments from frog skeletal muscle. *J Mol Biol.* **192**:831-851.

Stewart M, McLachlan AD (1975) 14 actin-binding sites on tropomyosin? *Nature (London),* **257**:331-333.

Stewart M, Kensler RW, Levine RJC (1985) Three-dimensional reconstruction of thick filaments from *Limulus*  and scorpion muscle. *J Cell Biol.* **101**:402-411.

Stewart M, McLachlan AD, Calladine CR (1987)  A model to account for the elastic element in muscle crossbridges in terms of a bending myosin rod. *Proc Roy  Soc London, Ser B.* **229**:381-413.

Stone D & Smillie LB (1978). The amino acid sequence of rabbit skeletal alpha-tropomyosin. *J Biol Chem.* **253**:37-1148.

# The Self-Assembly of Nonsarcomeric Myosins

R.A.Cross

*MRC Laboratory of Molecular Biology, Hills Road, Cambridge CB2 2QH, U.K*

Myosin filaments generate tension between arrays of parallel actin filaments. This happens most obviously in muscles, but is required in the cell cycle of every eukaryotic cell at least once, at cytokinesis. Myosin filaments from striated muscle cells contain extra proteins and appear uniquely stable. Those from all other eukaryotic cells, including those of smooth muscle , are thought to assemble *ad hoc* from a pool of free molecules [Yumura and Fukui, 1985]. Cells appear to regulate this assembly by converting free molecules into and out of an assembly-blocked storage conformation.

Little is known about the subsequent steps of the assembly mechanism. There are several nonequivalent packing environments in a myosin filament, and definition of the kinetic mechanism of self-assembly consequently appears daunting. Small [1988] has outlined recent progress. I will suggest that in spite of this complexity, the assembly behaviour of nonsarcomeric myosins can be modelled using a simple nucleation-linear propagation mechanism. In other words, the myosin binding sites on a growing myosin filament are effectively all at the filament ends, and these sites fill up in a loosely sequential way so that *on average* the affinity of the filament ends for free myosin is constant.

## Propagation

The growth and shrinkage of myosin filaments could occur by many routes. In the simplest case, subunits (dimers?) would exchange only from the filament ends, and in strict sequence, so that any one filament end would have only one target site for an attacking subunit. Complications could include multiple target sites of different affinity, and the breakage and reannealing of filaments. Observations suggest however that these reactions are not significant.

The rate of disassembly of filaments can be measured using light scattering to report the mass concentration of myosin filaments. To measure purely the disassembly rate, conditions must be found in which the contribution of the assembly reaction to the measured rate becomes negligible. For smooth muscle myosin, this can be done by adding enough MgATP to saturate the high affinity binding sites in the myosin heads. MgATP stabilises the assembly-blocked folded monomer conformation of this myosin [Cross, 1988]. In the presence of MgATP, myosin molecules which dissociate from the filament go straight into the folded storage conformation, instead of going back on again. The filaments disassemble until the equilibrium free monomer concentration in MgATP is reached. Provided the total myosin concentration is well below this, disassembly goes to completion and the reverse reactions of assembly do not contribute significantly to the measured rate.
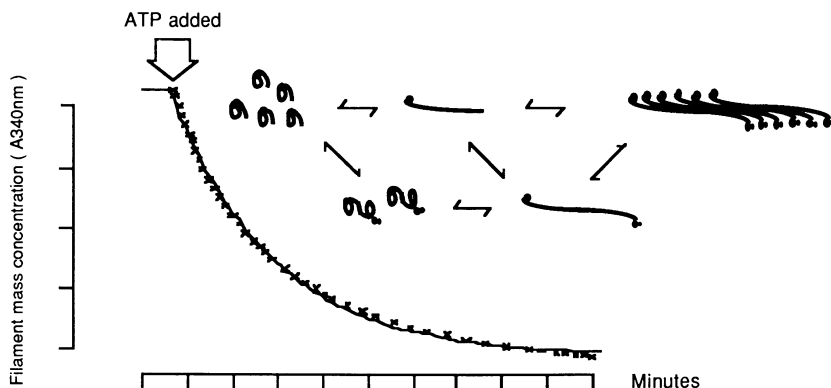
**Figure 1**. Disassembly of smooth muscle myosin filaments at 20 °C by MgATP. Addition of a fivefold molar excess of MgATP produces complete filament disassembly. *Conditions* 150 mM NaCl, 10 mM imidazole, 1 mM MgCl₂, 0.5 mm DTT, pH 7.3. The myosin filaments were 0.3 mg/ml. *Overlay* Assembly intermediates. MgATP drags the assembly equilibria to the left, disassembling the filaments.

Observed disassembly curves (fig. 1) are well fit by a single exponential, except at the end of the reaction, when large numbers of filaments are very short, and the linear relationship of turbidity to filament length breaks down [Berne, 1974]. This result is predicted if the initial filament length distribution is approximately exponential, and disassembly proceeds from each filament end only, at a constant rate [Purich et al.,1982].

Quite aside from this argument however, it is clear that the filament ends are the major sites of disassembly, because populations of short filaments disassemble faster than populations of long filaments, at constant myosin concentration [Cross, *in prep.*]. The more ends, the faster the disassembly.

The rate of disassembly is the same as the rate of assembly at equilibrium. For our standard filament preparation, the halftime for disassembly of an average filament (about 2 µm long) is about 30s at 20ºC (see figure). Calculation of the rate at which *molecules* dissociate must await a determination of filament mass/length.

## Nucleation

If myosin in solution at high ionic strength is rapidly diluted into filament-forming ionic conditions, the result is a large number of relatively short filaments, typically less than 1µm long, and often much shorter. A very different result is obtained when the filament formation conditions are approached more slowly, for example by a controlled slow decrease of ionic strength. Filaments of 10 µm or more are then produced [Sobieszek, 1972; Hinssen et al.,1978]. This behaviour can be explained if a high myosin monomer concentration favours the formation of many nucleii, whilst a low monomer concentration disfavours nucleation, but still allows the propagation of existing filaments to occur. The concentration of myosin monomers necessary to initiate a new filament would then be higher than that present in equilibrium with the assembled filaments. New nucleii would therefore not be formed at equilibrium. If this type of mechanism does operate, and if filament annealing is not a significant reaction, then deliberate shearing of the filaments should produce a permanent length redistribution. Fig 2 shows that myosin filaments

are indeed permanently shortened by shearing, in marked contrast to actin or tubulin, which recover an equilibrium length distribution after shearing.
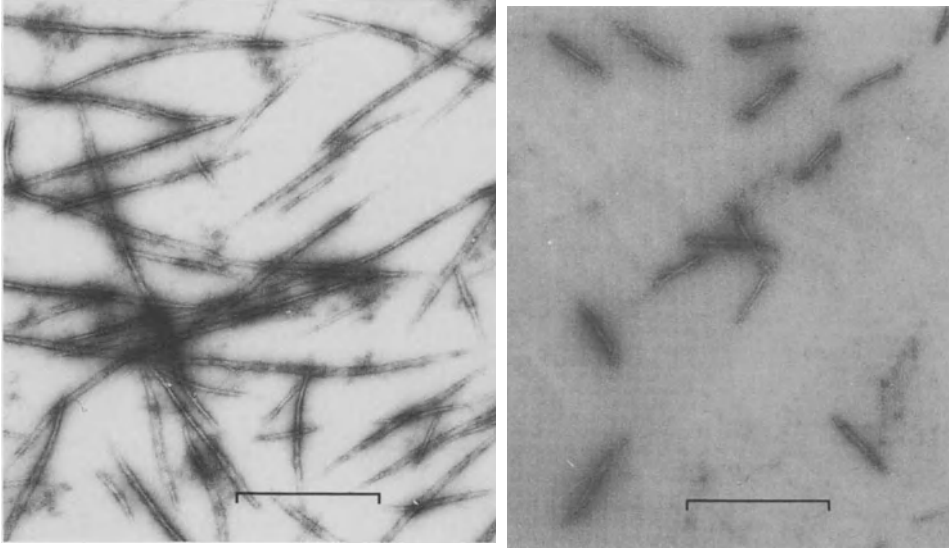


**Figure 2**. In vitro-assembled smooth muscle myosin filaments, negatively stained with 1% uranyl acetate. [A] Long filaments. [B] The same preparation of filaments after 7 passes through a 26 gauge needle. The grid was made 50 minutes after the shearing. The myosin concentration was 0.5 mg/ml in both cases. The buffer and temperature were as for figure 1. The scale bars represent 1 μm.

## Conclusions

None of the data so far exclude that myosin molecules can flip into and out of the body of a filament, but they do suggest that this process is considerably slower than addition to and loss of molecules from the filament ends. Filament initiation appears to depend on an unfavourable nucleation reaction which occurs only once in the history of a filament, and rarely if at all at equilibrium.

### References

Berne, B.J. (1974) Interpretation of the light scattering from long rods, J. Mol. Biol. **89** 755

Cross, R.A. (1988) What is 10S myosin for ? J. Mus. Res. Cell Mot. **9** 108-110

Hinssen,H., D'Haese,J., Small, J.V. and Sobieszek,A. Mode of filament assembly of myosins from muscle and nonmuscle cells, J. Ultrastruc. Res. **64** 282-302

Purich, D.L., Karr, T.L. and Kristofferson,D. (1982) Microtubule disassembly: A quantatative kinetic approach to defining endwise linear depolymerisation, Met. Enzymol. **85** 439-450

Small, J.V. (1988) Myosin filaments on the move, Nature **331** 568-569

Sobieszek (1972) Crossbridges on synthetic smooth muscle myosin filaments, J. Mol. Biol. **70** 741-744

Yumura ,S.and Fukuii ,Y.(1985) Reversible cyclic-AMP-dependent change in distribution of myosin filaments in Dictyostelium, Nature **314** 194-196

# Shape Changes in Myosin Induced by the Regulatory Light Chain Subunits

M.C.Schaub, A.Jauch, P.Huber, U.T.Brunner and T.Wallimann*

Pharmacological Institute, University of Zürich, Gloriastrasse 32,
CH-8006 Zürich, and Institute of Cell Biology*, Swiss Federal Institute
of Technology, Hönggerberg, CH-8093 Zürich, Switzerland

Myosin is a hexamer comprising two heavy chains (HC) of around 200 kDa and 4
light chains (LC) in the range of 16-22 kDa. Roughly half of the HC are alpha-
helical towards their C-terminal and form together the coiled-coil rod of 145 nm
length. The N-terminal halfs curl up into the globular head portions each bearing
a catalytic and an actin binding site. An alkali-type LC and a regulatory LC
(RLC) is non-covalently associated with each head. Even if the two HC are
identical in structure, the heads cannot simultaneously undergo identical
interactions with an actin filament during contraction. In fact, one-headed
myosin or proteolytically isolated heads (subfragment-1) are able to support
actin filament movement when attached to a solid surface (Harada et al., 1987;
Toyoshima et al., 1987). If the capability for movement is localized in the head
moiety, the two heads of a myosin must function together in some cooperative
manner. Our results indicate that in skeletal muscle myosin the RLC may be
involved in coordinating the functioning of the two heads in a crossbridge.


## Materials and Methods

Myosin (Watterson et al., 1975) and purified actomyosin devoid of troponin and
tropomyosin (Schaub et al., 1967) was prepared from rabbit fast-twitch skeletal
muscles. RLC was removed from myosin by limited proteolysis of the actomyosin by
alpha-chymotrypsin (ratio to RLC = 1:1'000) in the presence of 0.5-1.0 mM
dithio-bis-nitrobenzoic acid (DTNB), 5 mM EDTA at low salt concentrations and pH
7.5, followed by washings, reduction with dithiothreitol, dissociation from actin
by Mg-ATP at 0.7 M KCl and fractionation at 35-68% ammonium sulfate saturation.
Subfragment-1 (isolated myosin heads), rods and light meromyosin (LMM) were
prepared by proteolysis with alpha-chymotrypsin (Weeds & Taylor, 1975). Gel
permeation was performed on Sepharose-4B columns (1.5 x 90 cm) in 0.7 M KCl and
2mM EDTA. Electron microscope graphs of myosin spread on mica sheets were taken
after air-drying and rotary shadowing with platinum and evaluated as described
elsewhere (Walzthöny et al., 1984).

## Results and Discussion

The actin activated ATPase of myosin devoid of both RLC is the same as with intact myosin. After dissociation from actin the RLC-free myosin tends to form aggregates, mainly dimers, some trimers and few higher oligomers as revealed by electron microscopy (EM) and gel filtration. The aggregated molecules stick together in the head region with their tails projecting apart separately. Quantitation of the intermolecular aggregates agreed between gel filtration and EM counting techniques. Also the monomeric fraction of RLC-free myosin displays altered gel filtration properties. It elutes significantly ahead of intact myosin ($p < 0.001$ with $n1 = n2 = 17$) as if it had a larger mass, yet its mass is 8% lower because it lacks the two RLC. These differing elution properties were affected neither by ATP nor by reducing agents. The Stokes' radius was determined by the gel permeation technique for intact myosin, monomeric RLC-free myosin, isolated heads, the entire rod portion and LMM (Table). This allowed to derive the maximal axial ratio according to Perrin, i.e. the degree of asymmetry of the anhydrous proteins (Cantor & Schimmel, 1980). The results indicate that RLC-free myosin is more asymmetric than intact myosin. The degree of asymmetry for RLC-free myosin is very similar to that for isolated rod and for LMM. The maximal axial ratio and length corresponds to a cross-sectional diameter of 14-15 Å for the straight LMM portion. The rod with the same molecular diameter as LMM but a contour length of 145 nm ought to have an axial ratio of around 104. Its lower axial ratio of only 68 indicates that the rod cannot be straight but must be bent. In fact, light scattering and proton nuclear magnetic resonance data are consistent with a rigid rod once bent in the hinge region between LMM and the

Table: Molecular parameters for intact myosin, myosin devoid of regulatory light chains (RLC) and for its subfragments (Stokes' radii are derived from gel permeation experiments at high salt concentrations)

| Symbol for corresponding protein preparation | Molecular mass (kDa) | Molecular length (nm) | Stokes radius (Å) | Maximal axial ratio |
|---|---|---|---|---|
| Myosin | 470 | 160 | 156 | 53 |
| Myosin devoid of RLC | 432 | 160 | 169 | 66 |
| Rod | 220 | 145 | 137 | 68 |
| Light meromyosin (LMM) | 140 | 90 | 113 | 64 |
| Subfragment-1 (isolated head) | 110 | 18 | 50 | 11 |

shorter subfragment-2 portion, adopting an average angle of 128 degrees between them (Highsmith et al., 1982). Assuming the rod portion having identical dimensions the results imply that in RLC-free myosin the masses of the two heads must be drawn closer towards the rod axis. If the disposition of the RLC-free heads were not altered only a significantly longer rod, or else, a rigid and much striaghter rod could explain the higher axial ratio of 66 as opposed to 53 for intact myosin. In EM studies the head portions of RLC-free myosin are 18% shorter (p < 0.001 with n1 = 124 and n2 = 92) and some mass seems to be missing in the neck region between the two heads while their width is the same as in intact myosin. The RLC-free heads appear close together as if they interacted with one another. These shape changes in monomeric RLC-free myosin as well as the intermolecular aggregations are reversible upon reconstitution with exogenous RLC. Isolated rods never aggregated nor did isolated heads which lack the RLC when prepared by alpha-chymotrypsin. The sticky patch responsible for the hydrophobic intra- and intermolecular interactions seems to reside in a HC region near the base of the heads where they are joined to the rod and which is lost during proteolytic fragmentation. The head HC bears almost no net charges as judged from isoelectrofocusing. On the other hand, each RLC contains an excess of 8 negative charges. Since the RLC are bound by hydrophobic forces mainly they are expected to introduce negative charges on both head moieties. This could result in repulsion keeping the two heads apart. This, in turn, may prevent hydrophobic interaction between the sticky patches in myosin heads within individual molecules as well as between adjacent molecules in the filament.

## References

Cantor CR, Schimmel PR (1980) Biophysical chemistry. W.H.Freeman Co, San Francisco

Harada Y, Noguchi A, Kishino A, Yanagida T (1987) Sliding movement of single actin filaments on one-headed myosin filaments. Nature 326:805-808

Highsmith S, Wang CC, Zero K, Pecora R, Jardetzky O (1982) Bending motions and internal motions in myosin rod. Biochemistry 21:1192-1197

Schaub MC, Perry SV, Hartshorne DJ (1967) The effect of tropomyosin on the adenosine triphosphatase activity of desensitized actomyosin. Biochem J 105:1235-1243

Toyoshima YY, Kron SJ, McNally EM, Niebling KR, Toyoshima C, Spudich JA (1987) Myosin subfragment-1 is sufficient to move actin filaments in vitro. Nature 328:536-539

Walzthöny D, Eppenberger HM, Wallimann T (1984) Shadowing of elongated helical molecules (myosin, tropomyosin, collagen and DNA) yields regular molecule-dependent heavy metal grain patterns. Eur J Cell Biol 35:216-225

Watterson JG, Schaub MC, Locher R, DiPierri S, Kutzer M (1975) Temperature-induced transitions in the conformation of intermediates in the hydrolytic cycle of myosin. Eur J Biochem 56:79-90

Weeds AG, Taylor RS (1975) Separation of subfragment-1 isoenzymes from rabbit skeletal muscle myosin. Nature 257:54-56

# Plectin/Vimentin Interaction: Molecular Binding Domains and Regulation by Phosphorylation

R. Foisner, B. Feldman and G. Wiche

Institute of Biochemistry

University of Vienna

A-1090 Vienna, Austria

## Introduction

Plectin is a high molecular weight cytomatrix protein of widespread occurrence. In most cultured cell lines it was found to be part of cytoplasmic network arrays that appeared more dense and delicate than those of vimentin filaments after conventional fixation. Plectin and vimentin arrays appeared nearly identical, however, after extraction of cells with detergent, causing the release of a sizable fraction of cellular plectin (Herrmann and Wiche, 1983). These observations suggested that only part of the cytoplasmic plectin is associated with intermediate filaments while the rest is bound to more soluble structures or is forming a network of its own. There is, indeed, evidence that plectin interacts with several distinct cellular structures and that it acts as a general crosslinker of the cytomatrix (for review see Wiche, 1988). Here we report on molecular aspects of plectin's interaction with vimentin.

## *In Situ* and *In Vitro* Localization of Plectin on Vimentin Filaments

The association of plectin with vimentin filaments was demonstrated *in situ* by gold immunoelectron microscopy of microtubule- and actin-depleted as well as of quick frozen/deep etched cytoskeletons of fibroblast cells (Foisner et al. 1988a). In both cases, plectin was visualized primarily at junctions and cross-over sites of filaments rather than along their entire surface. Rotary shadowing electron microscopy of intermediate filaments reconstituted *in vitro* from purified samples of vimentin and plectin confirmed these observations. This technique also revealed that oligomeric and polymeric plectin structures (Foisner and Wiche, 1987), rather than single molecules, were attached to vimentin filaments.

## Molecular Domains Involved in the Binding of Plectin to Vimentin

To analyze, which of the molecular domains of vimentin were interacting with plectin molecules, vimentin was subjected to limited chymotryptic digestion, yielding fragments of known size and structure (Geisler et. al, 1982, Nelson and Traub, 1983). Plectin overlays onto these fragments transblotted to nitrocellulose revealed binding to both, intact vimentin and fragments containing the central rod domain of the molecule (Foisner et al. 1988a), which is well conserverd in structure and common to all intermediate filament proteins (Geisler et al. 1982, Steinert et al. 1985). Plectin molecules consist in solution of four 300 kDa polypeptide chains arranged in a dumb bell-shaped structure. To determine, which of the molecular domains of plectin interact with vimentin, defined plectin fragments obtained after digestion of plectin with elastase, protease V8 or trypsin were overlaid with vimentin. Binding of vimentin was observed to intact plectin and to plectin fragments of Mr between 300,000 and 100,000 (Foisner et al. 1988b). Characterization of these fragments by rotary shadowing electron microscopy and by immunoreaction with monoclonal antibodies specific for plectin's rod domain suggested that these fragments contain the intact rod domain of plectin molecules. Therefore the rod domain of plectin seems to be involved in the interaction with vimentin. Since the rod domains of both vimentin and plectin display a α-helical double stranded coiled coil conformation, the binding of plectin to vimentin seems to occur via the interaction of two α-helical coiled coil domains.

## Regulation of the Plectin Vimentin Interaction by Phosphorylation

A role of phosphorylation in plectin's interaction with the cytoskeleton has previously been suggested by the observation that cytoskeleton-bound plectin was about three times higher phosphorylated than the soluble protein species (Herrmann and Wiche, 1983). Furthermore, the *in situ* phosphorylation of plectin in detergent resistant cytoskeletons revealed it as a substrate of cAMP-independent, cAMP-dependent and Ca/Calmodulin-dependent kinases (Herrmann and Wiche, 1983, 1987). In addition, purified plectin was phosphorylated *in vitro* to an extent of 0.8 to 1 mol P/mol of plectin by cAMP-dependent kinases as well as protein kinase C. To test the influence of phosphorylation on plectin's interaction with vimentin, plectin samples that had been phosphorylated either by cAMP-dependent kinase or protein kinase C or had been dephosphorylated by alkaline phosphatase, were transblotted to nitrocelulose and overlaid with vimentin. An increase in vimentin binding of 30-60% was observed for plectin phosphorylated by cAMP-dependent kinases as compared to untreated or

dephosphorylated samples. Kinase C, on the other hand, caused a decrease in vimentin binding of about 30%. Similar results were obtained when plectin already immobilized on nitrocellulose was phosphorylated prior to the overlay. In contrast, phosphorylation of vimentin by cAMP-dependent kinase, which occurs primarily at the aminoterminal domain of the molecule (Geisler and Weber, 1988, Evans, 1988) and regulates vimentin-vimentin interaction (Inagaki et al.), was found to have no effect on the interaction of vimentin with plectin.

## References

Evans RM (1988) The intermediate filament proteins vimentin and desmin are phosphorylated in specific domains. Europ J Cell Biol 46:152-160

Foisner R, Wiche G (1987) Structure and hydrodynamic properties of plectin. J Mol Biol 198:515-531

Foisner R, Leichtfried FE, Herrmann H, Small JV, Lawson D, Wiche G (1988a) Cytoskeleton associated plectin: In situ localization, *in vitro* reconstitution, and binding to immobilized intermediate filament proteins. J Cell Biol 106:723-733

Foisner R, Feldman B, Wiche G (1988b) Partial proteolysis and localization of self-interaction and vimemtin binding sites on separate molecular domains. Protoplasma: in press

Geisler N, Kaufmann E, Weber K (1982) Proteinchemical characterization of three structurally distinct domains along the protofilament unit of desmin 10nm filaments. Cell 30:277-286

Geisler N, Weber K (1988) Phosphorylation of desmin *in vitro* inhibits formation of intermediate filaments; identification of three kinase A sites in the aminoterminal head domain. EMBO J 7:15-20

Herrmann H, Wiche G (1983) Specific *in situ* phosphorylation of plectin in detergent-resistant cytoskeletons from cultured chinese hamster ovary cells. J Biol Chem 258:14610-14618

Herrmann H, Wiche G (1987) Plectin and IFAP-300 are homologeous proteins binding to microtubule-associated proteins 1 and 2 and to the 240 kilodalton subunit of spectrin. J Biol Chem 262:1320- 1325

Inagaki M, Nishi Y, Nishizawa K, Matsuyama M, Sato C (1987) Site- specific phosphorylation induced disassembly of vimentin filaments *in vitro*. Nature 328:649-652

Nelson WJ, Traub P (1983) Proteolysis of vimentin and desmin by a Ca activated proteinase specific for these intermediate filament proteins. Mol Cell Biol 3:1146-1156

Steinert PM, Steven AC, Roop DR (1985) The molecular biology of intermediate filaments. Cell 42:411-419

Wiche G (1988) Plectin: General overview and appraisal of its potential role as a subunit protein of the cytomatrix. CRC Critical Reviews in Biochemistry: in press

# Interaction of Phosphoproteins with Calcium Phosphate

C. Holt and R.T. Bailey[a]
Hannah Research Institute
Ayr, KA6 5HL, UK.

Highly phosphorylated phosphoproteins are associated with many types of mineralization processes in biology. The binding of phosphoproteins to mineral surfaces and their action in controlling the precipitation of salts from solution are little understood, particularly with regard to the influence of the structure of the proteins on their biological function. The casein phosphoproteins occur naturally in milk as large particles called casein micelles which scatter light strongly. In these micelles, the caseins are linked through their phosphate groups to a very highly dispersed amorphous calcium phosphate which cements the protein monomers together. It is possible, therefore, that the proteins have a different conformation in the native casein micelle than in solution, free of calcium phosphate. Accordingly, a study of the infrared spectra of casein micelles and casein in free solution has begun and preliminary results are available.

Infrared spectra were recorded using a Nicolet 20 SXB spectrometer equipped with a mercury cadmium telluride detector. Spectra of casein micelles, suspended in aqueous or $^2H_2O$ buffers, were obtained using a Specac zinc selenide crystal attenuated total reflection cell, modified to allow solutions to be introduced from outside the spectrometer. This modification was required to enable sample, buffer and solvent to be replaced in the cell without perturbing the optical path length or purging gas composition. The spectrum of casein, free of calcium phosphate, was also recorded in the aqueous buffer. Buffers were designed specifically to ensure that the casein micelles were stable during the whole experiment. The $Ca^{2+}$ and phosphate ion concentrations were adjusted to produce a free $Ca^{2+}$ concentration of 3.5 mM and a buffer which was close to saturation with respect to the micellar calcium phosphate.

The spectrum of casein micelles differed from that of whole casein in free solution in the amide I, amide III and phosphate stretching regions. The change in the phosphate stretching region allows the infrared spectrum of the micellar calcium phosphate to be obtained by difference. Moreover, the changes in the amide I and amide III bands demonstrate a change in conformation of the protein on complexation with calcium phosphate.

---

[a] Department of Chemistry, Strathclyde University, Glasgow G1 1XL
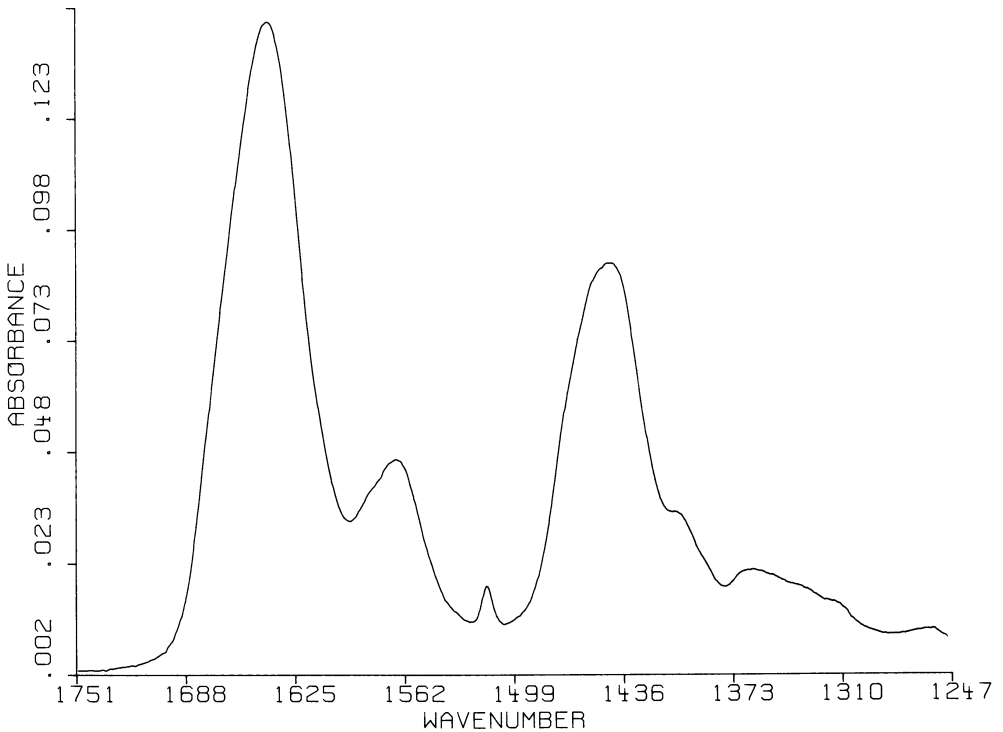
Fig. 1    Spectrum of bovine casein micelles in $^2H_2O$ buffer.

Compared to $H_2O$ solution, the $^2H_2O$ spectrum shows a substantial reduction in the intensity at 1550 cm$^{-1}$, suggesting that while the conformation of the casein changes on binding to the calcium phosphate, most of the peptide bonds remain accessible to the solvent.

It has been proposed (Holt and Sawyer, 1988; Holt and van Kemenade, 1989) that one of the principal functions of many highly phosphorylated phosphoproteins in calcifying systems is to modulate the precipitation of calcium phosphate from solution. The relatively flexible conformation and low content of regular secondary structures of the caseins in free solution may therefore facilitate rapid and non-stereospecific binding to the surface of calcium phosphate nuclei.

Holt C and van Kemenade MJJM (1989) The interaction of phosphoproteins with calcium phosphate. In: Hukins DWL (ed) Calcified Tissue. Macmillan, Basingstoke, Hants, in the press

Holt C and Sawyer L (1988) Primary and predicted secondary structures of the caseins in relation to their biological functions. Protein Engineering 4: in the press

# Thermal Stability and Folding of the Triple Helices of Interstitial and Basement Membrane Collagens

Hans Peter Bächinger, Nicholas P. Morris and Janice M. Davis
Research Unit, The Shriners Hospital for Crippled Children and
Department of Biochemistry, Oregon Health Sciences University
3101 SW Sam Jackson Park Road
Portland, OR 97201
USA

## Introduction

Vertebrate collagens comprise a family of extracellular matrix proteins which form fibrils or networks containing one type (homotypic) or multiple types (heterotypic) of molecules. Each of the twelve genetically distinct types of collagen contains multiple structural domains. By definition, one or more of these domains is the unique collagen triple helix. The collagen structural motif can be generalized as three colinear polypeptides forming a central triple helix flanked at both the amino and carboxyl ends by non-helical domains. Where these flanking regions are subsequently removed by specific proteolysis, the parent molecule is called a procollagen. The triple helix then provides an extended conformation which forms higher order aggregates through lateral associations. In some cases, end to end interactions are mediated through retained non helical domains flanking the helix.

Variations in this motif provide a basis for classification of the different collagen types (Miller 1985). A primary distinction is whether the triple helix is continuous or contains interspersed nonhelical regions. The interstitial collagens, types I, II, III, V, and XI, have in common a continuous triple helix with a length of approximately 300 nm and proteolytic processing of the globular domains. Not surprisingly, these collagens are functionally related in that they all appear to participate in the formation of the classical quarter stagger, banded collagen fibril. The function(s) of the globular domains is not well understood. The carboxyl propeptide directs the association of the correct combinations of pro$\alpha$ chains into the appropriate homopolymer or heteropolymer and sets the stage for folding of the triple helix. The amino propeptide, once removed, may participate in feedback regulation of collagen synthesis. The members of this group are distinguished by their tissue distribution and the rate, sequence, and extent of removal of globular domains. These latter features appear to regulate fibril assembly.

The triple helical domain of type IV collagen is divided into subdomains by short (less than 20 amino acids) non helical interruptions. Type IV collagen forms a network restricted to basement membranes. The carboxyl globular domain (NC1) forms dimeric intermolecular associations with another carboxyl globular domain. The amino terminal domain, referred to as "7S", is composed of helical and non helical elements and forms intermolecular tetrameric associations.


## Thermal stability of the triple helix

The collagen triple helix is formed by three polypeptide chains with a repetitive sequence of Gly-Xaa-Yaa, where Xaa is often proline and Yaa is often hydroxyproline. Each of these chains forms a left-handed polyproline II helix, which interact with two other helices to form a right-handed superhelix. An interesting feature of the triple helix is that it undergoes a sharp helix to coil transition at a temperature close to body temperature. What forces contribute to the stability of the triple helix? Hydrophobic interactions are unlikely because there are not many nonpolar residues, which could form extended clusters. Also, van der Waals contacts contribute little because the collagen triple helix is not a compact structure. Finally electrostatic interactions do contribute somewhat to the stability, but only minor changes in stability are observed by changes in pH and ionic strength. By elimination it is evident that most of the stability of the triple helix comes from hydrogen bonding (Privalov 1982). Hydrogen exchange studies reveal that there are two classes of hydrogen bonds in the triple helix. There are $1.0\pm0.1$ very slowly and $0.7\pm0.1$ slowly exchangeable hydrogen per tripeptide unit (Privalov et al. 1979). X-ray diffraction studies confirm a hydrogen bond between the amino group of glycine and the carbonyl group of the Xaa residue and additional stabilization involving water molecules and the carbonyl group of the Yaa residue. If the Xaa and Yaa residues are not imino acids further hydrogen bonds between the amino groups and water molecules can be formed (Fraser et al. 1979). Because of the correlation of the stability of the triple helix of various collagens with the hydroxyproline content (Burjanadze 1979), several models were proposed that involve hydrogen bonds between the hydroxyl group of hydroxyproline and water molecules. It was also found that the proline content correlates with thermal stability, but not as well as the

hydroxyproline content (Privalov 1982).

The thermal stability of collagen molecules is expressed as the melting temperature ($T_m$), i.e. the midpoint of the triple helix to random coil transition. This transition can be measured by monitoring optical properties like circular dichroism (CD), optical rotatory dispersion (ORD) or difference UV spectroscopy, by changes in hydrodynamic parameters such as the sedimentation coefficient or intrinsic viscosity, or by light scattering experiments (Engel 1987). The increased susceptibility to proteases upon denaturation has also been used to monitor the thermal stability of collagens (Bruckner and Prockop 1981). Several monoclonal antibodies recognizing triple helical epitopes have been successfully employed to determine the stability of triple helices in situ (Linsenmayer et al. 1984). For the evaluation of thermodynamic parameters the most direct method to monitor the stability is differential scanning calorimetry. The enthalpy and entropy changes of the triple helix coil transition depend on the type of collagen and from what species it was extracted. Both enthalpy and entropy changes increase with increasing stability (Privalov 1982).

Measurements of type I collagen by optical methods show a sharp single transition. The same results are obtained when viscosity is used to monitor unfolding, indicating a highly cooperative all-or-none process. However calorimetric measurements show a transition enthalpy of 19,500 kJ $mol^{-1}$ whereas the effective van't Hoff enthalpy is only 1,600 kJ $mol^{-1}$. From the ratio of the calorimetrically determined transition enthalpy and the van't Hoff enthalpy the size of a cooperative block was determined to be about 250 amino acid residues or a triple helical segment about 80 residues long (Privalov 1982). Interestingly a "predenaturational" transition is observed by calorimetric measurements in certain buffers, although it was not detected by optical methods (Privalov and Tiktopulo 1970). This suggests that major conformational changes occur in the molecule before the cooperative unfolding. The triple helix may therefore contain micro-unfolded states at a temperature range below the melting temperature. Hydrogen exchange studies also show that at the "predenaturational" transition, regions of about four amino acid residues unfold (Privalov et al. 1979). The large transition enthalpy of the triple helix can not be accounted for by one or two hydrogen bonds per tripeptide unit, but it seems likely that the structure of the solvent molecules (water) around the triple helix contribute additional stability (Privalov 1982).
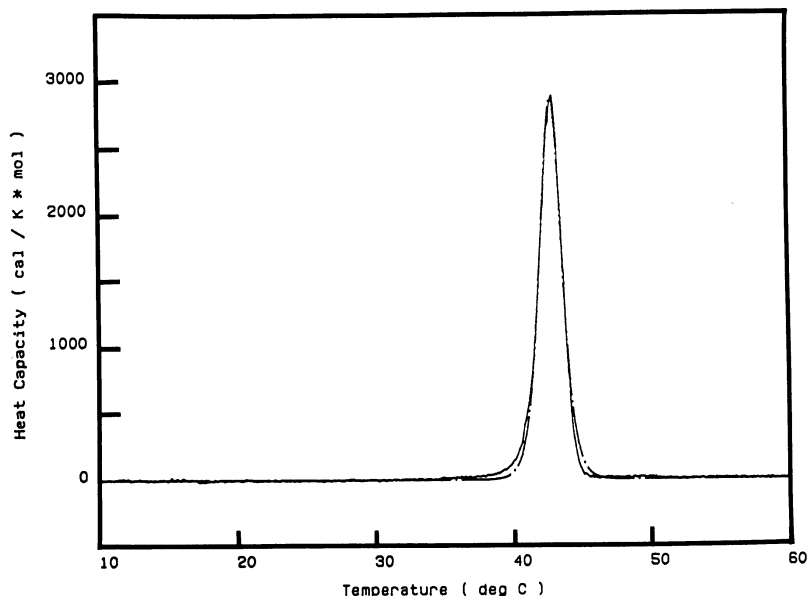
Figure 1. Differential scanning calorimetry of type II collagen.

   Experiments in our laboratory now show that differences exist in the thermal stability of different types of collagens and that for several collagen types a very complex melting behavior is observed. Figure 1 shows the calorimetric analysis of calf cartilage type II collagen in 50 mM Tris/HCl buffer, pH 7.4, containing 0.4 M NaCl. The rate of heating was 12.5 °C/h. The transition enthalpy for this single transition is $\Delta H_{res}$ = 8.5 kJ mol$^{-1}$ per residue and the van't Hoff enthalpy is 1500 kJ mol$^{-1}$. The effective enthalpy is very similar to type I collagen, whereas the calorimetrically determined change in enthalpy is significantly higher. In this buffer system type II collagen does not show a pretransition. This is in contrast to pepsinized calf skin type III collagen in the same buffer, which is shown in Figure 2. Two transitions are observed, a "pretransition" at 36.8 °C and the main transition at 40.6 °C. The total transition enthalpy equals $\Delta H_{res}$ = 6.7 kJ mol$^{-1}$.
   Type XI collagen from calf cartilage shows a complex melting profile, when monitored by circular dichroism at 221 nm. A biphasic transition with transition midpoints at 37.5 °C and 40 °C is found in 50 mM Tris/HCl buffer, pH 7.5, containing 0.4 M NaCl. In addition when the stability is observed by trypsin digestion several fragments of intermediate size are seen on polyacrylamide gels
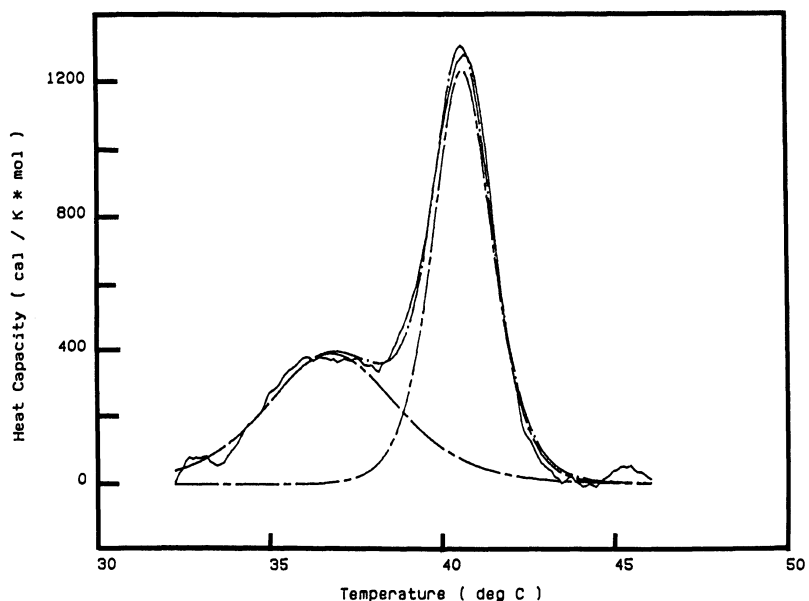
<u>Figure 2.</u> Differential scanning calorimetry of pepsinized type III collagen.

(Morris and Bächinger 1987). The occurrence of these fragments is not seen with type I, II and III collagen. Figure 3 shows a calorimetric analysis of the melting of type XI collagen in Tris/HCl buffer, pH 7.4, containing 0.4 M NaCl. Two major transitions are seen with $T_m$ of 38.5 °C and 41.5 °C. The transition enthalpy is $\Delta H_{res} = 6.1$ kJ mol$^{-1}$, when the data is analyzed as independent transitions. Because of the lack of information on the primary structure of type XI collagen we assumed that all residues are part of the triple helix.

A close structural relationship between type XI and type V collagen has been described. Our experiments with type V collagen ($\alpha 1_2 \alpha 2$) confirm that. All the features described for type XI collagen were also found for type V collagen. Figure 4 shows the thermal unfolding of type V collagen in 50 mM Tris/HCl buffer, pH 7.5, containing 0.4 M NaCl. Again a biphasic melting profile is observed with $T_m$ of 37 °C and 41 °C. The calorimetric analysis reveals a very similar pattern as type XI collagen (data not shown). To rule out kinetic effects upon unfolding, the temperature was raised at 1 °C/h. Basically an identical melting profile is observed shifted about 1 °C towards lower temperatures, but still showing two major transitions. Figure 5 confirms the existence of stable
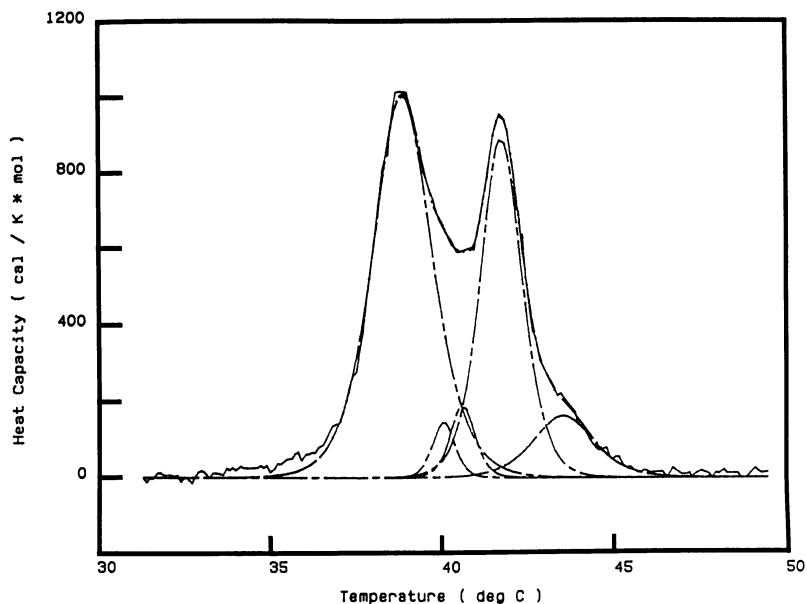
Figure 3. Differential scanning calorimetry of type XI collagen.

intermediates, when analyzed by tryptic digestion. We are now in process of isolating these fragments and sequencing their aminotermini to try to correlate differences in local stability with primary structure. These results indicate that the thermal stability of uninterrupted triple helices of about 300 nm in length is quite varied.

Type IV collagen, which was purified from the medium of a mouse tumor cell line (PF-HR9), contains interruptions in the Gly-Xaa-Yaa sequence of its 415 nm triple helix. These interruptions range from single deletions or insertions to regions up to twenty amino acid residues (Brazel et al. 1987, Brazel et al. 1988). It has been shown that procollagen IV has a multiphasic transition curve (Bächinger et al. 1982). In 50 mM Tris/HCl buffer, pH 7.4, containing 0.4 M NaCl there is a complex transition between 35 $^{\circ}$C and 42 $^{\circ}$C and an additional transition with a $T_m$ at 48 $^{\circ}$C (Davis et al. 1988). The transition at 48 $^{\circ}$C is associated with the melting of the aminoterminal 7S region (Risteli et al. 1980). Calorimetry reveals at least two separate transitions with midpoints at 36.5 $^{\circ}$C and 41 $^{\circ}$C in addition to the transition of the 7S region at 48 $^{\circ}$C. The total enthalpy change equals $\Delta H_{res}$ = 5.7 kJ mol$^{-1}$ per residue.
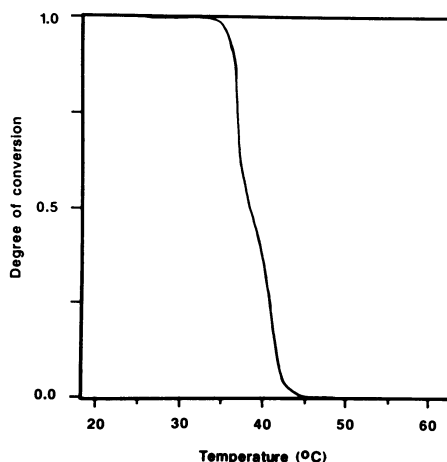
**Figure 4.** Thermal unfolding of type V collagen monitored by CD. The heating rate was 10 °C/h.

Tryptic digests at various temperatures in the transition range show that stable intermediate peptides exist. In the case of the type IV procollagen the interruptions lead to independently unfolding regions within the molecule (Davis et al. 1988).


## Folding of the triple helix

The folding of type I collagen has been studied quite extensively. Refolding was incomplete, because mismatched chains formed partial triple helices which were less stable. Aggregation occurred when chains formed triple helical regions with more than two other chains at different segments of the molecule (for a review see Engel 1987). It was recognized that the chains must be kept in register to refold completely and there is growing evidence that the carboxyterminal propeptide is responsible for this association. Experiments with collagens, procollagens, or fragments of procollagens which contain interchain disulfide bonds, suggest the following mechanism for the folding of the collagen triple helix (Bächinger et al. 1978 and many others). After complete synthesis of the proα-chains, chain selection and chain association is determined by the folded carboxy-terminal propeptides, which may or may not form interchain disulfide bonds. The associated carboxyterminal propeptides provide an efficient nucleus for triple helix formation which proceeds towards

C 25 35 36 37 38 39 40 41 42 43
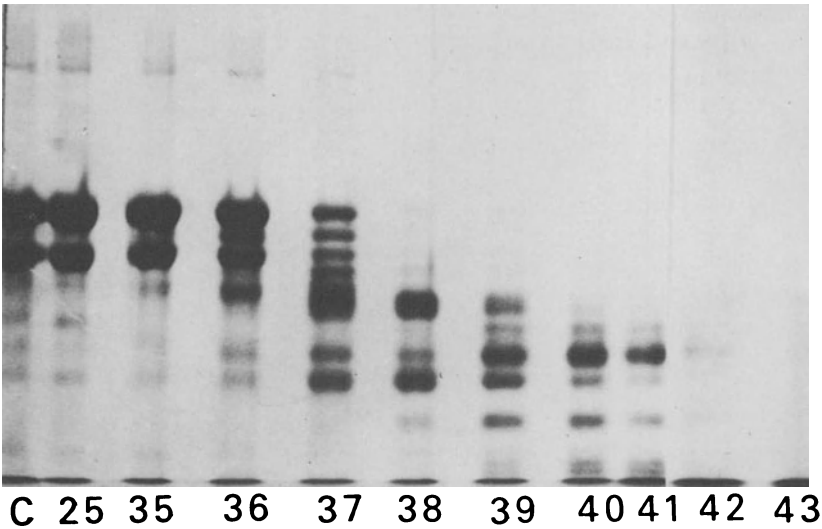
Figure 5. Thermal stability of type V collagen analyzed by resistance to trypsin digestion. Fragments generated at the indicated temperatures are resolved on a 5 % polyacrylamide gel run under reducing conditions.
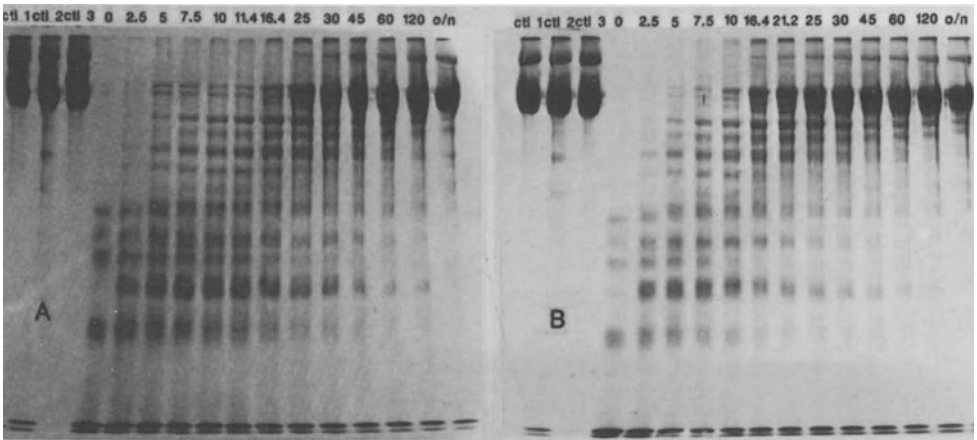


Figure 6. Refolding of type IV procollagen at 25 °C in the presence and absence of peptidyl-prolyl cis-trans isomerase extracted from E. coli. Panel A: Refolding after denaturation at 55 °C for 20 minutes. Samples were analyzed at the indicated timepoints on a 10 % polyacrylamide gel run under reducing conditions. Panel B: Refolding in the presence of peptidyl-prolyl cis-trans isomerase (final concentration of enzyme was 25 µg/ml total protein).

the aminoterminal end. Because the triple helical structure can only accommodate trans peptide bonds, refolding is "stopped" when a cis peptide bond is encountered and can only proceed after the cis-trans isomerization of this bond. The isomerization allows helix formation to proceed rapidly until the next cis peptide bond is encountered. These cis-trans isomerizations are the rate limiting step in the triple helix formation. This is confirmed by the high activation energy found for triple helix formation. After folding of the main triple helix, the aminoterminal propeptides associate. This "zipper" mechanism is further supported by the chain length dependence of the initial rate of folding (Bächinger et al. 1980). For procollagen type III without the carboxyterminal propeptide an initial rate of $v_0 = 0.028$ min$^{-1}$ was found at 25 $^o$C. At equilibrium in the random coil state on average every 25th tripeptide unit contains a cis peptide bond, i.e. on average about 25 tripeptide units can be incorporated into the triple helix without a cis-trans isomerization.

All these studies were performed with uninterrupted triple helices. We now have extended these studies to type IV procollagen. Type IV procollagen in 50 mM Tris/HCl buffer, pH 7.5, containing 0.4 M NaCl, refolds with an initial rate of $v_0 = 0.041$ min$^{-1}$ at 25 $^o$C, when monitored by ORD at 365 nm. Refolding is nearly complete. Figure 6 shows refolding at 25 $^o$C monitored by resistance to trypsin. As in type III collagen, fragments of increasing length are observed, protected from trypsin digestion by the triple helical conformation. The interruptions in type IV procollagen do not decrease the rate of triple helix formation. By electron microscopic analysis it is shown that in the denatured state most of the carboxyterminal propeptides are monomeric. After 10 min of refolding partial triple helices containing the trimeric carboxyterminal pro-peptides and a stretch of helix are observed (Davis et al. 1988). However in contrast to studies with proteolytic fragments of type IV collagen (Dölz et al 1988), we also observe stretches of triple helix which are not associated with trimeric carboxyterminal pro-peptides. It is likely that the 7S region of type IV procollagen, which contains interchain disulfide bonds can fold independently. This leads to an increase in the in vitro initial rate of folding, because two effective nuclei are present. In our experiments we show that monomeric carboxyterminal propeptides associate to form trimers, whereas in the experiments with the proteolytic fragments the single nucleus consisted of hexameric carboxyterminal

propeptides formed by the supramolecular association of type IV procollagen in the basement membrane (Dölz et al. 1988). These hexamers did not dissociate during the refolding studies. But both studies are in agreement that triple helix formation is not influenced by the interruptions in the triple helical sequence. It seems that renucleation of the triple helix after interruptions is faster than cis-trans isomerization.

Recently it was shown that the triple helix formation can be catalyzed in vitro by peptidyl-prolyl cis-trans isomerase (Bächinger 1987). Figure 6 shows that this is also the case for type IV procollagen.

Various genetic diseases involve the introduction of discontinuities into the continuous triple helix of type I procollagen. It was postulated that the observed overmodification (hydroxylation, glycosylation) in the type I triple helix is due to mutations of glycine residues, which is believed to impair folding (Bonadio et al. 1985). Our results with type IV procollagen suggest that interruptions, per se, have no major effect on the rate of folding.

## Acknowledgement

## References

Bächinger HP, Bruckner P, Timpl R, Engel J (1978) The role of cis-trans isomerization of peptide bonds in the coil triple helix conversion of collagen. Eur J Biochem 90:605-613

Bächinger HP, Bruckner P, Timpl R, Prockop DJ, Engel J (1980) Folding mechanism of the triple helix in type-III collagen and type-III pN-collagen: role of disulfide bridges and peptide bond isomerization. Eur J Biochem 106: 619-632

Bächinger HP, Fessler LI, Fessler JH (1982) Mouse procollagen IV: characterization and supramolecular association. J Biol Chem 257:9796-9803

Bächinger HP (1987) The influence of peptidyl-prolyl cis-trans isomerase on the in vitro folding of type III collagen. J Biol Chem 262:17144-17148

Bonadio J, Holbrook KA, Gelinas RE, Jacob J, Byers PH (1985) Altered triple helical structure of type I procollagen in lethal perinatal osteogenesis imperfecta. J Biol Chem 260:1734-1742

Brazel D, Oberbäumer I, Dieringer H, Babel W, Glanville RW, Deutzmann R, Kühn K (1987) Completion of the amino acid sequence of the α1 chain of human basement membrane collagen (type IV) reveals 21 non-triplet interruptions located within the collagenous domain. Eur J Biochem 168:529–536

Brazel D, Pollner R, Oberbäumer I, Kühn K (1988) Human basement membrane collagen (type IV) 172:35–42

Bruckner P, Prockop DJ (1981) Proteolytic enzymes as probes for the triple-helical conformation of procollagen. Anal Biochem 110:360–368

Burjanadze TV (1979) Hydroxyproline content and location in relation to collagen thermal stability. Biopolymers 18:931–938

Davis JM, Boswell BA, Bächinger HP (1988 In preparation) Thermal stability and folding of type IV procollagen and effect of peptidyl-prolyl cis-trans isomerase on the folding of the triple helix.

Dölz R, Engel J, Kühn K (1988 Submitted) Folding of collagen IV. Eur J Biochem

Engel J (1987) Folding and unfolding of collagen triple helices. Adv Meat Res 4:145–161

Fraser RDB, MacRae TP, Suzuki E (1979) Chain conformation in the collagen molecule. J Mol Biol 129:463–481

Linsenmayer TF, Gibney E, Fitch JM, Gross J, Mayne R (1984) Thermal stability of the helical structure of type IV collagen within basement membranes in situ: determination with a conformation-dependent monoclonal antibody. J Cell Biol 99:1405–1409

Miller EJ (1985) The structure of fibril forming collagens. In: Fleischmajer R, Olsen BR, and Kühn K (eds) Biology, Chemistry and Pathology of Collagen: Annals of the New York Academy of Sciences, vol. 460. The New York Academy of Sciences, New York, p1

Morris NP, Bächinger HP (1987) Type XI collagen is a heterotrimer with the composition (1α, 2α, 3α) retaining non-triple-helical domains. J Biol Chem 262:11345–11350

Privalov PL, Tiktopulo EI (1970) Thermal conformational transformation of tropocollagen. I. Calorimetric study. Biopolymers 9:127–139

Privalov PL, Tiktopulo EI, Tischenko VM (1979) Stability and mobility of the collagen structure. J Mol Biol 127:203–216

Privalov PL (1982) Stability of proteins: proteins which do not present a single cooperative system. Adv Prot Chem 35:1–104

Risteli J, Bächinger HP, Engel J, Furthmayr H, Timpl R (1980) 7-S collagen: Characterization of an unusual basement membrane structure. Eur J Biochem 108:239–250

# Refolding of Collagen IV and Other Collagens as Monitored by Electron Microscopy

R.Dölz, J.Engel, Biocenter, CH-4056 Basel, Switzerland,
K.Kühn, MPI, D-8033 Martinsried, FRG

In vivo, the formation of the triple helical structure is one of the important post translational events leading to the collagen precursor molecule. A prerequisite for the correct folding to an intact triple helix is a correct alignment and association of three polypeptide chains. As demonstrated for collagen I and III (Bächinger et al., Eur.J.Biochem. (1980) 106, 619; Bruckner et al., Eur.J.Biochem. (1978) 90, 595) this is facilitated by carboxyterminal crosslinks or peptides. The mechanism of collagen folding was described by a zipper model which proceeds from the C- to the N- terminus in a rather uniform rate being determined by the cis/trans isomerisation of proline peptide bonds.

In this study, we show that the folding process of collagens may be monitored with the electron microscope. We investigated collagen I and III, which show a continuous triple helix, a collagen I mutant possessing one interruption and collagen IV, which shows numerous interruptions in the triple helix. The collagens further possessed putative nucleation sites for triple helical folding at either none (processed  I), the carboxyterminal end (pro I, processed III, partially reduced IV) , the aminoterminal end (pepsinized IV) or on both ends (IV).

*Material and Methods:*

Processed Collagen I extracted from calf skin was obtained from Freudenberg (FRG). Procollagen I and Osteogenesis Imperfecta modified procollagen I was prepared by B.E.Vogel, K.E.Kadler, Y.Hojima and D.J.Prockop, Jefferson Institute for Molecular Medicine, Jefferson Medical College, Philadelphia. Collagen III was extracted from fetal bovine skin.  Collagen IV was isolated (Dölz et al.,Eur.J.Biochem., in press) from non- lathyritic EHS tumor material with collagenase purified from clostridium histolyticum at 4°C overnight  after EDTA-preextraction (Paulsson et al., Eur. J. Biochem. (1987) 166, 11). NaCl precipitation and heparin agarose chromatography yielded pure material. It consisted of the major triple helical part (about 80%) and the NC1 domain. At non- reducing conditions, the material migrated as one band in SDS electrophoresis with an apparent molecular weight of ca. 900000. This material then was digested with pepsin at mild conditions in order to cleave off the NC1 domain. Electron microscopy was carried out as follows: Samples were diluted to 20 - 50 µg/ml and dialyzed against  TBS. After heating for 15 minutes at 50 °C (Collagen IV (non-pepsinized): 30 minutes in the presence of 10 mM DTT), samples were cooled to

25°C. At different times, aliquots (25μl) were diluted with glycerol (25μl) of the same temperature (volume ratio 1:1) and sprayed on freshly cleaved mica disks. Specimen were dried in high vacuum, rotary shadowed with platinum/carbon at low angle, coated with a carbon film and floated onto water. Examination in the electron microscope (EM) at a magnification of 16000 was followed by enlarging the pictures to a final magnification of 300000. The micrographs of collagen III and IV (partially reduced collagenase fragment) were manually traced with a digitizer and histograms were calculated on a VAX 8800. Refolding of collagens I,III and IV was further monitored with circular dichroism spectroscopy. The data (not shown here) are in quantitative agreement with the data obtained with EM.

*Results from EM data:*

| Collagen type | N-terminal crosslinks | triple-helical interruptions | C-terminal crosslinks | Reformation of intact molecules |
|---|---|---|---|---|
| processed I | no | no | no | not observed |
| pro I | no | no | S-S & glob. | complete (but aggr.) |
| processed III | no | no | S-S | complete |
| IV (part.red.) | no | >15, var.len. | glob. | nearly complete |
| IV (frag.) | S-S | >15,var.len. | glob | nearly complete |
| IV (pepsin.) | S-S | >15,var.len. | no | not observed |
| pro I (OI) | no | 1 (Gly -> Cys) | S-S & glob. | partially complete |

*S-S refer to interchain, intramolecular crosslinks, glob. refers to a globular domain serving as "structural" crosslink. The collagen IV used was isolated as dimer (see materials & methods).*

*Conclusions:*

Refolding of collagen requires a correct alignment of polypeptide chains (insufficient refolding of processed I, correct refolding of processed III, pro I, and  fragment of IV).

The carboxyterminal globular domains are indeed starting point of triple helical growth in vitro (pro I, fragment of IV) .

The aminoterminal end of the triple helix may not serve as nucleation site for triple helical growth in vitro even if it is crosslinked (pepsinized  fragment of IV) .

The triple helical growth is delayed if a single glycine residue in the Gly-Xaa-Yaa repeat is substituted by a different amino acid (Osteogenesis imperfecta mutant of pro I).

The triple helical growth is not delayed if the Gly-Xaa-Yaa repeat is interrupted by several amino acids (fragment of IV). The cis/trans isomerisation (presumably) remains the rate-limiting step.

**SECTION IV**
**Biophysical Methods for Elucidation of the Structure and Assembly of Cytoskeletal and Extracellular Constituents**

# Scanned and Fixed Beam Microscopy of Cytoskeletal Components

A. Engel and R. Reichelt
M.E. Müller-Institute for High-Resolution Electron Microscopy
at the Biocenter, University of Basel
CH-4056 Basel, Switzerland

## Introduction

Fixed beam light microscopy is the oldest technique used to reveal the structure of living organisms. The origin of the light microscope is uncertain, but it is connected to the discovery of the telescope by Lippershey in 1608 and its first application by Galilei in the years to follow. The first description of a light microscope and its application to study the world of the very small is by Hooke in his *Micrographica* (1665). Due to a continuous development of light microscopes {which today provide a resolution given by the theoretical limit ($\delta = 0.61 \cdot \lambda$ /NA; $\lambda =$ wavelength, NA = numerical aperture)} and the use of fluorescent immunolabelling (Fujiwara and Pollard, 1976), the substructure of cells can now be directly visualised *in vivo* . Exploiting this resolution as well as the outstanding dynamic range, sensitivity and linearity of charge coupled device (CCD) imaging systems and combining these with digital image processing techniques, cellular organelles can be imaged in three dimensions (Agard et al., 1988). Very recently the combination of high resolution interference contrast light microscopy with video technique and image processing (Allen, 1985; Inoue, 1981) has allowed the motion of single organelles to be followed at a nm-scale resolution (Gelles et al.,1988). Much shorter is the history of the electron microscope which was invented by Ruska and his collaborators in Berlin (Knoll and Ruska, 1932). The extremely short wavelength of electrons accelerated by an electric field ($\lambda = 0.037$ Ångstoms (Å) for an acceleration voltage of 100 kV) provides the basis for a resolution of some Å that is currently attained by commercial high resolution instruments, and that allows single atoms to be visualised. The major disadvantages of electron microscopy for biological structure research are (i) the necessary dehydration of the sample to be introduced into the high vacuum of the electron optical system, and (ii) the beam damage created by a high energy electron beam. They have by no means prevented the elucidation of the fine structure of cellular organelles and their components down to a molecular level. Electron microscopy thus has provided us with an insight into the cellular architecture which, in turn, has stimulated many of the key experiments revealing basic cell functions.

Scanned beam microscopy includes the youngest imaging techniques available today. Motivated by the developments of electron microscopy and television, v. Ardenne was the first to build a scanning electron microscope for transmission in 1938. Scanning electron microscopes were then developed for observing the surfaces of bulk samples by collecting secondary and backscattered electrons. It took some time until these instruments became commercially available but today they are widely used tools in many fields including the one of cell biology. A most important, although perhaps less recognised development was carried out by Crewe and his collaborators in Chicago during the late sixties and early seventies (Crewe, 1970). This group built the first field emission scanning transmission electron microscope (STEM), an instrument of brilliant simplicity capable of visualising single heavy atoms with unprecedented clarity (Crewe et al., 1970). On the other hand,

scanning light microscopy was developed only very recently ( White et al.,1987) although pioneering work was carried out by Brakenhoff in the late seventies (Brakenhoff et al., 1979). The major advantage of this technique is the possibility to eliminate stray light emanating from out-of-focus planes. This allows sub-micron thin sections of cells and similar transparent structures to be recorded in a non-invasive manner. The most recent scanning instrument is the scanning tunneling microscope (STM) invented by Binnig and Rohrer in 1982. This microscope is, in its concept, even simpler than the STEM, and it has also demonstrated the capability to visualise single atoms, however, as yet on conducting surfaces only. In spite of the optimism prevailing in this young field, it is still not clear in which way the STM can be successfully used to reveal the structure of cellular components at atomic resolution. The invention of the STM has fostered the development of many other scanning sensor microscopes such as the atomic force microscope (AFM) (Binnig et al., 1986; Martin et al.,1988), the scanning thermal probe microscope (Williams and Wickramasinghe, 1986), the scanning magnetic tip microscope (Martin and Wickramasinghe, 1987), as well as the scanning light pipette microscope (Harootunian et al., 1986).

The primary aim of this contribution is to present a limited selection of electron microscopical methods and their biological applications in order to demonstrate their potential as well as their limitations. In addition, a short review of scanning sensor microscopes and their possible role in future studies of biological systems is presented.

## Electron microscopy

Fig.1 displays the configuration of the most simple electron microscope one could think of which consists of an electron source, a lens and a detector system. Furthermore, the electron beam-sample interactions which are responsible for the transfer of structural information to the observer, are shown schematically in the inset for thin and for thick samples.
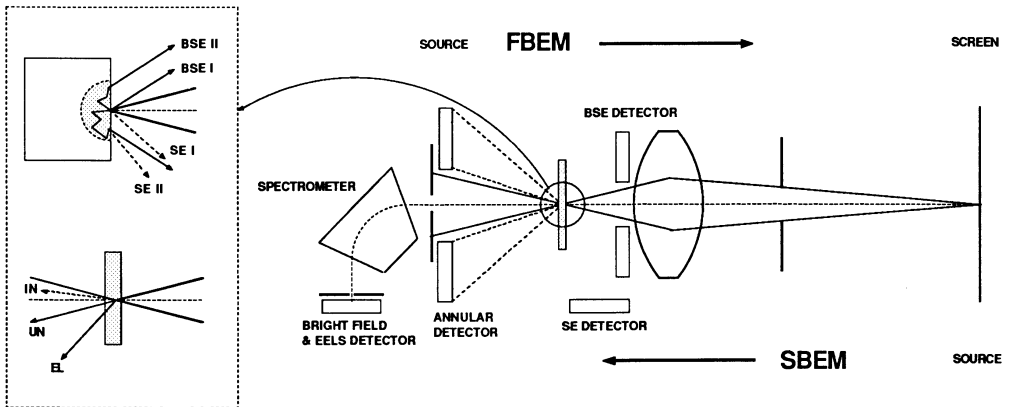


Fig.1  Optical system of fixed (FBEM) and scanned beam electron microscopes (SBEM). The inset shows the interactions between primary electrons and thick or thin samples, illustrating the various types of scattered electrons: backscattered (BSE), secondary (SE), inelastic (IN), elastic (EL) and unscattered (UN) electrons.

It is interesting to note that there is a remarkable similarity between fixed beam (FBEM) and scanned beam electron microscopes (SBEM), as one converts into the other simply by inverting the trajectories. Thus, the ray inversion theorem defines the equivalence of the FBEM source and the SBEM detector on the one hand and the FBEM detector and the SBEM source on the other (Engel, 1974) which we will use in the following to understand some of the more pertinent properties of the microscopes discussed.

**Scanning Electron Microscopy (SEM)**

In the SEM images of a conductive coat deposited on critical point - or freeze dried, large biological structures mounted on a bulk substrate are generated by scanning a focused electron beam over the specimen surface and collecting electrons escaping from the small irradiated volume. The SEM exploits (i) the secondary electrons which are generated and ejected from the sample due to inelastic collisions of the impinging electrons at the specimen surface and (ii) the backscattered primary electrons (Fig.1, inset). Contrast formation is not a simple matter as plural scattering is involved. Three types of signals need to be considered (Seiler, 1983; Peters, 1985): type I signals (secondary electrons (SE) and backscattered electrons (BSE)) which are due to the first scattering events at the point of incidence and which escape from a volume that extends only a few nm into the sample, type II signals which are generated sufficiently close to the surface to escape from the sample but rather far away from the point of incidence by electrons elastically scattered at large angles, and type III signals which are produced by BSE hitting the surfaces of the electron optical components.
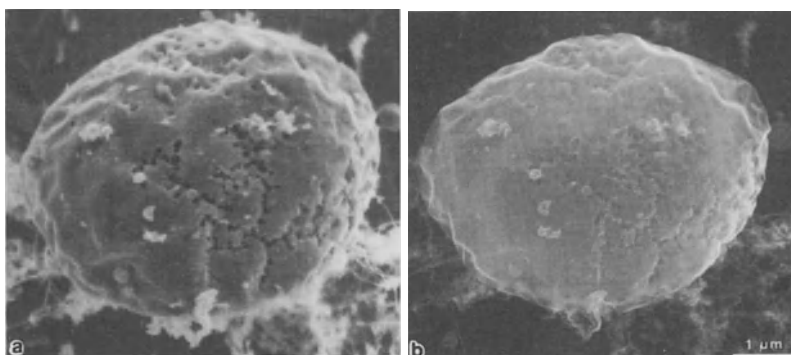


**Fig. 2** Topography of a freeze dried red blood cell ghost as recorded by the SE signal at 2 kV (a) and at 30 kV (b) primary beam energy. Due to the significantly reduced penetration depth at low energy, topographic contrast is pronounced in (a), although the sample has been coated by carbon rather than a heavy metal.

Signals of the second and third type contribute to a background signal that obscures the high resolution image from type I signals and should therefore be minimised by appropriate sample preparation techniques and microscope design (Peters, 1985). Since the electron stopping power of the coat determines the volume at the sample surface from which SE can escape, heavy metals such as Pt(C), Cr or Ta yielding homogeneous conducting films are deposited on the sample by sputtering or evaporation. These layers need to be thin compared to the penetration depth of the uncoated sample

but sufficiently thick to reduce the type II SE signal. Such samples allow topographic features of some nm diameter to be visualised using the SE signal (Peters, 1985; Müller and Hermann, 1988). Alternatively, the energy of the primary electrons can be decreased to reduce the interaction volume from which SE emanate. The effect of small penetration depth of low energy electrons compared to high energy electrons is illustrated in Fig. 2. In addition, low energy electrons allow bad conductors to be observed, since the (SE+BSE) yield is close to 1 so that no electric charge is deposited (Pawley, 1984). However, at low acceleration voltages the design of an appropriate electron optical system becomes difficult due to the strong influence of lens aberrations for low energy electrons (Crewe, 1986). Current efforts in improving the instrumentation for low energy electron microscopy promise that its limit is not as yet reached in practice.
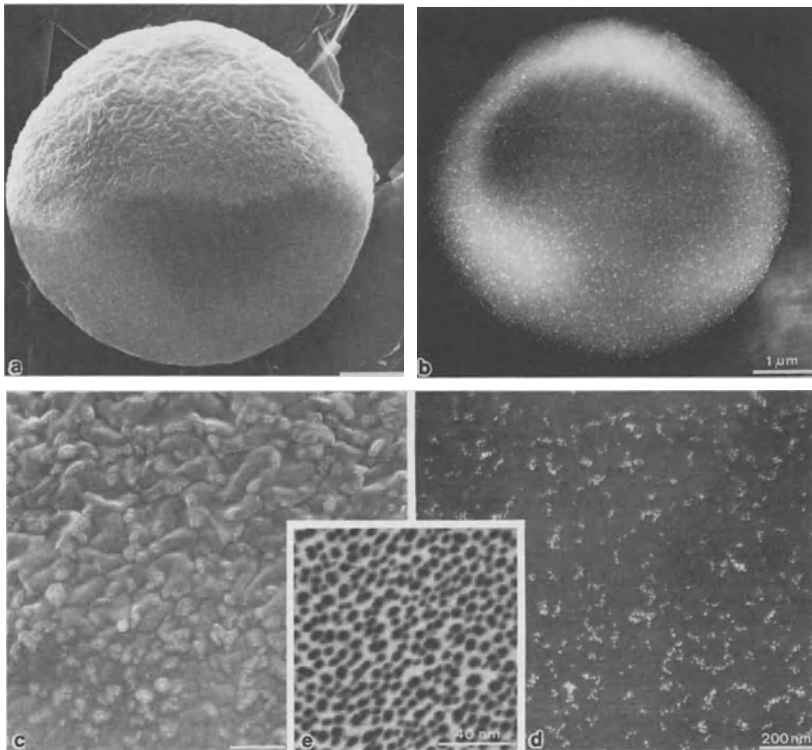


Fig.3 The visibility of immuno-gold labels is illustrated by a red blood cell (RBC) labelled by a rabbit anti-RBC, which in turn was decorated by anti-rabbit gold labels of 10 nm diameter before freeze drying and carbon coating. The topography is visible in the SE images at low (a) and high magnification (c), whereas the gold labels are clearly discernible in the BSE image at high magnification only (d). Close comparison of (c) and (d) reveals that some gold labels are not visible in the SE image which are present in the BSE image. The gold island displayed in the inset (e) illustrate that the resolution of a field emission SEM (Hitachi S-800) operated in the axial bright field mode is better than 2 nm. This implies that differential labelling with gold spheres of distinctly different diameters should be feasible.

The BSE signal is more material dependent than the SE signal, as the cross-section for backscattering is strongly dependent on the atomic number. The SEM thus offers an interesting possibility to localise specific components of a cell by immuno-gold labelling them before critical point - or freeze drying and coating with a thin carbon layer. Simultaneous acquisition of an SE image (which does not depict the gold particles unequivocally but reveals the surface features) and a BSE image then yields an image pair that allows 10 nm gold labels to be precisely localised at a cell surface (Fig.3 c,d). The resolution that can ultimately be obtained by a modern high resolution SEM is demonstrated by the gold islands shown in Fig.3 e which were evaporated onto a 4 nm carbon film and were recorded using the transmission mode.

**Scanning Transmission Electron Microscopy (STEM)**

Contrary to the SEM, the STEM is designed to observe thin samples at the highest possible resolution. To this end the scanning probe is generated by focussing the beam emitted by a field emission source with a high resolution objective lens. Electrons elastically scattered by the few atoms within the irradiated volume are collected by an annular detector over a wide angle, while inelastically scattered electrons are analysed by a spectrometer (Fig.1). In addition, the interference of unscattered electrons with electrons scattered elastically in forward direction can be recorded through a small aperture on the optical axis. According to the ray inversion theorem, the annular dark field image in the STEM corresponds to a hollow cone dark field image in the FBEM, whereas the STEM image recorded by an axial aperture corresponds to the axial bright field image of the FBEM. Thus, the annular dark field mode in the STEM is an almost perfectly incoherent imaging mode, while the coherence of the STEM bright field mode is determined by the size of the aperture, which corresponds to the aperture of the FBEM illumination system.
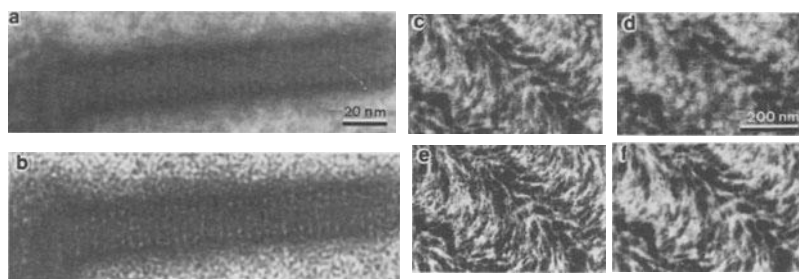


Fig.4  Various imaging modes of the STEM. (a) Elastic dark field image of an uranyl acetate stained giant T4 tail recorded by the annular detector; (b) coherent bright field image of the same structure recorded simultaneously with the elastic dark field image (a) through a small aperture at the spectrometer entrance (Fig.1). Although the bright field image appears to be sharper, close inspection of both images shows that the smoother dark field image can more easily be interpreted. Unstained sections of HM20 low temperature embedded *Dinoflagellate Prorocentrum micans E* illustrate the effect of signal mixing (c-f) : elastic dark field image (c); the delocalization is evident in the inelastic dark field image collected through an energy loss window extending from 10 to 80 eV (d); the ratio image (e) is the crispest of the four, but it does not provide a linear representation of the atomic number distribution; a weighted difference (EL-w·IN) reduces blurred background without introducing nonlinearities (f). Bright shades show protein in (a,b) and DNA in (c-f).

The characteristic features of these two imaging modes are illustrated in Fig.4 a and b. Micrographs generated by inelastically scattered electrons are, in general, more blurred than those from elastically scattered electrons due to the delocalisation of the inelastic collision (Reichelt and Engel,1986; Fig.4 d). Inelastic events however, provide a further kind of information on the irradiated matter.Firstly, the ratio of the elastic : inelastic signal is to a first approximation linearly related to the atomic number of the irradiated atoms (Crewe, 1970). This ratio can be generated on-line by the STEM which records both signals simultaneously via the annular detector and the spectrometer, respectively. Atomic number contrast (frequently referred to as Z-contrast) has fostered considerable interest as it has demonstrated its potential to depict proteins and nucleic acids embedded in a resin matrix without the necessity of heavy atom staining (Carlemalm and Kellenberger, 1982; Fig.4 e). Secondly, inner shell ionisation occurs if the inelastically scattered electron transfers an element specific minimum energy to an inner shell (core) electron. Thus, the energy loss spectrum reveals specific 'core-loss edges' that allow to identify the elements within the irradiated volume element and to determine their concentrations (Egerton, 1986).

While atomic resolution has been demonstrated with several STEMs (Wall et al., 1978; Isaacson et al., 1977; Cole et al., 1977) and a series of pleasing micrographs from typical biological samples has been recorded (Crewe, 1970; Engel et al., 1976; Carlemalm and Kellenberger, 1982; Engel and Reichelt, 1984) a quite different aspect appears to be of particular use for the structural biologist : the STEM is the instrument of choice for quantitative electron microscopy. As the scanning probe illuminates one sample volume element after the other, the scattered electrons are counted and stored for each of them by the annular detector as well as by the detectors appropriately placed behind the spectrometer. Each set of numbers thus represents the result of a scattering experiment. With little additional information (such as the average elemental composition), the number of atoms in the irradiated volume can be determined from the fraction of electrons scattered onto the annular detector. Since the ensemble of all these scattering experiments are conveniently represented as one (or several) dark field pictures, a single macromolecule can be discerned and hence its mass be evaluated simply by integration over all the picture elements (pixels) within the contour delimiting the molecule (Engel, 1978; Wall, 1979 ). Besides the appropriate instrumentation the prerequisite for such a mass determination is an unstained, well preserved dehydrated sample adsorbed to a thin carbon film. Freeze drying within the STEM is the least destructive preparation method available, but glycerol spraying and drying in air often provides a more homogeneous preservation of filigree like molecules in their extended form (Fig.5).

To illustrate the power of mass determination by the STEM, selected examples are presented in Figs. 5 - 8 and detailed in the legends. The technique exhibits several advantages:

(i)     less than 10 µg protein are required to prepare a grid.

(ii)    since molecules to be evaluated can in many cases be discerned by their shape, the preparation does not need to be pure.

(iii)   the mass range extends from 1 to $10^6$ kD; the lower end being feasible only if the images of many molecules can be averaged.

(iv)    domains or discernible morphological subunits can be measured individually and the results compared to sequence data (Fig.5).

(v)     supramolecular assemblies can be studied to determine parameters such as the mass per length (MPL) or the mass per area (MPA) characterising filaments and membrane-like structures, respectively (Fig.6,7).

(vi)    membrane protein complexes and fragile organelles can be measured *in situ* (Fig.8). In addition, mass determination by STEM is very precise (the main source of errors in fact is related to difficulties with sample preparation) and thus represents a valid alternative to the ultracentrifuge.
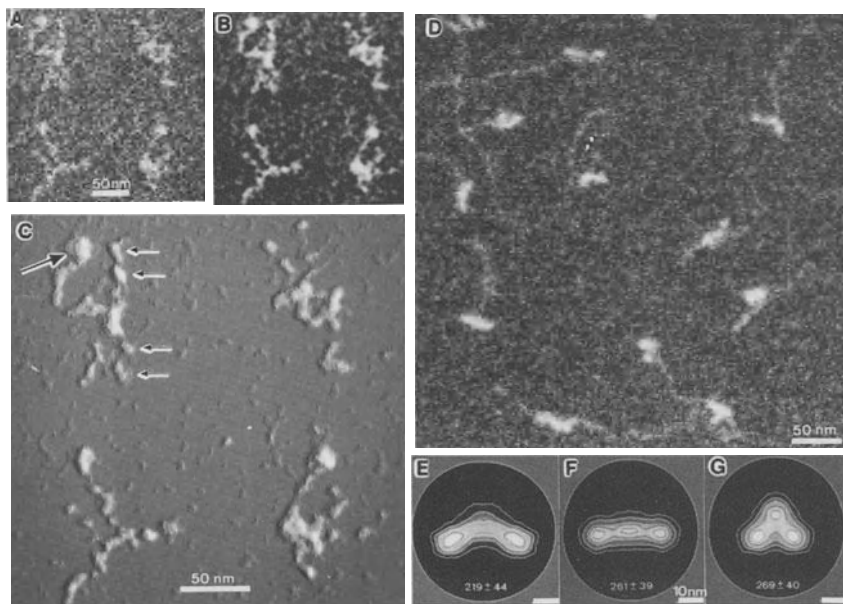


Fig.5  Mass determination of two glycerol sprayed macromolecules : laminin (a-c) and myosin (d-g). A detailed mass analysis of the domains and morphological units is possible by measuring the domains of many molecules (c) or by averaging many molecules exhibiting a similar conformation to obtain  mass-maps (e-g). Unprocessed laminin molecules illustrate the noise due to  counting statistics and carbon film irregularities (a). After low-pass filtering the molecules become distinctly visible (b). In (c) the mass above average background is shown by a shaded view. The mass values of the laminin large end domain (large arrow in (c)) exhibits a bimodal distribution with an average of 150±50 kD (n=46), while the dumb-bell shaped morphological units (small arrows in (c)) yield a single peak at 114±26 kD (n=43). In addition, the MPL of the long arm, which is thought to consist of a triple $\alpha$ helix turns out to be 4.6±1.2 kD/nm. This relatively high value could be explained by glycerol preferentially adsorbed at the thin rod, but it could also be due to additional small domains interrupting the triple helix. Myosin molecules sprayed onto 3 nm carbon film exhibit a variety of head conformations (d). Three types of myosin heads can be classified, aligned and averaged to produce the maps shown in (e-g). Mass determination of all three head types indicate that the classical pear-shaped head (e) has lost one pair of light chains of 20 kD each, which are distinctly visible in the two other head conformations as central domains ((f,g); Walzthöni et al., 1985).
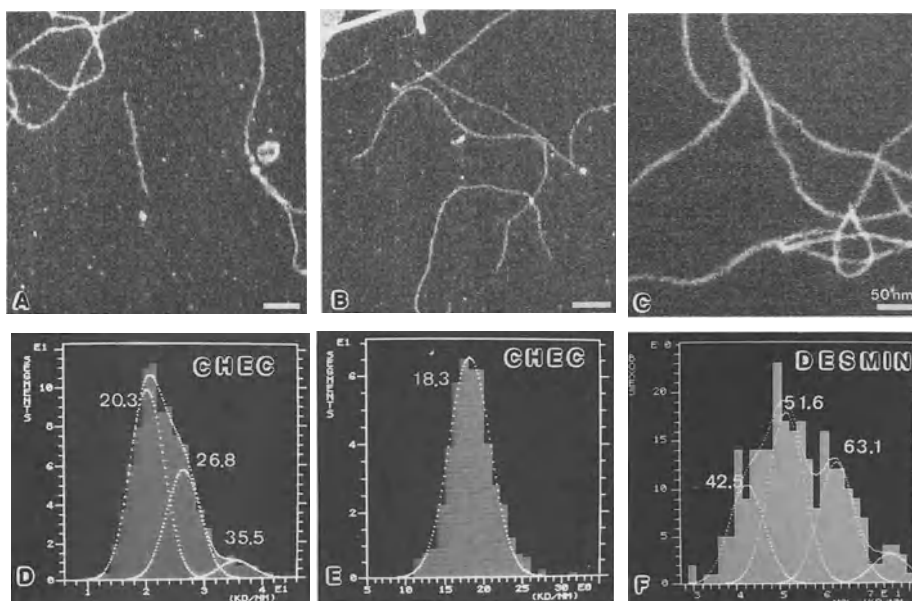
Fig.6   Mass per length (MPL) analysis by STEM has revealed polymorphic variants of intermediate filaments (IF) (Steven et al., 1983). This MPL variability is apparently common to all types of IF and possibly related to the specific purification and reassembly conditions, as illustrated by 3 different samples shown in (a-f). The heterogeneity of the filament mass is visible on the cultured human epidermis (CHEC) IFs shown in (a) and expresses itself in the MPL histogram (d). The peaks fitted correspond to a variable, but distinct number of protofibrils building the IF. From their positions, the average molecular weight of the IF polypeptides and the axial repeat (46.5 nm), the protofibrils were found to comprise approximately 8 subunits (Engel et al., 1985). In a different experiment the CHEC IFs turned out to be rather homogeneous (b) yielding a single peak which matches a MPL of two protofibrils (e). Desmin, the prototype IF consisting of a single polypeptide of 55 kD exhibits a distinct mass heterogeneity as well (c). The peaks in the related histogram (f) agree with the MPL of 4, 5 and 6 protofibrils.

As the elemental composition of the irradiated volume can be determined from the electron energy loss spectrum (Egerton, 1986; Fig.9) the acquisition of element maps is possible in a STEM equipped with a spectrometer (Colliex, 1984). The main limitation of this method is due to the small scattering cross section for the element specific core losses: a 10 nm thick carbon film eg. scatters only a fraction of $5 \cdot 10^{-4}$ of the incident beam into a 30 eV window positioned at the carbon K-edge. Thus, to collect 50 counts from a volume element of 1 nm diameter, a dose of $10^5$ electrons/nm$^2$ is required. As the core loss scattering cross sections for other elements and different electron shells are less favourable than that of the carbon K-edge, the recording doses used in practice are usually even higher ($10^8$-$10^{10}$ electrons/nm$^2$). The relevance of element maps recorded under these conditions have yet to be proved by evaluating the redistribution of the elements during such extreme electron irradiation. The STEM provides a unique possibility for this as well, since the simultaneously recorded annular dark field image allows the alignment parameters for averaging a

large number of molecules or lattice units to be determined. This should make element mapping of periodic structures feasible at a recording dose of $10^3$ electrons/nm$^2$ and a resolution of some nm.
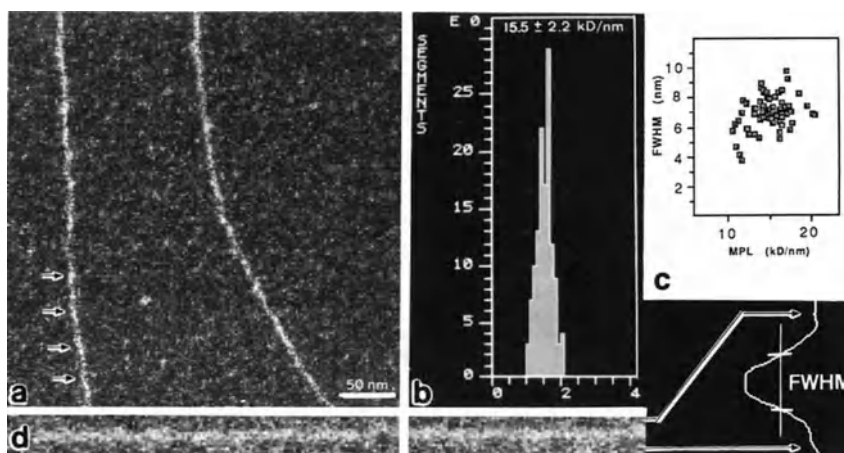


Fig.7 Freeze dried actin filaments reveal dense cross over points of the 2 strands regularly spaced by 36 nm (arrows in (a)). The MPL histogram consists of a single sharp peak (b) in spite of mass-density variations along the filament. This is explained by a pronounced variation of the width (full width half maximum (FWHM)) along the filament plotted in (c) versus the MPL values. The lack of a FWHM-MPL correlation indicates that the MPL is measured independently of the relative position of the 2 helical strands. The average FWHM can be obtained by measuring many short filament stretches during a mass analysis (c) but it also can be determined by projecting a straightened filament along its axis (d).
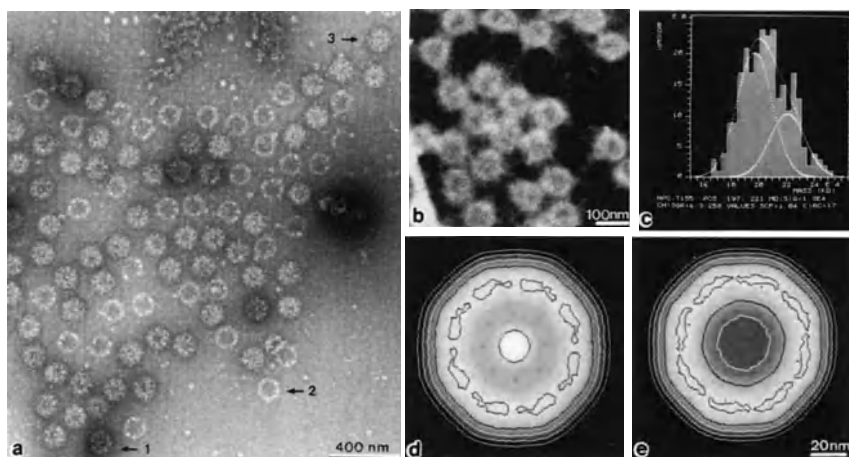


Fig.8 The nuclear pore complex (NPC) responsible for the nucleocytoplasmic molecular exchange can be prepared by spreading *Xenopus laevis* oocytes nuclear envelopes on a grid, partially or completely removing of the membrane by detergent extraction, and crosslinking (a). After thorough detergent extraction negative staining with uranyl formate

reveals three distinct conformations (Holzenburg et al, 1988): the native organelle (1), a ring-shaped unit (2), and a plug-spoke complex (3). The 'central plug' is frequently missing . Native NPCs with and without plugs are obtained by extensively washing the nuclear envelope in distilled water and freeze drying. These complexes, held together by the nuclear lamina meshwork sometimes hang freely over a hole in the supporting film and can be recorded without background at low dose in the STEM (b). A preliminary mass analysis of 258 NPCs yields a histogram fitted by two Gaussians positioned at 200 and 220 MD (d). The heterogeneity of the mass histogram is presumably related to the nuclear lamina meshwork which comprises almost 50% of the mass within the circular window fitted over the NPC. Averaging a set of 51 well preserved unstained NPCs images after angular and translational orientation with respect to a reference NPC reveals an 8-fold rotational symmetry that is directly visible in negatively stained images. The symmetrized mass-maps of the native (d) and the plug-free NPC (e) show the two structures to match closely in a radial interval extending from 20 to 60 nm. (The micrograph shown in (a) was recorded by A. Holzenburg).

<u>Fig.9</u>  The electron energy loss spectrum (EELS) of an unstained membrane reconstituted from E.coli porin and phospholipids shows the presence of phosphrous (P) by the $P_{L2,3}$ signal starting at 132 eV, of carbon (C) by the prominent $C_K$ signal starting at 284 eV, and of nitrogen (N) by the $N_K$ signal at 401 eV. After stripping the background, the $P_{L2,3}$ signal exhibits a characteristic fine structure. An analysis of the intensities of these 3 signals reveals the relative concentrations of P, N and C to be: $P/N = .07\pm.01$ (.08) and $P/C = .008\pm.002$ (.005), with the values expected from the current membrane model in brakets. (Experimental data kindly provided by R.D. Leapman).
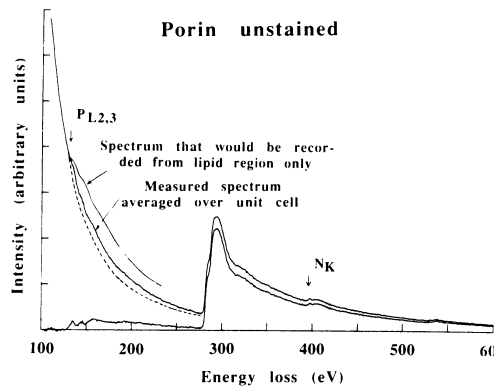


## Fixed beam transmission electron microscopy.

Most of the high resolution structural information on those cytoskeletal components that were not amenable to X-ray crystallographic analysis so far has been obtained by FBEM of negatively stained samples. Image formation in this instrument is - at least in a linear approximation - conveniently described by the theory of linear systems used in optics (Goodman, 1967). Two mechanisms contribute to the contrast in a bright field image:

(i)     the interference of scattered waves with the unscattered beam (phase contrast) and

(ii)    the loss of electrons scattered at large angles and hence cut off by the objective aperture (amplitude contrast).

The phase contrast transfer function is always zero for very low spatial frequencies and the position of the main frequency band transmitted can be appropriately adjusted by underfocussing the objective lens. Amplitude contrast however, is predominant at low frequencies. For large objective apertures or weakly scattering samples a negligible fraction of incident electrons is cut off so that the image is largely due to phase contrast. This readily explains the typical crisp appearance of bright field micrographs which is related to the suppression of low and the enhancement of high spatial frequencies in the image (Fig. 4b).

Negative staining has proved to be one of the most convenient and widely used preparation methods. The heavy metal salt used supports biomacromolecules adsorbed to a thin film during air drying and reduces their collapse due to surface tension effects. After drying, the biological structure is embedded in a solid, strongly scattering cast of dried salt which outlines the molecular envelope at a resolution of typically 2 nm. Electron microscopic projections of such three dimensional (3D) stain distributions allow the 3D molecular envelope to be determined by digital image processing methods (for a review cf. Aebi et al., 1984). The steps involved in a complete 3D reconstruction of a curved actin filament are displayed in Fig.10. Although most convenient, negative staining has several disadvantages to be considered. Firstly, microcrystals which are likely to distort the fine structure of biomacromolecules may form during dehydration and electron irradiation. Secondly, certain charged sites of the biomacromolecule may become positively stained thereby obscuring the idealised image of the molecular envelope. Thirdly, the sample is not necessarily homogeneously penetrated by and wrapped into the stain layer but is predominantly stained at the side facing the hydrophilic support film due to capillarity. Last but not least, all stains generate rather non-physiological ionic conditions and some require quite acidic pH values. Therefore, advances in the preparation and observation of frozen hydrated samples (Dubochet et al., 1988) has promised significant progress. Although these techniques are established in several laboratories by now, they will probably never completely replace negative staining in spite of its obvious shortcomings.
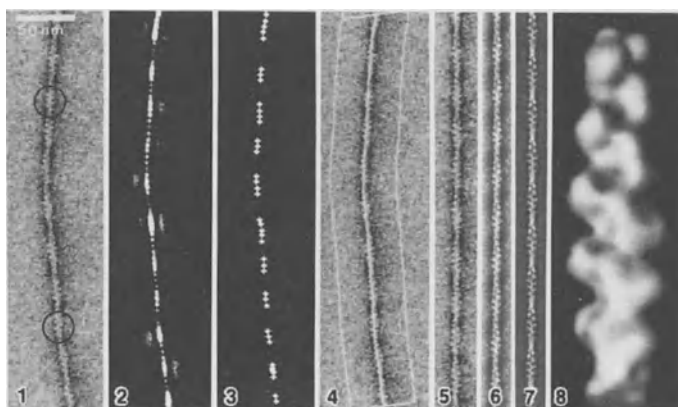


Fig.10 The essential steps of the three dimensional (3D) reconstruction of an actin filament. A negatively stained filament (1) is first straightened using the cross-correlation function of the filament computed with a suitable reference (2). Two patches (marked in 1) are aligned and averaged to provide a reference that is insensitive to the filament curvature. A peak search algorithm marks the highest correlation peaks approximately centered at the filament axis. A smooth spline function (Dierckx, 1980) is fitted through the peak positions and the image is reinterpolated along lines that run perpendicular to the spline (4). The thus straightened filament (5) can be submitted to a Markham averaging procedure which allows the helical repeat to be determined within a fraction of a pixel. The averaged filament (6) is then D(Z,k) filtered (Smith and Aebi,1974) to eliminate residual signals that are incompatible with the helical selection rule $l = -6 n + 13 m$ (7). From this clean projection a 3D model is calculated that can be represented by surface shading (8). (Micrograph kindly provided by U. Aebi. Processing steps 2-5 and 8 were done using SEMPER, steps 6-7 using MDP)

## Scanning Sensor Microscopy

The invention of the scanning tunneling microscope (STM) by Binnig and Rohrer (1982), has fostered a significant enthusiasm - not only among solid state physicists - but also among structural biologists interested in new, non destructive methods for gathering structural information of biomacromolecules and their supramolecular assemblies at high resolution (for a review cf. Quate (1986); for the principle of operation cf. Fig.11).

Fig.11 When the tip approaches the surface of the sample sufficiently closely, a tunneling current ($I_t$) starts to flow (a). $I_t$ is critically dependent on the gap distance s. As the tip is moved along the surface by a piezodrive, a feedback circuit keeps the current constant (const. $I_t$) by forcing the tip to follow the surface at a constant distance. The correction signal then provides information on the surface topography. If the tip height (z) is kept constant, $I_t$ will vary as the tip is scanned thus reflecting the topography as well (const. z). A signal related to the work function Ø (which shows typical values of 1 to 5 eV on a clean sample) is obtained by oscillating the tip along the z-axis. The voltage dependence of $I_t$ is related to the accessible empty electronic states at the sample surface as illustrated in (b). As V is increased, some electrons in the conducting band of the tip may also tunnel into states above the Fermi energy ($E_f$) of the sample. Therefore, $I_t$ does not linearly increase with V but exhibits kinks related to the specific electronic states at the sample surface probed by the tip.

**a**

$$I_t \ = \ f(V) \cdot \exp(-A \cdot \sqrt{Ø} \cdot s)$$

$$A \ = \ 1.025 \ / \ (\sqrt{eV} \cdot \text{Å})$$

const. $I_t$:  z = z (x)

const. z :  $I_t = I_t$ (x)

$z = z_0 + dz \cdot \cos(\Omega t)$ :  Ø = Ø (x)

**b**
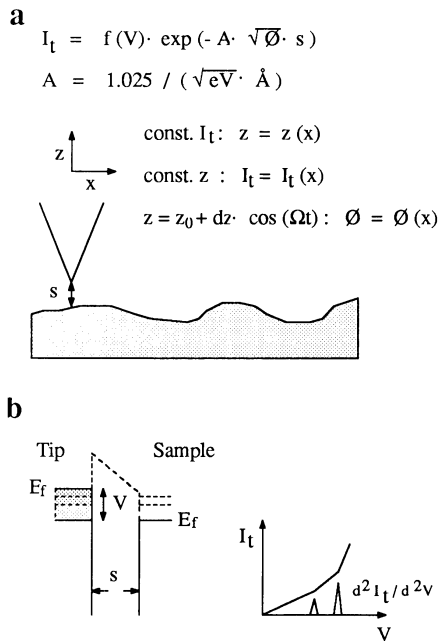
The STM seems to be of particular use, since it allows surfaces to be scanned in water or even weak buffers and spectroscopic measurements to be done at high spatial resolution. Unfortunately, however, the STM requires conducting and very flat samples which are usually found in solid state physics but not in biology. Nonetheless, several attempts to visualise native air dried biomacromolecules yielded results that indicated the feasibility of recording STM topographs from such samples in spite of their low conductance (Baro et al., 1985; Stemmer et al., 1987; Travaglini et al., 1987). These results initiated further work in several laboratories but the dream of recording a topograph of e.g. a protein lipid membrane in water has, so far, not been realised. What has been successfully reproduced are scans over Pt/C or Pt/Ir coated air - or freeze - dried supramolecular assemblies (Amrein et al., 1988; Guckenberger et al., 1988; Stemmer et al., 1988; Fig.12 b) or Pt/C replicas of freeze-fractured samples (Zasadzinski et al., 1988). The success of this approach is presently perhaps somewhat overrated as in fact it provides essentially no information that could not be just as easily obtained by electron microscopy. It is therefore important to further pursue the

avenue of observing biostructures in their native environment. To document the feasibility of this approach the STM topograph of an air dried porin membrane is displayed in Fig.12 a.
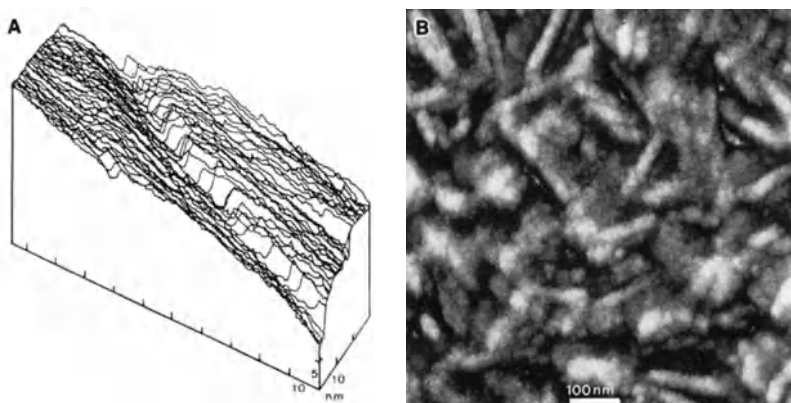


Fig.12 Topographs of two kinds of biological sturctures recorded in the STM : a membrane reconstituted from *E.coli* porin and phospholipids air dried on a thin carbon film (a; Stemmer et al., 1987) and tobacco mosaic virus (TMV) rods (b) adsorbed to a Pt/C coated cover slip, dried in air and shadowed by a 1 nm thick layer of Pt/C. The steps at the edge of the uncoated native membranes are 5 nm high in agreement with measurements on frozen hydrated porin membranes viewed edge on (A. Engel, unpublished) and point out that tunneling is possible at ambient pressure on native protein-lipid membranes. A second step suggesting a further membrane layer is discernible at the top right of the scan shown in (a). That this step is less sharp can be explained by the disruption of the folded membrane during air drying. In spite of many attempts, no unambiguous topographs of uncoated TMV rods could be obtained and doubts arose whether TMV was present at all. Shadowing one sample with a conducting layer instantly revealed that TMVs were densely packed at the cover slip surface, indicating that these structures are not suited for STM without metal coat. (The topographs were kindly given to the authors by A. Stemmer).

In this context the rapid development of a variety of scanning sensor microscopes (SSM) is most interesting since one or several of them could be particularly suited for the observation of biological samples. A comparative compilation of present SSM with some speculative applications is given in Table 1. They all exploit the possibility to position and move a sensor at subnanometer precision by piezo-elements and have in common that the sensor is of macroscopic size and shape which may obscure the image recorded. From a practical point of view SSM also has the disadvantage of depicting small areas ($1\mu m^2$) at a reasonable speed (1 frame/min) thus requiring additional tools for searching the sample. Irrespective of the related instrumental developments, the aim to observe biomacromolecules in water requires entirely new preparation procedures that warrant the fixation of the sample at a well defined surface suitable for scanning with a nanoprobe. While the preparation of single macromolecules in this manner may be difficult, the fixation of supramolecular assemblies such as filaments or membranes to an appropriate substrate may become possible.

| Scanning microscope type | Principle | Applications in Cell and Structural Biology |
|---|---|---|
| **Tunneling**<br>[Binnig and Rohrer, 1985] | A sharp metal tip is scanned so close to a surface that a tunneling current $I_t$ flows. A servo regulating the height of the tip is used to keep $I_t$ constant. | Determination of the topography of biological macromolecules and assemblies thereof, possibly in physiological solutions.<br>Spectroscopy to differentiate between characteristic macromolecules such as proteins, DNA, lipids (or, ultimately, residues thereof). |
| **Atomic force**<br>[Binnig et al., 1986] | A very flexible cantilever in mechanical contact with a surface is scanned and its deflection measured. | Determination of the topography, difficult to be performed in physiological solutions.<br>Determination of mechanical properties of flexible domains and hinge regions identified in the topograph. |
| **Magnetic force, Potentiometry**<br>[Martin and Wickra-masinghe, 1987;<br>Martin et al, 1988] | The force induced by local magnetic fields on a magnetic tip or electro-static forces between tip and sample are measured. | Likely to be used in physics and material sciences. A spatial resolution of 100 nm has been demonstrated. |
| **Thermal probe**<br>[Williams and Wickra-masinghe, 1986] | The tip consists of a microfabricated thermo-couple capable of resol-ving 0.1 millidegree. | Determination of cellular surface profiles by monitoring the thermal coupling between tip and sample. A spatial resolution of 100 nm has been demonstrated. |
| **Light pipette**<br>[Harootunian et al., 1986] | A capillary pipette drawn to a diameter of 60 nm at the end is used as light guide and is scanned over the sample. | Noninvasive observation of cellular attachment and movement on thin planar films. A spatial resolution of 60 nm has been demonstrated provided the pipette remains within a distance from the sample of 2-5 nm to warrant the near field condition. |
| **Ion pipette**<br>[Hansma et al., 1988] | A similar pipette is used to measure ion currents through an aperture of some nm diameter. | Direct observation of conducting states of membrane channels at high spatial resolution.<br>Determination of the topography of nonconductors. |

<u>Table 1</u>  Scanning sensor microsocpes and their possible applications

## Acknowledgments

## References

U. Aebi, W.E. Fowler, E.L. Buhle and P.R. Smith (1984), J. Ultrastruct. Res. 88, 143

D.A. Agard et al. (1988), Methods in Cell Biol. 30 (in press)

R. D. Allen (1985), Ann. Rev. Biophys. Biophys. Chem. 14, 265

M. Amrein, A. Stasiak, H. Gross, E. Stoll and G. Travaglini (1988), Science 240, 514

M. v. Ardenne (1938), Z. tech. Phys. 109, 533

A.M. Baró, R. Miranda, J. Alamán, N. Garcia, G. Binnig, H. Rohrer, Ch. Gerber and J.L. Carrascosa (1985), Nature 315, 253.

G. Binnig and H. Rohrer (1982), Helv. Phys. Acta 55, 726

G. Binnig & H. Rohrer (1985), Sci. Am. 235, 40

G. Binnig, C.F. Quate and Ch. Gerber (1986), Phys. Rev. Lett. 56, 930

G.J. Brakenhoff, P. Blom and P. Barends (1979), J. Microsc. 117, 219

E. Carlemalm and E. Kellenberger (1982), EMBO J. 1, 63

M.D. Cole, J.W. Wiggins and M. Beer (1977), J. Mol. Biol. 117, 387

C. Colliex (1984), in: Advances in Optical and Electron Microscopy, Vol 9, p. 66 (eds R. Barer and V.E. Coslett), Academic Press

A.V. Crewe (1970), Quart. Rev. Biophys. 3, 137

A.V. Crewe, J. Wall and J. Langmore (1970), Science 168, 1338

A.V. Crewe (1986), Proc. XIth Int. Cong. Electr. Micr. Kyoto, 2105

P. Dierckx (1980), Computing 24, 349

J. Dubochet , M. Adrian, J.J. Chang, J.C. Homo, J. Lepault, A.W. McDowall and P. Schultz (1988), Quart. Rev. Biophys. 21, 129

R.F. Egerton (1986), EELS in the Electron Microscope, Plenum Press

A. Engel (1974), Optik 41,117

A. Engel, J. Dubochet and E. Kellenberger (1976), J. Ultrastruct. Res. 57, 322

A. Engel (1978), Ultramicroscopy 3, 273

A. Engel and R. Reichelt (1984), J. Ulstrastruct. Res. 88, 105

A. Engel, R. Eichner and U. Aebi (1985), J. Ultrastruct. Res. 90, 323

K. Fujiwara and T.D. Pollard (1976), J. Cell Biol. 71, 848

J. Gelles, B.J. Schnapp and M.P. Scheetz (1988), Nature 331, 450

R. Guckenberger, C. Kösslinger, R. Gatz, H. Breu, N. Levai and W. Baumeister (1988), Ultramicroscopy 25, 111

P.K. Hansma et al. (1988), III Int. Conf. on STM (Abstract)

A. Harootunian, E. Betzig, M. Isaacson and A. Lewis (1986), Appl. Phys. Lett. 49, 674

A. Holzenburg, R. Reichelt, U. Aebi and A. Engel (1988), submitted

S. Inoue (1981), J. Cell Biol. 89, 346

M. Isaacson, D. Kopf, M. Utlaut, N.W. Parker and A.V. Crewe (1977), Proc. Nat. Acad. Sci. (USA) 74, 1802

M. Knoll and E. Ruska (1932) Ann. Phys. 12, 607

Y. Martin and H.K. Wickramasinghe (1987), Appl. Phys. Lett. 50, 1455

Y. Martin, D.W. Abraham and H.K. Wickramasinghe (1988), Appl. Phys. Lett. 52, 1103

M. Müller and R. Hermann (1988), Proc. 46th Ann. Meet. EMSA, 186 (ed A.W. Bailey)

J. Pawley (1984), J. Microsc. 136, 45

C.F. Quate (1986), Phys. Today 39, 26.

K.-R. Peters (1985), Scanning Electron Microscopy /1985/IV, 1519

H. Seiler (1983), J. Appl. Phys. 54, R1

P.R. Smith and U. Aebi (1974), J. Phys. A: Gen. Phys. 7, 1627

A. Stemmer, R. Reichelt, A. Engel, J.P. Rosenbusch, M. Ringger, H.R. Hidber and H.-J. Güntherodt (1987), Surf. Sci. 181, 394.

A.Stemmer, A. Engel, R. Häring, R. Reichelt and U. Aebi (1988), Ultramicroscopy 25, 171

A.C. Steven , J.F. Hainfeld, B.L. Trus, J.S. Wall and P.M. Steinert (1983), J. Biol. Chem. 258, 8323

G. Travaglini, H. Rohrer, M. Amrein and H. Gross (1987), Surf. Sci. 181, 380.

J.S. Wall, J.F. Hainfeld, J.W. Bittner (1978), Ultramicroscopy 3, 81

J.S. Wall (1979), Scanning Electron Microscopy /1979/II, 291

D. Walzthöni, M. Bähler, H.M. Eppenberger, T. Wallimann and A. Engel (1984), EMBO J. 3, 2621

J.G. White, W.B. Amos and M. Fordham (1987), J. Cell Biol. 105, 41

C.C. Williams and H.K. Wickramasinghe (1986), Appl. Phys. Lett. 49, 1587

J.A.N. Zasadzinski, J. Schneir, J. Gurley, V. Elings and P.K. Hansma (1988), Science 239, 1013.

# Diffraction Studies of Glycated Collagen

Eric F. Eikenberry[1], Gad Avigad[2] and Shizuko Tanaka[2]
[1]Departments of Pathology and [2]Biochemistry
Robert Wood Johnson Medical School
University of Medicine and Dentistry of New Jersey
Piscataway, NJ 08854 USA

Glycation is a non-enzymatic condensation between an amino group, such as an $\alpha$- or $\epsilon$-amino group of a protein, and the carbonyl group of a reducing sugar. The reaction begins with the formation of a Schiff base which undergoes Amadori rearrangement to form a relatively stable ketoamine. Subsequent interactions involving the ketoamine adducts affect the chemical, physical and biological properties of the protein. Glycation occurs spontaneously in living animal tissues with the consequence that long-lived proteins normally have measurable amounts of glucose attached to them by this reaction. Hemoglobin $A_{1c}$ is the best characterized product of glycation in humans, but other proteins also participate in this reaction. The rate of glycation under physiological conditions is normally very low, but is elevated in the chronic hyperglycemic state associated with diabetes mellitus. It has been hypothesized that glycation plays a role in the effects of aging and in the pathophysiology of diabetes (Cerami, *et al.*, 1985; Brownlee, *et al.*, 1988).

Collagen, the major structural protein in higher animals, is a substrate for glycation *in vivo*. Glycated collagen undergoes further reactions that result in the formation of covalent cross-links between the polypeptide chains. The cross-linked protein has a characteristic fluorescence, altered mechanical properties and greatly reduced extractability. For example, a 70 year old human dura mater is only 50 % solubilized by CNBr (Kohn, 1983).

We are investigating the biochemical and structural changes that occur in connective tissues subjected to glycation. Rat tail tendon was chosen for these studies because it is a highly homogeneous source of type I collagen and gives an excellent fiber x-ray diffraction pattern. Because of the very low reactivity of glucose as a glycating reagent, ribose was used in order to make the experiments feasible on a laboratory time scale.

The x-ray diffraction pattern of rat tail tendon contains a series of 70 or more strong meridional reflections parallel to the fiber axis, which derive from the 67 nm periodic axial structure of the specimen, and a set of equatorial and near equatorial reflections dominated by maxima at 12 - 14 nm which are derived from the three planes of the quasihexagonal structure that contain the centers of the collagen molecules (Hulmes & Miller, 1979). This x-ray pattern has been intensively investigated to give a fairly detailed picture of the structure of this type I collagen. In particular, we know the positions of the molecular centers

within the unit cell, the relative azimuthal orientation of the molecules and the average posi-
tions of the backbone atoms within the chains (Fraser, et al., 1979; Fraser, et al., 1983). But,
between these two levels of resolution there are still some features of the structure which
have remained inaccessible; namely, which of the chemically distinct segments of the
molecule are packed next to each other, which of the polypeptide chains, $\alpha 1$ and $\alpha 2$, occupy
the non-equivalent structural positions in the triple-helix, and which classes of amino acid
side chains interact along the "edges" of the molecules to determine the helix packing.  Lo-
calization of cross-linked triple-helical segments of the collagen molecule by both structural
and biochemical means could help to resolve these questions.

Exposure of rat tail tendon to ribose results in incorporation of the sugar into colla-
gen and in significant changes in the x-ray diffraction pattern, both of which increase with
time of incubation.  Upon incubation in 0.2 M ribose in physiological saline for several days,
the strong equatorial and near equatorial reflections move toward larger real spacings, indi-
cating an expansion of the structure.  Simultaneously, the equatorial reflections broaden and
there is an increase in diffuse scattering in that region of the pattern, consistent with a pro-
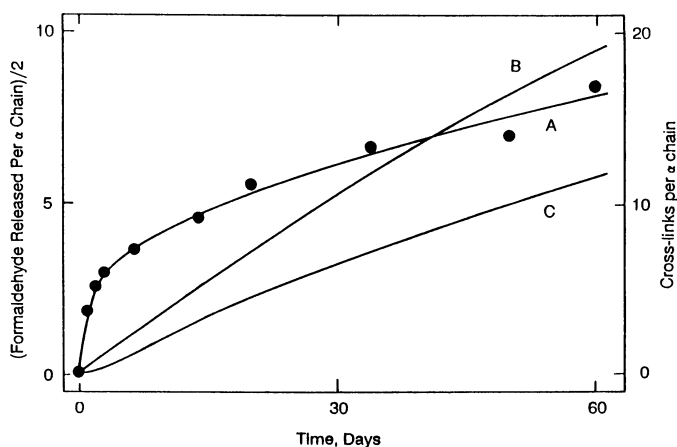


Fig. 1.  Glycation of rat tail tendon by ribose and kinetic models of glycation.  Sugar
incorporation was measured by an assay for release of formaldehyde upon periodate oxida-
tion (Tanaka, et al., 1988a).  It was assumed that two mols of sugar is released for each sugar
oxidized.  (•) Incorporation of sugar into rat tail tendon during incubation in 0.2 M ribose,
150 mM NaCl, 10 mM sodium phosphate, pH 7.5.  Tendons were incubated for various
times, then washed free of unbound sugar before assaying.  The initial rapid rise in
measurable formaldehyde falls off as the sugar becomes involved in cross-links, which makes
it partially inaccessible to the assay.  Similar curves showing proportionately lower rates of
incorporation were obtained with 0.1 M and 0.05 M ribose (Tanaka, et al., 1988a).  For
clarity, these data were omitted from the figure, but were used to find the best fit-kinetic
parameters.  (A) Best-fit kinetics from a model in which two glycated amino groups
condense to form a cross-link.  (B) Best-fit kinetics from the model described in the text.
The best-fit values of the rate constants were: $k_{+1} = 0.12$ M$^{-1}$ day$^{-1}$; $k_{-1} = 3.2$ day$^{-1}$; and $k_2$
$= 0.16$ (mol/mol $\alpha$ chain)$^{-1}$ day$^{-1}$.  (C) Cross-links formed according to the model shown in
(A).

gressive loss of long-range order as the glycation reaction continues (Tanaka, *et al.*, 1988a). There are also changes in the intensities of certain meridional reflections, notably the 13th - 19th orders, but the axial period remains unaltered at 67 nm.

As shown in Fig. 1, sugar is initially incorporated rapidly by rat tail tendon, but after a few days the measured rate declines. In contrast to the kinetics of sugar binding to the collagen, structural alteration is not immediately observable upon exposure to sugars. Axial and lateral changes both take place at an approximately uniform rate in time over 60 days of observation. The lateral expansion is not isotropic, but is directed parallel to the ($1\bar{2}0$) planes of the structure, one of the major planes of the quasihexagonal lattice. Over the course of a 17 day exposure to 0.2 M ribose, the lateral expansion results in a volume increase of about 12 % in the rat tail tendon unit cell (Tanaka, *et al.*, 1988a).

Four mechanisms were examined as possible explanations for the observed expansion: a change in electrostatic interactions caused by sugar binding to amino groups; a direct steric action by the incorporated sugar residues; an increase in hydration brought about by the presence of the sugar moieties; and, creation of cross-links in such positions as to push the chains apart. The first three of these were ruled out as being unable to explain fully the observations. Electrostatic changes are expected to be minimal because the secondary amine resulting from glycation of lysine retains a fairly basic $pK_a$, and would be completely charged at the pH of these experiments. A direct steric effect by the added sugars seems unlikely because the added steric volume of sugar is at most 3 % of the anhydrous volume of the protein. An explanation based on the water of hydration of sugars appears not to have the specificity to account for either the directional nature of the molecular expansion, or the specific changes in the meridional intensities. And, each of these mechanisms would predict structural changes proportional to the amount of sugar bound, whereas the observed changes are delayed considerably with respect sugar binding.

The fourth hypothesis, creation of intermolecular cross-links which serve to push the collagen molecules apart, is consistent with the observations. The creation of one, or at most a few, specific intermolecular cross-links could account for the directionality of the structural expansion, and the specificity of the changes in the meridional intensity pattern. Further, cross-link formation, which incorporates previously glycated lysine residues into more complex structures, can explain the apparent delay in the kinetics of structural change with respect to sugar incorporation.

A cross-link would act to join two neighboring $\epsilon$-amino groups of lysines at a fixed distance and thereby reduce the degrees of freedom through which they can move. Structures proposed for the cross-linking of lysine by aldoses and aldehydes suggest that the nitrogen atoms would be bridged by a single carbon atom (Pongor, *et al.*, 1984; Fraenkel-Conrat & Olcott, 1948). Such a cross-link between two residues at the same axial position would add a repulsive component to the lateral interactions between neighboring collagen triple-helices since the average intermolecular spacing in native tendon is about 1.5 nm, while

model building shows that fully extending the two linked lysines would require a center-to-center distance of almost 2.1 nm.  However, since the cross-link would exist under a compressive force, it should not be fully extended and the predicted expansion would be less than this.  Using the 234 residue overlap alignment of Chapman and Hulmes (1984), together with the relative azimuthal orientations of Fraser, *et al.* (1983), we found that there are only two positions in the overlap zone where lysine residues could directly oppose each other to create a cross-link of this kind:  $Lys_{270}$ to $Lys_{974}$; and $Lys_{290}$ to $Lys_{756}$.

As a step toward interpreting the x-ray diffraction pattern of glycated rat tail tendon, we have investigated with a computer model the changes expected in the equatorial pattern caused by disorder in the lateral structure introduced by glycation.  Disorder in structures is traditionally divided into two kinds: lattice disorder and substitution disorder.  Lattice disorder occurs when there is a lack of long range order in the lattice spacings because of variation in the effective size of the unit cells.  This causes reflections to broaden with a progressive increase in width of higher orders; higher orders may eventually blur together to form a continuous pattern.  Substitution disorder, in which the electron density profile within the unit cells varies, gives rise to diffuse scattering superimposed on the sampled scattering arising from the lattice.  This component typically increases in magnitude with scattering angle up to a maximum, and then falls off.  An additional important effect arises from the presence of crystalline domains of small size, which acts to broaden all reflections equally.

Schwartz, *et al.* (1975) derived an expression for the total scattered intensity from a disordered one-dimensional, i.e. lamellar, specimen:

$$I(s) = (1/d)|\overline{F_0(s)}|^2 \cdot [Z(s)_* |\Sigma(s)|^2] + N[\overline{|F_0(s)|^2} - |\overline{F_0(s)}|^2] \qquad (1)$$

where $s = 2\sin\theta/\lambda$ is the reciprocal space coordinate, d is the average unit cell nearest neighbor separation, N is the number of unit cells in a crystalline domain, $F_0(s)$ is the unit cell structure factor, $Z(s)$ is the interference function arising from the lattice, and $\Sigma(s)$ is the shape factor describing the size of a crystalline domain.  Bars over expressions indicate averaging.  The first term represents the sampled diffraction arising from the lattice, broadened by small crystallite size.  It predicts the occurrence of diffraction maxima as orders of a fundamental spacing given by the reciprocal of the average lattice dimension, d.  The second term is the variance of the electron density profile within the unit cells and describes the diffuse scattering.  An equivalent expression using a different formalism was obtained by Nelander and Blaurock (1978).  Guinier (1963) describes the extension of this approach to three dimensional ideal paracrystals, in which the fluctuations in structure along the three Cartesian axes are independent, a condition that is not met in the triclinic unit cell of collagen.  In a different approach specialized to the structural features of collagen, Woodhead-Galloway and Machin (1976) have modeled the lateral structure of rat tail tendon as a two-dimensional liquid crystal and have calculated the diffuse scatter along the equator.

This expression for the total scattered intensity was derived under the assumptions that the perturbation responsible for the disorder was small enough to permit averaging of structures, and that the lattice and substitution disorder were independent of each other and not correlated in spatial location. These assumptions probably are not valid in the case of glycated rat tail tendon because the perturbation may not be small enough and because the change in electron density represented by the cross-link would be fully correlated with the lattice disorder. Further, most calculations of scattered intensity rely on Gaussian distributions of lattice dimensions and of unit cell electron density profiles, whereas cross-links introduced by sugars would represent fixed size entities except for the strain introduced by inhomogeneity in the packing forces.
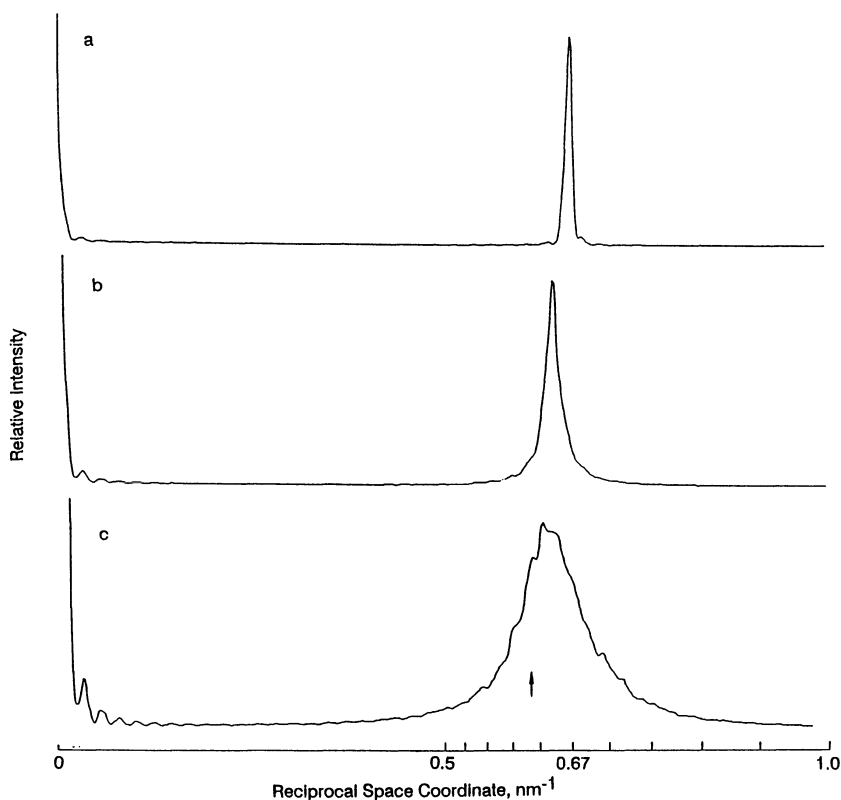


Fig. 2. One-dimensional simulation of the dominant equatorial diffraction maximum of rat tail tendon. (a) Profile predicted for 65 uniform unit cells at a spacing of 1.5 nm representing a diametral cross-section of an average coherent domain, broadened as described in the text. (b) Average of 300 randomly perturbed domains in which a perturbation of 0.3 nm was added to 20 % of the unit cells in each domain to give an average unit cell dimension of 1.56 nm. (c) Average of 300 randomly perturbed domains in which a perturbation of 0.6 nm was added to 20 % of the unit cells to give an average unit cell dimension of 1.62 nm (vertical arrow).

The current computer model accepts a one-dimensional profile sampled with a resolution of 4096 elements representing a section of the electron density along the ($1\overline{2}0$) plane through the center of a crystalline domain. Such a domain in rat tail tendon is about 100 nm in diameter, or about 65 molecules across, using the average intermolecular spacing in that direction of 1.544 nm. The perturbation caused by glycation is modeled as a stochastic process that causes a fraction, f, of randomly chosen nearest neighbor molecular spacings to increase by $\delta$. The diffraction pattern is computed and averaged for several hundred independently chosen domains of this sort. The result is convoluted with a Gaussian having a full width at half maximum of 1.5 mradian representing the point spread function of the x-ray camera. A typical result with f = 0.2 and $\delta$ = 0.3 nm is shown in Fig. 2b. This shows a single, broadened diffraction maximum positioned at the average unit cell dimension, as would be expected from Equation 1.

The simulation was used to explore the limitations of the approximations described above. Under a wide variety of circumstances, the predicted scattering profile was not a single symmetrical peak, but was skewed, displaced from the average unit cell dimension, and showed modulation that could potentially be resolved experimentally (Fig. 2c). The necessary conditions to retain a single maximum, as seen in current experiments, were that the fractional occupancy, f, not be more than about 25 % of all of the available unit cells; that the magnitude of the perturbation, $\delta$, not represent more than about 20 % of the intermolecular spacing; and that the instrumental broadening be introduced. The product $f\delta$ represents the average increase in nearest neighbor intermolecular spacing and hence predicts a linear dependence of the average unit cell size on the fractional occupancy of cross-link sites. Thus, the approximately linear change with time of the lattice spacing would be consistent with an approximately linear increase in the number of cross-links with time. We observe $f\delta$ to be 0.024 nm after 4 days of glycation in 0.2 M ribose, and 0.052 nm after 14 days, during which time the diffraction maxima are still fairly well resolved. If the magnitude of $\delta$ is about 0.3 nm, which is half of the increase that could be accomplished by fully extended lysine side chains, then f ranges from 8 % to 17 % during this period.

To understand the relations between the kinetics of glycation and those of the structural changes inferred from x-ray diffraction, it would be useful to have a kinetic model for the glycation reaction that predicts the time-course of cross-link formation. At present, such an analysis is difficult because the exact nature of the chemical reaction pathway leading to cross-link formation is unknown. However, since kinetic modeling depends primarily on the stoichiometry of reactants and products, evaluation of different kinds of models can be made with presently available data.

One analysis of glycation kinetics has been presented (Tanaka, *et al.*, 1988a). The essential features of this kinetic model were that a primary condensation occurs between the sugar moiety and the free amino group of lysine, and that two such glycated lysine residues undergo a second condensation to form a cross-link. This could be called the two sugar

residue model since other two sugar residue pathways will fit the data equally well with suitable rate constants. This mechanism gives a very good fit to our sugar incorporation data (Fig. 1, curve A) and predicts that cross-link formation is roughly linear with time (Fig. 1, curve C), which fits well with the time-course of the changes in structure. The two sugar residue model was based on schemes suggested by Pongor, *et al.* (1984) in their "routes" B and C. It has recently been found that the compound studied by Pongor, *et al.* (1984) was formed as a byproduct of the preparative procedure used to analyze the reaction and therefore does not represent the major final cross-link produced by glycation (Njoroge, *et al.*, 1988). Consequently, we have explored whether other kinetic models are compatible with the data.

One alternative model, the one sugar residue model, can be based on results from studies of cross-linking of lysine by formaldehyde (Fraenkel-Conrat & Olcott, 1948), which is analogous to route A of Pongor, *et al.* (1984). In this mechanism, a single aldehyde, or aldehydo group, acts to form a methylene bridge between amino groups of lysine. The primary condensation product of lysine with the aldehyde undergoes a further condensation with a free lysine amino group to form a stable cross-link:

$$\begin{array}{cccc} \text{Sugar,} & & \text{Rat Tail Tendon} & \xrightarrow[k_{-1}]{k_{+1}} \text{Glycated Amine} \\ \text{Aldehydo} & + & \text{Collagen } \epsilon\text{-Amine} & \text{(Schiff Base and} \\ \text{Form} & & & \text{Ketoimine Forms)} \end{array}$$

$$\begin{array}{cccc} \text{Glycated} & & \text{Rat Tail Tendon} & \xrightarrow{k_2} \text{Cross-Linked} \\ \text{Amine} & + & \text{Collagen } \epsilon\text{-Amine} & \text{Collagen} \end{array}$$
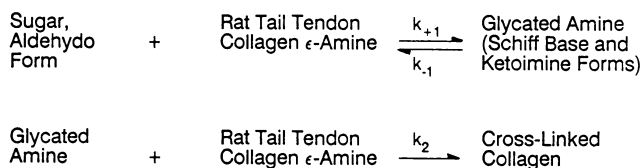
This model leads to the following set of equations:

$$\frac{dC}{dt} = -k_{+1}AC + k_{-1}G$$

$$\frac{dG}{dt} = k_{+1}AC - k_{-1}G - k_2GC$$

$$\frac{dX}{dt} = k_2GC$$

where C is the concentration of $\epsilon$-amino groups, t is time, A is the concentration of sugar aldehyde (assumed to remain constant), G is the concentration of glycated amino groups, and X is the concentration of cross-links. C, G and X are expressed in units of moles per mole of $\alpha$ chain. The equations were solved numerically and the best-fit values of the three adjustable constants were determined by non-linear least-squares analysis.

As shown in Fig. 1 curve B, this reaction scheme dramatically changes the allowed kinetics from the previous model, and in such a way that the sugar incorporation data can only be fit very poorly. We conclude that this kinetic model is ruled out by the data. Until a

fuller understanding of the chemistry of cross-linking is available, we will use the first kinetic model as a working hypothesis.

Thus, the model of the structural changes caused by glycation appears to be consistent with the experimental data at this time. We are extending the computer model to two dimensions to permit calculation of the full equatorial diffraction pattern from the transverse section of the fibril. The model also suggests that x-ray diffraction data from a camera with very high angular resolution could give insight into the statistics of the disorder that is present. In addition, biochemical studies have been initiated to determine the sites of cross-linking along the length of the collagen molecule. Fluorescent tryptic peptides have been isolated from dimers of collagen chains under conditions where essentially all cross-links are a result of exposure to sugar (Tanaka, *et al.*, 1988b). The structural information from x-ray diffraction studies combined with biochemical localization of cross-links within the amino acid sequence should give us new high resolution information about the structure of type I collagen.

## Acknowledgements

## References

Brownlee, M., Cerami, A., and Vlassara, H. (1988) Advanced glycosylation end products in tissue and the biochemical basis of diabetic complications. N. Engl. J. Med. **318**, 1315-1321.

Cerami, A., Vlassara, H., and Brownlee, M. (1985) Protein glycosylation and the pathogenesis of atherosclerosis. Metabolism **34**, Suppl 1. 37-44.

Chapman, J.A., and Hulmes, D.J.S. (1984) Electron microscopy of the collagen fibril. *in* Ultrastructure of the Connective Tissue Matrix. Ruggeri, A., and Motta, P.M., eds. Martinus Nijhoff, Boston, pp. 1-33.

Fraenkel-Conrat, H., and Olcott, H.S. (1948) The reaction of formaldehyde with proteins. J. Am. Chem. Soc. **70**, 2673-2684.

Fraser, R.D.B., MacRae, T.P., Miller, A., and Suzuki, E. (1983) Molecular conformation and packing in collagen fibrils. J. Mol. Biol. **167**, 497-521.

Fraser, R.D.B., MacRae, T.P., and Suzuki, E. (1979) Chain conformation in the collagen molecule. J. Mol. Biol. **129**, 463-481.

Guinier, A. (1963) X-ray Diffraction. W.H. Freeman and Co., San Francisco.

Hulmes, D.J.S., and Miller, A. (1979) Quasi-hexagonal molecular packing in collagen fibrils. Nature **282**, 878-880.

Kohn, R.R. (1983) Effects of age and diabetes mellitus on cyanogen bromide digestion of human dura mater. Connective Tissue Res. **11**, 169-173.

Nelander, J.C., and Blaurock, A.E. (1978) Disorder in nerve myelin: Phasing the higher order reflections by means of the diffuse scatter. J. Mol. Biol. **118**, 497-532.

Njoroge, F.G., Fernandes, A.A., and Monnier, V.M. (1988) Mechanism of formation of the putative advanced glycosylation end product and protein cross-link 2-(2-furoyl)-4(5)-(2-furanyl)-1H-imidazole. J. Biol. Chem. **263**, 10646-10652.

Pongor, S., Ulrich, P.C., Bencsath, F.A., and Cerami, A. (1984) Aging of proteins: Isolation and identification of a fluorescent chromophore from the reaction of polypeptides with glucose. Proc. Natl. Acad. Sci. USA **81**, 2684-2688.

Schwartz, S., Cain, J.E., Dratz, E.A., and Blasie, J.K. (1975) An analysis of lamellar x-ray diffraction from disordered membrane multilayers with application to data from retinal rod outer segments. Biophys. J. **15**, 1201-1233.

Tanaka, S., Avigad, G., Brodsky, B., and Eikenberry, E.F. (1988a) Glycation induces expansion of the molecular packing of collagen. J. Mol. Biol. **203**, 495-505.

Tanaka, S., Avigad, G., Eikenberry, E.F., and Brodsky, B. (1988b) Isolation and partial characterization of collagen chains dimerized by sugar-derived cross-links. J. Biol. Chem., in press.

Woodhead-Galloway, J., and Machin, P.A. (1976) Modern theories of liquids and the diffuse equatorial x-ray scattering from collagen. Acta Cryst. **A32**, 368-372.

# Oscillations in Microtubule Assembly Studied by Time-Resolved X-Ray Scattering

Eva-Maria Mandelkow, Gudrun Lange, Annette Jagla and Eckhard Mandelkow
Max-Planck-Unit for Structural Molecular Biology
c/o DESY, Notkestraße 85, D-2000 Hamburg 52, F.R.G.

## INTRODUCTION

Microtubules are hollow cylinders, about 25 nm in diameter, which form part of the cytoskeleton of eukaryotic cells. They perform a variety of functions, such as the beating of cilia, separation of chromosomes in mitosis, or transport of vesicles in nerve cells. They consist of the protein subunit tubulin (a heterodimer of molecular weight 100,000) and several microtubule-associated proteins (MAPs). Microtubules are often dynamic structures capable of assembly and disassembly. The protein can be isolated from cells (e.g. brain) and induced to self-assemble in vitro.

The biophysical methods for studying microtubule assembly have included mainly electron microscopy and light scattering. As an alternative we have applied the the method of time-resolved X-ray scattering from solutions using synchrotron radiation (Mandelkow et al., 1980; Bordas et al., 1983; Spann et al., 1987). An advantage of it is that it combines good structural and temporal resolution. This has allowed us to define several intermediate stages of assembly and disassembly. When the subunit protein of a biopolymer is induced to self-assemble (e.g. by a temperature jump) one generally observes pre-nucleation events, nucleation, and elongation. The latter is a pseudo-first order reaction so that the steady state of assembly is usually approached in an exponential fashion (see Oosawa & Asakura, 1975). However, microtubules show an additional and unique behavior that is not explained by the common nucleation/elongation models: They can be assembled into unstable states, showing overshoot and recovery, or even autonomous and synchronized oscillations

that are reminiscent of certain events in living cells. These features can be understood on the basis of the dynamic instability concept of Mitchison & Kirschner (1984). The system is remarkably simple; in principle it only requires energy in the form of GTP and the protein tubulin. Here we summarize the main features of this oscillator as seen by time-resolved X-ray scattering.

## METHODS

The protein preparation and other methods (electron microscopy, determination of protein-bound nucleotides) are described elsewhere (Mandelkow et al., 1988; Lange et al., 1988). The X-ray experiments were performed on instrument X33 of the EMBL Outstation at the DESY synchrotron, Hamburg (Koch & Bordas, 1983), equipped with a rapid temperature jump cell and a position-sensitive detector. The protein was filled into the chamber at 0-4°C, and the reaction was started by raising the temperature to 37°C within a few seconds. Scattering patterns were recorded in 2-6 sec intervals and analyzed as described (Bordas et al., 1983; Spann et al., 1987). Computer simulations of the time courses of assembly or oscillations were performed by numerical solution of a set of differential equations taking account of the reacting protein species (subunits, oligomers, polymers) and their interactions with other cofactors (nucleotides, metal ions, associated proteins), and then adding the various contributions after weighting with the form factors calculated from Debye's formula (Lange et al., 1988; and this volume).

## RESULTS AND DISCUSSION

Fig. 1 shows the X-ray scattering from an oscillating sample microtubule protein. The central scatter (left) is a measure of overall assembly, while the structures of the reacting species are deduced from the shape of the scattering patterns. For example, microtubules are recognized by a high central scatter and a subsidiary maximum around 0.05 nm$^{-1}$. The initial solution has a low central scatter and several side maxima; this arises from a mixture of tubulin

Fig. 1: Projection plot of the X-ray scattering from a solution of oscillating microtubules, showing the X-ray intensity as a function of scattering vector $(S = 2\sin\theta/\text{lambda})$ and time (traces shown are in 6 sec intervals) after a temperature jump from 4 to 37°C. The central scatter (left) indicates overall assembly, the subsidiary maximum arises from microtubules. From Mandelkow et al., 1988.
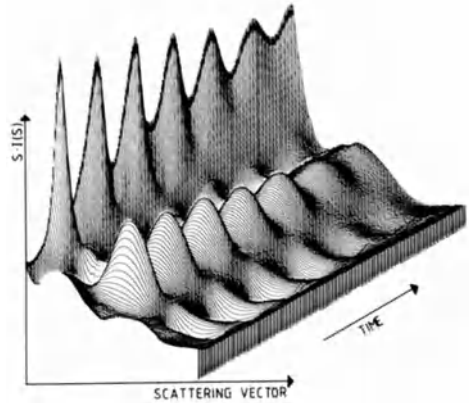
Fig. 2: Selected scattering traces observed between the first peak of an oscillation and the subsequent valley. The solid curve at the top of the central scatter (left) and at $S = 0.05$ nm$^{-1}$ is at the first assembly maximum, the bottom curve is at the subsequent valley, the others are at intermediate time points. Note the constant positions of the isosbestic points at $S = 0.025$, $0.041$, $0.062$, and $0.089$ nm$^{-1}$. The intermediate traces are accounted for by linear superpositions of the two extremes with varying ratios.
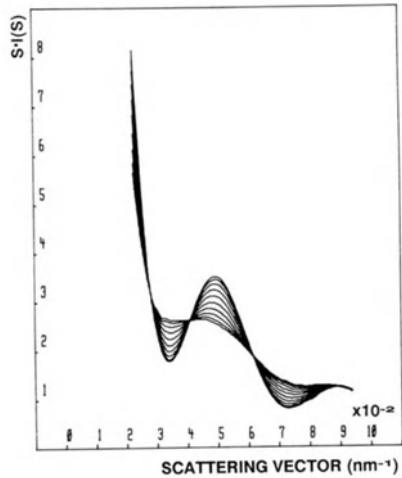
Fig. 3: Time dependence of X-ray scattering at three scattering angles. From top to bottom, $0.02$, $0.033$, and $0.05$ nm$^{-1}$. Note that the bottom curve oscillates in antiphase with the other two.
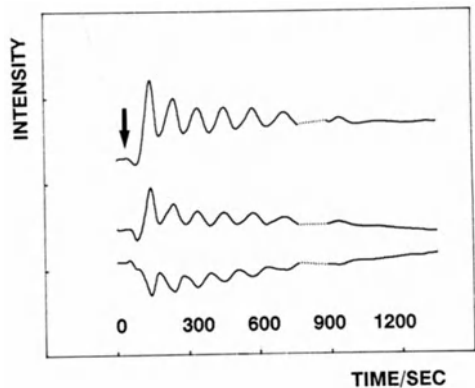
subunits and oligomers, many of which form closed rings in this preparation. The reaction is initiated by a rapid temperature jump from 4 to 37°C, leading to the rapid assembly of microtubules. However, they do not attain a steady state, as expected from a simple nucleation/condensation mechanism. Instead, the solution oscillates between a high and a low level of assembly. When the scattering curves observed during a cycle are superimposed they intersect at well-defined isosbestic points (Fig. 2). This indicates that the curves are dominated by the scattering from two main species whose contributions are mixed with varying ratios. Fig. 3 shows the time dependence of the oscillations at three different scattering angles. The central scatter (top) is roughly proportional to the overall degree of assembly, the middle curve shows the region where the microtubule form factor has its first side maximum, and the bottom curve corresponds to an angle where ring oligomers have their first side maximum. The two top curves oscillate in phase, the bottom one in antiphase. When the oscillations die out the two top curves slowly decrease, while the bottom one increases. A detailed comparison with model scattering curves suggests that the oscillations involve three species: Microtubules, oligomers, and tubulin subunits. The first two contribute noticeably to the scattering pattern in the observed angular region, while the contribution of subunits is comparatively weak (Mandelkow et al., 1988; Lange et al., 1988).

The X-ray data were complemented with biochemical and electron microscopical observations (Fig. 4). They show the following results: At the peak of oscillations the solution contains mainly microtubules, at the bottom the microtubules have largely disappeared, and instead one observes many oligomers (ring-like ones or smaller than rings, typically 80-100 nm long). These correspond to linear chains of tubulin subunits, equivalent to short protofilament fragments. The structure factors of these entities are compatible with the observed X-ray curves. Their appearance and disappearance can be correlated with the interaction between tubulin and its cofactor GTP which is necessary for assembly and is hydrolyzed to GDP in this process. The
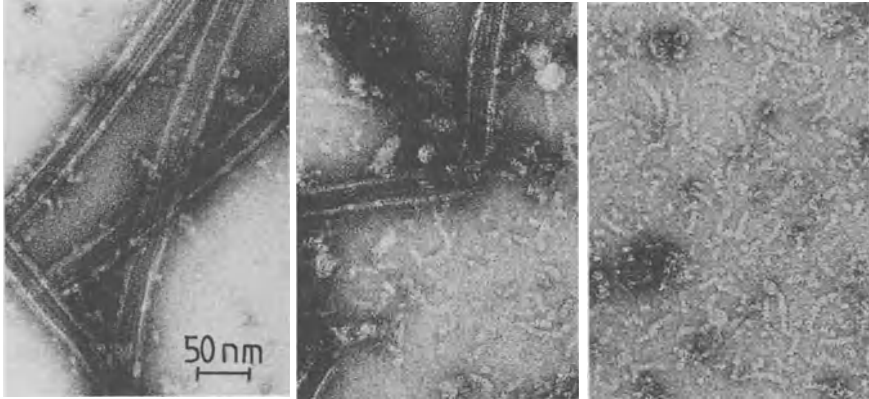
Fig. 4: Electron micrographs of tubulin at different stages of oscillations. Left, maximal assembly. One observes microtubules of normal appearance and oligomeric material in the background. Center, phase of disassembly. There is a noticeable increase in oligomers. Many microtubules appear broken. This may occur either during disassembly in solution or as a result of the preparations for electron microscopy (e.g. negative staining or drying), but in any case it indicates a lower stability of the microtubules. Right, field of oligomers at an assembly minimum. Typical lengths are between 20 and 100 nm, corresponding to 3-12 tubulin dimers. The longer ones clearly show the coiling characteristic of disassembled protofilament fragments that leads up to ring-like closure (see upper left). Complete rings are rare with PC-tubulin but frequent with microtubule protein, presumably due to the stabilization of oligomers by MAPs. From Mandelkow et al., 1988.

Fig. 5: Oscillations in tubulin-bound GTP (top) and oscillations in microtubule assembly (bottom). The curves are roughly in antiphase; assembled microtubules contain essentially tubulin with GDP bound to the exchangeable site, while tubulin subunits released from microtubules via oligomers are re-charged with GTP from the solution until they reach a level sufficient for the rescue from the disassembly phase. From Lange et al., 1988.
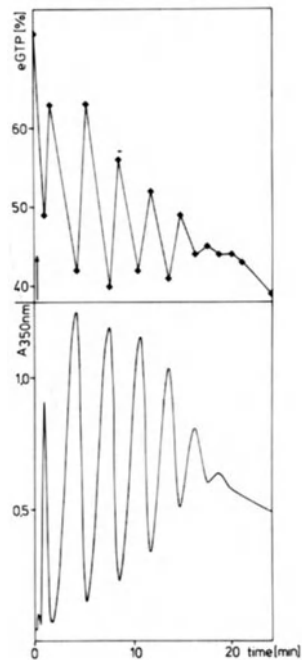
Fig. 6: Model of reaction mechanism for oscillations. There are three main species, subunits, microtubules, and oligomers. Only subunits can be activated for assembly by binding of GTP from the solution. Oligomers are the primary breakdown products of microtubules; they contain GDP and are not assembly-competent. The rescue from shrinking to growing microtubules is achieved by a buildup of active subunits (Tu.GTP). From Mandelkow et al., 1988.
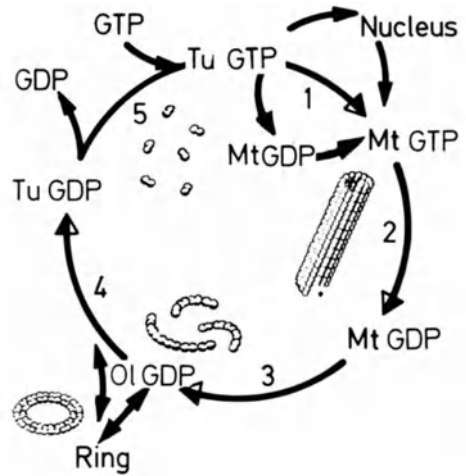


Fig. 7: (Top) Cryo-electron micrograph of disassembling microtubules, unstained and frozen in a layer of amorphous ice. Note that microtubules disintegrate by release of short protofilament fragments (oligomers). The oligomers can reassociate in a subsequent reaction to form closed rings (upper part). (Bottom) Disintegrating microtubule visualized by metal shadowing. From Mandelkow and Mandelkow, 1985.
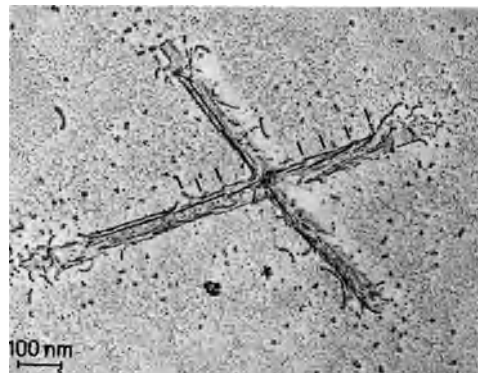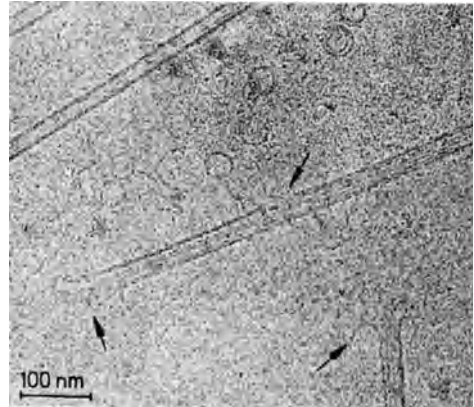
protein-bound GDP oscillates roughly in phase with the overall degree of assembly since the subunits incorporated into microtubules contain bound GDP. By contrast the protein-bound GTP oscillates roughly in antiphase Fig. 5); the buildup of tubulin.GTP serves to "rescue" the microtubules from the shrinkage phase into a new growth phase.

The combination of the above results can be explained by a cyclic reaction mechanism depicted in Fig. 6. In step 1 active tubulin subunits (tubulin.GTP) are incorporated into microtubules, either by elongation or de novo by nucleation; in step 2, the GTP bound to microtubules is hydrolyzed so that they become unstable; in step 3, microtubules disassemble into oligomers containing bound GDP (oligomer.GDP); in step 4, oligomers disintegrate into subunits with bound GDP (tubulin.GDP); in step 5, inactive subunits are re-activated by replacing GDP with GTP. The cycle is driven by the energy of GTP hydrolysis. Assembled microtubules are stable if the reactivation of subunits is rapid, compared with disassembly. Overshoot and oscillations occur if the protein is temporarily trapped in an inactive state such as oligomers. Thus the dynamic behavior depends on conditions that affect the relative rate constants of microtubule and oligomer formation.

The important point of the scheme is that the reaction involves not only subunits and polymers, but also a third assembly state, oligomers, which are generated from disassembling microtubules. This feature has been observed earlier by cryo-electron microscopy (Fig. 7; Mandelkow & Mandelkow, 1985). Oligomers contain bound GDP which renders them inactive with regard to microtubule assembly. Subunits can only be reactivated by GTP after they are released from oligomers (Fig. 6, step 4). For oscillations to occur, microtubules must remain in a measurable disassembly phase during which the factors that could lead to regrowth are inhibited. This is achieved by the slow dissolution of oligomers which represent a transient pool of assembly-incompetent tubulin.

Depending on conditions, oscillations can run for an extended period (up to an hour), or they can be strongly damped (up to the point where there is only an assembly maximum, decay, and rescue, see Mandelkow et al., 1983). The oscillations die out at the latest when GTP becomes exhausted, but usually much earlier, for reasons discussed elsewhere. These features can be reproduced by computer modelling of the reaction mechanism (see Lange et al., this volume). The calculations reproduce the observed effects, i.e. oscillations in all three components (subunits, microtubules, oligomers), and the peak in tubulin.GTP at the minimum of assembly. The rate constants can be adjusted to produce either steady state microtubules, oligomers, or oscillations. Damping of the oscillations is achieved by the depletion of GTP and buildup of GDP so that the rechargeable fraction of tubulin decreases. The final state is an equilibrium between oligomers and subunits.

Observations bearing on the dynamic instability of microtubules have been reported by several groups. For example, growth and shrinkage of individual microtubules has been monitored directly by light microscopy (Horio & Hotani, 1986; see also O'Brien & Erickson, this volume). In these experiments the microtubules are not synchronized, and the transitions between growth and shrinkage are not periodic. Because of the different experimental conditions (e.g. in protein concentration and other solution parameters) these results are not directly comparable to ours, although the underlying mechanism is likely to be similar. Using UV light scattering, synchronized oscillations have also been studied by Carlier et al. (1987) (see also this volume) and Pirollet et al. (1987). The conditions of the former study appear comparable to ours, but there are differences in interpretation (the authors did not include oligomers in the reaction mechanism). The latter study made use of a GTP regenerating system; these oscillations have a longer periodicity and can probably considered analogously to "forced oscillations", as discussed by Lange et al. (1988).

What can we learn from the oscillations in bulk solution? Microtubules show dynamic instability in living cells, i.e. there is a coexistence between shrinking and growing polymers (Mitchison & Kirschner, 1984). This occurs primarily in situations where new cellular structures are established. Roughly speaking the conversion between growing and shrinking phases provides a mechanism whereby a microtubule that self-assembles in the "wrong" direction can be retracted, and its subunits can be used elsewhere. In the usual experimental conditions in vitro the interplay between growth and shrinkage remains undetected, either because the amplitudes are too small or because the microtubules are not synchronized. In oscillating solutions the assembly and disassembly phases are strongly amplified and synchronized. This opens up the possibility of studying the biochemical and structural basis of microtubule dynamics.

# REFERENCES

Bordas, J., Mandelkow, E.-M. and Mandelkow, E. (1983). Stages of tubulin assembly and disassembly studied by time-resolved synchrotron X-ray scattering. J. Mol. Biol. 164, 89-135.

Carlier, M.F., Melki, R., Pantaloni, D., Hill, T.L. and Chen, Y. (1987). Synchronous oscillations in microtubule polymerization. Proc. Natl. Acad. Sci. U.S.A. 84, 5257-5261.

Horio, T. and Hotani, H. (1986). Visualization of the dynamic instability of individual microtubules by dark-field microscopy. Nature 321, 605-607.

Koch, M.H.J. and Bordas, J. (1983). X-ray diffraction and scattering on disordered systems using synchrotron radiation. Nucl. Instrum. Meth. 208, 461-469.

Lange, G., Mandelkow, E.-M., Jagla, A. & Mandelkow, E. (1988). Tubulin oligomers and microtubule oscillations: Antagonistic role of microtubule stabilizers and destabilizers. Eur. J. Biochem., in press.

Mandelkow, E.-M., Harmsen, A., Mandelkow, E. and Bordas, J. (1980). X-ray kinetic studies of microtubule assembly using synchrotron radiation. Nature 287, 595-599.

Mandelkow, E., Mandelkow, E.-M. and Bordas, J. (1983). Synchrotron radiation as a tool for studying microtubule self-assembly. TIBS 8, 374-377.

Mandelkow, E.-M. and Mandelkow, E. (1985). Unstained microtubules studied by cryo-electron microscopy: Substructure, supertwist, and disassembly. J. Mol. Biol. 181, 123-135.

Mandelkow, E.-M., Lange, G., Jagla, A., Spann, U. and Mandelkow, E. (1988). Dynamics of the microtubule oscillator: role of nucleotides and tubulin-MAP interactions. EMBO J. 7, 357-365.

Mitchison, T. and Kirschner, M. (1984). Dynamic instability of microtubule growth. Nature 312, 237-242.

Oosawa, F. and Asakura, S. (1975). Thermodynamics of the polymerisation of protein. Academic Press, London.

Pirollet, F., Job, D., Margolis, R.L. and Garel, J.R. (1987). An oscillatory mode for microtubule assembly. EMBO J. 6, 3247-3252.

Spann, U., Renner, W., Mandelkow, E.-M., Bordas, J. and Mandelkow, E. (1987). Tubulin oligomers and microtubule assembly studied by time-resolved X-ray scattering: Separation of prenucleation and nucleation events. Biochem. 26, 1123-1132.

# Study of the Secondary Structure of Tubulin in Solution and in Microtubules by Raman Spectroscopy

Engelborghs, Y., Audenaert, R., Heremans, L., and Heremans, K.

Laboratory of Chemical and Biological Dynamics
Katholieke Universiteit Leuven
Celestijnenlaan 200 D, B-3030, Leuven, Belgium

Microtubules are hollow fibers found in all eucariotic cells, which form the cytoskeleton or the spindle figure. They are formed by the polymerization of the protein tubulin, accompanied by GTP hydrolysis. Several experiments imply the existence of different conformations for tubulin. On the basis of the effect of GDP it can be suggested that T-GDP exists in a different conformation in solution and in the microtubule (Engelborghs and Van Houtte, 1981; Carlier and Pantaloni, 1987). This possibility necessitates a conformational study in the polymeric state. This can be done by Raman spectroscopy. Compared to CD, Raman spectroscopy has the advantage of being able to analyse turbid solutions, or even solid state samples.

## Materials and Methods

MTP preparation, purification of tubulin by ion exchange chromatography and buffer composition (MES buffer) is as described before (Lambeir and Engelborghs, 1981). For the pH-dependent study a sodium phosphate buffer system is used also at I = 0.1 M.

Microtubules are pelleted and Raman spectra are taken from the pellets with the backscattering configuration. Unpolymerized (pure) tubulin is concentrated up to 50 mg/ml by centrifuging for 1 hour at 5000 rpm on an Amicon Centricon 10 microconcentrator and studied in a thermostatted capillary.

Raman spectra are taken with a Spex 1403 double monochromator using the 514 nm line of an Ar+-laser (Spectra Physics series 2000) at 100 mW power at the sample. The secondary structure of the proteins is analysed from the Amide-I band by the method of Williams (1983). This method is similar to that applied in CD. The state of Tyr and Trp residues is deduced from their intensity ratio's.

## Results and discussion

Unpolymerized tubulin-GTP at 4 °C gives the following secondary structure: 18% α-helix (2 H-bonded), 12% α-helix (1 H-bonded), 37% β-sheet (antipar.), 4% β-sheet (par.), 18% β-turn, and 11% unordered. The total helix and β-sheet content correspond very well with the CD data of Lee et al. (1979). Replacing GTP by GDP induces a rearrangement of the secondary structure (decrease of 2 H-bonded α-helix with 8% and an increase of the antipar. β-sheet with 7%). Small differences in the CD spectra of T-GTP and T-GDP are also mentioned by Howard and Timasheff (1986). Small changes in the intensity ratio for tyrosine and for tryptophan are also observed.

Increasing the pH from 6.4 to pH 8.0 changes the tyrosine intensity ratio. The change in the tryptophan ratio's indicate that these residues become more exposed to the solvent when the pH is higher than 7.0. The secondary structure of tubulin changes significantly upon increasing the pH (2 H-bonded α-helix drops to 7% and the antiparallel β-sheet increases to 47% at pH 8).

The cytostatic colchicine is supposed to bind in two steps. Garland (1978) and Lambeir and Engelborghs (1981) provided kinetic evidence for the changes in tubulin conformation upon the binding of colchicine. The secondary structure of tubulin-demecolchine is similar to that of T-GDP (except for a slightly higher helix content).

Temperature has a very limited effect. The secondary structure analysis of microtubules shows a striking similarity between the parameters of tubulin-GDP and of microtubules. This is not surprising since (Weisenberg et al. 1976), it is known that hydrolysis of GTP occurs during or shortly after polymerization so that the tubulin dimer is bound with GDP in the microtubule.

The secondary structure of polymerized tubulin in the presence and absence of MAPs is the same. This is in full agreement with the findings of Clark et al. (1980). This raises the question of the contribution of the MAPs to the spectra.

These data prove that T-GDP in solution and in the microtubules has a very similar secondary structure.

## Acknowledgement

## References

Carlier MF, Pantaloni D. (1987) Microtubule Elongation and GTP Hydrolysis. Role of Guanine Nucleotides in Microtubule Dynamics. Biochemistry 20: 1918-1924.

Clark DC, Martin SR, Bayley PM (1980) A Study of Tubulin Dimer Conformation by Near-UV Circular Dichroism. Biochem. Biophys. Res. Comm. 97: 628-634.

Engelborghs Y, Van Houtte A (1981) Temperature Jump Relaxation Study of Microtubule Elongation in the Presence of GTP/GDP Mixtures. Biophys. Chem. 14: 195-202.

Garland DL (1978) Kinetics and Mechanism of Colchicine Binding to Tubulin: Evidence for Ligand-Induced Conformational Change. Biochemistry 17: 4266-4272.

Howard WD, Timasheff SN (1986) GDP State of Tubulin: Stabilization of Double Rings.

Lambeir A, Engelborghs Y (1981) A Fluorescence Stopped Flow Study of Colchine Binding to Tubulin. J. Biol. Chem. 256: 3279-3282.

Lee JC, Corfman D, Frigon RP, Timasheff SN (1979) Arch. Biochem. Biophys. 185: 4-14.

Weisenberg RC, Deery WJ, Dickinson PJ (1976) Tubulin-Nucleotide Interactions during the Polymerization and Depolymerization of Microtubules. Biochemistry 15: 4248-4254.

Williams RW (1983) Estimation of Protein Secondary Structure from Laser Raman Amide I Spectrum. J. Mol. Biol. 166: 581-603.

# Light Scattering Techniques

Martin Zulauf
Central Research Units
F. Hoffmann-La Roche & Co
CH-4002 Basel
Switzerland

## 1. Elastic light scattering (Bohren & Huffman, 1982)

The aim of light scattering experiments with solutions of macromolecules is to determine their size and shape. However, as a matter of fact, interactions among the macromolecules also affect light scattering, and the retrieval of information on size and shape may be complicated. This comes as follows. To analyze light scattering data, one has to solve a theoretical problem first: given a set of particles of known size, shape and optical properties, and distributed in the solvent in a defined way, find the field at all space points when they are illuminated by a monochromatic wave of arbitrary polarization. This problem entails the solution of Maxwell's equations with given boundary conditions. In the so-called Rayleigh-Debye-Gans approximation, which holds when the refractive index difference between particles and solvent is small compared to the solvent index and when the phase difference between a wave propagating inside the particle and one propagating outside is small in terms of the wavelength of the light, the problem reduces to the evaluation of interferences between scattering amplitudes emanating from all the volume elements in space. For spherical particles the result is easy to write down. The scattered intensity, or the scattering cross section $d\sigma$ into the solid angle $d\Omega$, divided by the scattering volume V, is

$$\frac{1}{V}\frac{d\sigma}{d\Omega} = cM\ H(\lambda,c)\ F^2(Q)\ S(Q)\ (\underline{f}_{in}\cdot\underline{\underline{\varepsilon}}\cdot\underline{f}_{out})^2 .$$

Thus, the scattered intensity is, first of all, proportional to the molecular weight of the macromolecules times their w/v concentration. $H(\lambda)$ is an experimentally accessible "contrast term" containing remnants of Maxwell's equations. $F(Q)$ is the so-called particle form factor, the Fourier transform of the particle density. (Q is the scattering vector, $Q = (4\pi/\lambda)n_{solvent}\sin\theta/2$, $\theta$ the scattering angle.) $S(Q)$, the so-called structure factor, takes into account the interferences of the scattering originating from distinct particles, hence it contains the distribution of the particles in space. It is the Fourier transform of the pair correlation function. Both in the limit of zero concentration and for $Q\to\infty$, $S(Q)\to 1$. But at finite concentrations, $S(0)>1$ when the particles attract each other, forming dynamical clusters, and $S(0)<1$ when they interact repulsively, trying to stay in quasicrystalline positions in space. Note that these effects do not vanish at zero angle. - Finally, the last term above describes depolarization, expressed by the tensor $\underline{\underline{\varepsilon}}$ incorporating optical properties of the molecules and projected on the incoming and outgoing polarization states.

All quantities above can be evaluated explicitly for spherical
particles. Particles need not be small compared to the wavelength
of the light. If they are, however, $F^2(Q)$ and $S(Q)$ are linear
functions of $Q^2$ and c and yield values for the radius of gyration
and the second virial coefficient. The weight of the macromolecules
is then obtained from extrapolations to zero angle and zero
concentration. When the particles are nonspherical, a slightly more
complicated formula can be worked out. It contains the single
particle form factor averaged over all orientations. For
polydisperse solutions, a rigorous treatment does not exist.
Unfortunately most solutions of macromolecules are polydisperse, be
it only because of the presence of large aggregates formed by
"damaged" particles or by dust in the solvent. Since these have
high molecular weights, they affect scattering even at very low
concentrations. Without fractionation the problem of polydispersity
cannot be handled in elastic light scattering, and the parameters
retrieved are averages (the weight, e.g., is the weight averaged
weight!).

## 2. Quasielastic light scattering (Berne & Pecora, 1976)

In this technique, properties of the structure factor $S(Q)$ are
exploited. When the light scattered from a solution of
macromolecules through a small aperture is recorded as a function
of time, one observes stochastic fluctuations of the intensity.
These fluctuations originate from the Brownian motion of the
particles, causing a ceaseless change in the interference pattern
between them. The speed of the fluctuation is related to the
particles' diffusion coefficient D. Since D depends only on their
size, not their weight, one can estimate this size by calculating
the hydrodynamic radius $R=kT/(6\pi\eta D)$ ($\eta$ is the solvent viscosity).
While elastic light scattering can measure radii of gyration only
down to 60-80nm, hydrodynamic radii as small as 1-2nm may be
obtained.

The practical determination of diffusion constants is possible by
autocorrelation of the fluctuating light intensity $I(t)$ and
performed by a correlator. Here, theory can cope with
polydispersity. If the solution contains different species of
particles with weights $M_i$, concentrations $c_i$ and diffusion
coefficients $D_i$, then the observable second order correlation
function is

$$g_2(\gamma) = \langle I(t)I(t+\gamma)\rangle/\langle I(t)\rangle$$

$$= 1 + B[\Sigma\alpha_i\exp(-D_iQ^2\gamma)]^2, \quad \alpha_i = c_iM_i/\Sigma c_iM_i.$$

(B is an instrumental constant.) There are various ways to analyze
measured correlation functions on the basis of the formula above.
In one (the moment analysis), data are fitted to a single
exponential with polynomial corrections; it yields an averaged
diffusion coefficient, the z-average. In another method, data are
fitted by nonlinear regression to two or three exponentials; it is
notoriously difficult to fit more exponentials without constraints.
In a third method, the computer is given a set of up to 30 $D_i$ test
values and evaluates the "amplitudes" of the corresponding
exponentials; this methods needs "regularization", but yields in
principle whole distributions.

The theory of dynamics of interacting particles has been developed in approximation, hydrodynamic drag corrections being the stumbling block. S(Q) determines the essence:

$$D_{apparent} \approx D_{true}/S(0).$$

## 3. Practice

The typical problems encountered by the light scattering practitioner are of the following kind. For a given protein solution it must be established whether the protein occurs as monomers, dimers or higher oligomers. Quasielastic light scattering gives a first impression of the polydispersity of the solution. After having determined the hydrodynamic radius of the most prominent species (usually the smallest), one can calculate from that radius what the weight is if the particles were globular, using the relation

$$(4\pi/3)R^3 = M\bar{v}(1+h)/N_{av},$$

where $\bar{v}$ is the specific volume ($0.73 cm^3/g$), h the hydration (usually $h \approx 0.3$) and $N_{av}$ Avogadro's number. If the weight is that of the monomer, then the solution contains these monomers and they are globular. If the weight is larger than that of the monomer, then we have either oligomers or the monomers are nonspherical. Intensity measurements from elastic light scattering, possibly corrected according to the observed distribution in quasielastic scattering, provide a determination of the weight. If we have oligomers, the hydrodynamic radius tells us whether they are globular or not. If not, we may use one of the many formula that allow calculation of D for nonspherical shape (e.g. ellipsoids of revolution). The parameters of these models are then adjusted such as to give the observed diffusion constant and the observed weight.

Sometimes it happens that the hydrodynamic radius is smaller than that expected for a monomer. To my experience this happens when the solvent contains no counterions such that the proteins develop strong Coulomb repulsions. In this case also the weight determined from elastic scattering is smaller than expected. By varying the protein concentration and by adding salt, this case can easily be diagnosed.

In conclusion, the combination of elastic and quasielastic light scattering provides a useful tool to investigate size, shape and interaction of macromolecules in solution. The concepts outlined above will be illustrated by results obtained with micelles.

Berne BJ, Pecora R (1976) Dynamic Light Scattering. John Wiley & Sons, New York London Sidney Toronto

Bohren CF, Huffman DR (1983) Absorption and Scattering of Light by Small Particles. John Wiley & Sons, New York Chichester Brisbane Toronto Singapore

# Chain Dynamics, Transport and Structural Properties of Actin Networks: A Quasielastic Light Scattering and Microfluorescence Study

C. F. Schmidt, H. E. Gaub, G. Isenberg and E. Sackmann,

Physics Department - Technical University München, Biophysics Group,

D - 8046 Garching - München, FRG

The role of actin filaments in the control of viscoelastic behaviour and motility of cells is based on two outstanding properties of the protein: (1) the fast assembly and disassembly kinetics of the filaments owing to the dissipative (ATP-consuming) nature of the polymerization mechanism and the regulation of the network structure by a variety of control proteins (Pollard & Cooper 1986) and (2) the flexibility of the actin filaments which allows a high degree of dynamics under thermal excitation.

On the other hand, actin gels exhibit typical features of conventional macromolecular solutions on a mesoscopic scale (with a coil radius of some 10 μm or more). They thus have a fundamental significance as a model system for the study of polymer structure and dynamics. This report is concerned principally with the latter aspect. The dynamics of networks of fully polymerized actin was studied by quasielastic light scattering. Structural and transport properties of the networks were studied by microfluorescence techniques.

## DYNAMIC LIGHT SCATTERING (QELS) STUDIES OF INTERNAL CHAIN DYNAMICS – ACTIN AS A ROUSE-ZIMM CHAIN ON A MESOSCOPIC SCALE

The internal motion of the actin filaments has been studied by dynamic light scattering (for details see Schmidt 1988). The scattering vector q (related to the scattering angle $\theta$, the wavelength of light $\lambda$ and the index of refraction n by: $q = 4\pi\,n\,\sin(\theta/2)/\lambda$) ranges from $5.6*10^4$ cm$^{-1}$ at a scattering angle of 20° to $3.1*10^5$ cm$^{-1}$ at a scattering angle of 150°. Its inverse, $2\pi/q$, is smaller than the average distance between the filaments, or the average mesh size of the network as seen in Figs. 1 and 4, and very small compared to the radius of gyration $R_G$ of a whole filament (see below). Thus the decay of the intensity autocorrelation function ($I_2(q,t)$) of the scattered light is determined entirely by internal modes of motion of the filaments. Essential results are presented in Fig. 2. On the left hand side, the normalized dynamic structure function, $K(q,t) = g(q,t)/g(q,0)$, calculated from $I_2(q,t)$, of actin networks at various actin concentrations is shown. The initial decay rate of $K(q,t)$, in contrast to the long time tail, shows no systematic dependence on the protein concentration from 0.4 to 0.1 mg/ml. This suggests strongly that the dynamic structure factor is dominated by the internal dynamics of a single chain rather than by concentration fluctuations involving different chains. At still lower actin concentrations (0.02 mg/ml) $K(q,t)$ decays faster, because, approaching the critical monomer concentration, the measured dynamics become dominated by monomer diffusion. On the right hand side of Fig. 2, the initial decay rate of the normalized dynamic structure factor $K(q,t)$: $\Gamma_k^{(0)} = d(\ln K(q,t))/dt\,|_{t=0}$ is shown as a function of the scattering vector q.

**5000 Å**
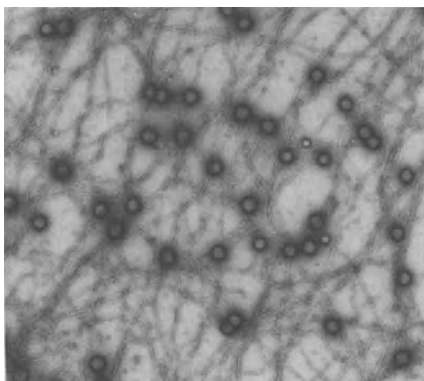


**Fig. 1:** Electron micrograph of an actin network. The actin concentration was 0.15 mg/ml. The round spots are latex beads of 0.1 μm diameter (cf. Fig. 4).
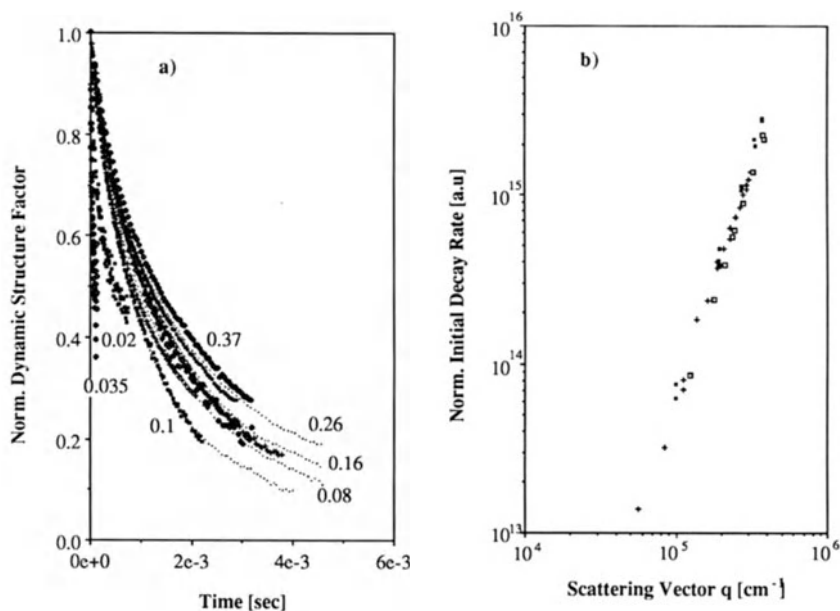


**Fig. 2:** a) Time dependence of the normalized dynamic structure factor $K(q,t) = g(q,t)/g(q,0)$ of actin networks with various actin concentrations, indicated in mg/ml in the figure.
b) +: Dependence of the initial decay rate $\Gamma_k^{(0)} = d(\ln K(q,t))/dt \big|_{t=0}$ of the dynamic structure factor, normalized by temperature and viscosity, $(\Gamma_k^{(0)} \eta_S/k_B T)$, on the scattering vector q for a concentration of 0.16 mg of actin per ml solution.
For comparison data obtained with polystyrene in organic solvent by Nemoto et al.(1984) (■) and by Adam and Delsanti (1977) (□) are shown in the plot.

It is apparent from the plot that $\Gamma_k^{(0)}$ obeys a power law of the form: $\Gamma_k^{(0)} = C(T,\eta) \, q^{2.76}$. This behavior is in good agreement with the result of quasielastic light scattering measurements using synthetic macromolecules in good solvents.

This permits the following conclusions: 1) QELS data from actin solutions can be described by the universal law of Dubois-Violette and DeGennes (1967). This law is based on the Rouse-Zimm model of polymer dynamics where the elasticity is described in terms of an elastic spring model and the damping of the excitations is governed by the hydrodynamic interaction between segments of the chain (actin monomers) (Schmidt, 1988).

2) On the nearly macroscopic scale of their overall size (radius of gyration of some 100 µm) actin filaments must be considered as Gaussian-coils.

Actin gels can thus be treated as greatly scaled up macromolecular networks.

## Translational Diffusion of Actin Filaments

The translational diffusion of actin chains in semidilute solutions was studied by fluorescence recovery after photobleaching (FRAP). An argon laser beam is focussed at the center of a 1 mm deep layer of polymerized actin in a sample chamber on a quartz slide. To follow the course of polymerization, the actin solution (containing 5% of NBD labeled actin) with freshly added polymerization buffer is pumped into the chamber just prior to the first measurement. Fig. 3a shows typical fluorescence recovery curves taken during the polymerization. These curves show a fast and a very slow component. The former decreases in amplitude with ongoing polymerization while the latter increases. Comparing the halftime of recovery of the fast component with that of monomeric actin, the fast component can be shown to be due to unpolymerized actin, the amount of which approaches the critical monomer concentration. The relative amplitude of the monomer contribution to the fluorescence intensity decreases in a complementary fashion to the increase of the amount of polymerized actin. The latter can be independently calculated from the rise in the absolute (prebleach) fluorescence intensity which is due to the increase in quantum yield of the fluorophores upon polymerization.(Detmers et al. 1981) The diffusion coefficients of monomeric ($D_G$) and of polymeric ($D_F$) actin were obtained from the halftimes ($t_{1/2}$) of recovery of the fast and slow components according to $D = 0{,}22\, r^2/t_{1/2}$ (Axelrod 1976) where r is the radius of the bleached cylindrical volume (here: $r = 11$ µm). From the very slow fluorescence recovery of the polymer component, $D_F$ was estimated as: $D_F < 1*10^{-10}$ cm$^2$/sec.

The fact that the recovery curves reflect only two populations with widely different mobilities is in agreement with current models of actin polymerization according to which the chains grow very fast to very long filaments once nuclei of a critical size have formed. For QELS-studies actin gels can therefore be considered as monodisperse systems.

This is further illustrated by contrast with the time course of mobilities during polymerization of actin in the presence of cytochalasin B (CB). The recovery curves in Fig. 3c show a continuous distribution of diffusion coefficients during the initial state of polymerization, changing to a distinctly bimodal distribution once a steady state is reached. The slow component which is then discernible, however, recovers much faster (100 % recovery after 30 minutes) than the one seen without CB (cf. Fig. 3c). The recovery curves in the steady state with CB can be approximately analyzed in terms of two exponentials giving an average diffusion coefficient of $D_F^{(CB)} = 1{,}35 * 10^{-9}$ cm$^2$/sec for the slow component. By assuming that the oligomers of actin behave as rigid rods of length L, this

length can be estimated from the diffusion coefficient according to: $D = k_B T \ln(L/b)/(2\pi \eta_S L)$ ($\eta_S$ = viscosity of solvent, b = rod diameter; Doi and Edwards 1987). For a filament cross section of 7 nm an average length of L = 41$\mu$m is obtained for actin oligomers stabilized by 16 mol% of cytochalasin.
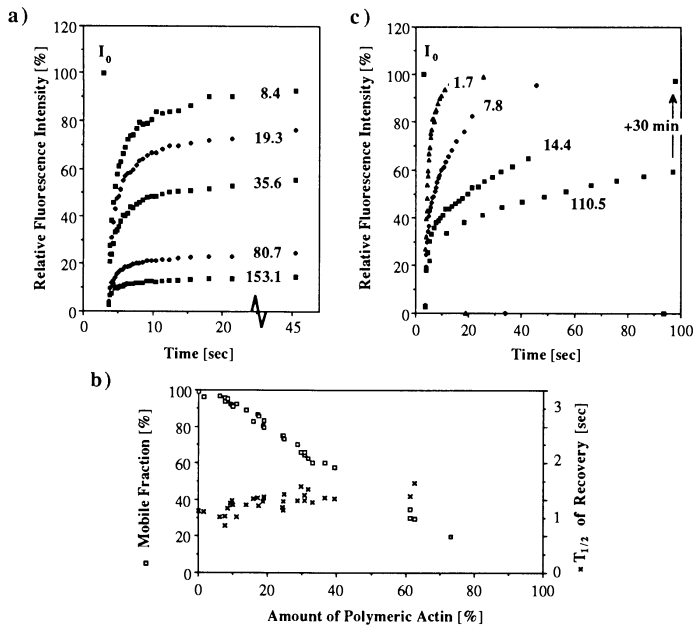


**Fig. 3:** **a)** Recovery of fluorescence intensity F(t) after photobleaching during the polymerization of 1 mg/ml actin, including 5% NBD labeled actin, with buffer containing 1.5 mM Mg$^{2+}$. The numbers at the curves give the time after the start of the polymerization in minutes.
**b)** □, scale on the left hand side: relative amount, $F_G$, of the fast recovering component, assumed to be monomeric actin, plotted against relative amount of polymeric actin, determined from the increase of the absolute prebleach intensity due to the increase of the quantum yield of the fluorophores upon polymerization.
✗, scale on the right hand side: halftime of recovery of the fast component.
**c)** Fluorescence recovery curves during polymerization of actin in the presence of 16 mol% cytochalasin B (with respect to actin), the numbers at the curves give the time after the start of the polymerization in minutes.

## DETERMINATION OF MESH SIZE FROM PARTICLE DIFFUSION IN ACTIN NETWORKS

The average mesh size of actin gels has been determined from diffusion measurements of fluorescent latex spheres of various diameters in actin solutions by the application of scaling laws. The diffusion coefficients D(c) were measured first by the conventional photobleaching technique and second via direct measurement of the mean square displacement of the latex spheres using a fast digital image processing system. From the data in Fig. 4a it is apparent that the latex sphere diffusion coefficient shows an exponential dependence on the actin concentration of the form:

$$D = D_0 \exp(\text{const} * c). \qquad (1)$$

$D_0$ is the diffusion coefficient obtained by extrapolation to zero concentration. Such a power law was in fact predicted by DeGennes et al. (quoted by Langevin & Rondelez 1978) for a polymer network formed from non-crosslinked filaments .These authors assume that the ratio of diffusion coefficients $D/D_0$ for a meshwork of mesh size $\xi$ is of the form:

$$D/D_0 = const' + exp -\{(R/\xi)^\delta\}. \qquad (2)$$

The exponent $\delta$ is expected to be $\delta = 2.5$ for cross linked and $\delta = 2.0$ for non cross-linked chains. This law is shown to be verified from a plot of $\ln\{\ln(D_o/D)\}$ versus the logarithm of the latex sphere radius (Fig. 4b) with $\delta \approx 2$. Another scaling law (De Gennes et al., 1976) predicts that the mesh size $\xi$ of a network of nearly rigid rods varies with the rod concentration c as: $\xi \propto c^{-1/2}$. Therefore:

$$D/D_o = exp (const'' R^2 c). \qquad (3)$$

Data (Fig.4a) are in agreement with this formula. The mesh size is thus determined from (2)(Fig.4c).
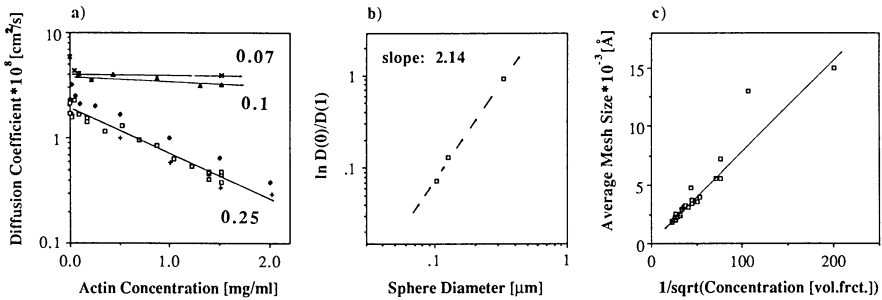


**Fig. 4:** a) Logarithmic plot of the diffusion coefficient of latex spheres of various diameters as a function of actin concentration. Sphere diameters in μm are given in the plot.
b) Plot of $\ln\{\ln[D(0)/D(1)]\}$ versus logarithm of Radius, R, of the spheres, where D(0) is the extrapolated diffusion coefficient for zero actin concentration and D(1) the interpolated value at c = 1 mg actin per ml of solution.

c) Mesh size $\xi$ of actin networks, determined from the relative decrease of the diffusion coefficient with the actin concentration.

## REFERENCES

Adam M, Delsanti M (1977) Dynamical Properties of Polymer Solutions in Good Solvent by Rayleigh Scattering Experiments. Macromolecules 10:1229-1237

De Gennes PG, Pincus P, Velasco RM (1976) Remarks on polyelectrolyte conformation. J Phys (Paris) 37:1461-1473

Detmers P, Weber A, Elzinga M, Stephens RE (1981) 7-Chloro-4-nitrobenzeno-2-oxa-1,3-diazole Actin As a Probe for Actin Polymerization. J Biol Chem 256:99-105

Doi M, Edwards SF (1986) The theory of polymer dynamics. Oxford University Press, Oxford

Dubois-Violette E, De Gennes PG (1967) Quasielastic scattering by dilute, ideal, polymer solutions: II. Effects of hydrodynamic interaction. Physics (Long Island City, N.Y.) 3:181-198

Langevin D, Rondelez F (1978) Sedimentation of large colloidal particles through semidilute solutions. Polymer 19:875-882

Nemoto N, Makita Y, Tsunashima Y, Kurata M (1984) Dynamic Light Scattering Studies of Polymer Solutions. 3. Translational Diffusion and Internal Motion of High Molecular Weight Polystyrenes in Benzene at Infinite Dilution. Macromolecules 17:425-430

Pollard TD, Cooper JA (1986) Actin and actin-binding proteins. A critical evaluation of mechanisms and functions. Ann Rev Biochem 55:987-1035

Schmidt CF (1988) Dynamik und Struktur polymerer Aktin-Netzwerke und ihre Wechselwirkung mit Modellmembranen. Dissertation, Technische Universität München

# Polymerization of Actin on Supported Lipid Bilayers

R. Zimmermann, Ch. F. Schmidt, M. Bärmann, G. Isenberg & H.E. Gaub

Physikdepartment E22, Technische Universität München,

D-8046 Garching, Federal Republic of Germany

Membrane/protein interactions play a significant role in the regulation and organization of the cytoskeleton. As a part of this complex system, we have investigated the interaction of actin with lipid membranes on solid supports.

Using a combination of microfluorimetry and fluorescence recovery after photo-bleaching in the evanescent field of a totally internal reflected wave, we have measured the adsorption and polymerization kinetics of actin at supported lipid bilayers of various compositions and at different solid surfaces.
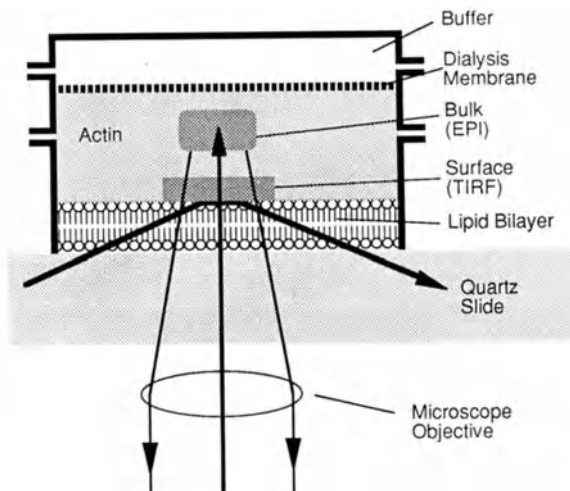


***Cartoon of the experimental set up***
*Above a certain angle an electromagnetic wave is totally internal reflected at an interface to a medium with lower refractive index but an evanescent wave penetrates some fraction of the wavelength into the medium. In our case this evanescent field is used to excite the fluorescence of labelled actin molecules exclusively at the interface which in our case is represented by the supported lipid bilayer (TIRF). Alternatively the path of the exciting laser is optically switched in order to allow the excitation of molecules in the bulk phase (EPI). This allows the direct comparison of events close to or at the membrane with those in the bulk.*
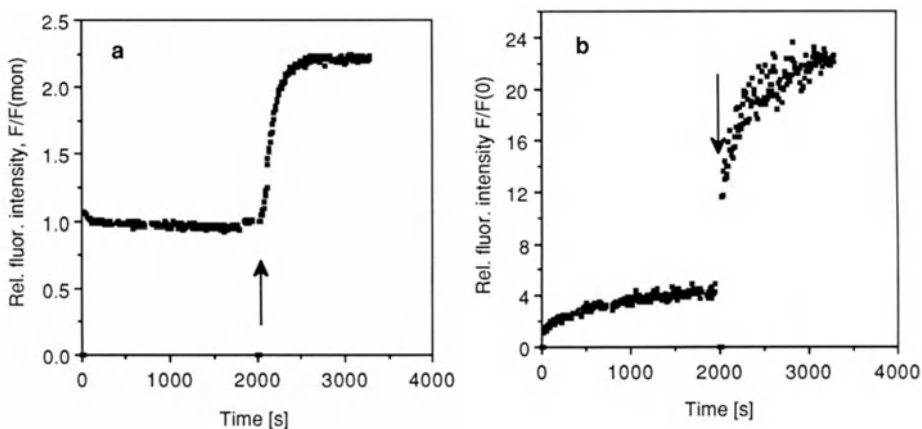
***Typical parallel time scan*** *of the bulk fluorescence (a) and the surface fluorescence intensity (b) of an actin sample (1mg/ml, 5% NBD labeled) on an argon plasma cleaned quartz slide. The arrows mark the time when Mg-ions were added to a final concentration of 2mg/ml.*

In our experiments monomeric actin did not significantly bind to either plain quartz (see fig. above) or a neutral (phosphatidyl choline) or negatively charged membrane (PC containing 50% phosphatidyl glycerol). In contrast, we found marked differences of actin/membrane interaction under conditions where actin polymerizes slowly (0.5mM Mg,<10mM PBS). In the proximity (closer than 1200 Å) of the DMPC bilayer actin polymerization, as measured by the fluorescence increase of a 5% fraction of NBD-labeled actin, was hindered with respect to the bulk phase, whereas polymerization near the DMPG containing membrane was enhanced. In the polymerized state lateral as well as on-off kinetics of actin were reduced by several orders of magnitude. By addition of severin  the polymer could be removed from the membrane. The same could be achieved by dialysis against low salt buffer for several hours. After addition (stirring) of Mg to a final concentration of 2mM  the surface fluorescence on both, DMPC and DMPG containing bilayers was approximately the same, but significantly more than expected from the polymerization-induced increase in quantum yield only.

Surface plasmon spectroscopy was employed to quantify the surface coverage on the membrane. The measured increase in surface coverage agrees well with the surface fluorescence increase, corrected for the polymerization effect. Thus it seems likely that the protein does not penetrate into the aliphatic membrane region.

The above findings suggest that the polymerization of actin in the vicinity of the membrane can be modulated by the lipid composition. Further investigations should show to what extent these mechanisms might play a role for the organization of the cytoskeleton in the proximity of cellular membranes.

# Macrophage Intracellular Motility and Its Correlation with Cell-Substrate Adhesion

Peter Gehr[*], Samuel Schuerch[***], Richard Marugg[*], Marianne Geiser[*], Vinzenz Im Hof[**]

[*]Institute of Anatomy, University of Berne, Buehlstrasse 26, CH-3000 Berne 9, Switzerland; [**]Inselspital, Department of Pneumology, University of Berne, Berne, Switzerland; [***]Department of Physiology, Faculty of Medicine, The University of Calgary, Calgary, Alberta, Canada.

## INTRODUCTION

Cell spreading and cell adhesion are influenced by the nature of the cell membrane and the structure of the cytoskeleton. The cell membrane with its surface glycopolymers, in combination with the cytoskeleton, may control interactions between the cell and its environment. Particularly the membrane-bound cytoskeleton appears to be involved in the organization of the membrane, and the formation of cell-substrate and cell-cell contacts (Traas and Ramaekers, 1986).

In the present work we demonstrate a combination of three approaches which have been applied to investigate these interrelationships: (1) cytomagnetometry to estimate cell motility, (2) interference reflection microscopy (IRM), to obtain information about the intensity of cell-substrate interaction, and (3) aqueous phase separated polymer solution of dextran and polyethylene glycol (PEG) to determine the affinity (work of adhesion) of the cell to the aqueous polymer phases.

## MATERIALS AND METHODS

### 1. Applied techniques

In <u>cytomagnetometry</u> submicrometric magnetic particles ($Fe_3O_4$) are used as probes for intracellular motility. After phagocytosis by cultured alveolar and airway macrophages, the particles are located

in phagosomes and later in secondary lysosomes which have been found
to be an integrated part of the cytoskeleton by electron microscopic
techniques. If a magnetic field is applied to such cells the
particles are magnetized and aligned; they produce a cellular,
remanent magnetic field. Upon removal of the magnetizing field a
decay of the remanent field can be observed. This is called
relaxation which is caused by the particles that are misaligned by
some intracellular forces, exerted on them (Fig. 1). Evidence has
been obtained that these forces are generated by filamentous elements
of the cytoskeleton. Therefore the rate of relaxation may be an
estimate of cytoskeletal filament activity (Gehr et al., 1983, 1985).
Relaxation is not caused by passive processes such as Brownian
movement and elastic recoil (Valberg and Albertini, 1985; Nemoto et
al., 1987).
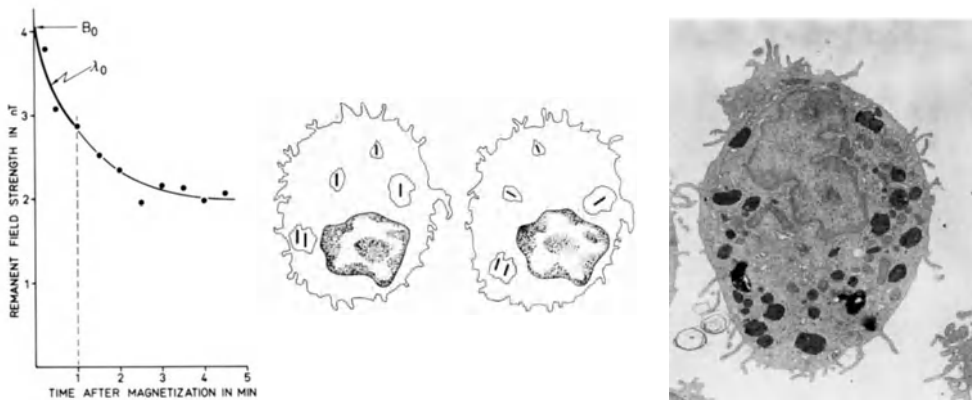


**Figure 1.** a) Relaxation curve. Points are magnetometric measurements
of individual cell culture dishes; $\lambda_0$ is the initial relaxation rate.
b) Schematic representation of alignment and misalignment of
phagosomes/secondary lysosomes in a cell. c) Transmission electron
micrograph of alveolar macrophage with secondary lysosomes containing
$Fe_3O_4$ particles (arrow).

Interference reflection microscopy (IRM) produces a cell-substratum
interference image of cultured cells which are illuminated by a cone
of monochromatic light of solid angle 0-100 degrees, corresponding to
an illuminating numerical aperture of 0-1.2. Adhesive zones of
macrophages appear as black-grey areas (Fig. 2) (Gingell and Todd,
1979; Verschueren, 1985). The intensity of adhesion of the cell
culture has been established by determining the fraction of cells
with such black-grey areas.
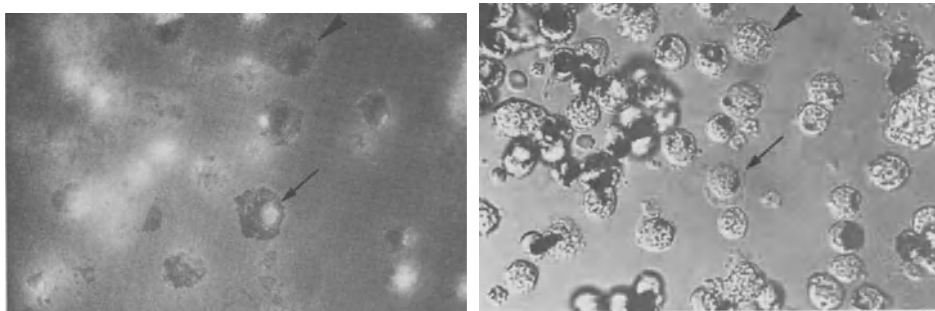
**Figure 2.** a) Adhesion of the macrophages on the bottom of the culture dish. Arrows and arrow heads, respectively, show the same cell in: a) IRM (white spots are $Fe_3O_4$), b) DIC (black spots are $Fe_3O_4$). From Gehr et al., 1988.

Further, we we have used <u>aqueous phase separated polymer solutions of dextran and polyethylene glycol (PEG)</u> to determine the affinity, i.e the work of adhesion of the cultured macrophages` surface glycopolymers to these dextran and PEG phases by measuring the contact angle $\theta$ of the dextran phase droplet spread on the cell surface (Fig. 3) (McIver and Schuerch. 1987).
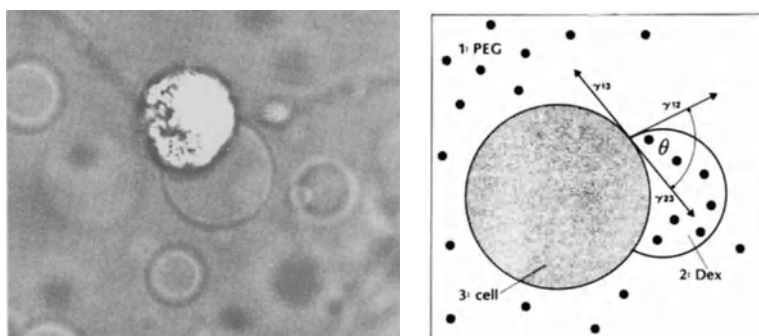


**Figure 3.** Dextran droplet spread on a macrophage in PEG. a) DIC picture; b) Principle of measurement of contact angle. $\gamma$ = free energies of the interfaces between the phases indicated. From Gehr et al., 1988.

## 2. Experiments

Alveolar and airway macrophages were collected from hamster lungs by repeated pulmonary lavage. The cells were centrifuged and resuspended

in culture medium ($10^6$ cells/ml Dulbecco's MEM, 10% newborn calf
serum, gentamycin, mycostatin) and incubated at $37^{\circ}$C for half an hour
in specially prepared culture dishes with glass coverslips at the
bottom. Non-adherent cells were rinsed off and the remaining
monolayer culture (approximately 2000-3000 cells per $mm^2$) was
reincubated with magnetic ($Fe_3O_4$) particles for 1 hour.

Afterwards the dish, maintained at $37^{\circ}$C, was placed in a magnetic
field of .5-1 T for 1-2 msec. The decaying remanent field was then
measured with a fluxgate magnetometer probe (Magnetoscop F 1.067,
Foerster Instruments) and the initial relaxation rate, $\lambda_0$ , i.e. the
rate of decay during the first minute after magnetization was
determined.

Thereafter the adhesiveness of the cells was investigated with a
Zeiss IM 35 inverted microscope equipped for interference reflection
microscopy (IRM) by determining the fraction of cells with black-grey
areas (Fig. 2).

Additionally, the surface affinity of the cells was estimated, as
previously described (Schürch et al., 1981), except, the contact
angles ($\theta$) of the dextran-phase droplets were determined on single
cells, using the differential interference (DIC) attachment of the
microscope (Fig. 3).

Cell adhesion and intracellular motility are dependant on the surface
properties of the substrate (Gehr et al., 1988). A variety of
surfaces with widely differing surface properties have been prepared:
Clean glass (G); siliconized glass (S); siliconized glass exposed for
30 min. at $22^{\circ}$C to a 1% L-alpha phosphatidylcholine (from Soybean)
solution and 1% Pluronic F68, 1:1 by volume, both agents suspended in
water (PC); glass coated with 0.01% poly-L-lysin for 1 min (L).

Some macrophages, grown on different surfaces were stimulated by
Zymosan, a particulate stimulus and cytochalasin B (cyt. B), a
soluble stimulus, before the three investigations have been
performed. Zymosan was prepared as previously described and used at a
concentration of $2mg/10^7$ cells (Paterson et al., 1985). Cyt. B was
used at a concentration of 20 $\mu$M (Gehr et al., 1985).

RESULTS

The substrate surface effect on the magnetic field relaxation and the contact angles are summarized in Table 1.

**Table 1.** Magnetic field relaxation, cell-substrate adhesion and cell affinity to 2-phase polymers. Numbers are means $\pm 1$ S.E., (n) = sample size.

| Surfaces | $\lambda 0$ $[-10^{-4} \ sec^{-1}]$ | Cells IRM areas % | $\theta$ Degrees |
|---|---|---|---|
| L | $34.0 \pm 2.2$ (11) | $67.3 \pm 7.1$ (7) | $87.6 \pm 2.6$ (12) |
| G | $37.8 \pm 2.2$ (17) | $48.0 \pm 5.9$ (7) | $91.8 \pm 1.7$ (25) |
| S | $37.2 \pm 2.7$ (10) | $4.6 \pm 1.3$ (5) | $92.0 \pm 1.6$ (12) |
| PC | $44.7 \pm 2.4$ (8) | approx. 2 | $90.3 \pm 2.0$ (11) |
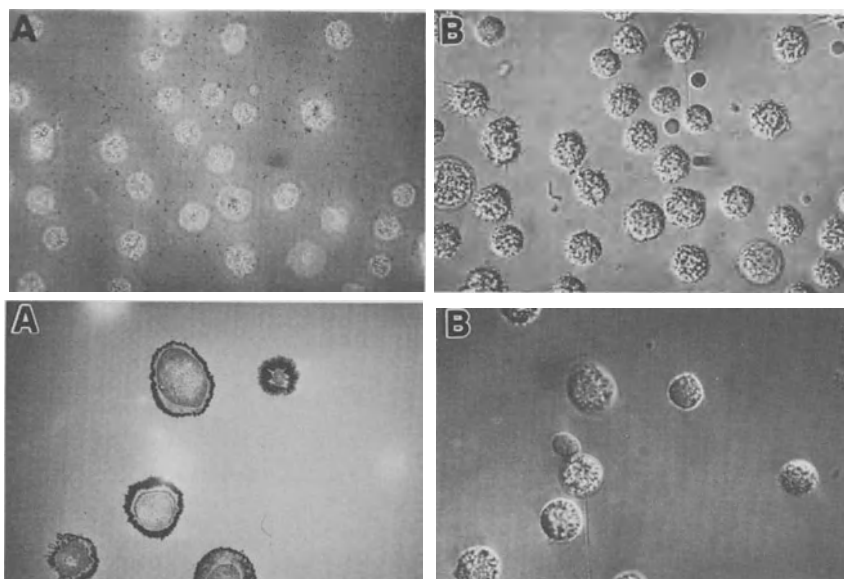


**Figure 4.** Substrate surface effect. Top: Siliconized glass exposed to L-alpha phosphatidylcholine and Pluronic F68; a) IRM picture, no reflection areas; b) DIC picture. Bottom: Clean glass; a) IRM picture, many reflection areas; b) DIC picture.

Only the PC substrate produced a significantly higher $\lambda_0$. The
fraction of macrophages with IRM areas was highest for the L surface,
and lowest for the PC substrate. There was no surface effect on the
cell's affinity as determined by the contact angles.

Table 2 shows a decrease by 50% and more in the relaxation rate,
depending on the nature of the substrate, due to Zymosan stimulation
of the cells. This change is accompanied by a substantial change of $\theta$
from about $92^O$ to $68^O$. For cyt. B the change in $\lambda_0$ was less
pronounced but still significant. However, $\theta$ was the same, i.e. there
was no change in the surface affinity of the macrophages to the
polymer phases.

**Table 2.** Influence of stimulus. Numbers are measn $\pm$ 1 S.E., (n) =
sample size; * not significantly different.

| | $\lambda_0$ $[-10^{-4} sec^{-1}]$ | | Cells IRM areas % | $\theta$ Degrees |
|---|---|---|---|---|
| Stimulus | S u r f a c e s | | | |
| | G | S | G | G, S |
| Control | 37.8 ± 2.2 (17) | 37.2 ± 2.7 (10) | 37.4 ± 6.8 (10) | 91.8 ± 1.7 (25) |
| Zymosan | no relaxation (5) | 17.5 ± 3 9 (4) | 57.0 ± 10.2 (4) | 68.3 ± 1.4 (18) |
| Cyt. B | 30.6 ± 2.3 (10) | —— | 31.8 ± 4.6 (6)* | 87.9 ± 1.8 (22)* |

There was no relaxation following stimulation by Zymosan of
macrophages adherent to a clean glass substrate. These cells on glass
demonstrated a considerable greater number of IRM areas than control
or cyt. B treated macrophages.

Cytochalasin, on the other hand had no measurable effect on the cell
surface affinity in the PEG-Dextran system, neither was the surface
affinity affected by the nature of the substrate e.g. glass or
siliconized glass.

DISCUSSION


The relaxation rate, $\lambda_0$, of the magnetic field was the same for all
surfaces except for PC, where a phosphatidyl monolayer was adsorbed
onto siliconized glass in association with Pluronic F68 (Table 1).
The relaxation rate, $\lambda_0$, was highest for this surface which was,
however, the least adhesive. This high $\lambda_0$ was associated with the
smallest fraction of interference reflection areas (Fig. 4), although
the cells do adhere to the surface. A minimal adherence is necessary
for the measurement of the relaxation of the magnetic field.

Pluronic F68 is a non-ionic block polymer surfactant that may
modulate cell adhesion by limiting protein adsorption to the surface
from the cell culture medium. Non-ionic surfactants have been shown
to diminish adsorption of bovine serum albumin to liquid-liquid
interfaces (Schürch et al., 1981).

Zymosan has been widely used as a particulate stimulus (Paterson et
al. 1985). In the present study we have found that $\lambda_0$ of alveolar and
airway macrophages stimulated with Zymosan was substantially
decreased as compared to non-stimulated cells (Table 2). This effect,
however, was strongly dependent on the nature of the substrate. On
clean glass, Zymosan stimulated macrophages showed a very high ratio
of IRM areas but there was no measurable magnetic field relaxation.
The considerable extend of the macrophages` spreading accompanied by
the thinning of the cells may interfere with the phagosomal motility,
the movement that is likely reponsible for the field relaxation (Fig.
1) (Gehr et al., 1985).

A less adhesive surface such as siliconized glass had to be chosen to
study a change in cell motility following Zymosan stimulation. The
change in $\lambda_0$ following Zymosan stimulation was accompanied by a
considerable change in the macrophage surface affinity for the
aqueous polymer phases as shown by a change in $\theta$ and thus in the work
of adhesion (Table 2). Zymosan, therefore, affects cell motility as
well as the cell surface glycopolymers. It is, furthermore,
speculated that Zymosan may promote molecular transport from the
interior of the cell to its surface (McIver and Schuerch, 1987).

242

From these findings it can be concluded that, on the one hand, the
intracellular motility for non-stimulated cells, as shown by $\lambda_0$, is
essentially independent of the substrate. This has been demonstrated
with the experiments with widely different surfaces such as
siliconized glass, a relatively non-adhesive surface, or glass coated
with poly-L-lysine, a highly adhesive surface. On the other hand,
stimulated cells may be restricted in their motility if the substrate
causes intensive cell spreading.

These experiments demonstrate that there is an interrelationship
between the cytoskeleton and the plasma membrane during cell-
substrate interaction, and that there exists a correlation between
cell motility and cell-substrate interaction.

REFERENCES

Gehr P, Schuerch S, Geiser M, Im Hof V, Furter Ch (1988) Magnetic
    field relaxation and its correlation with cell-substrate
    adhesive interactions. Proc. 6th Int. Conf. Biomag. Tokyo, Aug.
    27-30 1987 (in press)
Gehr P, Brain JD, Nemoto I, Bloom SB (1985) Organelle movements of
    alveolar macrophages studied by cytomagnetometry. In: Weinberg
    H, Stroink G, Katila T (eds) Biomagnetism: Applications and
    theory. Pergamon Press, New York, p 433-437
Gehr P, Brain JD, Nemoto I, Bloom SB, Valberg PA (1983) Magnetic
    particles in the liver: A probe for intracellular movement.
    Nature 302:336-338
Gingell D, Todd I (1979) Interference reflection microscopy. A
    quantitative theory for image interpretation and its application
    to cell-substrate separation measurement. Biophys J 26:507-526
McIver DJL, Schuerch S (1987) Polymer mixing and the thermodynamics
    of cell adhesion at fluid interfaces. J Adhesion 22:253-289
Nemoto I, Toyotama H, Brain JD, Gehr P (1988) Behaviour of
    ferrimagnetic particles in hamster pulmonary macrophages in
    vitro; magnetometric estimation of cell motility. Japan J Biomed
    Eng (submitted)

Paterson NAM, McIver DJL, Schuerch, S (1985) Zymosan enhances
     leukotriene $D_4$ metabolism by porcine alveolar macrophages.
     Immunology 56:153-159
Schuerch S, Gerson DF, McIver DJL (1981) Determination of cell-
     mediated interfacial tensions from contact angles in aqueous
     polymer systems. Biochim Biophys Acta 640:557-571
Traas J, Ramaekers F (1986) The membrane-associated cytoskeleton in
     cultured lens cells. Electron microscopical visualization in
     cleaved whole-mount preparations and platinum replicas. Exp Eyr
     Res 43:519-528
Valberg PA, Albertini DF (1985) Cytoplasmic motions, rheology, and
     structure probed by a novel magnetic particle method. J Cell
     Biol 101:130-140
Verschueren H (1985) Interference reflection microscopy in cell
     biology: methodology and applications.  J Cell Sci 75:279-301

# Adhesion of Pulmonary Macrophages to Langmuir-Blodgett Films, Investigated by Interference Reflection Microscopy

S. Schürch
Department of Medical Physiology
University of Calgary
3330 Hospital Drive N.W.
Calgary, Alberta, Canada T2N 4N1

One major part of macrophage function is to clear foreign particles
from the lung surface, a process that involves particle-cell adhesion
followed by particle phagocytosis.  Since adhesion is a crucial step
preceding phagocytosis, we have been developing methods for quanti-
tating macrophage adherence to various substrates using interference
reflection microscopy (IRM) in combination with computerized image
analysis.  The image visible in IRM is produced by reflections on
optical boundary faces and their interferences.  Therefore, the
intensity of monochromatic light reflected at the cell's underface
contains information about the closeness of contact between the cell
and the substrate (Verschueren, 1985).  We studied cell adhesion and
the extent of cell spreading continuously for up to 40 minutes on
various substrates in culture dishes at $37^{\circ}$ on a heating stage of a
Zeiss IM 35 microscope.  The substrates were prepared by coating the
glass coverslips with Langmuir-Blodgett bilayers of dipalmitoylphos-
phatidylcholine (DPPC) from air-water monolayers held at differing
surface tensions.  Some of the bilayers were further treated with
polymeric surfactant Pluronic F68 by allowing this substance to be
adsorbed onto the bilayer-water interface.  IRM images are usually
evaluated in a semi-quantitative way according to Izzard and Lochner
(1976), who differentiate between "close contacts" and "focal con-
tacts".  To the close contacts they apply a cell-substrate distance
of 30-40nm and to the focal contacts a distance of 10-15nm.  Close
contacts appear dark grey over relatively large areas of the cell;
focal contacts are small, almost black spots and appear to be asso-
ciated with the distal end of actin filament bundles.  We chose,
relatively to the background, the grey levels that include more
than 95% of typical close and focal adhesion areas (see Table 1).
The most adhesive surface investigated proved to be a DPPC bilayer
that was deposited at a monolayer surface tension of approximately

F. Green, M. Schoel and P. Gehr, Department of Pathology and
Medicine, University of Calgary and Department of Anatomy,
University of Berne, 3000 Berne, Switzerland

50 mN/m. The least adhesive surface was the DPPC bilayer in association with Pluronic F68.

|  | Glass | Pluronic F68 on glass | DPPC 48 mN/m | DPPC 28 mN/m | DPPC 48 mN/m + Pluronic F68 |
|---|---|---|---|---|---|
| Adhesion Ratio (AR) (Mean ± SEM) x $10^{-3}$ | 65±34 (6) | 1.5±0.9 (8) | 198±32 (8) | 94±24 (9) | 0.3±0.1 (8) |

Table 1. Macrophage adhesion intensities after 14 min. of incubation on various substrates. The adhesion ratios are the grey levels in numbers of pixels equal to or greater than eight standard deviations, of the mean grey level of the background divided by the total IRM area of the cell. In parentheses: number of cells investigated. Note: The most adhesive surface is the DPPC bilayer deposited at a monolayer surface tension of 48 mN/m. The more compact bilayer, formed at a monolayer surface tension of 28 mN/m, has an AR of about 50% of that formed at 48 mN/m. The least adhesive surface is the bilayer (48 mN/m) in association with an adsorbed coating of Pluronic F68, while Pluronic adsorbed to plain glass is more adhesive but still considerably less than plain glass or the DPPC bilayers.
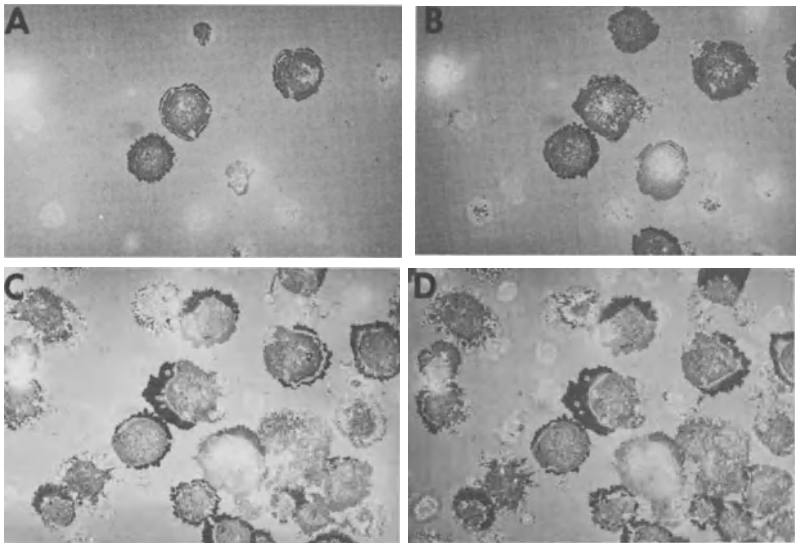


Fig. 1   IRM macrophage adhesion images at 3(A), 6(B), 12(C) and 16(D) minutes after placing the cells on a glass slide coated with a DPPC bilayer formed at a monolayer surface tension of 48 mN/m. Note: Adhesion appears to increase with time as can be seen from the darker images as well as from the increased number of cells that adhere to the surface.

Izzard CS, Lochner LR (1976)  Cell-to-substrate contacts in living fibroblasts: an interference reflection study with an evaluation of the technique.  J Cell Sci 21:129-159
Verschueren H (1985)  Interference reflection microscopy in cell biology: methodology and applications.  J Cell Sci 75:279-301

# SECTION V
## Thermodynamics and Kinetics of Assembly

# Microtubule Dynamics: Experimental Evidence and Numerical Modelling

P.M.Bayley, V.Gal, P.Karecla, S.R.Martin, M.J.Schilstra and
Y.Engelborghs[+].


National Institute for Medical Research, Mill Hill, London NW7 1AA
and [+]Laboratory of Chemical and Biological Dynamics,
University of Leuven, Celestijnenlaan, B-3030 Leuven, Belgium.

The involvement of GTP hydrolysis in microtubule assembly
introduces a number of characteristic observable properties
in the steady-state system, namely a time-dependent length
redistribution process, a high level of steady-state GTP
hydrolysis, unusually fast tubulin exchange kinetics, and,
most significantly, the coexistence of interconverting
growing and shrinking microtubules within the population.
We evaluate and model the implications of these dynamic
properties and we present a "Lateral Cap" model in which
co-operative interactions in the microtubule end account
for observed dynamic properties under both steady-state and
extreme non-steady state conditions. We examine the ways in
which factors such as metal ions, drugs, and microtubule
associated proteins can exert different degrees of control
of the behaviour of dynamic microtubule populations
appropriate for regulation of their biological function.

Tubulin, an $\alpha$-$\beta$ heterodimeric protein of molecular weight 100,000,
forms the major component of the microtubule system present in most
eukaryotic cells. The protein, which can be obtained in pure form
by conventional separation techniques can be assembled in vitro to
form microtubules which are effectively identical with those found
in vivo. This therefore comprises an important biological self-
assembly system, which has attracted widespread interest and
intensive experimentation, ([1], review).

The involvement and hydrolysis of GTP in microtubule assembly means
that the microtubule is strictly not a true equilibrium polymer,
although it may have this appearance since assembly is generally
performed in the presence of excess GTP or in the presence of an

enzymic GTP regenerating system. The hydrolysis to tubulin-GDP introduces a fundamental asymmetry in the process; it is basically tubulin-GTP which elongates, but tubulin-GDP which dissociates. Tubulin-GDP is incapable of assembly under normal solution conditions; i.e. $[T-GDP]_{ss}$ >> $[T-GTP]_{ss}$; (ss = steady-state). The paradox of how the (pseudo)-equilibrium polymer is maintained has been resolved by various models in which terminal residues of T-GTP confer stability, unless dissociating conditions cause their removal, when the polymer disassembles by loss of T-GDP, [see 2].

This capacity for rapid disassembly was formulated as microtubule "dynamic instability", [3], in observations of changes in length distribution in steady-state microtubule populations following limited dilution. The mean length increased whereas the value of **m** decreased. From this came the postulate of the co-existence (at constant polymer mass) of both growing and shrinking microtubules, with the loss of short microtubules (and decrease in **m**), and the growth of remaining microtubules to maintain mass balance. These deductions were largely confirmed by Horio & Hotani, [4]; dark-field microscopic observations of individual microtubules showed that growing and shrinking microtubules interconvert, that one end of the microtubule is more active, and that the states of microtubule ends change at random (cf. [5,6]). See Scheme A :
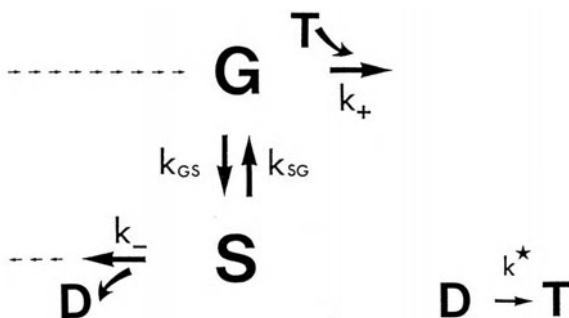


**Scheme A : Formulation of the dynamic behaviour of microtubules at steady-state, based on the observations of Horio & Hotani, [4].** An individual end is in either the growing state, **G**, in which it adds on T-GTP, (**T**) with bimolecular rate constant $k_+$, or in the shrinking state, **S**, in which it loses T-GDP, (**D**), with rate constant $k_-$. Interconversions between states occur with rate constants $k_{GS}$ and $k_{SG}$, which are constants at steady state. **T** regenerates from **D** _via_ the first-order process, $k^*$, see text.

**Table I – Parameters for the dynamic instability of microtubules.**

| End | Growth rate, $R_G$ ($\mu m$/min) | Shrinkage rate, $R_S$ ($\mu m$/min) | Lifetimes | | Ref. |
|---|---|---|---|---|---|
| | | | $T_G$ (min) | $T_S$ (min) | |
| "Active" | 0.63 | 7.9 | 2.9 | 0.3 | [4] |
| | 1.6 | 25.0 | 4.2 | 0.7 | [5] |
| "Inactive" | 0.20 | 15.2 | 6.0 | 0.05 | [4] |
| | 0.70 | 25.0 | 8.3 | 0.12 | [5] |

The growth rate, $R_G = k_+ \cdot [\text{T-GTP}]_{SS}$, and shrinking rate, $R_S = k_-$ are characteristic of the two states. Likewise, the lifetimes of each state $T_G$ ($=1/k_{GS}$) and $T_S$ ($=1/k_{SG}$) characterise the average length of time spent in either G or S state before switching to the other. Of the four rate parameters of Scheme A, only three are independent at steady state, when $[\text{T-GTP}]_{SS} = (f_S \cdot k_-)/(f_G \cdot k_+)$, where $f_G$ and $f_S$ are fractions, ($f_G + f_S = 1$) related by $f_G \cdot R_G = f_S \cdot R_S$.

Representative values are given in **Table I**; the rates may be translated to conventional rate constants, assuming 1625 tubulin molecules per $\mu m$, (i.e. 13 protofilaments), and with $[\text{T-GTP}]_{SS} = 10$ $\mu M$. The rates of 0.63 $\mu m \cdot min^{-1}$ and 7.9 $\mu m \cdot min^{-1}$ correspond to rate constants $k_+ = 2.10^{+6}$ $M^{-1}$ $s^{-1}$ and $k_- = 210$ $s^{-1}$ respectively. Although the rates in **Table I** vary significantly, possibly due to different solution conditions and measurement protocols, both [4] and [5] show one end to be more active in growth and shrinking. In [4] both ends appear to be relatively close to steady state, given the substantial experimental error, and it is interesting to note that MAPs effectively suppressed the dynamic properties.

We note here the importance of reliable values of the parameters $k_+$ and $k_-$ in **Scheme A**. Values based on observations of bulk microtubule properties depend on an additional parameter, namely m. This is usually determined by measurement of the length distribution of the microtubules using ultrastructural methods, which are time-consuming and often problematical due to sampling, shearing, [7] and aberrant structures [8,9]. Even given these limitations, there is clear evidence that the values of $k_-$ reported in the literature show variation due to the conditions of measurement. We found [10] that increasing $Mg^{2+}$ from 0.5 to 2.5 mM

caused a 5-fold increase in the dissociation rate at $5^{o}C$ from microtubules at constant $\mathbf{m}$. Recent work [11] has shown that $[Mg^{2+}]$ up to 20 mM and $[Ca^{2+}]$ up to 8 mM cause an enhancement of this rate from 200 $s^{-1}$ to more than 2000 $s^{-1}$ at $25^{o}C$. Under conditions of partial disassembly, electron microscopy confirms the presence of bona-fide microtubules. Since $k_-$ is found to be independent of microtubule length, this shows that the disassembly is an end-dependent process. Thus, $k_-$ varies markedly with ionic composition, and the value assigned must be appropriate to the conditions.

These observations have important implications for the treatment of tubulin microtubules in solution, both at steady state of assembly, and also, as will be shown, to systems far from the steady state, such as de novo assembly, and disassembly at high dilution. We have recently shown [12,13] that the simple formulation of Scheme A may be used to simulate several experimental observations on a steady-state population of microtubules using only three independent parameters deriving from experiment. These properties include a) microtubule length redistribution; b) fast tubulin incorporation; c) steady-state hydrolysis of GTP; d) the time-dependent behaviour of individual microtubules; e) the stochastic nature of label incorporation into steady-state microtubules; f) the complex properties of isotopic "pulse-chase" kinetics; and g) control of microtubule length distribution via rapid changes in $\mathbf{m}$.

The stochastic (random) nature of the switching process in a microtubule population has particular importance for pulse-chase experiments. Firstly the pulse is incorporated into microtubules to an extent which is totally uncorrelated with microtubule length. The "chase" process involves similarly stochastic dissociation processes, and there is no correlation of the extent of chase achieved in a given microtubule with the extent of label previously incorporated. This means that it is relatively inefficient to chase out all the pulse in the population. The result is a complex kinetic process, continuing several-fold longer than the pulse phase. The experimentally observed effects are of a portion of the pulse which is displaced only slowly. This has been attributed [14] to treadmilling, which is strictly the consequence of different affinities for addition at each end of the polymer. As with F-actin this is manifested as one end of the polymer undergoing net growth while the other undergoes a balancing net loss at steady state.

Evidence relating to this mechanism comes from double labelled GTP experiments; when ^{14}C-GTP tubulin is assembled, pulsed with ^{3}H-GTP tubulin, and then cold chased with GTP, the kinetics of the chase are observed to be relatively slow and different for the two isotopes. However, in **Figure 1**, these phenomena are seen to be an intrinsic feature of the stochastic nature of the pulse-chase incorporation in dynamic microtubules, without the need to invoke treadmilling. It would require extremely high (and so far unattained) precision in direct observations in order to determine whether net growth or shrinking occurs at steady-state, correlated with the polarity of a dynamic microtubule. In the absence of such definitive evidence, treadmilling as such is not required to rationalise slow chase kinetics; they are the effect of the dynamic nature of the pulse and chase processes in the linear polymer. Thus the evaluation of the relative contributions of microtubule dynamic instability and treadmilling remains an open question.
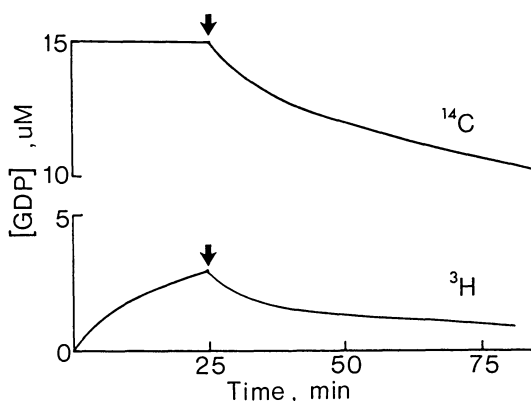


**Figure 1 : Simulation of double-label microtubule pulse-chase experiments**, showing different kinetics for displacement of the two isotopes by the cold chase (arrow). Mean microtubule length, 40 $\mu$m; [MT] = 15 $\mu$M; pulse = 25 min.

What factors control the switching between G and S states? In dilution experiments, all microtubules dissociate rapidly, and $k_{GS}$ is then fast. In direct observations, [5,6], the switching is strongly dependent on the concentration of free tubulin-GTP. We have therefore developed a model [13,15] which incorporates a co-operative mechanism for the switch. This involves a limited, lateral cap of **n** molecules of tubulin-GTP, with one important assumption, namely that the addition of one T-GTP molecule in an

elongation step causes the hydrolysis of the previously terminal T-GTP residue. (A similar principle is discussed by O'Brien et al, [16].) Thus the cap remains at constant size, and the processes required to bring about transition into S from G are unrelated to microtubule length. This model has the virtue of maintaining the relationship of one GTP hydrolysis for each T-GTP added. The co-operativity resides in the relationships of species intermediate between $T_n$ and $T_0$.

The model is shown in **Scheme B** : this is a formal model only, serving to illustrate the principles involved in the co-operative transitions between G and S. Given the complex, multi-strand nature of the microtubule lattice, it is unlikely that there is a single exact description of the growing end. However, simulation indicates how, at low [T-GTP], the lifetime of G, $(T_n)$ decreases sharply, and the proportion of intermediate states increases. These potentially inactive species could correspond to microtubules in a stationary state, as have been observed [5,6].

$$G \equiv T_5 \underset{k_a f_2}{\overset{k_b f_1}{\rightleftharpoons}} T_4 \underset{k_a}{\overset{k_b}{\rightleftharpoons}} T_3 \underset{k_a}{\overset{k_b}{\rightleftharpoons}} T_2 \underset{k_a}{\overset{k_b}{\rightleftharpoons}} T_1 \underset{k_a f_4}{\overset{k_b f_3}{\rightleftharpoons}} T_0 \equiv S$$
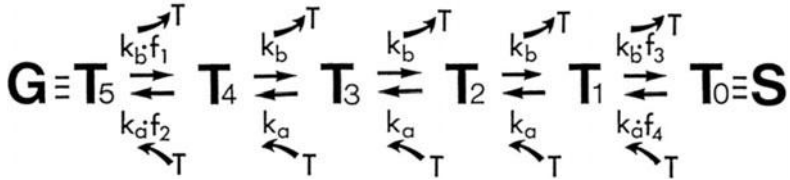
**Scheme B : The Lateral Cap model for a microtubule end**, illustrated for n = 5, (see text). The growing state **G**, **($T_n$)** is linked to the shrinking state **S**, **($T_0$)**, via reactions with intermediate species involving T-GTP, **(T)**. Coefficients $f_i$ determine the co-operative nature of the G-S transition; typically $f_1 < 1$ and $f_3 > 1$ with $k_a = k_+$ and $k_b << k_-$.

The course of assembly of microtubules at high [T-GTP] is also readily interpreted by this model. After initiation of growth the system is effectively 100% G; at high [T-GTP], the rate constants of the G to S transition mechanism readily allow the system to overshoot the ultimate $[T\text{-}GTP]_{ss}$, strongly depleting [T-GTP], and

hence inducing a kinetically-determined, synchronous switch to S
via $k_{GS}$. The system continues to oscillate until the synchrony is
destroyed by the stochastic nature of the processes, and finally
attains the expected steady-state. The essential initial condition
for imbalance is attributed to the concentration dependence of $k_{GS}$
in the dynamic instability mechanism; the relative slowness of
other coupled reactions serves to amplify the oscillatory
behaviour. This is illustrated in Figure 2. The fact that the final
(experimental) plateau value in such assemblies is substantially
attenuated [17-18], suggests that there is a significant proportion
of residual T-GDP, possibly present as oligomers [19], also
inducible by elevated $[Mg^{2+}]$, [20]. The slowness of nucleotide
exchange processes, (eg. in oligomeric species) determines the rate
at which T-GTP becomes available to cause the switch back from S to
G, and hence increases the amplitude of oscillation, (compare Fig
2A and B).
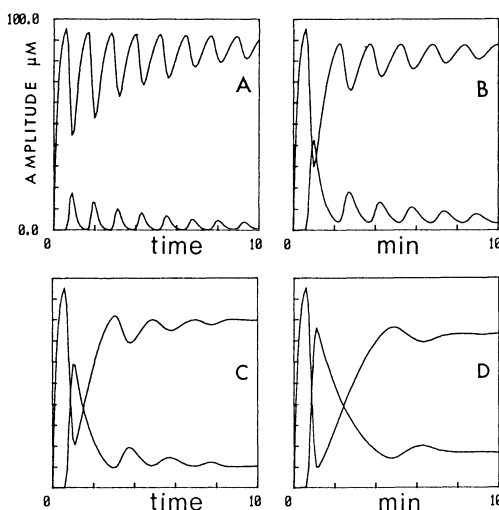


**Figure 2 : Simulation of microtubule self-assembly at high
protein concentration** (100 $\mu$M), showing initial assembly overshoot
and subsequent oscillations, with corresponding [T-GDP] levels.
Simulated from **Scheme A**, (with nucleation and co-operative G-S
transitions via the dependence of $k_{GS}$, $k_{SG}$ on [T-GTP] as **Scheme B**),
and a slow regeneration of [T-GTP] from [T-GDP] via a first-order
$k^*$, with (A-D) $k^* = 5$, 2, 1, and 0.5 $min^{-1}$, respectively.

Other molecules which can dramatically affect the behaviour of
microtubule populations include a range of drugs, such as the
mitotic poisons, colchicine and podophyllotoxin. We have recently

shown [21,22] that podophyllotoxin causes inhibition of microtubule dynamics, as judged by the cessation of the tubulin exchange reaction at sub-stoichiometric concentrations. Excess drug causes full disassembly at the unperturbed rate (ca. 200 s-1); it appears that the lower levels of the drug induce a third state (designated I) and that the species G,S and I are in a dynamic equilibrium. The fact that growth can be inhibited without causing total disassembly recalls the fact that cellular processes, including mitosis, are arrested in vivo at concentrations of drugs which would be ineffective for disassembly in vitro. While there may be several mechanisms operative, it is an interesting possibility that the suppression of microtubule dynamics provides one such means of inhibition without the disorganising and energy-expensive consequence of major disruption of the cytoplasmic network.

The effect of colchicine also shows striking differences between the behaviour in vitro and in vivo. Due to the quasi-irreversible binding of colchicine to tubulin (to form the TC complex), the effects of colchicine and TC can be distinguished. In vivo, both induce a rapid disassembly of spindle microtubules [23], whereas in vitro, addition of excess colchicine induces only a limited extent of disassembly in steady-state microtubules or isolated spindles [24]. TC inhibits elongation, binding to the ends of steady state microtubules with a dissociation constant of 0.3 $\mu$M [25]. When TC is added prior to nucleation, this inhibition produces more, but shorter, microtubules [26]. At steady-state, the uptake of labelled nucleotide is reduced to 50% by 0.13$\mu$M TC, [27], with a mean stoichiometry of 0.5 TC bound per end [28]. (At full saturation, up to 9 TC molecules may be bound per end). This shows that TC in a terminal position has a disproportionately large effect in the inhibition of growth; the binding of a single TC molecule appears capable of inhibiting growth of an individual microtubule.

The TC complex may also be incorporated in the interior of the microtubules [29]. The extent of this uptake shows an optimum TC concentration (ca. 0.13 $\mu$M), indicating that co-polymerisation of tubulin and TC is occurring [27]. This internal incorporation shows that a small number of terminal TC molecules can in fact be overgrown under suitable conditions. The effect of colchicine is at least partly determined by the microtubule polarity. Microtubules grown from flagella fragments in the presence of TC showed 50% inhibition at 0.27 $\mu$M [30]. When these microtubules, with TC

incorporated, were subjected to dilution, the disassembly of the minus end was strongly inhibited, whereas the plus end was almost unaffected. Microtubule dynamics have also been observed to have a similar strong end-dependence. The difference between the _in vitro_ and _in vivo_ behaviour with colchicine certainly reflects the inherent differential stability of the microtubules in question, including their polarity, and may well involve differences due to their dynamic properties.

**Conclusions** : the observation of the dynamics at steady state of a microtubule population has introduced a new dimension into the formulation and modelling of such properties. We show here that such modelling is indeed successful with relatively simple formulations. While the fuller picture will undoubtedly be more complex, the principles of a co-operative "Lateral Cap" model enumerated here appear to account for several fundamental dynamic properties. In particular we note three levels of control which appear to be exercised on the dynamic population by additional factors. (1) MAPs appear to suppress transitions, but allow slow growth and possibly slow shrinking. (2) High concentrations of cations appear able to switch the system rapidly into full disassembly, in a manner which could be useful for the wholesale disassembly of the MT network, whereas (3) certain drugs are able to switch off dynamics without interfering with the overall microtubule structure. Added to this other factors, in particular the number of nucleating sites, or **m**, assume great importance in system of constant microtubule mass, since modulation of **m** can bring about extensive changes in length redistribution, as required for different parts of the cell cycle. Likewise modulation of the fundamental kinetic parameters modifies the degree of exchange, and hence turnover of the assembled microtubule system. Finally, there appears to be a common mechanism of control through the level of tubulin-GTP, excess of which can promote oscillatory behaviour, and depletion causing rapid disassembly. These suggest potential regulatory mechanisms through nucleotide and energy sources, as well as at a more fundamental level _via_ the size of tubulin pools created under genetic control.

# References.

[1]   Engelborghs YE (1988) In : Avila J (ed) Microtubule Proteins. CRC Press, (In Press).
[2]   Carlier MF (1988) Cell Biophysics 11,105-117.
[3]   Mitchison T, Kirschner MW (1984) Nature 312,232-237 & 237-242.
[4]   Horio T, Hotani H (1986) Nature 321,605-607.
[5]   Cassimeris LU, Walker RA, Pryer NK, Salmon ED (1987) Bioessays 7,149-154
[6]   Walker RA, O'Brien ET, Pryer NK, Soboeiro MF, Voter WA, Erickson HP, Salmon ED (1988) J.Cell.Biol (in Press).
[7]   Hallett FR, Keates R.(1985) Biopolymers 24,2403-2415.
[8]   Carlier MF, Pantaloni D (1978) Biochemistry 17,1908-1915.
[9]   Karecla PI (1988) Ph.D.Thesis, London University.
[10]  Martin SR, Butler FMM, Clark DC, Zhou JM, Bayley PM (1987) Biochim.Biophys.Acta 914,96-100.
[11]  Gal V, Martin SR, Bayley PM (1988) Biochem.Biophys.Res.Commun. (in Press).
[12]  Martin SR, Schilstra MJ, Bayley PM (1987) Biochem.Biophys. Res.Commun.149, 461-467
[13]  Bayley PM, Martin SR (Submitted).
[14]  Farrell KW, Jordan MA, Miller HP, Wilson L. (1987) J.Cell Biol. 104,1035-1046.
[15]  Bayley PM, Schilstra MJ, Martin SR (1988) Biophys.J. 53,29a.
[16]  O'Brien ET, Voter WA, Erickson HP (1987) Biochemistry 26, 4148-4156.
[17]  Carlier MF, Melki R, Pantaloni D, Hill TL, Chen Y (1987) Proc.Natl.Acad.Sci. U.S.A. 84,5257-5261.
[18]  Pirollet WD, Job D, Margolis RL, Garel JR (1987) EMBO J. 6,3247-3252.
[19]  Mandelkow EM, Lange G, Jagla A, Spann U, Mandelkow E (1988) EMBO J. 7,357-365.
[20]  Howard WD, Timasheff SN (1986) Biochemistry 25,8292-8300.
[21]  Schilstra MJ, Martin SR, Bayley PM (1988) Proceedings: 4th Meeting, European Cytoskeletal Club,(In press).
[22]  Schilstra MJ, Martin SR, Bayley PM (submitted)
[23]  Salmon ED, McKeel M, Hays TS (1984) J.Cell Biol. 99,1066-1075.
[24]  Hays TS, Salmon ED (1986) Cell Motil.Cytoskel. 6,282-290.
[25]  Lambeir AM, Engelborghs Y (1980) Eur.J.Biochem. 109,619-624.
[26]  Lambeir AM, Engelborghs Y (1983) Eur.J.Biochem. 132,369-373.
[27]  Farrell KW, Wilson L (1980) Biochemistry 19,3048-3045.
[28]  Margolis RL, Rauch CT, Wilson L (1980) Biochemistry 19,5550-57.
[29]  Sternlicht H, Ringel I (1979) J.Biol.Chem. 254,10540-10550.
[30]  Bergen JG, Borisy GG (1983) J.Biol.Chem. 258,4190-4194.

# The Effects of Magnesium on the Dynamic Instability of Individual Microtubules

E.T. O'Brien, R.A. Walker*, E.D. Salmon* and H.P. Erickson

Department of Cell Biology, Duke University Medical Center

Durham, North Carolina, 27710, USA

Microtubules have been shown to exhibit two contrasting states: slow growth and rapid shortening. Recently, we have characterized how the transitions between these phases change with tubulin concentration, and determined the rate constants for the slow elongation phase for each microtuble end (Walker et al., 1988). These studies, as well as the original study that proposed the existance of these two phases (Mitchison and Kirschner, 1984), were done in the presence of 1mM magnesium (Mg). Recent work has demonstrated that Mg can have dramatic effects on both the assembly and disassembly phases of microtubule growth (O'Brien and Erickson, 1988; Gal et al., 1988), and that high Mg can promote bizarre microtubule behaviors, such as synchronous oscillations (Pirollet et al., 1987; Carlier et al., 1988; Mandelkow et al., 1988). However, these experiments were done in bulk solution, where the properties of individual microtubules, and differences between the ends, could not be determined. We therefore investigated the effects of Mg on the assembly and disassembly of individual microtubules.

Microtubules were prepared using pure tubulin, and grown onto sea urchin sperm axonemal seeds at 37° C in a buffer of 100 mM Pipes, 2 mM EGTA, 1 mM GTP, pH 6.9, and 1-12.5 mM magnesium sulfate. Individual microtubules were imaged using video-enhanced DIC microscopy and digital image processing, as described in Walker et al. (1988). The results reported here were obtained using 10-12 µM free, active tubulin, a concentration that allowed robust assembly without spontaneous nucleation of free microtubules.

**Effect on elongation.** The rate of microtubule growth during the elongation phase was dramatically affected by increasing the magnesium concentration. At 2.5 mM Mg, no appreciable effect of magnesium was seen. At 5 mM, the rate of elongation was approximately doubled at both ends, being approximately 4 µm/min at plus ends (108 subunits/sec) and 2.4 µm/min at minus ends (65 subunits/sec). Increasing Mg to 7.5 mM, however, did not increase the elongation rate, but rather decreased this rate somewhat, to 3.6 and 1.7 µm/min respectively. Since we have evaluated only one tubulin concentration, we could not determine whether the increased net elongation rate at 5 mM was a result of a diminished dissociation, or enhanced association rate constant. However, the fastest rates observed were very close to those expected if the dissociation rates for both ends (see Walker et al., 1988), during the elongation phase, had been eliminated.

**Effect on the rapid shortening phase.** Mg concentrations above 1 mM produced dramatic changes in the kinetics of rapid shortening. At 1 mM Mg, rates of shortening were between 10-40 µm/min at each end, as observed previously (Walker et al. 1988). At 2.5 mM

Mg, rates as high as 180 µm/min were observed at the more slowly growing (minus) ends, while the faster growing (plus) ends seemed to be limited to 60-90 µm/min. At 5 mM Mg, minus ends often shortened at near the maximum observed rate, 210-260 µm/min, and the presumed plus ends at only 90-130 µm/min. Suprisingly, at both 2.5 and 5 mM Mg, periods of extremely fast disassembly usually changed abruptly to relatively slower shortening. At 2.5 mM, these slower periods were comparable to those seen at 1 mM Mg (20-30 µm/min), while at 5 mM, the slower periods were somewhat faster (45-90 µm/min). At 7.5 mM Mg and above, the slower phases of disassembly were suppressed, and only one rate of rapid shortening, per catastrophe, was observed. The slower-growing end, presumed to be the minus end, disassembled at 220-300 µm/min, while the maximum rate of shortening at the plus ends was again limited to 60-90 µm/min. Thus, the increase in the rate of rapid shortening induced by Mg was not a smooth, gradual transition, but appeared to have both a gradual and a quantal component; rates did increase for both the fast and slower shortening stages as Mg was increased, but, more importantly, the fraction of time spent in the fastest state of rapid disassembly increased with increasing Mg. Data collected at 1 (A), 2.5 (B), 5 (C), and 7.5 (D) mM Mg are shown in the Figure. Data points represent a microtubule end just before and during a rapid shortening phase, while the lines drawn are least squares linear regression lines. Note the change in time scale between graphs. Rates of rapid shortening range from 12 and 14 µm/min at 1 mM Mg (A), to 310 µm/min at 7.5 mM (D). At these concentrations, rapid shortening was almost always monotonic, while at 2.5 and 5 mM Mg we almost always observed multiple stages of shortening, at markedly different rates. The rates of shortening in Figure **B** were, in order, 166, 40 and 102 µm/min, while the rates in C were 111 and 40 µm/min.
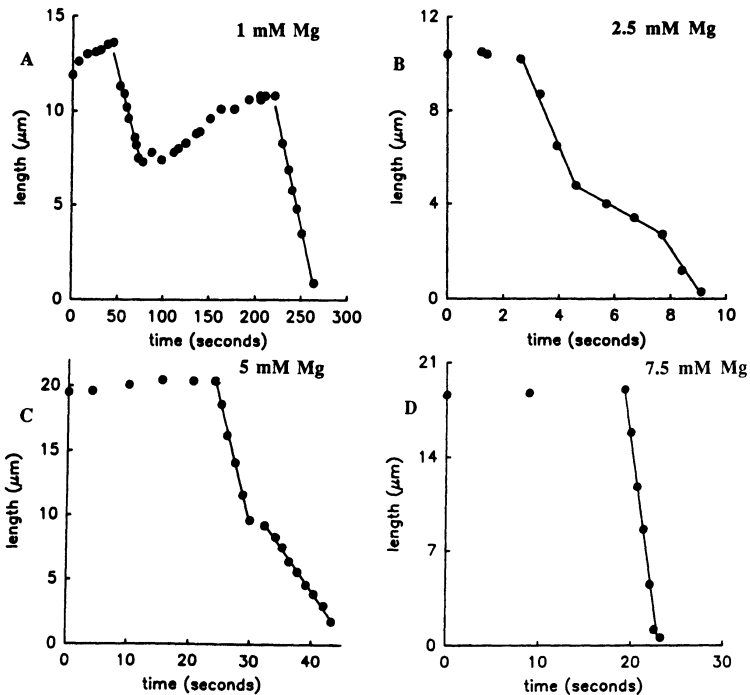
**Effect on the transitions between elongation and rapid shortening.** At 2.5 mM Mg, rescue (the transition from disassembly to elongation phases) was not observed during the 80 rapid shortening events analyzed. In contrast, the frequency of catastrophe (the transition from elongation to rapid shortening) seemed to be increased, particularly at the minus end. At tubulin concentrations less than 10 μM, minus ended microtubules were observed only rarely, evidence that slow growth, coupled with the extremely rapid disassembly observed at the minus ends, severely limited our ability to observe these microtubules. This is an interesting contrast to our observation at 1 mM Mg, where minus ended microtubules persisted longer than plus ends due to a higher frequency of rescue and lower frequency of catastrophe.

**Conclusions.** Our results demonstrate interesting new properties of microtubule dynamics, most of which cannot be explained solely within the context of the GTP-cap model of dynamic instability. Plus end disassembly rates appeared limited to 60-100 μm/min (1600-2700 s$^{-1}$), while minus end rates of 250-310 μm/min (6700-8100 s$^{-1}$) were common above 5 mM Mg. This implies an entire microtubule could disassemble in the range of 10000 s$^{-1}$. This extremely high rate of disassembly, coupled with an apparent supression of the rescue reaction, helps to explain the extremely dynamic behavior observed in the studies on oscillatory assembly/disassembly behavior mentioned above. Enhancement of elongation reaches a maximum at 5 mM Mg, while effects on rapid shortening appears maximal at 7.5 mM. Mg concentrations of 2.5-5 mM produced not only higher rates of shortening, but also exposed an unexpected property of microtubules in the shortening phase: the presence of multiple periods of disassembly, of differing but constant velocity. These multiple shortening states may correspond to different regions of the polymer, perhaps changing from an A to a B lattice, or 13 to 14 protofilaments. Whatever the underlying cause of the multiplicity of disassembly rates, it is clear that Mg exaggerates some unexpected, subtle difference in the polymer that is not apparent at either high or very low Mg. Similarly, Mg also seems to exaggerate dynamic instability, prehaps by increasing the difference in the affinity of subunits for a microtubule end depending on whether or not the microtubule end is capped (GTP-tubulin at the end) or not, thus increasing the rates of assembly during the elongation phase, and disassembly during shortening.

# References.

Carlier, M.F., Didry, D., Melki, M., Chabre, M., and Pantaloni, D. (1988) Biochemistry 27: 3555-3559.
Gal, V. Martin, S. and Bayley, P. (1988). Biochem. Biophys. Res. Comm. 155: 1464-1470.
Mandelkow, E.-M., Lange, G., Jagla, A. Spann, U. and Mandelkow, E. (1988) EMBO J. 7:357-365.
Mitchison, T. and Kirschner, M.W. (1984). Nature (Lond.) 312: 232-237.
O'Brien, E.T. and Erickson, H.P. (1988). Biochemistry (in press).
Pirollet, F., Job, D., Margolis, R.L. and Garel, J.R. (1987) EMBO J. 6: 3247-3252.
Walker, R.A., O'Brien, E.T., Pryer, N.K., Soboeiro, M.F., Voter, W.A., Erickson, H.P. and Salmon, E.D. (1988). J. Cell Biology 107: 1437-1448.

# About the Recognition of Colchicine by Tubulin

A. Vandecandelaere and Y. Engelborghs
Katholieke Universiteit te Leuven
Laboratory of Chemical and Biological Dynamics
Celestijnenlaan 200 D, B-3030 Leuven, Belgium

Colchicine is a well known cytostatic agent due to its inhibition of the assembly of microtubules. As a result of the kinetic analysis under pseudo first-order conditions of its binding to tubulin, the reaction was identified as a two step mechanism: a fast preequilibrium followed by a rate determining second step (Garland, 1978; Lambeir, Engelborghs, 1981).

$$T + C \; \underset{}{\overset{K_1}{\rightleftharpoons}} \; TC \; \xrightarrow{k_2} \; TC^*$$
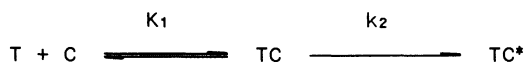
According to the model proposed by Andreu and Timasheff (1982) the first step is due to the binding of the tropolone (C) ring. This is followed by a conformational change and the binding of the trimethoxybenzene (A) ring. This model is based on the finding that the thermodynamic parameters of the fast preequilibrium are identical with those of tropolone binding to tubulin. However, the results with the bicyclic analog (AC) show a different behaviour (Engelborghs, Fitzgerald, 1987). Binding still occurs in two steps, but the thermodynamic parameters are rather different.

Here a kinetic study is presented of the binding of colchicine and AC in the presence of an analog of the A ring: trimethoxyacetophenon (TMA). According to the two site model, the presence of TMA should only slow down the second step proportional to the saturation of the subsite. This is under the assumption of a rapid exchange of TMA on this site. Our experiments, however, indicate that in the presence of a large excess of TMA, colchicine as well as AC bind in a single step. The slope of the pseudo first order plot is decreased relative to the initial slope in the absence of TMA. The bimolecular rate constant is only $2.8 \times 10^{-5}$ $M^{-1}s^{-1}$ at 30 °C. This indicates that in the presence of TMA, colchicine binds extremely slowly but in a single step.

Fluorescence titration of AC binding in the presence of TMA shows a decreased affinity, probably due to competition.

Different mechanisms are possible to explain these results. One such mechanism would imply hysteresis: the altered conformation of tubulin, induced by the binding of TMA would return to its original conformation much slower than the dissociation of TMA.

Another, more plausible, possibility is the formation of a ternary complex: colchicine as well as AC can bind to the tubulin-TMA complex although with a rather low affinity. However, the initial ternary complex can form the final complex at a much higher rate than in the case of pure tubulin.

Although evidence exists for a second low affinity site for colchicine (Ringel, Sternlicht, 1984), it is not plausible that TMA acts through this site, since colchicine would be supposed to do the same.

## Acknowledgement

## References

Andreu JM, Timasheff SN (1982) Interaction of Tubulin with Single Ring Analogues of Colchicine. Biochemistry 21: 534-543.

Engelborghs Y, Fitzgerald TJ (1987) A Fluorescence Stopped Flow Study of the Competition and Displacement Kinetics of Podophyllotoxin and the Colchicine Analog AC on Tubulin. J. Biol. Chem. 262: 5204-5209.

Garland DL (1978) Kinetics and Mechanism of Colchicine Binding to Tubulin: Evidence for Ligand-Induced Conformational Change. Biochemistry 17: 4266-4272.

Lambeir A, Engelborghs Y (1981) A Fluorescence Stopped Flow Study of Colchicine Binding to Tubulin. J. Biol. Chem. 256: 3279-3282.

Ringel I, Sternlicht H (1984) Carbon-13 Nuclear Magnetic Resonance Study of Microtubule Protein: Evidence for a Second Colchicine Site Involved in the Inhibition of Microtubule Assembly. Biochemistry 23: 5644-5653.

# Phosphate Release Following Nucleotide Hydrolysis Regulates the Dynamics of Actin Filaments and Microtubules

Marie-France Carlier, Ronald Melki, Cécile Combeau and D. Pantaloni

Laboratoire d'Enzymologie, C.N.R.S., 91198 Gif-sur-Yvette, France

Microtubules and actin filaments are the two major components of the eukaryotic cytoskeleton, and their reactions of assembly-disassembly constitute the basis of many motile reactions in the cell. Microtubules in particular are highly dynamic in vivo ; their property of "dynamic instability", describing their ability to undergo phase transitions between states of steady growth and catastrophic depolymerization, has raised a wave of interest in the recent years.

Microtubules and actin filaments share a number of functional analogies especially regarding the mechanism of polymerization and of the accompanying hydrolysis of the bound nucleotide. These analogies are summarized below.

1. ATP is hydrolyzed on the subunits of the actin filament and GTP is hydrolyzed on tubulin subunits of the microtubule following their incorporation in the polymer (Carlier and Pantaloni, 1981 ; Pardee and Spudich, 1982 ; Pollard and Weeds, 1984 ; Carlier et al., 1984a).

2. Nucleotide hydrolysis proceeds vectorially toward the tip of the polymer, as proposed for microtubules by Carlier et al., 1984b) and Brylawski and Caplow (1985) and experimentally demonstrated for both microtubules and Mg-F-actin (Carlier et al., 1987a,b).

3. Once XTP has been hydrolyzed and $P_i$ released in the medium, the resulting polymer composed of XDP-subunits is unstable and depolymerizes

spontaneously in the absence of free XTP (Carlier and Pantaloni, 1978 ; Carlier et al., 1984c).

4. In the presence of XTP, a steady state is established ; the stability of the polymer is maintained via the continuous feeding of the ends with XTP-subunits. Evidence for a regulation of assembly by XTP hydrolysis has been obtained in kinetic experiments demonstrating that subunits present at the ends of growing actin filaments and microtubules dissociate at a slower rate than internal XDP-subunits, and form a stabilizing cap, initially thought to be a XTP-cap (Carlier, 1982 ; Hill and Carlier, 1983 ; Carlier et al., 1984 a,b). This difference between terminal and internal subunits does not appear if polymerization takes place in the presence of a non hydrolyzable nucleotide ; it is more pronounced for microtubules than for actin filaments. The loss of a statilizing GTP cap has been proposed by Mitchison and Kirschner (1984) as the basis for the dynamic instability of microtubules.

In order to understand how the elementary reactions of nucleotide hydrolysis exert a regulatory switch from the state of strong interaction to the state of weak interaction between polymer subunits, we have undertaken a kinetic analysis of the XTP hydrolysis reaction and carried out the characterization of the dynamic properties of the transient complexes involved (for reviews see Korn et al., 1987 ; Carlier, 1988). The following conclusions have been reached.

1. ATP hydrolysis takes place on F-actin within two sequential steps, cleavage of the $\gamma$-phosphate followed by the slower release of $P_i$ (Carlier and Pantaloni, 1986 ; Carlier, 1987) according to the following scheme : G-ATP $\rightleftharpoons$ F-ATP $\xrightarrow{\leftarrow}$ F-ADP-$P_i$ $\rightleftharpoons$ F-ADP + $P_i$

2. $P_i$ binds (1:1) to F-ADP subunits, reconstituting a F-ADP-$P_i$ filament. Both the transient and reconstituted F-ADP-$P_i$ filaments have a higher stability than the filament made of ADP subunits, due to the slow rate

of dissociation of F-ADP-P$_i$ subunits (Carlier and Pantaloni, 1988). The slow rate of dissociation of F-ADP-P$_i$ subunits explains the decrease in critical concentration promoted by P$_i$ in the presence of ADP and cytochalasin D (Rickard and Sheterline, 1986). Therefore P$_i$ release, and not cleavage of ATP, is the chemical regulatory switch linked to a structural change of the polymer from a stable state, in which F-ADP-P$_i$ actin subunits interact strongly, to an unstable state in which F-ADP-actin subunits interact weakly. A large free energy change is associated to P$_i$ release. Correlatively, the two ends are energetically closer in the F-ADP-P$_i$ state : phosphate, at physiological concentrations, decreases the efficiency of treadmilling and may regulate actin dynamics in cells.

3. In contrast to actin, the GDP-P$_i$ microtubule is not a long lived intermediate in microtubule assembly. However P$_i$ as a stabilizing effect on microtubules and slow down 25-fold the rate of subunits dissociation from microtubule ends. The properties of the GDP-P$_i$-microtubule transient have been investigated using the structural analogs of phosphate aluminum and beryllium fluoride recently discovered by Bigay et al. (1985). These analogs bind (1:1) to GDP-tubulin subunits of the microtubule and to F-ADP actin subunits in competition with P$_i$ and with an affinity three orders of magnitude higher than P$_i$, reconstituting the transient XDP-P$_i$ state of the polymer, which exhibits very strong subunit-subunit interactions and depolymerizes very slowly (Carlier et al., 1988 ; Carlier and Combeau, 1988). AIF$_4^-$ and BeF$_3^-$ inhibit all aspects of dynamic instability in particular they abolish the oscillatory tubulin polymerization kinetics originally discovered in our laboratory (Carlier et al., 1987c). P$_i$ release following cleavage of GTP therefore appears the crucial step regulating dynamic instability. A cap of slowly dissociating GDP-P$_i$ subunits maintains the stability of GDP microtubules

at steady-state and accounts for the absence of GTP cap at steady-state (Carlier et al. 1987b ; Schilstra et al., 1987 ; O'Brien et al., 1987).

The regulatory role played by phosphate release in the dynamics of actin filaments and microtubules has a general bearing in the mechanism of other nucleotidases involved in force production or signal transduction. In all of these cases, nucleotide hydrolysis is associated to the interaction between the nucleotidase and an effector (that can be a protein or a nucleic acid) and destabilization of this interaction is linked to the liberation of phosphate.

## References

Bigay, J., Deterre, P., Pfister, C. and Chabre, M. (1985) FEBS Lett. 191, 181-185.

Caplow, M., Shanks, J. and Brylawski, B.P. (1985) Can. J. Biochem. 63, 422-429.

Carlier, M.F. and Pantaloni, D. (1978) Biochem. 17, 1908-1915.

Carlier, M.F. and Pantaloni, D. (1981) Biochem. 20, 1924-1932.

Carlier, M.F. (1982) Mol. Cell Biochem. 47, 97-113.

Carlier, M.F., Pantaloni, D. and Korn, E.D. (1984a) J. Biol. Chem. 259, 9983-9986.

Carlier, M.F., Hill, T.L. and Chen, Y. (1984b) Proc. Nat. Acad. Sci. USA 81, 771-775.

Carlier, M.F., Pantaloni, D., Coué, M., Lal, A., Brenner, S. and Korn, E.D. (1984c) J. Biol. Chem. 259, 6274-6283.

Carlier, M.F. and Pantaloni, D. (1986) Biochemistry 25, 7789-7792.

Carlier, M.F. (1987) Biochem. Biophys. Res. Comm. 143, 1069-1075.

Carlier, M.F., Pantaloni, D. and Korn, E. (1987a) J. Biol. Chem. 262, 3052-3059.

Carlier, M.F., Didry, D. and Pantaloni, D. (1987b) Biochem. 26, 4428-4437.

Carlier, M.F., Melki, R., Pantaloni, D., Hill, T.L. and Chen, Y. (1987c) Proc. Nat. Acad. Sci. USA 84, 5257-5261.

Carlier, M.F. (1988) Int. Rev. Cytology, in the press.

Carlier, M.F. and Pantaloni, D. (1988) J. Biol. Chem. 263, 817-825.

Carlier, M.F. and Combeau, C. (1988) J. Biol. Chem. 263, in the press.

Carlier, M.F., Didry, D., Melki, R. and Pantaloni, D. (1988) Biochem. 27, 3555-3558.

Hill, T.L. and Carlier, M.F. (1983) Proc. Nat. Acad. Sci. USA 80,

Korn, E.D., Carlier, M.F. and Pantaloni, D. (1987) Science 238, 638-644.

Mitchison, T. and Kirschner, M.W. (1984) Nature 312, 232-237.

O'Brien, E.T., Voter, W.A. and Erickson, H.P. (1987) Biochem. 26, 4148-4156.

Pardee, J. and Spudich, J.A. (1982) J. Cell Biol. 93, 648-654.

Pollard, T.D. and Weeds, A. (1984) FEBS Lett. 170, 94-98.

Rickard, J. and Sheterline, P. (1986) J. Mol. Biol. 191, 273-280.

Schilstra, M.J., Martin, S.R. and Bayley, P.M. (1987) Biochem. Biophys. Res. Comm. 147, 588-595.

# Self-Assembly of Supramolecular Structures: The Role of Fluctuations

M.B. Palma-Vittorelli and M.U. Palma
Dept. of Physics of the University and CNR
Institute for Interdisciplinary Applications of Physics
Via Archirafi 36
I-90123 Palermo
Italy

This is a short review of experiments performed at our Laboratory on the self-assembly of supramolecular structures in vitro. The experiments show that fluctuations of a relevant parameter driven from outside, as well as spontaneous fluctuations of local concentration occurring under or near thermodynamic instability, and non-linear interactions between these two types of fluctuations, can trigger or enhance the self-assembly of supramolecular order. The pattern generated by spontaneous fluctuations is capable of setting the canvas for the resulting self-assembled structure. Experiments performed so far concern two diverse systems: a polysaccharide widely found in nature, which makes firm aqueous biostructural gels (agarose), and a synthetic model system of bioelastomers, the polypentapeptide (Val-Pro-Gly-Val-Gly)$_n$ which represents the most significant sequence of the bioelastomeric protein, elastin. Work on the latter system was and is being done in collaboration with D.W. Urry's group of Birmingham, AL.

A set of experiments (Sciortino et al., 1986) was prompted by the remark that self-assembly of biostructures in vivo usually occurs under more or less random fluctuations of relevant parameters, such as pH, temperature, ionic strength etc. (for a review, see Palma-Vittorelli and Palma, 1987; Palma-Vittorelli, 1988). Self-assembly of supramolecular order in agarose-water systems was studied under randomly fluctuating temperature (Sciortino et al., 1986). Comparison of the structural order obtained in the presence of "temperature-noise", with that obtained in isothermal conditions showed the existence of an additional noise-induced order, well above theoretical predictions (Fig.1, left).

The role of spontaneous concentration fluctuations occurring when the same system is in its region of thermodynamic instability was investigated by low-angle light scattering, high-
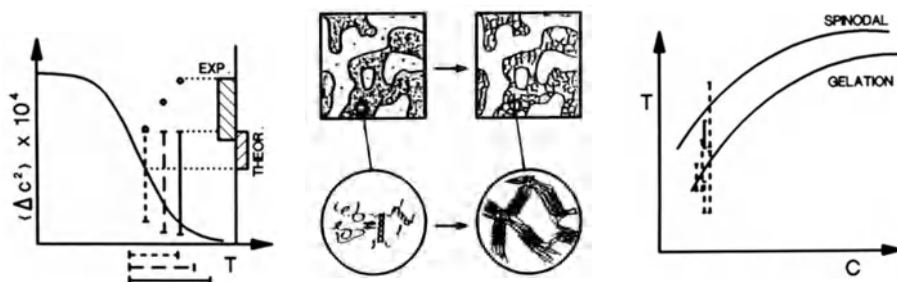
Fig.1. Left: The order parameter of the self-assembled supramolecular structure of 2% w/w agarose in water, obtained in the presence of a fluctuating temperature (dots) is compared with that obtained at a steady temperature (full line). Amplitudes of temperature fluctuations in the three experiments are indicated by segments parallel to the temperature axis. Center: In the same system, the spinodal separation is shown to set the canvas for the structure of the supramolecularly ordered, firm gel. Right: Spinodal and gelation lines delimiting the instability region (for the same system). Ranges of temperature fluctuations in different experiments are indicated by vertical segments. Noise-induced order is substantially amplified when temperature fluctuates within the instability region (continuous segment), where spontaneous concentration fluctuations are also present.

sensitivity turbidity spectra, quasi-elastic light scattering, and viscosity measurements. Fluctuations growing within a narrow wavelength window generate a spinodal decomposition, whose structural pattern is maintained in the gel (Fig.1, center). Self-organization is thus preceeded and triggered by self-sustained fluctuations of concentration leading to spinodal decomposition (San Biagio et al., 1986a, 1986b, Leone et al., 1987, Palma-Vittorelli and Palma, 1987, Palma-Vittorelli, 1988).

Another set of experiments (Carollo, 1986, Trapanese, 1988, M.B. Palma-Vittorelli et al., unpublished) on noise-induced order in different regions of the phase diagram has revealed a striking enhancement of the ordering effect of noise in the case of non-linear-interactions between spontaneous fluctuations and the externally driven random changes of temperature (Fig.1, right).

Finally, anomalous concentration fluctuations occurring in the region of thermodynamic stability, but close to the instability region, have been recently shown to have a triggering role in the supramolecular self-assembly process leading to bioelastogenesis (Sciortino, 1988; Sciortino et al., 1988). Indeed, as an effect of these fluctuations, the overlap of elastomeric coils required for the self-assembly of a bioelastomeric structure (San Biagio et al., 1988) becomes possible even in the region of thermodynamic stability, when the instability region is

approached closely enough for the damped concentration fluctuations to reach the sufficient amplitude.

In conclusion, from the experimental results available so far, it appears that: i) undamped fluctuations occurring in conditions of thermodynamic instability; ii) damped fluctuations occurring in the vicinity of an instability region; iii) externally imposed fluctuations of a relevant parameter, and iv) their joint operation, all show a positive role in triggering and enhancing the self-organization of supramolecular order. Specific features of the latter may conceivably reflect specific recognition and attachment patterns at a molecular level. This is a question addressed by an ongoing computer simulation study of spinodal decomposition on a system of some 8000 particles having a non-spherically symmetric attachment pattern (Fornili et al.1988).

References

Carollo CM (1986) Thesis. Palermo

Fornili SL, Bruge' F, Madonia R, Martorana V, Palma-Vittorelli MB (to be published)

Leone M, Sciortino F, Migliore M, Fornili SL, Palma-Vittorelli MB (1987) Order Parameters of Gels and Gelation Kinetics of Aqueous Agarose Systems: Relation to the Spinodal Decomposition of the Sol. Biopolymers 26: 743-761

Palma-Vittorelli MB, Palma MU (1987) Thermodynamic and Microscopic Aspects of Stability and Functional Interactions of Biomolecules in Solutions. In: Schowen RL and Barth A (eds) Adv. in Bioscences vol 65. Pergamon Press, New York, pp. 281-289

Palma-Vittorelli MB (1988) Molecular Interactions in Aqueous Solutions: the Role of Random Fluctuations of external Parameters and of their Thermodynamic Instabilities. Int'l J. of Quantum Chemistry (to appear in the Dec. issue)

Palma-Vittorelli MB, Carollo MC, Trapanese M (to be published)

San Biagio PL, Madonia F, Newmann J, Palma MU (1986a) Sol-Sol Structural transition of Aqueous Agarose Systems. Biopolymers 25: 2255-2269

San Biagio PL, Newman J, Madonia F, Palma MU (1986b) A Sol-Sol Transition as the First Step in the Gelation of Agarose Sols. Biomol. Str. Dyn. 3: 277-285

San Biagio PL, Madonia F, Trapane TL, Urry DW (1988) Overlap of Elastomeric Polypeptide Coils in Solution, required for Single-Phase Initiation of Elastogenesis. Chem. Phys. Lett. (in the press)

Sciortino F, Lapis M, Carollo CM, Fornili SL, Palma-Vittorelli MB (1986) Self-assembly of Supramolecular Structures: Experiments on Noise-induced Order. Biomol. Str. Dyn. 3: 287-297

Sciortino F, Prasad KU, Urry DW, Palma MU (1988) (submitted for publication) Spontaneous Concentration Fluctuations initiate Bioelastogenesis

Sciortino F (1988) Ph.D. Thesis (in preparation) Palermo

Trapanese M (1988) Thesis. Palermo

# Structure-Function Studies of the Actin Filament System of *Acanthamoeba*

Thomas D. Pollard

Karen A. Magnus[*]

Stephen Doberstein

Pascal Goldschmidt-Clermont

Donald A. Kaiser

Laura Machesky

Sutherland Maciver

David L. Rimm

Daniel Wachsstock

Department of Cell Biology and Anatomy
[*]Department of Biophysics
The Johns Hopkins Medical School
Baltimore, MD 21205, USA

Work in many laboratories on actin polymerization and the accessory proteins that regulate its assembly has progressed to the stage where we now can focus in detail on the structures and mechanisms of action of these essential protein components of the cytoplasmic matrix. The overall mechanism of actin polymerization is clear and the rate constants for the main steps are known. The inventory of the regulatory proteins is now large enough that we likely have in hand, from one cell or another, representatives of the major functional classes. The primary structures of actin and many of the regulatory proteins are known and their mechanisms of action partially deciphered. The long-term goal of research in the field is to provide an explanation at the molecular and cellular levels of how the actin system is assembled and remodeled during the life of the cell.

One of the major impediments to progress in the field is a lack of information about the 3-dimensional structures of these proteins including actin and myosin. This deficiency is particularly acute because the assembly and regulation of the actin cytoskeleton is largely a problem in macromolecular structure. We have started to fill this void by determining the structure of an Acanthamoeba profilin at atomic resolution and have crystallized a second Acanthamoeba actin-binding protein called actophorin. By combining this structural data with biophysical and biochemical studies of these proteins, we are beginning to understand how they work. Further, our work together with data from other investigators on the primary structure of a variety of actin binding proteins suggests how the family of actin-binding proteins may have evolved from a few small precursor proteins.

## Assembly of actin

The polymerization of actin is now understood in enough detail, that the process of spontaneous polymerization can be described by a few differential equations and rate constants (Reviewed by Pollard and Cooper, 1986). There are 5 main steps:

-NUCLEATION where actin monomers form dimers and then trimers (the nuclei)

-ELONGATION where actin monomers bind or dissociate from the ends of filaments

-FRAGMENTATION/ANNEALING where whole filaments break or join end to end

-NUCLEOTIDE HYDROLYSIS where ATP is split and the phosphate dissociates

-NUCLEOTIDE EXCHANGE where ATP or ADP bind to and dissociate from monomers.

It is generally agreed that the formation of trimer nuclei is highly unfavorable, but the nucleation reactions are poorly understood owing to the lack of assays for the intermediates in the process. We believe that the instability of dimers and trimers is due to very large dissociation rate constants, on the order of $10^5$ $s^{-1}$ for dimers, but this needs to be verified experimentally.

Nucleation is affected by at least 3 of the Acanthamoeba actin binding proteins. The complex of an actin monomer with profilin cannot participate in nucleation (Pollard and Cooper, 1984). Consequently profilin profoundly inhibits nucleation since the reactions are highly dependent on the concentration of actin monomers. Actobindin also inhibits nucleation, likely by binding to an intermediate such as dimers (Lambooy and Korn, 1986). On the other hand, capping protein strongly promotes nucleation by stabilizing intermediates in the normal reaction, most likely actin dimers (Cooper and Pollard, 1985). In the cell, profilin and actobindin may suppress spontaneous nucleation, so that all filaments formed can be initiated specifically by capping protein and other proteins that favor nucleation such as vertebrate gelsolin.

Elongation is understood in detail since there are good assays available to measure reaction rates and to provide absolute values for the rate constants for each reaction (e.g. Pollard, 1986). The filament has 2 distinct ends, named "barbed" and "pointed", from the polarity of myosin binding. At the barbed end, the association of ATP-actin is a rapid, diffusion-limited reaction with a rate constant of $10^7$ $M^{-1}s^{-1}$. Association at the pointed end is about 5 times slower. The dissociation of ATP-actin from both ends occurs at a rate of about 1 $s^{-1}$, so at steady state the concentration of ATP-actin ($= k_-/k_+$) required for growth (the critical concentration) is higher at the pointed end than the barbed end. At the barbed end ADP-actin binds more slowly but dissociates faster than ATP-actin, while at the pointed end ADP-actin binds and dissociates more slowly than ATP-actin. Given that ATP hydrolysis occurs subsequent to the incorporation of subunits, the dominant reactions at steady state are the association and dissociation of ATP-actin at both ends with rates of about 1 molecule $s^{-1}$. However, at steady state, the monomer concentration will be intermediate between the critical concentrations at the 2 ends, so that there will be net addition of subunits at the barbed end balanced by net dissociation at the pointed end. The elongation rate constants indicate that this subunit flux is very slow and damped to an unknown extent by the fact that ADP-actin dissociates more slowly than ATP-actin at the pointed end. The available information predicts that under

physiological conditions the filaments should be stable and constant in length over periods of minutes to hours even in the absence of regulatory proteins.

Elongation is regulated by several Acanthamoeba actin-binding proteins. Actin-profilin complexes do not add to the pointed end, but both the complexes and profilin seem to bind to and cap the barbed end (Pollard and Cooper, 1984). The binding of profilin to the barbed end is exceptionally weak ($K_d$ = 50 uM), so that low concentrations of profilin have little effect on barbed end elongation. However, in the cell the total concentration of profilin concentration is 100 uM, so if it is free, profilin may inhibit growth at the barbed end. Actophorin binds to actin monomers and inhibits their incorporation at both ends of filaments (Cooper et al, 1986). Capping protein binds to the barbed end with high affinity ($K_d < 10^{-9}$M) and blocks actin monomer addition (Cooper et al, 1984). In the cell at steady state, we expect that most of the filaments are capped by capping protein and that most of the unpolymerized actin molecules are tied up by profilin and actophorin. This further suggests that most of the cytoplasmic actin filaments are relatively stable.

Actin filaments are fairly strong, but even in unstirred samples at room temperature they occasionally break. This is detected by careful analysis of the time course of polymerization (Wegner and Savko, 1982; Cooper et al 1983) and can be inhibited by tropomyosin, which binds along the length of the filaments and stabilizes them (Hitchcock-DeGregori et al, 1988). Actophorin strongly promotes the fragmentation of actin filaments, presumably by destabilizing bonds within the polymer and thus increasing the likelihood that thermal forces will fracture the filament. Actin filaments can also anneal end to end, but this is detected only when the filaments are short and their number concentration is high, such as after shearing long filaments into short pieces. Under these conditions there is a rapid, transient burst of annealing with an association rate constant in the diffusion limited range that persists until the diffusion of the filaments becomes restricted by their increasing length (Murphy et al, 1988).

When ATP-actin polymerizes, the bound nucleotide is slowly hydrolyzed to ADP and $P_i$ after each subunit is incorporated into the polymer (Pollard and Weeds, 1984; reveiwed by Korn et al, 1987). Remarkably, the $P_i$ remains tightly bound to the polymer for long times (Carlier and Pantaloni, 1986) and transiently gives the filament some of the properties of an ATP-actin polymer (Rickard and Sheterline, 1986; Carlier and Pantaloni, 1988).

Since the nucleotide content of the actin subunits affects assembly, the exchange of nucleotides by monomers can be considered a step in the assembly reaction. These exchange reactions are exceedingly complicated and modulated by the effects of divalent cations on the conformation of the actin (Frieden and Patane, 1988). In the cytoplasm, the ionic milieu and ATP concentration should assure that the bulk of the actin monomers have a bound ATP.

## The structure and function of Acanthamoeba profilin

The primary structures of the profilin isoforms called profilin-I and profilin-II were first determined by amino acid sequencing (Ampe et al, 1985; Ampe et al 1987) and the nucleotide sequences of cloned cDNAs have provided some minor corrections (Pollard and Rimm, unpublished

data). Southern blots revealed single genes for profilin-I and profilin-II, so it seems likely that the initial impression (Ampe et al, 1985) that there are 2 profilin-I isoforms may have been due to contamination by profilin-II. Comparison of the amoeba profilin sequences with those of yeast (Oschsner et al, 1987), bovine and human (Kwiatkowski and Bruns, 1988) profilins reveals that all can be aligned from end to end. There are several potential sites in the C-terminal half of the invertebrate profilins for the extra 14 amino acids in the vertebrate profilins. It seems likely that all of these profilins have similar structures, although the primary structures of the known profilins have diverged enough from each other during evolution that the overall homology was not appreciated initially. The various profilins also differ somewhat in their properties. For example, human platelet profilin inhibits barbed end elongation of platelet actin filaments more efficiently than Acanthamoeba profilin inhibits elongation of Acanthamoeba actin filaments.

Acanthamoeba profilin-I readily crystallizes out of ammonium sulfate and yields high quality x-ray diffraction patterns (Figure 1; Magnus et al, 1986). We have also crystallized Acanthamoeba profilin-II (Figure 2) and human platelet profilin. We used multiple heavy atom isomorphous replacement to calculate phases of the profilin-I reflections and to calculate the initial electron density maps. Through model building and refinement, we have improved these phases and obtained a provisional model of profilin-I at 2.4 A resolution. Determination of this structure was slowed by the absence of cysteine and methionine for heavy atom labeling and as landmarks in the heavy atom map and by the small average size of the amino acid side chains (the average residue molecular weight is only 106). In spite of the fact that secondary structure predictions anticipated no alpha- or beta-structure, virtually the whole molecule appears to consist of alpha-helices and beta-sheets. Beginning at the N-terminus, there are 6 beta sheets, an alpha helix, 2 more sheets and 5 more helices. The bottom of the molecule consists of 5 sheets, the middle section consists of 2 helices and 3 sheets and the top 4 helices. In this model the bottom half is largely uncharged, while the top half has a cluster of positively charged side chains.
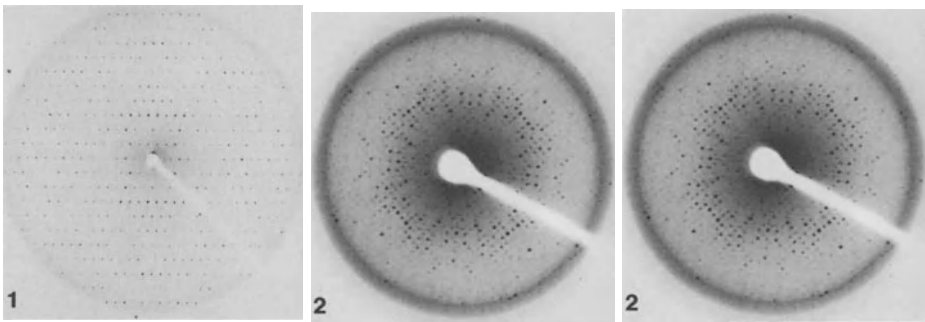


Figures: X-ray diffraction patterns. (1) A screened precession photograph of the hko zone of a crystal of profilin-I. The edge of the pattern corresponds to 3 A resolution. (2) A screened hko precession photograph of a crystal of profilin-II. The edge of the pattern is at a resolution of 5.5 A. (3) A screened precession photograph of the hol zone of a crystal of actophorin. The edge of the pattern is at a resolution of 3 A.

We have established an actin binding site on the profilin by chemical crosslinking and sequencing of the crosslinked peptides (Pollard et al, 1989). A water soluble carbodiimide forms a

zero length isopeptide bond between profilin lysine-115 and actin glutamic acid-365. Lysine-115 is located in the positively charged, alpha-helical region on the top of the profilin molecule. Remarkably, 2 larger actin filament capping proteins, vertebrate gelsolin and Physarum fragmin, have a stretch of primary sequence homology that flanks lysine-115 of the amoeba profilins (Ampe and Vandekerckhove, 1987). We speculate that this is a common site where all three of these proteins bind to the barbed end of actin filaments. Further, the fact that fragmin consists of 3 homologous domains (Ampe and Vandekerckhove, 1988) and gelsolin of 6 homologous domains (Kwiatkowski et al, 1986), suggests that both molecules may have arisen from a primitive profilin-like actin binding protein by multiple cycles of gene duplication. If true, these larger molecules may have a linear structure composed of profilin-like domains.

We speculate that acidic lipid micelles inhibit the binding of actin to profilin by competing directly for the actin binding site on the positively charged top surface of the profilin molecule. We confirmed the observation of Lassing and Lindberg (1985) that micelles of acidic phospholipids, especially phosphatidylinositol 4,5-bisphosphate (PIP$_2$), can inhibit the action of profilin on actin polymerization. Both vertebrate (Goldschmidt et al, unpublished) and Acanthamoeba (Machesky et al, unpublished) profilins bind to PIP$_2$ micelles with a stoichiometry of 1 profilin per 6-10 lipid molecules. In the case of human profilin the binding to PIP$_2$ is very strong. Since the lipid micelles have a negative surface charge, we predict that they bind ionically to the positively charged top half of the amphipathic profilin molecule and compete directly with actin for binding to profilin. Given the high concentration of profilin in amoebas (100 uM) and platelets (50 uM), this new information about the stoichiometry, affinity and mechanism of profilin binding to PIP$_2$ suggests that profilin may also regulate lipid metabolism by modulating the availability of PIP$_2$ as a substrate for phospholipases.


## Structure and function of actophorin

Acanthamoeba actophorin is a 15 kD protein that inhibits actin polymerization by sequestering actin monomers, but paradoxically it also stimulates that late stages of spontaneous polymerization (Cooper et al, 1986). We have attributed the stimulation of spontaneous polymerization to the ability of the protein to fragment actin filaments. In these ways, actophorin resembles depactin from echinoderm eggs (Mabuchi, 1983).

From the sequences of isolated peptides and cloned cDNAs, we have established the primary structure of actophorin. Although antibodies to actophorin and depactin fail to crossreact (Mabuchi and Pollard, unpublished data), there is extensive sequence similarity between the 2 proteins (Maciver et al, unpublished), with 30% identities and 54% conservative substitutions (Takagi et al, 1988). There is also sequence similarity between actophorin and the consensus repeating domain of dystrophin, the high molecular weight protein product of the gene responsible for muscular dystrophy. As in the case of profilin, actophorin may be a prototype for the domain structure of some of the larger actin-binding proteins.

Actophorin rapidly grows into large crystals suitable for x-ray diffraction analysis (Figure 3; Magnus et al, 1988). Given the presence of a reactive cysteine and 3 methionines, we anticipate that structure determination using multiple isomorphous heavy atom derivatives should be more straightforward for actophorin than profilin. Since we already have in hand a 1:1 complex of actin and actophorin crosslinked by carbodiimide, we hope to be able to identify the site on the actin molecule where filament destabilization occurs.

## Interaction of alpha-actinin and actophorin in crosslinking actinin filaments

Alpha-actinin is the major actin filament crosslinking protein of Acanthamoeba (Pollard et al, 1986) and it has a remarkable effect on the mechanical properties of the filaments (Sato et al, 1987). At high rates of deformation, it causes a large increase in the viscosity and stiffness of actin filaments, while at low rates of deformation it has little or no effect. We believe that the explanation lies in the weak binding of alpha-actinin to actin filaments, resulting at equilibrium in the binding and dissociation of crosslinks on a millisecond time scale. Hence, at low rates of deformation, the physical connections between the polymers can rearrange more rapidly than the displacement of the filaments.

Actophorin modulates this interaction in a fascinating way. At optimal concentrations, it can increase the viscosity and stiffness of the alpha-actinin/actin filament network by more than an order of magnitude, while at lower or higher concentrations, it has a smaller to no effect on the physical properties. This was unexpected, since all concentrations of actophorin reduce the viscosity and stiffness of actin filaments alone, presumably by fragmenting the filaments, and since capping protein, another protein that limits the length of actin filaments, only reduces the viscosity and stiffness of alpha-actinin/actin. The explanation of this paradoxical behavior seems to lie in the ability of these optimal concentrations of actophorin to promote the bundling of actin filaments by alpha-actinin. These bundles are large enough to be visualized by light microscopy and appear to be exceedingly stiff. Presumably, a modest reduction in the size of the actin filaments by actophorin favors their lateral alignment by alpha-actinin. Since the local concentration of actin in these bundles is higher than in random networks, the formation of bundles may secondarily strengthen the crosslinking process.

## Concluding remarks

Our experience to date suggests that new information about the 3-dimensional structures of the proteins in the actin system will provide considerable new insight into their functions and will stimulate new biochemical and biophysical work on their mechanisms of action. One presumes that this approach will reveal how the system works in the cell. Although unproven at this time, we expect that information about molecular structure will also reveal how the actin-binding proteins are related to each other by evolutionary gene duplication and mutation. We anticipate that such

insights will allow one to summarize how the actin cytoskeleton works in a few general principles that will greatly simplify the apparent diversity and complexity that we must now contend with in the field.

Literature References

Ampe C, Sato M, Pollard TD, Vandekerckhove J (1987) The primary structure of the basic isoform of Acanthamoeba. Eur J Biochem 170:597-601

Ampe C, Vandekerckhove J (1987) The F-actin capping proteins of Physarum-polycephalum - CAP42(A) is very similar, if not identical, to fragmin and is structurally and functionally very homologous to gelsolin - CAP42(B) is Physarum actin. EMBO J 6:4149-4157

Ampe C, Vandekerckhove J, Brenner SL, Tobacman L, Korn ED (1985) The amino acid sequence of Acanthamoeba profilin. J Biol Chem 260:834-840

Carlier MF, Pantaloni D (1986) Direct evidence for ADP-Pi-F-actin as the major intermediate in ATP-actin polymerization - rate of dissociation of Pi from actin-filaments. Biochem 25:7789-7792

Carlier MF, Pantaloni D (1988) Binding of phosphate to F-ADP-actin and role of F-ADP-Pi-actin in ATP-actin polymerization. J Biol Chem 263:817-825

Cooper, JA, Blum, JD, Pollard TD (1984) Acanthamoeba capping protein properties, mechanism of actin, immunologic cross-reactivity, and localization. J Cell Biol 99:217-225

Cooper JA, Blum JD, Williams RCJr, Pollard TD (1986) Purification and characterization of actophorin, a new 15,000 dalton actin binding protein from Acanthamoeba castellanii. J Biol Chem 261:477-485

Cooper JA, Buhle EL, Jr, Walker SB, Tsong TY, Pollard TD (1983) Kinetic evidence for a monomer activation step in actin polymerization. Biochemistry 22:2193-2202

Cooper JA, Pollard TD (1985) Effects of capping protein on the kinetics of actin polymerization. Biochemistry 24:793-799

Frieden C, Patane K (1988) Mechanism of nucleotide exchange in monomeric actin. Biochemistry 27:3812-3820

Hitchcock-DeGregori SE, Sampath P, Pollard TD (to be published) Tropomyosin inhibits the rate of actin polymerization by stabilizing actin filaments. Biochemistry

Korn, ED, Carlier, MF and Pantaloni, D (1987) Actin polymerization and ATP hydrolysis Sceince 238:638-644.

Kwiatkowski DJ, Bruns GAP (1988) Human profilin - molecular-cloning, sequence comparison, and chromosomal analysis. J Biol Chem 263:5910-5915

Kwiatkowski DJ, Stossel TP, Orkin SH, Mole JE, Colten HR, Yin HL (1986) Plasma and cytoplasmic gelsolins are encoded by a single gene and contain a duplicated actin-binding domain.  Nature 323:455-458

Lambooy PK, Korn ED (1986) Purification and characterization of actobindin, a new actin monomer-binding protein from Acanthamoeba-castellanii.  J Biol Chem 261:7150-7155

Lassing I, Lindberg U (1985) Specific interaction between phosphatidylinositol 4,5-biphosphate and profilactin.  Nature 314:472-474

Mabuchi I (1983) An actin depolymerizing protein (depactin) from starfish oocytes: properties and interactions with actins.  J Cell Biol 97:1612-1621

Magnus KA, Lattman EE, Sato M, Pollard TD (1986) Crystallization of Acanthamoeba profilin-I.  J Biol Chem 261:13360-13361

Magnus KA, Maciver SK, Pollard TD (to be published) Crystallization of actophorin, an actin filament severing protein from Acanthamoeba J Biol Chem

Murphy DB, Gray RV, Grasser WA, Pollard TD (1988) Direct demonsration of actin filament annealing in vitro.  J. Cell Biol 106:1947-1954

Oechsner U, Magdolen V, Bandlow W (1987) The cDNA and deduced amino acid sequence of profilin from Saccharomyces cerevisiae.  Nucleic Acids Res 15:9078

Pollard TD (1986) Rate constants for the reactions of ATP- and ADP-actin with the ends of actin filaments.  J Cell Biol 103:2747-2754

Pollard TD, Cooper JA (1984) Quantitative analysis of the effect of Acanthamoeba profilin on actin filament nucleation and elongation.  Biochemistry 23:6631-6641

Pollard TD, Cooper JA (1986) Actin and actin-binding proteins.  Ann Rev Biochem 55:987-1035

Pollard TD, Tseng PC-H, Rimm DL, Bichell DP, Williams RC Jr, Sinard J and Sato M (1986) Characterization of alpha-actinin from Acanthamoeba.  Cell Motil & Cytoskeleton 6:649-661

Pollard TD, Kaiser DA, Vandekerckhove J (to be published) Identification of an actin-profilin-I contact by chemical crosslinking and sequencing

Pollard TD, Weeds AG (1984) The rate constant for ATP hydrolysis by polarized actin.  FEBS Lett 170:94-98

Rickard JE, Sheterline P (1986) Cytoplasmic concentrations of inorganic phosphate affect the critical concentration for assembly of actin in the presence of cytochalasin D or ADP J Mol Biol 191:273-280

Sato M, Schwarz WH, Pollard TD (1987) Dependence of the mechanical-properties of actin alpha-actinin gels on deformation rate.  Nature 325:828-830

Takagi T, Konishi K, Mabuchi I (1988) Amino-acid sequence of starfish oocyte depactin.  J Biol Chem 263:3097-3102

Wegner A, Savko P (1982) Fragmentation of actin filaments.  Biochemistry 21:1909-1913

# Equilibrium and Kinetics of the Assembly of Capping Proteins with the Ends of Actin Filaments

Albrecht Wegner

Institute of Physiological Chemistry

Ruhr-University Bochum

D-4630 Bochum

Federal Republic of Germany

Abstract

We report on the determination of equilibrium and rate constants and of the stoichiometry of binding of capping proteins to the barbed ends of actin filaments. Equilibrium constants can be measured by the depolymerizing effect of capping proteins on actin filaments. When a capping protein blocks monomer consumption at the polymerizing barbed ends of treadmilling actin filaments, monomers continue to be produced at the depolymerizing pointed ends until a new steady state is reached in which monomer production at the pointed ends is balanced by monomer consumption at uncapped barbed ends. This method was applied to determination of the equilibrium constants $K_g$ for binding of the gelsolin-actin complex in the presence of micromolar $Ca^{2+}$-concentrations ($K_g$ above $10^{11}$ $M^{-1}$) and in excess EGTA ($K_g = 10^{10}$ $M^{-1}$) and for binding of the capping protein from bovine brain ($K_g = 2 \times 10^9$ $M^{-1}$). Retardation of nucleated actin polymerization brought about by highly purified vinculin was analyzed in terms of the number of vinculin molecules bound to the ends of actin filaments. The fraction of barbed ends of actin filaments occupied by vinculin was determined based on the decrease of the rate of polymerization. A plot of the fraction of barbed ends occupied by vinculin versus the free vinculin concentration was sigmoidal, indicating that vinculin binds cooperatively to the barbed ends of actin filaments. According to a Hill plot representation at least three vinculin molecules were found to bind to a barbed end in a cooperative manner. Rates of capping can be measured by inhibition of polymerization of actin filaments. Possible formation by capping proteins of new filaments

which polymerize toward the pointed ends, can be prevented by
keeping the monomer concentration below the critical monomer
concentration of the pointed ends where the barbed ends of
treadmilling filaments polymerize and the pointed ends depolymerize.
By using this method the gelsolin-actin complex was found to bind
fourfold faster to the barbed ends in the presence of micromolar
$Ca^{2+}$ ($10x10^6$ $M^{-1}$ $s^{-1}$) than in excess EGTA ($2.5x10^6$ $M^{-1}$ $s^{-1}$).


## Introduction

A number of capping proteins has been isolated during the last
years. Most of these proteins, if not all, bind to the barbed ends
of actin filaments to inhibit polymerization and depolymerization
at these ends. Some of these capping proteins have additional
functions. They can nucleate new actin filaments which polymerize
toward the pointed ends, or they can sever actin filaments. It is
still unclear whether or not capping proteins which bind to the
pointed ends, occur in cells (Oosawa et al., 1987). In our
laboratory we investigated binding of the capping protein from
bovine brain, of the gelsolin-actin complex and of vinculin to the
barbed filament ends in terms of equilibrium and rate constants and
of the stoichiometry. Major contributions to quantitative studies
on capping reactions have been reported also by other laboratories
(Cooper et al., 1985; Northrop et el., 1986).


## Equilibrium constants for binding of capping proteins to barbed filament ends

For determination of binding of capping proteins we utilized the
ability of actin filaments to treadmill, i. e. to polymerize
preferentially at the barbed ends and to depolymerize simultaneously
at the pointed ends. When a capping protein binds to a polymerizing
barbed filament end, monomer consumption is inhibited at these ends
while monomers are still produced at the depolymerizing pointed
ends. A graphic representation of the depolymerizing effect of
capping proteins is depicted in Fig. 1. On capping the monomer
concentration increases until a new steady-state monomer
concentration $c_1$ is reached at which monomer consumption at uncapped
barbed ends is balanced by monomer production at the pointed ends.
Thus, the monomer concentration reached following addition of a
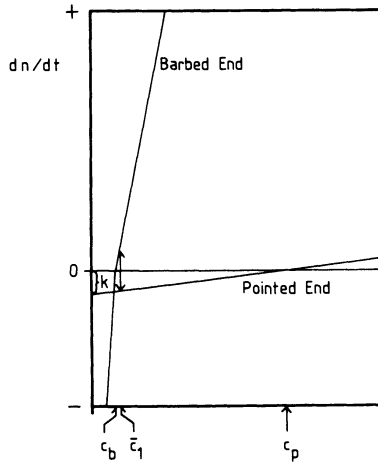
Fig. 1: Plot of the polymerization rate (number of subunits n per time t) versus monomer concentration. $c_p$, critical monomer concentration of the pointed end. $\bar{c}_1$, steady-state monomer concentration at which filaments polymerize at the barbed end at the same rate as they depolymerize at the pointed ends. When all barbed ends are capped, only the pointed ends contribute to consumption and production of monomers, so that the monomer concentration increases from $\bar{c}_1$ to $c_p$.

capping protein depends on the fraction of uncapped barbed ends of filaments. One can set up an equation which correlates the equilibrium constant for binding of a capping protein to a filament end $K_g$ with the actin monomer concentration $c_1$ and the rate constants of actin polymerization:

$$c_1 - \bar{c}_1 = \frac{(k_b^+ \bar{c}_1 - k_b^-) \, K_g \, P_{tot}}{k_b^+ + k_p^+ + k_p^+ K_g \, P_{tot}} \tag{1}$$

The rate constants are defined in Fig. 2. $P_{tot}$ is the total concentration of capping protein. Details of the derivation of eqn. (1) have been discussed by Wanger and Wegner (1985) and by Selve and Wegner (1986b). The rate constants $k_b^+$, $k_p^+$ and $k_b^-$ have been determined (Pollard, 1986; Selve and Wegner, 1986b) and can be used for determination of the equilibrium constant according to eqn. (1). However, it is also possible to determine the rate constants newly. A relatively simple method for determination of $k_b^+$, $k_p^+$ and $k_b^-$ has been described by Selve and Wegner (1986b).

$$\xrightleftharpoons[k_b^-]{k_b^+} \quad \ggg\ggg\ggg \quad \frac{k_p^+}{k_p^-}$$

$$K_g \quad k_g^+ \,\big\|\, k_g^-$$

$$\bullet\!\!\ggg\ggg\ggg \quad \frac{k_p^+}{k_p^-}$$
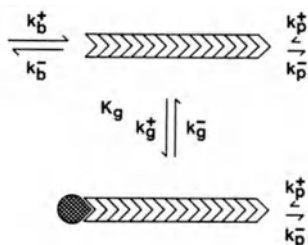
Fig. 2: Reaction scheme of binding of a capping protein to the barbed end of a treadmilling actin filament. The polar structure of actin filaments is indicated by the chevron symbol of the subunits. $K_g$, equilibrium constant for binding of the capping protein to the barbed end. $k_g^+$, rate constant for binding of the capping protein, $k_g^-$, rate constant for dissociation of the capping protein. $k_b^+$, $k_p^+$, rate constants of binding of an actin monomer to the barbed or pointed end, respectively. $k_b^-$, $k_p^-$, rate constants of dissociation of a subunit from the barbed or pointed end, respectively.

A plot of the concentration of the capping protein from bovine brain versus the actin monomer concentration is displayed in Fig. 3. Also curves calculated according to eqn. (1) are depicted. A good fit was obtained for $K_g = 2\times10^9$ $M^{-1}$. At first sight it is surprising that at half saturation of filaments with capping protein ($1/K_g = 0.5$ nM) almost no increase of the monomer concentration is observed. This has to do with the fast association and dissociation of actin molecules at the barbed ends compared to association and dissociation at the pointed ends. Thus, the barbed ends have a great weight in determining the monomer concentration (Wanger and Wegner, 1985). Fig. 3 shows that 25 nM capping protein are necessary for half maximal increase of the monomer concentration. At that concentration 99 percent of the barbed ends are capped. Thus, capping of a substantial fraction of filaments is required for a detectable increase of the monomer concentration. The equilibrium constant $K_g$ for capping of actin filaments by the gelsolin-actin complex was determined in a similar manner. $K_g$ turned out to be about $10^{10}$ $M^{-1}$ in excess EGTA and in the range of or above $10^{11}$ $M^{-1}$ if micromolar $Ca^{2+}$ concentrations were present (Selve and Wegner, 1986b). Based on an analogous type of approach the equibrium constant for capping by villin has been estimated to be higher than $10^{11}$ $M^{-1}$ (Walsh et al., 1984).
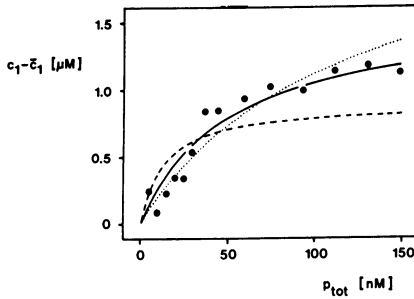
Fig. 3 : Monomer concentration $c_1$ versus the total concentration of capping protein from bovine brain $p_{tot}$. $\bar{c}_1$, steady-state monomer concentration (see Fig. 1). ● , experimental results. Continuous line, curve calculated for $K_g = 2 \times 10^5$ $M^{-1}$. The two other curves are displayed in order to show the sensitivity of the fit to the choice of $K_g$ and the parameters $k_b^+$, $k_p^+$ and $k_b^-$ (see Wanger and Wegner, 1985).

## Stoichiometry of binding of vinculin to the barbed filament ends

Investigations on the mode of interaction of vinculin with actin have been controversial. It has been doubted even if vinculin is an actin-binding protein. However, more recently evidence has been provided for the suggestion that vinculin is an actin-binding protein which retards actin polymerization by binding to the barbed ends of actin filaments (Ruhnau and Wegner, 1988; Wilkins and Lin, 1982; Gaertner et al., 1988). Vinculin has been shown not to nucleate or sever actin filaments. This protein is particularly easy to be analyzed because no side reactions interfere with the capping reaction. As vinculin does not change the cancentration of actin filaments, one can analyze the rate of actin polymerization nucleated by a constant concentration of filament ends in terms of the fraction of actin filaments occupied by vinculin. The fraction y of actin filaments occupied by vinculin has been shown to be given by (Gaertner et al., 1988):

$$y = \frac{t_i - t_a}{t_i} \frac{k_b^+ + k_p^+}{k_p^+} \tag{2}$$

where $t_i$ and $t_a$ are the times necessary for half maximal polymerization in the presence or absence of vinculin, repectively. The rate constants $k_b^+$ and $k_p^+$ are defined in Fig. 2. In Fig. 4 a plot of the fraction y of filaments occupied by vinculin versus the vinculin concentration is depicted. This binding curve is not hyperbolic as
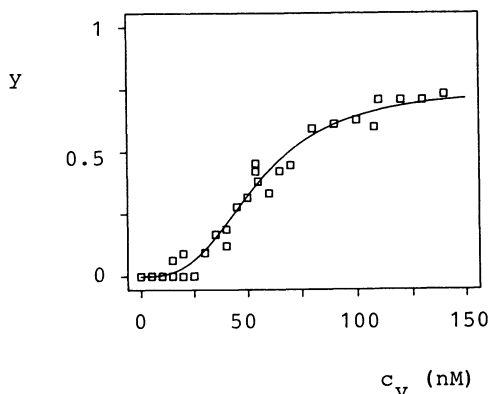
Fig. 4: Binding curve of vinculin to actin filaments. $c_v$, vinculin concentration. y, fraction of barbed ends of actin filaments occupied by vinculin. □ , experimentally determined values. Continuous line, binding curve calculated for the assumption that three vinculin molecules bind to the barbed end in a highly cooperative manner.

expected for binding of a single vinculin molecule to the barbed end. The sigmoidal shape of the binding curve suggests that several vinculin molecules bind to a barbed end of an actin filament in a cooperative manner (Gaertner et al., 1988).

Rate constants of the capping reaction

The rate of binding of capping proteins to filament ends can be determined in principle easily. The rate at which actin polymerization is inhibited by binding of capping proteins, has to be measured. An example for inhibition of polymerization by the gelsolin-actin complex is depicted in Fig. 5. One has to take into account a few points: (i) Some capping proteins have also other functions. For instance, gelsolin severs and nucleates actin filaments and the gelsolin-actin complex nucleates actin filaments which polymerize toward the pointed ends. When one measures inhibition of actin polymerization by capping, one has to exclude interferences from other activities of the capping proteins. Nucleation activity can be easily suppressed by keeping the monomer concentration below the critical monomer concentration of the pointed ends. Under this condition polymerization at the pointed ends of nuclei does not occur. There is no way to overcome severing activity. (ii) As
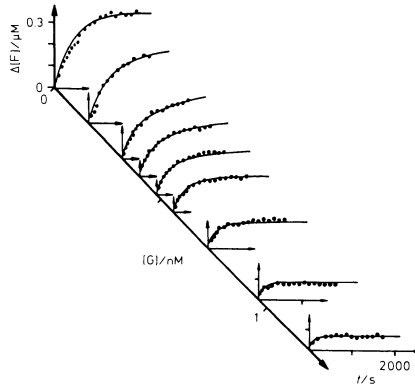
Fig. 5: Inhibition of actin polymerization by the gelsolin-actin complex. The polymerization of 0.5 $\mu M$ monomeric actin was nucleated by 0.4 $\mu M$ polymeric actin.$\Delta [F]$, increase of the concentration of polymeric actin. $[G]$ , concentration of the gelsolin-actin complex. The continuous lines were calculated for a rate constant of capping $k_g^+ = 1.1 \times 10^7 \ M^{-1} \ s^{-1}$.

binding of the capping protein to the barbed ends of filaments is followed by inhibition of polymerization, binding of the capping protein and actin polymerization should proceed at similar rates. Therefore, one has to explore experimental conditions where actin polymerizes at a similar rate as the capping protein binds. The rate of polymerization can be altered by changing the concentration of filament ends and the rate of capping can be varied over a wide range by using different concentrations of capping protein.

The rates of capping and of actin polymerization at the barbed ends can be expressed in terms of concentrations of capping protein p, of uncapped filament ends $c_e$, of the total concentration of filament ends $c_{etot}$ and of the actin monomer concentration $c_1$ (Fig. 2):

$$\frac{d \ p}{d \ t} = \frac{d \ c_e}{d \ t} = -k_g^+ \ p \ c_e + k_g^- \ (c_{etot} - c_e) \qquad (3)$$

$$\frac{d \ c_1}{d \ t} = -k_b^+ \ c_1 \ c_e + k_b^- \ c_e \qquad (4)$$

In deriving eqn. (4) it has been assumed that the contribution of the pointed ends to the change of the monomer concentration is negligible. This approximation is justified as the rate constants of the pointed ends are at least ten-fold lower than those of the

barbed ends (Pollard, 1986; Selve and Wegner, 1986b). Polymerization curves can be fitted by numerically solving eqns. (3) and (4) and fitting the rate constants $k_g^+$, $k_g^-$, $k_b^+$ and $k_b^-$. It is also possible to determine $k_b^+$ and $k_b^-$ independently by described methods (Selve and Wegner, 1986b). One can also take into account monomer production at the pointed ends as described by Selve and Wegner (1986b).

The rate of capping by the gelsolin-actin complex has been determined. 0.5 µM monomeric actin which is below the critical monomer concentration of the pointed ends, was polymerized onto polymeric actin in the presence of nanomolar concentrations of gelsolin-actin complex. Fig. 5 shows that with increasing gelsolin-actin complex concentrations actin polymerization is more and more inhibited. Curves fitted according to eqns. (3) and (4) are depicted in Fig. 5, too. The curves were calculated for irreversible binding ($k_g^- = 0$). The rate constant $k_g^+$ turned out to be $10^7$ $M^{-1}$ $s^{-1}$ at micromolar $Ca^{2+}$-concentrations. In excess EGTA $k_g^+$ was found to be $2.5 \times 10^6$ $M^{-1}$ $s^{-1}$ (Selve and Wegner, 1986a; Selve and Wegner, 1986b).

## Conclusions

The methods described in this paper permit quantification of the capping reaction. Quantitative analysis of this reaction may lead to a better understanding of the regulation of actin polymerization and organization by regulatory proteins. Perhaps, when more rates of reactions occuring during assembly and disassembly of the cytoskeleton are measured, one will obtain more insight into the sequence of molecular events during the turnover of actin filaments.

## References

Cooper, J. A., and Pollard, T. D. (1985) Biochemistry 24, 793-799.

Gaertner, A., Ruhnau, K., and Wegner, A. (1988) Eur. J. Biochem., in press.

Northrop, J., Weber, A., Mooseker, M. S., Franzini-Armstrong, C., Bishop, M. F., Dubyak, G. R., Tucker, M., and Walsh, T. P. (1986) J. Biol. Chem. 261, 9274-9286.

Oosawa, M., Shimaoka, S., Funatsu, T., Ishiwata, S., and Maruyama, K. (1987) J. Biochem. (Tokyo) 101, 1481-1483.

Pollard, T. D. (1986) J. Cell Biol. 103, 2747-2754.

Ruhnau, K., and Wegner, A. (1988) FEBS Lett. 228, 105-108.

Selve, N., and Wegner, A. (1986a) Eur. J. Biochem. 155, 397-401.

Selve, N., and Wegner, A. (1986b) Eur. J. Biochem. 160, 379-387.

Walsh, T. P., Weber, A., Higgins, J., Bonder, E. M., and Mooseker, M. S. (1984) Biochemistry 23, 2613-2621.

Wanger, M., and Wegner, A. (1985) Biochemistry 24, 1035-1038.

Wilkins, J. A., and Lin, S. (1982) Cell 28, 83-90.

# Lithium, Thiocyanate and Actin Assembly

New insights into an old concept from chemical embryology.

R.Colombo, A.Milzani
Dept.of Biology, Univ.of Milan, Via Celoria 26, 20133 MILAN (Italy)

S.Doglia
Dept.of Physics, Univ.of Milan, Via Celoria 16, 20133 MILAN (Italy)

P.Giordano
Italian Biotechn.Foundation, Via Hajech 10, 20129 MILAN (Italy)

Chemical embryologists demonstrated that morphogenetic patterns can be disarranged by treating whole eggs with chemical agents.

As shown by Herbst (1892), $Li^+$ promotes the development of entoderm while other agents, like thiocyanate, induce entoderm disappearance. At present, chemical animalization and vegetalization of embryo were not clearly explained.

We demonstrated here that LiCl and NaCNS, chemicals with antithetical influence on embryonic development, also have an opposite effect on actin polymerization.

As shown in Table 1, LiCl (100mM) polymerizes actin more efficiently than KCl (as also stated by Pan and Ware, 1988).

### TABLE 1
Ion-dependence of actin polymerization maximum rate

| Ion | $Mg^{++}$ 2mM | $Ca^{++}$ 2mM | $Li^+$ 100mM | $K^+$ 100mM |
|---|---|---|---|---|
| Max increase of fuoresc. intensity (a.u./min) | 0.235 | 0.071 | 0.046 | 0.035 |

TABLE 1: G-actin samples (0.5mg/ml; 10% was pyrene-actin) were polymerized by addition of different salts. Rabbit muscle actin was obtained according to Spudich & Watt (1971) and then gel-filtered on Sephadex G-150 as suggested by McLean-Fletcher & Pollard (1982). Pyrene-actin was prepared according to Tellam & Frieden (1982).

NaCNS, on the contrary, inhibits actin assembly (Table 2)

TABLE 2
Inhibitory effect on actin polymerization by NaCNS

| NaCNS concentration | 0.05M | 0.1M | 0.5M |
|---|---|---|---|
| % inhibition of the max fluorescence increase | 77 | 94 | 99 |

TABLE 2: Actin samples $(0.5\text{mg/ml}; 10\%$ was pyrene-actin) were polymerized by addition of 2mM $MgCl_2$ + 100mM KCl and in the presence of different concentrations of NaCNS. The maximum rate of fluorescence increase of control samples was assumed as 100%. The percentage inhibition values, relative to each different NaCNS concentration, were obtained by difference. Informations on the actin extraction procedure and the preparation of the fluorescent protein are reported in the legend of Table1.

and markedly depolymerizes F-actin (as summarized in Fig.1).
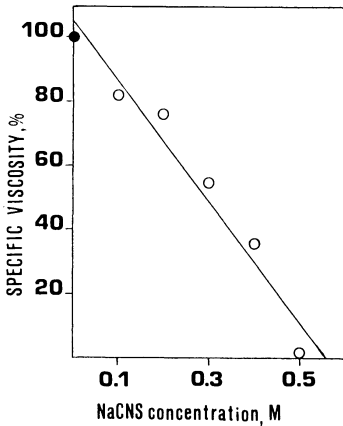


Fig.1 - G-actin samples $(0.5\text{mg/ml})$ were polymerized overnight by the addition of 2mM $MgCl_2$ + 100mM KCl. The steady-state specific viscosity was determined in several control samples. Other identical steady-state samples, treated with different concentrations of NaCNS (treated samples) and then (after 20 min) the specific viscosity was further tested.
In the diagram the specific viscosity of control is assumed as 100%.
The stright-line represents the linear regression calculated on viscosity values of treated samples.
Pure actin was obtained as in Table 1.

We obtained comparable results by viscometric, spectrofluorometric and electron microscopic experiments. Also cell cultures, treated with the considered chemicals and then stained to evidence F-actin, showed the sensitiveness of polymeric actin structures to the action of the two mentioned chemical compounds (not shown).

Since F-actin has a key role in generating mechanical forces which lead to the establishment of morphogenetic patterns (Shimizu, 1986), we suggest that LiCl and NaCNS could disarrange early embryonic development by their strong action on the G-actin/F-actin steady-state. Not all chemicals which interfere with the correct establishment of the animal/vegetal embryonic axis, could likely disarrange early embryonic development by affecting actin assembly.

In our opinion, it should be considered that the ooplasmic segregation process includes two main mechanisms: 1) Actin-mediated transport (AMT) of organelles and/or macromolecules through egg cytoplasm. 2) Localized specific activity (LSA) of transported cytoplasmic material.

It is clear that two chemically unrelated compounds, one of which inhibits the AMT of a determined organelle or macromolecule and the other which affects the LSA of the same biological entity, could disarrange to a similar extent, though by different ways, the correct embryonic development.

## REFERENCES

Herbst C. (1892) Exp.Unters.uber den Einfluss der veranderten Chemischen Zusammensetzung des ungebenden Mediums auf die Entwicklung der Tiere.
Zeitschr.f.wiss.Zool., 55, 446.

McLean-Fletcher S. & Pollard T.D. (1980) Identification of a factor in conventional muscle actin preparations which inhibits actin filament self-association.
Biochem.Biophys.Res.Comm., 96, 18-27.

Pan X.X. & Ware B.R. (1988) Actin assembly by lithium ions.
Biophys.J., 53, 11-16.

Shimizu T. (1986) Bipolar segregation of mitochondria, actin network and surface in Tubifex eggs: role of cortical polarity.
Dev.Biol., 116, 241-251.

Tellam R. & Frieden C. (1982) Cytochalasin D and platelet gelsolin accelerate actin polymer formation. A model for regulation of the extent of actin polymer formation in vivo.
Biochemistry, 21, 3207-3214.

# Procollagen Processing Control of Type I Collagen Fibril Assembly

David J S Hulmes[1], A Paul Mould[2], Karl E Kadler[3], John A Chapman[2] & Darwin J Prockop[3]

[1]Department of Biochemistry, University of Edinburgh, George Square, Edinburgh EH8 9XD, UK
[2]Departments of Medical Biophysics/ Biochemistry & Molecular Biology, University of Manchester, Oxford Road, Manchester M13 9PT, UK
[3]Department of Biochemistry & Molecular Biology, Jefferson Medical College, Thomas Jefferson University, Philadelphia 19107, USA

1. Introduction

Vertebrate collagens constitute a family of at least twelve genetic types that shows remarkable diversity in molecular structure and supramolecular assembly (Mayne & Burgeson, 1987). Types I, II and III collagens assemble *in vivo* to form fibrils of uniform diameter, near circular cross-section and with a characteristic axial periodicity of 65 to 67 nm (D). Fibrils *in vivo* are long (several μm) and diameters range from 8 nm to 500 nm, depending on collagen type, species, age and tissue of origin (Parry & Craig, 1984). The mechanisms that control fibril shape and diameter *in vivo* are poorly understood.

As an *in vitro* model for collagen fibril formation *in vivo*, the reconstitution of fibrils from extracted and purified collagens has been studied for several years (Holmes et al., 1986). On neutralisation and warming of cold, acidic solutions of collagen, fibrils form spontaneously that closely resemble the fibrils observed in tissues. Such reconstitution of fibrils *in vitro*, as monitored by turbidity at 313 nm, is accompanied by an initial lag phase followed by a sigmoidal growth phase. This curve, which is characteristic of many polymerisation reactions, has been interpreted in terms of classical nucleation and growth models (Wallace & Thompson, 1983) with multiple stages of assembly (Farber et al., 1986). The critical concentration for assembly is low (Williams et al., 1978) but finite (Na, 1988).

Reconstitution studies have shown that many factors may contribute to the control of fibril formation *in vivo*, e.g. temperature (Wood & Keech,1960), interactions with proteoglycans (Chandrasekhar et al., 1984; Vogel et al., 1987) or interactions between different collagen types (Lapiere et al., 1977; Adachi & Hayashi, 1986; Wotton et al., 1988). But the reconstitution approach is inherently limited, since fibril forming collagens assemble *in vivo* from their biosynthetic precursors, procollagens (Fig. 1; Prockop & Kivirikko, 1984). Procollagen molecules are secreted into the extracellular matrix where enzymatic processing to collagen occurs with the removal of N- and C-terminal propeptides by specific N- and C-terminal procollagen proteinases (Tanzawa et al., 1985; Hojima et al., 1985; Kessler et al., 1986; Halila & Peltonen, 1986). According to the pathway of processing different processing intermediates pN-collagen and pC-collagen are produced (Fig. 1). The exact site of processing, in relation to the cell surface, is unknown.

TYPE I PROCOLLAGEN MOLECULE

pN-COLLAGEN

pC-COLLAGEN

COLLAGEN MOLECULE
(300 nm)
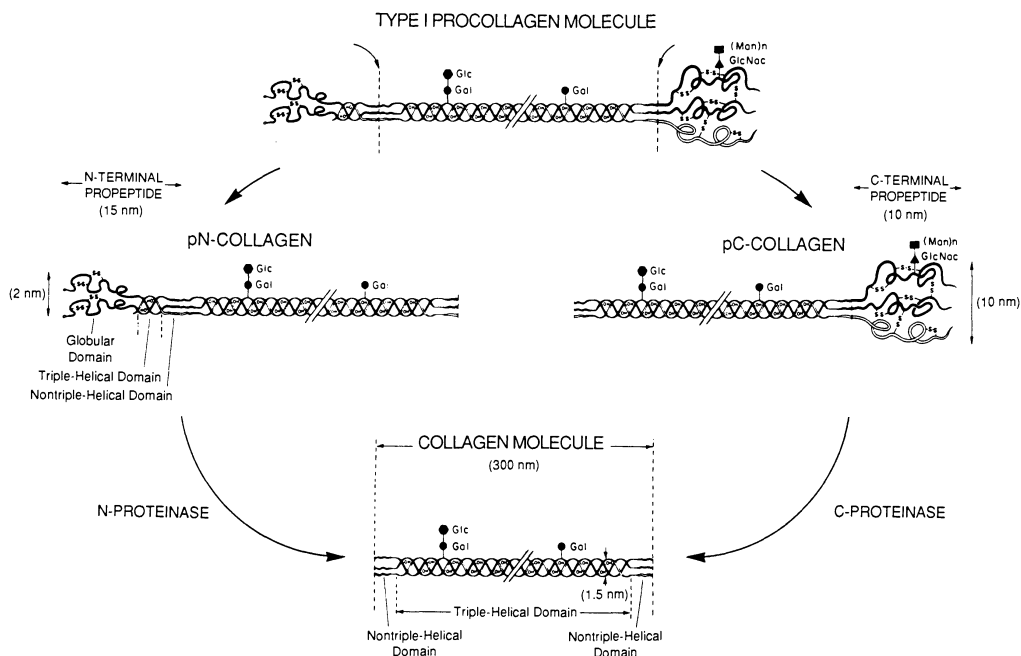
Fig. 1. Structure and enzymatic processing of the type I procollagen molecule (based on Prockop et al. (1979), with permission).

The pathway of procollagen processing appears to vary with collagen genetic type (Uitto et al., 1979; Fessler et al., 1981) and stage in development (Mellor, Atkins & Hulmes, unpublished observations). Processing intermediates can persist in normal tissue (Veis et al.,1973) and ultrastructural immunolocalisation studies have revealed an association of N-propeptides and C-propeptides with small and large diameter fibrils, respectively (Fleischmajer et al.,1987). These and other observations (Hulmes et al., 1983; Mould & Hulmes, 1987) have prompted the suggestion that procollagen propeptides can control assembly *in vivo*, and, according to the pathway of processing, determine collagen fibril diameter.

## 2. Fibril formation *de novo*

The hypothesis that procollagen processing controls fibril formation *in vivo* can now be tested *in vitro* with a system for the study of fibril formation *de novo* (Miyahara et al., 1982; Kadler et al., 1987, 1988; Prockop et al., this volume). In this system, purified type I procollagen may be exposed to highly purified N- and C-terminal procollagen proteinases, either separately or in combination, for subsequent monitoring of processing and assembly under physiological buffer conditions.

The most thoroughly characterised version of the *de novo* system is the assembly of collagen fibrils from pC-collagen in the presence of C-proteinase (Kadler et al., 1987, 1988). The pC-collagen is prepared by N-proteinase digestion of procollagen and purified by gel filtration chromatography.

Fig. 2 shows the results of a typical experiment, where the extent of processing is plotted at various times during assembly. The turbidity curve has a lag phase and sigmoidal growth phase that is reminiscent of the results obtained when fibrils are reconstituted from extracted collagen. Hence the mechanism of collagen assembly from pC-collagen in the presence of C-proteinase may share similar features to earlier reconstitution systems. But the rate of assembly *de novo* can be further controlled by the rate of enzyme processing of the C-propeptide (Kadler, Hojima & Prockop, unpublished observations).
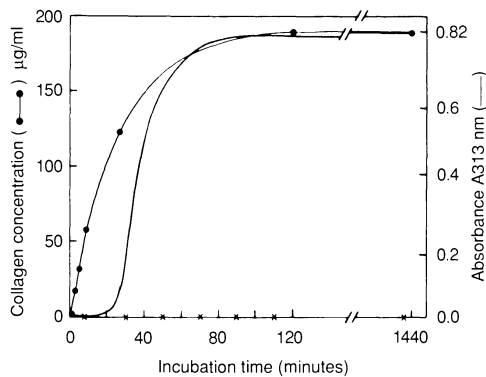


Fig. 2. Formation of type I collagen fibrils *de novo* . Incubation of purified human type I pC-collagen (250 μg/ml) with purified C-proteinase (100 units/ml) at $34^0$ C results in cleavage of the C-propeptide (●—●) and an increase in turbidity (——). In the absence of C-proteinase, there was no cleavage of C-propeptide or increase in turbidity (X—X). (From Kadler et al. (1987), with permission.)

Equilibrium studies with the pC-collagen to collagen system have enabled the critical concentrations for assembly to be monitored at a range of temperatures (Kadler et al., 1987). Critical concentrations were measured directly using a simple centrifugation procedure to pellet the large, fibrillar aggregates. At $37^0$ C, the critical concentration for type I collagen assembly in physiological conditions is approximately 0.4 μg/ml. Similar results have recently been obtained from classical reconstitution studies (Na, 1988).

Electron microscopy of the fibrils formed in the pC-collagen to collagen system revealed a native, D-periodic banding pattern in longitudinal section and approximately circular outlines in cross-section (Fig. 3(a)). Diameters at equilibrium can be very large (>1μm) but these are inversely related to temperature (Hulmes, Kadler, Hojima, Chapman & Prockop, unpublished observations). At $37^0$ C diameters are typically 200 to 600 nm starting with a pC-collagen concentration of 100 μg/ml. This is still an order of magnitude greater than found *in vivo*.

Fig. 2 also shows that when pC-collagen is incubated at 250 μg/ml and at $34^0$ C in the absence of C-proteinase there is no turbidity change or cleavage of the C-propeptide. Hence pC-collagen does not appear to assemble at this concentration, as limited by the sensitivity of turbidimetry.
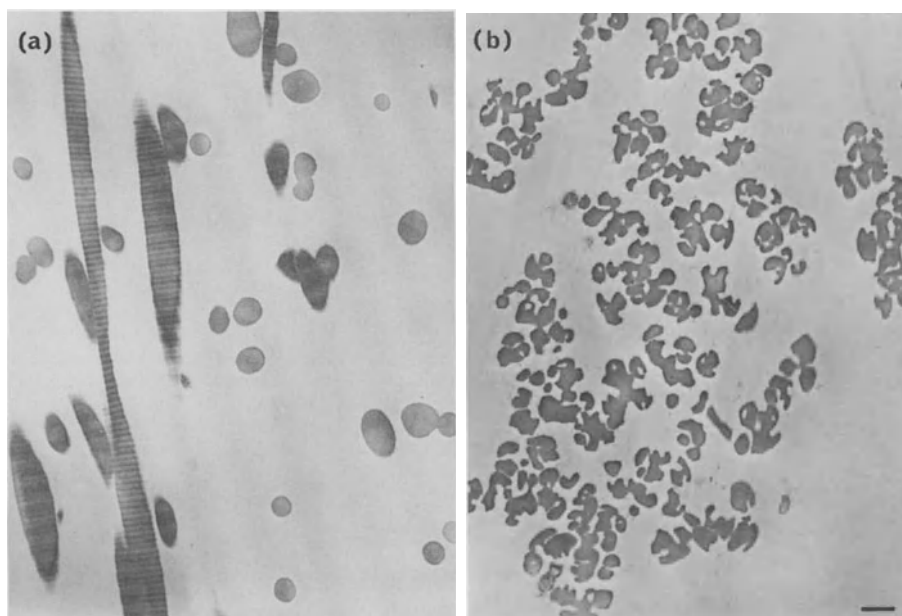
Fig. 3. Electron micrographs of sectioned pellets of fibrillar structures produced *in vitro* with the *de novo* procollagen processing system. (a) Near cylindrical fibrils at various angles of sectioning produced by incubating human type I pC-collagen (320 µg/ml) with C-proteinase (5 units/ml) at 37$^0$ C for 24 h. (b) Fluted fibrils in near transverse section produced by incubating equimolar mixtures of human type I procollagen (60 µg/ml) and human type I pC-collagen (53 µg/ml) with C-proteinase (20 units/ml). Scale bar 300 nm.

### 3. pN-collagen

The properties of newly formed pN-collagen can also be studied *in vitro* by incubation of type I procollagen with C-proteinase (Mould, Kadler, Hulmes, Hojima, Chapman & Prockop, unpublished observations). The solubility of pN-collagen differs markedly from that of pC-collagen.

Fig. 4 shows turbidity curves for pN-collagen assembly when different concentrations of type I procollagen were incubated with C-proteinase, using the same buffer conditions as described by Kadler et al (1987). There is an initial lag phase followed by a sigmoidal growth phase. The proportion of total pN-collagen forming large, light scattering aggregates increases with concentration. Using centrifugation to pellet the aggregates (4 minutes at 13,000 g, room temperature), the limit of solubility for type I pN-collagen at 37$^0$ C in physiological conditions is in the range 150 to 200 µg/ml. In contrast, procollagen and pC-collagen do not appear to assemble in solution at these concentrations.

Electron microscopy revealed that the products of pN-collagen assembly were strikingly different in structure from normal collagen fibrils. The structures are D-periodic but , rather than cylinders, they resemble wide sheets (Fig. 5). The sheets are often folded (as in Fig. 5), they have a uniform thickness of approximately 8 nm and widths up to several micrometres. These structures
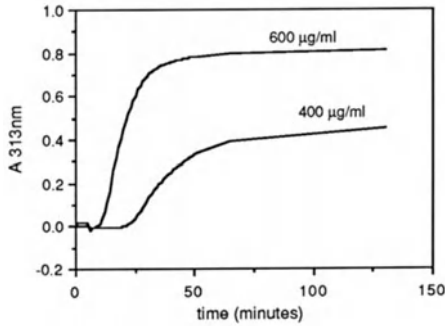
Fig. 4. Assembly of human type I pN-collagen showing the increase in turbidity when different concentrations of human type I procollagen were incubated at $37^0$ C with 50 units/ml C-proteinase. The enzyme was prepared according to the procedure of Hojima et al. (1985).
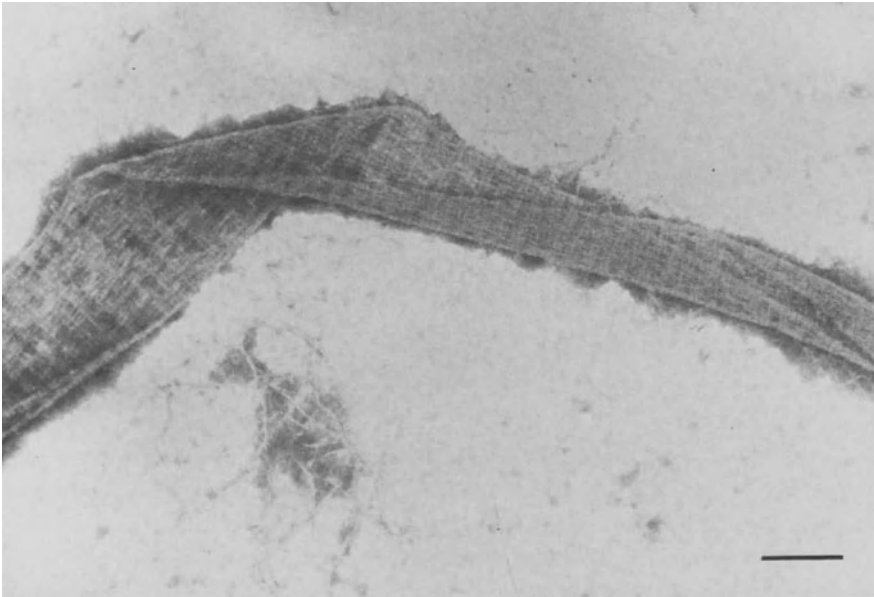


Fig. 5. Electron micrograph of a folded, sheet-like, D-periodic structure produced by *de novo* assembly of human type I pN-collagen. Negatively stained with phosphotungstic acid. Scale bar 300 nm.

differ from previous observations of pN-collagen assemblies reconstituted from extracted pN-collagen (Miyahara et al., 1983), where narrow and irregular fibrils were formed. The observations of Miyahara et al (1983) were based on heterogeneous preparations that contained considerable amounts of cross-linked pN-collagen, collagen and other components. The results illustrated in Figure 5 demonstrate that type I pN-collagen generated *de novo* from procollagen in the

presence of C-proteinase does not form narrow fibrils but instead forms wide sheets. Hence persistence of the N-propeptide markedly affects morphology.

By incubating mixtures of type I procollagen and pC-collagen with C-proteinase, it is possible to study co-precipitation of pN-collagen and collagen (Hulmes, Kadler, Mould, Hojima, Holmes, Cummings, Chapman & Prockop, unpublished observations). Structures assembled after prolonged incubation were collected by centrifugation and analysed by gel electrophoresis (to determine the composition of the pellets) and electron microscopy. Depending on the ratio of pN-collagen to collagen in the pellets, a continuum of D-periodic structures were found from near cylindrical fibrils (collagen alone) to wide sheets (pN-collagen alone). Between these extremes, fibrils were fluted and became progressively more distorted as the proportion of pN-collagen increased. Fig. 3(b) shows examples of such pN-collagen/ collagen fluted fibrils in cross-section. By computer image analysis, a monotonic increase was found in the ratio of fibril perimeter to cross-sectional area with increasing pN-collagen content. The formation of fluted pN-collagen/ collagen hybrid fibrils suggests that pN-collagen can bind to collagen and distort normal collagen fibril morphology.

4. Procollagen

The assembly of type I procollagen into supramolecular structures has been the subject of much research in recent years (Gross & Bruns, 1984; Mould & Hulmes, 1987). Early observations (summarised by Mould & Hulmes, 1987) of filamentous bundles in secretory vesicles, with dimensions corresponding to in-register assemblies of procollagen molecules, led to the hypothesis that the presence of procollagen propeptides gives rise to non-staggered rather than staggered assembly. The presence of similar structures (so called segment-long-spacing (SLS) aggregates) in negatively stained or pelleted and sectioned fibroblast culture medium (Hulmes et al., 1983) supported this hypothesis. Though proteinase inhibitors were added to the otherwise crude culture medium in these experiments, the medium was collected after at least 24h of culture, and so the procollagen had been processed to mixtures of pC-collagen and collagen (Hulmes et al., 1983). Centrifugation studies on the non-concentrated culture medium were inconsistent with the formation of supramolecular assemblies. It was concluded that SLS bundle formation occurs during concentration by prolonged ultracentrifugation or drying on the electron microscope grid.

Studies on purified type I procollagen have also demonstrated non-staggered aggregation, by rotary shadowing (Mould & Hulmes, 1987). Again hydrodynamic studies were inconsistent with aggregation up to a concentration of 800 μg/ml and it was concluded that procollagen aggregation can be a surface-induced phenomenon. These results were in conflict with light scattering observations of procollagen aggregates in solution with particle weights corresponding to approximately 5 procollagen molecules (Berg et al., 1986).

The assembly properties of purified type I procollagen have recently been extended to higher concentrations (Mould & Hulmes, unpublished observations). Fig. 6 shows turbidity curves obtained when concentrated solutions of purified chick procollagen, initially at $4^0$ C, were incubated at $37^0$ C in phosphate buffered saline (10 mM phosphate, 150 mM NaCl, 0.01% $NaN_3$, pH 7.2). Turbidity increased with time in a concentration dependent manner. Using centrifugation to pellet the

298
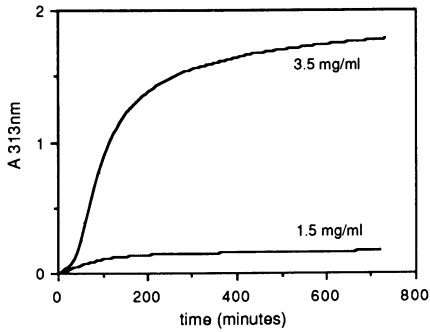


Fig. 6. Assembly of purified chick type I procollagen showing the increase in turbidity when different concentrations of procollagen, initially at $4^0$ C, were incubated in phosphate buffered saline at $37^0$ C.
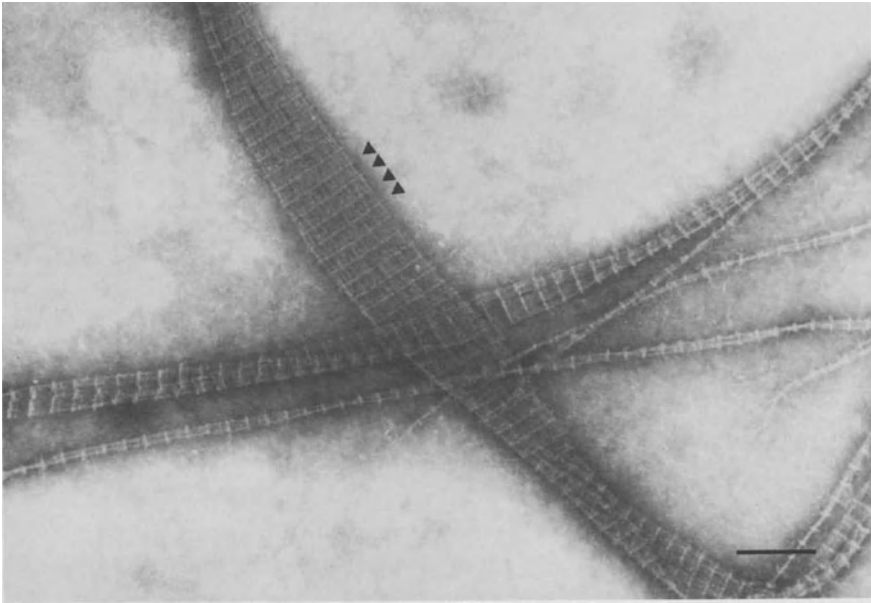


Fig. 7. Electron micrograph of D-periodic procollagen structures produced by incubation of purified chick type I procollagen at high concentration in phosphate buffered saline at $37^0$ C. The prominent stain excluding band at the position expected for the C-propeptide is indicated. Negatively stained with phosphotungstic acid. Scale bar 300 nm.

aggregates, the limit of solubility for chick type I procollagen at $37^0$ C in phosphate buffered saline was found to be in the range 1 to 1.5 mg/ml.

Remarkably, electron microscopy of the products of procollagen assembly revealed D-periodic structures (Fig. 7). SDS gel electrophoresis confirmed that the preparations contained almost entirely

procollagen chains with trace amounts of pC-collagen. The electron microscopic banding pattern after negative staining showed a periodic, prominent stain excluding band in the position expected for the C-propeptide (Fig. 7).

In summary, at sufficiently high concentration, even type I procollagen appears to form D-periodic structures, though possible copolymerisation with trace amounts of processed forms of procollagen cannot be excluded. Similar electron microscopic results and solubility data have been obtained in preliminary studies on purified type I pC-collagen (Mould, Kadler, Hulmes, Chapman & Prockop, unpublished observations).

While SLS aggregates may be intermediates in the formation of D-periodic supramolecular assemblies of procollagen, surface phenomena (Mould & Hulmes, 1987) or interactions with other components of crude culture medium (Hulmes et al., 1983) may give rise to preferential non-staggered assembly in some circumstances.

## 5. Conclusions

Procollagen processing control of type I collagen fibril assembly is probably a highly complex process. Not only collagen but also procollagen and both processing intermediates, pN-collagen and pC-collagen, can undergo concentration dependent supramolecular assembly. Furthermore, the nature of the three-dimensional structures formed is influenced by the persistence or removal of covalently attached N- and/or C-propeptides. For example, persistence of the N-propeptide and removal of the C-propeptide leads to wide sheet-like structures.

Fig. 8 shows a diagrammatic representation of the apparent solubilities of collagen, procollagen and the two processing intermediates at $37^0$ C in physiological conditions. The solubilities of collagen and procollagen differ by over three orders of magnitude. Within this range pN-collagen has an intermediate solubility which is less than that of pC-collagen. Hence, according to the concentrations of these various macromolecules that are present in the extracellular matrix (concentrations which may approach several mg/ml) a variety of different supramolecular structures may form. For example, below protein concentrations of 100 µg/ml only collagen would be expected to assemble. As the protein concentration increases, first pN-collagen then pC-collagen and procollagen would begin to assemble. When mixtures of different macromolecules are present, the complexity increases with possible copolymerisation and the formation of pleomorphic hybrid structures (e.g. pN-collagen and collagen). Furthermore, there may be multiple stages of assembly for each macromolecular species, rather than the simple monomer-aggregate equilibrium depicted in Fig. 8. The solubilities shown correspond to supernatant concentrations after centrifugation for 4 minutes at 13,000 g, a procedure that would not be expected to pellet small sub-assemblies consisting of only a few molecules. Finally, procollagen in the extracellular matrix is subject to continuous enzymatic processing and hence the extent of supramolecular assembly will also be influenced by the assembly kinetics and lifetimes of procollagen and its processing intermediates.

As mentioned in the introduction, several authors have suggested that the pathway of procollagen processing, i.e. the relative rates at which the N- and C-propeptides are enzymatically

300
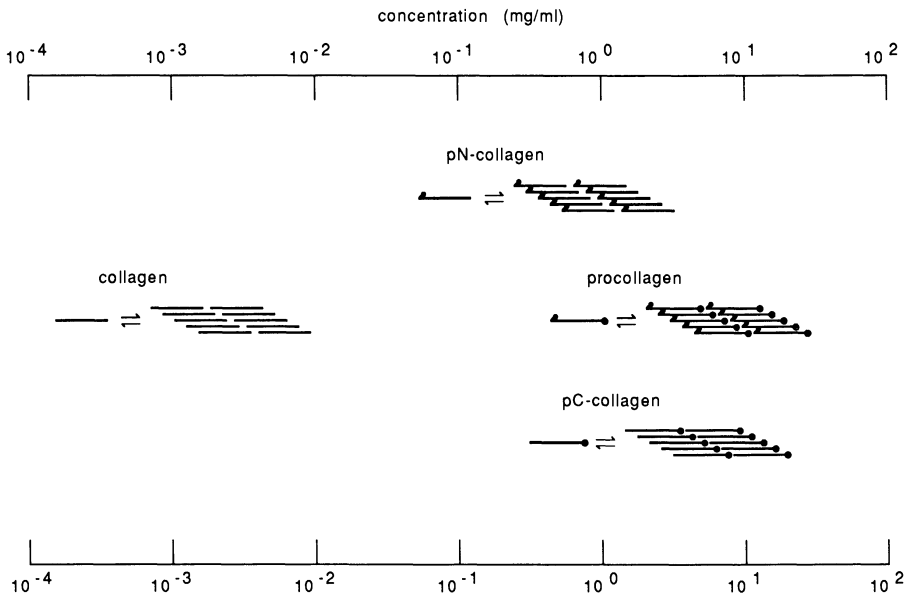


Fig. 8. Diagrammatic representation of the apparent solubilities of type I procollagen, pN-collagen, pC-collagen and collagen plotted on a logarithmic scale. Monomers are depicted in equilibrium with D-periodic assemblies. The mid-points of the equilibria correspond to the observed solubilities in physiological buffers at $37^0$ C. For clarity, possible multiple stages of assembly are not shown. The N-propeptide and C-propeptide are represented as a sharp kink and a large filled circle respectively.

removed, may control collagen fibril diameter. From the above discussion, it is likely that any such control will depend on the particular concentrations of procollagen substrate and the N- and C-terminal processing enzymes. Preliminary results with the *de novo* system (Hulmes, Kadler, Hojima & Prockop, unpublished observations) indicate that such a control mechanism can exist *in vitro* under certain conditions, but a complete understanding of procollagen processing control of type I collagen fibril assembly will take some time yet.

Adachi E, Hayashi, T (1986) *In vitro* formation of hybrid fibrils of type V collagen and type I collagen. Connect Tiss Res 14:257-266

Berg RA, Birk DE, Silver FH (1986) Physical characterization of type I procollagen in solution: evidence that the propeptides limit self-assembly. Int J Biol Macromol 8:177-182

Chandrasekhar S, Kleinman HK, Hassell JR, Martin GR, Termine JD, Trelstad RL (1984) Regulation of type I collagen fibril assembly by link proteins and proteoglycans. Collagen Rel Res 4:323-338

Farber S, Garg A, Birk DE, Silver FH (1986) Collagen fibrillogenesis *in vitro*: evidence for prenucleation and nucleation steps. Int J Biol Macromol 8:37-42

Fessler LI, Timpl R, Fessler JH (1981) Assembly and processing of procollagen type III in chick embryo blood vessels. J Biol Chem 256:2531-2537

Fleischmajer R, Perlish JS, Olsen BR (1987) The carboxylpropeptide of type I procollagen in skin fibrillogenesis. J Invest Dermatol 89:212-215

Gross J, Bruns RR (1984) Another look at fibrillogenesis. In: Trelstad RL (ed) The role of the extracellular matrix in development. Alan R Liss, New York, p 479

Halila R, Peltonen L (1986) Purification of human procollagen type III N-proteinase from placenta and preparation of antiserum. Biochem J 239:47-52

Holmes DF, Capaldi MJ, Chapman JA (1986) Reconstitution of collagen fibrils in vitro; the assembly process depends on the initiation procedure. Int J Biol Macromol 8:161-166

Hojima Y, van der Rest M, Prockop DJ (1985) Type I procollagen carboxyl-terminal proteinase from chick embryo tendons. J Biol Chem 260:15996-16003

Hulmes DJS, Bruns RR, Gross J (1983) On the state of aggregation of newly secreted procollagen. Proc Nat Acad Sci USA 80:388-392

Kadler KE, Hojima Y, Prockop DJ (1987) Assembly of collagen fibrils de novo by cleavage of type I pC-collagen with C-proteinase. J Biol Chem 262:15696-15701

Kadler KE, Hojima Y, Prockop DJ (1988) Assembly of type I collagen fibrils de novo. J Biol Chem 263:10517-10523

Kessler E, Adar R, Goldberg B, Niece R (1986) Partial purification and characterisation of a procollagen C-proteinase from the culture medium of mouse fibroblasts. Collagen Rel Res 6:249-266

Lapiere Ch M, Nusgens B, Pierard GE (1977) Interaction between collagen type I and III in conditioning bundles organisation. Connect Tiss Res 5:21-29

Mayne R, Burgeson RE (1987) Structure and function of collagen types. Academic Press, New York London

Miyahara M, Njieha FK, Prockop DJ (1982) Formation of collagen fibrils in vitro by cleavage of procollagen with procollagen proteinases. J Biol Chem 257:8442-8448

Miyahara M, Bruckner P, Helle O, Prockop DJ (1983) Aggregation of a type I collagen precursor containing N-terminal propeptides. Collagen Rel Res 3:279-293

Mould AP, Hulmes DJS (1987) Surface-induced aggregation of type I procollagen. J Mol Biol 195:543-553

Na GC (1988) UV spectroscopic characterisation of type I collagen. Collagen Rel Res 8:315-330

Parry DAD, Craig AS (1984) Growth and development of collagen fibrils in connective tissue. In: Ruggeri A, Motta PM (eds) Ultrastructure of the connective tissue matrix. Martinus Nijhoff, Boston The Hague, p 34

Prockop DJ, Kivirikko KI, Tuderman L, Guzman NA (1979) The biosynthesis of collagen and its disorders. New Engl J Med 301:13-23,77-85

Prockop DJ Kivirikko KI (1984) Heritable diseases of collagen. New Engl J Med 311:376-386

Tanzawa K, Berger J, Prockop DJ (1985) Type I procollagen N-proteinase from whole chick embryos. J Biol Chem 260:120-1126

Uitto J, Allan RE, Polak KL (1979) Conversion of type II procollagen to collagen. Eur J Biochem 99:97-103

Veis A, Anesey J, Yuan L, Levy SJ (1973) Evidence for an amino-terminal extension in high molecular weight collagens from mature bovine skin. Proc Nat Acad Sci USA 70:1464-1467

Vogel KG, Trotter JA (1987) The effect of proteoglycans on the morphology of collagen fibrils formed in vitro. Collagen Rel Res 7:105-114

Wallace DG, Thompson A (1983) Description of collagen fibril formation by a theory of polymer crystallization. Biopolymers 22:1793-1881

Williams BR, Gelman RA, Poppke DC, Piez KA (1978) Collagen fibril formation. J Biol Chem 253:6578-6585

Wood GC, Keech MK (1960) The formation of fibrils from collagen solutions. Biochem J 75:588-598

Wotton SF, Duance V, Fryer PR (1988) Type IX collagen: a possible function in articular cartilage. FEBS Lett 234:79-82

# Supramolecular Organization of Extracellular Matrices: Analogy with Liquid Crystals

Françoise Gaill
Centre CNRS de Biologie cellulaire
67 rue Maurice Gunsbourg
94205 Ivry cedex 05
France

Three dimensional distributions of collagen fibrils may present configurations similar to those of liquid crystalline phases. There are several types of liquid crystals but the analogy concerns mainly cholesteric liquid crystals (Fig.1a).

This analogy provides a useful approach towards understanding the organization of extracellular matrices. The collagen fibril network of the cuticle of annelids consisting of superimposed layers of collagen fibrils forms an orthogonal plywood (Fig. 1b). This network was suggested to be analogous to the "blue phase" (Gaill and Bouligand 1985)(Fig.1d), a fact demonstrated by Lepescheux (1988).
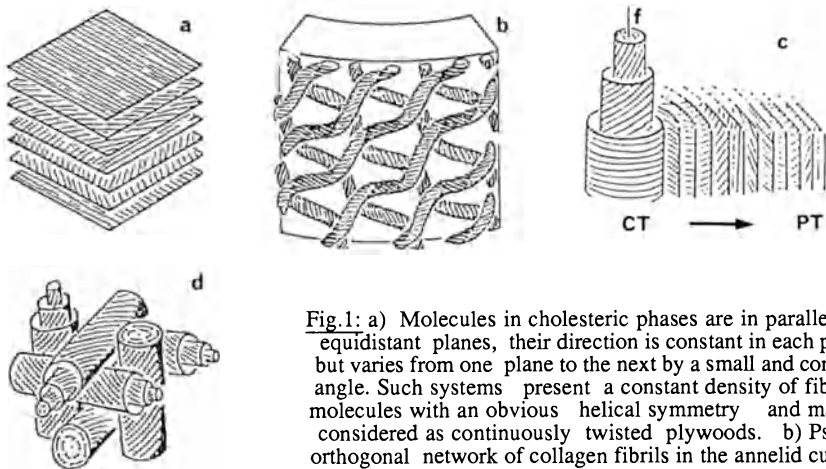


Fig.1: a) Molecules in cholesteric phases are in parallel and equidistant planes, their direction is constant in each plane, but varies from one plane to the next by a small and constant angle. Such systems present a constant density of fibrillar molecules with an obvious helical symmetry and may be considered as continuously twisted plywoods. b) Pseudo orthogonal network of collagen fibrils in the annelid cuticle. The fibrils are supercoiled and are parallel in each layer but their orientation rotates by 90° from one layer to the next. c) One of the model of the blue phase, an organization which appears at the transition from isotropic to cholesteric phases. d) Cuticular fibrils are in fact bundles of microfibrils wrapped around coaxial cylinders and the intrafibrillar organization of the collagen fibrils is that of a double twist: at long distances the cylindrical (or double) twist (CT) is transformed into a planar (or simple) twist(PT). Classical cholesteric systems are frustrated whereas the cuticular fibril is a defrustrated system.

The analogy with the blue phase allow us to explain the regulation of the collagen fibril diameter, using the "frustration" concept ( Fig.1d) : a double twist situation of the collagen microfibrils may occur only locally and cannot be extended to tile space. In this respect, the radius of the fibril cannot increase without modifying the topological relationships between collagen molecules. This is another way to understand the fact that the "twisting of fibrin fibers limits their radial growth" (Weisel et al,1987). Moreover, the increase in collagen fibril length may be explained by the presence of defects which are also observed in liquid crystalline phases ( Lepescheux,1988).

Two broad categories of mechanisms have been suggested to explain the arrangement of the collagen fibril: self assembly or cellular control.

Cuticular microfibrils of annelids are in close relationship with the cell membrane; they are parallel to the microvilli axis and it is possible that the cell play a part in the control of the first step of fibrillogenesis. The cytoskeleton, namely actin, may orientate fibrils via fibronectin (Zylbelberg et al,1988).

Studies on the microvilli density of the cuticle show that the number of fibril orientation decreases as does the fibril diameter when the microvilli density increases, a fact which may result from biomechanical constraints. These constraints may be macroscopic. Generally the collagen fibrils are straight but they are coiled in the annelid cuticle. Using the study of the surface volume ratio of the worm, it has been shown that the variation shape of the worm explained the occurence of supercoiling in the collagen fibrils (Gaill and Bouligand,1987).

The different patterns we describe have been observed *in vivo* in numerous extracellular matrices ( Bouligand and Giraud Guille, 1985, Trelstad and Coulombre,1971, Bard and Bansal,1987, Giraud-Guille,1988; Gaill et al 1988) as well as *in vitro* (Bouligand et al ,1985, Giraud Guille,1987)). These results show that the same constraints organize assemblies of collagen molecules *in vivo* and *in vitro*. The fact that all these types of organization present analogies with liquid crystals leads us to think that the same principle, a self assembly process, is acting in liquid crystal systems and in biological systems.

Some organization types observed *in vitro* are not observed *in vivo* and we think that this may be explained by the fact that the self assembly of collagen molecules is regulated by both biomechanical constraints and cellular control (Fig.2).

304

Fig. 2: Studies on the collagen
fibrils of the cuticle of annelids
have shown that the assembly
of collagen fibrils is
a self assembly process regulated
by two main types of factors:
biomechanical constraints and
cellular information.
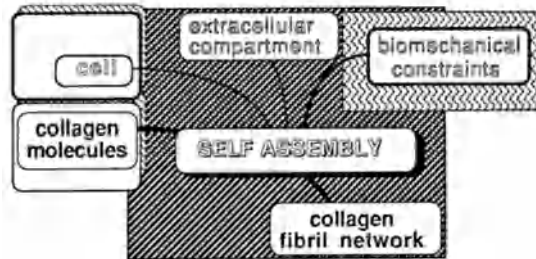
Bard JBL, Bansal MK (1987) The morhogenesis of the chick primary corneal stroma:I New observations on collagen organization in vivo help explain stromal deposition and growth Development 100:135-145

Bouligand Y,Giraud-Guille MM (1985) Spatial organization of collagen fibrils in skeletal tissues: analogies with liquid crystals. In Bairati A and Garrone R (ed) Biology of Invertebrate and Lower Vertebrate Collagens, Plenum Publishing Corporation, New York London, 93:115-134

Bouligand Y, Denèfle JP, Lechaire JP, Maillard M (1985) Twisted architecture in cell-free assembled collagen gels: study of collagen substrates used for cultures.Biol Cell 54:143-162

Gaill F, Bouligand Y (1985) Long pitch helices in invertebrate collagens. In Bairati A and Garrone R (ed) Biology of Invertebrate and Lower Vertebrate Collagens, Plenum Publishing Corporation, New York London, 93:267-276

Gaill F, Bouligand Y (1987) Supercoiled of collagen fibrils in the integument of an abyssal annelid.Tiss Cell 19: 625-642

Gaill F, Herbage D, Lepescheux L (1988) Cuticule structure and composition of two invertebrates.Oceanol Acta in press

Giraud-Guille M.M. (1987) Cholesteric twist of collagen *in vivo* and *in vitro*.Mol Cryst Liq Cryst 153:15-30

Giraud-Guille MM (1988) Twisted plywood architecture of collagen fibrils in human compact bone osteons. Calcif Tissue Int 42:167-180

Lepescheux L (1988) Spatial organization of collagen in annelid cuticle: order and defetcs. Biol Cell,62:17-31

Trelstad RL, Coulombre AJ (1971) Morphogenesis of the chick cornea.J Cell Biol 50:840-858

Weisel JW, Nagaswami C,Makowski L (1987) Twisting of fibrin fibers limit their radial growth Proc N Acad Sci USA 84:8991-8995

Zylberberg L,Bereiter-Hahn J,Sire JY (1988) Cytoskeletal organization and collagen orientation in the fish scales Cell Tissue Res 253:597-607

**SECTION VI**
**Complex Supramolecular Structures**

# A Modular Model of the Nuclear Pore Complex

Christopher W. Akey
MRC Laboratory of Molecular Biology
Hills Rd., Cambridge   CB2 2QH
England

The nuclear pore complex (NPC) is a singular assembly which spans the double membrane of the nuclear envelope and mediates nucleocytoplasmic transport (for a review see Newport & Forbes,1987). In order to understand these transport processes, I am currently devising methods to solve the 3-dimensional structures of various NPCs, including forms with a dilated central channel (transporter). The first step in this process is determining the 2-dimensional structures and possible inter-relationships of the different classes of NPCs observed in isolated amphibian nuclear envelopes. Cryo-electron microscopy of frozen-hydrated specimens, coupled with image analysis of a 4700 particle globally aligned database, has allowed verification of the NPC model proposed by Unwin & Milligan (1982). The model has been extended to 50-60 angstrom resolution and new features relevant to the *in vivo* function of the assembly have been observed. Significantly, projected structures of the NPC-transporter in different transport-related states have been obtained and an initial model is proposed.

## Model of the pore complex proper

Conceptually, the NPC can be thought of as being comprised of 2 structural entities, the outer structural framework (pore complex proper) and the central channel which has been named the NPC-transporter. The 2 entities appear to be functionally divided as well. The pore complex proper apparently provides a framework which maintains the incompletely fused state of the nuclear envelope, while the central spokes form an "artificial membrane" in which the transporter resides. The transporter is the active site of nucleocytoplasmic transport (Feldherr et al., 1984), a process which involves macromolecular translocation; hence the transporter is a "macromolecular pump".

A diagram demonstrating the modular architecture of the NPC is presented in Figures 1a & b. The detergent-extracted NPC, ignoring attachments to the lamina, is built from 3 co-axial rings along architectural principles consistent with point group symmetry [822] (Milligan, 1986). A centrally-located ring of massive spokes is connected circumferentially at inner radii to form an inner spoke ring (ISR), and is attached to and framed by 2 thin co-axial rings (NR & CR), which appear to be co-planar with the inner (INM) and outer nuclear membranes (ONM). The spokes are further divided radially into 3 domains including the inner spoke domain (IS), the outer spoke domain (OS) which abuts the nuclear envelope and the vertical supports (VS), which are attached to the nucleoplasmic and cytoplasmic thin rings. Furthermore, amphibian NPCs appear to be anchored to the

nuclear envelope in 2 ways. First, a specific interaction between the nucleoplasmic thin ring and the lamina appears to exist. Second, a new feature, the radial arms (RA), projects out past the membrane border giving the NPC an effective diameter of about 1500 angstroms and appear to be candidates for direct membrane anchoring sites.
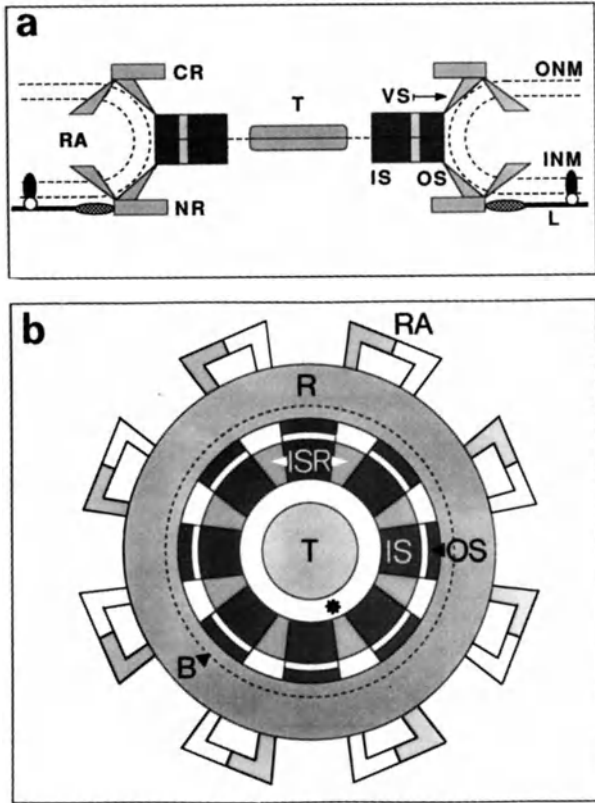


**Figure 1.** **a)** Modular model of the NPC viewed in central cross-section. The position of the radial arms (RA), along the z-axis, has been chosen to minimize the size needed by this structure to project out past the border of the NPC proper to a radius of about 750 angstroms. See text for further details on the model. **b)** The model viewed *en face* . The membrane border is indicated as a dashed circle (B) and a low density feature in the region of the central transporter, is labeled (T). Work on resolving the structure of the transporter is in progress (but see text).

## Model of the NPC-transporter

Global averages from the 4700 particle database have been used to obtain detailed information on the interactions, structure and

conformational flexibility of the pore complex proper (CWA, submitted). However, individual structures within the database consisting of about 200 NPCs, usually demonstrate a weak modulation of the central density, in the region previously identified as the central plug or granule (Unwin & Milligan,1982). A preliminary manual classification of the NPCs from a single micrograph (about 150 total), indicated that the blurred central density is in fact comprised of a superposition of the transporter in different transport-related states. Reconstructions of 2 of these states from the initial analyses are presented in Figure 2 (protein is white). In Figure 2a, the central transporter (labeled T) is apparently closed and has 8 arms radiating from a bright ring of density (A) whose center is hollow (P), giving the impression of an 8-sided star. In Figure 2b, the transporter densities are re-arranged into a strong annulus of 8 peaks, located at higher radii (labeled A'). Additional evidence for this remarkable transformation from a closed to an open state has been obtained from direct observation of individual 8-fold rotationally enforced images in the 4700 particle database (work in progress) and from studies of NPCs caught in the act of translocating nucleoplasmin-gold (CWA & D. S. Goldfarb, submitted).
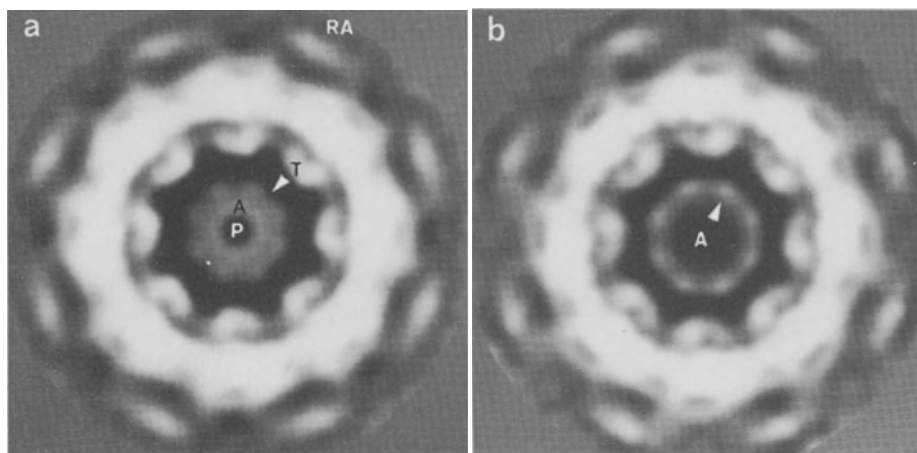


**Figure 2.** Reconstructions of membrane-associated NPCs embedded in vitreous ice which have been manually classified into differing transport states. **a)** In the closed state, the transporter (T) demonstrates an 8-sided star shape with a central bright ring of density (A) which surrounds a pore of about 90 angstroms diameter. The central pore is labeled (P). **b)** In the open state, the transporter density is arranged in an annulus (A') of 8 bright densities at higher radius.

A preliminary model of the transporter has been constructed, based on the observed features of the projection maps coupled with structural considerations of the elements necessary in a macromolecular pump (see Figure 3). The model consists of a disk-like structure of 2 apposed

(possibly puckered) layers oriented in a head-to-head manner, with each layer comprised of 8 subunits radially aligned to form a supramolecular iris. The model can therefore be thought of as a "double-lock" which may control the fidelity of the nuclear transport process and prevent back-streaming of complexes *in transit*. The individual transporter subunit may be composed, in part, of an as yet unidentified mechano-ATPase, which acts in a concerted and cooperative manner to produce the iris-like dilation. The iris subunit also appears to contain some members of the GlcNAc nucleoporins (Akey, C.W. & D.S. Goldfarb, submitted). This model is not meant to be space filling as precise details of the subunit shapes and packing must await a complete analyses of the 2-dimensional database coupled with a 3-dimensional structure determination of at least one transporter state. However, the general features of the model closely mimic observed structural and physiological data. Notably, the model can dilate about 3.5 "f-stops", presumably via a molecular conformational change or hinge-like motion near the radial tips of the subunits, resulting in a range of open states consistent with those needed in nucleocytoplasmic transport *in vivo*. Details of the model, including the number and positions of the pivot points, are currently being refined; however, the model should provide an initial structural framework with which to integrate the results of labeling and transport studies and should allow the rational design of experiments to probe the role of the NPC-transporter in intra-cellular communications processes.
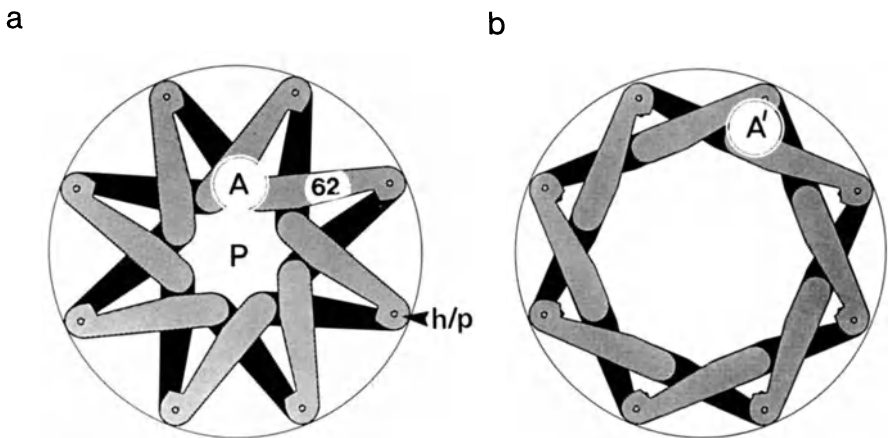


**Figure 3.** A preliminary model of the NPC-transporter: **a)** The closed state consists of 2 layers of 8 subunits, radially aligned as 2 apposed supramolecular irises. Note that the bright ring of density round the central pore in Figure 2a originates from the juxtaposition of 4 subunits at inner radii, labeled (A). The central pore and probable location of np62 are marked (P) & (62), respectively. The location of a pivot or hinge region is also indicated (h/p). **b)** In the fully dilated state, the transporter subunits in each layer have irised open in a motion which can be described

mechanically as a pivot about their distal ends, resulting in the juxtaposition of 4 subunits at larger radii, labeled (A'), to give the bright annulus observed in Figure 2b. No data are currently available on the absolute hand of the individual iris layers.


## Future prospects

The modular architecture of the NPC, as described herein, may reflect an important facet of the intriguing and unknown principles which govern the assembly and disassembly of the complex during mitosis in most eukaryotic cells. Work is now in progress to determine the 3-dimensional structure of this assembly in different transport-related states and should give further insights into the fundamental process of nucleocytoplasmic transport, at molecular dimensions.

## Acknowledgements

## References

Akey, C.W. (submitted) Interactions, structure and conformational flexibility of the Nuclear Pore Complex revealed by cryo-electron microscopy.

Akey, C.W. & D.S. Goldfarb (submitted). Nuclear import requires docking and subsequent dilation of the Nuclear Pore Complex-Transporter.

Feldherr, C.M., Kallenbach,E. & Schultz, N. (1984). Movement of a karyophilic protein through the Nuclear Pores of oocytes. J. Cell Biol. 99:2216-2222.

Milligan, R.A. (1986). A structural model of the Nuclear Pore Complex. In Nucleocytoplasmic Transport (ed. R. Peters & M. Trendelenburg), Springer-Verlag, pp. 113-122.

Newport, J.W. & Forbes, D.J. (1987). The nucleus: structure, function and dynamics. Ann. Rev. Biochem. 56:535-565.

Unwin, P.N.T. & Milligan, R.A. (1982). A large particle associated with the perimeter of the nuclear pore complex. J. Cell Biol. 93:63-75.

# Maps in all Varieties – The Cytoskeleton of *Trypanosoma Brucei*

T. Seebeck, A.K. Schlaeppi, A. Hemphill, M. Affolter, L. Rindisbacher
Institut für Allgemeine Mikrobiologie
Baltzerstrasse 4
3012 BERN    Switzerland

## INTRODUCTION

African trypanosomes, the causative agents of sleeping sickness in man and of Nagana in cattle are an old scourge of mankind, but a new entry to the field of cell biology. These flagellate protozoa have long been the subject of clinical, veterinary and epidemiological research. However, it is not very long since their attraction as model organisms for cell biology has been appreciated. Several reviews have recently appeared which summarize the progress  made in different areas of trypanosomal cell biology, such as glycolysis (Opperdoes, 1987), the lipid-anchoring of external membrane proteins (Ferguson et al., 1988), the genetics of the variable surface glycoproteins (Van der Ploeg, 1987), the organization of the mitochondrial genes (Simpson, 1987), the phenomenon of RNA trans-splicing (Borst, 1986) and posttranscriptional RNA editing (Maizels and Weiner, 1988).

## THE CYTOSKELETON

Early investigations of the cellular architecture of trypanosomes (reviewed by Vickerman and Preston, 1976) have demonstrated that this organism contains a fairly simple cytoskeleton, consisting essentially of three structures:
(i) a prominent microtubular membrane skeleton, which consists of a tight array of closely spaced microtubules which are associated to the cell membrane, and which are laterally connected to each other by a host of yet undefined linker proteins. This membrane skeleton is the only cytoskeletal structure identified so far in the trypanosomal cell body. No transcellular structures have yet been detected.
(ii) the single flagellum contains an axoneme which is very similar to other orthodox eukaryotic flagellar axonemes.
(iii) in addition to the axoneme, the flagellum contains a second prominent structure, the paraflagellar rod. In contrast to the axoneme, with which it is tightly associated, this structure is unique to trypanosomes and euglenoids. Its  function is unclear at present.

TUBULIN

The trypanosomal cell contains a number of different microtubule populations (membrane skeleton, mitotic apparatus, flagellar axoneme) which differ in function, in-vivo turnover rates and in-vitro stability. On the other hand, the trypanosomal genome contains 10 $\alpha$-tubulin genes and 10 ß-tubulin genes which are all arranged in a single large cluster of tightly packed, tandemly repeated alternating $\alpha$- and ß-tubulin genes (Thomashow et al., 1983; Seebeck et al., 1983). However, these genes apparently do not code for different tubulin isotypes, since they are all very similar or identical, and only a single species of $\alpha$- and of ß-tubulin mRNA is produced. The primary translation product from the $\alpha$-tubulin mRNA undergoes posttranslational modification by reversible detyrosination of the C-terminus, and by acetylation (Schneider et al., 1987; Sherwin et al., 1987; Dolan et al., 1986). Overall, a very simple isotype pattern of tubulin is found in trypanosomes, consisting of two $\alpha$-tubulin isotypes ($\alpha$1 and $\alpha$3, which is the acetylated derivative of $\alpha$1), and a single ß-tubulin isotype corresponding to the primary translation product. The distribution of isotypes is not specific for individual microtubule populations, and the different stoichiometry between the two $\alpha$-isotypes which is observed in different microtubule populations is most likely correlated to the turnover rate of the each population, rather than to its particular function.

From the analysis of the microtubular cytoskeleton of trypanosomes, a picture has emerged where microtubules are most liklely constructed all alike, irrespective of their later functions in the cellular context. What thenspecifies their biological half-life and their function are the microtubule-associated proteins (MAPs) which confer functional specificity upon the different microtubule populations.

MICROTUBULE-ASSOCIATED PROTEINS

A number of putative MAPs have recently been identified and characterized to various extents in different laboratories (Balaban et al., 1988; Jensen and Smaill, 1986; Bramlett et al., 1987). Recent progress of our own laboratory in this area is summarized briefly.

**Acylated MAP p41**

A minor cytoskeletal protein has recently been identified as a MAP which binds to microtubules in vitro in a strictly $Ca^{2+}$ dependent manner. This protein is covalently modified by fatty acid residues (Schneider et al., 1988a). Considering the close interaction between microtubules and the cell membrane, this protein

might serve as a microtubule/membrane linker within the membrane skeleton. Its precise intracellular localization has not yet been determined.

## High-molecular weight MAPs

A family of high molecular weight MAPs (300 - 400 kDa) are prominent components of the membrane skeleton. At least two of them consist of highly repetitive amino acid sequences which are closely related to each other, but bear no sequence similarity to other eukaryotic MAPs. One member of this trypanosomal MAP family, p320, consists of at least 50 tandemly repeated near-identical blocks of 38 amino acids (Schneider et al., 1988b). This high degree of repetition is stunning, even considering the growing evidence that a certain degree of repetitiveness is apparently a common theme for many eukaryotic MAPs. The high molecular weight MAPs colocalize in situ with the microtubules of the membrane skeleton, but are absent in the flagellum.

## The paraflagellar rod

This structure is associated with the flagellar axoneme through an intricate network of connecting proteins, and it may be regarded in its entirety as a microtubule-associated structure. Its major components are two proteins of 68 and 72 kDa, which appear closely related immunologically and biochemically, but which are coded for by distinct genes. In addition to these major components, a host of minor proteins are part of the complex. These include calmodulin (Ruben and Patton, 1987) and a set of spectrin-like proteins (Schneider et al., 1988c). The function of the paraflagellar rod complex is not understood, but it is hoped that a closer insight into its structure might provide clues towards understanding its function.

## CONCLUSIONS

The cytoskeleton of Trypanosoma brucei is an attractive subject for analyzing several lines of questions of cell biology. Its basic structure is very simple, consisting almost entirely of microtubules, and it is very stable, which facilitates many biochemical approaches. Besides the potential of offering new insights into the inner workings of a microtubule-based structure and its interactions with cell membranes, the cytoskeleton may also prove a suitable target for novel chemotherapeutics. This long-range prospect is not to be neglected since trypanosomes, as mentioned above, may be newcomers to cell biology, but they have been a deadly threat for man all along since the early days when Lucy took her first steps in prehistoric East Africa.

# LITERATURE REFERENCES

Balaban N, Waithaka HK, Njogu AR, Goldman R (1988) Isolation of subpellicular microtubule proteins from trypanosomatidae which mediate crosslinking of microtubules. Submitted

Borst P (1986) Discontinuous transcription and antigenic variation in trypanosomes. Ann Rev Biochem 55: 701-732

Bramlett GT, Chang S, Flavin M (1987) Periodic crosslinking of microtubules by cytoplasmic microtubule-associated and microtubule-corset proteins from a trypanosomatid. Proc Natl Acad Sci USA 84: 3259-3263

Dolan MT, Reid CG, Voorheis HP (1986) Calcium ions initiate the selective depolymerization of the pellicular microtubules in bloodstream forms of Trypanosoma brucei. J Cell Sci 80: 123-140

Ferguson MAJ, Mormans SW, Dwek RA, Rademacher TW (1988) Glycosyl-phosphatidyl inositol moiety that anchors Trypanosoma brucei variant surface glycoprotein to the membrane. Science 239: 753-759

Imboden MA, Blum B, DeLange T, Braun R, Seebeck T (1986) Tubulin mRNAs of Trypanosoma brucei. J Mol Biol 188: 393-402

Jensen CG, Smaill BH (1986) A technique for analyzing the spatial organization of microtubular arms and bridges. Ann NY Acad Sci 446: 417-419

Maizels N, Weiner A (1988) In search of a template. Nature 334: 469-470

Opperdoes FR (1987) Compartmentation of carbohydrate metabolism in trypanosomes. Ann Rev Microbiol 41: 127-152

Ruben L, Patton CL (1987) Calmodulin from Trypanosoma brucei: Immunological analysis and genomic organization. Meth Enzymol 139: 262-276

Schneider A, Eichenberger W, Seebeck T (1988a) A microtubule-binding protein of Trypanosoma brucei which contains covalently bound fatty acid. J Biol Chem 263: 6472-6475

Schneider A, Hemphill A, Wyler T, Seebeck T (1988b) High-molecular weight microtubule-associated protein from T. brucei contains tandemly repeated, near-identical sequences. Science 241: 459-462

Schneider A, Lutz HU, Marugg R, Gehr P, Seebeck T (1988c) Spectrin-like proteins in the paraflagellar rod structure of Trypanosoma brucei. J Cell Sci 90: 307-315

Schneider A, Sherwin T, Sasse R, Russell DG, Gull K, Seebeck T (1987) Subpellicular and flagellar microtubules of Trypanosoma brucei brucei contain the same alpha-tubulin isotypes. J Cell Biol 104: 431-438

Sherwin T, Schneider A, Sasse R, Seebeck T, Gull K (1987) Distinct localization and cell cycle dependence of C-terminally tyrosinolated alpha-tubulin in the microtubules of Trypanosoma brucei brucei. J Cell Biol 104: 439-446

Seebeck T, Whittaker P, Imboden MA, Hardman N, Braun R (1983) Tubulin genes of Trypanosoma brucei: A tightly clustered family of alternating genes. Proc Natl Acad Sci USA 80: 4634-4638

Simpson L (1987) The mitochondrial genome of kinetoplastoid protozoa: Genomic organization, transcription, replication and evolution. Ann Rev Microbiol 41: 363-382

Thomashow LS, Milhausen M, Rutter WJ, Agabian N (1983) Tubulin genes are tandemly linked and clustered in the genome of Trypanosoma brucei. Cell 32: 35-43

Van der Ploeg LHT (1987) Control of variant surface antigen switching. Cell 51: 159-161

Vickerman K, Preston TM (1976) Comparative cell biology of the kinetoplastid flagellates. In: Lumsden WHR, Evans DA (eds) Biology of the Kinetoplastida. Academic Press, New York, pp 35-130

# Isolation and Partial Characterization of Ciliary Rootlets from *Paramecium Tetraurelia*

Linda Sperling
Centre de Génétique Moléculaire
Centre National de la Recherche Scientifique
91190 Gif-sur-Yvette
FRANCE

## introduction

The cortical cytoskeleton of *Paramecium* is a fabric of distinct fibrous elements organized with precise geometry in 2 μm square repeating units (cortical units) which cover the surface of the organism in a regular pattern (Allen, 1971; Cohen & Beisson, 1988). The ciliary rootlet, also known as the kinetodesmal fibre, is one element of the cortical cytoskeleton of *Paramecium*. Each rootlet is anchored at the base of a cilium with precise orientation; it grows from the right side of the basal body and curves forwards to run anteriorly the length of several cortical units, interacting side-to-side with other ciliary rootlets to constitute a rigid rope-like scaffold clearly defining the anterior posterior axis of the cell and assuring alignment of the basal bodies and hence of the cortical units.

All flagella and cilia bear striated rootlets at their bases, and in each organism they are thought to play a role in anchoring and especially in orienting the cilia or flagella, a notion well-supported by studies of *Chlamydomonas* mutants lacking normal flagellar rootlets (Hoops et al, 1984). Yet the composition and dynamic properties of these analogous structures vary widely. For example, molecular masses for rootlet polypeptides of 20 kD (*Tetraselmis striata*; Salisbury et al, 1984), 47 kD (*Tetrahymena thermophilus*; Hyams & King, 1985), 170 kD (*Naegleria gruberi*; Larson & Dingle, 1981) and of 30-36 kD (*Paramecium*; this study) have been reported. The rootlets of some species are contractile (Salisbury et al, 1984) while others, including those of *Paramecium*, are not. Finally, although all rootlets are striated, the spacings and detailed banding patterns differ.

We report here the purification of ciliary rootlets from *Paramecium tetraurelia*. Our aim is to understand their structure and assembly, especially as the behaviour of the rootlets at cell division suggests that they play an important role in the morphogenesis of *Paramecium*.

## experimental results

The method employed for obtaining a highly purified fraction of ciliary rootlets involves three steps: 1- lysis of the cells in 1% Triton X-100 at low ionic strength, in the presence of EGTA (5 mM) and $Mg^{++}$ (2 mM), 2- detachment of the rootlets from the cortex with 100 mM $Mg^{++}$ and 3- separation of the rootlets from other cellular components on self-forming Percoll density gradients. The only contaminant in the preparations, as judged by phase contrast light microscopy and SDS-PAGE, was basal bodies. In situ each ciliary rootlet is tightly attached to a basal body and in most preparations, basal bodies were associated with a few of the rootlets.

The isolated rootlets appear intact and are about 8 -10 μm long and on average 0.1 μm wide. They have a polarity and a definite shape, being thickest and curved at the basal body end and

tapering progressively along their entire length. The striations which characterize thin section e.m. images are also found upon negative staining of isolated rootlets. Images of negatively stained rootlets diffract to at least 8 orders of a 330 Å spacing in the fibre direction and sharp equatorial spots at c. 1/(35 Å) visible in some views arise from the side to side packing of the constituent fibrils. In general, the images are reminiscent of paracrystals of fibrous proteins. If we imagine that the rootlets are built up by end-to-end packing of $\alpha$-helical polypeptides, then the molecular mass of the rod-shaped domains would be about 27 kD. However, it is important to note that the structure does not have 2-fold symmetry and does have a polarity; in addition, at the tapered end, the rootlets are frayed into fibrils rather than displaying a sharp break at a specific position in the banding pattern as might be expected for a paracrystal of molecules aligned end-to-end in some simple staggered arrangement.

On SDS-PAGE, the isolated rootlets are resolved into a series of polypeptides of molecular mass 31 to 36 kD. There are no intermolecular disulfide bridges as the same pattern is found in the absence or in the presence of a reducing agent. A polyclonal antibody was prepared by injecting the series of 31-36 kD bands cut out of SDS-polyacrylamide gels into a rabbit. The immune serum reveals the entire series of polypeptides on Western blots, even of whole cells. The serum also decorates the ciliary rootlets in situ.

The availability of an antibody directed against *Paramecium* ciliary rootlets has allowed us to verify the important observations of Fernandez-Galiano (1978) who sudied the dynamics of the rootlets through cell division using a silver staining technique. The surface of *Paramecium* consists of some 4000 repeating (cortical or ciliary) units organized in antero-posterior rows (kineties). Growth and (mitotic) division in *Paramecium* involves global doubling of the number of cortical units and remodeling of the surface to give two identical daughter cells. New units are inserted anteriorly to old units within each row (kinety). Fernandez-Galiano found that the ciliary rootlets regress/disassemble at the beginning of division, as appearance of the new cortical units begins, and regrow/reassemble late in division, as surface remodeling occurs. Fernandez-Galiano (1978) first suggested, and recent work in our laboratory has confirmed (Iftode et al, submitted) the existence of transcellular signals which control the growth and remodeling of the cortex; they are manifest as waves of activity originating primarily from the gullet.

The transcellular signal which controls cortical growth and reorganization through the cell cycle may be protein phosphorylation, at least as concerns the ciliary rootlets. Evidence in favor of such an hypothesis was obtained using the monoclonal antibody MPM-2 of Davis et al (1983) which specifically recognizes phosphorylated polypeptides. Keryer et al (1987) and Beisson (unpublished observations) have shown by immunofluorescence and immunoelectron microscopy experiments that the ciliary rootlets are decorated by MPM-2 only at cell division, just before the rootlets regress. We are at present trying to determine whether the structural proteins of the rootlets themselves are phosphorylated and whether the phosphorylation modulates their assembly into ciliary rootlets, just as phosphorylation of the nuclear lamins is implicated in nuclear envelope assembly (Gerace and Blobel, 1980).

## acknowledgements

## references

Allen RD (1971) Fine structure of membranous and microfibrillar systems in the cortex of Paramecium caudatum. J Cell Biol 49:1-20

Cohen J, Beisson J (1988) The cytoskeleton. In: Görtz H-D (ed) Paramecium. Springer-Verlag, Berlin Heidelberg, p 363

Davis FM, Tsao T, Fowler SK, Rao PN (1983) Monoclonal antibodies to mitotic cells. Proc Natl Acad Sci USA 80:2926-2930

Fernandez-Galiano D (1978) Le comportement des cinétodesmes pendant la division de Paramecium caudatum. Protistologica 14:291-294

Gerace L, Blobel G (1980) The nuclear envelope lamina is reversibly depolymerized during mitosis. Cell 19:277-287

Hoops HJ, Wright RL, Jarvik JW, Witman GB (1984) Flagellar waveform and rotational orientation in a Chlamydomonas mutant lacking normal striated fibres. J Cell Biol 98:818-824

Hyams JS, King CA (1985) Identification of proteins of the striated rootlets of Tetrahymena by immunofluorescence microscopy and immunoblotting with an anti-rootlet serum. Eur J Cell Biol 38:102-105

Keryer G, Davis FM, Rao PN, Beisson J (1987) Protein phosphorylation and dynamics of cytoskeletal structures associated with basal bodies in Paramecium. Cell Motil Cytoskel 8:44-54

Larson DE, Dingle AD (1981) Isolation, ultrastructure, and protein composition of the flagellar rootlet of Naegleria gruberi. J Cell Biol 89:424-432

Salisbury JL, Baron A, Surek B, Melkonian M (1984) Striated flagellar roots: isolation and partial characterization of a calcium-modulated contractile organelle. J Cell Biol 99:962-970

# Strategies in Regulation of Protein Associations of the Spectrin-Based Membrane Skeleton

V. Bennett, J. Steiner, J. Davis, H. Kaiser, and E. Kordeli
Howard Hughes Medical Institute and Department of Biochemistry
Duke University Medical Center
Durham, North Carolina 27710
USA

ABSTRACT

The spectrin-based membrane skeleton of nonerythroid cells exhibits an unsuspected variety in protein interactions and regulatory mechanisms. Spectrin has at least two options in linkage to the membrane: ankyrin-mediated interaction with integral membrane proteins and direct linkages with ankyrin-independent sites. Ankyrin includes at least two families of functionally distinct isoforms, a general isoform expressed in many cells and a specialized isoform expressed in a limited number of cells and localized in a highly polarized distribution in these cells. Proteins likely to associate with the specialized isoforms of ankyrin based on association in vitro assays and co-localization in cells include the anion exchanger of erythrocytes and collecting ducts of kidney, the Na/K ATPase in distal tubule cells of kidney, and the voltage-dependent sodium channel in neurons. An additional mechanism for ankyrin diversity is processed variants of ankyrin with deleted regulatory domains that express binding sites unavailable to unprocessed ankyrin. Spectrin also can interact with high affinity with protein sites in synaptosomes and other membranes that are independent of ankyrin. Calmodulin in the presence of submicromolar concentrations of calcium is a competitive inhibitor of direct binding of spectrin to synaptosomal membranes but does not affect spectrin-ankyrin interactions. Thus the potential exists for differential regulation of spectrin-membrane interactions. The assembly state of the spectrin-actin lattice may also vary in certain cells. Adducin, a protein that promotes spectrin-actin interactions, is concentrated at sites of cell-cell contact in certain epithelial cells. These studies provide a low-resolution view of the spectrin skeleton and emphasize the possibilities for participation of this structure in a variety of functions including maintenance of specialized cell domains and participation in dynamic calcium-regulated processes.

INTRODUCTION

The spectrin-based membrane skeleton is an assembly of structural proteins associated with the plasma membranes of many vertebrate cells (for reviews, see Marchesi, 1985; Bennett, 1985, 1989; Goodman and Zagon, 1986). Spectrin and the membrane skeleton were first discovered in erythrocytes and this is the system

where the structure is best understood. Spectrin, the principal component of the
skeleton, is a flexible, rod-shaped protein about 200 nm in length containing two
subunits, termed alpha and beta. The subunits are aligned anti-parallel to form
tetramers which are the major form of spectrin in cells.

Spectrin tetramers are associated at their ends with actin oligomers in a
ratio of 5-6 spectrins per actin oligomer, and are arranged as a two-dimensional
network (Byers and Branton, 1985; Shen et al., 1986; Liu et al., 1987). Association
of spectrin and actin involve accessory proteins such as protein 4.1, protein 4.9,
and tropomyosin that stabilize and also may regulate spectrin-actin interactions.
Adducin is another candidate to interact with spectrin-actin complexes and will be
discussed below. The spectrin-actin network is attached to the membrane through
high affinity association of the beta subunit of spectrin with ankyrin, which in
turn, is linked to the cytoplasmic domain of the anion exchanger (also referred to
as band 3). An additional membrane linkage for the network is provided by binding
of protein 4.1 to glycophorin C, another integral protein.

A major function of the spectrin skeleton in erythrocytes is to stabilize the
lipid bilayer. Defects or deficiencies in spectrin and associated proteins result
in cells with abnormal shapes and reduced mechanical stability in diseases such as
hereditary spherocytosis and elliptocytosis (Agre et al., 1985; Marchesi et al.,
1987; Conboy et al., 1986).

Proteins closely related to erythrocyte spectrin, also referred to as fodrin,
are expressed in many cells and organisms. Spectrin is especially prominent in
brain where it comprises about 3 per cent of the total membrane protein. In most
tissues spectrin is distributed uniformly along the plasma membrane (Levine and
Willard, 1981; Repasky et al., 1982; Glenney and Glenney, 1983; Drenckhahn and
Bennett, 1987). Such a nonpolarized distribution of spectrin suggests a fairly
simple organization analogous to the erythrocyte membrane. The purpose of this
review is to present a low-resolution view of protein associations of spectrin in
nonerythroid cells and of several mechanisms for regulation of these interactions.
A recurring theme will be the diversity of potential protein interactions available
to spectrin, and the complexity of the organization of the spectrin skeleton in
tissues compared to the highly specialized and homogeneous erythrocyte membrane.

## Mechanisms of ankyrin diversity

Ankyrin isoforms.  Two isoforms of ankyrin have been purified from erythrocytes
and brain that have many biochemical properties in common (Bennett and Stenbuck,
1980; Davis and Bennett, 1984). Brain and erythrocyte ankyrin a) bind to the beta
subunit of spectrin in the midregion of spectrin tetramers; b) associate with the
cytoplasmic domain of the anion exchanger; c) have similar domain structures with
a $M_r$=72,000 fragment that associates with spectrin and a $M_r$=90,000-95,000 fragment

that associates with membrane sites; d) share antigenic sites; e) have similar physical properties and are asymmetric monomers in solution. Recent work indicates that brain and erythrocyte ankyrin are prototypes of two families of ankyrin that have major differences in expression and localization in cells (Davis et al., 1989; Kordeli et al., 1989). These families will be referred to as specialized and general forms of ankyrin and can be distinguished by antibodies against erythrocyte and brain ankyrin.

Specialized ankyrins react better with antibody against the erythrocyte protein, are expressed in a limited number of cells, and exhibit a highly polarized distribution in these cells. In kidney, the specialized iscform is present in high concentrations in distal tubule cells and intercalated cells of the collecting duct (Drenckhahn et al., 1985; Drenckhahn and Bennett, 1987; Davis et al., 1989), but is absent or present in much lower amounts in other cell types. In brain, this form of ankyrin is present primarily in neurons and is absent from glial cells (Drenckhahn and Bennett, 1987; Kordeli et al., 1989). Specialized ankyrin is confined to the basolateral domains of kidney distal tubule and intercalated cells, and is absent from apical domains. In brain, a striking finding has been the localization of specialized ankyrin at the node of Ranvier (Kordeli et al., 1989) as well as at focal sites in dendrites and neuronal cell bodies (Drenckhahn and Bennett, 1987).

The general form of ankyrin reacts better with antibody against brain ankyrin, and is present in most cell types in a nonpolarized distribution. In kidney, this form of ankyrin is present in proximal and distal tubule cells, the collecting duct, thin loops of Henle and glomeruli. General ankyrin is present on apical as well as basolateral membranes. In brain, general ankyrin does not exhibit the localization at nodes of Ranvier noted with specialized ankyrin, but is present uniformly along axons.

Specialized and general isoforms of ankyrin are likely to interact with different integral membrane proteins. The specialized form of ankyrin has been demonstrated in _in vitro_ assays to bind to the Na/K ATPase (Nelson and Veshnock, 1987) and to the voltage-dependent sodium channel (Srinivasan et al., 1988). These test-tube assays are likely to have physiological relevance since the specialized isoform of ankyrin is colocalized with the ATPase in distal tubule cells of kidney (Koob et al., 1988) and with the sodium channel at the node of Ranvier (Kordeli et al., 1989). In contrast to the specialized ankyrin, no proteins have been identified yet that interact with the general isoform of ankyrin.

Direct evidence for diversity of membrane binding sites among ankyrin isoforms is provided by comparison of binding of brain and erythrocyte ankyrins to kidney microsomes (Davis et al., 1989). Brain and erythrocyte ankyrin each associate with high affinity ($K_d$=100-200 nM) with distinct membrane sites. The specificity of these sites is not absolute but reflects 2.5-10-fold differences in relative

affinities. Further evidence that the binding sites of different ankyrins share some common features is that the cytoplasmic domain of the erythrocyte anion exchanger associates with both isoforms and displaces their binding to kidney membranes. The system of ankyrins and their membrane sites thus is formally analogous to the situation with catecholamines where a number of chemically related but distinct ligands interact with a variety of membrane receptors.

Processed variants of ankyrin. Another potential source for diversity among ankyrins is provided by processed variants of ankyrin missing regulatory domains. Human erythrocytes contain a form of ankyrin of lower molecular weight referred to as protein 2.2 (nomenclature based on mobility on SDS-gels) that is missing a $M_r$= 29,000 regulatory domain but retains binding domains for spectrin and the anion exchanger (Hall and Bennett, 1987). The mechanism for deletion of this domain is not established, although differential splicing of mRNA is a possibility. Protein 2.2 is of interest since it is an activated form of ankyrin with enhanced binding to spectrin and to erythrocyte membrane sites.

Binding of protein 2.2 to kidney microsomes was measured as part of the study with brain and erythrocyte ankyrin isoforms (Davis et al., 1989). Protein 2.2 associated with kidney membranes with 3-6-fold greater capacity than unprocessed erythrocyte ankyrin, and also was capable of binding to the same sites as brain ankyrin. Protein 2.2 thus expresses a binding site that is absent from unprocessed ankyrin. The most likely explanation for this difference is the deletion of the $M_r$=29,000 regulatory domain in protein 2.2, since in other respects, including amino-terminal sequence, these ankyrins are identical. The regulatory domain could alter the conformation of ankyrin. Alternatively, this domain may directly interact with the binding site and act as a "pseudosubstrate". Ankyrin may thus be analogous to enzymes such as protein kinase C and myosin light chain kinase that contain regulatory domains that are competitive inhibitors of enzyme activity (Howe and Kemp, 1987; Kemp et al., 1987).

Isoform-specific ankyrin protease activity that deletes regulatory domains. A leupeptin-sensitive protease activity has been discovered in kidney that has potential to selectively activate the specialized isoform of ankyrin (Davis et al., 1989). The kidney protease has no effect on brain ankyrin but selectively cleaves two regulatory domains from erythrocyte ankyrin. The digested erythrocyte ankyrin retains binding domains for spectrin and the membrane, and is activated with respect to binding to kidney membranes.

The biological function of this interesting protease is not yet known. It will be important to determine if the protease plays a role in processing of the specialized isoform of kidney ankyrin during its synthesis and assembly. The protease activity is confined to membranes and potentially could function as a mechanism for site-directed activation of ankyrin in the vicinity of the membrane attachment protein.

## Direct association of spectrin with membrane protein sites distinct from ankyrin

In tissues more complex than erythrocytes spectrin is likely to fulfill additional roles and interact with proteins not found in red cells. Recently brain spectrin has been discovered to associate with high affinity ($K_d$=5-10 nM) with protease-sensitive sites in highly extracted brain membranes completely depleted of ankyrin (Steiner and Bennett, 1988). Erythrocyte spectrin also associates with brain membranes, although with 3-4-fold lower capacity. The binding sites for erythrocyte spectrin may reflect the presence of erythroid isoforms of spectrin that have been found in brain (Riederer et al., 1986; Lazarides and Nelson, 1983). The binding of spectrin to these membrane sites is likely to be biologically important since the capacity of membranes for brain spectrin (20-30 pMole per milligram of membrane protein) is close to the amount of spectrin in brain (30 pMoles per milligram) and binding was optimal at physiological pH (6.8-7.0) and ionic strength (50 mM). The beta subunit of spectrin mediates the high affinity association with brain membranes, and interacts with membranes at a site distinct from the ankyrin-binding site. Thus, spectrin could associate with both ankyrin and the membrane site at the same time. A small number of ankyrin-independent sites could be measured in erythrocytes (5-8 per cent of the number of copies of ankyrin), although these sites associated with brain spectrin with higher affinity than with erythrocyte spectrin. Ankyrin-independent association of spectrin therefore is not a significant feature of mature erythrocytes, although such an interaction may have been important during assembly of the membrane skeleton.

The existence of two mechanisms for spectrin-membrane interactions suggests the possibility that these interactions may be regulated independently of each other. Direct evidence for differential regulation of spectrin-membrane linkages is the finding that calmodulin, in the presence of calcium, has no effect on spectrin-ankyrin interactions but inhibits binding of spectrin to brain synaptosomal membranes (Steiner et al., 1989). Calmodulin is a competitive inhibitor with a $K_i$= 1.3 uM, and with half-maximal effects at 0.1-0.3 uM calcium. Inhibition is due to a reversible calmodulin-binding interaction since the effect of calcium/calmodulin is reversed by the calmodulin antagonist, trifluoperazine, and by chelation of calcium with Na EGTA. The target for calmodulin is most likely the membrane attachment protein(s) rather than spectrin itself since calmodulin inhibits membrane binding of brain spectrin beta subunit which does not associate with calmodulin.

Modulation of spectrin-membrane interactions by calmodulin provides the first biochemical evidence that spectrin can exist in a dynamic state under metabolic control and distinct from the mechanically stable membrane skeleton of erythrocytes. A consequence of independent regulation of these membrane attachment mechanisms is that calcium/calmodulin can dissociate direct spectrin-membrane interactions locally or regionally without disassembly of the areas of the membrane

skeleton stabilized by linkage of spectrin to ankyrin. A possible physiological
role for a regulated spectrin structure, suggested by Perrin and coworkers (Perrin,
1987), could be as a barrier that separates secretory vesicles from the plasma
membrane and prevents vesicle-membrane fusion events. Calcium/calmodulin-induced
disassembly of such spectrin structures would allow access of secretory vesicles
to the membrane and could be an important step in regulation of exocytosis. Disso-
ciation of spectrin could also modulate slower events such as endocytosis and
vesicle recycling.

A membrane protein of $M_r$=88,000 has been identified in brain membranes that
is dissociated from spectrin affinity columns by calcium/calmodulin and is a can-
didate for a calmodulin-sensitive spectrin binding site in brain. An interesting
possibility is that this spectrin-binding protein may function as a channel for
ions such as calcium or potassium, and that such a channel activity could be regu-
lated by calmodulin in concert with the modulation of spectrin binding. It will be
important in future work to purify this protein, determine its cellular localiza-
tion, and evaluate other functions in addition to linkage of spectrin to membranes.

## Implications of multiple spectrin-membrane linkages

The studies summarized above indicate that spectrin has many options in
association with membrane proteins with different linkages provided by ankyrin
isoforms, processed forms of ankyrin, and ankyrin-independent sites. The multipli-
city of linkages has some theoretical implications for assembly and function of
spectrin. Assembly of the spectrin-skeleton could occur in stages, with different
linkages occuring in early and mature structures. For example, during erythroid
differentiation spectrin associates with the plasma membrane prior to synthesis of
the specialized ankyrin isoform (Hanspal and Palek, 1987). It is possible that
initial linkage of spectrin to the membrane is provided either by the general
ankyrin isoform or by an ankyrin-independent mechanism. The specialized isoform of
ankyrin thus may associate with spectrin on the membrane followed by loss of the
initial attachment protein(s). A consequence of such an assembly pathway is that
ankyrin could utilize a pre-existing membrane skeleton for placement of the anion
exchanger, without participation in the initial construction of the skeleton.

Different spectrin linkages could be segregated to different regions of polar-
ized cells and have distinct functions. As discussed above, the differential regu-
lation of direct linkages by calmodulin indicates the possibility of coexisting
dynamic and stable spectrin structures. Moreover, the multiple ankyrin variants
would permit association of spectrin with specialized integral proteins in differ-
ent membrane domains.

## Localization of adducin at sites of cell-cell contact

Results described above have focused on diversity of membrane linkages of the spectrin-skeleton. The interaction of spectrin with actin also is important as an essential linkage in construction of a spectrin network. Adducin is a protein recently discovered and purified from erythrocytes (Gardner and Bennett, 1986) that promotes association of spectrin with actin (Gardner and Bennett, 1987; Mische et al., 1987). A protein closely related to erythrocyte adducin has also been purified from brain (Bennett et al., 1988). Adducin is of special interest as a regulatory protein since it binds to calmodulin, its association with spectrin-actin complexes is inhibited by calmodulin, and since adducin is a substrate for protein kinase C (Gardner and Bennett, 1986; Bennett et al., 1988; Ling et al., 1986).

Adducin in brain is colocalized with spectrin along axons and in cell bodies of neurons (Kaiser et al., 1989). Adducin also is expressed in certain epithelial tissues such as small intestine, and has been localized in frozen sections of these tissues to sites of cell-cell contacts on the lateral cell borders (Kaiser et al., 1989). Spectrin, in contrast is present uniformly along the plasma membrane. The localization of adducin has been studied in more detail in cultured keratinocytes (Kaiser et al., 1989). Adducin is randomly distributed on membranes of isolated cells but becomes highly concentrated at sites of cell contact once cells associate, while spectrin remains randomly associated over the cell membrane in isolated and confluent cells.

The targeting of adducin to specialized cell domains suggests the possibility of a special recognition site for adducin that is unique to sites of cell-cell contact. It will be of interest to determine if adducin associates with known cell adhesion molecules. A consequence of association of adducin in these domains could be to promote spectrin-actin interactions and promote assembly of a stable membrane skeleton.

## Summary

The spectrin-based membrane skeleton of nonerythroid cells exhibits an unsuspected variety in protein interactions and regulatory mechanisms. Spectrin has multiple options in linkage to integral membrane proteins through ankyrin mediated interaction with integral membrane proteins. Spectrin also can interact with high affinity with membrane sites in synaptosomes and other membranes that are independent of ankyrin. Calmodulin in the presence of submicromolar concentrations of calcium is a competitive inhibitor of direct binding of spectrin to synaptosomal membranes but does not affect spectrin-ankyrin interactions. Thus the potential exists for differential regulation of spectrin-membrane interactions. The assembly state of the spectrin-actin lattice may also vary in certain cells. Adducin, a protein that promotes spectrin-actin interactions, is concentrated at sites of cell-cell contact in certain epithelial cells. These studies provide a low-resolu-

tion view of the spectrin skeleton and emphasize the possibilities for participation of this structure in a variety of functions including maintenance of specialized cell domains and participation in dynamic calcium-regulated processes.

References
Agre P, Casella J, Zinkham W, McMillan C and Bennett V (1985) Erythrocyte spectrin is partially deficient in hereditary spherocytosis. Nature 314:380-383
Bennett V (1985) The membrane skeleton of human erythrocytes and its implications for more complex cells. Ann Rev Biochem 54:273-304
Bennett V, Gardner K and Steiner J (1988) Brain adducin:A protein kinase C substrate that may mediate site-directed assembly at the spectrin-actin junction. J Biol Chem 263:5860-5869
Bennett V and Stenbuck PJ (1980) Human erythrocyte ankyrin. Purification and properties. J Biol Chem 255:2540-2548
Byers TJ and Branton D (1985) Visualization of the protein associations in the erythrocyte membrane skeleton. Proc Nat Acad Sci USA 82:6153-6157
Conboy J, Mohandas N, Tchernia G and Kan Y (1986) Molecular basis of hereditary elliptocytosis due to protein 4.1 deficiency. New Eng J Med 315:680-685
Davis J and Bennett V (1984) Brain ankyrin-a membrane associated protein with binding sites for spectrin, tubulin and the cytoplasmic domain of the erythrocyte anion channel. J Biol Chem 259:13550-13559
Davis J, Davis L and Bennett V (1989) Functionally distinct ankyrin isoforms in kidney:Cellular localization and identification of an isoform-specific ankyrin protease activity. J Cell Biol, abstract
Drenckhahn D and Bennett V (1987) Polarized distribution of $M_r$ 210,000 and 190,000 analogs of erythrocyte ankyrin along the plasma membrane of transporting epithelia, neurons and photoreceptors. Eur J Cell Biol 43:479-486
Drenckhahn D, Schluter K, Allen D and Bennett V (1985) Colocalization of band 3 with ankyrin and spectrin at the basal membrane of intercalated cells in the rat kidney. Science 230:1287-1289
Gardner K and Bennett V (1987) Modulation of spectrin-actin assembly by erythrocyte adducin. Nature 328:359-362
Gardner K and Bennett V (1986) A new erythrocyte membrane-associated protein with calmodulin binding activity:identification and purification. J Biol Chem 261:1339-1348
Glenney JR and Glenney P (1983) Fodrin is the general spectrin-like protein found in most cells whereas spectrin and the TW protein have a restricted distribution. Cell 34:503-512
Goodman SR and Zagon IS (1986) The neural cell spectrin skeleton:A review. Am J Physiol 250:C347
Hall TG and Bennett V (1987) Regulatory domains of erythrocyte ankyrin. J Biol Chem 262:10537-10545
Hanspal M and Palek J (1987) Synthesis and assembly of membrane skeletal proteins in mammalian red cell precursors. J Cell Biol 105:1417-1424
Howe C and Kemp B (1987) Protein kinase C contains a pseudosubstrate prototope in its regulatory domain. Science 238:1726-1728
Kaiser HW, O'Keefe EJ and Bennett V (1989) Adducin, a protein that promotes assembly of spectrin-actin complexes, is localized at sites of cell-cell contact and is redistributed by treatment with phorbol ester. J Cell Biol, abstract
Kemp B, Pearson R, Guerriero V, Bagchi I and Means A (1987) The calmodulin binding domain of chicken smooth muscle myosin light chain kinase contains a pseudo-substrate sequence. J Biol Chem 262:2542-2548
Koob R, Zimmermann M, Schoner W and Drenckhahn D (1987) Colocalization and coprecipitation of ankyrin and Na/K ATPase in kidney epithelial cells. Eur J Cell Biol 45:230-237
Kordeli E, Davis J, Trapp B and Bennett V (1989) Localization of the erythroid isoform of ankyrin at the node of Ranvier in myelinated nerve fibers. J Cell Biol, abstract

Lazarides E and Nelson W (1983) Erythrocyte and brain forms of spectrin in cerebellum:Distinct membrane-cytoskeletal domains in neurons. Science 220:1295-1296

Levine J and Willard M (1981) Fodrin:axonally transported polypeptides associated with the internal periphery of many cells. J Cell Biol 90:631-643

Ling E, Gardner K and Bennett V (1986) Protein kinase C phosphorylates a recently identified membrane skeleton-associated calmodulin-binding protein in human erythrocytes. J Biol Chem 261:13875-13878

Liu S-C, Derick LH and Palek J (1987) Visualization of the hexagonal lattice in the erythrocyte membrane skeleton. J Cell Biol 104:527-536

Marchesi SL, Letsinger JT, Speicher DW, Marchesi VT, Agre P, Hyun B and Guiati G (1987) Mutant forms of spectrin alpha-subunits in hereditary elliptocytosis. J Clin Invest 80:191-198

Marchesi VT (1985) Stabilizing infrastructure of cell membranes. Ann Rev Cell Biol 1:531-561

Mische S, Mooseker M and Morrow J (1987) Erythrocyte adducin:A calmodulin regulated actin-bundling protein that stimulated spectrin-actin binding. J Cell Biol 105:2837-2849

Nelson WJ and Veshnock PJ (1987) Ankyrin binding to the $(Na^+ + K^+)$ATPase and implications for the organization of membrane domains in polarized cells. Nature 328:533-535

O'Keefe EJ and Bennett V (1989) Desmoplakin 1 and 2:Purification and characterization. J Cell Biol, abstract

Perrin D, Langely OK and Aunis D (1987) Anti-alpha fodrin inhibits secretion from permeabilized chromaffin cells. Nature 326:498-501

Repasky E, Granger B and Lazarides E (1982) Widespread occurrence of avian spectrin in nonerythroid cells. Cell 29:821-833

Riederer BM, Zagon IS and Goodman SR (1980) Brain spectrin (240/235) and brain spectrin (240/235E). Two distinct spectrin subtypes with different locations within mammalian neural cells. J Cell Biol 102:2088-2097

Shen BW, Josephs R and Steck TL (1986) Ultrastructure of the intact skeleton of the human erythrocyte membrane. J Cell Biol 102:997-1006

Srinivasan Y, Elmer L, Davis J, Bennett V and Angelides K (1988) Ankyrin and spectrin associate with voltage-dependent sodium channels in brain. Nature 333:177-180

Steiner JP and Bennett V (1988) Ankyrin-independent membrane protein binding sites for brain and erythrocyte spectrin. J Biol Chem, in press

Steiner JP, Walke HT and Bennett V (1989) Calcium/calmodulin inhibits direct binding of spectrin to synaptosomal membranes. J Cell Biol, abstract

# A cAmp-Dependent Phosphorylation Alters Spectrin Binding Properties

Hans U. Lutz, Dieter Maretzki, and Mariagabriella Mariani

Dept. of Biochemistry, ETH-Zentrum

CH 8092 Zurich, Switzerland

## Summary

A cAMP-dependent process conveys to a limited number of spectrin molecules an altered binding property. They become resistant to both low and high ionic strength extractions. These modified spectrin molecules are selectively extracted from KCl-stripped IOV by urea at low ionic strength. The urea-extractable spectrin is antigenically similar to low ionic strength-extractable spectrin. It contains, however, additional phosphopeptides not found in low ionic strength - extracted spectrin. Its tight association with the membrane is most likely due to fatty acid-acylation, since its specific labeling by [9,10(n)-$^3$H]-palmitate was highest among high molecular weight proteins and occurred in both spectrin subunits, but preferentially in band 2. Whether a cAMP-dependent phosphorylation of spectrin is required for spectrin to become fatty acid-acylated and thereby membrane-associated is not yet established . This is likely, since cAMP increased the amount of IOV-associated spectrin, its fatty acid-acylation and its unique phosphorylation.

## Introduction

The red cell membrane has become a paradigma in membrane biochemistry, for characterization of integral and peripheral membrane proteins (for review see Branton et al.1981). Application of the red cell-based methods to other cell types has revealed a more complex situation than originally found in red cells. The variety of membrane proteins was extended, namely by the discovery of lipid-anchored proteins, like Thy 1 (Low, Kincade, 1985), and of membrane skeletal proteins which existed in several forms, a peripheral or even cytoplasmic form and a membrane-associated one which was fatty acid-acylated (e.g. vinculin) (Kellie, Wigglesworth, 1987). In the meantime lipid anchored proteins were also found in red cells: decay accelerating factor (DAF) (Medof et al.1987) and acetylcholinesterase (Taguchi et al.1984). So far no red cell protein has been described which altered its binding properties in response to a modification and thus showed dynamics. We report on a fraction of spectrin which fulfills these criteria:

Peripheral proteins are operationally defined as those components that are extracted from membranes by buffers of either low or high ionic strength. Spectrin, the major membrane skeletal protein, is extracted from membranes by low ionic strength solutions (Bennett, Stenbuck, 1979), while ankyrin, one of the linker proteins between the

spectrin/actin meshwork and the bilayer, is extracted by solutions of high ionic strength (0.6 M or more) (Hargreaves et al.1980). The selective extractability of these proteins has been confirmed in many investigations. Thus the results leave no doubt that the bulk of spectrin is soluble in low ionic strength solutions. We (Lutz et al.1986) noticed, however, that low ionic strength buffers do not completely extract spectrin from membranes. The membrane inverts during extraction with low salt solutions and forms small, inside-out vesicles (IOV). These IOV retain 5-10 % of spectrin which resists extraction. We have studied this minor fraction of spectrin in more detail, since it has dynamic properties. Its amount is under control of a cAMP-dependent phosphorylation and is greatly diminished in IOV from old red cells. We report on the selective extraction of this spectrin from the membrane and show that it is tightly associated with the membrane, presumably because it is fatty acid-acylated.

## Materials and Methods

*Extraction procedures*
Human blood collected in heparin was obtained from the Swiss Red Cross. Young, middle-aged and old red cells were isolated by density centrifugation on self-forming Percoll gradients, as outlined elsewhere (Lutz et al.1984; Lutz, 1988). The creatine contents of the cells were measured to verify the quality of density separation. Density separated or unseparated red cells were washed three times in PBS containing 1mM EDTA. Membranes were obtained by hypotonic lysis. They were washed once with PBS containing 0.4 mM diisopropylfluorophosphate and once more with hemolysis buffer. Membranes were further washed twice with low ionic strength buffer (0.3 mM phosphate and 0.2 mM EDTA, pH 8.0) and spectrin was extracted by incubating membranes in 10 volumes of the same buffer for 30 min at 37° C (Bennett, Stenbuck, 1979). Spectrin extracts were concentrated and purified by gel filtration (Lutz, 1984). The generated inside-out-vesicles (IOV) were washed once in low ionic strength buffer and ankyrin was extracted by incubating IOV with 10 volumes of 1M KCl and 0.4 mM diisopropylfluorophosphate (Hargreaves et al.1980). The supernates containing ankyrin were concentrated with Centricon 30 (Amicon) and stored at 4° C. KCl-stripped IOV were washed and resuspended in 5mM phosphate (pH 7.4) to a protein concentration of 4-5 mg/ml. These suspensions were diluted 5-fold and adjusted to 2.5 mM phosphate, 1 mM dithiothreitol, 30 μg /ml phenyl methyl sulfonyl fluoride, and 5 M urea (pH 7.4). Samples were incubated for 15 min at 37° C. Extraction was terminated by ultracentrifugation for 15 min at 100,000g. The pellets were washed in 5mM phosphate and the supernates were concentrated to a final concentration of 1-2 mg/ml. Aliquots of each sample (membranes and extracted proteins) were stored frozen after addition of 1% SDS and 5mM N-ethylmaleimide for subsequent electrophoresis analysis.

*Labeling of whole cells and of isolated spectrin.*
Density-separated red cells were washed and $^{32}$P-phosphate labeled as described (Lutz
et al.1986) by incubation in the presence of 50 µM phosphate, 0.2 mCi/ml of carrier-free
$^{32}$P-phosphate, and 0-200 µM cAMP, under ATP-maintaining conditions. The incubation
buffer was slightly modified: it contained 40 mM imidazole, 100 mM NaCl, 5 mM KCl, 1
mM MgCl$_2$, 15 mM D-glucose, 30 mM sucrose, 50 µg/ml PMSF and 200 units/ml of
penicillin G ( pH 7.4, 310-320 mOsM). Labeling with [9,10(n)-$^3$H]-palmitic acid was carried
out as follows: red cells were incubated for 2-14 h at 37˚ C and 29 % Hct in the buffer
given  containing in addition 0.2 mCi/ml of labeled palmitic acid, 1 mM phosphate, 0.5 mM
EGTA, 5 µM coenzyme A (Calbiochem), 5 mM sodium pyruvate. Membranes were
prepared, spectrin, ankyrin, and urea-extractable spectrin were obtained as outlined
before.
Purified spectrin dimer from unlabeled cells was in vitro phosphorylated by incubation with
123 mCi/mmol of [γ$^{32}$P] ATP in the presence of the catalytic subunit of a cAMP-
dependent protein kinase from bovine heart (Sigma) (Lutz, 1984; Maretzki, Lutz, 1986).

*SDS-PAGE and two-dimensional electrophoresis*
SDS-PAGE was performed as described (Lutz, 1978).  The samples were reduced with
40 mM dithiothreitol for 30 min at 37˚ C and alkylated with an excess of N-ethylmaleimide,
before subjecting them to electrophoresis. Two-dimensional separation (IEF and SDS
PAGE) of tryptic peptides from spectrin was carried out essentially as described
(Speicher et al.1980).

*Immunoblotting*
Human, naturally occurring anti-spectrin antibodies were affinity purified as described in
(Lutz et al.1984) from pooled human IgG (Sandoglobulin[R]) and labeled with $^{125}$I-iodine by
chloramine-T. Blots from SDS-PAGE were incubated overnight at room temperature with
labeled anti-spectrin at 3 x 10$^5$ cpm/ml in 1% gelatine, 10 mg/ml IgG which was adsorbed
on band 3 and spectrin (Lutz et al. 1987). Blots were washed, dried and
autoradiographed.

**Results and Discussion**

Extraction of red cell membranes with low salt solutions at 37˚  C yields spectrin
dimer in the supernate and mainly inverted vesicles (IOV)  in the pellet.The polypeptide
pattern of IOV shows ankyrin, band 3 protein, band 4.1, 4.2 and among high molecular
weight proteins two weakly stained bands with apparent molecular weights corresponding
to those of spectrin band 1 and 2. The two polypeptides represent residual amounts of
spectrin, since affinity-purified anti-spectrin antibodies reacted with these bands. In Fig. 1

B a naturally occurring, human anti-spectrin antibody that primarily reacted with spectrin band 1 is shown to bind to spectrin band 1 in IOV and KCl-stripped IOV. Thus, a small
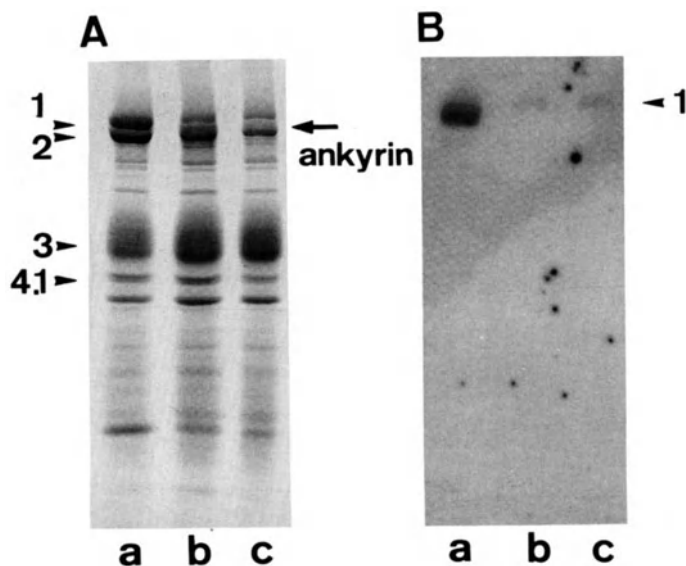


**Fig. 1. Low and high ionic strength-resistant spectrin.** Membranes (a); IOV (b); and KCl-stripped IOV (c) were prepared from unseparated red blood cells as outlined. Equal volumes of IOV and KCl-stripped IOV were electrophoresed in parallel to 20 µg of whole control membranes (a). **A:** stained gel; **B,** immunoblot that was incubated with labeled, naturally occurring anti-spectrin antibodies. **1,2,** spectrin subunits.

fraction (5-10 % ) of spectrin resists extraction by low ionic strength buffers. IOV-associated spectrin also resisted extraction by 1 M KCl. This was unique, because the harsh treatment extracted most of ankyrin and a large portion of band 4.1 (Fig. 1 A).

The amount of IOV-associated spectrin changed in characteristic ways with dynamic properties of the cell:

**1)** It was almost twice as high as in controls when IOV were obtained from red cells that were incubated with 10- 200 µM cAMP under ATP-maintaining conditions (Fig. 2 A).

**2)** It was high in samples from young but low in those from old cells (not shown).

**3)** Furthermore, the capacity of a cell to generate IOV-associated spectrin from normal spectrin in response to added cAMP was high in young and absent in old cells. Thus, IOV-associated spectrin does not represent a residual amount of spectrin that remained associated with IOV because of imperfections in extraction procedures or because it was sealed within right-side-out vesicles.

**4)** Increased generation of IOV-associated spectrin in response to cAMP was due to a cAMP-dependent phosphorylation, since the amount of IOV-associated spectrin was

also increased by incubation of membranes with ATP and the catalytic subunit of a cAMP-dependent protein kinase (not shown).

**5)** IOV-associated spectrin was also generated from exogenously added $^{125}$I-iodinated spectrin dimer by resealing it in membranes with ATP and the catalytic subunit of a cAMP-dependent protein kinase.

**6)** Catalytic subunit similarly increased the amount of IOV-associated spectrin on membranes of young and old cells, while cAMP together with endogenous enzymes of the membrane was only active on membranes from young cells.
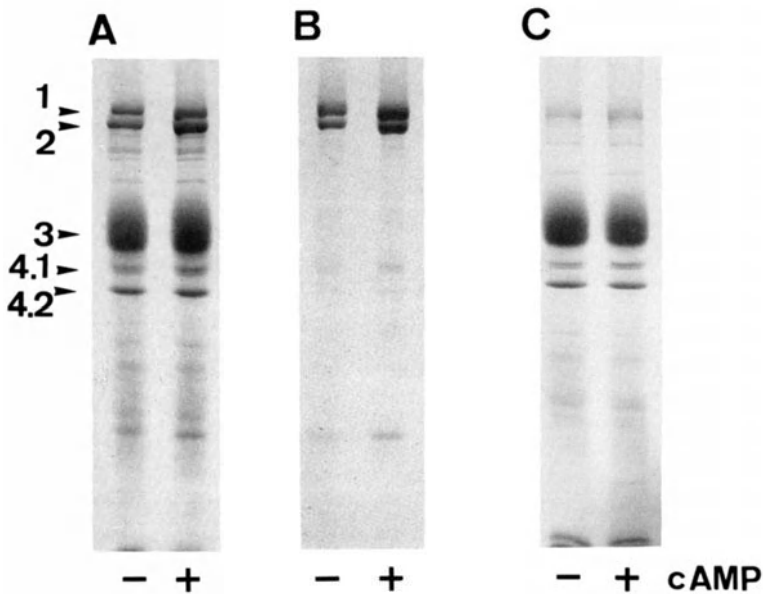


Fig. 2. **Enhanced generation of IOV-associated spectrin in young red cells in response to 200 µM cAMP.** Young red cells with a creatine content of 187 µg /$10^{10}$ red cells were incubated for 14 h under ATP-maintaining conditions either in the absence (-) or the presence (+) of 200 µM cAMP. KCl-stripped IOV (**A**) were prepared from both types of cells. Membrane-associated spectrin was extracted by urea (**B**). Urea-extracted vesicles (**C**) were washed in 5 mM phosphate. Equal volumes of each preparation. were run on SDS PAGE. Stained gels are shown.

Hence, generation of IOV-associated spectrin from low ionic strength-extractable spectrin appears a cAMP-dependent process. As adenylate cyclase and most kinase activities decay exponentially from reticulocytes to mature red cells , it is not surprising to find that old red cells are no longer capable of generating IOV-associated spectrin. These properties strongly suggest that spectrin molecules associated with IOV differ from the bulk in their binding properties and their dynamics.

In order to compare this interesting subpopulation of spectrin with normal spectrin dimer we aimed at purifying it. Selective extraction of spectrin from IOV was not an easy problem. The best and reproducible results were obtained by extracting KCl-stripped IOV with 4 - 5 M urea at low ionic strength (Fig. 2 B). Extraction of spectrin from KCl-stripped membranes was complete (Fig. 2 C), irrespective of whether cells were pretreated with or without cAMP. Thus, both the preexisting portion of IOV-associated spectrin and the one generated by cAMP have the same properties and were coextracted. The two high molecular weight bands (Fig. 2 B) from these extracts reacted similarly with anti-spectrin antibodies as low ionic strength extracted spectrin (not shown).

Two-dimensional peptide maps of urea-extractable spectrin revealed a high similarity and a few distinct differences to those of low ionic strength extractable spectrin (not shown). The two phosphopeptide maps differed greatly and both differed from the one obtained from spectrin that was in vitro phosphorylated by ATP and the catalytic subunit of a cAMP-dependent protein kinase (Lutz, 1984; Maretzki and Lutz, 1986). The complexity of these maps and the finding that many strongly labeled phophopeptides represented weakly stained peptides call for caution, particularly because the preparation used for this analysis was yet only 90 % pure. We have since purified urea extractable spectrin and will report on its peptide and phosphopeptide composition elsewhere (Mariani and Lutz, unpublished result). So far we can conclude that urea-extractable material is mainly composed of spectrin and contains additional phosphopeptides as compared to low ionic strength extractable spectrin .

The difficulties in extracting IOV-associated spectrin prompted us to study whether this subpopulation of spectrin was fatty acid-acylated. Results obtained with [9,10(n)$^3$H]-palmitate showed a slow incorporation of label, with saturation being reached beyond 5 hours. Autoradiographs from the high molecular weight region of SDS PAGE show even on overloaded gels no incorporation into low ionic strength-extractable spectrin (Fig. 3A). Likewise, the highest molecular weight species of ankyrin was devoid of label. Breakdown products of ankyrin contained, however, label and their labeling was not increased by adding cAMP. On the contrary, the minute amounts of urea-extractable spectrin were labeled in both bands. The specific labeling of urea-extractable spectrin was by far the highest among high molecular weight proteins. Its labeling increased proportionally to the amount of protein in extract. Fatty acid-acylation of urea-extractable spectrin was found in 4 experiments, but the extent of labeling in spectrin band 1 was variable. Label was indeed associated with spectrin, since one-dimensional peptide maps of spectrin band 2 allowed to identify 4 labeled peptides which coincided with stained peptides. Two of these peptides also showed a cAMP-dependent increase in $^{32}$P-phosphate labeling (not shown).
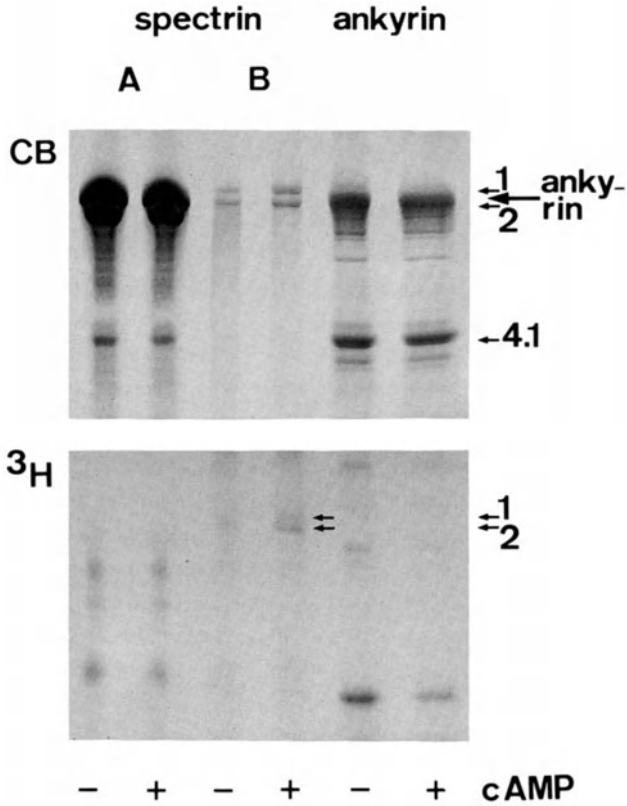
**Fig. 3. Labeling of IOV-associated, urea-extractable spectrin by [9,10(n) $^3$H] palmitate.** Unseparated red cells were incubated with labeled palmitate as outlined and with (+) or without (-) 200 µM cAMP. The reactions were stopped, membranes isolated. The following extracts were prepared and run on SDS PAGE: low ionic strength-extractable spectrin (**A**); urea-extractable spectrin (**B**); extract obtained with 1 M KCl from IOV, containing primarily ankyrin and band 4.1. **CB**, stained gel: $^3$**H,** fluorograph; 1,2 refer to spectrin subunits. The small arrows on the fluorograph point to acylated spectrin band 1 and 2.

## Conclusions

The results suggest that a limited number of spectrin molecules alters its binding properties in response to cAMP. This is a novel aspect for red cells and may have functional implications in maintenance of red cell shape. It is for example conceivable that this membrane-associated spectrin molecules are equally spread over the inner surface and directly mediate the contact of the skeleton with the bilayer in contrast to the bulk of spectrin which binds via ankyrin to the membrane. This would result in at least two types of spectrin-mediated, skeleton-membrane interactions. This hypothesis is in fact well supported by physiological phenomena: formation of "macrobuds" in early echinocytosis occurs without a release of spectrin from the bilayer (Ziparo et al.1978). Generation of "microbuds" in the course of extended ATP-depletion occurs regularly over the surface

and terminates in the release of "spectrin-free vesicles" (Lutz et al.1977; Müller et al.1981; Lutz, 1978). These vesicles are not only free of spectrin, but likewise of ankyrin, a phenomenon that up to now could not be explained on the basis of a spectrin-ankyrin membrane connnection. Furthermore, these vesicles bud of primarily from young cells (Snyder et al.1985).  We speculate: areas of membranes that potentially can bud off as spectrin-free vesicles are those that contain fatty acid-acylated spectrin. The observed loss of membrane-associated (IOV-associated) spectrin with cell age (not shown), may occur by in vivo release of spectrin-free vesicles  (Lutz, 1978; Dumaswala, Greenwalt, 1984) or/and by substitution of these links by ankyrin-spectrin mediated anchorage of the membrane skeleton.

**References**

Bennett V, Stenbuck PJ (1979) Identification and partial purification of ankyrin, the high affinity membrane attachment site for human erythrocyte spectrin. J Biol Chem 254:2533-2541

Branton D, Cohen CM, Tyler J (1981) Interaction of cytoskeletal proteins on the human erythrocyte membrane. Cell 24:24-32

Dumaswala UJ, Greenwalt TJ (1984) Human erythrocytes shed exocytic vesicles in vivo. Transfusion 24:490-492

Hargreaves WR, Giedd KN, Verkleij A, Branton D (1980) Reassociation of ankyrin with band 3 in erythrocyte membranes and lipid vesicles. J Biol Chem  255:11965-11972

Kellie S, Wigglesworth NM (1987) The cytoskeletal protein vinculin is acylated by myristic acid. FEBS Lett 213:428-432

Low MG, Kincade PW (1985) Phosphatidylinositol is the membrane anchoring domain of the Thy-1 glycoprotein. Nature 318:62-64

Lutz HU, Liu S-C, Palek J (1977) Release of spectrin-free vesicles from human erythrocytes during ATP depletion. J  Cell Biol 73:548-560

Lutz HU (1978) Vesicles isolated from ATP-depleted erythrocytes and out of thrombocyte-rich plasma. J Supramol Struct 8:375-389

Lutz HU, Flepp R, Stringaro-Wipf G (1984) Naturally occurring autoantibodies to exoplasmic and cryptic regions of band 3 protein of human red blood cells. J Immunol 133:2610-2618

Lutz HU (1984) A cyclic AMP-dependent phosphorylation of spectrin dimer. FEBS Lett 169:323-329

Lutz HU, Stringaro-Wipf G, Maretzki D (1986) Red cell spectrin phosphorylation and cytoskeletal anchorage. J Cardiovasc Pharmacol 8(Suppl.8):76-79

Lutz HU, Bussolino F, Flepp R, et al (1987) Naturally occurring anti-band 3 antibodies and complement together mediate phagocytosis of oxidatively stressed human red blood cells. Proc Natl Acad Sci USA 84:7368-7372

Lutz HU (1988) Commentary to "The relationship of red cell enzymes to cell life-span by E. Beutler. Blood Cells 14:76-80

Maretzki D, Lutz HU (1986) Calmodulin inhibits the phosphorylation of spectrin in vitro. Arch Biochem Biophys 246:469-477

Medof ME, Lublin DM, Holers VM, et al (1987) Cloning and characterization of cDNAs encoding the complete sequence of decay-accelerating factor of human complement. Proc Natl Acad Sci USA 84:2007-2011

Müller H, Schmidt U, Lutz HU (1981) On the mechanism of vesicle release from ATP-depleted human red blood cells. Biochim Biophys Acta 649:462-470

Snyder LM, Fairbanks G, Trainor J, Fortier NL, Jacobs JB, Leb L (1985) Properties and characterization of vesicles released by young and old human red cells. Br J Haematol 54:513-522

Speicher DW, Morrow JS, Knowles WJ, Marchesi VT (1980) Identification of proteolytically resistant domains of human erythrocyte spectrin. Proc Natl Acad Sci USA 77:5673-5677

Taguchi R, Suzuki K, Nakabayashi T, Ikezawa H (1984) Acetylcholinesterase release from mammalian erythrocytes by phosphoinositol-specific phospholipase C of Bacillus thuringensis and characterization of the released enzyme. J Biochem 96:437-444

Ziparo E, Lemay A, Marchesi VT (1978) The distribution of spectrin along the membranes of normal and echinocytic human erythrocytes. J Cell Sci 34:91-101

# Inhibition of Tropomyosin Binding to F-Actin by Tropomodulin, a New Tropomyosin-Binding Protein from the Human Erythrocyte Membrane

Velia M. Fowler

Department of Molecular Biology

Research Institute of Scripps Clinic

10666 North Torrey Pines Road

La Jolla, CA 92037

U.S.A.

Tropomyosins in non-muscle cells are thought to influence actin filament organization and function by binding to actin and blocking the action of severing, cross-linking or bundling proteins on actin filaments (Burgess et al., 1987; Côté, 1983; Matsumura and Yamashiro-Matsumura, 1986; Payne and Rudnick, 1985; Prulière et al., 1986). A role for tropomyosin in regulation of actomyosin ATPase in non-muscle cells is less certain due to the absence (to date) of proteins analogous to the muscle troponins that bind tropomyosin and directly influence its interaction with actin (Côté, 1983; Payne and Rudnick, 1985).

We have discovered a new $M_r$ 43,000 non-actin tropomyosin-binding protein that we have named tropomodulin on the basis of its ability to inhibit tropomyosin binding to actin. This protein was initially identified by binding of ^{125}I-labeled tropomyosin to nitrocellulose blots of erythrocyte membrane proteins separated by SDS-gel electrophoresis and was shown to be present in the membrane skeleton in a ratio of 1 for every 2 tropomyosin molecules (Fowler, 1987). This protein is not related to actin, a tropomyosin binding protein with a similar subunit molecular weight because (1) ^{125}I-tropomyosin does not bind to actin on blots, (2) its mobility is distinct from actin on SDS gels in the presence of 4M urea ($M_r$ 45,000) or on SDS gels with a pH 9.1 separating gel ($M_r$ 39,000), (3) its hydrodynamic properties are distinct from those of actin, and indicate that it is a somewhat asymmetric monomer (2.8S, $R_s$ = 3.7 nm; f/fo = 1.5), (4) only two $M_r$ 43,000 tropomodulin monomers bind to each tropomyosin molecule at saturation, whereas between 6 and 7 actin subunits in an actin filament interact with each erythrocyte tropomyosin molecule (Fowler and Bennett, 1984a), (5) unlike actin, tropomodulin does not appear to self-associate into filaments (or otherwise) under physiological

salt conditions, and (6) antibodies specific for tropomodulin do not cross-react with actin and vice versa (Fowler, 1987).

Originally, tropomodulin was purified from a 1M Tris extract of tropomyosin-depleted erythrocyte membranes (Fowler, 1987). However, the yields of protein obtained by this procedure were poor (about 50 $\mu$g from 300 ml of membranes), primarily due to inefficient extraction from the membranes. We have found that tropomodulin can be completely solubilized from Triton X-100 extracted erythrocyte membranes by treatment with 0.8M sodium bromide at 4°C, without appreciably extracting either the spectrin or the erythrocyte actin. Starting with 300 mls of membranes, approximately 500 $\mu$g of tropomodulin, 95% pure, can be purified from this extract by sequential steps of ion exchange chromatography on DEAE cellulose, gel filtration on Ultrogel AcA 34, and sedimentation on 5-20% sucrose gradients (Fowler and Smith, 1989).

Tropomodulin is a potent non-competitive inhibitor of erythrocyte tropomyosin binding to F-actin ($K_i \approx 0.8$ $\mu$M), and is equally effective whether or not the tropomyosin is preincubated with the actin before addition of the protein. Unlike other proteins from non-muscle cells which influence tropomyosin binding to actin (e.g., caldesmon, filamin), tropomodulin itself does not bind to F-actin (Fowler and Smith, 1989). This implies that binding of tropomodulin to tropomyosin induces a conformational change in the tropomyosin which interferes with the ability of tropomyosin to bind to F-actin. This idea is consistent with the inability of a large excess of F-actin to block ^{125}I-tropomyosin binding to tropomodulin on blots (Fowler, 1987). The interaction of tropomodulin with tropomyosin is also qualitatively different from that with the muscle troponins, which enhance the binding of non-muscle tropomyosins to F-actin (Côté, 1983), and are unable to compete for binding of ^{125}I-tropomyosin to tropomodulin (Fowler, 1987).

In muscle tropomyosins, the C-terminal end of one tropomyosin molecule binds to the N-terminal end of another, mediating the head-to-tail self-association of the tropomyosin molecules along the actin filament (Côté, 1983; Leavis and Gergely, 1984). Although it has been reported that erythrocyte tropomyosin is incapable of head-to-tail self-association using a viscometric assay (Mak et al., 1987), ^{125}I-labelled

erythrocyte tropomyosin binds to itself on nitrocellulose blots (Fowler, 1987), and binding of erythrocyte tropomyosin to F-actin is highly cooperative, as is muscle tropomyosin, implying that it self-associates along the actin filament (Fowler and Bennett, 1984). Thus, it is tempting to speculate that tropomodulin could bind to (one of) the ends of the tropomyosin molecule, blocking the ability of erythrocyte tropomyosin to self-associate along the actin filament, thereby weakening its binding to actin.

Erythrocyte tropomodulin is anticipated to be a representative of a new class of tropomyosin-binding proteins since immunoreactive polypeptides have been detected in a variety of non-erythroid cells and tissues, including skeletal muscle, brain, lens, neutrophils and endothelial cells (Fowler and Smith, 1989). In erythrocytes, we propose that tropomodulin functions with tropomyosin to regulate the interaction of the membrane-associated actin filaments with spectrin or other erythrocyte actin-binding proteins (Fowler and Bennett, 1984b; Mak et al, 1987) and, thus, influences the assembly and organization of the erythrocyte membrane skeleton. Alternatively, since erythrocytes contain myosin (Fowler et al., 1985; Wong et al., 1985), tropomodulin could function with tropomyosin to regulate erythrocyte actomyosin ATPase activity and influence erythrocyte shape.

REFERENCES

Burgess DR, Broschat KO, Hayden JM (1987) Tropomyosin distinguishes between the two actin-binding sites of villin and affects actin-binding properties of other brush border proteins. J Cell Biol 104:29-40

Côté GP (1983) Structure and function of non-muscle tropomyosins. Molec Cell Biochem 57:127-146

Fowler VM (1987) Identification and purification of a novel $M_r$ 43,000 tropomyosin-binding protein from human erythrocyte membranes. J Biol Chem 262:12792-12800

Fowler VM, Bennett V (1984a) Erythyrocyte membrane tropomyosin: Purification and properties. J Biol Chem 259:5978-5989

Fowler VM, Bennett V (1984b) Tropomyosin:  A new component of the erythrocyte membrane skeleton.  In:  Brewer GJ (ed) Erythrocyte Membranes 3:  Recent Clinical and Experimental Advances.  Alan R Liss, Inc, New York, 57-71

Fowler VM, Davis JQ, Bennett V (1985) Human erythrocyte myosin: Identification and purification.  J Cell Biol 100:47-55

Fowler VM, Smith CM (1989) Tropomodulin, a new tropomyosin-binding protein from the human erythrocyte membrane that regulates tropomyosin binding to F-actin, manuscript in preparation.

Leavis PC, Gergely J (1984) Thin filament proteins and thin filament linked regulation of vertebrate muscle contraction.  CRC Crit Rev Biochem 16:235-305

Mak AS, Roseborough G, Baker H (1987) Tropomyosin from human erythrocyte membrane polymerizes poorly but binds F-actin effectively in the presence or absence of spectrin.  Biochem Biophys Acta 912:157-166

Matsumura F, Yamashiro-Matsumura S (1986) Modulation of actin-bundling activity of 55-KDa protein by multiple isoforms of tropomyosin.  J Biol Chem 261:4655-4659.

Payne MR, Rudnick SE (1985)  Tropomyosin.  Structural and functional diversity. In: Shay JW (ed) Cell and Muscle Motility.  Plenum Press, New York, 6:141-184

Prulière G, d'Albis, A, der Terrossian E (1986) Effect of tropomyosin on the interactions of actin with actin-binding proteins isolated from pig platelets.  Eur J Biochem 159:535-547

Wong AJ, Kiehart DP, Pollard TD (1985) Myosin from human erythrocytes.  J Biol Chem 260:46-49

Yamashiro-Matsumura S, Matsumura F (1988)  Characterization of 83-kilodalton non-muscle caldesmon from culture rat cells: Stimulation of actin binding of non-muscle tropomyosin and periodic localization along microfilaments-like tropomyosin.  J Cell Biol 106:1973-1983

# A Model for Protein-Protein Interactions Involved in the Linkage of the Actin Cytoskeleton to Transmembrane Receptors for Extracellular Matrix Proteins

Shin Lin, Mary A. Risinger, and James A. Butler

Department of Biophysics

Johns Hopkins University

Baltimore, MD 21218

U.S.A.

Actin filament bundles in cultured fibroblasts can be seen by electron microscopy to emanate from specialized regions of the cell membrane where the cell adheres tightly to the underlying substratum -- the adhesion plaques or focal adhesions (see Chen and Singer, 1982, for discussion). Results from immunofluorescence and protein binding experiments have implicated a number of proteins in the anchorage of the actin filaments (F-actin) to the membrane at these locations (see Burridge, 1986, for a recent review). A schematic model of possible interactions among these proteins based on current information is presented in Figure 1.
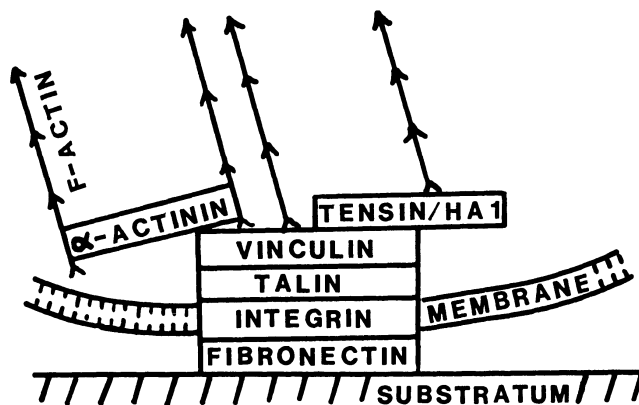


Figure 1. A schematic model of protein interactions at the adhesion plaque of a fibroblast.

We have focussed our research in this general area on the protein vinculin, which had previously been shown by Geiger et al. (1980) to be localized at the adhesion plaques. To test whether the protein interacts directly with actin, we examined its effect on F-actin elongation in vitro. Initial results showed that substoichiometric amounts of the vinculin preparation used inhibited monomer addition at the barbed end of the filaments (Wilkins and Lin, 1982). Subsequent

studies indicated that much of this activity is attributed to minor amounts of contaminating polypeptides designated as HA1 (Wilkins and Lin, 1986). More highly purified vinculin, however, was found to retain a low level of activity (Wilkins et al., 1986), a result confirmed by more detailed studies by Wegner (1988). The conclusion that vinculin interacts with low affinity with the barbed ends of F-actin is consistent with studies showing binding of ^{3}H-labelled vinculin to F-actin at a molar ratio of $1:10^3$ actin monomers (Wilkins and Lin, 1982).
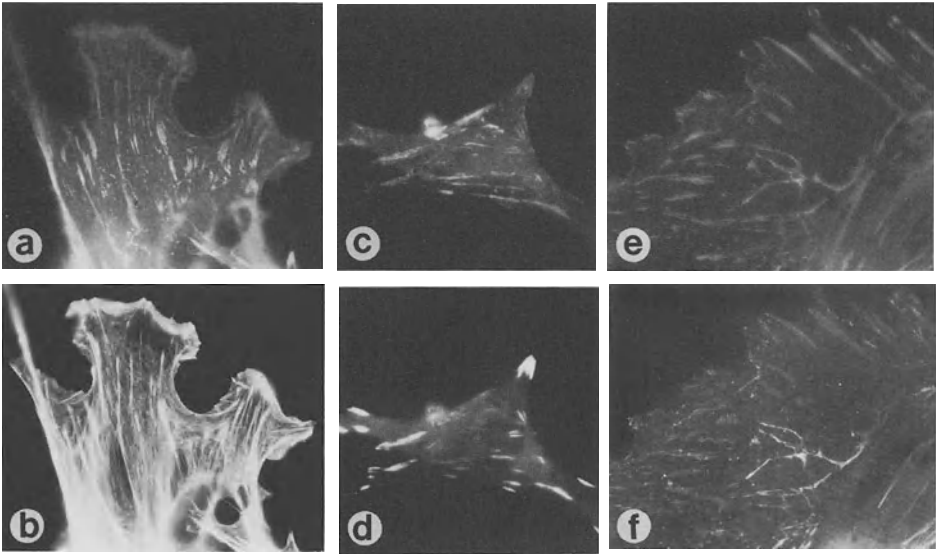


Figure 2.   Fluorescence localization of adhesion plaque proteins in chicken embryo fibroblasts.   F-actin was stained with fluorescently labelled phalloidin. The other proteins were stained with specific antibodies, followed with secondary antibodies labelled with fluorescein or rhodamine.   (a) and (b), cell double-stained for tensin and F-actin, respectively.   (c) and (d), cell double-stained for tensin and vinculin, respectively.   (e) and (f), cell double-stained for talin and integrin, respectively.

Further work on HA1, a heterogenous group of polypeptides with Mr of 25,000 to 45,000, led to the isolation of an immunologically related protein, designated as tensin (Mr = 150,000) (Wilkins et al., 1987). Antibodies against either HA1 or tensin were found to stain the ends of actin filament bundles of fibroblasts in a manner similar to anti-vinculin antibodies (Wilkins et al., 1986, and Figure 2a-d). Moreover, consistent with the co-localization of the two proteins at the adhesion plaques (Figure 2 c, d), we found in a blot-overlay experiment that ^{125}I-labelled tensin binds with saturability to vinculin transferred from SDS gel to nitrocellulose blots, indicating the capability of these proteins to interact

with each other (Wilkins et al., 1987).  On the other hand, we found that the purified tensin preparation has little or no activity in actin polymerization assays.  The structural and functional relationship between tensin and HA1 is unclear at this time.

The blot-overlay assay had also been used to show that ^{125}I-labelled vinculin binds with saturability to polypeptides in the 200,000 dalton range present in extracts of smooth muscle and platelets (Wilkins et al., 1983). Subsequent studies revealed that these polypeptides are related to the protein talin (Burridge and Mangeat, 1984), also localized at the adhesion plaques of fibroblasts (Burridge and Cornell, 1983).  Talin, in turn, had been shown with an equilibrium gel filtration assay to interact with integrin (also referred to as CSAT antigen) (Horwitz et al., 1986), a transmembrane receptor for the extracellular matrix protein fibronectin at adhesion plaques (Horwitz et al., 1985).  These results are consistent with the co-localization of the two proteins in the cell (Figure 2 e, f).

The blot-overlay experiment described above also revealed low affinity binding of ^{125}I-labelled vinculin to  alpha-actinin (Wilkins et al., 1973), a protein known to bind along the sides of F-actin (Goll et al., 1972) and to be concentrated at adhesion plaques (Geiger, 1979).  Subsequently, we used the technique of fluorescence energy transfer to measure binding of fluorescently labelled vinculin and alpha-actinin under equilibrium conditions.  We found that much of the binding is saturable and can be inhibited by reaction of the vinculin with a sulfhydryl reagent (Wachsstock et al., 1987).

In summary, the picture that is emerging at this time shows that multiple interactions among a growing list of proteins contribute to the total force holding actin filaments to the cell membrane at the adhesion plaques.  As shown in Figure 1, F-actin can attach directly to vinculin, or indirectly through its interactions with  alpha-actinin and with HA1/tensin.  Vinculin, in turn, can be linked to the talin-integrin-fibronectin chain.  In considering this model, however, one should be aware that further investigations may very well reveal additional protein components and linkages not described here.  In addition, one should keep in mind that the binding experiments described here were done with purified proteins from muscle.  Further studies have to be performed to see if analogous proteins from fibrobalsts have the same properties and whether the interactions of the proteins are influenced by cytoplasmic factors.

## REFERENCES


Burridge K (1986) Substrate adhesion in normal and transformed fibroblasts: organization and regulation of cytoskeletal, membrane and extracellular matrix components at focal contacts.  Cancer Res 4:18-78

Burridge K, Connell L (1983) A new protein of adhesion plaques and ruffling membranes. J Cell Bio 97:359-367

Burridge K, Mangeat P (1984) An interaction between vinculin and talin. Nature 308:744-746

Chen W-T, Singer SJ (1982) Immunoelectron microscopic studies of the sites of cell-substratum and cell-cell contacts in cultured fibroblasts. J Cell Biol 95:205-222

Geiger B (1979) A 130K protein from chicken gizzard: its localization at the termini of microfilament bundles in cultured chicken cells.  Cell 18:193-205

Geiger B, Tokuyasu KT, Dutton AH, Singer SJ (1980) Vinculin, an intracellular protein localized at specialized sites where microfilament bundles terminate at cell membranes. Proc Natl Acad Sci USA 77:4127-4131

Goll DE, Suzuki A, Temple J, Holmes GR (1972) Studies on purified alpha-actinin. J Mol Biol 67:469-488

Horwitz A, Duggan K, Buck C, Beckerle MC, Burridge K (1986) Interaction of plasma membrane fibronectin receptor with talin -- a transmembrane linkage.  Nature 320:531-533

Horwitz A, Duggan K, Greggs R, Decker C, Buck CJ (1985) The CSAT antigen has properties of a receptor for laminin and fibronectin.  J Cell Biol 101:2134-2144

Wachsstock DH, Wilkins JA, Lin S (1987) Specific interaction of vinculin with alpha-actinin.  Biochem Biophys Res Comm 146:554-560

Wegner A (1988) this volume

Wilkins JA, Chen KY, Lin S (1983) Detection of high molecular weight vinculin binding proteins in muscle and non-muscle tissues with an electroblot-overlay technique. Biochem Biophys Res Comm 116:1026-1032

Wilkins JA, Lin S (1986) A re-examination of the interaction of vinculin with actin. J Cell Biol 102:1085-1092

Wilkins JA, Lin S (1982) High-affinity interaction of vinculin with actin filaments in vitro. Cell 28:83-90

Wilkins JA, Risinger MA, Lin S (1987) Purification of a vinculin binding protein from smooth muscle.  J Cell Biol 105:130a

Wilkins JA, Risinger MA, Lin S (1986) Studies on proteins that co-purify with smooth muscle vinculin.  Identification of immunologically related species in focal adhesions of nonmuscle and Z-lines of muscle cells.  J Cell Biol 103:1483-1494

# The Anchorage of the Cytoskeleton to the Plasma Membrane: Interaction of Vinculin with Membranes In Vitro and In Situ

V. Niggli, L. Sommer[1], J. Brunner[1] and M.M. Burger[1]
Dept. of Pathology, University of Bern
Freiburgstr. 30, 3010 Bern, Switzerland

The widely distributed cytoskeletal protein vinculin has been impli-
cated to participate in actin-membrane linkage. This hypothesis is
mainly based on the highly specific location of vinculin in areas
where this linkage occurs. However, conclusive evidence confirming
this hypothesis is yet lacking, and the molecular mechanism of the
proposed linkage of vinculin to both actin filaments and the plasma
membrane has not yet been clarified.

We have now shown by hydrophobic photolabeling that vinculin inter-
acts in vitro directly with bilayers of acidic phospholipids (Niggli
et al., 1986). In order to investigate whether such an interaction
occurs also in intact cells, chicken embryo fibroblasts were incuba-
ted for two hours with a $^3$H-labeled photoactivatable fatty acid
(11-[4-[3-(trifluoromethyl)diazirinyl]phenyl]-[2-$^3$H]-undecanoic acid
= [$^3$H]TUA). This fatty acid exhibits identical photochemical proper-
ties as the phospholipid used in the in vitro studies. Part of the
fatty acid added to the cells was incorporated into cellular phospho-
lipids and diglycerides. The cells were then photolyzed at 360 nm.
This procedure did not change the morphology of the cells and pro-
tein synthesis was not affected. Subcellular fractions were isolated
both from photolyzed and non-photolyzed cells by high-speed centrifu-
gation of cellular homogenates. Vinculin was immunoprecipitated from
a crude membrane fraction and from a soluble fraction using a speci-
fic polyclonal anti-vinculin antibody. The immunoprecipitates were
analyzed on 7.5% SDS-polyacrylamide gels, followed by autoradiogra-
phy. Scans of the vinculin bands on the Coomassie blue-stained gel
and autoradiograph of a typical experiment are shown in Fig. 1. Vin-
culin was recovered from both fractions, the cytosolic fraction con-
taining 2-3-fold more vinculin than the membrane fraction (Fig. 1A).
Significant incorporation of label was restricted to membrane-asso-
ciated vinculin isolated from photolyzed cells (Fig. 1B). Cytosolic

[1]L.S.: Biocenter, Basel; J.B.: Lab. of Biochemistry, ETH-Z, Zürich;
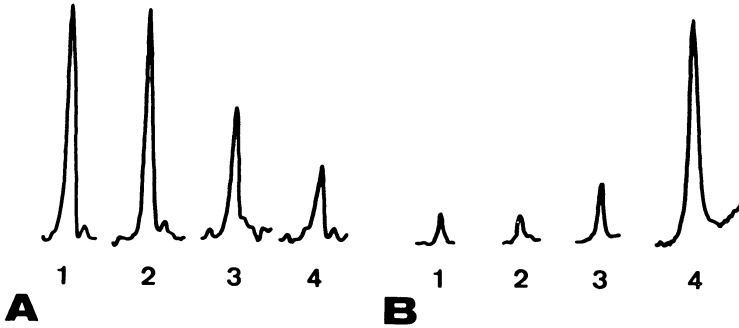M.M.B.: Friedrich Miescher Institute, Basel, Switzerland

Fig. 1: Labeling of vinculin by [$^3$H]TUA in intact cells
Incubation of the chicken embryo fibroblasts with the label, photolysis and immunoprecipitation of vinculin from subcellular fractions were carried out as described in the text. Scans of the vinculin bands on the Coomassie blue-stained gel of the immunoprecipitates (A) and scans of the vinculin bands on the corresponding autoradiograph (B) are shown. 1,3: fractions isolated from non-photolyzed cells; 2,4: fractions from photolyzed cells; 1,2: soluble fraction; 3,4: crude membrane fraction.

vinculin was much less labeled, and photolysis had no effect on incorporation of label. For a quantitative evaluation of the experiments, specific vinculin labeling was calculated from the peak areas of the scans. Photolysis increased labeling of membrane-associated vinculin 4-8-fold, as determined in three experiments. Moreover, specific labeling of the membrane-bound protein was 8-30-fold higher than that of the cytosolic protein, after photolysis. These results strongly suggest, that vinculin interacts also in intact cells directly with the hydrophobic part of bilayers. The molecular mechanism and the functional relevance of this interaction are not yet known.

Recently, several cytoskeleton associated soluble proteins have been shown to interact directly with lipids which in some cases may regulate their function (reviewed in: Niggli and Burger, 1987). The technique described above may allow the verification of this new concept in intact cells.

REFERENCES

Niggli V, Burger MM (1987) Interaction of the cytoskeleton with the plasma membrane. J Membrane Biol 100:97-121

Niggli V, Dimitrov DP, Brunner J, Burger MM (1986) Interaction of the cytoskeletal component vinculin with bilayer structures analyzed with a photoactivatable phospholipid. J Biol Chem 261:6912-6918

# Connectors of Supramolecular Assemblies

J.H. Fessler, B. Blumberg, A.G. Campbell, K. Garrison, A.J. MacKrell, R.E. Nelson,
P.F. Olson and L.I. Fessler
Molecular Biology Institute and the Department of Biology
University of California, Los Angeles
405 Hilgard Avenue
Los Angeles, California  90024
USA

## INTRODUCTION

An underlying theme of this meeting is the search for potential biophysical relationships between the extracellular matrix and the cytoskeleton.  We found that the fruit fly, Drosophila melanogaster, shares with vertebrates some major extracellular matrix components that are adjacent to cell surfaces, and also a transmembrane receptor of the integrin type.  Actin filaments are probably indirectly linked to the cytoplasmic portion of such receptors in vertebrates and very similar actins exist in Drosophila.  This suggests that parts of the molecular relationships between the extracellular matrix and the cytoplasm have been conserved during evolution, and that these mechanisms are likely to have important roles in cell biology.

The advantages of the Drosophila melanogaster system for this study are the potential for genetic manipulation, both by breeding and by recombinant DNA techniques.  We have isolated several of the genes and will insert modified forms of them into cultured cells and into the germline of animal stocks.  We wish to see the effect of modifying key molecules on the processes of supramolecular assembly, and can also observe the de novo normal or abnormal assembly during embryological development.

We characterized the basement membrane glycoproteins collagen IV (Blumberg et al., 1988; Lunstrum et al., 1988), laminin (Fessler et al., 1987), a proteoglycan called papilin (Campbell et al., 1987), and glutactin (Olson et al., 1988).  Cross-adsorbed antibodies against each purified component stain common, basement membrane locations in Drosophila embryos, larvae and adults.  Collagen IV and laminin molecules share the same domain structures as their vertebrate equivalents.  This is strikingly apparent in the appearance of sprayed and rotary shadowed molecules in the electron microscope (Fessler et al., 1987; Lunstrum et al., 1988), and has also been seen in laminins from other evolutionary distant animals (McCarthy et al., 1987).

DROSOPHILA COLLAGEN IV

 Comparison of the amino acid sequences that are deduced from cloned cDNA sug-
gest that evolutionary conservation is probably highest in those domains of these
macromolecules that are important in their functional interaction with each other,
and with other components. The NC1 domain of collagen IV is specially adapted for
joining the carboxyl ends of two collagen IV molecules to each other (Timpl et al.,
1985). Each molecule consists of three chains, and the carboxyl-most 230 amino
acids of each chain are folded into a compact, disulfide-linked structure that is
juxtaposed to the other carboxyl ends of the triplet. In the mouse, two of the
three chains are identical, and are called α1(IV), and the third chain is from ano-
ther gene called α2(IV). The junction between the carboxyl ends of two trimeric
collagen molecules is therefore a heteromeric hexamer. Sweet and Eisenberg (1983)
defined a hydrophobic correlation coefficient which reliably predicts whether two
aligned sequences share the same three-dimensional structure. Proteins with close-
ly similar three-dimensional structures have a hydrophobic correlation coefficient
greater than 0.4. For example, the coefficient for horse alpha and beta globins is
0.68. The correlation coefficient between the two mouse carboxyl sequences that
make up the hexameric junction is 0.82. Drosophila collagen IV molecules are most-
ly homotrimeric. The hydrophobic correlation coefficient between the Drosophila
carboxyl sequence and that of mouse α1(IV) is 0.78, and with mouse α2(IV) is 0.72.
Thus the three-dimensional structure of this key junctional domain of Drosophila
basement membrane collagen is almost as closely related to either of the two mouse
sequences that form a heterohexamer, as the two mouse sequences are to each other.
This is also shown in a 59% identity of amino acids of this part of the Drosophila
chain with either mouse chain, and in the conservation of the positions of all 12
cysteine residues (Blumberg et al., 1987; Cecchini et al., 1987).

 In contrast, the amino acid sequences that form the collagen helical part of
the Drosophila basement membrane collagen IV are poorly conserved relative to those
of mouse, except for the Gly-X-Y motif that is essential for the collagen triple
helical fold. The collagen thread also has a different number of amino acids, and
correspondingly a different length in the electron microscope (Blumberg et al.,
1988; Lunstrum et al., 1988).

 At the amino end of vertebrate collagen IV is a junctional domain of about
30nm of collagen helix. The amino domains of four collagen triple helices overlap
to form a 30nm-long tetramer called a 7S junction, in which the N-to-C peptide di-
rection of two molecules is the same and antiparallel to the other two molecules.
Strategically placed cysteine residues at the boundaries of the 30nm overlap spon-
taneously form disulfide bridges between adjacent molecules (Timpl et al., 1981;
Duncan et al., 1983). Drosophila collagen IV has a modulated form of the same

junctional domain, with equivalently placed cysteine residues. The sequence simi-
larity between Drosophila and mouse over this domain is distinctly higher than over
any other parts of their collagen helical regions, which are otherwise relatively
poorly conserved. There are also several lysine residues that are potential
bridgeheads for lysine-derived cross links, such as are known to exist in the ver-
tebrate 7S junction. Interestingly, however, three small changes between verte-
brates and Drosophila may cause appreciable differences in the final supramolecular
assemblies that are formed from these similar collagen molecules (Blumberg et al.,
1988).

First, the vertebrate 7S junctional domain clearly joins four molecules, and
while dimers and trimers appear at low concentrations during the assembly process,
these are only intermediates for the final, dominant, tetrameric junction. In con-
trast, the major Drosophila collagen IV polymer extracted from embryos, larvae and
cell cultures is the dimer, with progressively decreasing amounts of 7S-linked tri-
mers, tetramers, and higher forms. Siebold et al. (1987) showed that the distribu-
tion of hydrophobic amino acid residues favors the juxtapositioning of four ver-
tebrate collagen IV helices into a self-limiting tetrameric 7S junction. The un-
derlying asymmetric distribution of hydrophobic residues along the cylindrical sur-
face of a vertebrate collagen IV molecule depends critically on the heterotrimeric
combination of $\alpha 1$(IV) and $\alpha 2$(IV) chains. A homotrimeric collagen molecule could
not share this property. The association of Drosophila collagen IV molecules at
the corresponding junctional domain is not self-limited to tetramers, and this
would be consistent with a mostly homotrimeric composition.

Second, the 7S-like junctional domain is symmetrically duplicated at the amino
end of each Drosophila collagen chain. This provides the potential for, nominally,
both 30nm-long and 60nm-long junctional overlaps between two Drosophila collagen IV
molecules. Probably both forms exist, and there are several possibilities for the
junctions between three or more amino ends of Drosophila collagen IV molecules.
The diagram of Fig. 1 illustrates some of the possible relationships of two anti-
parallel Drosophila collagen IV molecules, though the locations of the cysteine
residues would also allow other disulfide-linked arrangements. Corresponding rela-
tionships are possible for two parallel molecules.

Third, the pattern of cysteine residues that defines the "double 7S" domain at
the amino end of Drosophila collagen IV is repeated at another position of the col-
lagen molecule in slightly modulated form. The distance between the two complex
domains is just one-third of the length of the collagen thread. While vertebrate
collagen IV has only a single 7S domain, there are also a few cysteine residues in
the vertebrate collagen thread that occupy equivalent positions to the Drosophila
cysteine residues in the more centrally placed junctional domain. The potential of
forming additional segment junctions one-third of the way along the Drosophila col-

lagen helix provides opportunities for a variety of multimolecular assemblies. These could be various networks, and/or microfibrillar structures, and the cysteine residues become remarkably well juxtaposed for extensive intermolecular disulfide bonding. Conceptually, a microfibril that is periodically disulfide cross-linked along its length can be expanded perpendicularly to its axis into a network of the same connectivity.
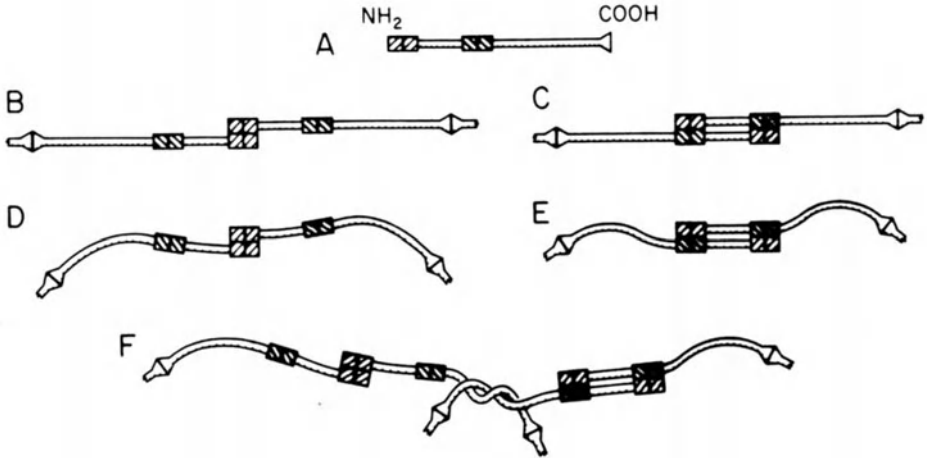


FIGURE 1

(A): Diagramatic _Drosophila_ collagen IV molecule with a highly conserved NCI junctional element (◁) at its carboxyl end, reduplicated "7S" junctional element (▨) at its NH$_2$ end, and a modulated copy of this (▧) at one-third of the collagen thread length.
(B) and (C): Diagrams of some of the ordered possible ways of joining two molecules.
(D) and (E): Same ordered junctional structures as (B) and (C), but with spatial disorder introduced by flexible linkages between the junctional domains.
(F): Same structures as (D) and (E), but illustrating the possibilities of topological linkage between polymerised flexible assemblies.

The interesting electron microscopic observations of Yurchenko and Ruben (1987) show that in some vertebrate basement membranes collagen IV molecules entwine around each other to form a topological linkage. It is not known whether this is related to the imperfections of collagen helical Gly-X-Y sequence that are scattered along the length of the collagen helical thread. The relative positions along the thread of half of the approximately 20 imperfections are remarkably exactly conserved in _Drosophila_, human and mouse, and most of the others are also closely matched. Yet the actual amino acid sequence that constitutes a given imperfection has not been conserved in _Drosophila_ relative to the vertebrates, and may significantly differ in kind and number of residues. Quantitative evaluation

of the flexibility of _Drosophila_ collagen IV molecules from electron micrographs indicates that there are not any fixed bends, and that some of the more flexible regions roughly correspond to locations of several imperfections. Our interim conclusion is that some evolutionary constraint has maintained the positions of the imperfections of helix, and may correspond to a requirement for supramolecular assembly. However, we do not know whether the actual amino acid residues within imperfections serve any specific functions.

It may be very difficult to provide an exact description of the network arrangements of collagen IV molecules in any basement membrane, and we do not have one for _Drosophila_. However, our studies of _Drosophila_ basement membrane collagen suggest that even a moderate number of possible connectivities could rapidly lead to an apparently complex arrangement, which might vary in detail from location to location. Nevertheless, such structures would not be random, and would obey an underlying order that is dictated by the arrangement of covalent junctions between molecules. The locations of cysteine residues along the collagen thread of _Drosophila_ collagen IV molecules potentially allow the formation of several different, interesting arrays of mutually disulfide-linked molecules. Combinations of parallel and antiparallel molecules, staggered by one-third of the collagen thread length, could form regularly disulfide-linked microfibrils (Blumberg et al., 1988). Similar arrays, splayed out perpendicularly to the microfibril axis, could form a network of the same connectivity. However, if the network were locally deformed to accomodate an adjacent cell surface then it might appear much less ordered than a microfibril of the same connectivity. Further variety might be introduced by connecting other combinations of cysteine residues either in different basement membranes or in various regions of a single basement membrane. Such combinations might be particularly suitable for a flexible basement membrane that needs to be able to interact intimately with varying cell surfaces. We suggest that there can be meaningful order in supramolecular assemblies of biopolymers without the repetitive regularity of a crystalline array, and that this may be more suitable for some biological needs.


## DROSOPHILA PAPILIN

This proteoglycan-like glycoprotein of _Drosophila_ basement membranes shows another type of connectivity (Campbell et al., 1987). As seen in the electron microscope, each molecule consists of a major loop from which a pair of fine threads protrude at one point. Upon reduction, the loop opens into a linear molecule of the same length, 225±15 nm. Disulfide bridges not only join the ends of individual molecules into loops, but also join loops into oligomers of loops. We do not know how the loops of papilin are connected to other basement membrane components.

## DROSOPHILA BETA INTEGRIN

We have found one of the potential connectors of basement membranes to cell surfaces of Drosophila (MacKrell et al., 1988). In the recessive embryonic lethal mutant myospheroid muscles pull clear of their enveloping basement membranes, and basement membranes rupture. We determined the cDNA sequence of the normal gene whose mutation gave rise to these defects. The translated amino acid sequence corresponds, with over 40% identity of amino acids, to a group of vertebrate cell surface receptors known as integrins (Hynes, 1987; Ruoslahti and Pierschbacher, 1987). A common theme of these receptors is recognition of a sequence related to Arg-Gly-Asp-Ser in various macromolecular, extracellular ligands such as fibronectin. All integrins are made up of two chains, called alpha and beta, which belong to variously related gene families. This Drosophila gene codes for a beta chain, which has a transmembrane region. The extracellular portion consists of several domains that have good homologies to the human and chick chains, and a characteristically cysteine-rich repetitive region. In the total molecule there are 56 cysteine residues, after cleavage of the signal peptide, and all have counterparts in the vertebrate analog chains. Of particular interest for the purposes of this conference are the transmembrane and cytoplasmic domains. Seventeen of the 23 residues of the transmembrane domain are identical in Drosophila, human and chick. This indicates that this transmembrane domain is likely to have a specific, conserved structure. The first 33 residues of the 46 amino acid long cytoplasmic domain are 88% identical between Drosophila and chick. The length of the cytoplasmic domain is highly conserved and most of the differences in amino acid residues are conservative substitutions. This suggests conservation of functional interactions of this domain with adjacent molecules. An indirect connection with actin filaments was indicated by in vitro reconstitution experiments with vertebrate receptors. This is influenced in transformed vertebrate cells by phosphorylation of a tyrosine residue (Hirst et al., 1986), that has also been conserved in the Drosophila protein's cytoplasmic domain.

Our in situ hybridization with nucleic acid probes show that many embryonic cells produce this integrin beta chain. It forms receptors in combinations with different alpha chains. Wilcox and associates (Bogaert et al., 1987; Leptin et al., 1987) found that position specific antigens, which are integrin chains, appear and disappear during Drosophila development in interesting correlation with some changes of cell patterns during development.

## POTENTIAL ASSEMBLY MECHANISM OF BASEMENT MEMBRANES

At present we do not know the extracellular macromolecular ligands of this integrin receptor. As loss of functional integrin in the myospheroid mutant may affect not only adhesion of muscle cells to basement membranes but also the assem-

bly of basement membranes (Newman and Wright, 1981), the receptor may also serve to assure adequate local concentrations of the assembly components. Basement membrane formation may necessitate cooperation between juxtaposed vertebrate cells (Kuhl et al., 1984). Both staining with antibodies and _in situ_ hybridization with nucleic acid probes for specific mRNAs indicate that potentially wandering Drosophila cells, called lamellocytes, produce collagen IV in regions where basement membranes form (Lunstrum et al., 1988; Mirre et al., 1988). We also find that these cells produce laminin and some other extracellular components. If these cells need to adhere to locations where basement membranes are to form, then one would expect some initial selective adhesion mechanism. We find both by immunostaining (Fessler et al., 1987) and by analyses of total embryos that during development distinct amounts of laminin appear a short time before substantial collagen IV synthesis starts.

## DROSOPHILA GLUTACTIN

The electrophoretic migration and some other properties of this basement membrane glycoprotein are quite similar to entactin, and we regarded it as the putative Drosophila equivalent of vertebrate entactin. From the cDNA sequence we determined the 1023 residue long amino acid sequence, and verified this by direct amino acid sequencing of several parts of the purified protein. Comparison with the sequence of vertebrate entactin, which was recently determined by Drs. Durkin and Chung and kindly made available to us, showed that these proteins were not homologous, and we have renamed the Drosophila protein glutactin. Glutamic acid and glutamine make up about 45% of the residues of its carboxyl domain, which is separated from the major two-thirds of the molecule by a stretch of 13 consecutive Thr residues. The protein is strongly acidic and contains several residues of tyrosine sulfate. It is likely to bind calcium, though not necessarily specifically, and gives a strong periodic acid Schiff's reaction. Antibodies locate it in all the major basement membranes. It lacks entactin's avidity to bind to laminin. We do not know its functional role in basement membranes.

## CONCLUSIONS

Our concepts of supramolecular assemblies are influenced by how we view the components and what we know of their abilities to link to each other. The successes of X-ray diffraction crystallography cause us to think of proteins as rigidly defined structures, and of the supramolecular assemblies of proteins as having a crystalline-like order. Yet polymer science has shown the utility of regarding some molecules as flexible, near-random chains. The large extracellular glycoproteins consist of several domains, with relatively flexible connectors between them. Supramolecular assemblies of such large proteins may themselves be flexible, and

while the nature of such assemblies will be ruled by the interactions between the components, the overall, physiologically functioning structure may differ from crystalline regularity. However, such an assembly has an underlying order that is determined by the pattern of connections between the component molecules. At least some of the connecting interfaces of basement membrane components have remained remarkably unchanged during evolution.

## REFERENCES

Blumberg B, MacKrell AJ, Fessler JH (1988, in press) J Biol Chem
Blumberg B, MacKrell AJ, Olson PF, Kurkinen M, Monson JM, Natzle JE, Fessler JH (1987) J Biol Chem 262:5947-5950
Bogaert T, Brown N, Wilcox M (1987) Cell 51:929-940
Campbell AG, Fessler LI, Salo T, Fessler JH (1987) J Biol Chem 262:17605-17612
Cecchini JP, Knibiehler B, Mirre C, LeParco Y (1987) Eur J Biochem 165:587-593
Duncan KG, Fessler LI, Bächinger H-P, Fessler JH (1983) J Biol Chem 258:5869-5877
Fessler LI, Campbell AG, Duncan KG, Fessler JH (1987) J Cell Biol 105:2383-2391
Hirst R, Horwitz A, Buck C, Rohrschneider L (1986) Proc Natl Acad Sci USA 83:6470-6474
Hynes RO (1987) Cell 48:549-554
Kuhl U, Ocalan M, Timpl R, Mayne R, Hay E, von der Mark K (1984) Differentiation 28:164-172
Leptin M, Aebersold R, Wilcox M (1987) EMBO J 6:1037-1043
Lunstrum GP, Bächinger H-P, Fessler LI, Duncan KG, Nelson RE, Fessler JH (1988, in press) J Biol Chem
MacKrell AJ, Blumberg B, Haynes SR, Fessler JH (1988) Proc Natl Acad Sci USA 85:2633-2637
McCarthy RA, Beck K, Burger MM (1987) EMBO J 6:1587-1593
Mirre C, Cecchini J-P, LeParco Y, Knibiehler B (1988) Development 102:369-376
Newman SM Jr, Wright TRF (1981) Dev Biol 86:393-402
Olson PF, Fessler LI, Nelson RE, Sterne R, Campbell AG, Fessler JH (in preparation for publication)
Ruoslahti E, Pierschbacher MD (1987) Science 238:491-497
Siebold B, Qian RA, Glanville RW, Hofmann H, Deutzmann R, Kühn K (1987) Eur J Biochem 168:569-575
Sweet RM, Eisenberg D (1983) J Mol Biol 171:479-488
Timpl R, Oberbaumer I, Von Der Mark H, Bode W, Wick G, Weber S, Engel J (1985) Ann NY Acad Sci 460:58-72
Timpl R, Wiedemann H, Van Delden V, Furthmayr H, Kühn K (1981) Eur J Biochem 120:203-211
Yurchenko PD, Ruben GC (1987) J Cell Biol 105:2559-2568

# Basement Membrane Synthesis in *Drosophila:* Indications for more than One Assembly Mechanism for Basement Membranes

L.I. Fessler, P. Olson, K. Garrison, A. MacKrell, A. Blumberg and J.H. Fessler
Department of Biology and the Molecular Biology Institute
University of California, Los Angeles
405 Hilgard Avenue
Los Angeles, California  90024
USA

Components of basement membranes such as collagen IV and laminin have been high-ly conserved during evolution.  We have characterized collagen IV (Blumberg et al., 1987; Blumberg et al., in press; Lunstrum et al., in press), laminin (Fessler et al., 1987), a proteoglycan called Papilin (Campbell et al., 1987), and glutactin, isolated from *Drosophila melanogaster* cell culture media and embryos.  The amino acid sequences derived from cDNA sequences of some of these components have been determined (Blumberg et al., 1987; Montell and Goodman, 1988; Blumberg et al., in press), and some domains of these molecules show a high degree of identity with the equivalent molecules from vertebrates.

Similarly, the transmembrane receptors (integrins) have been found in *Drosophila* (Bogaert et al., 1987; MacKrell et al., 1988), and the amino acid sequence, derived from the cDNA sequence, of the integrins shows extensive evolutionary conservation.

The macromolecular constituents of basement membranes can either be synthesized by those cells which are immediately adjacent to them, and remain attached to them, or by other cells which do not remain in contact with the newly formed basement membrane.

We investigated the formation of basement membranes in *Drosophila melanogaster* embryos.  *In situ* hybridization with nucleic acid probes specific for *Drosophila* basement membrane procollagen IV show that the mRNA occurs in two categories of cells.  One of these are the cells that are eventually attached to basement mem-branes, and the other group consists of wandering cells which are only transiently associated with the nascent basement membranes.  The latter cells, called lamel-locytes, also strongly stain intracellularly with purified antibodies against *Dro-sophila* collagen IV, *Drosophila* laminin, and another glycoprotein of basement mem-branes, provisionally called X.  We conclude that these wandering cells make base-ment membrane constituents and deposit them as basement membranes, but these cells are not themselves permanently associated with the final structure.

Basement membrane formation is impaired in a *Drosophila* mutant, l(1)mys, in

which the defect is in a transmembrane receptor protein, integrin-$\beta$ (MacKrell et al., 1988). This suggests that such receptors may not only function to anchor cells to adjacent extracellular matrix, but that they also assist in the initial capture and nucleation of basement membrane components.

Different final extracellular matrices could arise from the same set of starting components, if in one case they are supplied through a cell surface that contains receptors for them, and in another they are delivered from an external source.

Blumberg B, MacKrell AJ, Fessler JH (to be published) *Drosophila* basement membrane procollagen $\alpha$1(IV): Complete cDNA sequence, genomic structure and general implications for supramolecular assemblies. J Biol Chem

Blumberg B, MacKrell AJ, Olson PF, Kurkinen M, Monson JM, Natzle JE, Fessler JH (1987) Basement membrane procollagen IV and its specialized carboxyl domain are conserved in *Drosophila*, mouse and human. J Biol Chem 262:5947-5950

Bogaert T, Brown N, Wilcox M (1987) The Drosophila PS2 antigen is an invertebrate integrin that, like the fibronectin receptor, becomes localized to muscle attachments. Cell 51:929-940

Campbell AG, Fessler LI, Salo T, Fessler JH (1987) Papilin: A *Drosophila* proteoglycan-like sulfated glycoprotein from basement membranes. J Biol Chem 262:17605-17612

Fessler LI, Campbell AG, Duncan KG, Fessler JH (1987) Drosophila laminin: Characterization and localization. J Cell Biol 105:2383-2391

Lunstrum GP, Bächinger H-P, Fessler LI, Duncan KG, Nelson RE, Fessler JH (to be published) *Drosophila* basement membrane procollagen IV: Protein characterization and distribution. J Biol Chem

MacKrell AJ, Blumberg B, Haynes SR, Fessler JH (1988) The lethal myospheroid gene of *Drosophila* encodes a membrane protein homologous to vertebrate integrin $\beta$ subunits. Proc Natl Acad Sci USA 85:2633-2637

Montell DJ, Goodman CS (1988) Drosophila substrate adhesion molecule: Sequence of laminin B1 chain reveals domains of homology with mouse. Cell 53:463-473

# Laminin Polymerization and Binding to Glycosaminoglycans: A Hypothesis for Modulation of Basement Membrane Structure

Peter D. Yurchenco

Department of Pathology
Robert Wood Johnson Medical School
Piscataway, N.J. 08854
U.S.A.

Typical basement membranes (BMs) are sheet-like extracellular matrices composed of a lamina lucida and lamina densa. They support and anchor cells, regulate growth and differentiation, divide tissue compartments and selectively filter the passage of macromolecules from one side to the other. Common to most BMs are a set of protomers, or "building blocks", which assemble into a biological matrix: these include type IV collagen, laminin, nidogen and heparan sulfate proteoglycans and smaller amounts of other components. These components self-assemble with specific binding interactions into one or more molecular architectures [Yurchenco et al.,1986; Yurchenco & Ruben,1988]. Functions of BMs such as support and sieving are expected to be dependent on both the presence of protein domain determinants as well as their supramolecular arrangement in three-dimensional space. Similarly cell-matrix interactions are probably dependent on architecture as well. A matrix protein with a cell binding domain, for example, cannot interact with the cell if its domain is inaccessible by virtue of its geometrical position in the matrix: evidence has been presented that this is the case with the central cell-binding domain of laminin in the corneal epithelial BM [Schittny et al.,1988].

Architectural heterogeneity, reflecting different functional needs, can be identified in different tissues. The lens capsule, for example, is extremely thick with a relatively parallel alignment of very fine filaments [Cammarata et al.,1986], lacks a lamina lucida, and is transparent. Glomerular BM, the main filtration barrier of the renal glomerulus, has three layers. Descemet's membrane, another light-transmitting BM, possesses regular hexagonal arrays. Heterogeneity is also seen at a biochemical level. While most BMs share similar basic components, different ratios of these components are found in different BMs with collagen, for example, ranging from 25% in Reichert's membrane to at least 90% in lens capsule [Kefalides et al.,1981; Kefalides,1981]. The thermal stability of type IV collagen in situ is dependent on the BM in which it is located, reflecting variations in structural milieu [Linsenmeyer et al.,1984]. Molecular variability also appears to exist in collagen and laminin depending on tissue source [Edgar et al.,1988; Langeveld et al.,1988].

BM heterogeneity may provide a mechanism to respond to different developmental or physiological needs. Both in early embryonic development and in the capillary angiogenesis of wound repair, for example, laminin is deposited before type IV collagen in newly formed BM [Leivo et al.,1980; Wu et al.,1983; Form et al., 1986]. Here the initial BMs may furnish a different set of signals to adjacent cells and may have different physical properties (e.g. more flexible or permeable). During acute inflammation, when the post-capillary venule must accommodate a flux of large amounts of solutes as well as mobile cells, the BM structure may change to accommodate this flux.

How might the BM-forming cell create and regulate heterogeneity? One possibility is that the constituent macromolecules, despite overall similarities, are different for each BM (e.g. different post-translational modifications) and assemble into different architectures. This would require a large repertoire of protomer variants to cover the structural heterogeneity in both space and time. A second possibility is that the common components always self-assemble into the identical supramolecular structure while heterogeneity is generated by the further addition of structure with components unique to a specific BM. A third possibility is that there is assembly polymorphism [Oosawa & Asakura, 1975] in which the same protomers can assemble into different supramolecular arrays as a result of the modifying influence of other components (e.g. changes in their relative concentrations). A classical system in which this had been observed is that of the cytoskeleton where actin, depending on its interactions with associated proteins can form different varieties of polymerized filaments and thereby respond to different physiological needs. Assembly polymorphism also operates in the extracellular matrix. For example, type I collagen fiber diameter can be modified to meet different tissue requirements by the intercalation of smaller amounts of type V collagen [Birk et al.,1988]. Our recent findings indicate polymorphic structural regulation may exist in the BM as well.

*Laminin:* This large glycoprotein ($M_r$ = 850 - 1000 kDa) plays a central role in basement membranes, both structurally and functionally. By electron microscopy laminin is visualized as an asymmetrical cross, 110 nm in its greatest dimension, possessing two globular domains in each short arm and a larger globule at the end of the long arm [Engel et al., 1981]. The protein is composed of three polypeptide chains (A, B1, B2) which are bound together by disulfide interactions [Cooper et al.,1981; Kurkinen et al.,1983]. A current view of laminin native structure is that the N-terminal moieties of each chain form the three short arms: these chains join to form the cross and run together to form the long arm with the terminal globule formed only by the larger A chain [Timpl & Dziadek, 1986]. As extracted from tissue with chelating agents in physiological buffers [Paulsson et al.,1987] laminin is tightly complexed with nidogen, a 150 kDa dumbbell-shaped glycoprotein. Laminin's multidomain structure provides for a series

of binding interactions with other macromolecules. Laminin, in addition to its association with nidogen, has been found to bind heparin [Del Rosso *et al.* 1981; Sakashita *et al.*,1980], basement membrane heparan sulfate [Fujiwara *et al.*,1984], type IV collagen both directly [Charonis *et al.*,1985] and through a nidogen bridge [Dziadek, Paulsson & Timpl,1985], and to itself [Yurchenco *et al.*,1985]. Laminin appears to employ specific protein domains in these interactions: the inner cross region interacts with nidogen, the end of the long arm binds glycosaminoglycans, and the ends of both arms provide for interactions with collagen and other molecules. It is believed that these specific interactions produce one or several three-dimensional geometries which are in significant part responsible for functions of basement membranes.
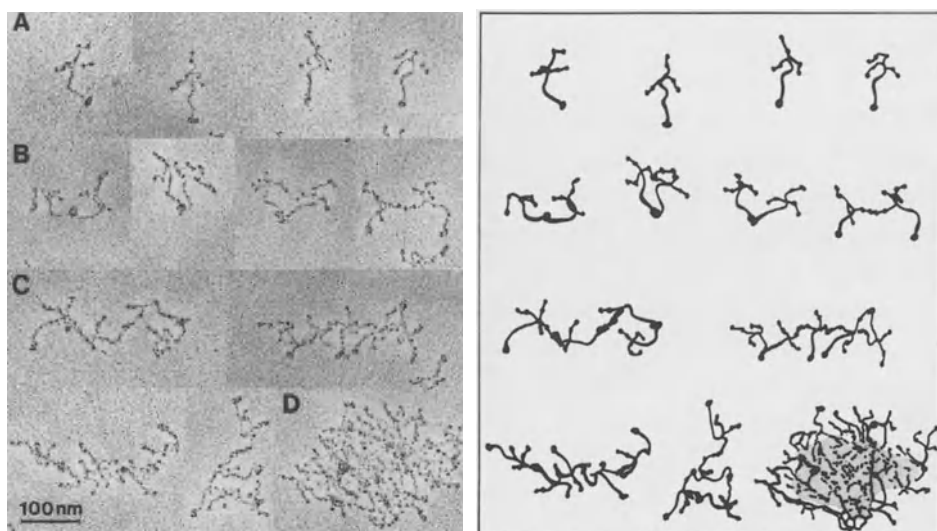


**Figure 1.** *Laminin and its aggregates.* Electron micrographs of rotary shadowed Pt/C replicas of laminin monomers (**A**), dimers (**B**), oligomers (**C**), and polymers (**D**). Interpretive drawings shown on right side. Terminal interactions of the long and short arms of laminin can be identified in dimers and many oligomers; however, molecular organization in larger complexes is unclear by this technique.

*Laminin Polymerization:* Laminin will aggregate *in vitro* [Yurchenco *et al.*,1985] in a temperature, time- and concentration-dependent manner. This aggregation can be analyzed by turbidity, sedimentation, viscosity and by electron microscopy (Fig.1). Assembly appears to occur cooperatively in two steps by a process of *nucleation-propagation*. A plot of either sedimentable aggregate or turbidity against total protein concentration reveals an apparent critical concentration of 0.1 $\mu$M (0.05 $\mu$M for laminin-nidogen) below which polymerization does not occur. In addition, upon warming laminin in the absence of divalent cation, turbidity development is blocked and only oligomeric forms are visualized in the electron microscope: addition of a molar excess of calcium (and to a lesser degree with magnesium) will restore the

development of turbidity and the appearance of large aggregates by electron microscopy [Yurchenco et al.,1985]. Thus we identify a temperature-dependent oligomer forming step followed by a divalent cation-dependent polymer forming step. It has recently been reported [Paulsson, 1988] that half-maximal aggregation is achieved at approximately 10 $\mu$M $Ca^{2+}$ and that there are about 16 binding sites for calcium of varying affinities. The finding that EDTA or EGTA in neutral isotonic buffer will selectively liberate substantial amounts of soluble laminin from the EHS tumor matrix [Paulsson et al.,1987] and other BMs argues that this assembly process is physiologically relevant. At about 2.5 $\mu$M laminin undergoes a sol-to-gel transition upon incubation at 25-37°C (Fig. 2). Gelation, like aggregation, is thermally reversible: the clear gel returns to a sol if cooled on ice and can be cycled between the two states. If we assume a homogenous distribution of laminin molecules in this matrix, we would estimate the laminin centers are separated from each other by 80-90 nm at this minimal gelation concentration.

Which domains of laminin participate in this assembly process and what final polymer architecture is achieved? By electron microscopy (Fig. 1) both long and short arm ends are observed to be bound together in dimeric and larger oligomers [Yurchenco et al.,1985]; however, it is not possible to visualize the structural domains involved in forming the larger aggregates. Using proteo-



Figure 2. *Laminin Gelation*. Laminin/nidogen, in 10 mM Tris-HCl, pH 7.4, 127 mM NaCl, 1 mM $CaCl_2$, was adjusted to either 1 or 5 mg/ml, incubated at either 37° or 0°C for one hour in a tube in a upright position, and then tilted and photographed as above. Laminin gelled only at the higher temperature and concentration (middle tube).

lytically-generated protein fragments [Ott et al.,1982; Timpl et al.,1983; Paulsson,1988] as an experimental tool, there is now further evidence to support the hypothesis that the polymer is also held together by peripheral-domain interactions. First, polyclonal laminin antibody which does not bind P1' (cross region[1]) and which therefore reacts with more peripheral domains inhibits laminin aggregation while antibody which binds P1' has little effect (Fig.3). Second, it has been reported that antibody specific for the E3 domain of laminin (elastase-generated globule of long arm) will inhibit aggregation [Charonis et al.,1986]. Third, we find that the E3 fragment (but not fragment P1') will bind to a laminin affinity column. Fourth, the E4 fragment of laminin (globule of short arm, elastase generated) will inhibit laminin aggregation (Fig. 4) while the P1' fragment will not. These data are interpreted to indicate that the laminin polymer is held together by specific end-to-end interactions of the long and short arms with the formation
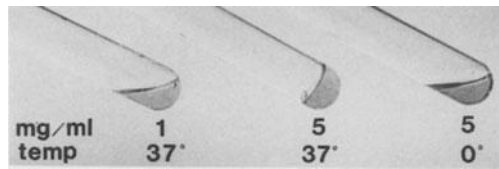
---

[1]We distinguish a pepsin-derived laminin cross fragment P1' from P1 [Rohde et al.,1980] and E1' [Paulsson,1988]: it is of intermediate size ($M_r$ of ~440 kDa vs 290 kDa for P1 and 530 kDa for E1') and shape (asymmetrical "Y"-shape with a longer arm and one or more diminished globules).

of a specific molecular architecture. However, it cannot be excluded that weaker secondary interactions, dependent on these primary bonds, also contribute to this structure.
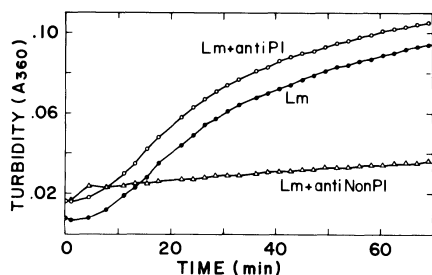


**Figure 3.** *Antibody inhibition of laminin aggregation.* Rabbit anti-laminin antisera was passed down a laminin P1' column, separated into P1'-binding and P1'-non-binding fractions, and digested with papain to form Fab fragments. Laminin (0.4 mg/ml) in 10 mM Tris-HCl, pH 7.4, 127 mM NaCl, 1 mM CaCl$_2$ (TBS/-Ca) was incubated at 35°C alone (closed circles) or in the presence of either anti-P1' Fab (open circles) or anti-nonP1' Fab (open triangles). Only antibody which did not bind to the cross region inhibited aggregation. (K Barkalow, honors thesis, laboratory of P Yurchenco).
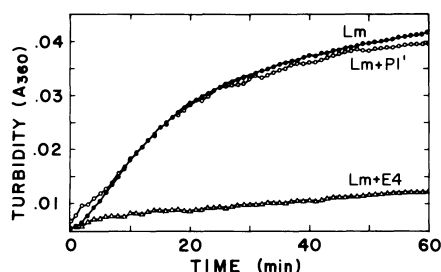
**Figure 4.** *Inhibition of laminin aggregation with proteo-lytic fragments.* Laminin domain fragments P1' and E4 were prepared as described [Yurchenco et al.,1985; Timpl et al.,1983; Paulsson,1988]. Laminin/nidogen complex (0.25 mg/ml in TBS/Ca) was incubated at 35°C alone (closed circles) or in the presence of fragments (0.4 mg/ml) P1' (open circles) and fragment E4 (open triangles). The terminal short arm domain (E4) selectively inhibited aggregation.

*Basement Membrane Heparan Sulfate Proteoglycan:* Both low and high density (high and low molecular weight) forms of HSPG have been identified and characterized in BMs [Fujiwara et al.,1984; Paulsson et al.,1987; Yurchenco et al.,1987]. The polyanionic glycosaminoglycan (GAG) chains of these components are believe to be important in regulating the charge-dependent selective filtration properties of BMs [Farquhar et al.,1982]. The larger HSPG has a single polypeptide chain core protein, is organized into a tandem array of globular domains, and usually has three GAG chains at one pole of the core [Paulsson et al.,1987; Yurchenco et al.,1987]. It appears that the core can bind to itself at one end to form dimers and oligomers [Yurchenco et al.,1987] and may have interactions with several other BM components.

*Laminin - Glycosaminoglycan Binding:* By affinity chromatography both heparin and heparan sulfate chains of low density BM proteoglycan bind to laminin [Del Rosso et al.,1981]. This interaction is believed to primarily be due to binding to the globule of the long arm of laminin [Ott et al.,1982]. Heparin binds to laminin-E3, as quantitated with a nitrocellulose assay, with a $K_D$ of about 0.1 $\mu$M [Yurchenco PD, Schittny JC, Cheng Y-S, Wong C, submitted]. BM heparan sulfate, on the other hand, exhibits substantially weaker interaction (between 50 and 100 fold higher concentration of heparan sulfate is required to produce a 50% inhibition of radiolabelled heparin binding to laminin domain E3 as compared to unlabelled heparin). Given these findings, we might expect that *in vivo* a low concentration of heparin would displace BM

heparan sulfate from laminin and therefore induce a reorganization of the surface polyanion charges.

*Effect of Glycosaminoglycan on Laminin Polymerization:* Heparin also has an effect on the polymerization of laminin (Fig. 5) and this effect is manifested in several ways [Yurchenco PD, Schittny JC, Cheng Y-S, Wong C, submitted]. *First,* when heparin (0.2 to 20 µg/ml) is incubated with laminin or laminin/nidogen and assembly followed by turbidity, it is found, in a concentration-dependent manner, to decrease both the time to achieve half-maximal turbidity and the apparent critical concentration for aggregation (from 50 µg/ml to

**Figure 5.** *Heparin effect on laminin aggregation.* Laminin in TBS/Ca was incubated alone (solid circles), or in the presence of either 10 µg/ml heparin (open circles) or EHS BM heparan sulfate (open triangles) at 35°C.

about 5 µg/ml using laminin/nidogen). The effect, which is seen in the physiological heparin concentration range, approaches saturation when heparin (15-16 kDa) is present in molar excess. The effect is highly specific for heparin and is inhibited by heparinase (preferentially degrades heparin) but not by heparitinase (preferentially degrades heparan sulfate). Furthermore the heparin co-factor, antithrombin III, inhibits the heparin-induced change in aggregation. By turbidity, BM heparan sulfate (EHS-derived), bovine kidney heparan sulfate, chondroitin sulfates, hyaluronic acid, low molecular weight heparin (4-6 kDa), and de-N-sulfated heparin have little or no effect on laminin aggregation. *Second,* heparin alters the macroscopic gelation properties of laminin. In the presence of heparin (10-40 µg/ml), the sol-to-gel transition concentration increases (2.6 to 4 mg/ml) and the apparent viscosity of the gel above this transition becomes lower. *Third,* heparin alters the requirement of laminin aggregation for calcium in a synergistic manner. In the absence of heparin, laminin will not aggregate in the usual concentration range studied unless calcium or other divalent cation is present. However, in the presence of heparin, laminin will aggregate in the absence of divalent cation (with EDTA). The level of turbidity achieved for both heparin and calcium is greater than that achieved for each separately.
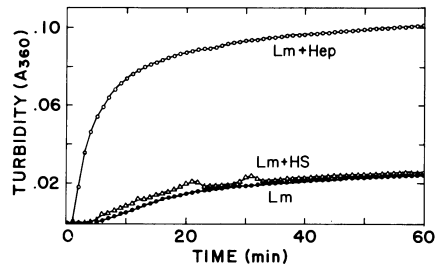
The data indicate that heparin specifically induces a change in the process of laminin self-assembly and in the polymer structure. While both the mechanism and molecular architecture of the heparin effect remain to be elucidated, we can consider possible models based on the data at hand. First the heparin effect appears to be dependent on both the density of sulfation as well as the length of the polysaccharide. The latter raises the possibility that heparin acts

as a bridge, or crosslink, between laminin molecules. However, it is also possible that heparin induces an allosteric-type modification in laminin, changing its self-assembly. In interacting with laminin, heparin alters the thermodynamics and probably the spatial relationships of protomers in the polymer. The increase in the gel transition concentration further suggests that laminin may become more plastic in the BM when heparin is present, possibly allowing larger macromolecules to penetrate laminin in BM.
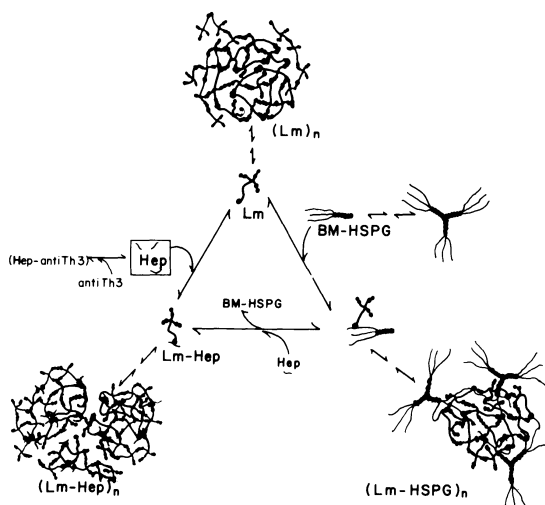


**Figure 6.** *Working hypothesis of laminin - heparin - HSPG interrelationships.* Extrinsic heparin (and possibly more highly sulfated cell heparan sulfates) binds laminin, alters its assembly and displaces BM-heparan sulfate proteoglycan GAG chains bound to laminin. Effect of heparin on laminin may be to drive self-assembly (with possible formation of crosslinks) but with formation of a more discontinuous (sol) polymer. This might, for example, increase permeability through the BM. These effects would be reversed both by loss of heparin through dilution as well as by inhibitors such

*A Hypothesis for Regulation of Laminin Supramolecular Structure in BM*:    Heparin is not generally considered a component of basement membranes; rather, it is released by platelets, mast cells and other inflammatory cells during thrombosis, inflammation, repair and development. On the other hand heparin can contact BM and hence potentially interact with it, *e.g.* when vascular BM is exposed to blood following endothelial injury and when new capillary BM is formed during angiogenesis. Therefore, given the interactions described, we have the possibility for the modification of BM structure with non-covalent, and hence reversible, interactions with an exogenous component. We have proposed from *in vitro* experiments that heparin can both disrupt HSPG--laminin binding and alter laminin self-assembly. Given the above specific and reversible interactions, that heparin is not apparently itself an intrinsic BM component, that the heparin binding site(s) on laminin is(are) the same as the binding site for other glycosaminoglycans, and that this site is on the same globule that

binds type IV collagen, heparin may serve the role as an extrinsic and transient regulator of several important BM interactions (assembly polymorphism). In angiogenesis, for example, it has been reported that mast cells release heparin in front of the leading edge of the growing capillary bud [Folkman,1986]: heparin, in addition to its chemotactic effect on endothelial cells, may act directly on the newly forming BM. The concentration of heparin may also locally increase (above a baseline of 1-2.5 $\mu$g/ml) in the BM of a microvessel following injury or during development. As a result BM mechanical and permeability properties as well as cell signalling could change as a consequence of [i] a heparin displacement of the chains of intrinsic BM HSPGs altering the topographical distribution of polyanionic charges and charge-dependent sieve properties and [ii] a heparin-induced alteration of the molecular architecture and physical properties of the laminin supramolecular complex. In addition [iii] heparin may dissociate other interactions such as cell surface heparan sulfate--laminin bonds. In short, intrinsic BM assembly and molecular architecture might be coordinately changed by a rise in concentration of a single extrinsic glycosaminoglycan. While heparin has been implicated in producing alterations of BM structure [Petorak et al.,1977; Turley et al.,1987] and function [Wardle & Uldall, 1972] no direct cause and effect has yet been established. The findings reported here raise the interesting possibility that such specific heparin mechanisms may exist and may be of biological importance.

## REFERENCES

Birk DE, Fitch JM, Babiarz JP, Linsenmeyer TF (1988). Collagen type I and V are present in the same fibrils in the avian corneal stroma. *J Cell Biol* **106**:999-1008.

Cammarata PR, Cant-Crouch D, Oakford L, Morrill A (1986) Macromolecular organization of bovine lens capsule. *Tissue & Cell* **18**:83-97.

Charonis AS, Tsilibary EC, Yurchenco PD, Furthmayr H (1985) Binding of laminin to type IV collagen: a morphological study. *J Cell Biol* **100**:1848-1853.

Charonis AS, Tsilibary EC, Saku T, Furthmayr H (1986) Inhibition of laminin self-assembly and interaction with type IV collagen by antibodies to the terminal domain of the long arm. *J Cell Biol* **103**:1689-1697.

Cooper AR, Kurkinen M, Taylor A, Hogan BLM (1981) Studies on the biosynthesis of laminin by murine parietal endoderm cells. *Eur J Biochem* **119**:189-197.

Del Rosso M, Cappelletti R, Viti M, Vannucchi S, Chiarugi V (1981) Binding of the basement-membrane glycoprotein laminin to glycosaminoglycans. *Biochem J* **199**:699-704.

Dziadek M, Paulsson M, Timpl R (1985) Identification and interaction repertoire of large forms of the basement membrane protein nidogen. *EMBO J* **4**:2513-2518.

Edgar D, Timpl R, Thoenen H (1988) Structural requirements for the stimulation of neurite outgrowth by two variants of laminin and their inhibition by antibodies. *J Cell Biol* **106**:1299-1306.

Farquhar MG, Courtoy PJ, Lemkin MC, Kanwar YS (1982). In Kühn K, Shoene HH, Timpl R (eds) *New Trends in Basement Membrane Research*, Raven Press, New York, p9.

Folkman J (1986) How is blood vessel growth regulated in normal and neoplastic tissue? *Cancer Res* **46**:467-473.

Form DM, Pratt BM, Madri JA (1982) Endothelial cell proliferation during angiogenesis: in vitro modulation by basement membrane components. *Lab Invest* **55**:521-530.

Fujiwara S, Wiedemann H, Timpl R, Lustig A, Engel J (1984) Structure and interactions of heparan sulfate proteoglycans from a mouse tumor basement membrane. *Eur J Biochem* **143**:145-157.

Kefalides NA, Alper R, Clark CC (1979) Biochemistry and metabolism of basement membranes. *Int Rev Cytol* **61**:167-228.

Kefalides NA (1981) Basement membranes: structure function relationships. *Renal Physiol* **4**:57-66.

Kefalides NA (1981) Biochemical properties of human glomerular basement membrane in normal and diabetic kidneys. *J Clin Invest* **53**:403.

Kurkinen M, Barlow DP, Jenkins JR, Hogan BLM (1983) In vitro synthesis of laminin and entactin polypeptides. *J Biol Chem* **258**:6543-6548.

Langeveld JPM, Wieslander J, Timoneda J, McKinney P, Butkowski RJ, Wisdom BJ, Hudson BG (1988) Structural heterogeneity of the noncollagenous domain of basement membrane collagen. *J Biol Chem* **263**:10481-10488.

Leivo I, Vaheri A, Timpl R, Wartiovaara J (1980) Appearance and distribution of collagens and laminin in the early mouse embryo. *Dev Biol* **76**:100-114.

Linsenmeyer TF, Gibney E, Fitch JM, Gross J, Mayne R (1984) Thermal stability of the helical structure of type IV collagen within basement membranes in situ: determination with a conformation-dependent monoclonal antibody. *J Cell Biol* **99**:1405-1409.

Oosawa F, Asakura S (1975) *Thermodynamics of the polymerization of protein.* Academic Press, London New York San Francisco.

Ott U, Odermatt E, Engel J, Furthmayr H, Timpl R (1982) Protease resistance and conformation of laminin. *Eur J Biochem* **123**:63-72.

Paulsson M, Aumailley M, Deutzmann R, Timpl R, Beck K, Engel J (1987) Laminin-nidogen complex: extraction with chelating agents and structural characterization. *Eur J Biochem* **166**:11-19.

Paulsson M, Yurchenco PD, Ruben GC, Engel J, Timpl R (1987) Structure of low density heparan sulfate proteoglycan isolated from a mouse tumor basement membrane. *J Mol Biol* **197**:297-313.

Paulsson M (1988) The role of $Ca^{2+}$ binding in the self-aggregation of laminin-nidogen complexes. *J Biol Chem* **283**: **263**: 5425-5430.

Petorak I, Imren H, Iplikçi A (1977) Electronmicroscopical investigations of the effects of heparin upon the structural elements of the rat glomerulus. *Exp Path* **14**:252-258.

Rohde H, Bächinger HP, Timpl R (1980) Characterization of pepsin fragments of laminin in a tumor basement membrane: evidence for the existence of related proteins. *Hoppe-Seyler's Physiol Chem* **361**:1651-1660.

Sakashita S, Engvall E, Ruoslahti E (1980) Basement membrane glycoprotein laminin binds to heparin. *FEBS Lett* **116**:243-246.

Schittny JC, Timpl R, Roth J, Engel J (1988) Localization of three domains of laminin, nidogen and low density heparan sulfate proteoglycan in basement membranes of the mouse cornea: a high resolution immunoelectron microscope study. *J Cell Biol* In press.

Timpl R, Johansson S, van Delden V, Oberbäumer, Höök M (1983) Characterization of protease-resistant fragments of laminin mediating attachment and spreading of rat hepatocytes. *J Biol Chem* **258**:8922-8927.

Timpl R, Dziadek M (1986) Structure, development and molecular pathology of basement membranes. *Int Rev Exp Pathol* **29**:1-112.

Turley E, Tretiak M, Tanguay K (1987) Effect of glycosaminoglycans and enzymes on the integrity of human placental amnion as a barrier to cell invasion. *J N C I* **78**:787-795.

Wardle EN, Uldall PR (1972) Effect of heparin on renal function in patients with oliguria. *Brit Med J* **4**:135-138.

Wu T-C, Wan Y-J, Chung AE, Damjanov I (1983) Immunohistochemical localization of entactin and laminin in mouse embryos and fetuses. *Dev Biol* **100**:496-505.

Yurchenco PD, Tsilibary EC, Charonis AS, Furthmayr H (1986) Models for the self-assembly of basement membrane. *J Histochem Cytochem* **34:**93-102.

Yurchenco PD, Tsilibary EC, Charonis AS, Furthmayr H (1985) Laminin polymerization in vitro: evidence for a two-step assembly with domain specificity. *J Biol Chem* **260:**7636-7644.

Yurchenco PD, Cheng YS, Ruben GC (1987) Self-assembly of a high molecular weight basement membrane heparan sulfate proteoglycan into dimers and oligomers. *J Biol Chem* **262:**17668-17676.

Yurchenco PD, Ruben GC (1988) Type IV collagen lateral associations in the EHS tumor matrix: comparison with amniotic and in vitro networks. *Am J Pathol* **132:**278-291.